

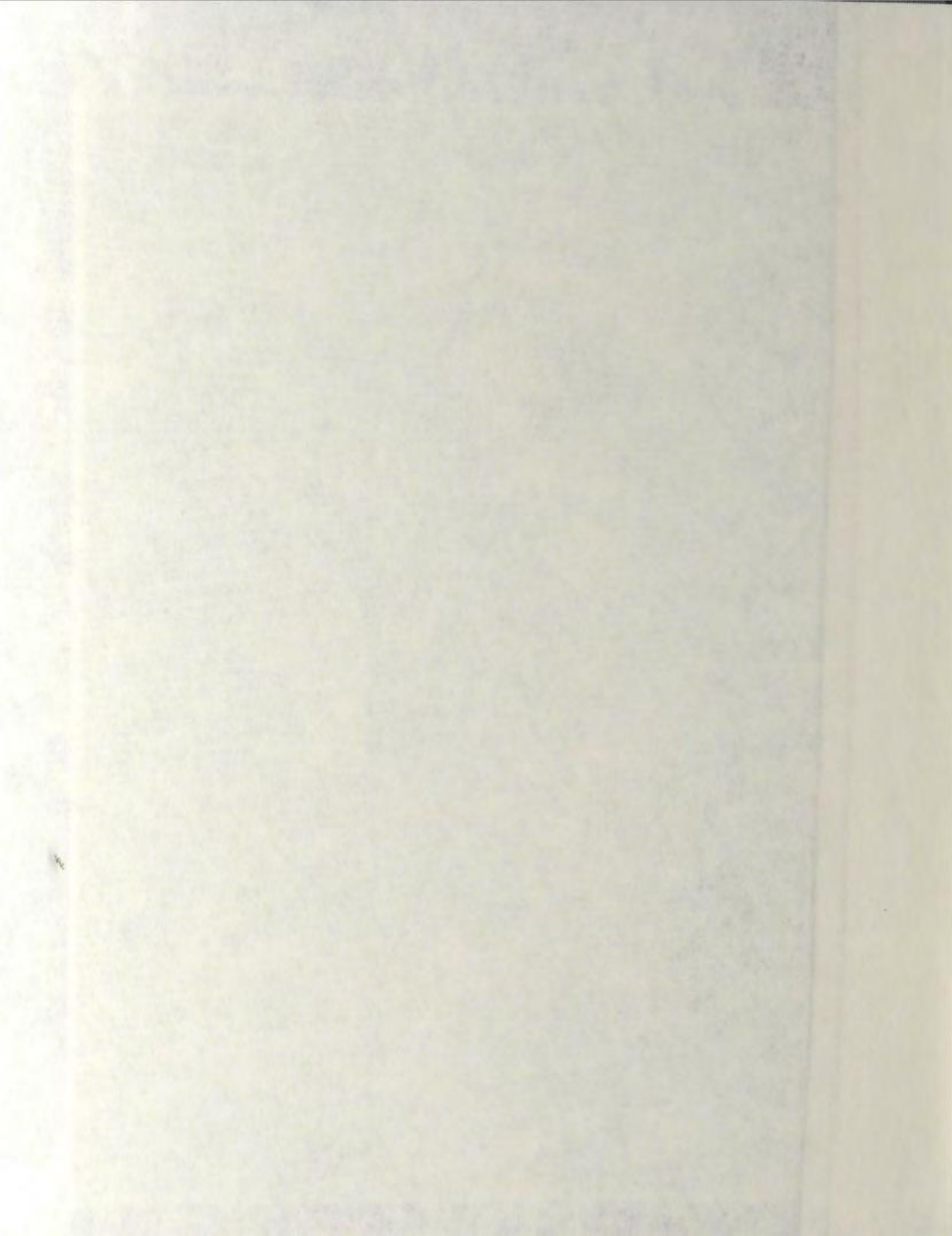
GEOCHEMICAL AND ISOTOPIC EVOLUTION OF THE
MAGGO GNEISS COMPONENT FROM THE HOPEDALE
BLOCK, LABRADOR: EVIDENCE FOR LATE-MIDDLE
ARCHAEAN CRUSTAL REWORKING

CENTRE FOR NEWFOUNDLAND STUDIES

TOTAL OF 10 PAGES ONLY
MAY BE XEROXED

(Without Author's Permission)

GREGORY CLEMENT FINN, B.Sc., M.Sc.





National Library
of Canada

Bibliothèque nationale
du Canada

Canadian Theses Service Service des thèses canadiennes

Ottawa, Canada
K1A 0N4

NOTICE

The quality of this microform is heavily dependent upon the quality of the original thesis submitted for microfilming. Every effort has been made to ensure the highest quality of reproduction possible.

If pages are missing, contact the university which granted the degree.

Some pages may have indistinct print especially if the original pages were typed with a poor typewriter ribbon or if the university sent us an inferior photocopy.

Reproduction in full or in part of this microform is governed by the Canadian Copyright Act, R.S.C. 1970; c. C-30, and subsequent amendments.

AVIS

La qualité de cette microforme dépend grandement de la qualité de la thèse soumise au microfilmage. Nous avons tout fait pour assurer une qualité supérieure de reproduction.

S'il manque des pages, veuillez communiquer avec l'université qui a conféré le grade.

La qualité d'impression de certaines pages peut laisser à désirer, surtout si les pages originales ont été dactylographiées à l'aide d'un ruban usé ou si l'université nous a fait parvenir une photocopie de qualité inférieure.

La reproduction, même partielle, de cette microforme est soumise à la Loi canadienne sur le droit d'auteur, SRC 1970, c. C-30, et ses amendements subséquents.

GEOCHEMICAL AND ISOTOPIC EVOLUTION OF
THE MAGGO GNEISS COMPONENT FROM
THE HOPEDALE BLOCK, LABRADOR: EVIDENCE FOR
LATE - MIDDLE ARCHAean CRUSTAL REWORKING

BY

© GREGORY CLEMENT FINN, B.Sc., M.Sc.

A thesis submitted to the School of Graduate
Studies in partial fulfillment of the
requirements for the degree of
Doctor of Philosophy

Department of Earth Sciences (Geology)
Memorial University of Newfoundland

June 1988

St. John's

Newfoundland

Permission has been granted to the National Library of Canada to microfilm this thesis and to lend or sell copies of the film.

The author (copyright owner) has reserved other publication rights, and neither the thesis nor extensive extracts from it may be printed or otherwise reproduced without his/her written permission.

L'autorisation a été accordée à la Bibliothèque nationale du Canada de microfilmer cette thèse et de prêter ou de vendre des exemplaires du film.

L'auteur (titulaire du droit d'auteur) se réserve les autres droits de publication; ni la thèse ni de longs extraits de celle-ci ne doivent être imprimés ou autrement reproduits sans son autorisation écrite.

ISBN 0-315-50463-3

ABSTRACT

The Hopedale Block, an informal name for the southern portion of the Nain Structural Province, Labrador, preserves evidence of a protracted Archaean to Proterozoic developmental history. This study examines the Archaean development of a segment of the Hopedale Block, centred at Hopedale village, as recorded in the Maggo gneiss, a typical grey gneiss of tonalitic to trondhjemitic composition. Following field mapping and petrographic examination of all lithologies within the study area, major, trace and rare earth element (REE) lithogeochemical analyses and Rb-Sr isotopic determinations were completed on the Maggo gneiss.

The geochronological development of the Maggo gneiss, based on the Rb-Sr isotopic studies of twelve suites, identified three distinct Archaean tectonothermal events. Isotopic evidence of the oldest event, the Pre-Hopedalian, dated at 3305 ± 75 Ma (1 sigma) is preserved at one locality, however structural evidence of this event can be recognized throughout the study area. Inclusions of supra-crustal material (Weekes association) and anorthosite within Maggo gneiss, preserve evidence of two periods of deformation prior to the Pre-Hopedalian event. The dominant component of the Maggo gneiss is preserved within the Hopedalian domain. Four sample suites yielding ages of $3,140 \pm 95$ Ma to $3,025 \pm 165$ Ma date this event. The

Hopedalian event produced a moderate to steeply dipping, NW-SE planar fabric within the gneiss. The Hopedale dykes, which predate the Hopedalian event were rotated into concordance with the Hopedalian fabric at this time.

The Flordian, a series of events, which marks the last major Archaean period of tectonism to affect the Hopedale Block lithologies occurred between 2,927 +/- 50 Ma and 2,632 +/- 285 Ma. The Flordian is divided into an early and late period characterized by reworking of preexisting crustal material separated by a period during which the Kanariktok intrusive suite was emplaced. In response to the Flordian reworking the Maggo gneiss exhibits the following characteristics:

- 1) reorientation of earlier fabrics into a NE-SW direction,
- 2) low to middle amphibolite facies metamorphism which retrogresses Hopedalian middle to upper amphibolite facies assemblages,
- 3) large ion lithophile element (LILE; Rb, Ba, K) depletion, high field strength (HFS) element (Ti, Zr, P, Y and V) enrichment and no change in either Sr or REE contents,
- 4) resetting of the Rb-Sr isotopic systematics of the gneiss in response to Rb depletion.

Geochemical reworking associated with the Flordian event occurs independently of structural reworking.

The application of the concept of areals and areal isochrons as applied to the Hopedalian and Flórdian suites yields ages of $3,366 \pm 212$ Ma and $2,930 \pm 82$ Ma, respectively. These ages date the timing for a common period of Sr homogenization for each group of suites at a specific point in their past.

Petrogenetic modelling, using LILE, REE and HFS element and a variety of possible lithologic compositions has been carried out to determine the source to the Maggo gneiss precursor. An intermediate composition parent, metamorphosed to granulite and/or amphibolite facies, on 25% melting will yield REE and HFS element abundances in agreement with those observed for the Maggo gneiss. The source compositions modelled all require trace amounts ($< 0.5\%$) of minor, residual, phases, e.g. apatite, titanite and zircon, which control single elements, e.g. P, Ti and Zr respectively, and REE abundances in the resulting melts. The major and trace element composition of the parent used is comparable to published results for Early Archaean crust as represented by the Amitsoq gneiss of southern West Greenland.

These results extend the history of the Hopedale Block beyond that presently recognized. A proposed correlation between the recorded development for other areas of the North Atlantic Craton (NAC) and the Hopedale Block is presented.

ACKNOWLEDGMENTS

The author wishes to acknowledge the assistance and support of the following people;

B.J. Fryer who suggested studying the affects of Flordian reworking on the Maggo Gneiss at Hopedale. Financial support, in the form of an NSERC grant to B.J.F., provided a graduate student stipend. Costs of field work were offset by an EMR Research Grant held by B.J.F. and G.C.F. and a Northern Science Training Grant to B.J.F.

Supervisory committee members B.J. Fryer, T. Rivers and R.K. Stevens.

I.F. Ermanovics introduced the author to the geology of the Hopedale Block.

G. (Dougle) Wong (1982) and P. Carracio (1983) provided able field assistance under often adverse conditions.

Technical assistance at MUN was provided by G. Andrews (AA analysis); T. Finn (isotope chemistry); D. Press and G. Veinott (XRF analysis); H. Longerich (microprobe); F. Thornhill, L. Warford and R. Soper (thin sections); G. Ford (anything and everything); A. Collins (drafting supplies); and at Brock University by P. Brown (drafting); D. Mucclante (photography).

The deepest thanks go to Trish; first, for saying yes and staying in Newfoundland longer than she planned; second, for all her help and encouragement during the course of this study, and lastly for understanding all the early mornings, late nights and weekends.

TABLE OF CONTENTS

	Page
Abstract.....	ii
Acknowledgments.....	v
Table of Contents.....	vi
List of Tables.....	xiv
List of Figures.....	xvii
List of Photographic Plates.....	xxii
Chapter 1 - INTRODUCTION.....	1
1.1 High Grade Gneiss Terrains.....	1
1.2 Reworking.....	3
1.3 Previous Work.....	7
1.4 Overview of Hopedale Block Geology.....	9
1.5 Scope and Aims of the Investigation.....	10
1.6 Location and Access.....	11
Chapter 2 - REGIONAL GEOLOGY AND STRUCTURAL SETTING.....	13
2.1 Introduction.....	13
2.2 Regional Geology.....	14
2.3 Model for the Development of the Hopedale Block.....	24
2.4 Structural Geology.....	30
2.4.1 Introduction.....	30
2.4.2 Pre-Pre-Hopedalian.....	32
2.4.3 Pre-Hopedalian.....	35
2.4.4 Hopedalian Structural Domain.....	35

2.4.5	Flordian Structural Domain.....	39
2.4.6	Proterozoic Events.....	45
2.4.7	Faults and Shear Planes.....	46
2.4.8	Summary of Structural Data.....	49
Chapter 3	- LITHOLOGIC DESCRIPTIONS AND METAMORPHISM.....	51
3.1	Introduction.....	51
3.2	Description of Lithologies.....	52
3.2.1	Weekes Association.....	52
3.2.1.1	Field Relationships-Weekes Association..	54
3.2.1.2	Amphibolite Subunits.....	56
3.2.1.3	Ultramafic Rocks.....	58
3.2.1.4	Marble.....	61
3.2.1.5	Pelitic and Metavolcaniclastic Rocks...	62
3.2.1.6	Endoskarn Lithology.....	65
3.2.2	Anorthosite and Related Rocks.....	66
3.2.2.1	Field Relationships.....	66
3.2.2.2	Mineralogy.....	67
3.2.3	Maggo Gneiss.....	68
3.2.3.1	Field Relationships.....	68
3.2.3.2	Mineralogy.....	73
3.2.4	Hopedale Dykes.....	78
3.2.4.1	Field Relationships.....	78
3.2.4.2	Mineralogy.....	81
3.2.5	Kikkertavaik Dykes.....	83
3.2.5.1	Field Relationships.....	83
3.2.5.2	Mineralogy.....	84

3.3 Metamorphism.....	85
3.3.1 Introduction.....	85
3.3.2 Maggo Gneiss.....	86
3.3.3 Hopedale Dykes.....	87
3.3.4 Weekes Association.....	92
3.3.4.1 Amphibolite Subunits.....	93
3.3.4.2 Ultramafic Rocks.....	95
3.3.5 Summary.....	98
 Chapter 4 - GEOCHRONOLOGY.....	 100
4.1 Introduction.....	100
4.1.1 Isochron vs. Errorchron.....	101
4.2 Manuel Island.....	102
4.3 Porphyritic Phase.....	102
4.4 Hypothesis Island.....	109
4.5 Southeast Double Island.....	109
4.6 Hopedale Harbour.....	109
4.7 Marsha's Cove.....	112
4.8 Hopedale Gneiss.....	116
4.9 Black Head Tickle.....	123
4.10 Dead Dog Point.....	124
4.11 Pilliarusik Bay.....	124
4.12 Dyke Island.....	127
4.13 Next Bay North.....	130
4.14 Discussion.....	131
4.14.1 Hopedalian Suites.....	132
4.14.2 Flordian Suites.....	136

4.14.2.1 Introduction.....	136
4.14.2.2 Flordian Fabric and Flordian Age.....	137
4.14.2.3 Hopedallian Fabric and Flordian Age.....	139
4.14.2.4 Flordian Fabric and Hopedallian Age.....	142
4.15 Areal Isochrons.....	143
4.15.1 Introduction.....	143
4.15.2 Hopedallian Areal.....	147
4.15.3 Flordian Areal.....	152
4.16 Summary.....	155
Chapter 5 - GEOCHEMISTRY.....	158
5.1 Introduction.....	158
5.2 Maggo Gneiss.....	159
5.2.1 Introduction.....	159
5.2.2 Major Elements.....	168
5.2.3 Element Mobility Studies - Background.....	177
5.2.4 Trace Elements.....	186
5.2.5 Rare Earth Elements.....	195
5.2.5.1 Discussion.....	212
5.2.5.2 Metamorphic Differentiation.....	218
5.2.5.3 Magmatic Differentiation.....	218
5.2.5.4 Comparison of REE with other NAC Grey Gneiss Complexes.....	219
5.3 Hopedale Dykes.....	223
5.3.1 Introduction.....	223
5.3.2 Major and Trace Elements.....	224
5.3.3 Rare Earth Elements.....	229

x
5.3.4 Summary.....235

Chapter 6 - DISCUSSION - ORIGIN AND EVOLUTION OF THE

MAGGO GNEISS.....236

6.1 Introduction.....236

6.2 Hopedalian vs. Flordian Domain Maggo Gneiss.....237

6.2.1 Introduction.....237

6.2.2 Major and Trace Elements.....237

6.2.2.1 Large Ion Lithophile Elements.....243

6.2.2.2 High Field Strength Elements.....250

6.2.2.3 Rare Earth Elements.....255

6.2.3 Quantitative Aspects of Flordian Reworking..283

6.2.3.1 Maggo Gneiss.....284

6.2.3.2 Hopedale Dykes.....272

6.3 Sr₀ Evolution of the Hopedale Block.....273

6.3.1 Maggo Gneiss.....273

6.3.1.1 Hopedalian Domain Suites.....277

6.3.1.2 Flordian Domain Suites.....283

6.3.2 Published Maggo Gneiss and Kanariktok
Intrusion Results.....284

6.4 Characteristics of the Flordian Event.....287

6.4.1 Introduction.....287

6.4.2 Role of the Kanariktok Intrusions.....288

6.4.3 Chemical and Physical Changes Accompanying
the Flordian Reworking.....289

6.4.4 Flordian Metamorphism and the Contemporaneous
NAC High Grade Event.....290

6.4.5 Nature and Role of the Flordian Fluid Phase.....	291
6.4.6 Observed Mineralogical Changes.....	295
6.4.7 Summary.....	297
6.5 Origin of the Maggo Gneiss Precursor.....	298
6.5.1 Introduction.....	298
6.5.2 Petrogenetic Modelling - Introduction.....	301
6.5.3 Mantle Source.....	302
6.5.4 Crustal Source.....	305
6.5.4.1 Metabasaltic Sources.....	308
6.5.4.1.1 Trace Mineral Control on the REE Contents.....	314
6.5.4.2 Intermediate Sources.....	316
6.5.4.2.1 Parent REE Composition.....	316
6.5.4.2.2 Granulite Facies Parent.....	317
6.5.4.2.3 Amphibolite Facies Parent.....	321
6.5.5 Discussion.....	326
6.5.6 Summary.....	332
6.6 Conclusions.....	333
 CHAPTER 7 - SIGNIFICANCE OF THE MAGGO GNEISS IN THE DEVELOPMENT OF THE NORTH ATLANTIC CRATON.....	 335
7.1 Field Relationships.....	335
7.2 Geochronological Relationships.....	341
7.3 Proposed Developmental History of the Maggo Gneiss.....	345
7.3.1 Early to Early Middle Archaean (> 2,900 Ma).....	345
7.3.2 Late Middle to Late Archaean (<2,900 Ma).....	354
7.4 Summary.....	357

PHOTOGRAPHIC PLATES.....	358
REFERENCES.....	381
APPENDIX A - FIELD LOCATIONS, GEOCHRONOLOGY SUITES.....	402
A.1 Introduction.....	402
A.2.1 Manuel Island.....	405
A.2.2 Porphyritic Phase.....	408
A.2.3 Hypothesis Island.....	408
A.2.4 Hopedale Harbour.....	409
A.2.5 Marsha's Cove.....	412
A.2.6 Hopedale Gneiss.....	419
A.2.7 Black Head Tickle.....	420
A.2.8 Dead Dog Point.....	423
A.2.9 Pilliarusik Bay.....	424
A.2.10 Dyke Island.....	425
A.2.11 South East Double Island.....	425
A.2.12 Next Bay North.....	426
APPENDIX B - SAMPLING AND ANALYTICAL TECHNIQUES.....	428
B.1 Sampling.....	428
B.2 Major Element Analysis.....	429
B.3 Trace Element Analysis.....	430
B.4 Rare Earth Element Analysis.....	432
APPENDIX C - RUBIDIUM - STRONTIUM ISOTOPIC DATING	
METHODS.....	440

C.1 Rubidium - Strontium Analysis.....440
C.2 Strontium Analysis.....443
C.3 Regression Analysis.....445

APPENDIX D - LISTING OF MAJOR, TRACE AND RARE EARTH
ELEMENT RESULTS FOR MAGGO GNEISS AND
HOPEDALE DYKES.....446

APPENDIX E - PARTITION COEFFICIENT DATA.....469

List of Tables

Table	Description	Page
2.1	Archaean and Proterozoic events of the Hopedale Block	21
2.2	Structural Chronology of the Study Area	31
3.1	Chronology of the Study Area	53
3.2	CaO(host rock)/CaO(olivine) Ratios for Olivine of Igneous and Metamorphic Origin	97
4.1	Rubidium - strontium regression results	105
4.2	Isotopic results for MI, PP, HI and SEDI geochronology suites	106
4.3	Isotopic results for HH, MC and NBN geochronology suites	113
4.4	Isotopic results for HG, BH, DP, PB and DI geochronology suites	119
4.5	Averaged isotopic data for Areal Isochron	148
5.1	Analyses of Tonalite Subgroup, Maggo Gneiss	163
5.2	Analyses of Trondhjemite Subgroup, Maggo Gneiss	164
5.3	Analyses of Granodiorite Subgroup, Maggo Gneiss	165
5.4	Analyses of Diorite Subgroup, Maggo Gneiss	166

5.5	Average compositions of chemically defined gneiss subgroups	167
5.6	REE concentrations, Diorite Subgroup	197
5.7	REE concentrations, Tonalite Subgroup	201
5.8	REE concentrations, Trondhjemite Subgroup	207
5.9	REE concentrations, Granodiorite Subgroup	211
5.10	Chemical composition of the Hopedale Dykes	225
6.1	Average compositions, geochronology suites	239
6.2	Mean compositions, Hopedalian and Flordian domain gneiss	242
6.3	Single analysis, Mass Balance calculations	265
6.4	Maggo Gneiss model ages	281
6.5	Metabasaltic source mineralogies	303
6.6	Intermediate composition source mineralogies	302
6.7	Estimates of bulk composition of Intermediate composition sources	322
B.1	Accuracy and Precision of AAS	431
B.2	REE Separation Procedure	433
C.1	Replicate Rb and Sr results for USGS Standard Sample W-1	441
C.2	Rb and Sr duplicate results	442
C.3	Sr Separation Procedure	444
E.1	Partition Coefficient Data, Mantle source	469

E.2	Partition Coefficient Data, Quartz Tholeiite Source	470
E.3	Partition Coefficient Data, Intermediate Composition Source	471

List of Figures

Figure	Description	Page
1.1	Location Map	6
2.1	Structural Provinces of Labrador	16
2.2	Geology of the Hopedale Block	19
2.3	Paleostress system of the Hopedale Block	28
2.4	Structural Geology of the study area	33
2.5	Equal area projections for Hopedalian planar and linear structures	37
2.6	Location of Hopedalian and Flordian domains	41
2.7	Equal area projection of Flordian planar structures	43
2.8	Equal area projection for shear planes within the study area	48
3.1	Geology of the study area	55
3.2	ACF triangular diagram of observed mineral assemblages in Hopedale Dykes	89
4.1	Distribution of ages within the study area	104
4.2	Manuel Island Isochron plot	108
4.3	Porphyroblastic Phase Isochron plot	108
4.4	Hypothesis Island errorchron plot	111
4.5	Southeast Double Island errorchron	111

4.6	Hopedale Harbour Isochron plot	115
4.7	SE end Marsha's Cove Isochron plot	115
4.8	SW end Marsha's Cove Isochron plot	118
4.9	Marsha's Cove all samples, errorchron	118
4.10	Hopedale Gneiss errorchron	122
4.11	Black Head Tickle errorchron	122
4.12	Dead Dog Point errorchron	126
4.13	Pilliarusik Bay errorchron	126
4.14	Dyke Island errorchron	129
4.15	Next Bay North errorchron	129
4.16	Pooled Hopedalian data Isochron	135
4.17	Pooled Flordian data errorchron	135
4.18	Areal Isochron for Hopedalian suites	151
4.19	Areal errorchron for Flordian suite	151
4.20	Flordian areal Isochron minus HH suite	154
5.1	Sample location map	160
5.2	Harker variation diagrams (major elements), Maggo Gneiss	170
5.3	Na_2O vs K_2O and $\text{Na}_2\text{O}/\text{K}_2\text{O}$ vs Al_2O_3	174
5.4	AFM plot, Maggo Gneiss data	176
5.5	$\text{Na}_2\text{O}-\text{K}_2\text{O}-\text{CaO}$ plot, Maggo Gneiss data	179
5.6	Normative Ab-An-Or projection for Maggo Gneiss	181
5.7	Harker variation diagrams (trace elements) Maggo Gneiss	189
5.8	Element ratio diagrams	193

5.9	REE distribution patterns, dioritic subgroup, Maggo Gneiss	199
5.10	REE distribution patterns, tonalitic subgroup, Maggo Gneiss	203
5.11	REE distribution patterns, trondhjemitic subgroup, Maggo Gneiss	206
5.12	REE distribution patterns, granodioritic subgroup, Maggo Gneiss	210
5.13	Fields of REE distribution for chemically defined Maggo Gneiss subgroups	214
5.14	REE patterns for two trondhjemite classes	217
5.15	NAC REE data compared with Maggo gneiss	222
5.16	Variation diagrams for Hopedale Dykes	227
5.17	CaO/Al ₂ O ₃ vs K ₂ O, Hopedale Dykes	231
5.18	REE distribution patterns, Hopedale Dykes	233
6.1	LILE variation diagrams, geochronology suites	245
6.2	HFS element variation diagrams, geochronology suites	252
6.3	Normalized LILE and HFS plots	257
6.4	REE distribution patterns, Hopedalian samples	260
6.5	REE distribution patterns, Flordian samples	262
6.6	Composition-volume relationships, individual Maggo Gneiss samples	268
6.7	Composition-volume relationships, mean gneiss compositions and Hopedale Dykes	271

6.8	Sr ₀ Evolution - errors and ⁸⁷ Rb/ ⁸⁶ Sr ratios	276
6.9	Sr ₀ Evolution - Hopedalian and Flordian paths	279
6.10	Sr ₀ Evolution - Maggo gneiss and Kanairiktok Intrusions	286
6.11	Partial melting results; mantle and eclogite	307
6.12	Partial melting results; garnet granulite and garnet amphibolite sources	311
6.13	Partial melting results; amphibolite source	313
6.14	Partial melting results; Intermediate composition at granulite facies	320
6.15	Partial melting results; Intermediate composition at amphibolite facies	324
6.16	Normalized LILE and HFS abundances for Amphibolite IV and Granulite II	330
7.1	NAC Reconstruction	337
7.1	Sr ₀ Evolution diagram, North Atlantic Craton	343
7.3	Summary of Hopedale Block development	347
7.4	Diagrammatic summary of Archaean development of the Hopedale Block	349
A.1	Field Locations of Geochronology Suites	404
A.2	Sample Locations and Geology, West Bay, Manuel Island	407
A.3	Geology of Hypothesis Island	411

A.4	Geology of Pilliarusik Bay	414
A.5	Geology and Sample locations, SW Marsha's Cove Geochronology Suite	418
A.6	Geology and Sample Location Black Head Geochronology Suite	422
B.1	REE determinations - Accuracy	436
B.2	REE determinations - Precision	438

List of Plates

Plate	Description	Page
1	A Weekes association Antiform	360
	B Weekes association Inclusion	360
	C Volcaniclastic Unit, Weekes association	360
	D Granoblastic, equigranular texture, in clinopyroxene bearing amphibolite	360
	E Lepidoblastic texture, normal amphibolite	360
	F Garnet porphyroblast, garnet bearing amphibolite	360
2	A Equilibrium texture cpx-hbl-pl	362
	B Plagioclase-hornblende coronas on garnet	362
	C Ultramafic unit, Weekes association, with harrisitic olivine	362
	D Composite Inclusion of Weekes association	362
	E Alteration of olivine porphyroblast	362
3	A Weekes association marble inclusion in Maggo Gneiss	364
	B Close up of layering in marble inclusion	364
	C Olivine porphyroblast in marble	364
	D Staurolite inclusion in garnet, pelitic, metasediment unit, Weekes association	364
	E Corundum bearing pelitic horizon, Weekes association	364

4	A	Cumingtonite-biotite-garnet assemblage in gellite unit, Weekes association	366
	B	Primary (?) layering in volcanoclastic unit, Weekes association	366
	C	Anthophyllite-garnet-plagioclase-quartz- biotite, from volcanoclastic unit	366
	D	Inclusions of anorthositic lithologies	366
	E	Anorthosite, anorthositic gabbro and hornblendite inclusions in Maggo Gneiss	366
5	A	Rootless intrafolial fold in Maggo Gneiss	368
	B	Discordant contact, Maggo Gneiss and Hopedale Dyke	368
	C	Hopedalian fabric within Maggo Gneiss	368
	D	Foliated tonalite inclusions in massive, tonalite phase of Maggo Gneiss	368
	E	Foliated tonalite inclusion in tonalite to trondhjemite phase of Maggo Gneiss	368
6	A	Various types of Hopedalian migmatites	370
	B	Lit-par-lit migmatites producing a banded Maggo Gneiss	370
	C	Diktyonitic migmatite cutting foliated biotite tonalite	370
	D	Diktyonitic and nebulitic migmatites	370
	E	Hornblende rich trondhjemitic phase, Maggo Gneiss	370

7	A	Biotite, foliated trondhjemitic Maggo Gneiss	372
	B	Interstitial K-feldspar	372
	C	Garnet bearing trondhjemitic Maggo Gneiss	372
	D	Folded Hopedale Dyke	372
	E	Boudinaged Hopedale Dyke	372
	F	Parallel limbs of folded Hopedale Dyke	372
8	A	Rectangular boudins of Hopedale Dyke	374
	B	Granoblastic, equigranular texture, Hopedale Dyke	374
	C	Plagioclase accumulations in Hopedale Dyke	374
	D	Cpx bearing Weekes association	374
	E	Retrogressed Hopedalian mineral assemblage in Hopedale Dyke	374
9	A	Thinned and folded Hopedale Dykes	376
	B	Gently folded foliated hornblende tonalite, Maggo Gneiss	376
	C	Homogeneous, foliated tonalite, Maggo Gneiss	376
	D	Location of samples 83-202 and 203	376
	E	Location of samples 83-204 and 205	376
	F	Location of samples 83-208 and 209	376

10	A	Location of samples 83-216 and 217	378
	B	Field location, samples from the Hopedale Gneiss geochronology suite	378
	C	Field location and relationships, Dead Dog Point samples	378
	D	Refolded isoclinal fold in Weekes association	378
	E	Hopedale Dyke displaying coplanar folding	378
11	A	Hopedalian domain Maggo Gneiss	380
	B	Weak Flordian overprinting on Maggo Gneiss	380
	C	Increased intensity of Flordian reworking of Maggo Gneiss	380
	D	Completely reoriented Maggo Gneiss resulting from the Flordian overprinting	380
	E	Faulted Kikkertavak Dyke	380

Chapter 1

INTRODUCTION

1.1 High Grade Gneiss Terrains

Archaean high grade gneiss terrains are presently exposed on all continents, comprising the cores of stable cratons. The most extensively studied areas are West Greenland (McGregor, 1973; O'Nions and Pankhurst, 1974; Griffin et al., 1980), South Africa (Anhaeusser et al., 1969; Davies and Allsop, 1976; Condie and Hunter, 1976; Hunter et al., 1978) and Australia (Wilson, 1968; Gluckson, 1972; Gray, 1977; Rutland, 1981).

Two contrasting schools of thought have evolved in interpreting the origin of Archaean high grade gneiss terrains (Gluckson, 1979). The first, or North Atlantic school, suggests that the early sialic crust predated development of greenstone belts (Windley, 1973). The Barberton - Pilbara school suggests that greenstone belts represent preserved primary crustal material into which granitic and gneissic terrains were later emplaced (Anhaeusser et al., 1969; Gluckson, 1972).

The fundamental difference between the two schools is whether the Earth's primeval crust was "basaltic" or "granitic" in composition. This question is related to the pre-Archaeon history of the Earth, about which little direct information exists.

A common feature of all high grade gneiss terrains is the predominance of granitic (sensu lato; s.l.) lithologies accounting for > 70% of these areas in combination with varying proportions of supracrustal units and layered igneous complexes (Bridgwater et al., 1973; Condie and Hunter, 1976). The large volumes of granitic material observed in high grade gneiss terrains raises an age old problem in geology - The Origin of Granitic Magmas, which has been debated for the past 200 years. Knowledge of where and how large volumes of granitic magma originate, in the Archaeon, is essential in interpreting the growth and development of the Earth's early continental crust.

Recent workers interpret granitic (s.l.) magmas to be derived by 1) partial melting (Wyllie, 1977; Huang and Wyllie, 1981), 2) closed system crystal-liquid fractionation (Leeman and Dasch, 1978), 3) coupled fractionation-melting (Hildreth, 1981), or 4) liquid immiscibility (Gellinas et al., 1976; Roedder, 1978). Closed system crystal-liquid fractionation and liquid immiscibility processes produce relatively minor amounts of granitic magma, e.g. approximately 10% granitic magma by crystal-liquid fractionation (Grout, 1926). Whether these

processes played a major role in the growth of the continental crust in the Archaean remains unknown. Partial melting, with or without excess H_2O present, of a variety of parental compositions, may generate sufficient amounts of granitic liquids (Wyllie, 1977) to account for their large volume recorded throughout geologic time.

1.2 Reworking

Archaean continental crust may have been derived by direct melting of basaltic (s.l.) material or by reworking of preexisting crustal material (Collerson et al., 1981). Both mechanisms involve partial to complete melting and require different parent compositions to yield the same daughter product. The first, introduces new material into the crust, resulting in an overall increase in crustal volume. The second mechanism, while not significantly enlarging the volume of crust, plays an important role in the development of the crust.

Reworking of crustal material may provide an effective means of contributing to the growth and development of sialic crust (Collerson et al., 1981). To account for the evolution of the Precambrian crust in Greenland, Moorbath (1975) defined reworking of preexisting sialic crust as:

"a process of partial to complete melting leading to mobilization and reconstitution, as an essentially new rock, and not in the frequently used but incorrect sense of isochemical recrystallization and/or deformation."

In describing the origin of high grade gneiss terrains Watson (1973), defined reworking as:

"reconstitution of older crystalline rocks ... by deformation in association with metamorphism and, on occasion, with partial melting of preexisting material and introduction of granitic material."

These workers are restrictive in their thinking as to why reworking, in any sense, occurs, as numerous factors e.g. lithologic composition, prevailing metamorphic grade fluid composition and abundance etc., are interrelated with the reworking process.

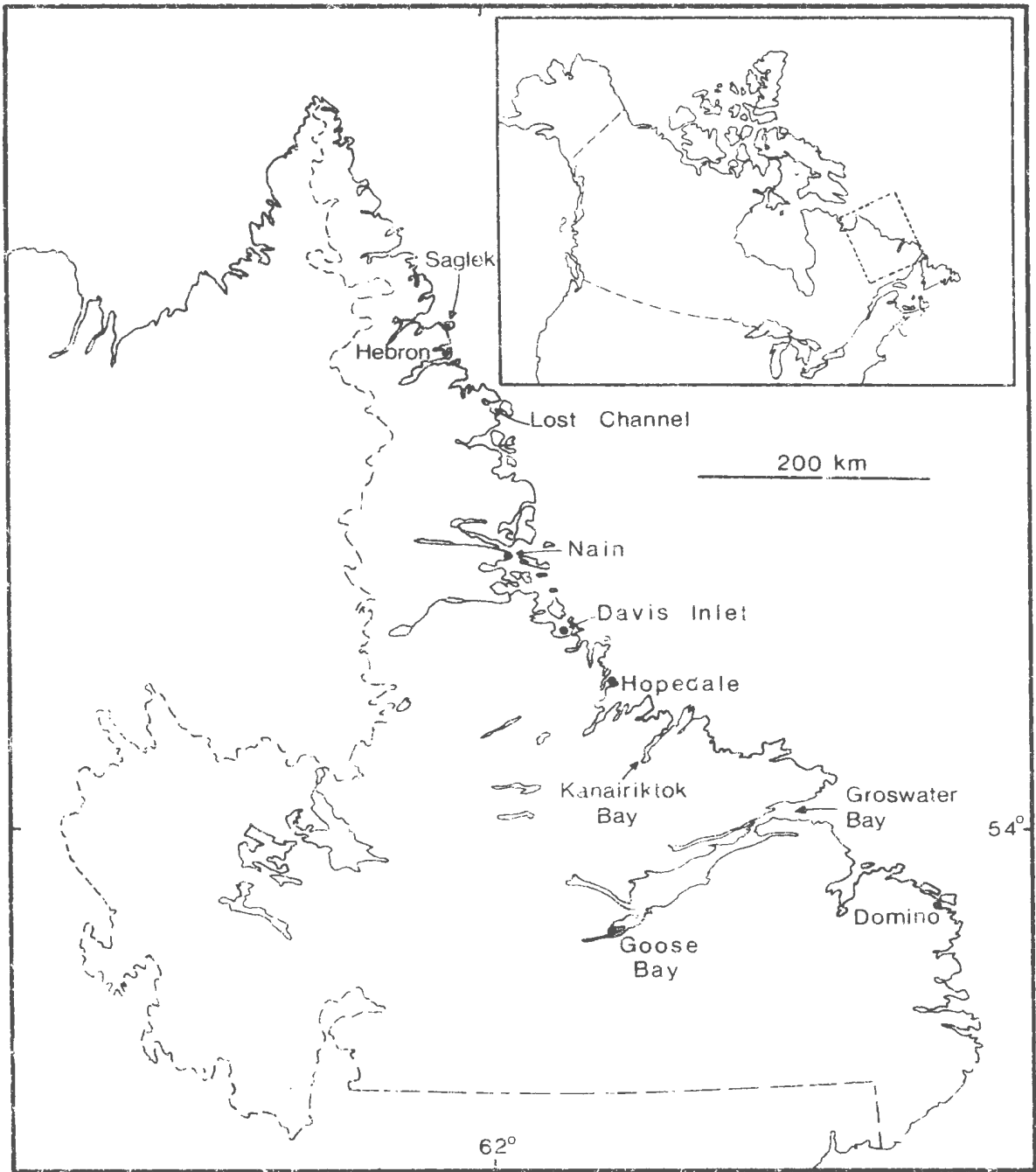
Reworking as defined in this study is considered to be "the large scale processes which reflect the interaction of metamorphism, deformation and melting as they affect preexisting continental crust".

The interrelated processes, individually, or in various combinations, may be significant in generating, altering or recycling sialic crust. The extent to which reworking can be effective in generating large volumes of new crustal material is unknown. If recycling of preexisting crustal material is responsible for crustal growth, the crucial question becomes, at which point in time was the original material formed, i.e. when and how did the preexisting crust originate?

The Archaean terrain at Hopedale (Figure 4.1), coastal Labrador, provides an exceptional opportunity to examine

17000

Figure 1.1: Map showing the location of Hopedale, Labrador with respect to Goose Bay. Other coastal communities mentioned in Section 1.3 are shown.



the metamorphic, structural and geochemical affects of reworking in the generation of continental crustal material.

1.3 Previous Work

Early work in Labrador was restricted to an examination of the geology exposed along its extremely indented coast. Inland regions remained inaccessible and unexamined until the late 1960's. Lieber (1860) described the rocks extending from Domino (south of Groswater Bay) to Davis Inlet as coarse quartzose gneisses, which he termed Domino gneiss. (The location of geographic localities mentioned in the text can be found in Figure 1.1.) The unit was subdivided by Packard (1891) into Domino and Hopedale gneiss, the boundary being Kanairiktok Bay, southeast of Hopedale. The terms Domino and Hopedale gneiss endured in the literature for three quarters of a century (Coleman, 1921; Christie et al., 1953; Douglas, 1953; Kranck, 1953).

During the 1967, 1969 and 1971 field seasons, Taylor (1969, 1970, 1972a, 1979) carried out the first regional mapping of the geology of Labrador and northeastern Quebec north of latitude 55° N. The recognition of early Archaean gneisses from Saglek (3622 Ma, Hurst et al., 1975), Hebron (3618 Ma, Barton, 1975) and Lost Channel (3460 Ma, Hurst, 1973) led to an increase in activity centred on Saglek Bay, northern Labrador. The area examined was restricted to coastal and island exposures with limited information from inland outcrops (Bridgwater et al., 1975;

Ryan, 1977; Kerr, 1980). Bridgwater and Collerson (1976) and Collerson and Bridgwater (1979) have interpreted the granitic (s.l.) gneisses of the Saglek area as representing reactivated polycrystalline basement rocks emplaced prior to 3622 Ma. This age represents the time of isotopic homogenization of the Ulvak gneiss (Collerson and Bridgwater, 1979) based on the Rb-Sr geochronometer. The northern Nain Province is now recognized to contain an early Archaean gneiss complex which has survived subsequent isotopic resetting.

In contrast to the northern Nain Province, the southern Nain Province or Hopedale Block has received little attention following Taylor's (1972a) work. Mineral exploration surveys by Brinex (1964, 1970) mapped portions of the Uqjuktok Bay and Florence Lake areas. (For locations within the Hopedale Block see Figure 2.2.)

Collerson et al. (1974) mapped the Flowers Bay and Hunt River areas. Ryan (1974) and Jesseau (1976) provide the only detailed studies of Hopedale Block geology until the work of Ermanovics and Raudsepp (1979). Subsequently Ermanovics (1980), Ermanovics and Korstgard (1981) and Ermanovics et al. (1982) have completed 1:50,000 scale mapping of the Hopedale Block. Ryan and Kay (1982) mapped the southeast margin of the Hopedale Block where it is in contact with the Makkovik Subprovince. Hill (1981) has mapped the intrusive contact between the Nain Igneous Complex and the Hopedale Block.

Following from the work of Ermanovics and Raudsepp (1979), Ermanovics (1980), Ermanovics and Korstgard (1981) and Ermanovics et al. (1982), Korstgard and Ermanovics (1984; 1985) have proposed a model, based on structural and metamorphic evidence to explain the development of the Hopedale Block. This model, outlined in Chapter 2, forms the starting point for the geochemical and geochronological work carried out in this study. Preliminary Rb-Sr (Marzano, 1981; Grant et al., 1983) and U-Pb (Loveridge et al., 1987) age determinations have been completed for Hopedale Block lithologies in support of the Korstgard and Ermanovics (1984; 1985) model.

1.4 Overview of the Geology of the Hopedale Block

In the Hopedale Block evidence exists for two periods of reworking. An older, Early to Early Middle Archaean event (Time classification divisions within the Archaean are after Stockwell (1982)), derived the grey gneiss precursors by reworking of preexisting sialic crust. Once stabilized the Hopedale Block crust underwent a second reworking in the Late Middle Archaean. The structural aspects of this later reworking have been studied by Korstgard and Ermanovics (1984; 1985).

The Hopedale Block grey gneiss component, informally termed Maggo gneiss (Ermanovics and Raudsepp, 1979), accounts for 55 to 60% of all exposed lithologies. In the area examined in this study Maggo gneiss accounts for 85 to 90% of all lithologies. Supracrustal material, of varying

ages, occurs as xenoliths and tectonic inclusions within Maggo gneiss. A suite of diabasic dykes, termed the Hopedale dykes (Ermanovics and Raudsepp, 1979), have been intruded into the Hopedale Block lithologies following emplacement and deformation of the Maggo gneiss.

The Hopedale Block is dominated by two structural domains. An older domain, the Hopedalian, displays a NW-SE trending fabric, postdating Hopedale dyke emplacement. After development of the older fabric, in Early Middle Archaean time, Hopedalian domain lithologies were reworked in the Late Middle Archaean. This event, the Flordian, is characterized by NE-SW trending planar fabrics.

1.5 Scope and Aims of This Investigation

Using the Korstgard and Ermanovics (1984; 1985) model as a base, this study aims to examine the geochemical and geochronological aspects of reworking of the Maggo gneiss in response to the Flordian event. Using whole rock major, trace and rare earth element litho-geochemistry and Rb-Sr geochronology, the following aspects of the growth and development of the Hopedale Block have been determined

- 1) the age of the Hopedalian and Flordian events.
- 2) the affects of the Flordian reworking on the major, trace and rare earth element distributions.
- 3) the evolution of the Rb-Sr isotopic systematics of Hopedale Block Maggo gneiss.
- 4) the nature of the Maggo gneiss precursor and the means by which the precursor was derived from its parent.

5) the affects of the Flordian reworking on the chemistry of the Hopedale dykes.

These results provide information on the geochemical changes associated with Flordian reworking and the importance of reworking of preexisting sialic crust in the growth, development, evolution and stabilization of the Earth's continental crust.

Field and petrographic relationships for Hopedale Block lithologies in the study area are presented and provide the first detailed examination of all lithologic units in this portion of the Hopedale Block. This framework is essential before undertaking geochemical studies dealing with the affects of reworking.

A comparison of lithologic units and geochronological events in the development of the Hopedale Block with the features preserved in West Greenland is presented. This comparison emphasizes both similarities and differences in the development of continental crust from the two areas.

1.6 Location and Access

The study area is centred on the village of Hopedale, located 230 km due north of Goose Bay, Labrador (Figure 1.1). The village of Hopedale may be reached by charter and/or regularly scheduled fixed wing aircraft service from Goose Bay. Hopedale is a port of call for seasonal Marine Atlantic (formerly CN Marine) coastal boat service along the north Labrador coast. This latter means of transportation provides an economical and occasionally

00012

efficient means of deploying field crews out of Goose Bay.

The study area is characterized by extensive outcrop, in most cases up to 95% exposure is common along the mainland shore and offshore islands. An extensive shoreline zone, up to 15 m wide, of ice scoured outcrop provides excellent exposure throughout the study area.

Chapter 2

REGIONAL GEOLOGY AND STRUCTURAL SETTING

2.1 Introduction

This chapter includes the background information necessary for the geochemical and geochronological analysis which is the main part of this study. It incorporates the following aspects:

- 1) the regional geologic setting of the Hopedale Block, and the relationships of the study area to the Hopedale Block as a whole;
- 2) the tectonic model of Korstgard and Ermanovics (1984; 1985) for the development and evolution of the Hopedale Block. This model formed the basis for the collection of geochemical and geochronological samples used in this study;
- 3) structural data, collected by the author within the study area, that document the two Archaean domains recognized regionally by Korstgard and Ermanovics (1984; 1985).

00013

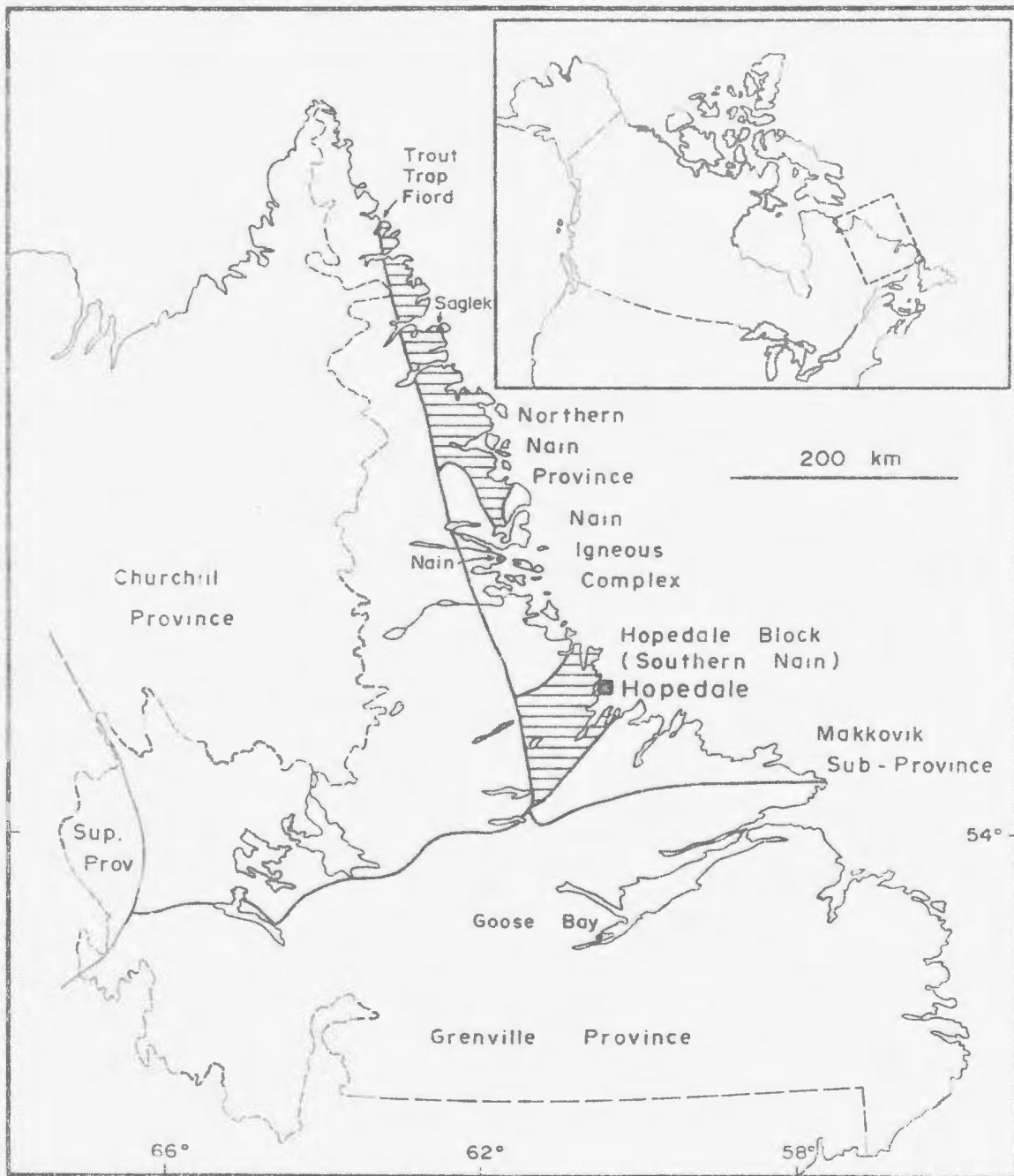
2.2 Regional Geology

The Nain Structural Province, defined by Taylor (1970), forms a thin wedge of Archaean gneisses and migmatites along the coast of Labrador (Figure 2.1). The province extends for > 500 km from Kanaiktok Bay in the south, to beyond Trout Trap Fjord in the north, reaching a maximum width of 100 km inland from Hopedale. The Nain Province is naturally divided into northern and southern parts, separated by the Nain Igneous Complex, which is composed of middle Proterozoic gabbroid to granitoid intrusions with intervening screens of Archaean gneiss that demonstrate lithologic continuity of Nain Province rocks through this central zone (Hill, 1981).

The presence of Early Archaean gneisses (>3,400 Ma) in the northern Nain Province between Saglek and Hebron Fjords was established by Bridgwater et al. (1975), Hurst et al. (1975) and Barton (1975). These old gneisses have been the subject of a number of studies (Bridgwater and Collerson, 1976; Collerson and Bridgwater, 1979; Collerson et al., 1981; Collerson et al., 1984) in which correlations between the Nain Province of Labrador, the Archaean terrains of southern Greenland and northwest Scotland were established and elaborated. Together these terrains form the North Atlantic Craton (NAC; Bridgwater et al., 1973).

In contrast to the northern Nain Province, the southern Nain Province, informally known as the Hopedale Block, has been the subject of few detailed studies. The Hopedale

Figure 2.1: Location of the Hopedale Block, of the Main Structural Province (ruled pattern), with respect to other structural provinces of Labrador.



Block has a trapezoidal shape and an area of approximately 12,000 km². Its northern and western boundaries are intrusive contacts with middle Proterozoic plutons of the Nain, Igneous Complex (NIC; Hill, 1981; see Figure 2.2) and the Harp Lake anorthosite complex (Emslie, 1980), respectively. The northwest boundary of the Hopedale Block is with gneisses of the Churchill Province, the boundary being placed where the local NE structural trend in the Nain Province is re-oriented into the north-south Hudsonian trend and accompanied by lower greenschist facies metamorphism (Ermanovics and Korstgard, 1981). The Kanairiktok shear (Ermanovics et al., 1982), a zone of Late Archean (1,847 +/- 50 Ma; Grant et al., 1983) reworking of Archean and Proterozoic lithologies marks the boundary between the Hopedale Block and the Makkovik Subprovince. In the south, Archean gneisses of the Hopedale Block have been overprinted by Grenvillian fabrics (Gower et al., 1980).

The spatial distribution of the lithologies and the relative chronology of the Hopedale Block were defined by Ermanovics and Raudsepp (1979), Ermanovics (1980), Ermanovics and Korstgard (1981), Ermanovics et al. (1982) and Korstgard and Ermanovics (1985). The chronology proposed by Ermanovics et al. (1982) bears many similarities, at least superficially, with other regions of the NAC. The chronological development of the Hopedale Block proposed by Ermanovics et al. (1982) and Korstgard


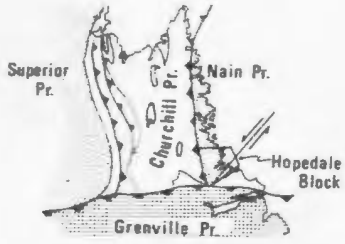


Figure 2.2: Geology of the Hopedale Block, Labrador (From Ermanovics et al., 1982). Place names mentioned in the text are shown (NIC - Nain Igneous Complex). The study area is centred on the village of Hopedale.



- | | | |
|-------------|--------------------|--|
| PROTEROZOIC | | Flowers River Igneous Complex |
| | | Seal Lake Group |
| | | Harp Lake Complex & Nain Igneous Complex |
| | | Island Harbour Granite |
| | | Makkovik Province Gneiss & Churchill Province Gneiss, Isograds: CHL-chlorite, HB-amphibole |
| | | Moran Lake Group & Ingrid Group |
| ARCHEAN | | Migmatites of Various Ages |
| | | Kanairiktok Intrusions |
| | | Florence Lake Group |
| | | Weekes Amphibolite |
| | | Hunt River Belt |
| | | Maggo Gneiss, Isograd: OPX-orthopyroxene |
| | Geological contact | |
| | Fault | |
| | Thrust fault | |
| | An Anorthosite | |

54°45'
60°15'

55°00'
59°30'

and Ermanovics (1985), is summarized below and presented in Table 2.1.

Supracrustal rocks of the Hunt River Belt were inferred to represent the oldest unit within the Hopedale Block by Korstgard and Ermanovics (1985). Lithologies within the Hunt River Belt, including amphibolites, meta-ultramafic rocks, metadiabase dykes and minor metasediments, are in fault contact with the enclosing gneisses (Jesseau, 1976) (see Table 2.1 and Figure 2.2). Inferred correlatives of the Hunt River Belt, informally referred to as the Weekes Amphibolite by Ermanovics et al. (1982), are found elsewhere in the Hopedale Block, although correlation between the two units is tenuous. In this study possible correlatives of the Hunt River Group are referred to by the non-generic term 'Weekes association', which describes supracrustal fragments of various lithologic types within the Maggo gneiss (see below). Gabbroic-anorthositic rocks also occur as inclusions and xenoliths within the Maggo gneiss. Age relationships between this latter group of lithologies and the supracrustal rocks are unknown.

The supracrustal and anorthositic lithologies are surrounded by tonalitic to trondhjemitic gneisses known as the Maggo gneiss (Ermanovics et al., 1982), which form the predominant lithology within the region. Maggo gneiss shows evidence of a protracted history of deformation and metamorphism, but exact age relationships between the Maggo gneiss and older lithologies (Hunt River Belt, Weekes

Table 2.1. Summary of Archaean and Early Proterozoic events in the Hopedale Block and the adjoining Makkovik Subprovince (modified from Ermanovics et al., 1982 and Korstgard and Ermanovics, 1985), as established before this study.

ARCHAEAN

- 1) (?) Deposition of basaltic supracrustal rocks, Weekes association (= Hunt River Belt?), and intrusion of gabbroic-anorthositic rocks.
- 2) (?) Intrusion of tonalite and porphyritic granodiorite, Maggo gneiss, followed by Pre-Hopedalian deformation and metamorphism.
- 3) Intrusion of doleritic Hopedale dykes.
- 4) Hopedalian deformation and metamorphism at upper amphibolite facies.
- 5) Deposition of mafic to felsic metavolcanic rocks, Florence Lake Group.
- 6) Intrusion of Kanariktok Suite (ca. 2,830 Ma).
- 7) Flordian deformation and metamorphism at lower amphibolite facies.

PROTEROZOIC

- 8) Intrusion of doleritic to diabasic dykes, Kikkertavak dykes (ca. 2,200 Ma).
- 9) Deposition of shallow-water, basinal sediments and lava flows of Moran Lake Group, subaerial lava flows and conglomerates of Ingrid Group.
- 10) Makkovikian deformation and metamorphism at lower amphibolite facies.
- 11) Intrusion of Island Harbour Bay Intrusive Suite. Early phases are syn-tectonic to Makkovikian deformation; the main phase is post-tectonic at ca. 1,810 Ma, but followed by shearing in Kanariktok Bay.
- 12) Intrusion of dioritic sills and dykes, Kokkovik dykes (ca. 1,635 Ma).

association and anorthositic rocks) were not well established by Ermanovics et al. (1982).

Ermanovics et al. (1982) considered that the Maggo gneiss contained evidence of the earliest tectonothermal event that they recognized in the study area, which they termed the Pre-Hopedalian event. Evidence for this early event is locally preserved at several localities near Hopedale village. A suite of diabase dykes (Hopedale dykes; Ermanovics et al., 1982) was subsequently emplaced into the gneiss-supracrustal complex. Discordant contacts between the dykes and the Pre-Hopedalian fabric within the gneiss are preserved in areas of low strain (Plate 5B). Postdating emplacement of the dyke swarm, Ermanovics et al. (1982) and Korstgard and Ermanovics (1985) recognized a second regional tectonothermal event, termed the Hopedalian, which affected the entire Hopedale Block.

The Florence Lake Group, occurring in the southern portion of the Hopedale Block and consisting of intermediate to felsic volcanoclastic rocks with subordinate mafic lavas and minor limestones was considered by Ermanovics et al. (1982) to postdate the Hopedalian event. Subsequently a third tectonothermal event known as the Flordian, resulted in the reorientation of earlier (i.e. Pre-Hopedalian and Hopedalian) fabrics into a NE-SW direction. This structural event was associated with the development of lower amphibolite facies mineral assemblages and shear zones displaying a sinistral sense of

displacement (Ermanovics et al., 1982). A pre- to syn-tectonic intrusive suite, (Kanairiktok Intrusives) was emplaced in the crust during the Flordian event. Contacts between the Kanairiktok Intrusives and the enclosing gneiss-supracrustal terrain are obscure. Ermanovics et al. (1982) reported that the margins of the plutons are foliated and their compositions are similar to the rocks into which they were emplaced. Diabasic to gabbroic dykes (Kikkertavak dykes, Harp Lake dykes and possibly Mesozoic or younger dykes) have subsequently been emplaced into the Hopedale Block.

A fourth deformation and metamorphism, termed the Makkovikian, of Late Aphebian age (Korstgard and Ermanovics, 1985) overprinted the southern portion of the Hopedale Block in the Makkovik Subprovince (Ryan and Kay, 1982). It is characterized by the development of transcurrent shear zones, (e.g. the Kanairiktok Shear Zone; Ermanovics et al., 1982) and retrogression of the Nain Province lithologies.

As a result of the present study, the chronology of Ermanovics et al. (1982) has been modified and a revised version is shown in Table 3.1. The major changes (discussed in more detail in Chapter 3) result from the identification of at least 2 tectonothermal events which predated emplacement of the Maggo gneiss protolith.

2.3 Model for Development of the Hopedale Block

Korstgard and Ermanovics (1984; 1985) proposed a model, based on the regional distribution of planar and linear structures, which attempted to explain the Archaean and Proterozoic structural development of the Hopedale Block. Using all available structural information (field data for planar and linear elements and structural trends taken from aerial photographs), Korstgard and Ermanovics (1984) defined two distinct structural domains within the Hopedale Block. The dominant structural trend, oriented NE-SW, paralleling the major bays and flords, was termed the Flordian trend and defines the Flordian Structural Domain (Ermanovics and Korstgard, 1981; Korstgard and Ermanovics, 1984). In the vicinity of Hopedale village Ermanovics and Korstgard (1981) and Korstgard and Ermanovics (1984) recognized older NW trending structures, discordant to the Flordian trend, that defined what they termed the Hopedale trend characteristic of the Hopedalian Structural Domain.

Within the Hopedalian domain, NW-SE trending planar structures have steep SW dips and are accompanied by shallow SE-plunging lineations (Korstgard and Ermanovics, 1984). Evidence for Pre-Hopedalian and older deformational events is preserved within the Hopedalian domain in the supracrustal rocks (Hunt River Belt and Weekes association) and in gabbroic-anorthositic inclusions within the Maggo gneiss.

The Maggo gneiss and older lithologies were intruded by a suite of diabasic dykes, the Hopedale dykes, prior to Hopedalian deformation (Ermanovics et al., 1982).

In passing from the Hopedalian to the Flordian domain, NW-SE trending Hopedalian structures become reoriented into NNE-SSW, subvertical Flordian planar fabrics that are accompanied by the development of moderate NE plunging linear fabrics (Korstgard and Ermanovics, 1984). Locally, Hopedalian structures are preserved in the Flordian domain, but generally regional NE plunging Flordian linear elements are well developed.

Korstgard and Ermanovics (1984) proposed a simple shear model for the development of the Hopedalian and Flordian structural domains, based on the following observations:

- 1) within both domains all linear structural elements are parallel and subhorizontal to gently plunging;
- 2) most planar structural elements are parallel and subvertical, where planar structures have been folded, linear structures are parallel;
- 3) where new planar fabrics have developed, geometric relationships indicate simple shear strain;
- 4) SE of Hopedale village, NW-SE planar structures are rotated into a NNE-SSW orientation indicating sinistral simple shear during the Flordian.

Korstgard and Ermanovics (1984; 1985) interpreted the Flordian domain to represent a portion of a major ductile shear belt having NNE striking, subvertical shear surfaces.

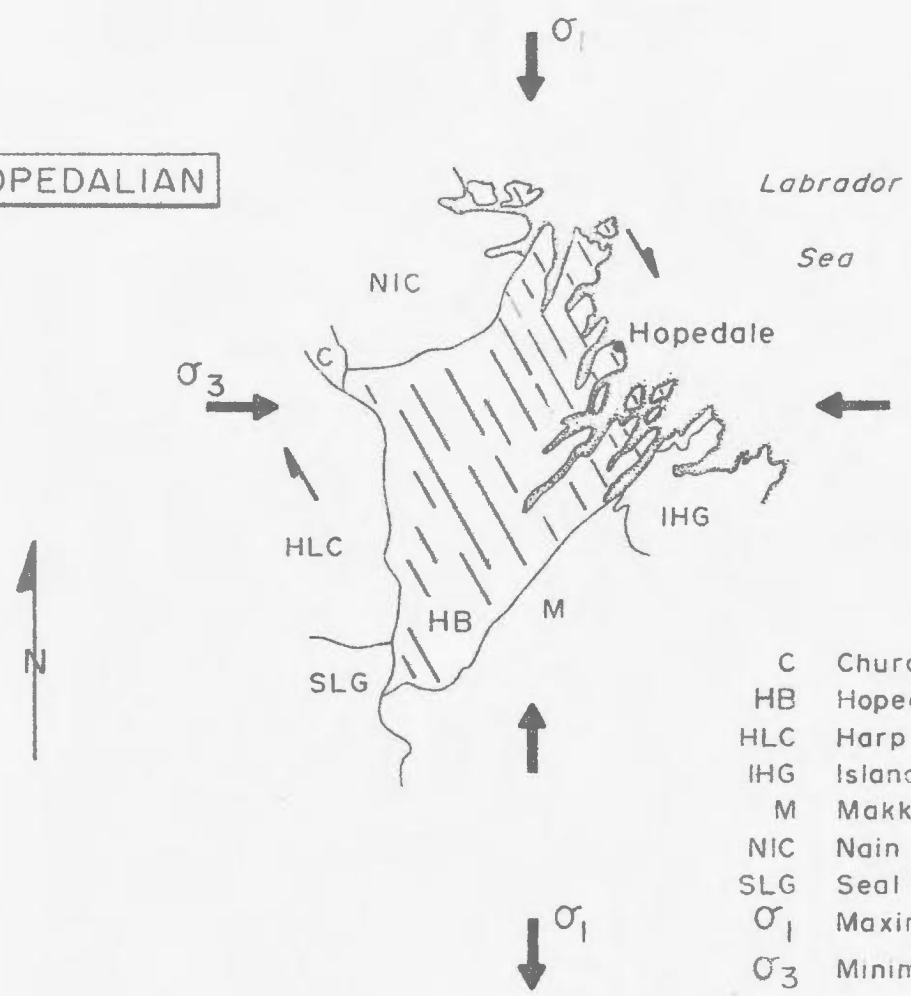
Movement direction within the shear belt was subhorizontal with a sinistral shear sense (Korstgard and Ermanovics, 1984; 1985). On the basis of these observations, these workers were able to suggest a possible orientation for the paleostress system which gave rise to the sinistral sense of shear observed in the Flordian domain (Figure 2.3)

Similarly the Hopedalian domain was interpreted to represent the remnants of a wide shear belt, with a NW striking shear surfaces along which subhorizontal movement took place. Korstgard and Ermanovics (1984) assumed a dextral sense of shear for the Hopedalian domain (Figure 2.3), resulting in an orientation for the principal stress system similar to that obtained for the Flordian.

The upper amphibolite facies mineral assemblages developed during the Hopedalian deformation are preserved within the Hopedalian domain (Korstgard and Ermanovics, 1985). Near the coast the assemblage hornblende + garnet + clinopyroxene (+/- biotite + plagioclase + quartz) is preserved in Maggø gneiss. Inland, near the Nain-Churchill boundary, hornblende granulite facies assemblages (hornblende + garnet + orthopyroxene or hornblende + garnet + clinopyroxene (+/- biotite + plagioclase + quartz)) are preserved in mafic lithologies (Korstgard and Ermanovics, 1985). The higher grade assemblages were interpreted by Ermanovics et al. (1982) and Korstgard and Ermanovics (1985) to represent a deeper crustal level of exposure.

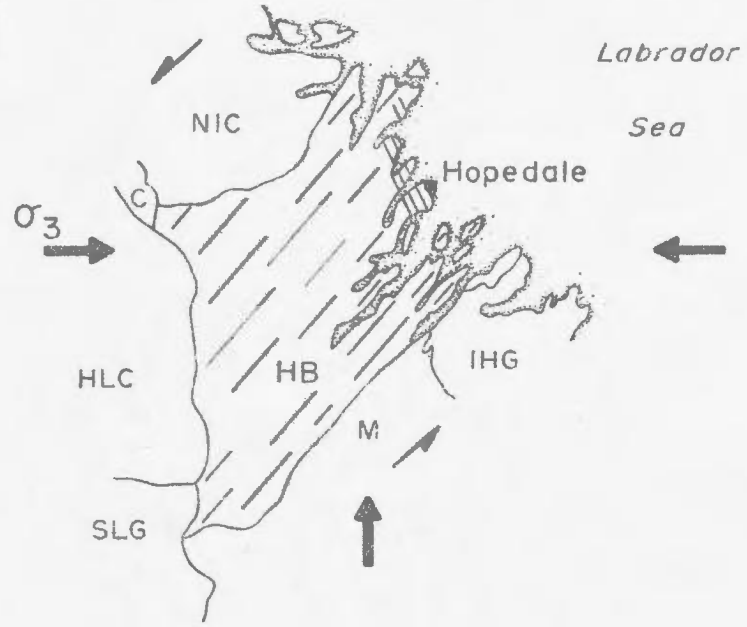
Figure 2.3: Orientation of the principal stress axes in the Hopedale Block during the Hopedalian and Flordian deformational events (after Korstgard and Ermanovics, 1984). A NW-SE trending planar fabric, produced during the Hopedalian event was overprinted by a NE-SW trending fabric during the Flordian deformation. The earlier fabric is preserved in the vicinity of Hopedale.

HOPEDALIAN



- C Churchill Province
- HB Hopedale Block
- HLC Harp Lake Complex
- IHG Island Harbour Granite
- M Makkovik Subprovince
- NIC Nain Igneous Complex
- SLG Seal Lake Group
- σ_1 Maximum compressive stress
- σ_3 Minimum compressive stress

FIORDIAN



Flordian deformation was accompanied by metamorphism under epidote amphibolite facies conditions (Grant et al., 1983) and resulted in the subassemblages hornblende + biotite and hornblende + garnet in felsic and mafic lithologies, respectively (Korstgard and Ermanovics, 1985). These assemblages resulted from retrogression of the older, higher grade Hopedalian assemblages.

Preliminary Rb-Sr and U-Pb isotopic age determinations for Hopedale Block lithologies were reported by Korstgard and Ermanovics (1984; 1985) which supported the chronology implied by their tectonic model. Lithologies dated included the Maggo gneiss within the Hopedalian and Flordian domains and the pre- to syn-Flordian Kanaliktok Intrusive suite. The Maggo gneiss within the Hopedalian domain yielded a Rb-Sr whole rock isochron age of 3,011 Ma (the Ulvak Point suite of Grant et al., 1983), and a minimum U-Pb zircon age of 3,105 Ma (Ermanovics, pers. comm., 1986). These ages were interpreted to date the timing of Hopedalian deformation (Grant et al., 1983). The pre- to syn-Flordian Kanaliktok Intrusions have yielded Rb-Sr whole rock and U-Pb zircon ages of 2,832 Ma (Marzano, 1981) and 2,830 Ma (Ermanovics et al., 1982), respectively, and were interpreted to date the upper limit of Flordian deformation (Grant et al., 1983).

Grant et al. (1983) pointed out a discrepancy between the preserved tectonic fabric and the Rb-Sr ages for Maggo gneiss suites from the Hopedale Block. The Maggo Island

suite (Grant et al., 1983), which yielded the youngest age (2,704 Ma) for the Maggo gneiss, was collected from an area in which there is a well developed Hopedalian trend with no apparent evidence of Flordian overprinting; whereas the oldest age of 3,226 Ma for the Hunt River suite was obtained from samples with a well developed Flordian trend and no evidence of relict Hopedalian structures.

Grant et al. (1983) interpreted these preliminary results as indicating that the Maggo gneiss was derived from two crustal segments, each with slightly different mantle extraction times. The two crustal segments were interpreted to date the timing of the Hopedalian and Flordian deformations (Grant et al., 1983), but these workers did not consider the role of reworking in the generation of the Hopedale Block crust.

2.4 Structural Geology of the Hopedale Area

2.4.1 Introduction

The tectonic model of Korstgard and Ermanovics (1984, 1985) was used as a starting point for the collection of geochemical and geochronological samples in this study, in which the effects of Flordian reworking on the Maggo gneiss are examined. In addition, the detailed examination of several critical localities permitted a greater understanding of the pre-Hopedalian history of the area.

Evidence for at least six periods of deformation affecting the Weekes association and younger lithologies has been recognized in the study area (Table 2.2). The

Table 2.2: Amended Structural Chronology of the Hopedale Block

EVENT	SCHISTOSITY	FOLDING	LINEATION
ARCHAEAN			
Deposition of Weekes association			
Folding of S_0 D_1	S_1	F_1	
Folding of S_0/S_1 D_2	S_2	F_2	L_2

Pre-Hopedalian D_{n+1}	S_{n+1}	F_{n+1}	
Hopedalian (3,200 Ma) D_{n+2}	S_{n+2}	F_{n+2}	L_{n+2}
Flordian (2,750 Ma) D_{n+3}	S_{n+3}	F_{n+3}	L_{n+3}
PROTEROZOIC			
Kanairiktok Shear D_{n+4}	S_{n+4}		L_{n+4}

relative timing of the youngest three of these events; i.e. the Hopedalian, Flordian and Makkovikian (early Proterozoic) are known (Korstgard and Ermanovics, 1984; 1985). The relationship of the remaining three events, which are recognized in inclusions and xenoliths within the Maggo gneiss, to the younger events remains unknown. The Makkovikian event, referred to as D_{n+4} , is associated with large scale, regional shear zones developed in the Makkovik Subprovince to the south of the study area (Korstgard and Ermanovics, 1985).

In Table 2.2 the break between events D_2 and D_{n+1} represents the lack of correlation between the S_1 and S_2 fabrics within the Weekes association with the oldest recognizable, S_{n+1} fabric in the Maggo gneiss. If 'n' = 1, then the Pre-Hopedalian event would have been responsible for the refolding of earlier fabrics observed in the Weekes association.

The structural data for the study area are shown in Figure 2.4, from which it can be seen that the dominant fabric is NW trending, corresponding to the Hopedalian domain, and is overprinted by Flordian fabrics, e.g. along the east side of Piliarusik Bay.

2.4.2 Pre- Pre-Hopedalian

At least two (unnamed) tectonothermal events affected the Weekes association prior to the incorporation of this unit within the Maggo gneiss. The S_1 and S_2 fabrics are observed in inclusions of Weekes association and

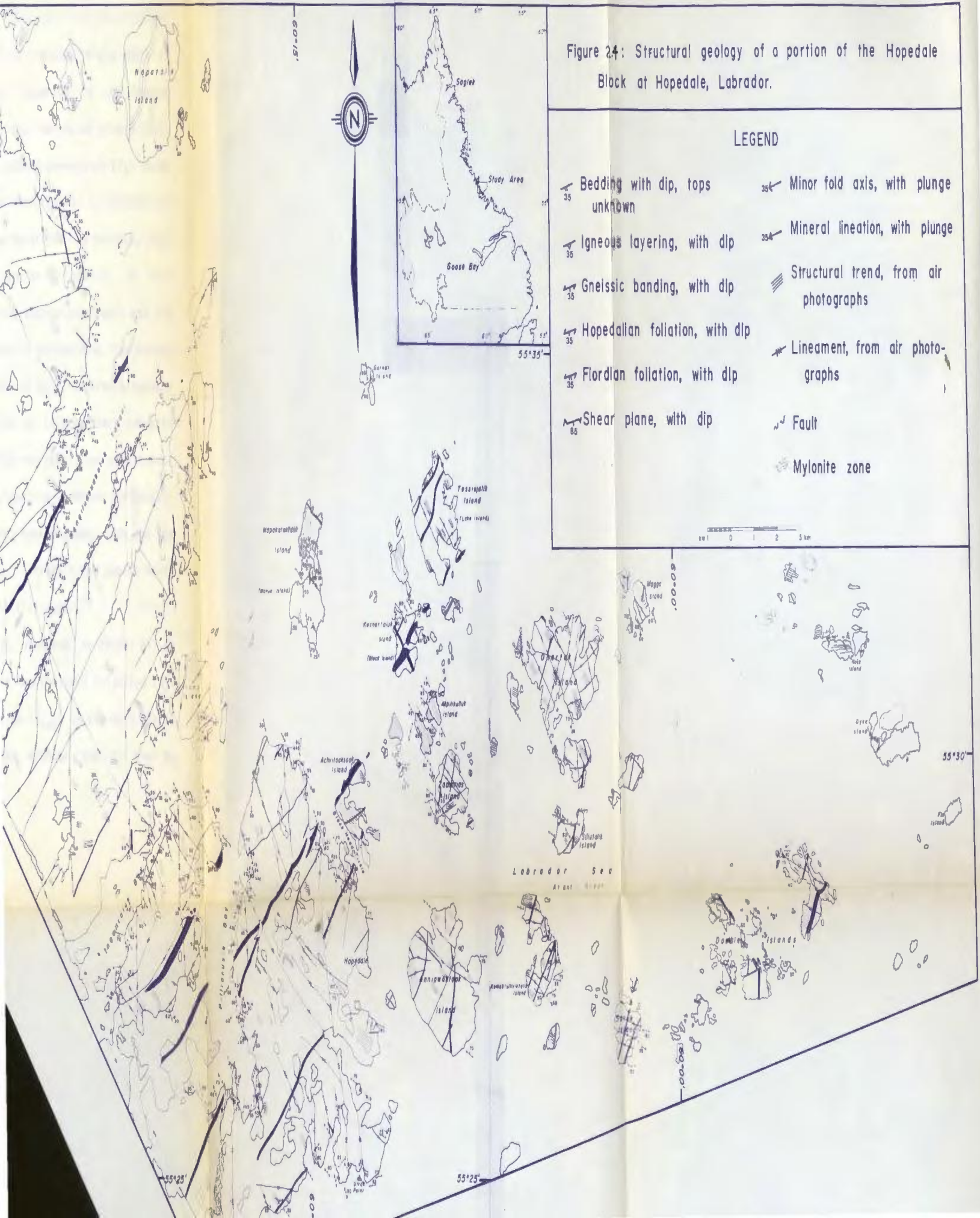


Figure 2.4: Structural geology of a portion of the Hopedale Block at Hopedale, Labrador.

LEGEND

- Bedding with dip, tops unknown
- Igneous layering, with dip
- Gneissic banding, with dip
- Hopedalian foliation, with dip
- Flordian foliation, with dip
- Shear plane, with dip
- Minor fold axis, with plunge
- Mineral lineation, with plunge
- Structural trend, from air photographs
- Lineament, from air photographs
- Fault
- Mylonite zone

0 1 2 3 km

anorthosite within Maggo gneiss. The relationship between these two events and the oldest, Pre-Hopedalian, fabric within Maggo gneiss remains unknown.

The earliest recognizable fabric within the Weekes association is interpreted to be reflect primary layering which was subsequently enhanced by metamorphic differentiation. Evidence for this early fabric exists on Zacharius (Plate 4B) and Manuel Islands (Plate 10D). At Manuel Island, compositional layering in the Weekes association displays refolded, isoclinal folds (Plate 10D). The relationship between the second generation (F_2) folds and the fabric within the enclosing gneiss is unknown, as the F_2 structure lies at the centre of the enclave, away from the contact with the enclosing gneiss. At this locality the contact between the supracrustal unit and the enclosing gneiss is interpreted to be tectonic. The Weekes association preserves evidence of D_2 structures elsewhere in the study area, e.g. Zacharius Island, where contacts with the gneiss are marked by recrystallized pegmatites. The disrupted contact relationships between the latest preserved fabric (S_2) in the Weekes association and the predominant, Hopedalian (S_{n+2}) fabric in the gneiss makes correlation of these two fabrics difficult.

Anorthositic enclaves also preserve evidence of an early fabric. In these rocks the dominant foliation (S_2) is discordant to the foliation (S_{n+2}) in the host gneiss (Plate 4D). It is not known whether the S_1 and S_2

fabrics are significantly older than those within the gneiss.

2.4.3 Pre-Hopedallian

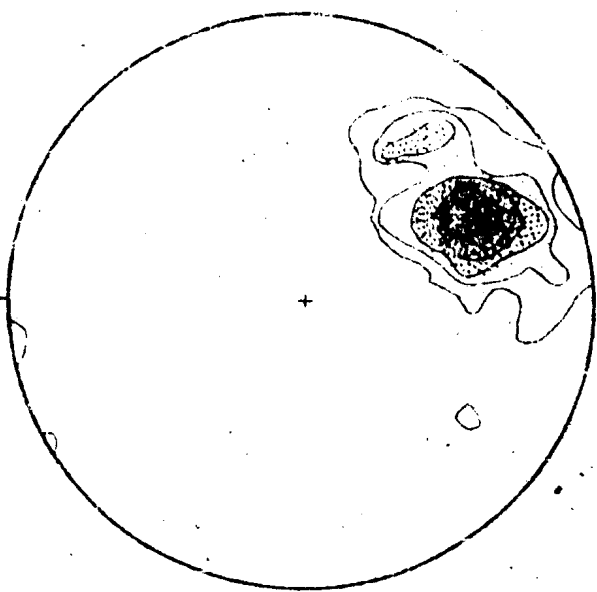
In Hopedallian low strain zones, north and east of Hopedale village, evidence of a Pre-Hopedallian (S_{n+1}) fabric is preserved within the Maggo gneiss. The Pre-Hopedallian fabric, characterized by a NW-SE trending planar fabric, is known to have been developed prior to intrusion of the Hopedale dykes. The S_{n+1} fabric is preserved as small rootless intrafolial folds within the Maggo gneiss (Plate 5A) and in Hopedallian low strain zones which preserve the discordancy between S_{n+1} and Hopedale dykes (Plate 5B).

2.4.4 Hopedallian Structural Domain

The Hopedallian Structural Domain, centred in the vicinity of Hopedale village (Korstgard and Ermanovics, 1984) is characterized by the Hopedallian (S_{n+2}) fabric, which is the most extensive, recognizable fabric within the study area. It is characterized by a NW-SE striking, steep, mainly SW dipping planar fabric combined with shallow SE plunging linear elements (Figure 2.5). During the Hopedallian deformation, Hopedale dykes were rotated into concordance with the S_{n+1} fabric in the Maggo gneiss and in areas of high strain, a second foliation in the gneiss and a first foliation (S_{n+2}) in the dykes was developed.

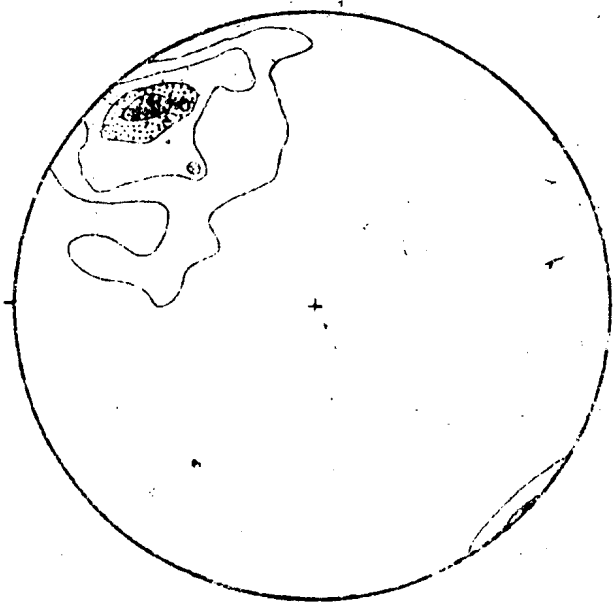
In response to Hopedallian (D_{n+2}) deformation, dykes were folded (Plates 7D and 9A) and boudinaged (Plates 7E

Figure 2.5. Orientation diagrams for (a) planar and (b) linear structures within the Hopedalian domain of the study area. (Equal area, lower hemisphere projection)



b

126 linear structures
 Contours - 2%, 4%, 6%, 8%, 10%
 per 1% area, maximum 16%



a

H-HOPEDALIAN DOMAIN

206 poles to planar structures
 Contours - 2%, 4%, 6%, 8% per
 1% area, maximum 12%

and 8A). The S_{N+2} fabric within the Maggo gneiss can be seen to cross-cut fold closures defined by Hopedale dykes (Plate 7D).

It has already been noted that the Hopedale dykes were emplaced after the Pre-Hopedalian and prior to the Hopedalian event. At several localities within the study area, Hopedale dykes define refolded, isoclinal folds, with axial planes parallel to the S_{N+2} fabric in the gneiss (Plate 10E).

Another response of Hopedale dykes to Hopedalian deformation was boudinage, which accompanied folding. The development of boudins is in part a function of ductility contrast, orientation with respect to strain axes, strain rate and total strain (Ramsay, 1967). Where visible in three dimensions the Hopedale dyke boudins appear as linear structures, plunging to the SE, parallel to L_{N+2} , on the S_{N+2} surface (Plate 7E and 8A).

The development of both rectangular boudins (Plate 8A) and necked blocks (Plate 7E), may reflect the variable ductility contrast between the dyke and host gneiss. Rectangular boudins appear to have formed where the ductility contrast was large, whereas necked boudins may have resulted from a lower ductility contrast (Ramsay, 1967). No regional change in boudin shape was observed in the study area.

The interboudin zones have been infilled by ductile flow of gneissic material (Plate 7E) producing scar folds

(Hobbs et al., 1976) and/or by injection of new material of granite (s.l.) melt composition, inferred to be derived from the enclosing gneiss.

2.4.5 Flordian Structural Domain

Three zones of Flordian overprinting have been identified within the study area, based on structural evidence (Figure 2.6). Within these zones the fabric defining the Flordian (S_{n+3}) overprint has a N-S orientation with steep easterly dips (Figure 2.7), resulting from the progressive reorientation of Hopedalian (S_{n+2}) fabrics. Flordian lineations (L_{n+3}) are only weakly developed in the study area, but are widespread elsewhere in the Hopedale Block (Korstgard and Ermanovics, 1984).

Flordian overprinting can be observed on outcrop to map scale and is characterized by the reorientation of Hopedalian structures into the Flordian orientation. At the outcrop scale the first effects of the Flordian overprinting on the Maggo gneiss are manifest by the development of small scale, sinistral shears and associated folds. Where shears developed, e.g. Zacharius Island, the Hopedalian fabric is folded, offset and partially reoriented into a NNE-SSW orientation (Plate 11B). At the terminations of these shears the Hopedalian fabric is folded (Plate 11B), but is unaffected away from the shear terminations.

07880

Figure 2.6. Map of the study area showing structural domains dominated by Hopedallian (H) and Flordian (F) structures. The solid and dashed lines mark assumed and inferred boundaries, respectively, between the two domains.

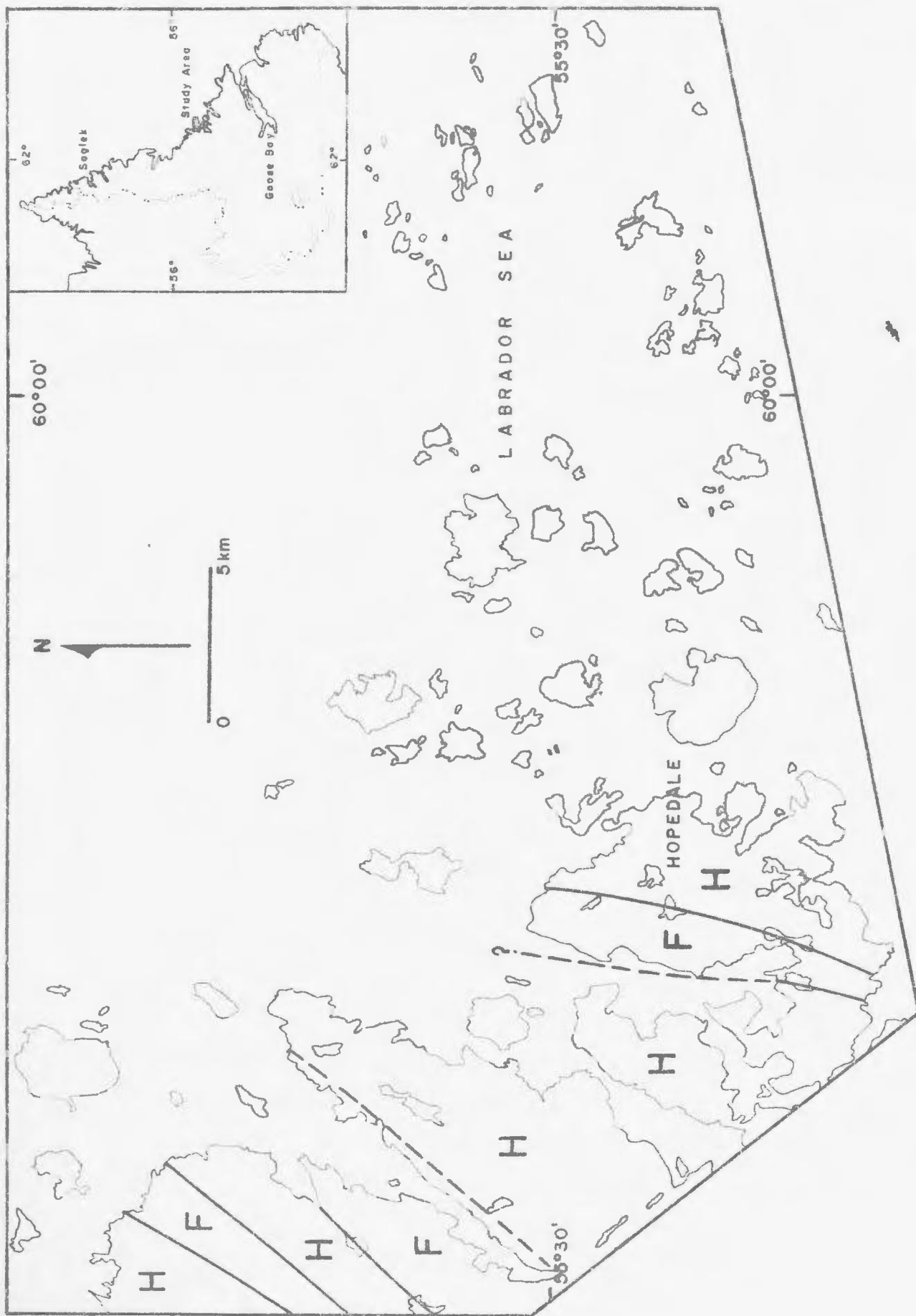
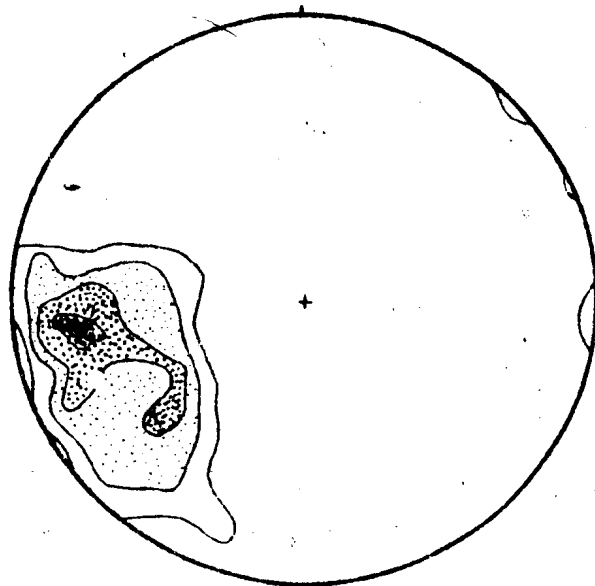


Figure 2.7. Orientation of planar structures within the Flordian domain. (Equal area, lower hemisphere projection)

00043



F - FIORDIAN DOMAIN

165 poles to planar structures

Contours - 2%, 4%, 6%, 8% per

1% area, maximum 12%

On a larger scale the progressive effects of Flordian reorientation of the Hopedallian fabric can be observed along the east side of Pilliarusik Bay. In this case the core of a large auge of Maggo gneiss, elongated into a NNE-SSW (Flordian) direction, maintains a Hopedallian "appearance" in terms of preserved structures, mineralogy and contact relationships (Plate 9D). Away from the core of this auge, the progressive effects of Flordian reworking of the Maggo gneiss are evident, firstly as 1 to 3 cm wide, dextral shear zones which exhibit a brittle-ductile character, across which the S_{n+2} fabric in the gneiss is offset (Plate 11C). The dextral shears are interpreted to represent the conjugate shear to the dominant sinistral component of the Flordian event. At this locality there is no evidence for the introduction of "new" material into the gneiss complex in response to the Flordian reorientation.

The outer margins of the augen are marked by the obliteration of the S_{n+2} fabric within the gneiss and all lithologies (Weekes association, Maggo gneiss and Hopedale dykes) exhibit a well developed Flordian, S_{n+3} , fabric.

Where Flordian fabrics predominate, the Maggo gneiss is recrystallized, with evidence of new hornblende growth. In Flordian low strain zones, blocks of Maggo gneiss with relict Hopedallian fabric are preserved (Plate 11D). These blocks can be recognized by the discordant relationship between the fabric (S_{n+3}) in the enclosing gneiss and the S_{n+2} fabric within the xenolith. The Hopedallian fabric

within the fragments invariably exhibits evidence of rotation, reflecting the sinistral shear component of the Flordian event.

Two types of migmatites are associated with the Flordian event. Diktyonitic migmatites (Mehnert, 1989) associated with Flordian shears, which offset the Hopedalian fabric, are inferred to be of local origin, derived from the enclosing gneisses. These exhibit a sigmoidal form with gradational margins. The Hopedalian fabric (S_{n+2}) is offset across the migmatite zones, and is folded by movement along the shear zone, providing a kinematic indicator of shear sense (Plate 6C and 6D). At their terminations these shears become concordant to the foliation and the migmatites become nebultic (Plate 6C and 6D).

Agmatitic migmatites (Mehnert, 1989) are common in zones of extensive Flordian reworking where the preexisting gneiss is brecciated and the migmatitic material has filled the void between the fragments. In these areas, the S_{n+2} fabric can be recognized in the clasts of Hopedalian domain gneiss.

2.4.6 Proterozoic Events

Proterozoic tectonic events (development of the Kanairiktok Shear Zone and the thrusting of Churchill Province gneisses onto the western portion of the Hopedale Block) are seen to affect Archaean lithologies at the margins of the Hopedale Block. These events are not recognized in the study area and are not discussed here.

2.4.7 Faults and Shear Planes

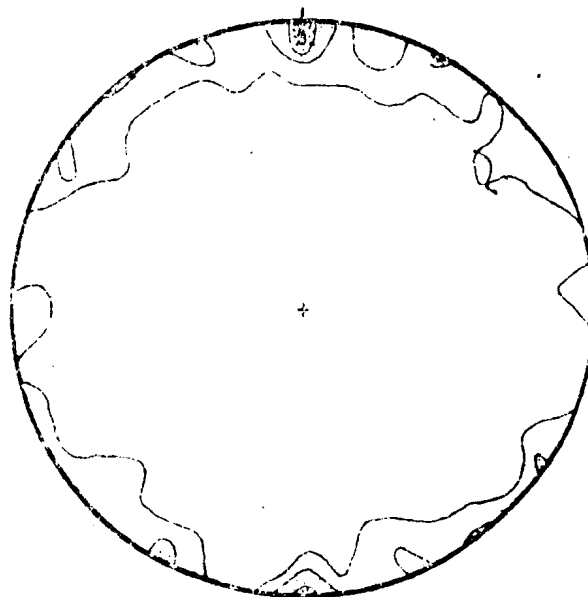
Major faults in the study area (Figure 2.4) occur along the trace of the NE-SW trending bays (Pilliarusik Bay and Kangliuasukoluk Tagani). The bays are aligned in the direction of the Flordian fabric, but sub-parallel to Proterozoic shear zones (i.e. Kanairiktok Shear Zone). At the head and mouth of Pilliarusik Bay, fault movement can be shown to have occurred after emplacement of the Kikkertavak dykes (Plate 11E). Along the east shore of Kangliuasukoluk Tagani, all lithologies have been brecciated during movement along the fault. Movement along these two major faults is interpreted to have occurred during the Proterozoic, synchronous with the development of the Kanairiktok Shear Zone.

Smaller scale faults observed in the study area are generally associated with topographic lineaments. These faults cut the gneisses as well as Kikkertavak dykes, again suggesting movement during the Proterozoic. The nature of small scale shear zones associated with the Flordian overprinting have previously been described (Section 2.4.6).

Shear plane orientation data are presented in Figure 2.8. The major shear direction in the area has an E-W orientation with vertical dips (Figure 2.8). Two submaxima corresponding to shear planes oriented at 070 and 110, about the maximum. A third small submaximum at 030, corresponds to the orientation of the Flordian shear direction defined by Korstgard and Ermanovics (1984).

Figure 2.8 Orientation of shear planes within the study area. (Equal area, lower hemisphere projection)

00048



SS poles to Shear Planes
Contours - 2%, 6%, 10% per 1%
area, maximum 14%

2.4.8 Summary of Structural Data

Within the study area evidence for six periods of deformation have been recognized. Two (D_1 and D_2) are preserved in inclusions within the Maggo gneiss. The older, D_1 , is characterized by the development of isoclinal folds within the Weekes association which were subsequently refolded during D_2 . This event also imparted a foliation to the gabbro-anorthositic rocks. The relationship between these early periods of deformation and the oldest fabric (D_{n+1}) observed in the Maggo gneiss is unknown.

Maggo gneiss preserves evidence of three Archaean deformational events - Pre-Hopedalian, Hopedalian and Flordian. The earliest recognizable fabric, the Pre-Hopedalian (D_{n+1}), is preserved in Hopedalian (D_{n+2}) low strain zones. The predominant structural grain of the area results from the Hopedalian event, characterized by NW-SE, moderately SW dipping, planar fabric and moderately SE plunging linear elements. During this event Hopedale dykes were rotated into concordant contact with the foliation in the gneiss. This event produced folds which are recognized by tracing Hopedale dykes, and is characterized by moderately SE plunging, near vertical axial surfaces.

The effects of the Flordian event (D_{n+3}) are observed as an overprinting on older fabrics. This event is characterized by NE-SW trending, moderate to steep SE dipping planar fabrics and moderate NE plunging linear

00050

elements. The Flordian has a sinistral shear sense recognized where the earlier, Hopedalian fabric is rotated into a NE-SW orientation. Associated with the Flordian deformation is the emplacement of diktyonitic, agmatitic and nebulitic migmatites. Major shear zones developed during the Flordian event were reactivated after emplacement of the Kikkertavak dykes, during the Proterozoic.

Chapter 3

LITHOLOGIC DESCRIPTIONS AND METAMORPHISM

3.1 Introduction

This chapter provides the following information on lithologies within the study area:

- 1) detailed lithologic descriptions of all units recognized (Section 3.2), and
- 2) data documenting the metamorphic conditions associated with the Hopedalian and Flordian events (Section 3.3).

The lithologic descriptions herein, based on field and petrographic relationships, are the first detailed descriptions of these lithologies from the Hopedale Block.

The last sections of this chapter document the observed metamorphic mineral parageneses for Hopedalian and Flordian domains as preserved within the Hopedale dykes, and to a lesser degree the Maggo gneiss. Mineral assemblages developed in the Weekes association are also presented (Section 3.4) to point out some of the problems with combining all supracrustal material into one unit.

00031

As a result of the present study the chronology proposed by Ermanovics et al. (1982) (see Table 2.1) has been modified and a revised version is shown in Table 3.1.

3.2 Description of Lithologies

3.2.1 Weekes Association

The Weekes association, the oldest lithologic unit within the study area (Table 3.1), occurs as widespread rafts of melanocratic rocks, dominantly amphibolites with a prominent metamorphic layering, within the Maggo gneiss (Ermanovics et al., 1982). All supracrustal fragments within the Maggo gneiss, collectively referred to as the Weekes association, have been interpreted to be lithostratigraphic equivalents of the Hunt River Group (Jesseau, 1976; Ermanovics and Raudsepp, 1979), although this has not been proven conclusively. Data presented in this chapter indicate the possibility that the Weekes association, as defined previously, is composed of two distinct supracrustal sequences, separable on the basis of mineralogical, structural and metamorphic criteria.

In this study the Weekes association has been lithologically subdivided into 2 classes comprising 8 subunits. Class I consists of various amphibolite types, subunits 1 to 4 (below), which are the most abundant lithologies. Class II subunits consist of minor amounts of ultramafic, metasedimentary (pelitic, volcanoclastic and marble) and endoskarn lithologies. The subunits of the Weekes association are:

Table 3.1 Archaean and Proterozoic chronology of the Hopedale Block as observed within the area shown in Figure 3.1.

EARLY ARCHAEOAN ?*

- | | |
|--|----------------|
| 1) Deposition of Weekes association Supracrustals | S ₀ |
| 2) Deformation | D ₁ |
| 3) Emplacement of <u>gabbroic-anorthositic</u> rocks | I ₁ |
| 4) Deformation | D ₂ |

EARLY MIDDLE ARCHAEOAN

- | | |
|---|------------------------------------|
| 5) Emplacement of Maggo gneiss protolith | I ₂ |
| 6) Deformation and metamorphism (?) Pre-Hopedalian | |
| 7) Intrusion of Hopedale dykes | D _{n+1} |
| 8) Deformation and metamorphism Hopedalian
3,140 - 3,025 Ma (Rb-Sr whole rock) | I ₃
D _{n+2} |

LATE MIDDLE - LATE ARCHAEOAN

- | | |
|---|------------------|
| 9) Intrusion of Kanairiktok Granitoids
2,830 Ma (U-Pb zircon)* | I ₄ |
| 10) Deformation and metamorphism Flordian
2,854 - 2,632 Ma (Rb-Sr whole rock)) | D _{n+3} |

PROTEROZOIC

- | | |
|--|------------------|
| 11) Intrusion of Kikkertavak dykes
2,200 Ma (Rb-Sr whole rock)+ | I ₅ |
| 12) Deformation and metamorphism Makkovikian | D _{n+4} |

* Subdivisions of the Precambrian time scale are after Stockwell (1982).

* Unpublished U-Pb age by D. Loveridge, GSC.

+ Unpublished Rb-Sr whole rock age by B.J. Fryer, MUN.

- 1) Hornblende (hbl)-plagioclase (plag) amphibolite
- 2) Clinopyroxene (cpx)-bearing amphibolite
- 3) Garnet (gt)-bearing amphibolite
- 4) Gt, cpx-bearing amphibolite
- 5) Ultramafic rocks
- 6) Marble
- 7) Meta-sedimentary (pelitic and volcaniclastic) rocks
- 8) Endoskarn rocks.

The four-fold mineralogical subdivision of the amphibolite types is similar to that used by Kalsbeek and Leake (1970) and Jesseau (1976) for amphibolites from the Ivigtut-Frederikshab area, SW Greenland and the Hunt River Belt, Labrador, respectively.

3.2.1.1 Field Relationships of the Weekes Association

The Weekes association inclusions within the Maggo gneiss (Figure 3.1), vary in size from mappable units at 1:50,000 scale to small (0.2 m X 1.0 m) enclaves (Plates 1A and 1B). Contact relationships between the Weekes association and the enclosing Maggo gneiss are variable, but nowhere in the study area was evidence found to indicate intrusion of the gneiss precursors into the Weekes association. At Zacharius Island the contact is marked by a band of recrystallized pegmatite, between 0.5 m to 3.5 m wide (Plate 1C), containing Weekes association inclusions. At other localities a mono-mineralic reaction rim or corona separates Weekes association enclaves from the enclosing gneiss.



LEGEND

- Pre-Hopedale Domain**
- Weekes Association
 - 1a Normal Amphibolite
 - 1b Clinopyroxene Amphibolite
 - 1c Garnet Amphibolite
 - 1d Garnet-Clinopyroxene Amphibolite
 - 1e Ultramafic
 - 1f Metasediments
 - 1g Skarn
 - 1h Carbonate rich Horizon
 - Anorthosite and Related Rocks
 - 2a Anorthosite
 - 2b Biotitic Anorthosite
 - 2c Hornblende
- Hopedale Domain**
- Moggo Gneiss
 - 3a plag-qtz-bio > hbl
 - 3b plag-qtz-bio > hbl-gt
 - 3c plag-qtz-hbl > bio
 - 3d plag-qtz-hbl > bio-gt
- Fiordian Domain**
- Moggo Gneiss
 - Tonalite Phase (K-feldspar present)
 - 4a plag-qtz-bio > hbl
 - 4b plag-qtz-bio > hbl-gt
 - 4c plag-qtz-hbl > bio
 - 4d plag-qtz-hbl > bio-gt
 - Trendyhemite Phase (no K-feldspar present)
 - 5a plag-qtz-bio > hbl
 - 5b plag-qtz-hbl > bio
 - 10 Kinkitic Granitoid Suite
- Proterozoic**
- 11 Kinkitic Dykes
- Geologic Symbols**
- Mylonite Zone

Figure 3.1: Solid geology of a portion of the Hopedale Block at Hopedale, Labrador.

The dominant orientation of the amphibolite inclusions is NW-SE, parallel with the Hopedalian fabric in the host Maggo gneiss. The prominent layering or banding within the Weekes association has the same orientation as the foliation in the surrounding gneiss, except locally where mesoscopic folds are present in the supracrustals (Plate 1A). The Weekes association is reoriented and retrogressed with the host Maggo gneiss in areas of Flordian reworking and as such is a useful marker for distinguishing reworked Maggo gneiss from the younger, foliated Kanairiktok intrusions.

3.2.1.2 Amphibolite Subunits (1-4)

Each of the amphibolite subunits (1 - 4) have similar field characteristics, and are distinguished on the basis of mineralogy, with a key feature being the presence or absence of garnet. Quartz is a common accessory mineral in all amphibolite subunits. Other accessories include biotite, titanite, zircon and opaque oxides. Secondary minerals include sericite, epidote, chlorite and actinolite.

Subunit 1 is the most abundant of the subunits. Layers or bands of hornblende-plagioclase amphibolite vary from 10 cm to > 1 m in width, often grading into other amphibolite types. The recognition of clinopyroxene in amphibolites (Subunits 2 and 4) is only possible in thin section.

Textures observed in Hopedalian domain amphibolites vary from a granoblastic equigranular mosaic (Plate 1D) to

a lepidoblastic mosaic defined by aligned hornblende crystals (Plate 1E). Grain size varies from 0.5 to 1.2 mm, with hornblende exhibiting the largest variation in subunit 1. The proportion of hornblende in the amphibolites varies from 40% to 80% (visual estimates). Hornblende exhibits the following pleochroic schemes within the amphibolite subunits:

X = straw brown, light green, green

Y = green, light green, green-brown

Z = green, green-brown, dark-green brown.

The light green to green pleochroism is common in Subunit 1 whereas the dark green to brown colours are prevalent in Subunit 4. Hornblende within Subunit 1 may have incomplete rims (<0.05 mm wide) of blue-green amphibole with no distinct line of demarcation between the two. Where the blue green amphibole is present there is a marked increase in the biotite content of the amphibolite, suggesting that some of the biotite may be a product of retrogression. The secondary biotite has a random orientation and is spatially associated with hornblende. Relict biotite elsewhere define a weak parallel alignment in the amphibolite.

Plagioclase (An 40 to An 65) occurs interstitially (Plate 1D) to hornblende, exhibits discontinuous twinning and is common as inclusions in hornblende.

The clinopyroxene is light green in colour, lacks pleochroism and has rounded shapes often embayed by hornblende (Plate 1D). Rational grain boundaries between

clinopyroxene, hornblende and plagioclase are prevalent in the Subunit 2 amphibolite. Alteration of the clinopyroxene to a non-pleochroic, pale green actinolitic amphibole is evident at grain contacts and along fractures cutting through grains.

Garnet, where present, occurs as poikiloblasts, up to 4 mm across, with quartz and opaque oxide inclusions, and exhibits irregular shapes with no discernible crystal faces (Plate 1F). Plagioclase is partially enclosed by garnet and forms discontinuous rims around garnet in subunit 3. Subunit 4, containing the assemblage garnet-clinopyroxene is interpreted to record the highest metamorphic grade attained by the Weekes association in the study area. In this unit the amphibolite has an equigranular interlocking mosaic texture, which becomes lepidoblastic with increasing amphibole content. Equilibrium textures, in the form of 120° triple point junctions and rational grain boundaries, are abundant (Plate 2A). In subunit 4 garnet is partially to completely surrounded by reaction rims of plagioclase (Plate 2B; See Section 3.3).

Within the Flordian domain the predominant amphibole within the amphibolites is actinolite produced by the retrogression of hornblende. Associated with the actinolite is epidote, formed by the breakdown of plagioclase.

3.1.3 Ultramafic Rocks

Ultramafic rocks constitute approximately 10% of the Weekes association within the study area. They have MgO

contents of > 20 wt% and occur as disrupted layers and blocks within other lithologies of the Weekes association (Plate 2C) and more rarely within the Maggo gneiss (Plate 2D). Ultramafic blocks have spheroidal to elliptical shapes and vary in size from 0.5 to 10's of m in length. Ultramafic inclusions in Maggo gneiss generally form solitary elliptical bodies, elongated in the direction of the foliation.

Due to their disrupted state, occurrences of the ultramafic subunit cannot be traced over great distances within the amphibolite. As such, the origin of the unit, whether intrusive into the amphibolite or disrupted cumulates cut by later basaltic/gabbroic magmas has not been determined.

Within some ultramafic bodies, relict igneous textures, i.e. harrisitic and cumulate features, are preserved, but these bodies lack igneous mineralogy. Heuristics textures have also been described from the Hunt River Belt by Collerson et al. (1976b) and Jesseau (1976).

Metamorphic assemblages observed in the ultramafic subunit are:

- 1) talc - tremolite
- 2) talc - tremolite - serpentine
- 3) talc - tremolite - serpentine - phlogopite
- 4) talc - tremolite - serpentine - olivine -
phlogopite
- 5) tremolite - phlogopite

6) olivine - anthophyllite - spinel

7) olivine - serpentine - phlogopite

Dolomite, calcite and opaque oxides (magnetite and pyrite) are the most common accessory/secondary minerals found in the ultramafic lithologies.

The mineralogy and texture of the ultramafic rocks is a combination of the relict igneous and metamorphic assemblages. The metamorphic assemblages observed span the range from lower greenschist facies to upper amphibolite facies.

Olivine porphyroblasts, up to 1 cm long, are invariably fractured and variably altered to fibrous serpentine (Plate 2E). Commonly the olivine is present as small (<0.05 mm) relict fragments within the serpentine. Where extensive serpentinization has occurred, two generations of serpentine may be seen, the younger occurring in fractures which cut the earlier formed phase (Plate 2E). Associated with the serpentinization of the olivine is the development of very fine grained magnetite intergrowths (Plate 2E).

The ultramafic bodies invariably exhibit evidence of reaction with the enclosing gneiss (Plate 2D) and to a lesser degree with amphibolite. Within the portion of the Hopedale Block examined here, the ultramafic bodies lack the complex zonation patterns observed elsewhere in the NAC (e.g. Windley, 1972; Mathews, 1967). The nature of the corona or rim on the ultramafic inclusion is dependent on the composition of the inclusion; talc-tremolite-serpentine

Inclusions have tremolite-actinolite rims, whereas carbonate-bearing ultramafic inclusions have phlogopite rims. Ultramafic blocks within the Weekes association do not generally show evidence of reaction between the inclusion and host during later, Flordian metamorphism.

3.2.1.4 Marble

Marble inclusions were observed at two localities in the study area within the Maggo gneiss and the ultramafic unit of the Weekes association just described.

The larger occurrence, located in West Bay of Manuel Island, is a single, layered, lens-shaped body (0.60 m X 2.3 m) within Maggo gneiss (Plate 3A). The lens, which is completely enclosed by a phlogopite rim, 4 to 15 cm wide, consists of alternating layers of phlogopite and dolomite, with minor calcite, up to 4 cm thick (Plate 3B). The following mineral assemblages are present:

- 1) phlogopite - magnetite - dolomite
- 2) phlogopite - dolomite - magnetite - calcite - spinel
- 3) dolomite - forsterite - phlogopite - magnetite - calcite.

Assemblage 1 characterizes the corona enclosing the lens, assemblages 2 and 3 the phlogopite-rich and dolomite-rich layers, respectively.

Phlogopite (X = colourless, Y = Z = light green brown), which is oriented parallel to the layering within the inclusion, has a grain size up to 2.5 mm and decreases in relative abundance from assemblage 1 to assemblages 2 and

3. Magnetite occurs interstitially to the phlogopite as rounded irregular shaped grains. The dolomite occurs as a granoblastic intergranular mosaic with interstitial magnetite and phlogopite, the latter exhibiting a preferred orientation. Forsterite grains, up to 4.0 mm in size, are fractured and variably serpentized (Plate 3C).

The smaller marble locality is situated on the peninsula separating Pilliarusik and Inganlaluk Bays (Figure 3.1). The marble is associated with boudinaged, ultramafic inclusions within Maggo gneiss.

Calcite accounts for 98% of the carbonate portion of the enclave with the remainder being pyrite. The calcite forms a granoblastic interlocking mosaic with serrated grain boundaries. The pyrite forms ididioblastic to subidioblastic grains throughout the calcite-rich portion of the inclusion, which grades into an ultramafic-rich lithology (talc-phlogopite-magnetite-calcite) over a distance of 3 cm. Inclusions have a mono-mineralic rim of Ca-rich amphibole (Plate 2D).

3.2.1.5 Pelitic and Volcaniclastic Meta-sedimentary Rocks

Meta-sedimentary lithologies form a minor component of the Weekes association within the study area. Clearly identifiable pelitic meta-sediments occur on Woody Island, whereas those on Zacharius Island are interpreted to be volcaniclastic in origin (see Figure 3.1 for locations). The meta-sedimentary lithologies occur as conformable lenses/layers within the amphibolites of the Weekes association.

Mineral assemblages recorded in the pelitic lithologies are:

plagioclase - biotite - rutile - quartz

garnet - plagioclase - biotite - corundum

garnet - plagioclase - biotite - cummingtonite - quartz.

Accessory minerals include opaque oxides, titanite and zircon. Retrograde chlorite was observed in all sections.

Garnet forms idioblastic to subidioblastic grains, 1 mm to 1 cm across. The garnet is poikiloblastic with inclusions of plagioclase, biotite and quartz. Within the corundum-bearing samples, staurolite forms anhedral inclusions in garnet (Plate 3D). Within the pelitic lithologies, garnets are predominantly almandine-pyrope mixtures, in the range 59-72 and 21-35 mole percent, respectively. Grossular and spessartine form minor components (4-5 and 1-3 mole percent, respectively) of the garnet.

Plagioclase (An 34-40) forms equidimensional grains interspersed with biotite. The latter displays a preferred orientation defining a well developed fabric in the pelitic unit.

Corundum occurs as lath shaped grains, 1 x 5 mm in size, interstitial to garnet and biotite (Plate 3E). Cummingtonite, displaying rare polysynthetic twinning, was observed in a single sample from Woody Island (Plate 4A). The cummingtonite is aligned in the fabric with biotite and,

defines the foliation which can be seen to wrap around garnet.

Rocks interpreted to be metavolcaniclastic lithologies, on Zacharius Island, occur as a 1.5 to 2 m thick coherent unit interbedded with amphibolite subunits. They possess a compositional layering (Plate 4B) defined by alternating amphibole-rich and amphibole-poor layers, which are interpreted to be a metamorphically enhanced primary feature. The melanocratic layers are more competent than the leucocratic layers and are boudinaged (Plate 4B).

Mineral assemblages in the metavolcaniclastic lithologies are:

garnet - plagioclase - hornblende

plagioclase - garnet - biotite - anthophyllite

plagioclase - garnet - biotite - hornblende -

anthophyllite - cummingtonite

Quartz, opaque oxides, titanite and calcite are present as accessory phases in all metavolcaniclastic rocks.

Plagioclase (An 40) and biotite in the metavolcaniclastic unit are similar to those in the pelitic lithology. Hornblende is abundant in the melanocratic layers associated with plagioclase, quartz and garnet. Garnet forms euhedral to subhedral, occasionally poikiloblastic grains within leucocratic and melanocratic layers (Plate 4C).

Garnet, within the leucocratic layers, consists of mixtures of almandine (61-53 mole percent), pyrope (22-35

mole percent) grossular (11-15 mole percent) and spessartine (1-2 mole percent). In the melanocratic layers the grossular and spessartine contents of the garnet (21-23 and 5-7 mole percent, respectively) increase at the expense of the pyrope component (9-10 mole percent). Garnet compositions are thus distinct from those in the pelitic unit.

Anthophyllite (Plate 4C) and cummingtonite occur together in the leucocratic layers as porphyroblasts and matrix grains. Inclusions of hornblende, plagioclase, quartz and garnet are common in both amphiboles.

3.2.1.6 Endoskarn Lithology

Endoskarn (Bates and Jackson, 1981) rocks occur along the mainland shore southwest of Napatalik Island. This lithology is developed in inferred equivalents to various amphibolite subunits of the Weekes association. At this locality a relatively undeformed phase of the Maggo gneiss, contains up to 15 m² endoskarn blocks, which exhibit a layering interpreted to represent layering or banding present in the original Weekes lithology. Mineralogically the endoskarn consists of the following assemblages;

- 1) K-feldspar - clinopyroxene - scapolite - tremolite - biotite - epidote - titanite - calcite
- 2) epidote - hornblende - scapolite - clinopyroxene / plagioclase.

Garnet (34 to 50 mole percent spessartine, 5 to 14 mole percent pyrope and 14 to 21 mole percent almandine) is

present in all endoskarn samples examined. Grain sizes in the endoskarn vary from 0.1 mm to 4.0 mm with grain boundaries often irregular, displaying embayed and serrated contacts. The clinopyroxene is retrogressed to an actinolitic amphibole. Symplectic intergrowths between amphibole - K-feldspar - quartz and epidote - K-feldspar - quartz are present. In the former, this intergrowth has the appearance of an exsolution feature.

3.2.2 Anorthosite and Related Rocks

Anorthosite and related rocks account for a minor component of Hopedale Block lithologies. In the regional chronology of the Hopedale Block, it can be seen that the anorthositic rocks were either associated with the Weekes association or emplaced after deposition of the Weekes association. There is a complete gradation from anorthositic through gabbroic compositions, with the former lithology being dominant. The gabbroic lithologies resemble the hornblende-plagioclase amphibolite, subunit 1 of the Weekes association.

3.2.2.1 Field Relationships

The anorthosite suite consists of blocks and fragments incorporated in the Maggo gneiss. Fragments (10 cm to 4 m across; Plate 4D) are invariably rounded and are easily recognizable in the field because of the presence of an S_2 fabric discordant to the S_{n+2} foliation in the enclosing gneiss together with the distinct orange-brown weathering colour of the plagioclase. The greatest

abundance of anorthosite fragments is found along the north shore of Kangiluasukoluk Tagani. At this locality a large (3.5 m wide) fragment of layered gabbro was observed. The layering within this fragment, which is parallel to the foliation within the enclosing Maggo gneiss, is interpreted to be a primary feature which was subsequently enhanced by metamorphic processes. At this same locality fragments of the anorthosite suite vary in composition from anorthosite with minor hornblende, to hornblendite with large recrystallized plagioclase accumulations (Plate 4D and 4E). Solitary enclaves of anorthosite are present at other localities throughout the study area.

3.2.2.2 Mineralogy

The anorthositic rocks within the Hopedale Block possess metamorphic mineralogies. The dominant end member mineral assemblages are:

plagioclase - hornblende - titanite

hornblende - plagioclase - clinopyroxene -
titanite.

Accessory minerals include apatite, zircon, opaque oxides and rutile. Epidote, biotite, sericite, carbonate and alkali feldspar are common secondary minerals.

Plagioclase and hornblende form an equigranular, granoblastic mosaic, exhibiting rational grain boundaries with 120° triple point junctions in most samples. Plagioclase compositions decrease from An 62 in the clinopyroxene-bearing lithologies to An 40 in the

retrogressed samples. Hornblende is pleochroic (X=olive green, Y=light green, Z=dark green) in the clinopyroxene-bearing anorthosite. In retrogressed samples of this lithology hornblende is rimmed by a blue-green amphibole. Clinopyroxene occurs as rounded and embayed grains with associated hornblende being coarser grained, up to 2.5 cm, than in samples lacking clinopyroxene.

It is not clear whether the mineral parageneses recorded in the anorthosite reflect Hopedalian retrogression of pre-Hopedalian assemblages or Flordian retrogression of Hopedalian assemblages.

In melanocratic layers within the anorthosite the retrogression produced epidote, blue-green amphibole and biotite. The epidote forms subidioblastic to xenoblastic grains in symplectic intergrowth with quartz. Hornblende is irregular in shape, fractured and altered to blue-green or colourless amphibole. In the leucocratic layers, the plagioclase alters to a mass of epidote-sericite, which partially to completely replaces plagioclase.

3.2.3 Maggo Gneiss

The Maggo gneiss is the most abundant lithology within the study area (Figure 3.1). It is a typical grey gneiss, similar in appearance to the Uivak, Amitsoq, Nuk and Scourian gneisses of the North Atlantic Craton.

3.2.3.1 Field Relationships

The Maggo gneiss consists of a homogeneous suite of quartzo-feldspathic gneisses and migmatites that preserve

evidence of Pre-Hopedalian and younger tectono-thermal events. Contact relationships between the Maggo gneiss and older lithologies vary from those with a tectonic origin to a reaction relationship. Evidence of a Pre-Hopedalian fabric (S_{n+1}) in the Maggo gneiss is preserved as rootless intra-folial folds (Plate 5A), foliations discordant to the younger Hopedalian fabric (S_{n+2}) and discordant Hopedale dykes (Plate 5B). At the latter localities the degree of discordancy is small, the dykes having subsequently been rotated during the Hopedalian event.

The Hopedalian S_{n+2} fabric, prevalent within the Maggo gneiss, varies from a weak foliation (foliated gneiss), defined by the alignment of biotite and to a lesser extent hornblende, to a well developed banded gneiss (Plate 5C), with individual segregations on a cm scale. Grain size variation within the gneiss is readily discernible in the field. Foliated gneiss is fine to medium grained and generally occurs as discontinuous layers within the medium grained banded gneiss (Plate 5D and 5E). Ermanovics et al. (1982) interpreted the foliated, finer grained lithology to be the oldest phase of the Maggo gneiss which was subsequently intruded by what is now the medium grained, weakly megacrystic, banded gneiss lithology. The megacrystic nature of the original lithology has been obliterated in the study area, but is preserved elsewhere in the Hopedale Block (Ermanovics, 1982, pers. comm.).

For descriptive purposes, the Maggo gneiss is subdivided into tonalitic and trondhjemitic varieties. The tonalite contains alkali feldspar as a minor phase with amphibole and/or biotite as the mafic minerals. The trondhjemite, which by definition lacks alkali feldspar, is a leucocratic rock with amphibole as the common mafic mineral (Arth and Hanson, 1972). Contacts between tonalitic and trondhjemitic gneiss are gradational. This subdivision of quartzo-feldspathic gneisses into tonalitic and trondhjemitic varieties was suggested previously for the Minnesota River Valley quartz-diorite gneiss (Arth and Hanson, 1972).

The relative distribution of the tonalite and trondhjemite phases of the Maggo gneiss is shown in Figure 3.1. It is unlikely that the observed distribution reflects the original disposition of these lithologies. The difference between the two phases most likely results from K mobility during post-placement metamorphism, e.g. the Hopedalian and/or Flordian events.

The Maggo gneiss has undergone at least three major periods of migmatization. Clear relationships for the development and emplacement of Hopedalian and Flordian migmatites can be established in the field. Pre-Hopedalian and older migmatites are recognizable in Hopedalian low strain zones. Terminology for migmatite description is after Mehnert (1968).

Hopedallian migmatites are commonly thin stromatic to phlebitic structures, emplaced lit-par-lit into a previously deformed, variably migmatized gneiss (Plate 5C and 11A). Contacts between the Maggo gneiss and Hopedallian migmatites are concordant, with the migmatites exhibiting pinch and swell structures developed during the Hopedallian event (D_{n+2}). Hopedallian and earlier migmatites were folded during the Hopedallian event (Plate 6A), with concordant migmatites displaying tight chevron folds (Plate 6B). Early Hopedallian migmatites were recrystallized, foliated and folded during later stages of the Hopedallian deformation (Plate 6A). At other localities, the concordant migmatites within the Maggo gneiss can be traced along strike where they become discordant and develop ptygmatic structures. In such cases the axial planes of the ptygmatic structures parallel the Maggo gneiss foliation (Plate 6A).

In contrast to the Hopedallian migmatites, the younger Flordian migmatites are relatively undeformed and irregular in shape. Flordian migmatization produces diktyonitic, nebulitic and minor schlieric structures not only in the Maggo gneiss, but in all lithologies. Diktyonitic structures are easily recognized in the field. They are associated with a sinistral shear component of the Flordian event (Plate 6C and 6D). These migmatites vary in width from 1 cm to 10 cm, with the S_{n+2} foliation in the adjacent gneiss offset by the associated shear. The diktyonitic migmatites vary in length from 20 cm to 3 m.

The terminations of the diktyonitic migmatites are marked by a ductile response of the S_{n+2} foliation to the sinistral shear, and by the development of nebulitic migmatites (Plate 6C and 6D). Contacts between both migmatite types and the surrounding gneisses are gradational.

The development of diktyonitic and nebulitic migmatites and associated sinistral shears is the first manifestation of Flordian reworking of the older, Hopedalian, Maggo gneiss. The relationships observed at outcrop scale are analogous to the large scale Flordian structures visible on a regional scale, i.e. the long narrow NE-SW trending Flords.

In local areas of more intense Flordian reworking agmatitic zones are common, however the characteristic Flordian shear component may be lacking. In agmatitic zones "marker layers" within the Maggo gneiss, e.g. Hopedale dykes, exhibit evidence of rotation, recrystallization and migmatization consistent with Flordian overprinting. An examination of the effects of the progressive overprinting of the Maggo gneiss during the Flordian event is given in Section 2.4.5.

Maggo gneiss may be further subdivided on the basis of its migmatitic character. Along the north shore of Kangluasuakoluk Tagani and Uivak Point, Maggo gneiss contains abundant anorthosite xenoliths in an extensively migmatized, banded to foliated gneiss. (Plate 4E). Away

from the anorthosite xenoliths the degree of migmatization affecting the gneiss decreases. The migmatites which cut the gneiss and anorthosite are interpreted to result from the Flordian event (D_{n+3}).

3.2.3.2 Mineralogy

Trondhjemitic Maggo gneiss throughout the study area, whether from the Hopedalian or Flordian domains, exhibits the following mineral assemblage:

plagioclase - quartz - biotite - hornblende.

Tonalitic gneiss is characterized by the addition of alkali feldspar to the above assemblage. Accessory minerals include titanite, apatite, zircon and opaque oxides. Secondary minerals within the Maggo gneiss are sericite, epidote group minerals, chlorite and calcite. Almandine garnet, a characteristic accessory mineral within the Hopedalian domain, is absent in Flordian reworked Maggo gneiss.

Textural relationships within the Maggo gneiss are characterized by granoblastic, inequigranular grains displaying irrational boundaries, commonly as embayed, irregular and serrated contacts (Plate 6E and 7A). These relationships are prevalent between plagioclase and quartz grains having amoeboid shapes.

Quartz is invariably strained, with the development of subgrains in response to the Hopedalian and Flordian deformations. Plagioclase displays discontinuous albite and periclinal twins, developed in response to the deformations.

Plagioclase compositions vary from oligoclase (An 25) to andesine (An 42). Alkali feldspar in the tonalitic gneiss is interstitial to the plagioclase and quartz (Plate 7B). A finer grained equilibrium texture is present between these three phases in the interstices between the larger grains. The alkali feldspar content varies from trace amounts to approximately 5 volume percent (visual estimate). Antiperthitic, granophyric and myrmekitic textures are common in the tonalite gneiss. The latter is commonly associated with the antiperthite.

The proportion of mafic minerals (i.e. biotite and hornblende) is less than 15 volume percent (visual estimate) in the Maggo gneiss. Tonalitic gneiss contains varying proportions of biotite and hornblende. Hornblende predominates in the trondhjemitic gneiss, with minor biotite.

Two generations of biotite were observed within the gneiss (Plate 7A). The more abundant type is characterized by the following pleochroic scheme:

X = light brown, pale olive brown

Y = Z = red-orange brown, dark brown.

This biotite defines the foliation within the gneiss, with the crystallographic c-axes of the mineral grains perpendicular to the foliation. This aligned biotite is variably retrogressed to chlorite. In the banded gneiss biotite is present in the leucocratic and melanocratic bands, having a greater concentration in the latter.

The second biotite results from reaction between the more abundant red-brown biotite and garnet. This biotite is characterized by the following pleochroism;

X = light green

Y = Z = dark green.

This green biotite is randomly oriented about the retrogressed garnet.

The red-brown biotite displays a characteristic, oriented, microstructural intergrowth of acicular rutile needles, - sagenitic texture. Hatch et al. (1972) interpreted the texture to result from the breakdown of complex Ti-bearing minerals. Collerson and Bridgwater (1979), examining the Ulvak I gneiss, carried this breakdown hypothesis further by suggesting that the sagenitic biotite resulted from the breakdown of high grade (granulite facies) hornblende. Sagenitic biotite may also be produced by the retrogression of other granulite facies minerals, i.e. clinopyroxene and orthopyroxene. Evidence for a granulite facies metamorphism affecting the Maggo gneiss is lacking in the study area. The sagenitic biotite within the Maggo gneiss is interpreted to result from the retrogression of hornblende produced at upper amphibolite facies during the Hopedalian event.

Hornblende within Maggo gneiss from both the Hopedalian and Flordian domains defines the prominent foliation and/or banding together with biotite. Hornblende is characterized by the following pleochroism;

X = pale green, straw brown

Y = green

Z = dark green, brown green.

Hornblende varies from 0.5 mm to 1.3 cm grains. The latter grains are porphyroblastic, with ididioblastic to subidioblastic shapes. Hornblende forms irregular, rounded grains, displaying irrational contacts with plagioclase, quartz and other hornblende grains (Plate 6E). Where hornblende is abundant in the gneiss it forms a lepidoblastic texture, most prevalent in Hopedalian domain Maggo gneiss. The hornblende is irregular in shape, often displaying rounded edges and poikiloblastic inclusions of plagioclase and quartz.

Garnet, present within Hopedalian domain Maggo gneiss, occurs as fragmented poikiloblastic grains. Original garnet shapes are impossible to determine due to post crystallization changes, i.e. deformation and retrogression. The garnet proportion in the Maggo gneiss varies from trace amounts to approximately 15 volume percent in some units of the gneiss (Plate 7C). Where garnet is least fragmented, inclusion trails are symmetrically positioned about the core, suggesting growth during times of minimal shearing stress.

Clinopyroxene (sillite) was observed in one Maggo gneiss sample (GF-83-162), from Black Head Tickle Cove, as anhedral, rounded grains (0.1 to 0.4 mm). The presence of the clinopyroxene reflects the bulk composition of this

particular sample, which chemically corresponds to a diorite composition (see Section 5.2.1). Hopedale dykes at this same locality contain clinopyroxene suggesting the area was at upper amphibolite facies during the Hopedalian deformational event. (see Section 3.2.4, and Section 3.3.3).

Alteration minerals within the Maggo gneiss result from re-equilibration during later stages of the Hopedalian deformational event and retrogression associated with the Flordian event. Epidote group minerals (epidote, zoisite and clinozoisite) vary in abundance in the gneiss, with epidote most abundant. Epidote within the Maggo gneiss occurs as a symplectic intergrowth with quartz or as quartz-free porphyroblasts. One possible means of producing the symplectite may be the breakdown of the anorthite component of plagioclase, e.g.:



Epidote often displays both habits in a single thin section where quartz-free epidote rims, with euhedral to subhedral outlines surround symplectic epidote. The reverse of the above, i.e. porphyroblastic cores with symplectic rims was also observed. The symplectic intergrowth of epidote is not restricted to the Maggo gneiss, and is also observed in the Weekes association and the Hopedale dyke lithologies.

3.2.4 Hopedale Dykes

3.2.4.1 Field Relationships

Hopedale dykes occur as strongly attenuated, dismembered pods of amphibolite, lacking primary textures and mineralogy, emplaced into the Maggo gneiss. In the Hopedale Block the dykes represent a significant time-stratigraphic marker, as they are discordant to the Early Middle Archaean fabric (Pre-Hopedalian; D_{n+1}) within the gneiss, and were emplaced prior to the Hopedalian event (D_{n+2}). Contact relationships between the dykes and host Maggo gneiss can be used to identify Hopedalian low strain zones where Pre-Hopedalian fabrics are preserved. In the Archaean of south West Greenland, McGregor (1973) used the Ameralik dykes to distinguish two ages of gneiss (Amitsoq and Nuk), although Chadwick and Coe (1976) urged that caution be used when subdividing and correlating lithologies from various areas using the presence or absence of mafic dykes.

Hopedale dykes are distinguished from the Weekes association amphibolites by: 1) the prominent layering in the Weekes association amphibolite, 2) the continuous nature of the dykes within the host gneiss and 3) the absence of garnet in the dykes. The dykes are ubiquitous, easily recognizable in the field, exhibit a range of sizes and a variety of contact relationships with the Maggo gneiss (Plate 7D, 7E, 7F and 8B). In Hopedalian low strain zones, discordant contacts between pre-Hopedalian (S_{n+1})

fabric and the dykes are preserved (Plate 5B). The degree of discordancy is small ($<10^\circ$) with the dykes exhibiting maximum thickness, up to 2 m. The majority of the dykes are concordant with the foliation in the gneiss, having been rotated into a NW-SE orientation during Hopedalian deformation (D_{n+2}). Original dimensions and the orientation of the Hopedale dyke swarm cannot be determined due to flattening and rotation associated with the Hopedalian deformation. Within the Flordian domain, Hopedale dykes were subjected to a second deformation resulting in further disruption of the dykes by shearing, recrystallization and retrogression.

In the Hopedalian domain, dykes can be traced for 10's of metres along strike, where they are thinned, exhibit pinch and swell structures, are boudinaged and folded, accompanied by recrystallization and assimilation by the host gneiss. The intensity of folding is variable, in most areas only fold limbs were observed with few hinge zones exposed. Within the hinge zones the S_{n+2} (Hopedalian) fabric is discordant to the dyke-gneiss contact (Plate 7D). Ermanovics (1982, pers. comm.) believes the dykes have been isoclinally folded with near vertical axial surfaces, parallel limbs and rarely exposed hinge zones. Where hinge zones are lacking the fold limbs could be interpreted to represent parallel, distinct dykes (Plate 7E). In response to the Hopedalian deformation the Hopedale dykes become boudinaged, reflecting the competency contrast between dyke

and host gneiss. The interboudin zones may be filled by host gneiss or by migmatitic material of minimum melt composition. The host gneiss has plastically flowed into the interboudin zone (Plate 7A) while the migmatites have migrated into the interboudin zone (Plate 8A). (See Section 2.4.4)

The final response of the Hopedale dykes to Hopedalian deformation was recrystallization and resorption, the extent of which is variable and localized. Dykes may thin to < 4 cm in width and resorption of the dykes by the surrounding gneiss occurs (Plate 7F). Accompanying recrystallization, is the injection of migmatitic material interpreted to be derived from the host gneisses. The injected material forms apophyses, penetrating 1-6 cm into, or completely cutting across the dyke. The injected material has an orientation parallel with the Hopedalian fabric (Plate 7D).

On Dyke and Garnet Islands, relict plagioclase aggregates are preserved within the Hopedale dyke lithology (Plate 8C), similar to type B and B' Ameralik dykes (Chadwick, 1981). The plagioclase aggregates are interpreted to represent relict glomeroporphyritic plagioclase in the original dyke. Where preserved, the aggregates exhibit extensive alteration to sericite, clinzoisite and chlorite with minor alkali feldspar. This variety of dyke, with plagioclase aggregates, is not common within the study area.

Flordian deformation further disrupted the Hopedale dykes mainly by shearing, with or without the introduction of migmatitic material. Evidence of the Flordian deformation is noticeable in the dykes due to lithologic and competency contrasts between the dykes and gneiss.

3.2.4.2 Mineralogy

The Hopedale dykes exhibit the following mineral assemblages:

hornblende-plagioclase (An 20-22) -epidote-actinolite

hornblende-plagioclase (An 20) +/- epidote

hornblende-plagioclase (An 25-31) - diopside +/- epidote

Accessory minerals include biotite, quartz, titanite, zircon, carbonate and opaques.

Hornblende, the dominant mineral in the dykes, may or may not define a fabric. In thin section hornblende is strongly pleochroic from:

X = straw brown to pale green

Y = green brown

Z = green to brown green.

Hornblende occurs as idioblastic to xenoblastic grains with subidioblastic grains dominant (Plate 8B). Subidioblastic hornblende defines a granoblastic, equigranular, interlobate mosaic with sharp, rational hornblende-hornblende boundaries and embayed, irrational hornblende-plagioclase and hornblende-clinopyroxene

contacts. Poikiloblastic hornblende, with inclusions of rounded plagioclase and clinopyroxene is common. Zircon forms small inclusions in all hornblende types. Hornblende defines a lepidoblastic texture in foliated samples and in samples displaying a strongly developed foliation subgrains of hornblende form. Hornblende also occurs in a symplectic intergrowth with epidote, the latter interpreted to result from retrogression of plagioclase.

Plagioclase in the Hopedale dykes, exhibit albite and to a lesser extent pericline twins. Plagioclase compositions vary from An 20 to An 23 in clinopyroxene-absent dykes and An 25 to An 32 in clinopyroxene-bearing dykes. The variation in plagioclase compositions is interpreted to reflect an increased metamorphic grade for the latter dykes, as the bulk chemical composition of all dykes are similar (see Section 3.3.3).

Clinopyroxene is pale green, in colour, occurs as rounded spherical to irregular shaped grains, completely to partially enclosed in hornblende (Plate 8B). Garnets within the Hopedale dyke lithology were observed at one locality (Dyke Island, Sample 83-192). These are isolated from clinopyroxene and hornblende in the dyke by a corona of plagioclase. This texture suggests the garnet is not in equilibrium with the dominant mineralogy of the dyke and is metastable. As with clinopyroxene, the garnet is interpreted as a relict mineral reflecting a higher P assemblage within the dyke. (See Section 3.3.3)

Epidote is colourless, forms subidioblastic grains and commonly forms a symplectic intergrowth with quartz (Plate 8E). The symplectite texture reflects the effects of Flordian retrogression of plagioclase (see Section 3.2.3.2 and Equation 3.1).

Actinolite is non-pleochroic, pale green and forms at the expense of hornblende due to Flordian retrogression (Plate 8E). Biotite appears to be produced by the retrogression of hornblende, presumably with the introduction of K and Al and liberation of Si and Ca.

3.2.5 Kikkertavak Dykes

All late, undeformed, mafic dykes have been assigned to the Kikkertavak dyke swarm. Ermanovics et al. (1982) suggest two Proterozoic dyke swarms were emplaced into the Hopedale Block (Kikkertavak and Harp Lake suites). An unpublished Rb/Sr age of $2,199 \pm 55$ Ma (Fryer, 1983; pers. comm.) has been determined for a Kikkertavak dyke from Cross Island, southeast of Hopedale. Grant et al. (1983) obtained a Rb/Sr age of $1,206 \pm 120$ Ma for a post Flordian dyke from the head of Kanariktok Bay. The Kikkertavak dyke swarm belongs to an Fe-tholeiite suite of mafic dykes intruded into the North Atlantic Craton in early Proterozoic time (Bridgewater et al., 1985).

3.2.5.1 Field Relationships

The Kikkertavak dykes have a predominately NE-SW orientation, with the larger dykes forming prominent ridges within the study area. The longest dyke (> 15 km) can be

traced from Pilliarusik Bay to the NE as far as Tesslujalik Island (Figure 3.1). The dykes have sharp contacts with the enclosing Maggo gneiss with dyke apophyses penetrating into the gneiss.

The Kikkertavak dykes have been affected by later Proterozoic faulting, e.g. the tip of Dead Dog Point (Plate 11E) and the south end of Pilliarusik Bay. At both localities the dykes have been retrogressed to greenschist facies assemblages as a result of faulting.

3.2.5.2 Mineralogy

Mineralogically the dykes consist of the following igneous mineral assemblage:

plagioclase - clinopyroxene - olivine -
orthopyroxene - opaque oxides.

Secondary minerals include sericite, amphibole and chlorite. Plagioclase forms euhedral to subhedral, compositionally zoned, twinned grains. Plagioclase cores are of bytownite composition (An 70 to An 75) with edges of andesine to labradorite (An 46 to An 51). The plagioclase varies in grain size from 0.3 mm to 1.2 cm. Coarse grained to very coarse grained plagioclase accumulations were observed in the larger dykes.

Clinopyroxene (diopside) and opaque oxides form an angular intergrowth interstitial to and surrounding plagioclase and olivine. Ophitic to sub-ophitic textures with plagioclase laths enclosed by single, large oikocrysts of diopside are common in coarser grained dykes. Olivine.

forms rounded, fractured, altered grains that vary in size from 0.2 to 2.0 mm. The olivine alteration varies in intensity from minor alteration along fractures to grains with only minor amounts of olivine preserved.

Along the dyke margins the primary mineralogy has been hydrated, possibly due to late Proterozoic activity, i.e. at the time of development of the Kanariktok Shear zone to the south. Along the margins of the dykes the diopside alters to a blue-green amphibole and the plagioclase to sericite. Rounded clots of chlorite - orthoamphibole - opaques, similar in size and appearance to the olivine in the fresh dyke are present.

3.3 Metamorphism

3.3.1 Introduction

Korstgard and Ermanovics (1985) have documented the prevailing metamorphic conditions associated with the Hopedalian (D_{n+2}) and younger tectonothermal events within the Hopedale Block and adjacent structural provinces. The evidence presented in this section for Maggo gneiss and Hopedale dykes is in agreement with the conclusions of Korstgard and Ermanovics (1985). In addition, data for the Weekes association amphibolite and ultramafic subunits are presented, to point out the problems encountered when all supracrustal material is lumped into a single unit.

3.3.2 Maggo Gneiss

The Maggo gneiss exhibits a relatively homogeneous mineralogical composition throughout the study area, regardless of the structural domain sampled.

Maggo gneiss is characterized by the mineral assemblage plagioclase-quartz-hornblende-biotite +/- alkali feldspar, placing it within the amphibolite facies (Miyashiro, 1973). Garnet is a common accessory mineral within Hopedalian domain gneiss. The presence or absence of garnet may be used as a broad indicator of the prevailing P-T conditions associated with each structural domain. Ermanovics (pers. comm., 1982) suggested that garnet is only present within those areas of the Hopedale Block where the Hopedalian fabric dominates, indicating Hopedalian metamorphism occurred at upper amphibolite facies. This generalization cannot be accepted since the presence or absence of garnet, in itself, is not a useful indicator of metamorphic grade, as many factors other than P and T, influence garnet stability (Deer et al., 1982).

Garnet appears to be an unstable phase, occurring as irregularly shaped, fractured grains, invariably exhibiting some degree of alteration (Plate 7C). The retrogression of garnet results from late Hopedalian and Flordian effects.

Maggo gneiss underwent retrogression within the Flordian domain resulting in lower amphibolite facies parageneses. This is supported by the predominance of hornblende, with minor biotite, and the lack of garnet in

Flordian domain gneiss samples within the study area. Hornblende occurs as porphyroblasts, up to 1 cm across, in Flordian domain Maggo gneiss and associated migmatites.

3.3.3 Hopedale Dykes

The Hopedale dykes exhibit a restricted compositional range, represented by the shaded region on Figure 3.2 and are interpreted to have undergone minor, post emplacement chemical alteration (see Section 5.3).

Three representative samples of the Hopedale dykes, from the Hopedalian and Flordian domains, can be examined to document the prevailing metamorphic grade associated with each tectonothermal event. Mineral analyses for Hopedale dyke parageneses, representing the stable assemblages observed in the dyke samples are shown in Figure 3.2.

Sample 83-192, from Garnet Island (See Figure 5.1 for sample locations), represents the highest grade assemblage preserved in the dykes. In the field this sample is characterized by the presence of garnet in the cores of plagioclase clots (Plate 8C). This locality is the only one in the Hopedale Block where garnet was observed within the dyke lithology (Ermanovics, pers. comm., 1982).

The dominant assemblage within the dyke is hornblende-plagioclase-clinopyroxene (Figure 3.2a), with the garnet-clinopyroxene-hornblende assemblage being unstable. A general reaction of the type:

Figure 3.2. ACF diagrams showing mineral assemblages observed in the Hopedale dyke lithology from the Hopedalian (a,b) and Flordian (c) domains. Shaded region - bulk composition of dykes.

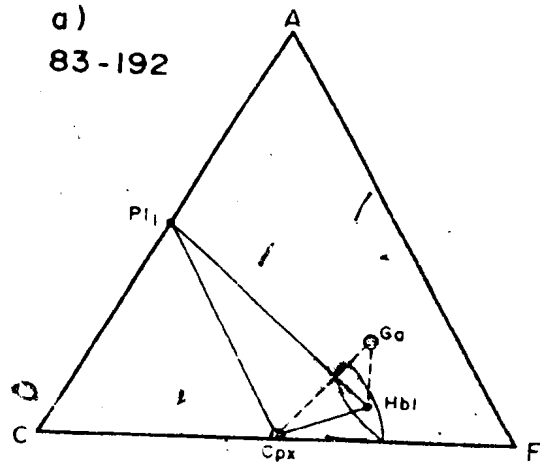
a) 83-192 - highest grade assemblage, garnet-clinopyroxene-hornblende (hornblende granulite facies) reacting to upper amphibolite facies.

Garnet-clinopyroxene-hornblende assemblage unstable (dashed line) replaced by plagioclase-hornblende-clinopyroxene.

b) 82-69A - middle amphibolite facies (plagioclase-hornblende), characteristic of Hopedalian metamorphism.

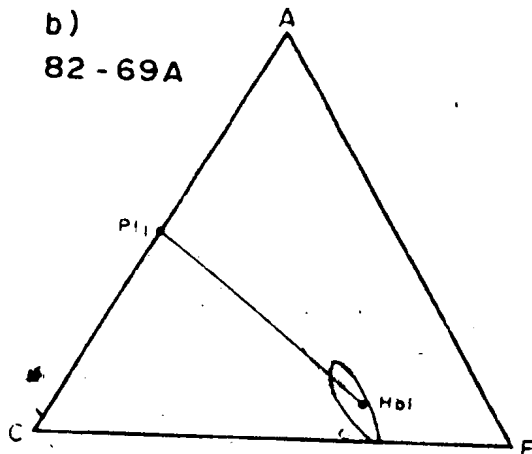
c) 83-212 - lower amphibolite facies epidote-actinolite-plagioclase replaces plagioclase-hornblende as a result of Flordian retrogression.

a)
83-192

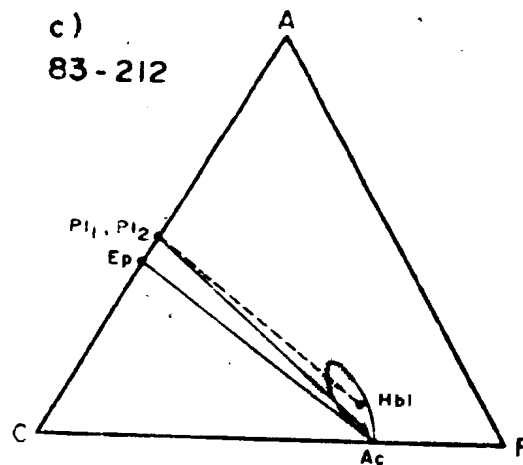


Go - Garnet
 Cpx - Clinopyroxene
 Hbl - Ferro Edenitic Hornblende
 Pl₁ - Plagioclase (An 27)
 Pl₂ - Plagioclase (An⁴ 21)
 Ep - Epidote
 Ac - Actinolite

b)
82-69A



c)
83-212



00000

garnet + clinopyroxene + H₂O

====> hornblende + plagioclase (3.2)

The garnet-clinopyroxene-hornblende assemblage in the dyke is interpreted to result from the peak of metamorphism associated with the Hopedalian (D_{n+2}) event. The same mineralogical and textural features have been observed in Weekes association subunit 4 at this locality and one other locality in the study area and corresponds to the garnet granulite facies.

Based on the textures and mineralogy observed in the Hopedale dyke, and the Weekes association, the reaction is retrogressive in nature and requires the presence of a hydrous fluid phase.

The clinopyroxene-hornblende-plagioclase assemblage (Plate 8B), observed in 6 Hopedale dyke samples, from widely separated localities, is indicative of upper amphibolite facies conditions (Figure 3.2a) during the Hopedalian event.

Subsequent to the development of the cpx-hbl-pl assemblage, clinzoisite forms as a result of retrogression of plagioclase, similar to equation 3.1. The clinzoisite forms a symplectic intergrowth with quartz, as the SiO₂ produced in excess by this reaction, does not diffuse away from the site of the reaction. This retrogression may result from either late Hopedalian effects or reflect Flordian overprinting on the dyke. Due to the lack of

retrogression of hornblende, characteristic of Flordian overprinting, and the presence of stable clinopyroxene, the epidote is interpreted to result from late Hopedalian effects. The fluid phase required to retrogress the stable cpx-hbl-pl assemblage in the dykes may be of the same source which resulted in the retrogression of the cpx-gt-hbl assemblage discussed above (Equation 3.2). The retrogression is inferred to have occurred under lower to middle amphibolite facies conditions.

The dominant mineral assemblage observed in Hopedale dykes within the Hopedalian domain, is plagioclase-hornblende-quartz as represented by Sample 82-69A (Figure 3.2b). This assemblage was observed within 11 dyke samples from throughout the study area and is interpreted to have developed at middle amphibolite facies conditions. Varying degrees of retrogression of this assemblage to sericite and epidote, with minor actinolite, are interpreted to have occurred after the peak Hopedalian metamorphism, but not necessarily as a result of the Flordian event.

Accompanying the structural reorientation of the Hopedale dykes in response to the Flordian (D_{n+3}) event is the retrogression of Hopedalian mineral parageneses. The dominant Flordian mineral assemblage, characterized by the formation of actinolite and epidote, can be represented by Sample 83-212 (Figure 3.2c). Based on petrographic evidence the retrogressed assemblage results from the breakdown of hornblende and plagioclase, e.g.;

hornblende + anorthite + H₂O

====> actinolite + clinzoisite + albite (3.3)

Actinolite replacement of hornblende is seen as a sharp change in colour and pleochroism at the margins of the amphibole. Symplectic intergrowths of epidote and quartz (Plate 8E) are well developed within the Flordian domain. The An content of the plagioclase within the Hopedale dykes from the Hopedalian and Flordian domains varies from An 27 to An 21, respectively. The relict Hopedalian assemblage (the dashed line in Figure 3.2c) unstable during Flordian metamorphism is replaced by the assemblage epidote-actinolite-plagioclase. The lower An content of the plagioclase, the stability of actinolite and epidote suggest that Flordian metamorphism occurred at lower amphibolite or greenschist facies.

3.3.4 Weekes Association

The wide range of bulk compositions recorded for the Weekes association points to this unit as the most useful indicator of preserved metamorphic conditions within the study area. However, the supracrustal rocks are not present throughout the study area and each lithology exhibits a wide variety of mineral parageneses.

The Weekes association, and its inferred correlative equivalents (Hunt River Group), have been interpreted to represent the oldest lithology within the Hopedale Block (Ermanovics et al., 1982). As such this lithology preserves evidence of two tectonothermal events, interpreted to have

developed prior to incorporation in the gneiss (See Table 3.1). The major problem in using this unit as an indicator of P-T- X_{H_2O} conditions is that the age of the preserved assemblage is unknown with respect to the Hopedalian event. Metamorphic parageneses for the amphibolite and ultramafic subunits, from the Hopedalian domain, are examined below and indicate that each subunit displays two distinct metamorphic assemblages. This indicates that the Weekes association, as defined by previous workers (Ermanovics et al., 1982; Korstgard and Ermanovics, 1984) consists of two distinct sequences of supracrustal material. It should be noted that these observations on the Weekes association mineral parageneses are of a preliminary nature.

3.3.4.1 Amphibolite Subunits

Within the amphibolite subunits the highest metamorphic grade is preserved in the garnet-clinopyroxene amphibolite (Plate 2A and 2B). Two samples (83-64 and 193) consist of garnet-clinopyroxene which are metastable and can be seen to be reacting out to produce hornblende-plagioclase coronas around garnet (Plate 2B). The interpretation of this reaction and the resulting textures is similar to that suggested for the Hopedale dykes (Reaction 3.2; Section 3.3.3).

Sample 83-64, characterized by a fine grained (0.1 to 0.5 mm), granoblastic, equigranular texture, displays a well developed equilibrium texture between plag-cpx, cpx-hbl, hbl-plag and plag-plag, progressing from the matrix

into the plagioclase corona around the garnet (Plate 2A and 2B). There is a progressive increase in grain size from the matrix towards the corona, most evident with the appearance of hornblende, up to 0.5 mm, in the corona. This sample comes from a large (50 to 150 m thick) layer of Weekes association (see Figure 5.1 for location) which may have been isolated from retrogression associated with Pre-Hopedalian and younger events.

Sample 83-193, taken from the same locality as the garnet-bearing Hopedale dyke (Sample 83-192), displays a medium grained (0.7 to 2.0 mm), lepidoblastic texture defined by aligned hornblende. Plagioclase is sericitized and the proportion of clinopyroxene is lower, approx. 5% vs. 30%, compared with Sample 83-64.

Whether the mineral assemblages present in these two samples result from the same metamorphic event has not been determined. The close field relationship between the Weekes association amphibolite and the Hopedale dyke lithology, samples 83-193 and 83-192, respectively, displaying similar textures and mineralogy, suggests that the preserved mineral assemblages resulted from Hopedalian metamorphism. The isolated position of Sample 83-64, with respect to the Hopedale dykes, makes a clear and unequivocal correlation between the preserved parageneses and the Hopedalian metamorphism tenuous.

The lowest grade assemblage preserved in the amphibolite subunits, for samples from Woody and Maggo

Islands, correspond to the almandine zone of the amphibolite facies (Turner, 1968). At both localities the amphibolite is characterized by the assemblage hornblende-plagioclase (An 36)-almandine +/- epidote. This lower grade assemblage is distinctly different than that recorded for the Weekes association samples (83-84, 193) above.

The Weekes association amphibolite samples preserving the low and high grade assemblages exhibit minimal differences in bulk chemical composition. The samples representing the extremes of metamorphism come from widely separated localities with no obvious demarcation line between the high and low grade assemblages. If the Weekes association amphibolite samples do belong to a single supracrustal sequence then the peak of metamorphism observed should be much closer than that recorded. Alternatively, it is tentatively suggested that the Weekes association amphibolite samples belong to two distinct supracrustal sequences, each of which retains evidence for a peak metamorphism corresponding to separate metamorphic events.

3.3.4.2 Ultramafic Rocks

The ultramafic subunit exhibits a distinct dichotomy of textures and mineralogy in the study area, reflecting separate igneous and metamorphic origins. Relict igneous, i.e. harrisitic (Plate 2C) and cumulate, textures are evident at some localities (Station 83-131 and Woody Island), whereas ultramafic lithologies from Manuel Island

and Ulvak Point are foliated to banded, displaying well developed metamorphic mineral parageneses.

One means of distinguishing between igneous mineralogy and metamorphic mineral parageneses is to examine olivine compositions. Collerson et al. (1976b) have proposed using the ratio $\text{CaO}(\text{host rock})/\text{CaO}(\text{olivine})$ to distinguish olivines of igneous or metamorphic origin. Table 3.2 presents the results of applying this ratio to olivine from the ultramafic subunit of the Weekes association. Also presented in Table 3.2 are the ratios for olivines of known igneous and metamorphic origin (from Collerson et al., 1976b).

Using this criterion, the olivine from sample BF-82-4A is igneous in origin. Both the olivine and orthopyroxene, in this sample are fractured, with serpentine along fractures cutting through the olivine grains. The ultramafic body from which this sample was collected is quite large (up to 75 m wide) and has been cut by numerous anastomosing fractures, resulting in individual blocks of the order of 2 to 3 m in size. The margins of the blocks are marked by the development of actinolite reaction rims, up to 20 cm thick, symmetrically distributed about the centre of the fracture. Sample BF-82-4A was taken from the central portion of one of these individual blocks.

The remaining two samples (BF-82-3, GF-83-51 in Table 3.2) from the study area indicate a metamorphic origin for the olivine. These samples, from ultramafic blocks, up to

Table 3.2: Comparison of $\text{CaO}_{(\text{host rock})}/\text{CaO}_{(\text{olivine})}$ ratios for olivine formed by igneous and metamorphic processes.

Locality	$\text{CaO}_{(\text{host rock})}/\text{CaO}_{(\text{olivine})}$	Source
Igneous Origin		
BF-82-4A	34.00	This Study
Hunt River	11.00	1
Munro Twp.	15.59	2
Barberton	61.39	3
Metamorphic Origin		
BF-82-3	>500	This Study
GF-83-51	>800	This Study
Malenco (Italy)	60.00	4
Malenco (Italy)	115.00	4
Malenco (Italy)	195.00	4

References - 1) Collerson et al. (1976b); 2) Pyke et al. (1973); 3) Nesbitt (1971); 4) Trommsdorff and Evans (1972).

10 m thick, within Weekes association amphibolite are characterized by:

- 1) coarse to very coarse grain size,
- 2) well developed mineralogical layering (possibly reflecting original layering),
- 3) strong mineral lineation, and
- 4) elongated, fractured and serpentized olivine.

Minerals found in association with the olivine are anthophyllite, magnetite and a green spinel.

The ultramafic sample containing olivine of inferred igneous origin comes from Woody Island, where the Weekes association amphibolite displays the lowest preserved metamorphic grade. Where olivine can be shown to be of metamorphic origin (Manuel Island; Sample BF-82-3), the metamorphic assemblages within the Weekes association amphibolite correspond to a higher metamorphic grade. These observations reinforce the conclusion that the Weekes association represents two distinct supracrustal sequences within the Hopedale Block.

3.3.5 Summary of Metamorphism

Due to the quartzo-feldspathic composition of the Maggo Gneiss, it is not a sensitive indicator of changing conditions of metamorphism. The gneiss can be broadly separated, on the basis of the presence or absence of garnet, into two groups corresponding to samples representative of Hopedalian and Flordian metamorphism, respectively.

↓

The Hopedale dykes provide the most sensitive indicators of changing metamorphic conditions within the study area. This lithology records mineral assemblages interpreted to result from Hopedalian metamorphism which were subsequently retrogressed during the Flordian event. The assemblage gt-cpx-hbl reacting to cpx-hbl-plag, with the addition of water, corresponds to the boundary between garnet granulite and amphibolite facies. The coexistence of the gt-cpx-hbl marks the highest grade attained for the Hopedale dykes during the Hopedalian metamorphism. The predominant mineral assemblage produced as a result of Hopedalian metamorphism is hbl-plag +/- cpx, characteristic of upper amphibolite facies. Flordian assemblages (actinolite-epidote-oligoclase) result from retrogression, at lower amphibolite facies, of the Hopedalian assemblage.

Mineral assemblages presented for the amphibolite and ultramafic subunits of the Weekes association indicate two distinct metamorphic grades for this lithology. More detailed field and petrographic work is required before the two metamorphic grades can be correlated with those recognized in the Maggo gneiss and Hopedale dykes. Preliminary conclusions indicate that the Weekes association may consist of two supracrustal sequences of differing ages.

Chapter 4

GEOCHRONOLOGY

4.1 Introduction

This chapter presents the results of Rb/Sr age determinations for twelve Maggo gneiss suites from the Hopedale Block. Field descriptions and locations for each suite can be found in Appendix A. The geochronological study was undertaken to: 1) date the timing of the Hopedalian deformational event; 2) date the Flordian reworking of the preexisting Hopedalian lithologies; and 3) examine the effects on the Hopedalian isotopic systematics of the Flordian reworking.

All isotopic determinations were carried out on whole rock powders of Maggo gneiss. Ion exchange separation procedures and an estimate of precision and accuracy for the determinations are presented in Appendix C. Errors quoted for Rb and Sr concentrations and $^{87}\text{Rb}/^{86}\text{Sr}$ ratios are ± 2 to 5% and $\leq 1\%$, respectively. Errors for $^{87}\text{Sr}/^{86}\text{Sr}$ ratios, ages and initial $^{87}\text{Sr}/^{86}\text{Sr}$ ratios are reported at the 1 sigma confidence level.

4.1.1 Isochron vs. Errorchron

The fitting of isochrons to yield ages and initial Sr ratios was carried out using a least squares regression method similar to that suggested by Brooks et al. (1972). The regression result for an individual suite yields a "date" which corresponds to the "age" at which time the Rb-Sr isotopic systematics for that suite closed. A measure of the geological error associated with an individual regression is given by the mean square of the weighted deviates (MSWD). The MSWD is a statistical function which evaluates the relative contribution of analytical error versus geological error to the age determination.

Brooks et al. (1972) suggested that for an MSWD > 2.5, the samples used in the regression define an errorchron rather than a true isochron. The cutoff point separating isochron and errorchron behaviour for an individual suite of analyses will be a function of the sample population size. Fryer and Taylor (1985) indicate that a MSWD of 8 for a three-point isochron is equivalent to a MSWD of 2.5 for an eight-point isochron, taking into account the number of degrees of freedom in each case.

An increase in the MSWD implies a greater degree of geological error rather than analytical error for the regression. In this work an MSWD of < 5, for small sample populations, is interpreted to reflect isochron behaviour for that particular suite.

The location of each suite analyzed and their resulting ages are shown on Figure 4.1. Regression results obtained for each Maggo gneiss suite are summarized in Table 4.1.

All ages quoted are based on a decay constant for ^{87}Rb of $1.42 \times 10^{-11} \text{ y}^{-1}$ (Steiger and Jaeger, 1977).

4.2 Manuel Island (MI)

Nine samples from Manuel Island (See Figure 4.1 for location) were analyzed (Table 4.2). Regression analysis of all points yields a date of $2,950 \pm 93 \text{ Ma}$ with an MSWD of 18.5. The high MSWD for this suite can be attributed to two samples which lie off the regression line.

At locality 82-78 the Maggo gneiss exhibits evidence of weak shearing and migmatization interpreted to result from Flordian reworking. Sample 83-305 is a recrystallized, foliated pegmatite, concordant to the Hopedalian fabric in the enclosing gneiss. The foliation within the pegmatite is discordant to the foliation in the enclosing gneiss, indicating a pre-Hopedalian origin for the fabric. Omission of these two analyses and regressing the remaining samples yields a date of $3,125 \pm 43 \text{ Ma}$ ($\text{Sr}_0 = 0.70163 \pm 0.00019$ ($\text{Sr}_0 = \text{initial } ^{87}\text{Sr}/^{86}\text{Sr} \text{ ratio}$)) and a MSWD of 2.3 (Figure 4.2).

4.3 Porphyroblastic Phase (PP)

Five samples of medium grained, porphyroblastic biotite tonalite gneiss from three widely separated localities are combined in this isochron (See Figure A.1 for locations). Results of the isotopic determinations (Table 4.2) are

0000

Figure 4.1: Location map and regression results for the twelve suites of Maggo gneiss examined in this study.

Abbreviations, referring to individual suites, are: BH - Black Head Tickle; DP - Dead Dog Point; DI - Dyke Island; HG - Hopedale Gneiss; HH - Hopedale Harbour; HI - Hypothesis Island; MC - Marsha's Cove; MI - Manuel Island; NBN - Next Bay North; PB - Pilliarusik Bay; PP - Porphyroblastic Phase; SEDI - Southeast Double Islands.

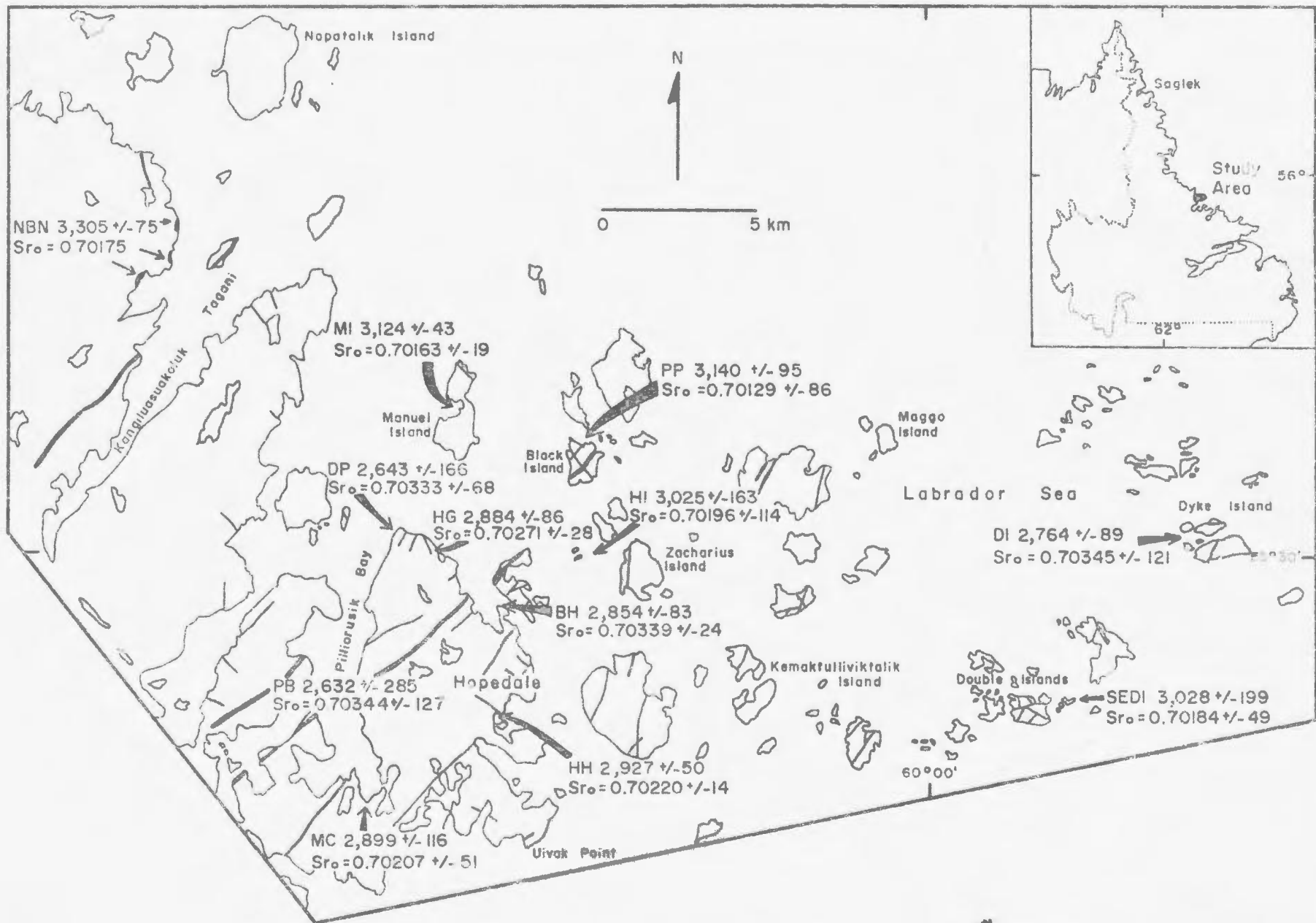


Table 4.1: Rubidium - strontium regression results for whole rock data from the Hopedale Block. N - number of samples; ages are quoted in Ma.

Suite	N	Age +/- 1 σ	Initial Ratio +/- 1 σ	MSWD
<u>PRE-HOPEDALIAN</u>				
Next Bay North ¹	6	3,133 +/- 170	0.70259 +/- 0.0009	9.9
Next Bay North ²	4	3,305 +/- 75	0.70175	1.3
<u>HOPEDALIAN</u>				
Manuel Island	7	3,125 +/- 43	0.70183 +/- 0.00019	2.29
Porphyroblastic Phase	5	3,140 +/- 95	0.70129 +/- 0.00088	1.04
Hypothesis Island	6	3,025 +/- 163	0.70198 +/- 0.00114	3.57
SE Double Island	6	3,028 +/- 199	0.70184 +/- 0.00049	2.62
<u>FLORDIAN</u>				
Hopedale Harbour	4	2,927 +/- 50	0.70220 +/- 0.00014	1.54
Marsha's Cove (SE) ^{1*}	8	2,888 +/- 150	0.70186 +/- 0.00084	48
Marsha's Cove (SE) ^{2*}	6	2,894 +/- 26	0.70199 +/- 0.00011	1.37
Marsha's Cove (SW)	4	2,865 +/- 81	0.70271 +/- 0.00038	4.53
Marsha's Cove (All)	12	2,899 +/- 116	0.70208 +/- 0.00051	38
Hopedale Gneiss	5	2,884 +/- 86	0.70271 +/- 0.00028	15.6
Black Head Tickle ¹	7	2,874 +/- 251	0.70298 +/- 0.00070	52
Black Head Tickle ²	5	2,854 +/- 83	0.70339 +/- 0.00024	5.66
Dead Dog Point ¹	5	2,643 +/- 166	0.70333 +/- 0.00068	13.9
Dead Dog Point ²	4	2,804 +/- 100	0.70282 +/- 0.00038	3.68
Pilliarusik Bay	4	2,632 +/- 285	0.70344 +/- 0.00127	13.0
Dyke Island	10	2,764 +/- 89	0.70345 +/- 0.00121	4.70

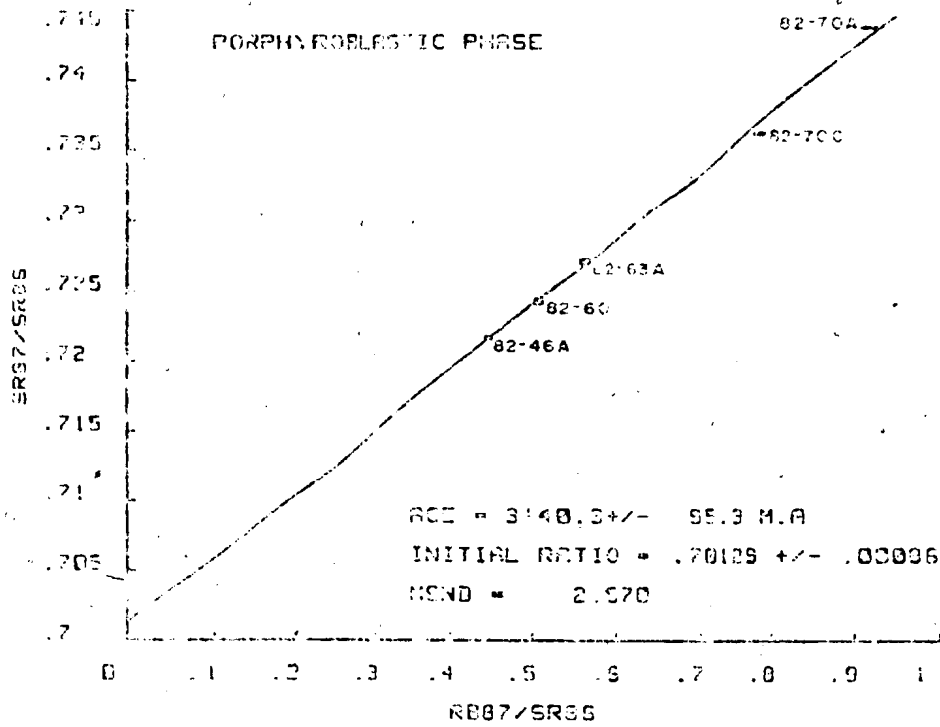
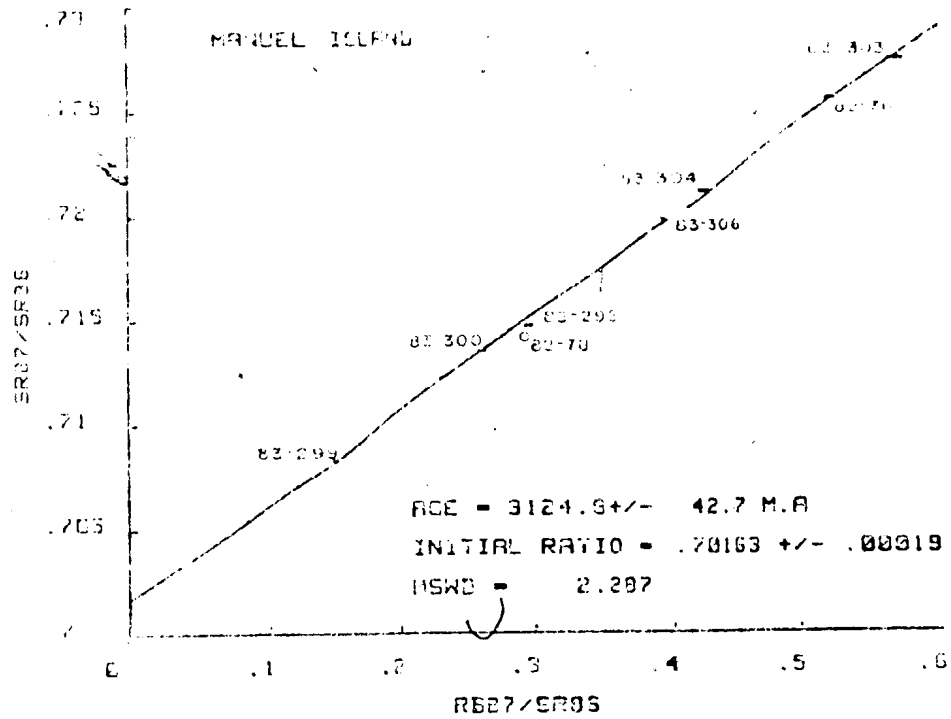
* - Numbers refer to regression results for all samples (1) and regression results obtained after elimination of discordant samples (2)

Table 4.2: Rb and Sr Contents and Isotopic Compositions for samples of Maggo Gneiss from the Hopedalian Domain. Errors are 2 to 5 % for Rb, Sr and <1% for $^{87}\text{Rb}/^{86}\text{Sr}$. The $^{87}\text{Sr}/^{86}\text{Sr}$ ratios are normalized to $^{87}\text{Sr}/^{86}\text{Sr} = 0.1194$ and corresponding errors, at 1 sigma, are quoted in terms of 10^{-5} . * - sample not used in regression analysis, D - duplicate analysis of $^{87}\text{Sr}/^{86}\text{Sr}$ ratio, carried out on separate aliquots of the same powder.

Sample No.	Rb	Sr	Rb/Sr	$^{87}\text{Rb}/^{86}\text{Sr}$	$^{87}\text{Sr}/^{86}\text{Sr}$	1 sigma
<u>Manuel Island</u>						
82-76	49	270	0.180	0.521	0.725450	6.7
82-78*	43	422	0.101	0.294	0.714162	9.5
83-298	59	581	0.102	0.296	0.714662	2.6
83-299	10	202	0.050	0.145	0.708274	3.4
83-299D*					0.708250	2.2
83-300	32	353	0.091	0.262	0.713487	4.3
83-303	63	319	0.196	0.569	0.727308	3.5
83-304	54	368	0.146	0.422	0.721045	6.1
83-305*	70	308	0.227	0.659	0.728348	2.3
83-305D*					0.728333	5.9
83-306	50	366	0.137	0.397	0.719758	2.9
<u>Porphyritic Phase</u>						
82-46A	47	307	0.154	0.445	0.721619	14.6
82-60	54	312	0.175	0.506	0.724232	21.3
82-63A	80	413	0.193	0.559	0.727090	19.7
82-70A	77	243	0.315	0.916	0.743698	6.0
82-70C	77	285	0.269	0.782	0.736176	9.4
<u>Hypothesis Island</u>						
82-64	62	340	0.181	0.525	0.725458	6.5
82-65A	55	332	0.164	0.478	0.723071	9.5
83-275	71	316	0.223	0.648	0.730079	5.8
83-276	49	330	0.148	0.429	0.720236	3.0
83-277	56	392	0.139	0.404	0.719848	5.8
83-277D*					0.719783	1.3
83-278	57	372	0.154	0.445	0.721632	8.3
<u>SE Double Island</u>						
82-74A	27	456	0.059	0.171	0.709488	13.7
82-74B	30	440	0.067	0.194	0.70186	9.0
82-74C	24	467	0.052	0.149	0.708494	6.1
82-74D	23	467	0.050	0.145	0.708252	6.6
82-74E	24	448	0.054	0.157	0.708461	10.4
82-74F	36	441	0.082	0.238	0.712503	14.8

Figure 4.2: Rb/Sr whole rock isochron for seven samples of Maggo gneiss from Manuel Island. Isotopic data used to construct the diagram may be found in Table 4.2. o - samples not used in regression analysis. (Sample 83-305, not used in the regression analysis, lies off the diagram.)

Figure 4.3: Rb/Sr whole rock isochron for five samples of the Porphyroblastic Phase of the Maggo gneiss. Isotopic data to construct the diagram may be found in Table 4.2.



plotted in Figure 4.3. Regression of all samples yields a date of 3,140 \pm 95 Ma, $Sr_0 = 0.70129 \pm 0.00086$ with an MSWD = 2.6. The collinearity, as evidenced by the low MSWD, of the samples reflects the homogenization effects of isotopic resetting over a wide area during the Hopedalian event.

4.4 Hypothesis Island (HI)

Six samples of the biotite tonalite phase of the Maggo gneiss from Hypothesis Island (Table 4.2) yield an age of 3,025 \pm 163 Ma with $Sr_0 = 0.70196 \pm 0.00114$ and an MSWD = 3.6 (Figure 4.4). The high error on the age and the initial Sr ratio for this suite can be attributed to the restricted range of $^{87}Rb/^{86}Sr$ ratios.

4.5 Southeast Double Island (SEDI)

The Southeast Double Island suite consists of six samples of homogeneous hornblende trondhjemite. The restricted lithological variation of the suite is reflected in the low range of $^{87}Rb/^{86}Sr$ ratios (Table 4.2). The date for this suite is 3,028 \pm 199 Ma ($Sr_0 = 0.70184 \pm 0.00049$, MSWD = 2.6; Figure 4.5). The low $^{87}Rb/^{86}Sr$ ratios, the lowest of all samples analyzed, reflect the low Rb and high Sr content of these samples compared with other analyzed samples (see Section 6.2.2).

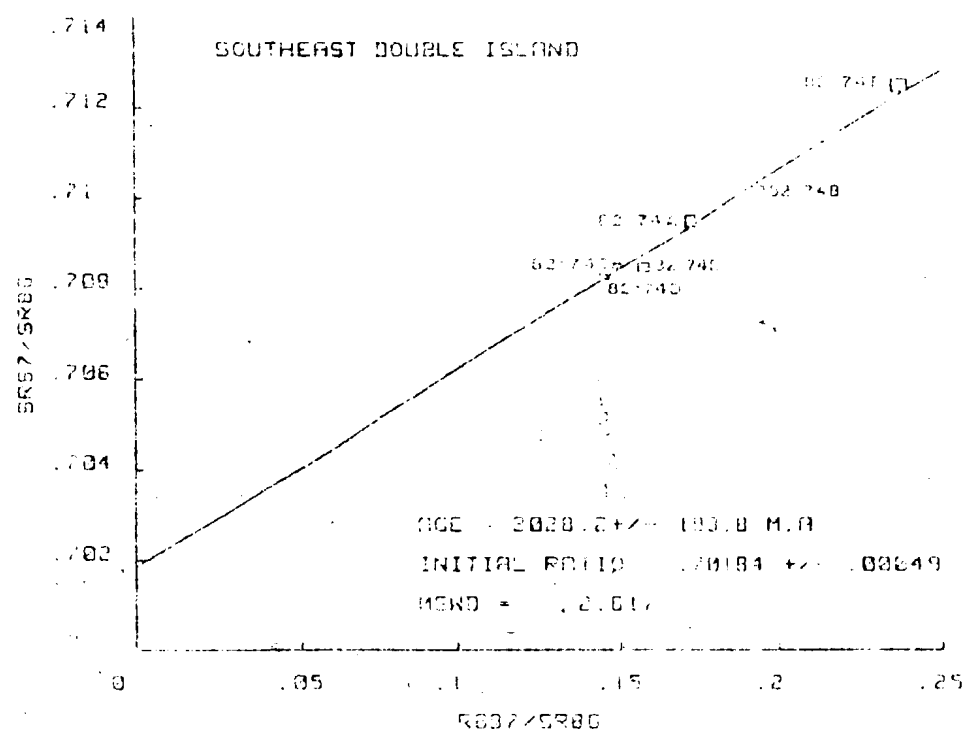
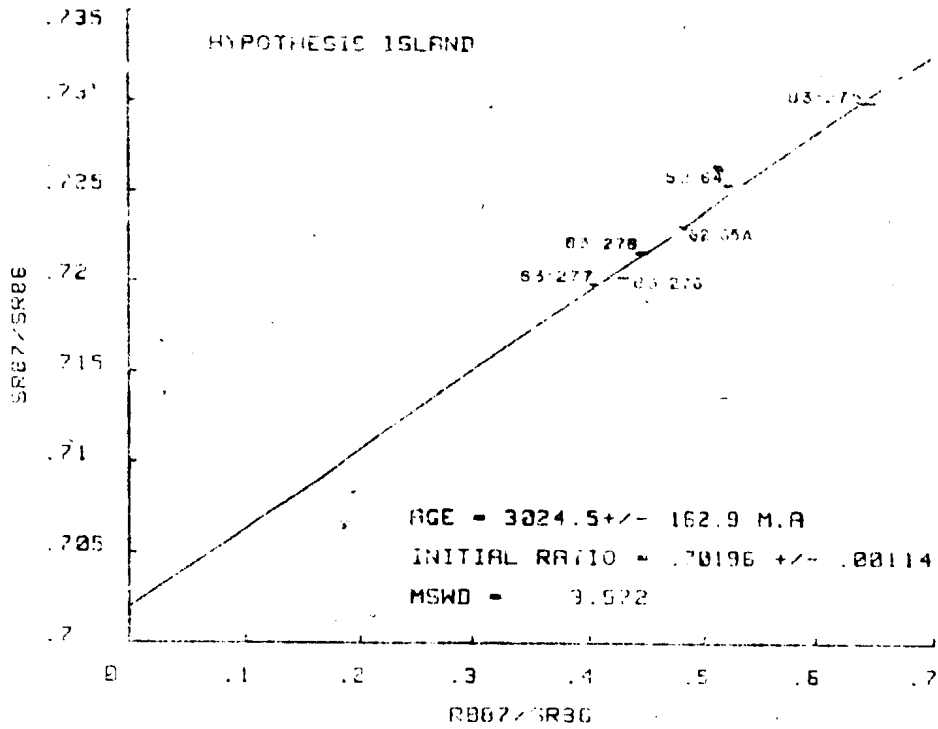
4.6 Hopedale Harbour (HH)

The Hopedale Harbour suite consists of four samples collected from the extreme western end of the harbour (Figure 4.1). Regression analysis of the samples (Table

Figure 4.4: Rb/Sr whole rock isochron for six samples of Maggo gneiss from Hypothesis Island. Isotopic data used to construct the diagram may be found in Table 4.2.

Figure 4.5: Rb/Sr whole rock isochron for five samples of Maggo gneiss from South East Double Island area. Isotopic data used to construct the diagram may be found in Table 4.2.

00111



4.3) yields a date of $2,927 \pm 50$ Ma with $Sr_0 = 0.70220 \pm 0.00014$ (Figure 4.6). The low MSWD (1.54) attests to the samples belonging to an isotopically homogeneous suite of Maggo gneiss.

4.7 Marsha's Cove (MC)

In Marsha's Cove, Ermanovics et al. (1982) recognized the progressive effects of Flordian reworking of the Maggo gneiss. All analyzed samples (Table 4.3) are from a recognizable augen of Maggo gneiss with preserved Hopedalian fabric (S_{n+2}). Along the margins of this large augen the foliation is progressively reoriented into a NE-SW direction (S_{n+3}) characteristic of the Flordian event. Sample locations are shown in Figures A.4 and A.5, and Plates 6D, 9D, 9E, 9F and 10A.

Samples from the SE end of Marsha's Cove (See Appendix A, Section A.2.5); come from two localities situated along strike and separated by < 100 m. Regressing eight samples yields a date of $2,888 \pm 150$ Ma ($Sr_0 = 0.70186 \pm 0.00064$) and an MSWD of 47.7. Eliminating the highly discordant samples, 83-202 and 83-203, from the regression reduces the errors on the age and initial ratio and lowers the MSWD to 1.37 (Figure 4.7). The new age ($2,893 \pm 26$ Ma) and initial ratio ($S_0 = 0.70199 \pm 0.00011$) are within error of the values obtained using all samples. There is no recognized geological basis for the elimination of these two samples.

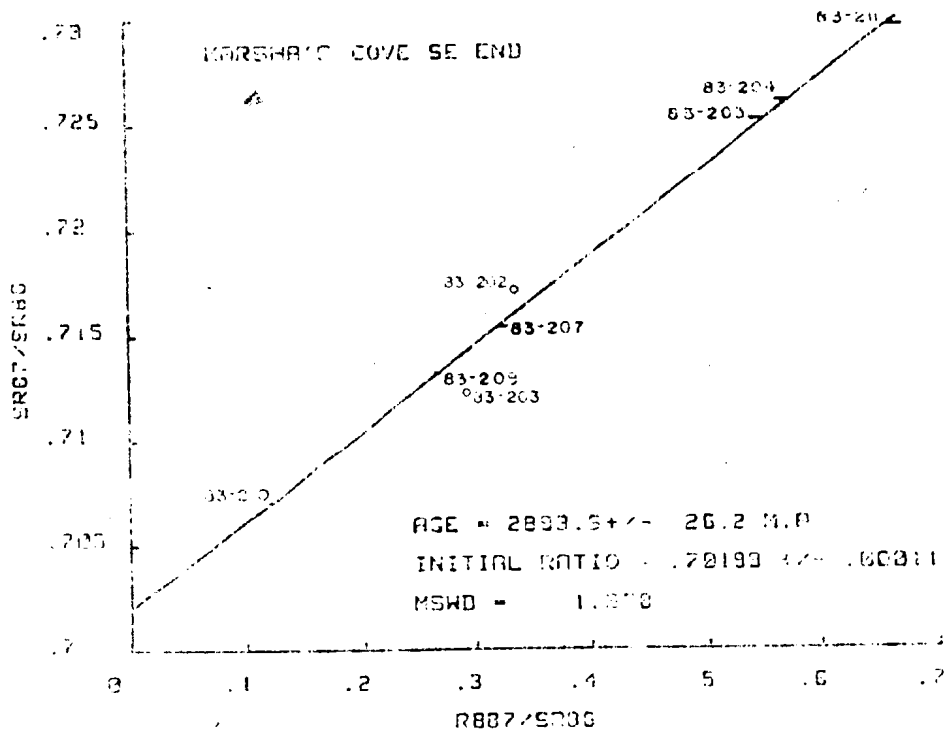
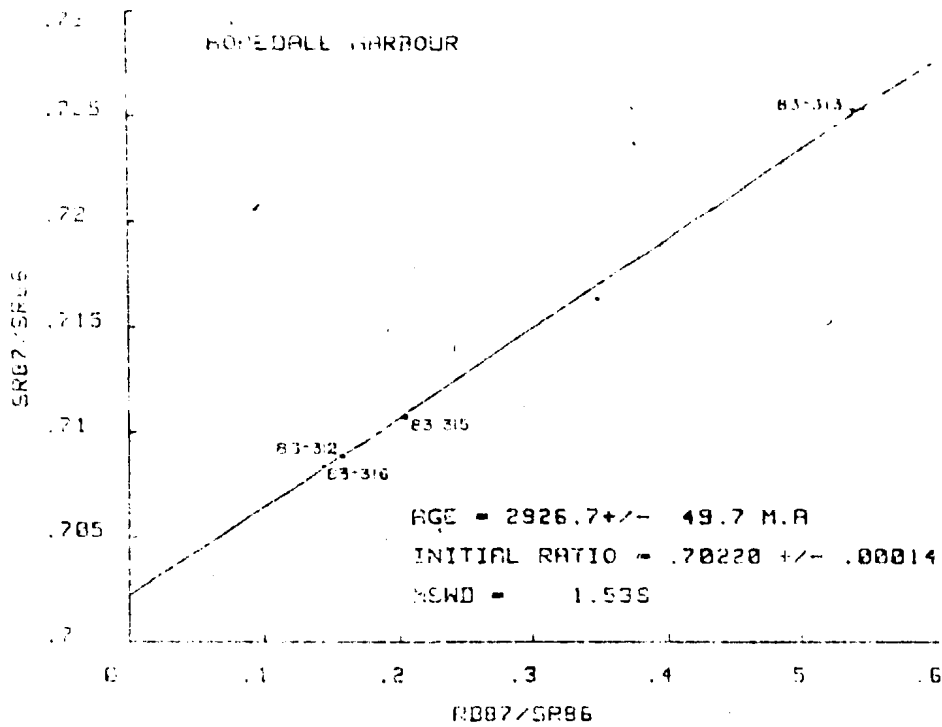
Table 4.3: Rb and Sr contents and isotopic composition of Maggo Gneiss from Hopedale Harbour, Marsha's Cove and Next Bay North.

Errors are 2 to 5 % for Rb, Sr and < 1% for $^{87}\text{Rb}/^{86}\text{Sr}$. The $^{87}\text{Sr}/^{86}\text{Sr}$ ratios are normalized to $^{87}\text{Sr}/^{86}\text{Sr} = 0.1194$ and corresponding errors (1 sigma) are quoted in terms of 10^{-5} . * - sample not used in regression analysis. D - duplicate analysis of $^{87}\text{Sr}/^{86}\text{Sr}$ ratio, carried out on separate aliquots of the same powder.

Sample No.	Rb	Sr	Rb/Sr	$^{87}\text{Rb}/^{86}\text{Sr}$	$^{87}\text{Sr}/^{86}\text{Sr}$	1 sigma
<u>Hopedale Harbour</u>						
83-312	38	703	0.054	0.157	0.708848	5.5
83-313	56	301	0.188	0.544	0.725395	4.1
83-313 D*					0.725458	3.9
83-315	46	650	0.070	0.204	0.710695	6.2
83-316	32	642	0.049	0.143	0.708321	2.1
<u>Marsha's Cove</u>						
83-202*	27	230	0.116	0.335	0.717110	2.6
83-203*	16	160	0.101	0.293	0.712229	4.6
83-204	39	199	0.196	0.569	0.726066	2.7
83-204 D*					0.726359	3.3
83-205	49	260	0.188	0.546	0.725191	3.9
83-207	25	220	0.112	0.325	0.715420	3.5
83-208	45	490	0.092	0.267	0.713175	2.5
83-208 D*					0.713067	2.3
83-210	12	284	0.041	0.119	0.707004	4.0
83-211	42	181	0.230	0.674	0.729634	5.2
83-211 D*					0.729427	8.3
83-214	20	320	0.063	0.181	0.710197	2.3
83-215	50	313	0.159	0.461	0.721394	2.3
83-216	42	253	0.167	0.483	0.723035	4.4
83-217*	42	251	0.166	0.482	0.713643	5.2
83-218*	43	372	0.116	0.337	0.716904	3.2
<u>Next Bay North</u>						
83-269	38	388	0.097	0.271	0.714639	12.3
83-272	33	239	0.138	0.401	0.720943	13.1
83-273	40	251	0.160	0.464	0.723573	6.6
83-274	38	255	0.151	0.437	0.721496	7.8
83-293	48	234	0.206	0.596	0.730449	3.2
83-294	36	349	0.102	0.296	0.716484	5.9

Figure 4.6: Rb/Sr whole rock isochron for four samples of Maggo gneiss from Hopedale Harbour. Isotopic data used to construct the diagram may be found in Table 4.3.

Figure 4.7: Rb/Sr whole rock isochron for six samples of Maggo gneiss from the southeast end of Marsha's Cove. Isotopic data used to construct the diagram may be found in Table 4.3. o - sample not used in regression analysis.



The third locality, SW end, Marsha's Cove provided five samples, four of which have been regressed (Figure 4.8) yielding an age of 2,865 \pm 81 Ma ($Sr_0 = 0.70271 \pm 0.00036$; MSWD = 4.5). The MSWD of 4.5 for this four-point isochron suggests that the error may be as much analytical as geological in origin.

Sample 83-217 was not included in the regression as it clearly crosscuts the remaining gneiss samples in outcrop. This age is within error of that for the SE end of Marsha's Cove, however the initial ratio for the latter suite is higher.

Figure 4.9 presents an errorchron plot for all 12 samples from Marsha's Cove. This composite errorchron yields an age of 2,899 \pm 116 Ma ($Sr_0 = 0.70206 \pm 0.00051$) and an MSWD of 38. This composite plot reflects what is interpreted to be the partial resetting of the isotopic systematics and the variable initial ratios for the Maggo gneiss suites from the enclave, preserved within an area of Flordian reworking (see Section 4.14.2.2).

4.8 Hopedale Gneiss (HG)

The Hopedale Gneiss locality (Plate 10B) represents three distinct lithologic compositions, reflected in the range of $^{87}\text{Rb}/^{86}\text{Sr}$ ratios (Table 4.4). Regression results for the five samples yields a date of 2,884 \pm 86 Ma, $Sr_0 = 0.70271 \pm 0.00028$ and an MSWD of 15.6 (Figure 4.10). The high MSWD implies that the samples are

Figure 4.8: Rb/Sr whole rock Isochron for four samples of Maggo gneiss from the southwest end of Marsha's Cove. Isotopic data used to construct the diagram may be found in Table 4.3. o - sample not used in regression analysis.

Figure 4.9: Rb/Sr whole rock errorchron combining all samples of Maggo gneiss from Marsha's Cove.

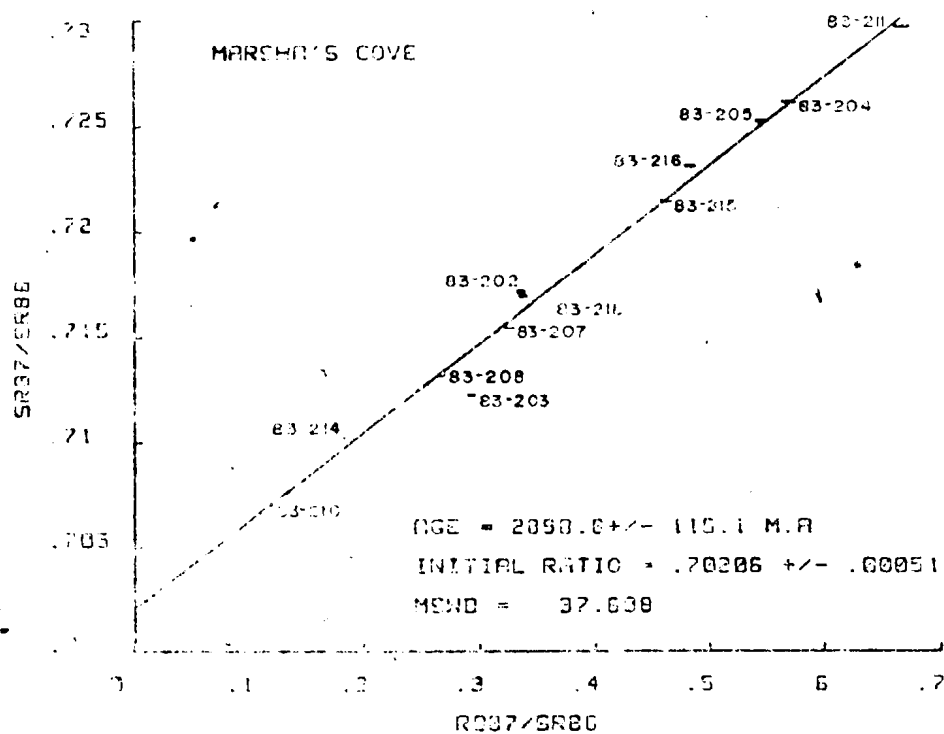
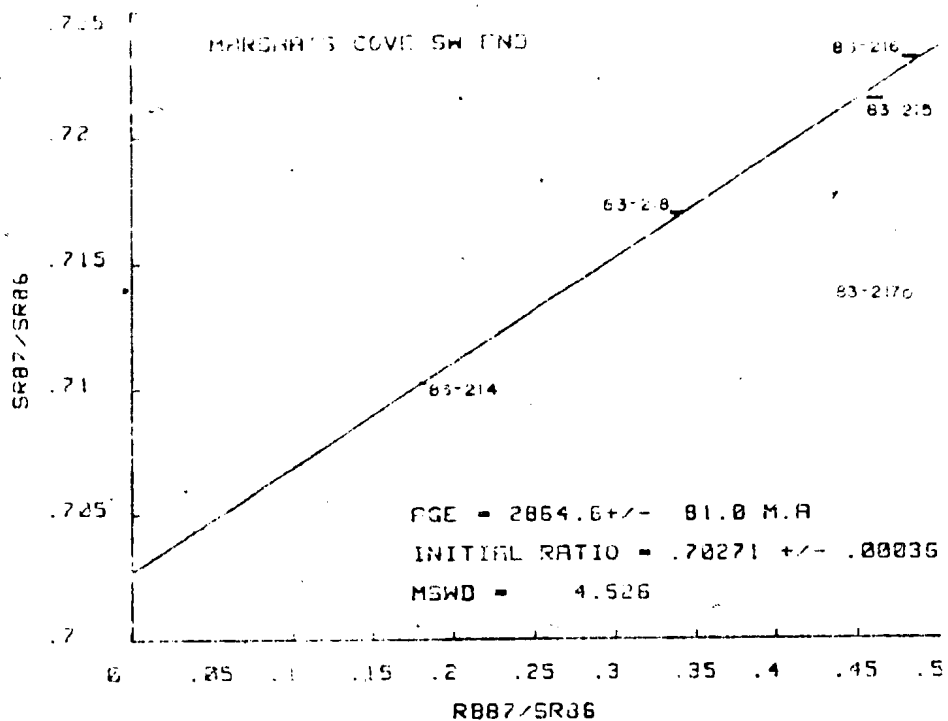


Table 4.4: Rb and Sr Contents and Isotopic Compositions for Maggo Gneiss samples from the Floridian Domain. Errors are 2 to 5 % for Rb, Sr and < 1% for $^{87}\text{Rb}/^{86}\text{Sr}$. The $^{87}\text{Sr}/^{86}\text{Sr}$ ratios are normalized to $^{87}\text{Sr}/^{86}\text{Sr} = 0.1194$ and corresponding errors, at 1 sigma, are quoted in terms of 10^{-5} . * - sample not used in regression analysis, D - duplicate analysis of $^{87}\text{Sr}/^{86}\text{Sr}$ ratio, carried out on separate aliquots of the same powder.

Sample No.	Rb	Sr	Rb/Sr	$^{87}\text{Rb}/^{86}\text{Sr}$	$^{87}\text{Sr}/^{86}\text{Sr}$	1 sigma
<u>Hopedale Gneiss, Black Head Cove</u>						
83-232	16	324	0.0480	0.139	0.708383	2.8
83-233	90	217	0.413	1.201	0.755042	2.3
83-234	95	402	0.236	0.684	0.730246	5.9
83-235	88	379	0.232	0.673	0.730484	28.4
83-237	13	331	0.041	0.117	0.707846	6.0
<u>Black Head Tickle</u>						
83-259	34	374	0.091	0.265	0.714238	3.7
83-261*	40	700	0.057	0.166	0.709498	3.5
83-262*	36	601	0.060	0.175	0.709182	3.0
83-263	15	367	0.041	0.119	0.708277	4.2
83-264	54	373	0.144	0.418	0.720359	4.4
83-265	29	314	0.091	0.264	0.714745	5.8
83-265 D*					0.714821	3.2
83-266	21	453	0.047	0.135	0.708953	6.3
<u>Dead Dog Point</u>						
83-238	50	432	0.115	0.333	0.716484	3.8
83-239*	48	435	0.133	0.386	0.717363	3.4
83-242	33	361	0.092	0.265	0.713330	2.5
83-243	46	367	0.124	0.359	0.717498	2.4
83-244	20	328	0.061	0.178	0.710122	3.2

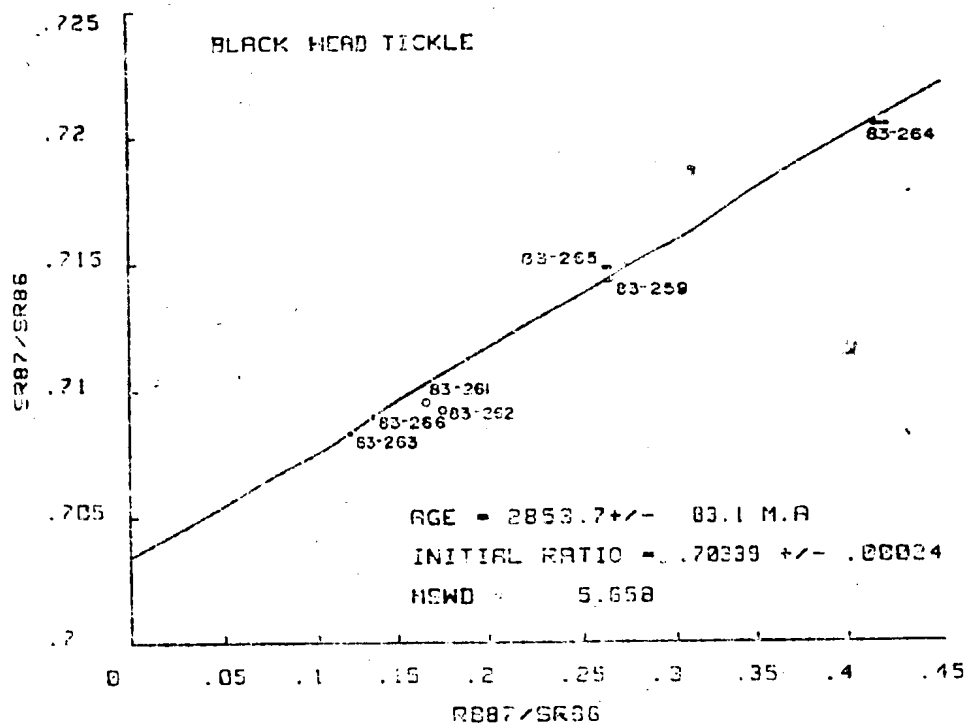
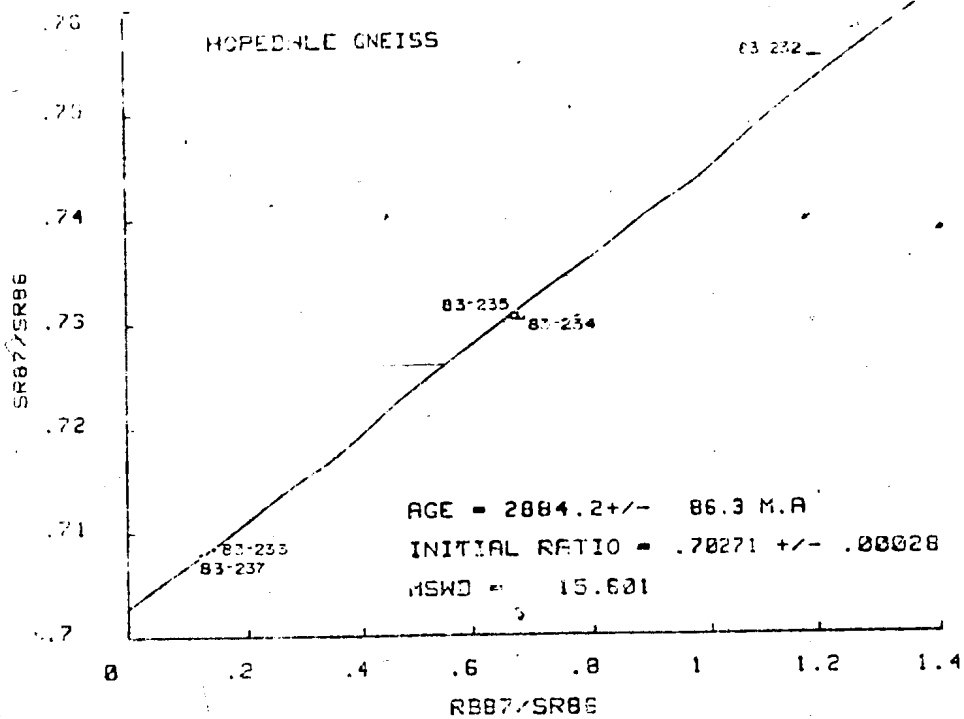
Table 4.4 (continued)

Sample No.	Rb	Sr	Rb/Sr	$\frac{87\text{Rb}}{86\text{Sr}}$	$\frac{87\text{Sr}}{86\text{Sr}}$	1 sigma
<u>Pilliarusik Bay, Flordian Mix Samples</u>						
83-142	36	262	0.136	0.393	0.718443	5.2
83-177*	15	543	0.028	0.082	0.709366	2.2
83-178	47	397	0.120	0.347	0.716539	1.9
83-179	39	450	0.088	0.253	0.712733	4.6
83-184	69	753	0.091	0.264	0.713936	5.4
83-184 D*					0.713933	2.8
<u>Dyke Island (B.J. Fryer analyst)</u>						
DB-81-1A	89	144	0.617	1.798	0.775930	6.4
DB-81-1B	55	199	0.274	0.795	0.735121	6.3
DB-81-1C	53	208	0.256	0.742	0.733403	4.2
DB-81-1D	52	193	0.270	0.782	0.735165	4.9
DB-81-1E	87	255	0.342	0.994	0.742746	5.6
DB-81-1F	63	192	0.326	0.946	0.740644	3.3
DB-81-1G*	54	188	0.287	0.832	0.735400	30.5
DB-81-1H	59	192	0.305	0.886	0.738624	6.4
DB-81-1I*	45	138	0.325	0.943	0.742877	3.4
DB-81-1J	79	176	0.443	1.288	0.764587	5.4

Figure 4.10: Rb/Sr whole rock errorchron for five samples comprising Hopedale Gneiss from northwest of Black Head Tickle. Isotopic data used to construct the diagram may be found in Table 4.4.

Figure 4.11: Rb/Sr whole rock errorchron for five samples of Maggo gneiss from Black Head Tickle. Isotopic data used to construct the diagram may be found in Table 4.4. o - sample not used in regression analysis.

00122



Isotopically inhomogeneous. The inhomogeneity may result from either an originally cogenetic suite having undergone an isotopic disturbance, or the samples do not have a genetic link. The relationships between the samples for this suite, outlined below, would tend to favour the latter possibility coupled with some disturbance attributable to post emplacement effects.

Two samples (83-232, 83-234) represent typical Maggo gneiss (biotite tonalite), samples 83-235 and 83-237 represent migmatitic material discordant to the foliation within the gneiss and one sample (83-233) is a melanocratic variety of gneiss. Sample 83-235 represents a thin, < 4 cm, phlebitic to stromatic migmatite injected lit-par-lit into the gneiss. Sample 83-237 is a nebulitic migmatite emplaced along the contact between the biotite tonalite and the melanocratic gneiss. This suite comes from an area that has been variably affected by Flordian structural overprinting.

4.9 Black Head Tickle (BH)

Seven samples of foliated biotite and hornblende tonalite were collected from the point of land immediately west of Black Head Tickle (Figures 4.1 and A.6). Regressing all samples (Table 4.4) yields a date of 2,874 +/- 251 Ma, $Sr_0 = 0.70298 \pm 0.00070$ and an MSWD of 52. The large error in the age and the high MSWD can be attributed to two samples (83-261, 262) which fall below the line. Sample 83-262 is a sigmoidal, dictyonitic migmatite cutting the foliation in sample 83-261 (Plate 6C). The migmatite was

interpreted to result from Flordian migmatization of Hopedalian gneiss.

Eliminating samples 83-261 and 83-262 from the data set and regressing the five remaining samples yields a date of 2,854 +/- 83 Ma, $Sr_0 = 0.70339 \pm 0.00024$ and an MSWD of 5.7 (Figure 4.11). As expected, the elimination of the two samples significantly lowers the MSWD, but still suggests errorchron behaviour for the suite. The revised age is within error of that obtained for all samples. The major effect of eliminating the discordant samples is to raise the Sr_0 value for the suite.

4.10 Dead Dog Point (DP)

Five samples from Dead Dog Point (See Figure 4.1 for location) have been regressed and yield an errorchron (MSWD = 14.0) age of 2,643 +/- 166 Ma and $Sr_0 = 0.70333 \pm 0.00068$ (Figure 4.12). Elimination of sample 83-239 reduces the MSWD to 3.7, the initial Sr ratio to 0.70282 ± 0.00038 and increases the age to 2,804 +/- 100 Ma. The basis for removing sample 83-239 from the errorchron is questionable. It is similar in mineralogy and field relationships to sample 83-238. The age obtained using all data points is interpreted to reflect partial resetting in response to Proterozoic metamorphism and deformation.

4.11 Pilliarusik Bay (PB)

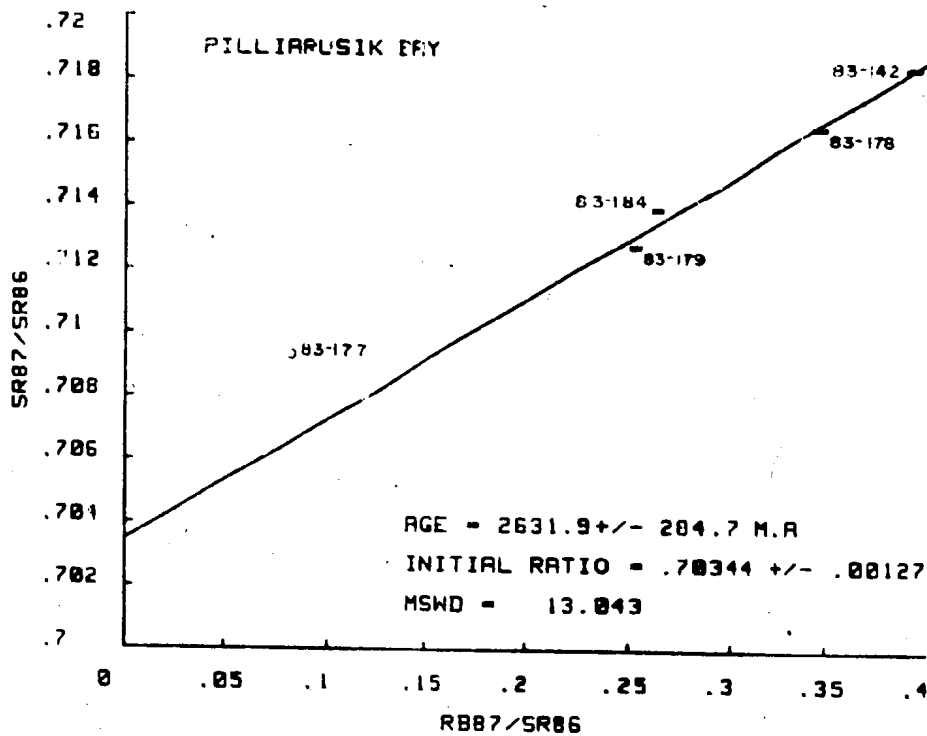
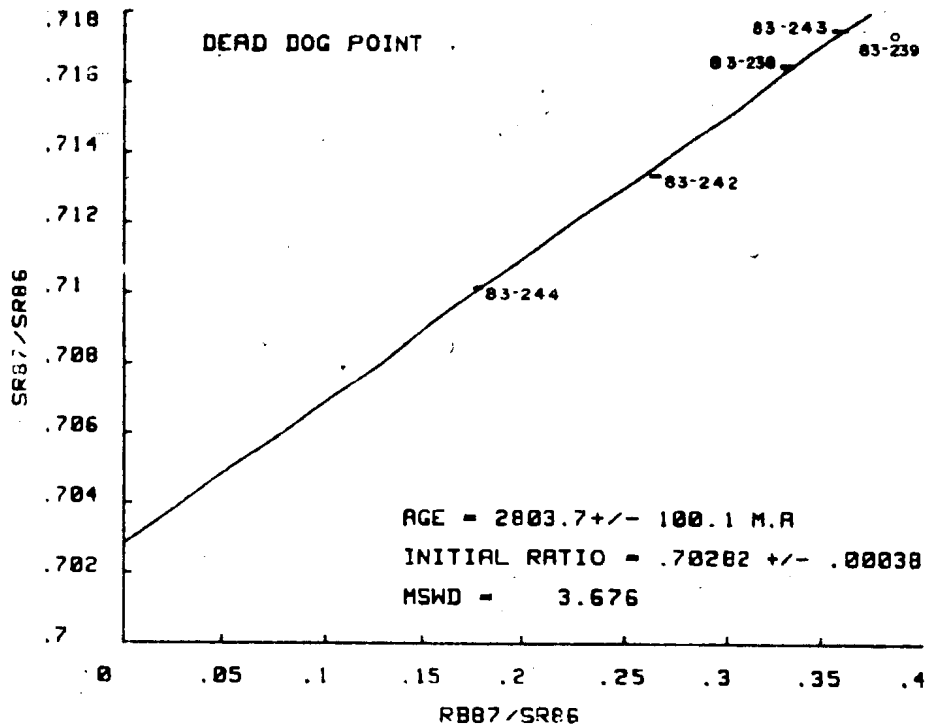
This suite of five samples was collected along the east shore of Pilliarusik Bay, west of Hopedale village (Figure 4.1, Table 4.4). Regressing all samples yields an unlikely

26/80

Figure 4.12: Rb/Sr whole rock errorchron for five samples of migmatized Maggo gneiss from Dead Dog Point. Isotopic data used to construct the diagram may be found in Table 4.4. o - sample not used in regression analysis.

Figure 4.13: Rb/Sr whole rock errorchron for four samples of Maggo gneiss from within the Flordian Domain, Pilliarusik Bay. Isotopic data used to construct the diagram may be found in Table 4.4. o - sample not used in regression analysis.

00126



age of 1,781 \pm 198 Ma, $Sr_0 = 0.70710 \pm 0.00068$ and an MSWD of 88. Removing sample 83-177 and regressing the remaining samples yields an age of 2,632 \pm 285 Ma ($Sr_0 = 0.70344 \pm 0.00127$, MSWD = 13; Figure 4.13).

The elimination of point 83-177 from the regression is supported by field evidence. The sample comes from an area cut by numerous small scale faults which offset the Flordian (S_{n+3}) fabric (Plate 11C). The samples are from the marginal zone of a large enclave of Maggo gneiss which retains Hopedalian mineralogy, but exhibits the progressive effects of Flordian reorientation.

4.12 Dyke Island (DI)

This suite of ten samples, collected by D. Bridgwater and analyzed by B.J. Fryer, is included here for the sake of completeness. The suite was collected, on the basis of field relationships, to yield a Hopedalian age. At the sample site there are no obvious manifestations of Flordian structural overprinting or the development of younger migmatites affecting the gneiss.

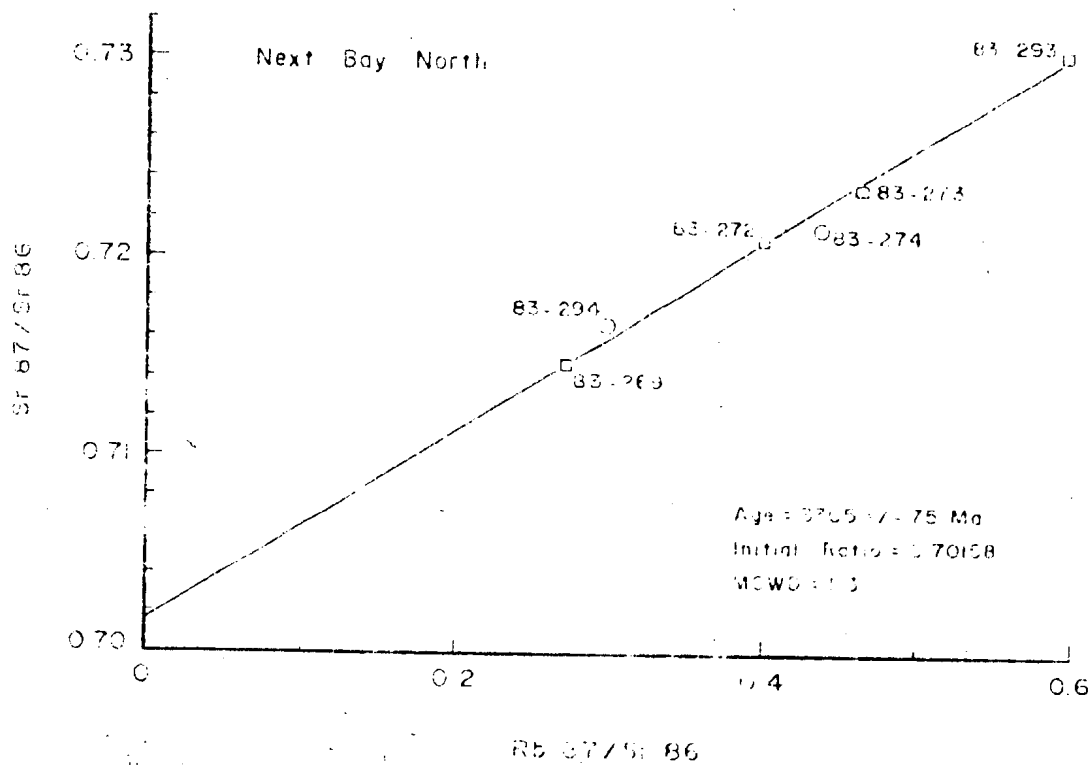
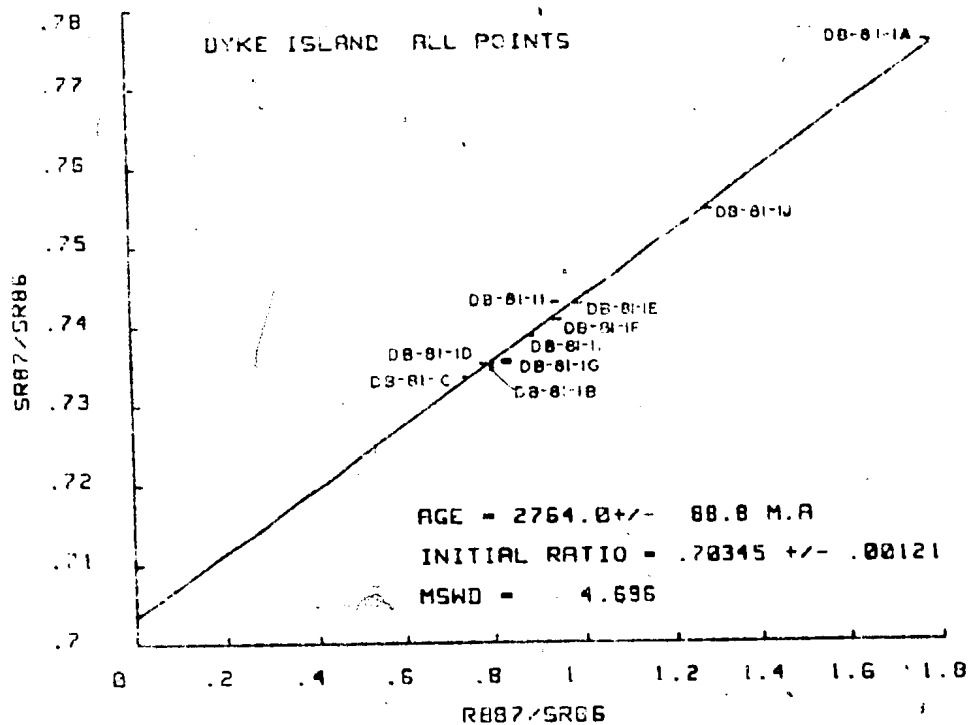
Regressing all samples (Table 4.4.) yields an age, initial ratio and MSWD of 2,764 \pm 89 Ma, 0.70345 \pm 0.00121 and 4.7, respectively (Figure 4.14). This regression includes one sample (DB-81-11) which Bridgwater (1982, pers. comm.) interprets to be a white pegmatite of Hopedalian age. Eliminating this sample lowers the age to 2,750 \pm 62 Ma, within error of that obtained for all samples, ($Sr_0 = 0.70344 \pm 0.00084$) and reduces the MSWD

Figure 4.14: Rb/Sr whole rock errorchron for ten samples of Maggo gneiss from Dyke Island. Isotopic data used to construct the diagram may be found in Table 4.4.

Figure 4.15: Rb/Sr whole rock Isochron for four samples of Maggo gneiss from north of Kangliuasukoluk Tagani (Next Bay North). Isotopic data used to construct the diagram may be found in Table 4.3.

o - sample not used in regression analysis.

00129



to 2.3. Examination of Figure 4.14 shows sample DB-81-1G to be discordant to the line. Eliminating this sample, along with DB-81-11, regression reduces the age to 2,740 +/- 48 Ma ($Sr_0 = 0.70388 \pm 0.00068$) and further reduces the MSWD to 1.4. All three dates and their corresponding initial ratios are within error of each other, the sole effect of deleting the samples being the reduction of the MSWD for the suite. There is no compelling geological evidence for the elimination of either sample.

4.13 Next Bay North (NBN)

The six samples analyzed (Table 4.3) in this suite come from three localities along the mainland shore north of Kangliuasukoluk Tagani (See Figure 4.1). Regressing all samples yields a date of 3,133 +/- 170 Ma, $Sr_0 = 0.70259 \pm 0.00097$ and an MSWD = 10. Two samples which lie off the regression line can be eliminated from the suite on the basis of their field and microscopic characteristics. Sample 83-274 is a mafic-rich layer, within the gneiss, which in the field was thought to represent a leucocratic phase of the Weekes association. Removal of Sample 83-294 is justified due to the following criteria when considered with respect to the remaining samples in the suite:

- 1) the leucocratic nature of this sample,
- 2) the presence of interstitial alkali feldspar, which is very minor to lacking in the other samples, and
- 3) the recrystallized nature of the sample.

In some respects this sample resembles what has been

Interpreted to represent a recrystallized pegmatite, at Manuel Island (Sample 83-305), which preserves evidence of a Pre-Hopedalian fabric.

Elimination of these two analyses and regressing the remaining four data points yields an age of $3,305 \pm 75$ Ma and an Sr_0 value of 0.70157 (Figure 4.15). The resulting MSWD for this regression is lowered to 1.3, indicating isochron behaviour for this suite.

4.14 Discussion

In high grade, polydeformed gneiss terrains, Rb-Sr whole rock isochrons are interpreted to either represent the "age" of the gneiss complex or reflect the timing of regional metamorphic events (Moorbath, 1975a). The latter interpretation implies large scale, regional homogenization of Sr isotopes at the isochron date. For the former, whole rock Rb-Sr isotopic systematics observed in grey gneiss complexes result from retention of the original isotopic systematics, even if the complex has undergone a later intense (to upper amphibolite facies) metamorphism. The preservation of the isotopic systematics is taken to indicate isochemical behaviour, on the whole rock scale, of Rb and Sr (Moorbath, 1975a). Evidence for later metamorphism can be detected using mineral dates. The Amitsoq gneiss of southwest Greenland preserves a whole rock Rb-Sr age of 3,700 Ma, even though the area subsequently underwent an amphibolite facies metamorphism and accompanying deformation at 2,800 Ma (Moorbath, 1975a).

Geochronological results for Maggo gneiss suites are subdivided into those interpreted to date the older, Hopedalian event and the younger, Flordian event. The ages obtained for Maggo gneiss suites, representing the Hopedalian and Flordian domains, will be discussed in terms of their significance to the development of Hopedale Block crust. The ages and initial $^{87}\text{Sr}/^{86}\text{Sr}$ ratios quoted are found in Table 4.1.

4.14.1 Hopedalian Suites

The MI, PP, HI and SEDI suites, all located N and E of Hopedale (see Figure 4.1), exhibit well developed NW-SE planar and SE plunging linear elements, characteristic of the Hopedalian (S_{n+2}) fabric as defined by Ermanovics et al. (1982) and Korstgard and Ermanovics (1984, 1985). Hopedale dykes, boundinaged and concordant to the S_{n+2} fabric in the gneiss, are characterized by the assemblages hbl-pl-cpx and hbl-pl, indicative of Hopedalian metamorphism, at these localities. The presence of the S_{n+2} fabric, concordant Hopedale dykes and preserved middle to upper amphibolite facies assemblages are taken to indicate that these suites equilibrated during the Hopedalian (D_{n+2}) event.

Ages obtained for these suites fall between 3,140 and 3,025 Ma. The ages, all within error of each other, are interpreted to date the timing of the Hopedalian deformational event (D_{n+2}) within the study area.

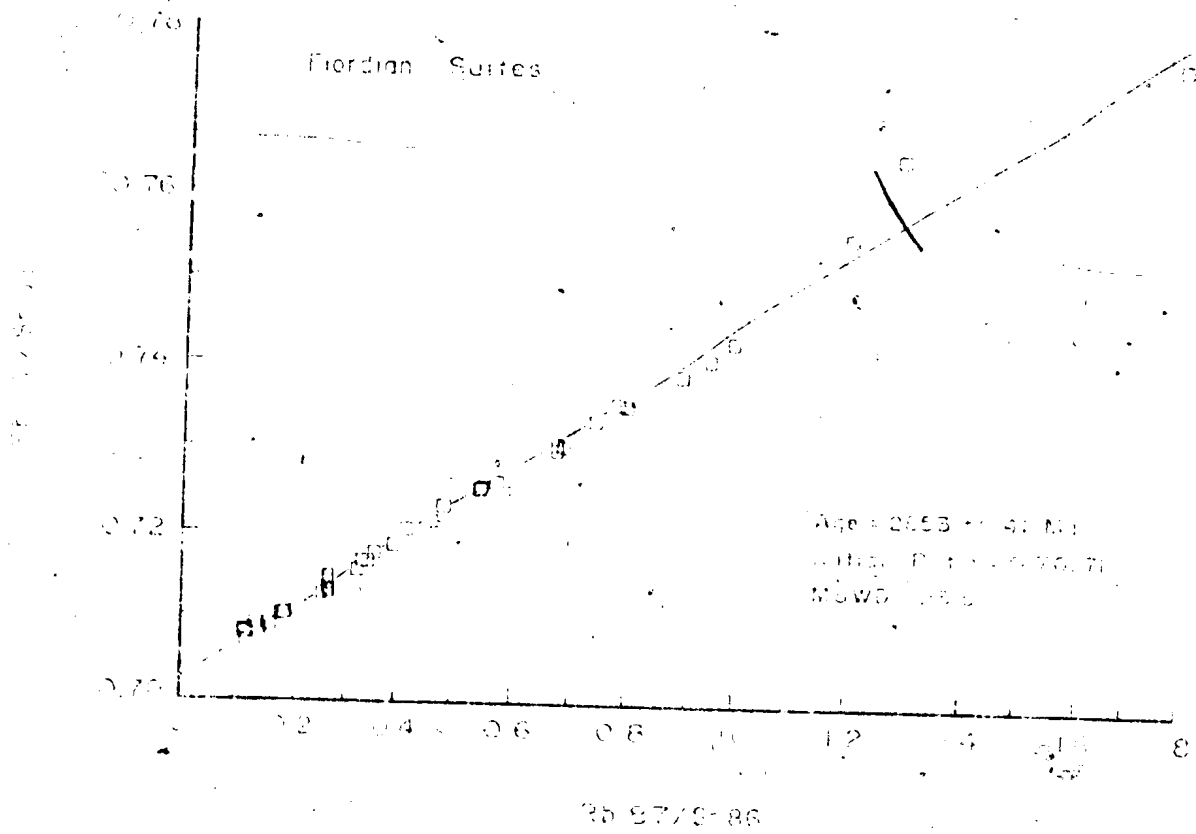
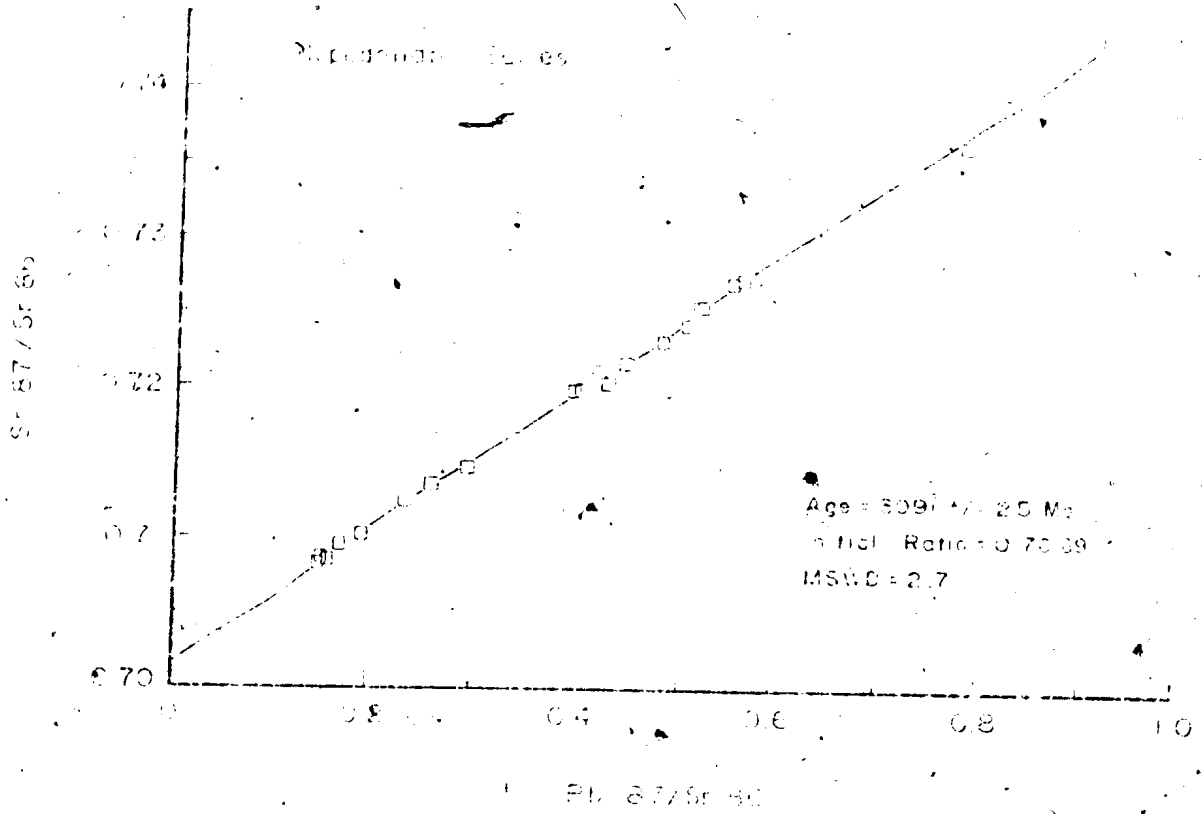
Pooling all the data for the 24 samples from the four Hopedalian suites and regressing them together yields a date of $3,091 \pm 25$ Ma and a $Sr_0 = 0.70169 \pm 0.00015$. (Figure 4.16). The low MSWD value (2.7) for this regression is interpreted to signify that the whole rock isotopic systematics equilibrated with their surroundings in response to the Hopedalian event, and have remained unaffected by later events.

Grant et al. (1983) report Rb-Sr whole rock ages for Maggo gneiss of 3,027 Ma for their Kanariktok Bay suite (KG), from south of the present study area, and 3,011 Ma for the Uivak Point suite (UP), situated within the study area. An unpublished, minimum U-Pb zircon age of 3,150 Ma (Ermanovics, pers. comm., 1986) has been obtained for the Uivak Point suite. These two suites are characterized by a well developed Hopedalian fabric (Grant et al., 1983). The resulting isotopic ages for the suites are indistinguishable from the pooled age for all Hopedalian samples from this study.

Isotopic results, from this study in conjunction with published data, for the Hopedalian suites indicate that the Hopedale Block was stabilized as a craton at 3,090 Ma. The stabilization of the crust, at least with respect to Rb and Sr, two highly mobile elements, at this time provides the starting point to begin examining the effects of Flordian reworking on the Maggo gneiss.

Figure 4.16: Rb/Sr whole rock isochron for pooled data from the MI, PP, HI and SEDI suites. Isotopic data used to construct the diagram can be found in Table 4.2

Figure 4.17: Rb/Sr whole rock errorchron for 39 samples from all Floridian Suites. Isotopic data used to construct the diagram may be found in Table 4.3 and 4.4



4.14.2 Flordian Suites

4.14.2.1 Introduction

The Flordian domain has been defined (Korstgard and Ermanovics, 1984) on the basis of the following structural and metamorphic characteristics:

- 1) prominent NE-SW trending, SE dipping planar fabrics,
- 2) moderate NE plunging linear elements,
- 3) lower to middle amphibolite facies mineral assemblages in metabasic lithologies.

The above characteristics result from the reorientation and retrogression of Hopedalian domain lithologies in response to the Flordian reworking (Sections 2.4 and 3.2.6).

Published field and geochronological results may be used to broadly fix the timing of the Flordian deformation. The Kanaiříktok intrusions of dioritic to granodioritic composition are interpreted by Ermanovics et al. (1982) and Korstgard and Ermanovics (1984) to have been emplaced into the Hopedale Block prior to, or in part synchronous with, the Flordian deformation and metamorphism. Grant et al. (1983) have examined the Rb-Sr isotopic systematics of three suites of Kanaiříktok intrusives. Two of these suites, KT and K suites (abbreviations are from Grant et al., 1983) yield ages of 2,832 Ma ($Sr_{87} = 0.7017$) and 2,763 Ma ($Sr_{87} = 0.7030$), respectively. The third suite (BT) yields an age of 2,453 Ma ($Sr_{87} = 0.7043$) which Grant et al. (1983) interpret to result from partial metamorphic resetting during the Proterozoic. A U-Pb zircon

concordia age of 2,830 Ma (Ermanovics et al., 1982) is in agreement with the Rb-Sr whole rock ages for the emplacement of the Kanariktok Intrusives and, based on established field relationships, the timing of the Flordian deformation.

The ages obtained for the remaining eight suites of Maggo gneiss, examined in this study are discussed in terms of the observed structural fabric exhibited at each locality and the resulting whole rock age. Suites which exhibit similar field relationships and ages are considered under the following headings:

- 1) Flordian fabric and Flordian age,
- 2) Hopedallian fabric and Flordian age, and
- 3) Flordian fabric and Hopedallian age.

4.14.2.2 Flordian Fabric and Flordian Age

Three suites (MC, DP, and PB), examined in this study, are from a clearly recognizable augen of Flordian reoriented Maggo gneiss exposed along the east shore of Pilliarusik Bay. (Figure 4.1). All suites yield Flordian ages (Table 4.1) similar to those reported by Ermanovics et al. (1982) and Grant et al. (1983).

MC suite samples were collected from the core of the augen, which on the outcrop scale resembles Hopedallian domain Maggo gneiss, but exhibits a Flordian fabric. The Hopedallian appearance is lacking, away from the augen core, where the gneiss is strongly reoriented in NNE-SSW direction. On a microscopic scale, Hopedallian mineral

assemblages within the Hopedale dykes can clearly be seen to be retrogressed to lower amphibolite facies assemblages in response to Flordian metamorphism (Plate 8E).

The composite plot for all 12 samples from Marsha's Cove (Figure 4.9) reflects the partial resetting of the Hopedalian isotopic systematics of the Maggo gneiss enclave preserved within an area of Flordian reworking. The lower initial Sr_0 ratio (0.70206) in contrast with those for other Flordian suites, both published (Grant *et al.*, 1983) and presented in this study, may reflect the partial resetting. There exists the possibility that there is a component of radiogenic Sr, derived from the syn-Flordian Kanariktok intrusives, mixed with Hopedalian Sr still present within the MC suite samples. The link between the MC suite, other Flordian suites and the Hopedalian suites is further discussed in Section 6.4, dealing with the Sr evolution of the Hopedale Block.

The DP suite yields a four point isochron age of 2,804 +/- 100 Ma for Maggo gneiss displaying a well developed Flordian fabric (S_{n+3}). In the field the S_{n+3} fabric can be shown to result from reorientation of the earlier S_{n+2} (Hopedalian) fabric (Plate 11C and D). This age, although younger than previously reported Flordian ages (Grant *et al.*, 1983), is interpreted to represent the final stages of the Flordian isotopic resetting at this locality.

The age recorded for the PB suite (2,632 +/- 285 Ma, $Sr_0 = 0.70344$, MSWD = 13) is interpreted to represent

the partial resetting of the isotopic systematics within this suite in response to Proterozoic activity.

Along the length of Pilliarusik Bay, where the samples for this suite were collected, evidence exists for movement along faults associated with the Proterozoic activity (see Section 2.4.8). This brittle deformation results in a minimum displacement of 2.5 km, based on the offset of Kikker-tavak dykes on opposite sides of the bay. Grant *et al.* (1980) suggest that an age of 2,453 Ma for a suite of the Kanariktok Intrusions from Ugjuktok Bay (their BT suite) reflects the partial resetting of the Rb-Sr systematics in response to Proterozoic metamorphic activity.

4.14.2.3 Hopedallian Fabric and Flordian Age

Based on field relationships the HH, HG, BH and DI suites were collected with the view that they would give a Hopedallian or possibly older age. Only the BH suite exhibits any visible evidence of reorientation in response to the Flordian event (Plate 6C). All of these suites yield whole rock ages which date the Flordian event, as defined above.

The HH suite samples an area of Maggo gneiss which displays evidence of a Pre-Hopedallian fabric (Plate 5B). The age for this suite, $2,927 \pm 50$ Ma (Figure 4.6), is within error of the age obtained for all samples from Marsna's Cove (Figure 4.9), placing it within the time frame of the Flordian event. The HH data points exhibit the best fit line (MSWD = 1.5) of all the suites in this

group, indicating that the Rb-Sr systematics of this suite underwent a major resetting and complete homogenization at 2,930 Ma. Even though this suite lacks visible Flordian deformational features, the recorded age may be interpreted to reflect the incipient chemical effects of the Flordian reworking on the isotopic systematics of the Maggo gneiss.

The HG and BH suites yield ages of 2,884 \pm 86 Ma and 2,854 \pm 83 Ma, respectively, indistinguishable from that obtained for the MC suite and previously reported Flordian ages (Grant et al., 1983). The high MSWD values for these suites (HG = 15.6, BH = 5.7) reflect the incomplete resetting of the isotopic systematics in response to the Flordian event at these localities.

The DI suite, displays a Hopedalian fabric and records a Flordian age which is indistinguishable from the other Flordian suites. The data for this suite, when regressed, yield an errorchron (MSWD = 4.7) again suggesting the inhomogeneous behaviour of Rb and Sr in response to the Flordian reworking.

The geologic setting and the geochronological results for this locality are incompatible. In terms of the geologic setting the Hopedale dykes at Dyke Island exhibit well developed relict plagioclase accumulations (see Figure 21.4a in Ermanovics et al., 1982) and retain a Hopedalian mineral assemblage (hbl-pl-cpx) with no evidence for Flordian retrogression. The Maggo gneiss at Dyke Island is characterized by the assemblage pl-qtz-biotite-hbl which

has a fresh appearance in thin section and does not exhibit any indications of having been retrogressed.

The D1 suite on a macro- and microscopic scale resembles Hopedalian domain Maggo gneiss, however the resetting of the isotopic systematics during the Flordian did not affect the appearance of the gneiss and associated lithologies, i.e. Hopedale dykes. The actual means or mechanism for the resetting of the isotopic systematics without disturbing the petrographic characteristics of the suite remains an enigma. This suggests that the Flordian resetting does not need to be defined by a structural change, indicating that this event could be dominantly thermal in nature and in effect be more complicated than previously thought.

The values in Table 4.3 and 4.4, used to determine the age for each of the Flordian suites, when pooled and regressed yield an errorchron (MSWD = 7.8) age of 2,835 +/- 26 Ma and an Sr_0 ratio of 0.70257 (Figure 4.17). This age and initial ratio are indistinguishable from those values for Flordian domain Maggo gneiss and Kanairiktok Intrusives reported by Ermanovics et al. (1982) and Grant et al. (1983).

Eliminating the five most discordant analyses from the composite plot and regressing the remaining analyses yields a date of 2,832 +/- 16 Ma ($Sr_0 = 0.70267$) and lowers the MSWD to 7.7. This age is within error of that obtained for all analyses (Figure 4.17). The removal of the discordant

analyses, based on their contribution to the MSWD, lowers the MSWD, however, the data still exhibit errorchron behaviour, suggesting that geological rather than analytical scatter is responsible for the high MSWD. Further removal of discordant points, up to 30 % of the total analyses, results in a lowering of the MSWD to 3.5 with no change in the age or Sr_0 value for the pooled data set.

The errorchron behaviour for the pooled data set, regardless of the number of discordant points removed, is to be expected as each individual suite exhibits only partial homogenization of the Rb-Sr systematics in response to the Flordian reworking.

The fact that five of six Flordian suites yield errorchrons, in the sense of Brooks et al. (1968), attests to the pervasive, incomplete resetting affects of the Flordian event on the Maggo gneiss. The ages of these five suites (MC, HG, BH, DP, DI) cluster between 2,899 and 2,794 Ma and are inferred to represent the re-equilibration of the gneiss in response to the Flordian reworking. Of these suites only PB and DP exhibit a well developed Flordian, S_{n+3} fabric.

4.14.2.4 Flordian Fabric and Hopedalian Age

The NBN suite records an age of 3,305 \pm 75 Ma, the oldest age reported for the Maggo gneiss within the Hopedale Block. This age is older than the pooled age for all Hopedalian suites (see Section 4.14.1) despite

possessing a Flordian fabric characterized by distorted NW-SE fabric (S_{n+2}) which is reoriented into a NE-SW (S_{n+3}), Flordian, direction. The gneiss also displays a mineral lineation which gently plunges to the NE, again characteristic of Flordian deformation (Korstgard and Ermanovics, 1985).

The relationship of this age with the preserved Flordian fabric is similar to that reported for the BR suite of Grant et al. (1983). Their BR suite records the oldest age (3.226 Ma) of all suites analyzed by these workers and like the NBN suite displays a Flordian fabric. The significance of the NBN age to the development of the Hopedale Block is that it dates the timing of an "isotopic event" older than the Hopedalian.

Unpublished U-Pb zircon ion probe ages (Schlotte via Ermanovics, pers. comm. 1988), for grains separated from a pelite collected at the same locality as the NBN suite, fall in the range 3,288 to 3,260 Ma. These ages imply the presence of "older" source material from which the pelite were derived. The most likely source would be the gneisses in the local area rather than deriving the zircons from further afield, i.e. northern Labrador or west Greenland.

4.15 Areal Isochrons

4.15.1 Introduction

Traditionally plots of $^{87}\text{Sr}/^{86}\text{Sr}$ vs. $^{87}\text{Rb}/^{86}\text{Sr}$ are used to present mineral and/or whole rock isochron data. Mineral isochrons yield ages which correspond to the

time the Rb/Sr isotopic systematics for cogenetic minerals closed. Whole rock isochrons for metamorphic rocks are interpreted to date either the time of metamorphism or anatexis. In either case the age records the time when the whole rock Rb/Sr systematics closed, although Rb and Sr exchange between minerals in a given sample may still occur (Koehler and Mueller-Sohnius, 1980). In terms of scale, mineral isochrons reflect systematics on the mm to cm scale, while whole rock isochrons generally deal with samples collected over dm to m intervals.

Koehler and Mueller-Sohnius (1980) enlarge the scale of Rb-Sr geochronology sampling by an order of magnitude or more in considering regions 100's of m to several km in diameter, with individual regions separated by distances in excess of 10 km. This larger sample size is termed an 'areal' by these authors. An areal must consist of cogenetic samples and at some point in the past the areal must have existed as a closed Rb-Sr system. Within the region defined by the areal, Rb and Sr transport between individual whole rock samples is permitted (Koehler and Mueller-Sohnius, 1980).

To demonstrate the principle of areals the following example, considered by Koehler and Mueller-Sohnius (1980) is presented. These authors examined the Rb-Sr data for a cogenetic paragneiss-anatexite body from the Bohemian Massif of East Bavaria. The paragneiss sequence, derived from greywackes and minor amphibolites, collected from five

distinct outcrop regions that were interpreted to have undergone similar geological histories: sedimentation, regional metamorphism, anatexis and regional cooling. Mineral isochrons yielded cooling ages of 310 to 315 Ma, while whole rock isochrons gave ages of the anatexis event ranging from 420 to 470 Ma (Koehler and Mueller-Sohnius, 1980).

The existence of whole rock isochrons from the five regions examined was interpreted by these authors to indicate total Sr isotope exchange between whole rock samples within each region. Distinctive initial Sr_0 ratios, ranging from 0.709 to 0.711, for the whole rock isochrons, were interpreted to suggest that Sr exchange did not occur between the widely separated regions (Koehler and Mueller-Sohnius, 1980). The lack of Sr exchange was interpreted to indicate that each region existed as a separate and closed system during anatexis. Taking the above considerations into account Koehler and Mueller-Sohnius (1980) considered each region to represent an areal.

The mean $^{87}Sr/^{86}Sr$ and $^{87}Rb/^{86}Sr$ values for each whole rock suite provide the respective 'X-Y' coordinates for each areal, such that when plotted on a conventional $^{87}Sr/^{86}Sr$ vs. $^{87}Rb/^{86}Sr$ diagram and regressed yield a straight line. In the case of the East Bavarian samples the resulting line corresponds to an age of 544 Ma and an initial $Sr_0 = 0.7048$ (Koehler and

Mueller-Sohnius, 1980). Can this straight line be regarded as an isochron and if so, how can the resulting age be interpreted?

Since all samples used to define the areals were subjected to the same geological events, Koehler and Mueller-Sohnius (1980) suggested that the linear array defined by the areal points was meaningful and interpreted the straight line as an isochron and term it an 'areal isochron'. In interpreting the significance of the resultant areal age Koehler and Mueller-Sohnius (1980) postulated that a pre-anatectic event which caused a uniform mean $^{87}\text{Sr}/^{86}\text{Sr}$ ratio for the areals. They were uncertain of the nature of the pre-anatectic event, but suggested that it could be related to either the original sedimentation or the subsequent regional metamorphism.

Application of the principal of areals and areal isochrons to the Maggo gneiss suites analyzed in this study can be justified on the following grounds: 1) all the suites represent various compositional phases of the Maggo gneiss; 2) based on regional and local chronology, each Hopedalian and Flordian suite can be shown to have undergone a comparable sequence of deformational and metamorphic development; and 3) the initial Sr ratios for each areal are comparable. The latter argument requires that exchange of Sr has not occurred between the areals at the time recorded for the Hopedalian and Flordian events. The homogenization giving rise to the similar initial Sr

ratios for the suites occurred at some point in time prior to the recorded tectonothermal events. The initial Sr_0 ratios for the Hopedalian and Flordian suites range from 0.7013 to 0.7019 and 0.7021 to 0.7035, respectively. The range of Sr_0 ratios for each geochronologically similar group of suites suggests that each group closed to further exchange and homogenization of Sr at the same time in their past.

The concept of areals and areal isochrons have previously been applied to Archaean lithologies (Marzano, 1981), Grenvillian gneisses (Mose, 1982) and Paleozoic granites (Haack *et al.*, 1982; Wilton, 1984).

Areal data for the Maggo gneiss suites examined in this study (Table 4.5) and the resulting areal isochrons for the Hopedalian and Flordian domains are discussed in the following sections.

4.15.2 Hopedalian Areal

The mean $^{87}Rb/^{86}Sr$ and $^{87}Sr/^{86}Sr$ ratios (Table 4.5) for the MI, HI, PP and SEDI suites of Maggo gneiss are used to derive the Hopedalian areal isochron. The age (3,059 +/- 83 Ma) and initial ratio ($Sr_0 = 0.70182$) resulting from the regression of these four areals is indistinguishable from the pooled age for all Hopedalian samples (see Section 4.14.1).

The areal concept requires that all samples used in determining the areal isochron closed to Sr exchange in response to the same event in their past (Koehler and

Table 4.5: Averaged Isochron data and respective errors (Δ), calculated using the method of Koehler and Mueller-Sohnlus (1980), used to construct the Areal Isochrons.

Suite	$^{87}\text{Rb}/^{86}\text{Sr}$	Δ	$^{87}\text{Sr}/^{86}\text{Sr}$	Δ
<u>HOPEDALIAN</u>				
Manuel Island	.349	0.023	0.716933	0.0008
Porphyroblastic Phase	.623	0.013	0.730563	0.0019
Hypothesis Island	.480	0.013	0.722872	0.0008
SE Double Island	.174	0.005	0.709584	0.00005
Next Bay North	.393	-----*	0.721264	-----
<u>FIORDIAN</u>				
Hopedale Harbour	.252	0.015	0.715743	0.0007
Marsha's Cove	.380	0.136	0.718741	0.0008
Hopedale Gneiss	.531	0.123	0.726400	0.0036
Black Head Tickle	.213	0.036	0.712509	0.0016
Dead Dog Point	.297	0.009	0.714959	0.0013
Pilliarusik Bay	.292	0.001	0.715097	0.0024
Dyke Island	.980	0.052	0.744450	0.0028

* - No errors were calculated for the NBN suite as the gradient angle of the areal isochron is required (see Koehler and Mueller-Sohnlus, 1980). This suite was not used in the areal treatment.

Mueller-Sohnius, 1980). The exchange of Sr at this time results in a homogenization of Sr ratios producing equivalent Sr_0 ratios for each suite defining the areal. The results for the Hopedalian areal suites imply that this was not the case. The SEDI suite is enriched in Sr with respect to other Hopedalian suites (450 ppm versus 355 ppm, respectively; Figure 6.1b). Additionally the SEDI suite exhibits a depletion in Rb compared to the other Hopedalian suites (27 ppm versus 55 ppm, respectively), and the corresponding Rb/Sr ratio (0.06) for the SEDI suite is the lowest recorded ratio for all suites analyzed in this study. Based on these differences, compared with the remaining Hopedalian suites, the removal of the SEDI suite from the areal isochron calculation is justified.

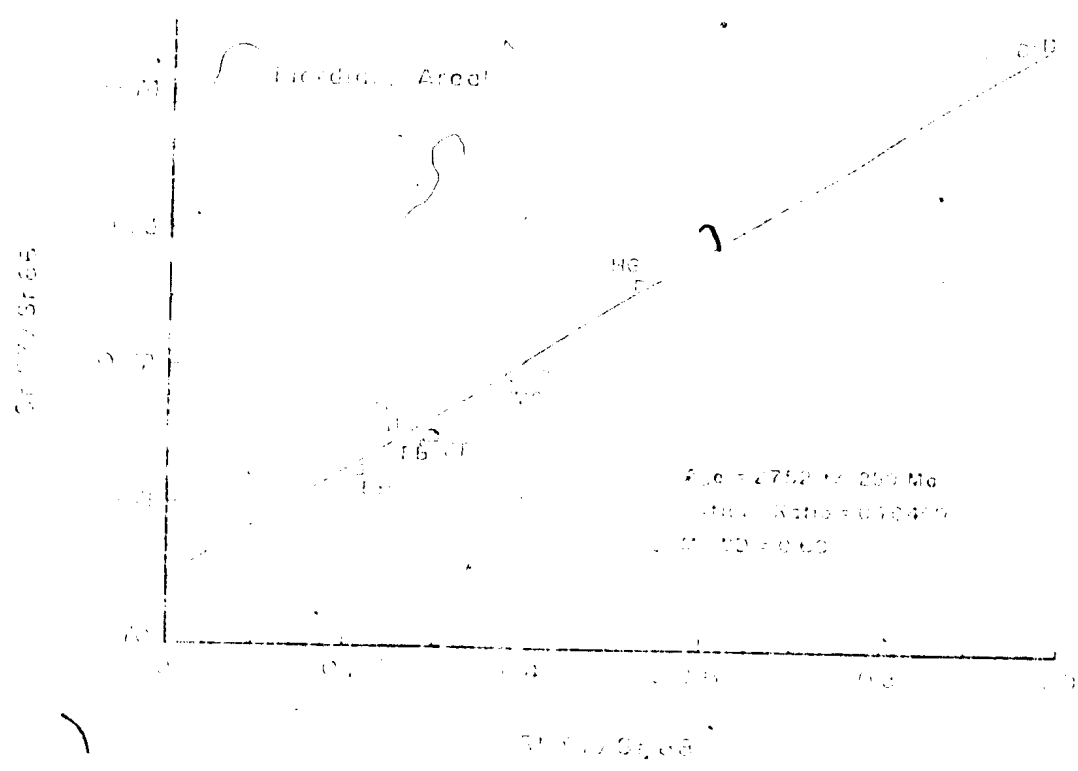
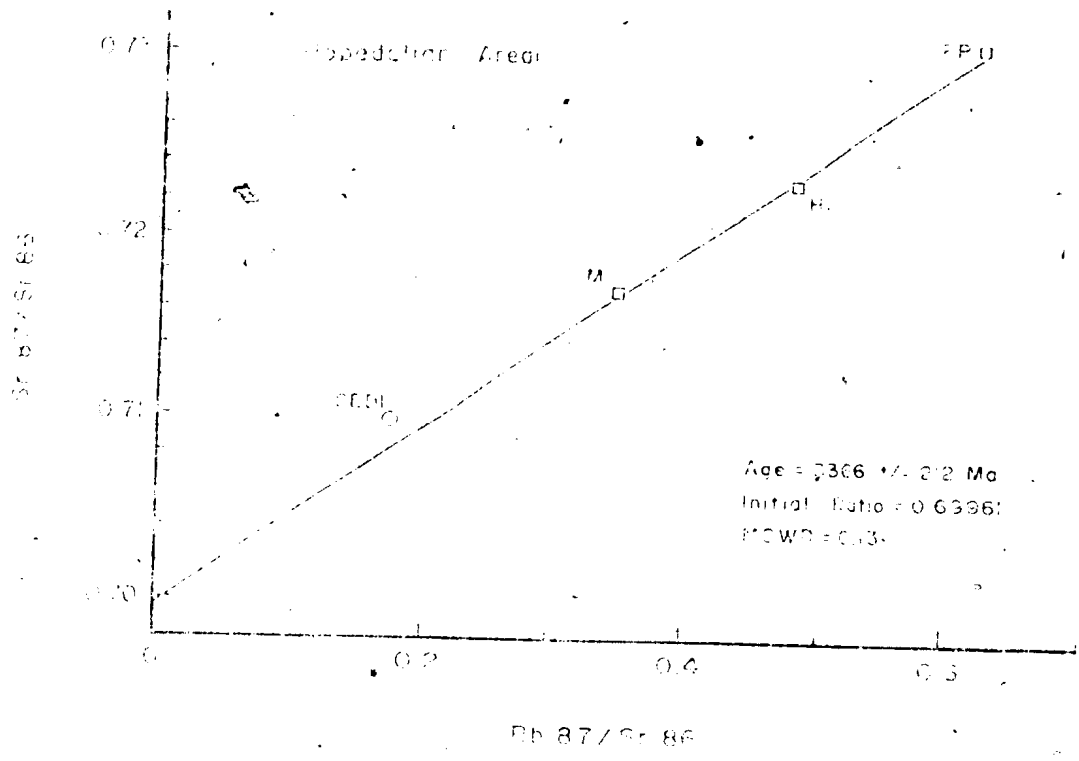
Regressing the remaining 3 Hopedalian areal suites (Figure 4.18) yields an age of $3,366 \pm 212$ Ma with a corresponding Sr_0 ratio of 0.6996 and an MSWD of 0.13. This age is interpreted as the best age for the Hopedalian areal. Observations which support this being the Hopedalian areal age are:

- 1) The similarity of this age to that for the NBN suite (Section 4.13). The NBN suite was collected over a much wider area than most conventional Rb-Sr geochronology suites and as such it may represent an areal isochron in itself.
- 2) Inclusion of the mean $^{87}\text{Rb}/^{86}\text{Sr}$ and $^{87}\text{Sr}/^{86}\text{Sr}$ ratios for the Ulvak Point suite of Grant

Figure 4.18: Areal Isochron for Hopedalian Suites. Isotopic data used to construct the diagram, based on mean Rb, Sr and $^{87}\text{SR}/^{86}\text{SR}$ values for each suite, may be found in Table 4.5. MI - Manuel Island, PP - Porphyroblastic Phase, HI - Hypothesis Island, SEDI - Southeast Double Island. o - areal not used in regression analysis.

Figure 4.19: Areal Isochron for Flordian suites. Isotopic data used to construct the diagram may be found in Table 4.5. MC - Marsha's Cove, HH - Hopedale Harbour, BH - Black Head tickle, DP - Dead Dog Point, PB - Pilliarusik Bay, HG - Hopedale Gneiss, DI - Dyke Island.

00151



et al. (1983; data from Marzano, 1981) with the areal data for the Hopedalian suites of this study (MI, HI, PP) yields a comparable age (3,288 +/- 234) initial Sr_0 (0.69983) and MSWD (0.18).

3) The agreement between the areal isochron age and the ion probe U-Pb zircon age (Schlotte, unpublished data) suggesting that "old" crust was being eroded in the Hopedale Block prior to the Hopedalian event.

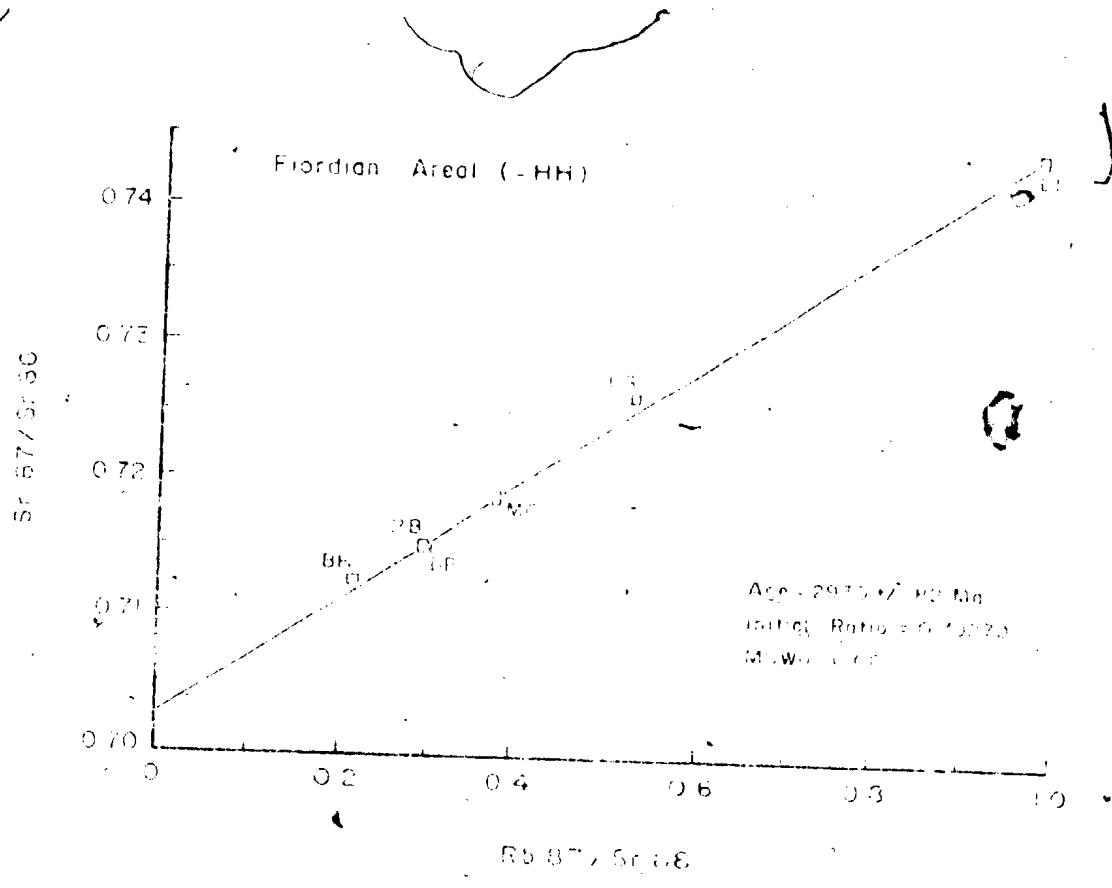
The Hopedalian areal isochron age indicates a Sr homogenization event has affected the Maggo gneiss which predates the Hopedalian event. The significance of the age obtained for the Hopedalian areal and its relationship to the development of the Maggo gneiss within the Hopedale Block are discussed in Section 6.4 and Chapter 7.

4.15.3 Flordian Areal

The remaining seven suites (MC, DP, PB, BH, HH, HG, DI) are considered in deriving the Flordian areal isochron. Regressing the areal values for these suites (Table 4.6) yields a date of 2,752 +/- 250 Ma (Sr_0 = 0.70469; MSWD = 0.60; Figure 4.19). The low MSWD for the areal isochron is a function of the large errors associated with the mean $^{87}Rb/^{86}Sr$ and $^{87}Sr/^{86}Sr$ ratios.

Eliminating the most discordant point (HH) from the regression analysis increases the age to 2,930 +/- 82 Ma (Sr_0 = 0.7027; MSWD = 0.06; Figure 4.20). Justification for the elimination of the HH areal is based on the lack of Sr homogenization with the remaining suites during the

Figure 4.20: Areal Isochron for Flordian suites after
elimination of HH suite (see text for details).



older Sr exchange event recorded by the Flordian areal. The HH suite is enriched in Sr (518 ppm) with respect to the remaining Flordian areal suites (mean Sr value = 389 ppm). The 2,930 Ma result is taken to represent the age for the Flordian areal isochron.

This age is identical to the result obtained for the HH whole rock isochron. The similarity between the ages would suggest that an alternate interpretation, than that suggested in Section 4.14.2.3, for the HH age is that this suite records the final imprint of the Hopedalian event on the Maggo gneiss at this locality. Based on the field relationships of this suite the latter interpretation is regarded as the more likely of the two.

The Flordian areal age overlaps with both the Hopedalian and Flordian isochron ages. The significance of this age is that it dates the timing of the last Sr homogenization/exchange within the Maggo gneiss which has subsequently been affected by the Flordian event and is indistinguishable from the Flordian pooled age (Figure 4.17). The initial Sr_0 ratios for the Flordian pooled and areal isochrons are identical.

4.16 Summary

An important result of this study is the documented discrepancy between the preserved tectonic fabric and the recorded Rb-Sr isotopic age for each suite, e.g. Hopedalian fabric and Flordian age, of Maggo gneiss. This discrepancy was first pointed out by Grant et al. (1983) for suites of Maggo gneiss from the Hopedale Block.

Combining the geochronological results with the previously determined structural and lithological chronology (Korstgard and Ermanovics, 1984; 1985) suggests that physical and chemical reworking associated with the Flordian event do not necessarily occur simultaneously. Visible evidence, i.e., development of the S_{n+3} fabric, and invisible effects, i.e. chemical changes especially in the Rb-Sr isotopic systematics, associated with the Flordian reworking occur independently of each other for the individual suites analyzed in this study. Collerson and Fryer (1978) pointed out that isotopic systems (Sr and Pb) close when large scale mantle and lower crust degassing ceases, irrespective of demonstrably different field and stratigraphic relationships.

Using the pooled isotopic data for the four suites analyzed in this study, the Hopedalian event occurred 3,091 +/- 25 Ma ago. Results for the NBN suite indicate that an event pre-dating the Hopedalian event affected the Maggo gneiss at 3,305 +/- 75 Ma. The pooled Hopedalian age is in agreement with the previously reported results for Maggo gneiss (Grant et al., 1983; Ermanovics, pers. comm., 1986) and supracrustal lithologies (Schlotte, pers. comm., 1988).

The remaining seven suites analyzed in this study yield ages between 2,927 and 2,632 Ma with a pooled age of 2,853 +/- 41 Ma, defining the mean time of the Flordian deformation. The Flordian suites are interpreted to represent varying degrees of retrogression and isotopic

resetting associated with the Flordian event. The pooled Flordian age result is in agreement with the results of Grant et al. (1983) for reworked Maggo gneiss and the pre- to syn- Flordian Kanariktok Intrusives.

Application of the areal concept to the Hopedallan domain Maggo gneiss suites indicates that these suites retain evidence of an older, pre-Hopedallan, isotopic resetting/homogenization event at $3,360 \pm 212$ Ma. This age is in agreement with single suite isochron results. The close agreement between the Flordian areal ($2,930 \pm 82$ Ma) and pooled ($2,853 \pm 41$ Ma) ages suggests that Flordian reworking has completely reset the isotopic systematics of the gneiss. The resetting has effectively obliterated any isotopic characteristics of an older event to have affected the Flordian domain Maggo gneiss.

Chapter 5

GEOCHEMISTRY

5.1 Introduction

In recent years the geochemical affinities of North Atlantic Archaean grey gneiss complexes have been investigated by numerous workers, including Drury (1973; 1978), Compton (1978a and b), Moorbath *et al.* (1975; 1981), Collerson and Bridgwater (1979), Tarney *et al.* (1979) and Moorbath and Taylor (1981). These detailed geochemical investigations have been carried out in regions extensively studied in the field. In each case it was concluded that the volume of preserved continental crust was increased as a result of either reworking of preexisting material (Collerson and Bridgwater, 1979) or by the addition of juvenile material to the crust (Moorbath and Taylor, 1981).

Visible effects of the Flórdian reworking on Hopedalian domain Maggo gneiss are the development of new planar and linear fabrics within the gneiss and retrogression of Hopedalian mineral assemblages. In this chapter the major, trace and rare earth element (REE) geochemistry of the Maggo gneiss will be presented.

The results of the geochemical study will be used to:

- 1) Define the chemical characteristics of the Maggo gneiss from the Hopedalian domain.
- 2) Define the changes in the chemical nature of the Maggo gneiss in response to Flordian overprinting.
- 3) Provide information on the origin and possible parental compositions of the gneiss.

Data for other lithologies will be presented in a supporting role.

Methods employed in the field for sample selection together with analytical techniques employed in the major, trace and rare earth element determinations are given in Appendix B. The relative precision and accuracy of the methods employed and the results of determinations on standard samples are also listed in the appropriate sections of Appendix B. Figure 5.1 provides the location of all samples analyzed in this study.

5.2 Maggo Gneiss

5.2.1 Introduction

A total of 138 gneiss samples were analyzed for major and trace elements by atomic absorption and X-ray fluorescence techniques, respectively. Due to the relatively restricted variation in mineralogy and given the considerable but continuous range in composition, the Maggo gneiss has been arbitrarily subdivided on the basis of its SiO_2 and K_2O contents. The following chemical subdivisions of the Maggo gneiss are used:

Dioritic gneiss $\text{SiO}_2 < 62 \text{ wt\%}$

Tonalitic gneiss $\text{SiO}_2 > 62 \text{ and } < 68 \text{ wt\%}$

$\text{K}_2\text{O} < 2 \text{ wt\%}$

Trondhjemitic gneiss $\text{SiO}_2 > 68 \text{ and } < 74 \text{ wt\%}$

$\text{K}_2\text{O} < 2 \text{ wt\%}$

Granodioritic gneiss $\text{SiO}_2 > 68 \text{ and } < 74 \text{ wt\%}$

$\text{K}_2\text{O} > 2 \text{ wt\%}$

Siliceous gneiss $\text{SiO}_2 > 74 \text{ wt\%}$

This subdivision of the Maggo gneiss is similar to that used by McGregor (1979) for the Nuk gneiss of SW Greenland. Trondhjemitic and tonalitic subgroups are the most abundant accounting for 52% and 25%, respectively, of all Maggo gneiss samples analyzed.

Subdivision of the Maggo gneiss on the basis of chemistry is reflected in the mineralogy. Trondhjemitic gneiss contains minor to negligible amounts of interstitial K-feldspar, displays a low mafic mineral content, with biotite $>$ hornblende. Tonalitic gneiss samples lack K-feldspar, have both hornblende and biotite with the former being more abundant. In the granodioritic subgroup biotite is the dominant mafic phase and K-feldspar is more abundant than in the trondhjemitic samples. The dioritic gneiss subgroup, the least common chemical group (8 samples) has a higher proportion of mafic minerals, with hornblende commonly more abundant than biotite.

The subdivision of the Maggo gneiss into chemically defined gneiss subgroups, based on increasing SiO_2 and K_2O contents corresponds to an increase in the degree of 'fractionation'. Fractionation is here taken to mean that an evolutionary link exists between the various subgroups, with no specific 'fractionation' mechanism implied. Regardless of what this process is there is an observed, gradual change in Maggo gneiss chemistry, i.e., increasing SiO_2 from diorite to granodiorite gneiss.

This chemical subdivision is applied to all gneiss samples irrespective of the structural domain from which they were collected. The differences in whole rock chemistry between samples from the Hopedalian and Flordian domains is discussed in Section 6.2

During the 'normal' crystallization of a primary magma the absolute abundance of any oxide or element will vary, i.e. increase or decrease in liquid in response to fractionation processes, depending on the phases involved. However, the ratio between elements, with similar partition coefficients, should remain relatively unchanged (Hart and Allegre, 1980; Zindler et al., 1984). For the Maggo gneiss any primary petrogenetic trends, based on geochemical data, must necessarily be more obscure when compared to suites which do not exhibit a similar protracted history.

Representative analyses of the chemically defined gneiss subgroups are presented in Tables 5.1 to 5.4. Table 5.5 presents average compositions for each gneiss subgroup.

Table 5.1: Representative analyses Tonalite Subgroup, Maggo Gneiss.

Sample	82-60	83-129	83-169	83-202	83-255	83-296
SiO ₂	67.60	66.0	65.70	66.40	65.60	64.90
TiO ₂	0.34	0.64	0.45	0.52	0.62	0.40
Al ₂ O ₃	16.80	15.50	15.00	14.80	16.10	14.60
Fe ₂ O ₃ *	3.54	4.47	4.49	4.96	4.34	5.3
MnO	0.06	0.07	0.06	0.08	0.05	0.11
MgO	1.46	1.91	2.68	2.07	1.04	3.31
CaO	4.41	4.27	4.92	4.99	3.81	5.25
Na ₂ O	4.46	4.11	3.87	4.17	4.68	3.61
K ₂ O	1.44	1.67	1.23	0.86	1.32	1.35
P ₂ O ₅	0.11	0.12	n.d.	0.08	0.15	0.06
LOI	0.41	0.47	0.92	0.76	0.27	0.67
TOTAL	100.63	99.23	99.32	99.69	97.98	99.56
Pb	9	10	11	3	6	4
Th	n.d.	9	7	3	7	1
U	n.d.	6	n.d.	n.d.	2	n.d.
Rb	56	64	32	28	9	33
Sr	301	368	331	220	274	199
Y	10	18	7	17	9	16
Zr	110	144	114	126	261	89
Nb	6	9	6	6	6	7
Zn	53	46	54	47	43	49
Cu	11	12	45	46	15	35
Ni	11	14	36	23	2	56
Ba	311	367	307	126	4	207
V	42	52	81	77	56	91
Cr	22	24	71	23	n.d.	175
Ga	18	17	21	16	18	17
Na ₂ O/K ₂ O	3.1	2.5	3.2	4.9	9.5	2.7
K/Rb	213	217	319	255	424	340
K/Ba	38.4	37.8	33.3	56.6	954.6	339.5

* - Total Fe as Fe₂O₃

n.d. - not detected

00164

Table 5.2: Representative analyses Trondhjemite subgroup, Maggo Gneiss.

Sample	82-32	83-26	83-172	83-218	83-249	83-279
SiO ₂	69.70	70.40	68.80	70.4	70.5	70.4
TiO ₂	0.42	0.30	0.47	0.29	0.20	0.34
Al ₂ O ₃ *	14.60	14.90	14.70	15.60	15.60	15.00
Fe ₂ O ₃ *	3.01	2.58	3.61	1.89	1.91	2.38
MnO	0.05	0.03	0.05	0.03	0.02	0.05
MgO	1.55	0.91	1.43	0.79	0.72	1.52
CaO	3.47	3.24	4.34	2.97	3.21	3.05
Na ₂ O	4.04	4.56	3.96	5.31	5.23	4.73
K ₂ O	1.47	1.49	1.22	1.29	1.59	1.49
P ₂ O ₅	0.09	n.d.	n.d.	0.18	0.15	0.12
LOI	0.47	0.54	0.89	0.5	0.24	0.45
TOTAL	98.87	98.95	99.47	99.25	99.37	99.53
Pb	5	10	5	9	3	8
Th	n.d.	6	4	n.d.	6	n.d.
U	n.d.	n.d.	n.d.	n.d.	n.d.	1
Rb	59	45	31	45	45	57
Sr	255	297	175	353	464	323
Y	17	2	9	1	n.d.	4
Zr	116	109	129	89	79	112
Nb	6	5	4	2	1	2
Zn	43	35	46	33	33	44
Cu	16	23	19	19	15	16
Ni	19	12	10	4	2	20
Ba	431	294	278	171	327	381
V	39	41	58	27	22	31
Cr	9	43	19	11	5	40
Ga	17	20	20	18	18	18
Na ₂ O/K ₂ O	2.8	3.1	3.3	4.1	3.3	3.2
K/Rb	206	274	327	238	293	217
K/Ba	28.3	42.1	36.4	62.6	40.4	34.3

* - Total Fe as Fe₂O₃
n.d. - not detected

00165

Table 5.3: Representative analyses Granodiorite subgroup, Maggo Gneiss.

Sample	82-44	83-176	83-194	83-197	83-243	83-288
SiO ₂	72.90	71.40	73.30	70.60	71.30	68.70
TiO ₂	0.23	0.20	0.18	0.45	0.28	0.56
Al ₂ O ₃ *	14.70	15.00	13.60	15.00	14.00	13.70
Fe ₂ O ₃ *	1.54	1.60	1.76	2.21	1.99	4.76
MnO	0.03	0.03	0.04	0.03	0.03	0.07
MgO	0.50	0.54	0.50	1.01	0.53	2.10
CaO	2.30	2.60	2.48	2.88	1.81	2.43
Na ₂ O	4.46	4.95	4.37	4.39	3.48	3.49
K ₂ O	2.56	2.48	2.32	2.18	4.46	2.54
P ₂ O ₅	0.04	0.06	0.06	0.14	0.12	0.05
LOI	0.67	0.78	0.25	0.57	0.29	0.40
Total	99.93	99.64	98.86	99.46	98.29	98.80
Pb	9	28	12	7	16	6
Th	n.d.	6	10	5	17	1
U	n.d.	n.d.	n.d.	n.d.	n.d.	n.d.
Rb	70	45	68	63	90	113
Sr	428	423	192	652	385	179
Y	6	4	11	4	1	2
Zr	94	95	102	143	216	136
Nb	2	6	5	5	3	9
Zn	35	58	31	50	36	77
Cu	16	12	14	20	14	16
Ni	n.d.	1	2	3	n.d.	35
Ba	608	832	494	699	1626	351
V	20	24	15	43	21	84
Cr	1	3	10	9	n.d.	138
Ga	18	20	15	21	16	20
Na ₂ O/K ₂ O	1.7	2.0	1.9	2.0	0.78	1.4
K/Rb	304	458	283	287	411	190
K/Ba	34.9	24.7	39	25.9	22.8	60.1

* - Total Fe as Fe₂O₃
n.d. - not detected

Table 5.4: Representative analyses of the Diorite and Siliceous Gneiss Subgroups, Maggo Gneiss.

Sample	Diorite				Siliceous Gneiss	
	83-78	83-182	83-274	83-297	82-698	DB-81-11
SiO ₂	58.70	57.20	60.20	53.70	75.50	78.40
TiO ₂	0.93	0.54	0.70	0.69	0.14	0.05
Al ₂ O ₃ *	15.80	18.70	15.50	15.10	13.20	13.00
Fe ₂ O ₃ *	8.51	5.01	6.83	7.97	1.62	0.73
MnO	0.10	0.04	0.12	0.14	0.03	0.02
MgO	3.71	3.97	3.73	7.52	0.52	0.25
CaO	5.72	7.74	5.88	7.8	2.75	2.59
Na ₂ O	4.69	5.12	4.23	3.10	4.34	3.97
K ₂ O	0.36	0.83	1.49	1.72	1.22	1.81
P ₂ O ₅	0.23	0.18	0.12	0.11	0.03	n.d.
LOI	0.44	0.34	0.41	0.75	0.69	0.70
Total	99.19	99.67	99.21	98.60	100.04	101.52
Pb	3	2	2	7	3	8
Th	n.d.	3	2	4	5	9
U	n.d.	n.d.	n.d.	n.d.	n.d.	2
Rb	4	7	37	55	35	47
Sr	258	446	245	74	151	134
Y	27	7	14	25	15	3
Zr	135	43	77	78	101	41
Nb	6	1	6	7	6	4
Zn	52	66	69	78	14	13
Cu	38	31	13	51	28	16
Ni	41	43	42	76	3	n.d.
Ba	51	73	132	166	239	339
V	132	110	117	257	17	2
Cr	42	17	69	116	n.d.	n.d.
Ga	19	22	21	21	15	14
Na ₂ O/K ₂ O	13.0	6.2	2.8	1.8	3.6	10.1
K/Rb	747	984	334	260	289	319
K/Ba	58.8	94.4	93.7	86	42.4	44.3

* - Total Fe as Fe₂O₃
n.d. - not detected

Table 5.5: Average analyses of the chemically defined subgroups of the Maggo Gneiss.

	1 (n=8)		2 (n=36)		3 (n=68)		4 (n=18)		5 (n=6)	
	\bar{x}	s	\bar{x}	s	\bar{x}	s	\bar{x}	s	\bar{x}	s
SiO ₂	58.83	2.3	65.16	1.7	70.83	1.4	71.59	1.6	74.72	3.6
TiO ₂	.71	.2	.51	.1	.3	.1	.25	.1	.15	.2
Al ₂ O ₃	15.66	1.3	15.48	.8	15.07	.6	14.72	.6	13.7	1.0
Fe ₂ O ₃	7.47	1.2	4.84	.9	2.31	.7	1.97	1.1	1.12	.9
MnO	.12	.04	.08	.02	.04	.01	.04	.02	.02	.01
MgO	4.42	1.3	2.37	.6	1.03	.4	.9	.6	.39	.4
CaO	6.67	1.0	4.92	.7	3.21	.5	2.59	.3	2.51	.6
Na ₂ O	4.01	.7	4.08	.3	4.61	.4	4.37	.4	4.25	.2
K ₂ O	1.21	.7	1.22	.3	1.47	.2	2.46	.6	1.89	1.0
P ₂ O ₅	.15	.06	.12	.04	.08	.04	.07	.04	.06	.01
Pb	4.8	3	6.3	3	6.9	3	10.6	7	6	3
Th	3.2	2	5.8	3	5.1	3	6.1	4	7.8	3
U	1.0	1	4.2	4	2.3	1	4.0	16	2	4
Rb	28.9	30	35.6	12	49.4	16	69.3	23	42.8	22
Sr	235.1	107	337.5	106	369.9	119	358.3	158	312	212
Y	19.9	7	13.3	5	6.0	4	6.8	4	7.7	6
Zr	90.3	36	111.1	34	104.3	33	106.4	36	74.5	47
Nb	6.4	3	5.1	2	4.2	2	6.1	3	3.8	1
Zn	73.5	13	55.6	8	36.4	11	39.6	16	18.5	21
Cu	27.9	15	25.9	12	18.5	10	16.4	7	21.2	5
Ni	57.6	19	26.6	18	11.5	8	9.9	10	3.0	0
Ba	110.1	48	253.9	110	334.3	130	587.5	318	590.0	614
V	160.6	49	78.9	20	30.8	14	31.1	22	15.4	17
Cr	83.6	53	45.8	32	18.1	16	21.7	36	4.0	2
Ga	18.9	3	17.9	3	17.6	2	17.6	2	15.3	2
Na ₂ O/K ₂ O ¹	3.3		3.3		3.1		1.8		2.2	
K/Rb ¹	347		284		245		295		366	
K/Ba ¹	91		40		37		35		27	

1. Diorite Subgroup. SiO₂ < 62 wt%.
2. Tonalite Subgroup. SiO₂ 62-68 wt%, K₂O < 2 wt%.
3. Trondhjemite Subgroup. SiO₂ 68-74 wt%, K₂O < 2 wt%.
4. Granodiorite Subgroup. SiO₂ 68-74 wt%, K₂O > 2 wt%.
5. Silica-rich Subgroup. SiO₂ > 74 wt%.

\bar{x} - Mean value for oxide/element.

s - Standard deviation (1 sigma confidence limits).

* - Total Fe as Fe₂O₃

1 - Ratios calculated using mean values above.

A complete listing of the results for all gneiss samples analyzed is given in Appendix D.

5.2.2 Major Elements

SiO_2 contents of the Maggo gneiss vary from 53.7 to 78.4 wt%. Harker-type variation diagrams (Figure 5.2) relating major elements to silica content display a variety of relationships. The alumina content of the gneiss varies from 13.0 wt% to 18.7 wt%, with the majority of samples clustering at 15.0 ± 1 wt% (Figure 5.2a). Overall there is a weak negative correlation of Al_2O_3 with increasing silica.

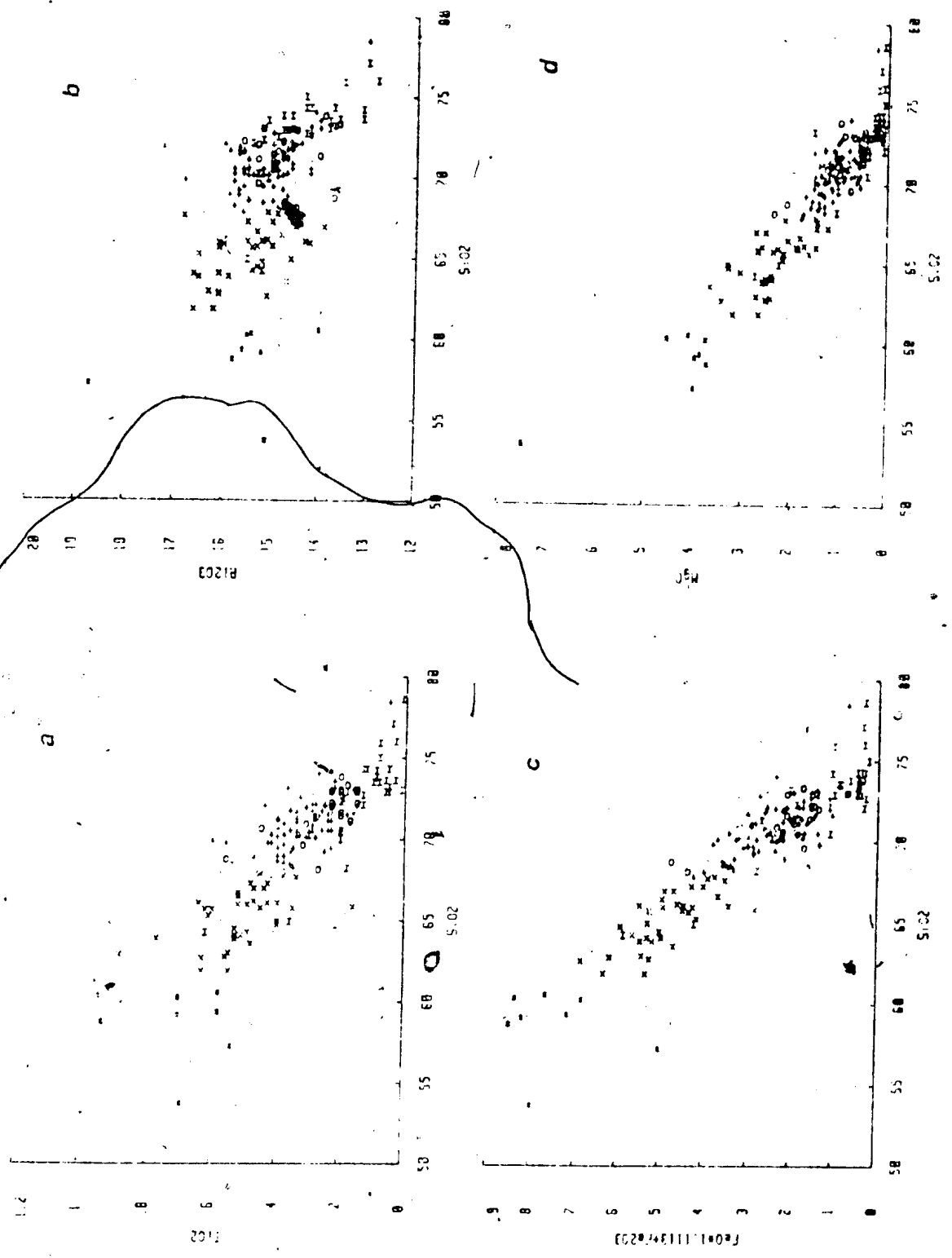
The oxides TiO_2 (0.03 - 0.94 wt%), $\text{Fe}_2\text{O}_3^{\text{Total}}$ (0.38 - 8.51 wt%), MgO (0.05 - 7.52 wt%) and CaO (1.39 - 7.80 wt%) all exhibit negative correlations with increasing silica content in the gneisses (see Figure 5.2 a, and c to e). The oxides, MnO (0.01 - 0.15 wt%; not shown) and P_2O_5 (0.01 - 0.23 wt%; Figure 5.2h) both exhibit negative correlations with silica, but there is a wide scatter in the distribution possibly related, at least in part, to low abundances and related analytical difficulties.

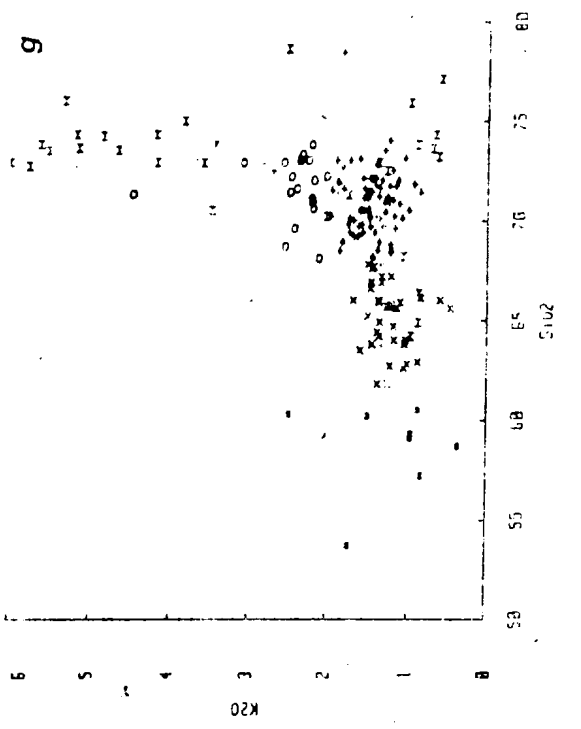
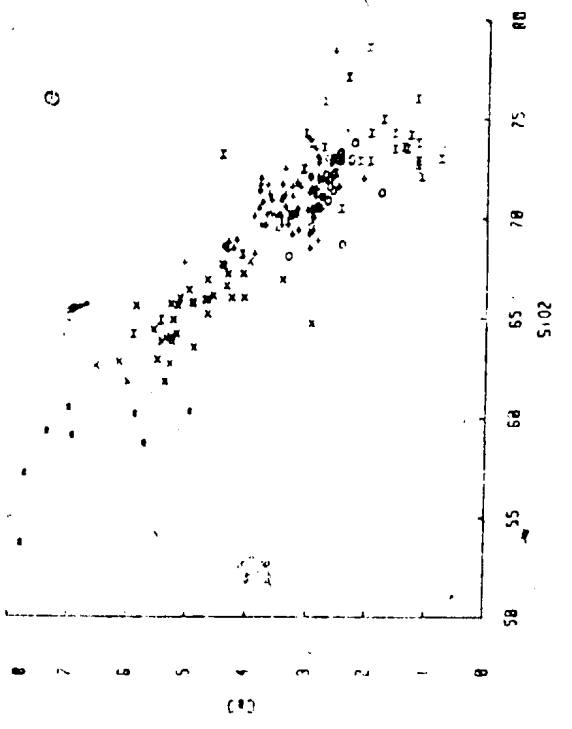
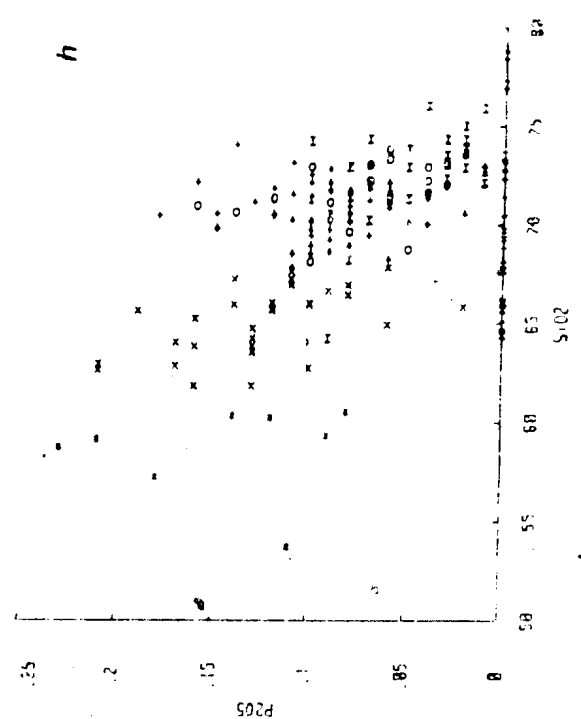
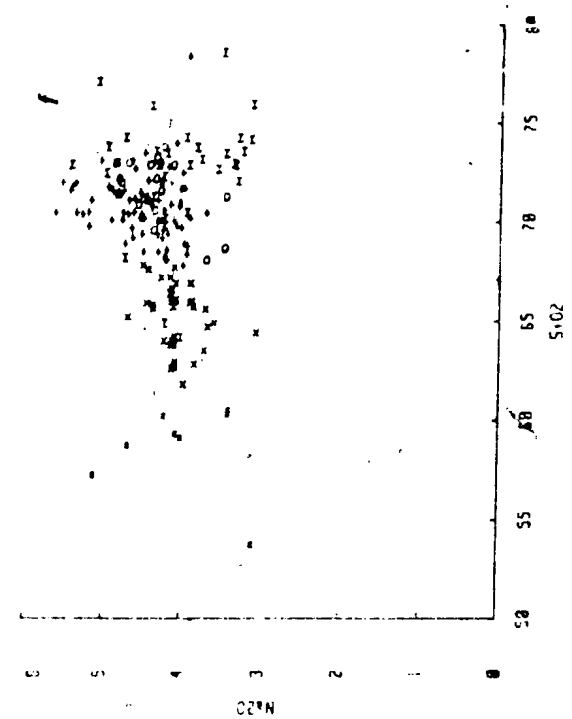
The remaining two major element oxides (Na_2O and K_2O) exhibit weak positive correlations with increasing silica content. Na_2O ranges from 3.08 to 5.65 wt% and exhibits an increase in the spread of values with increasing silica content (Figure 5.2f). K_2O values, range from 0.36 to 5.15 wt% and exhibit an even wider spread at high silica values (Figure 5.2g).

Figure 5.2: Harker variation diagrams (major elements) for Maggo gneiss samples, distinguished according to chemically defined gneiss groups: a) TiO_2 vs SiO_2 ; b) Al_2O_3 vs SiO_2 ; c) Fe_2O_3^* vs SiO_2 ; d) MgO vs SiO_2 ; e) CaO vs SiO_2 ; f) Na_2O vs SiO_2 ; g) K_2O vs SiO_2 ; h) P_2O_5 vs SiO_2 .

Symbols:

- * - dioritic gneiss
- x - tonalitic gneiss
- + - trondhjemitic gneiss
- o - granodioritic gneiss
- H - siliceous gneiss (with strongly migmatitic gneiss samples)





The $\text{Na}_2\text{O}/\text{K}_2\text{O}$ ratios for the gneisses vary from 0.75 to 6.17, with the majority having $\text{Na}_2\text{O}/\text{K}_2\text{O}$ values greater than 2.0 (Figure 5.3a). There is no clear relationship between the Al_2O_3 content of the gneisses and the $\text{Na}_2\text{O}/\text{K}_2\text{O}$ ratio (Figure 5.3b).

One interpretation of the variable Na_2O and K_2O contents and $\text{Na}_2\text{O}/\text{K}_2\text{O}$ ratios, depicted on Figure 5.3, is that these oxides have been mobile during post-solidification alteration events, i.e. metamorphism, affecting the Maggo gneiss. The wide spread of K_2O values at high silica contents is especially indicative of secondary redistribution, mainly the introduction of K, in response to metamorphism. Some trace elements, e.g. Rb, Ba and Sr, show similar patterns.

The range of composition exhibited for the Maggo gneiss is such that it defines a continuous trend, evident on an AFM diagram (Figure 5.4). The trend is linear and parallels the trondhjemite trend of Barker and Arth (1976) for Norwegian trondhjemite, with the Maggo gneiss samples lying within the calc-alkaline field defined by these authors. It is also evident from the AFM diagram that Maggo gneiss samples overlap the fields for both the Amitsoq Banded Grey Gneiss (ABGG) of southern West Greenland (Nutman *et al.*, 1984) and the Uivak I gneiss of northern Labrador (Collerson and Bridgwater, 1979).

It is not possible to distinguish between trends of calc-alkaline and trondhjemitic affinity from the AFM

Figure 5.3: a) Na_2O vs. K_2O . The majority of the Maggo gneiss samples have $\text{Na}_2\text{O}/\text{K}_2\text{O}$ values > 2 .

b) $\text{Na}_2\text{O}/\text{K}_2\text{O}$ ratio vs. Al_2O_3 .

Symbols as in Figure 5.2.

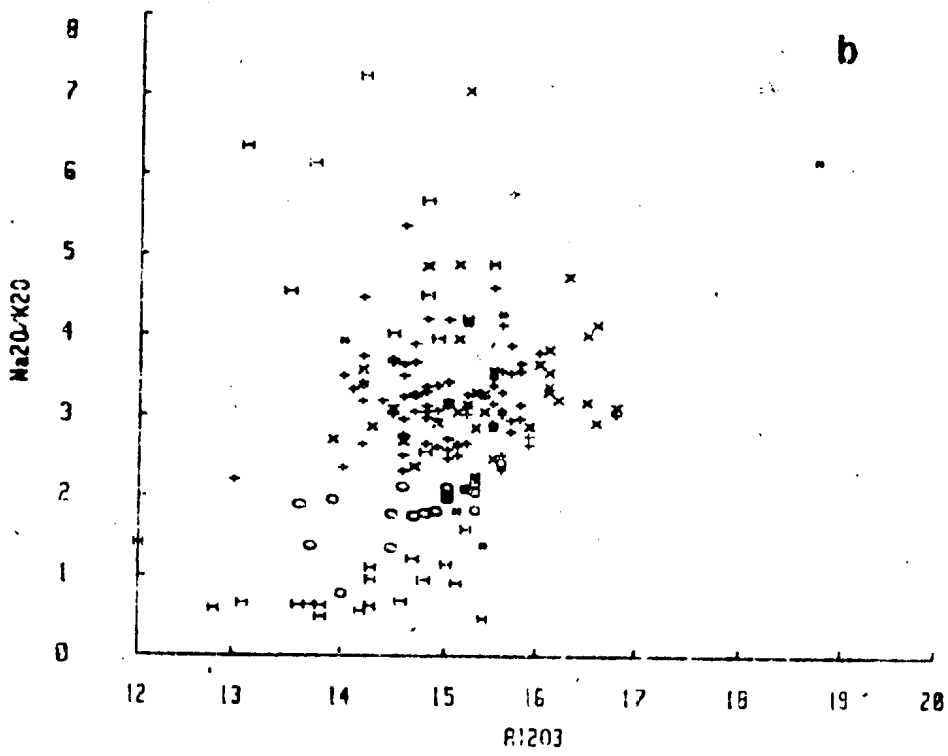
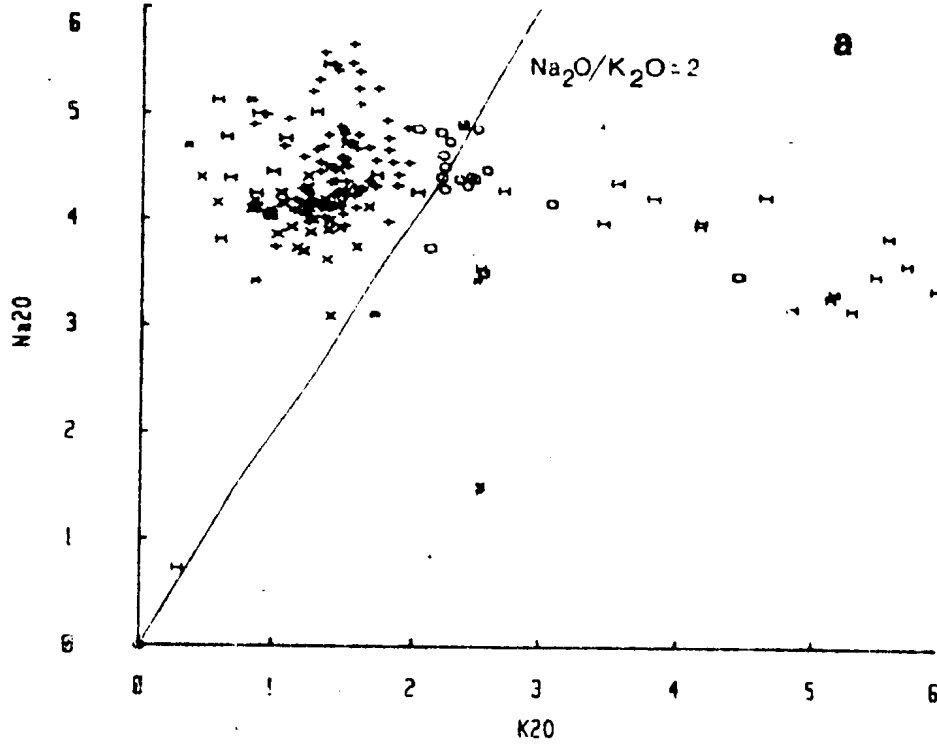


Figure 5.4: AFM ternary projection for the Maggo gneiss samples. The fields for Ulvak I Gneiss of northern Labrador (Collerson and Bridgwater, 1979) and Amitsoq Banded Grey Gneiss (ABGG: light stipple) from SW Greenland (Nutman et al., 1984) are shown for comparison. Solid line - trondhjemitic trend; Dashed lines - calc-alkaline field (From Barker and Arth, 1976).

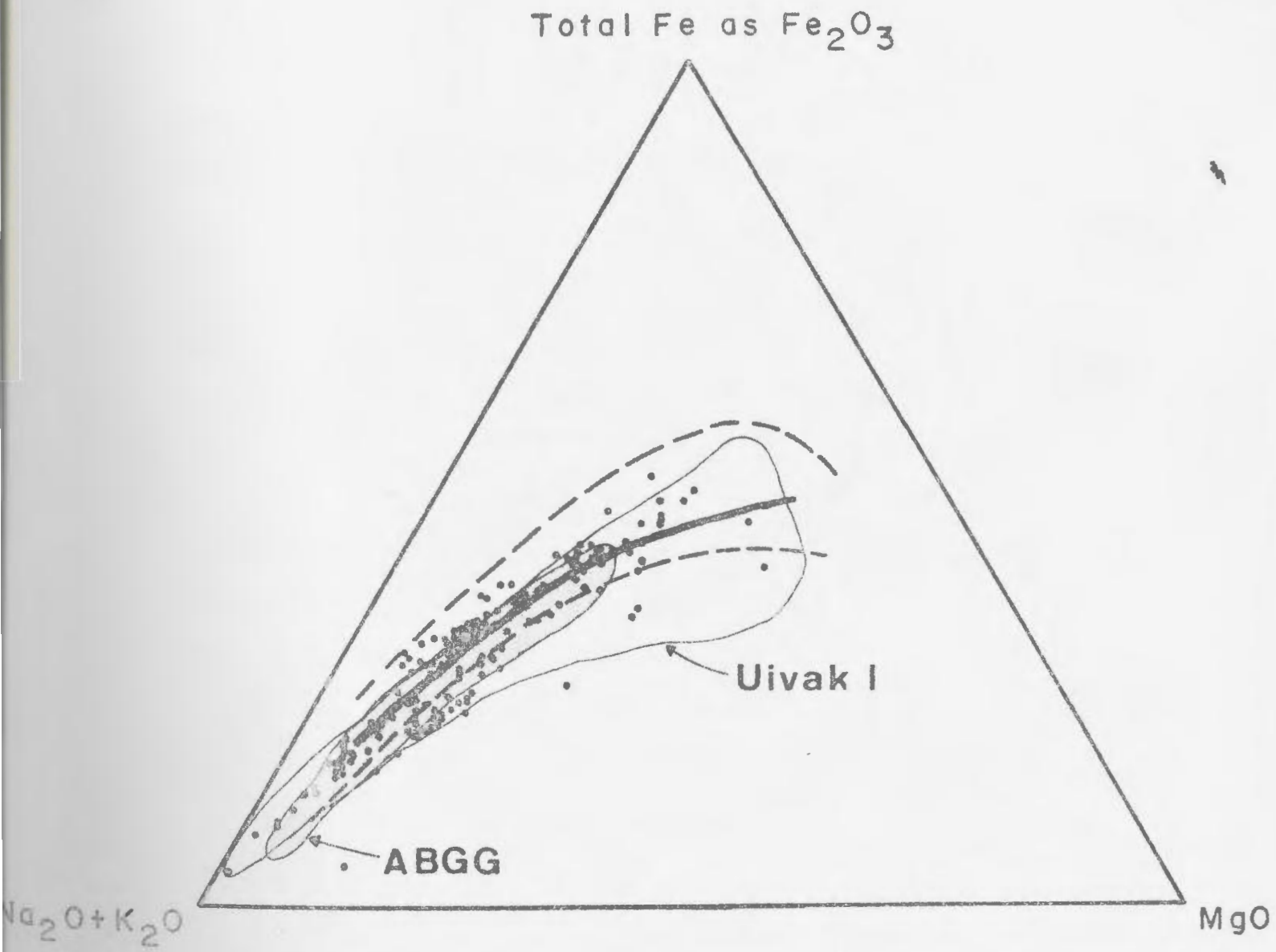


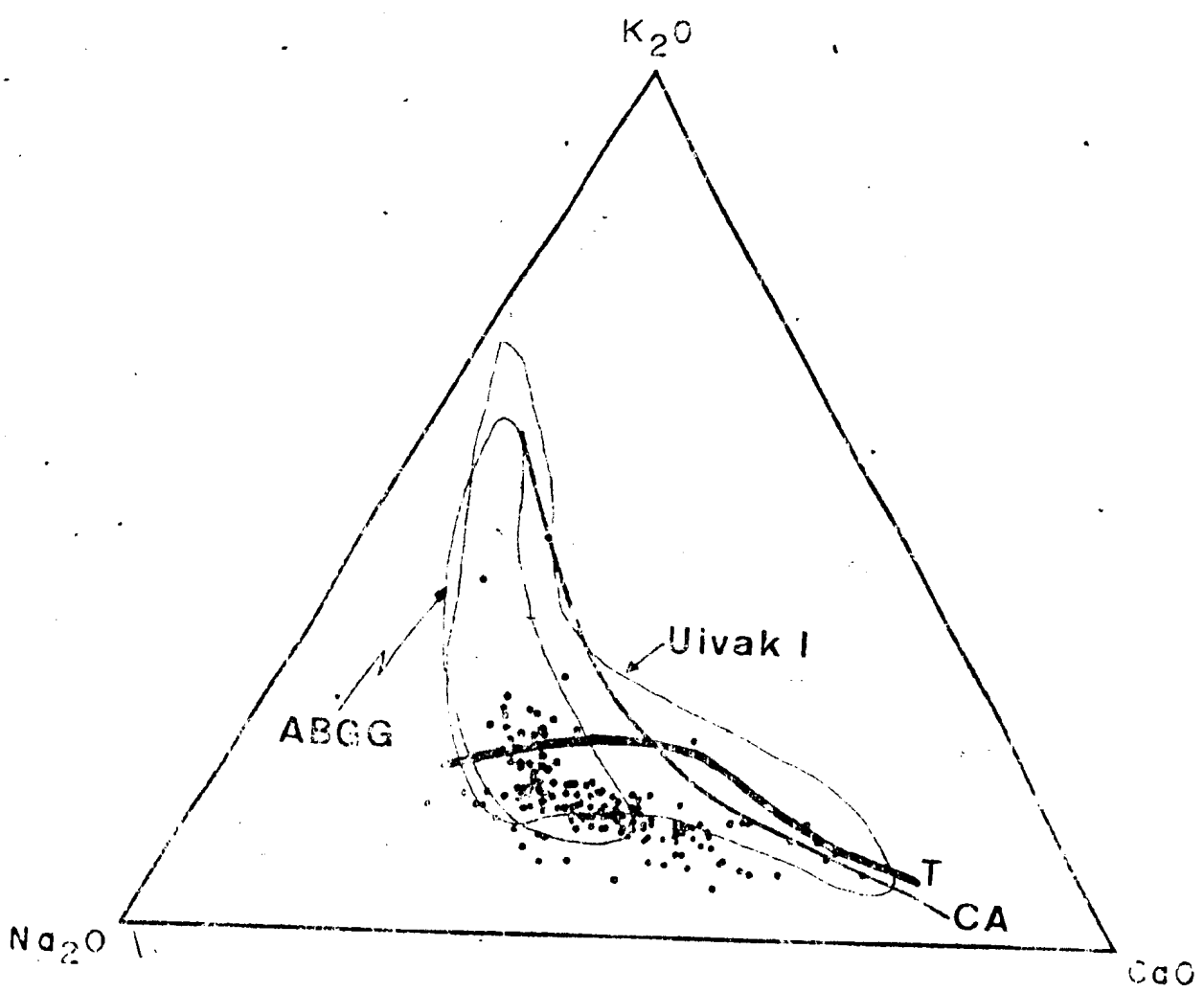
diagram. However, when Maggo gneiss results are plotted on a ternary $\text{Na}_2\text{O}-\text{K}_2\text{O}-\text{CaO}$ diagram (Figure 5.5) two trends, subparallel to the trondhjemite and calc-alkaline trends of Barker and Arth (1976), are apparent. A feature observable in Figure 5.5 is that the Maggo gneiss samples are displaced away from the K_2O apex compared to the trends defined by Barker and Arth (1976) and the fields for the Amitsoq Banded Grey Gneiss and Ulvåker Gneiss (Nutman *et al.*, 1984, Collerson and Bridgwater, 1979) presumably reflecting K_2O depletion (see Figure 5.5). The lower K_2O content, reflects either the primary protolith composition of the Maggo gneiss or subsequent depletion in response to metamorphism (Hopedalian and/or Flordian).

Normative analyses for Maggo gneiss samples, calculated using the method of Barth (1959, 1962) are plotted on the normative Ab-An-Or triangular diagram (Figure 5.6). The majority of the samples plot in the tonalite and trondhjemite fields of O'Connor (1955), away from the Or apex. The low normative Or contents directly reflect the low K_2O content of the Maggo gneiss.

5.2.3 Element Mobility Studies - Background

Essential to the interpretation of trace element data for the Maggo gneiss is the concept of element mobility-immobility in response to any alteration event, i.e. the Hopedalian and Flordian events. Elements of interest include the large ion lithophile elements (LILE; K, Rb, Ba, Sr) and the high field strength (HFS) elements (Ti, Zr, P, Nb, Y) and the rare earth elements (REE).

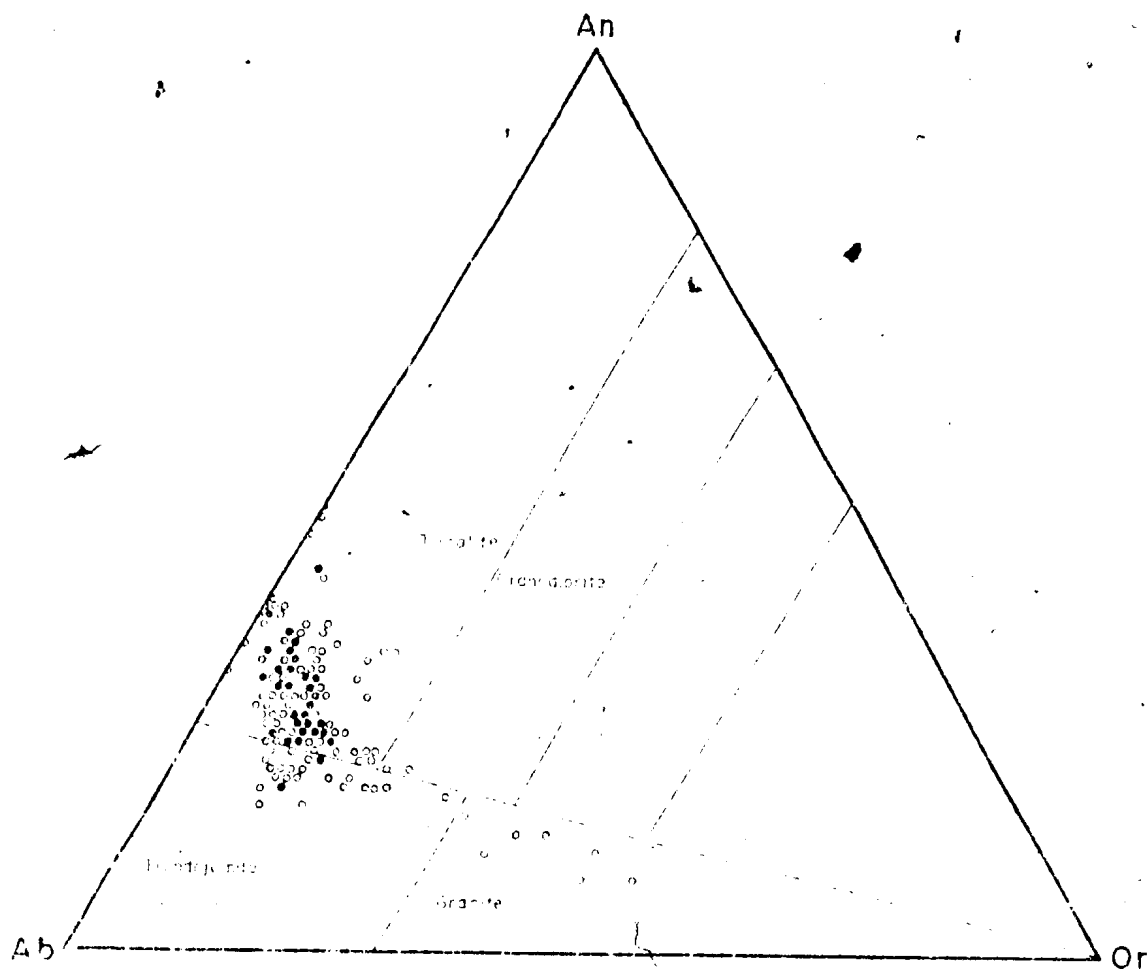
Figure 5.5: $\text{Na}_2\text{O}-\text{K}_2\text{O}-\text{CaO}$ ternary projection for Maggo gneiss samples. Uivak I and ABGG (light stipple) fields are shown for comparison. T - tholeiitic trend; CA - calc-alkaline trend (From Barker and Arth, 1976).



u

Figure 5.6: Normative (wt %) Ab-An-Or projection (after O'Connor, 1965) for Maggo gneiss samples. The majority of analysis plot within the tonalite and trondhjemite fields. Symbols: open circles - single analysis, solid circles - two or more analyses.

(



Investigations examining low temperature and pressure changes in metabasalts (Cann, 1970; Pearce and Cann, 1971; 1973; Graham, 1976) suggest that concentrations of Y, Zr, Hf, Nb, Ta and the REE remain unaffected during any alteration event. Discrimination plots for immobile elements produce high correlations with each other and are useful in identifying the source region for basaltic rocks. A similar type of discrimination diagram for granitic rocks (Pearce et al., 1984) has been proposed.

Hynes (1980) and Murphy and Hynes (1986) examined the effects of greenschist facies metamorphism on high field strength (HFS) elements (Ti, P, Zr, Y and Nb). These authors found that under conditions of high CO₂ contents in the accompanying fluid phase that the HFS elements become mobile during metamorphism, with Ti behaving independently and exhibiting both mobile and immobile behaviour.

At higher metamorphic grades, LILE mobility studies have concentrated on the granulite - amphibolite facies transition (Lambert and Heler, 1968; Heler and Thoresen, 1971; Green et al., 1972; Drury, 1973; Sheraton et al., 1973; Field and Clough, 1976; Kalsbeek, 1976). Low Rb contents, producing high K/Rb ratios, attributed to granulite facies metamorphism, are suggested to result in enrichment of the upper crust in Rb relative to lower crust. Applying K/Rb ratios, Shaw (1968) suggested upper crustal lithologies have a mean K/Rb value of 230, which

Increases with decreasing K content. In several Precambrian granulite facies terrains the K/Rb ratio increases to values > 1000 , (e.g. Buksefjorden region, SW Greenland (Compton, 1978b)).

The significance of K/Rb ratio trends is in dispute. Extreme variation in the K/Rb ratio has been interpreted to reflect a primary igneous trend (e.g. Norwegian metabasites, Field and Clough, 1976). Alternatively, Tarney (1976) believes the K/Rb ratio of Precambrian granulites results from secondary processes, as compositionally equivalent lithologies from adjacent amphibolite facies areas have normal K/Rb values. Under granulite facies metamorphism the large Rb ion is preferentially lost, compared with K, during :

- 1) anatexis, leaving a granulite facies residuum
- 2) the slow removal of hydrous fluids in the formation of an anhydrous assemblage,
- or 3) leaching by mantle derived fluids during high grade metamorphism (Tarney, 1976).

Tarney and Windley (1977), examining the evolution of the lower continental crust, conclude that K and Rb depletion observed in granulites is due to the development of a non K- or Rb-bearing mineral assemblage together with the presence of a metasomatic fluid capable of removing Rb and K. However, evidence for Polish and central European granulites suggests that it is equally possible for granulite facies conditions to be attained in a closed

system resulting in little Rb or K loss (Tarney and Windley, 1977).

Compton (1978b) suggests the K/Rb trend observed in the Nuk gneiss, resulted from igneous processes, with samples lying off this trend reflecting element mobility. Samples of Eqalit gneiss (a phase of the Nuk gneiss) with and without orthopyroxene, reflecting amphibolite and granulite facies metamorphism, respectively, are thoroughly mixed on a K vs Rb plot. This conclusion is in agreement with that of Tarney and Windley (1977) who suggested that Rb depletion is not dependent on the formation of an anhydrous assemblage, but that other factors, i.e. closed system, have an effect. Data presented by Tarney and Windley (1977) for Polish high pressure granulites display a wide range of K contents, but maintain low K/Rb ratios, even for low K contents. These authors conclude that the development of an anhydrous high pressure mineral assemblage does not necessarily lead to removal of Rb and K.

Alternatively, Compton (1978b) suggests all Eqalit Gneiss samples were metamorphosed to granulite facies and on retrogression only local chemical changes occurred. This involved either a general depletion in K and Rb during high grade metamorphism, with some areas escaping depletion, or selective addition of K and Rb during the subsequent retrogression.

As opposed to LILE, the REE are considered to remain relatively immobile during very low grade to low grade

metamorphism (Frey et al., 1968; Philipotts et al., 1969; Frey et al., 1974; Muecke et al., 1977). Frey et al. (1968) and Philipotts et al. (1969) examining mid-oceanic ridge basalts (MORB) found no significant differences in REE abundances between fresh and altered basalts. Palagonitization of glassy basalts results in depletion of La and HREE, with the HREE showing no relative fractionation (Frey et al., 1974). In this same study LREE were observed to be enriched during the alteration of crystalline basalt. Studies of low grade Archaean greenstone belts find these lithologies have REE abundances comparable to present day basalt types (Arth and Hanson, 1975; Condie, 1976).

Less data are available on the behaviour of REE during high grade metamorphism. Cullers et al. (1976) study of a pelitic schist, metamorphosed at greenschist to upper amphibolite facies, exhibited no change in REE concentration with increasing grade. Masuda et al. (1971) and Green et al. (1972) report REE patterns for metagabbros and eclogites, respectively, similar to ocean floor basalts.

Studies of the amphibolite to granulite transition in grey gneiss complexes show REE distributions to be unaffected by increased metamorphism (Green et al., 1969, 1972; Drury, 1978; Compton, 1978a, 1978b.)

In contrast to the above studies indicating REE immobility, numerous investigators conclude that REE are

mobile under specific geological conditions (Collerson and Fryer, 1978; Hellman et al., 1979; Nesbitt, 1979; Alderton et al., 1980; Taylor and Fryer, 1980; 1983; Nystrom, 1984).

All these investigators point to the requirement of a large volume of fluid with dissolved species which is responsible for REE mobility.

Hydrothermal and supergene alteration of granitic (s.l.) lithologies, associated with porphyry-type mineral deposits result in REE removal (Alderton et al., 1980; Taylor and Fryer, 1983). Anionic species (F^- , Cl^- , CO_3^{2-}) in the fluid phase complex with REE providing a transport mechanism for their removal. LREE are complexed with Cl^- under low fluid/rock ratios and high pH. With increasing fluid/rock ratios and decreasing pH, F^- and CO_3^{2-} become important anionic species, complexing with and removing HREE from the original lithology (Collerson and Fryer, 1978; Taylor and Fryer, 1983).

5.2.4 Trace Elements

The preceding discussion indicates that the LIL and REE exhibit varying degrees of element mobility under a variety of geologic conditions, reflecting metamorphic grade, fluid-rock interaction, PH_2O , etc. For Maggo gneiss samples the trace elements of interest, exhibiting evidence of mobility are Rb, Sr, Ba, Th and Pb. Trace element concentrations exhibit a much wider scatter of distribution compared with the major element data for the Maggo gneiss. In this section, discussion will be limited to the

distribution of these elements in all gneiss samples, while Section 8.2 considers the response of these elements to Floridian retrogression.

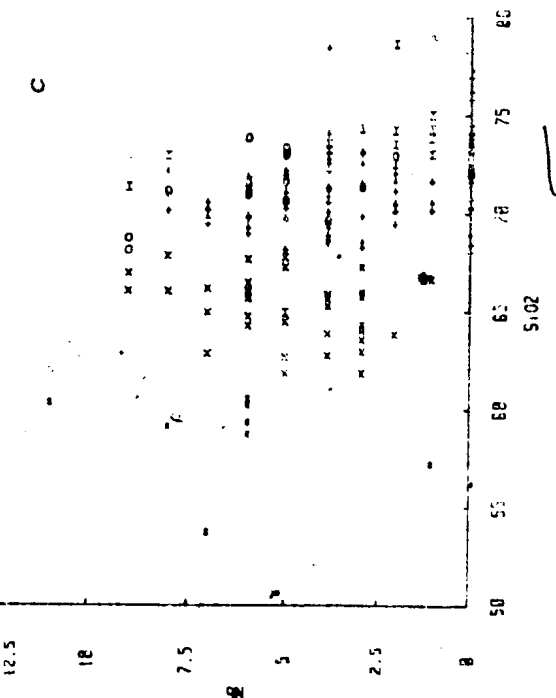
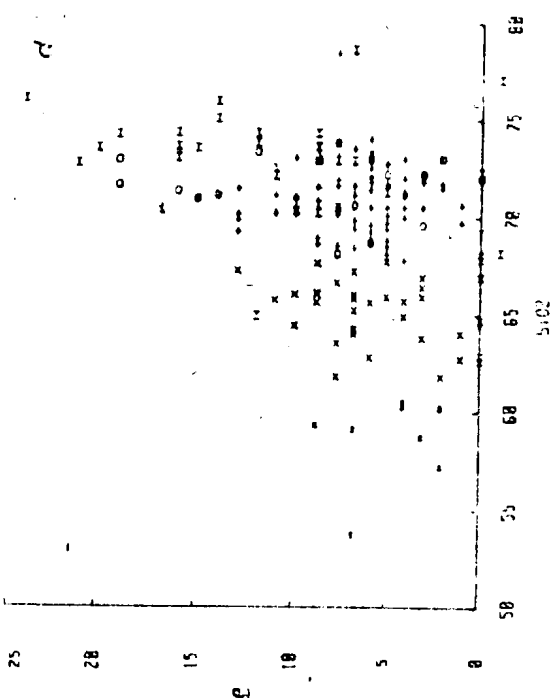
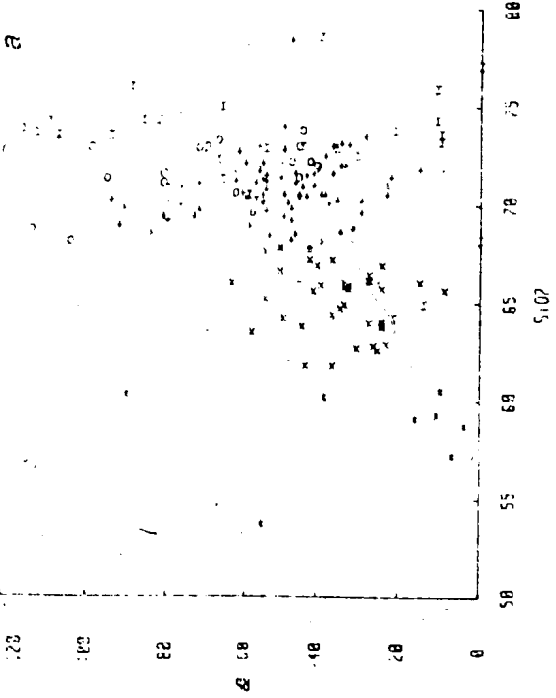
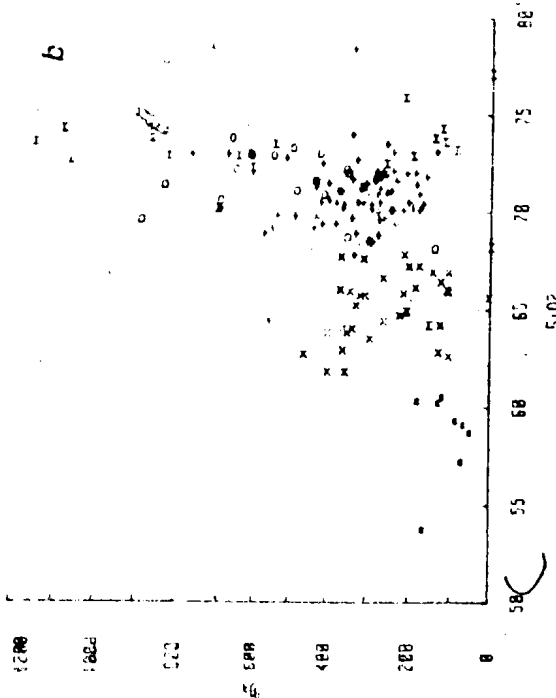
Figure 5.7 presents Harker-type variation diagrams, for Maggo gneiss samples, on which the majority of elements exhibit a scatter of distribution, without any clear correlation with silica content. The chemical subdivisions (based on whole rock chemistry) of the gneiss show no clear distinction between groups on the basis of trace element chemistry. Mean trace element contents for the subgroups have large standard deviations (Table 5.5).

Elements displaying a negative correlation with increasing silica content are Y and V (Figure 5.7 g and h). Cr and Ni (Figure 5.7 i and j) exhibit a negative correlation, however there is a much wider scatter associated with these elements. Other elements, Nb, Zr and Ga (Figure 5.7 c, f and k), define fields of distribution rather than linear trends. The U content (not shown) of the gneiss subgroups is low, < 12 ppm, with the majority of samples having U contents below detection limits for XRF (< 2 ppm).

The elements Rb, Ba, Pb and Sr (Figure 5.7 a, b, d and e) exhibit a weak positive correlation with increasing silica, although these elements all exhibit a wide scatter at high SiO_2 values.

Variations in the ratios K/Rb, CaO/Sr, and K/Ba are shown in Figure 5.8. The K/Rb ratio displays the largest

Figure 5.7: Harker variation diagrams (trace elements) for Maggo Gneiss samples, distinguished according to chemically defined gneiss subgroups, shown in order of increasing compatibility. a) Rb vs SiO_2 ; b) Ba vs SiO_2 ; c) Nb vs SiO_2 ; d) Pb vs SiO_2 ; e) Sr vs SiO_2 ; f) Zr vs SiO_2 ; g) Y vs SiO_2 ; h) V vs SiO_2 ; i) Cr vs SiO_2 ; j) Ni vs SiO_2 ; k) Ga vs SiO_2 . Symbols as in Figure 5.2.



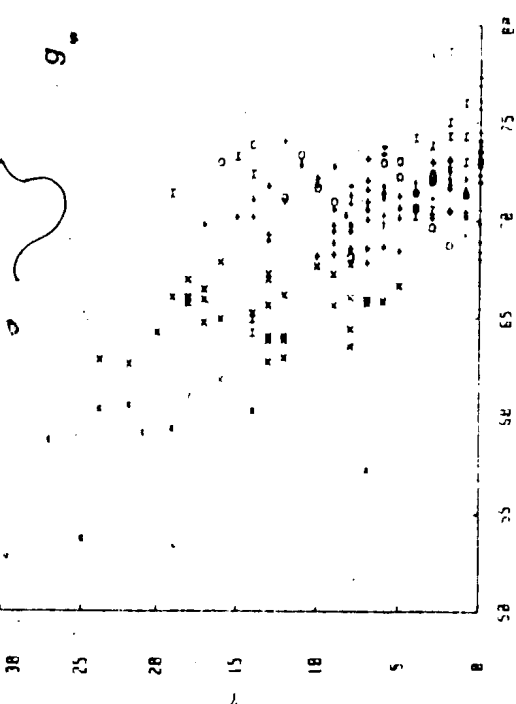
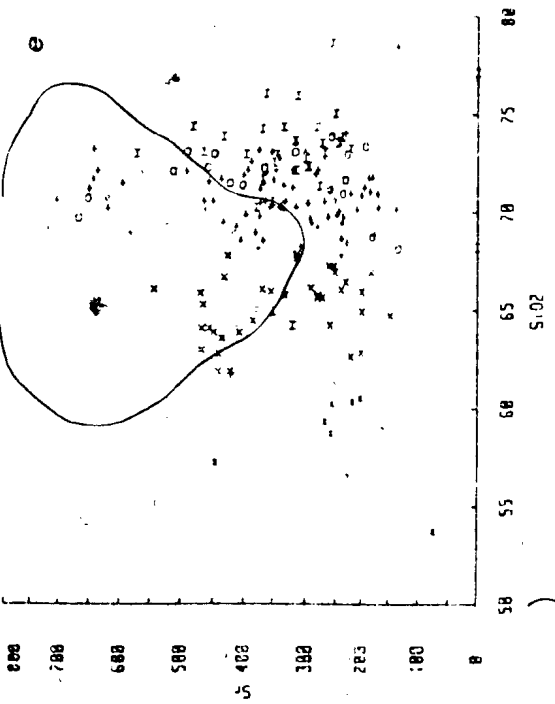
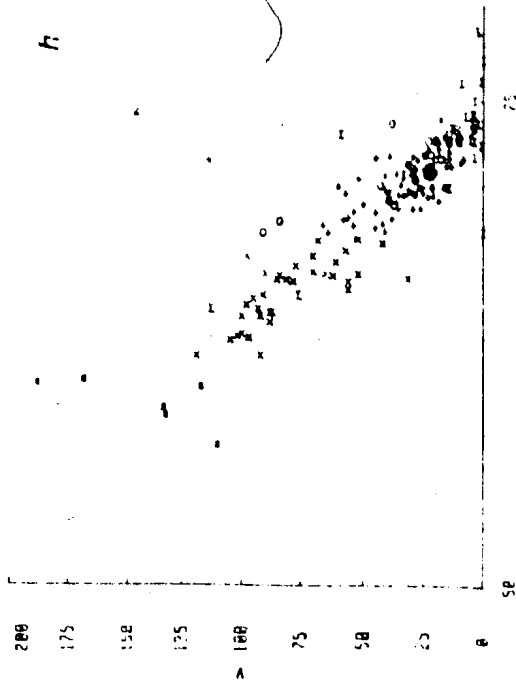
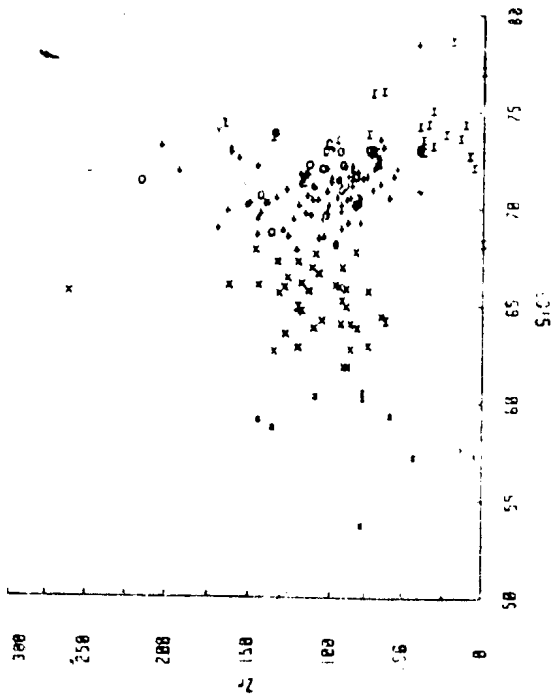
0
202
201
200
199
198
197

0
202
201
200
199
198
197

0
202
201
200
199
198
197

0
202
201
200
199
198
197

00190



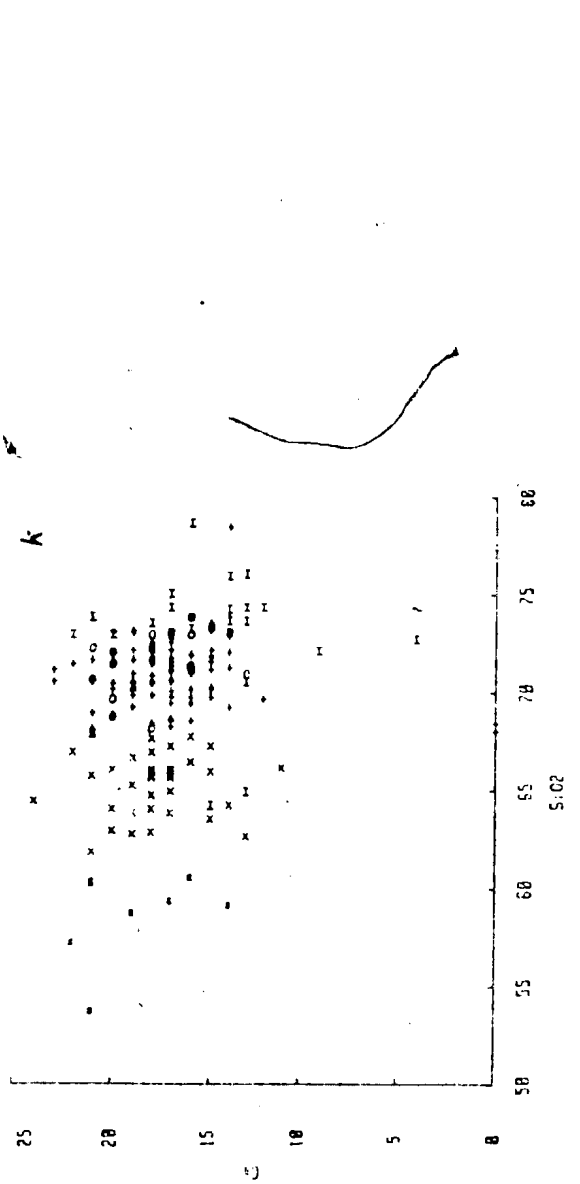
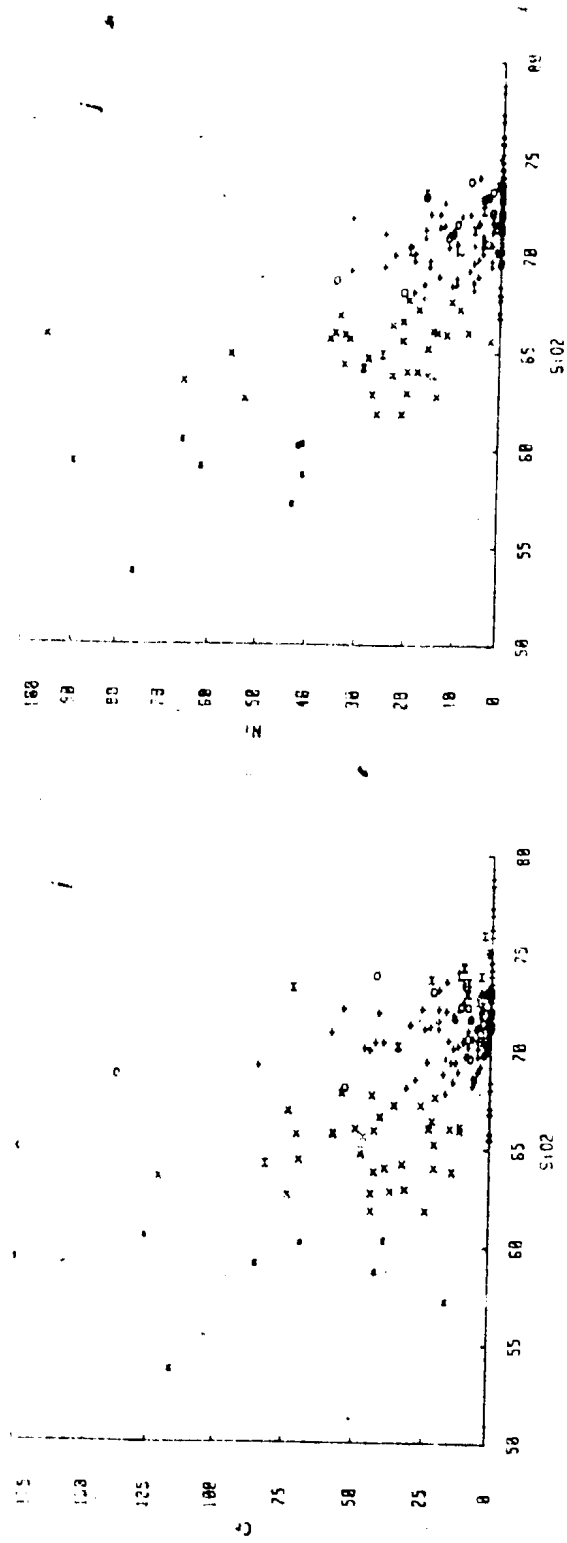
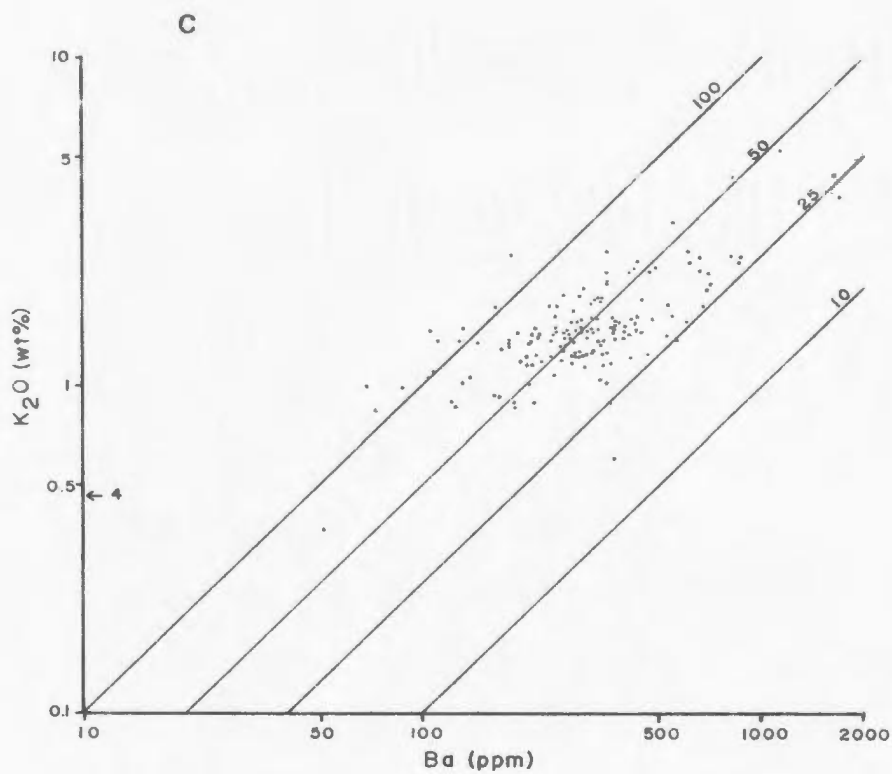
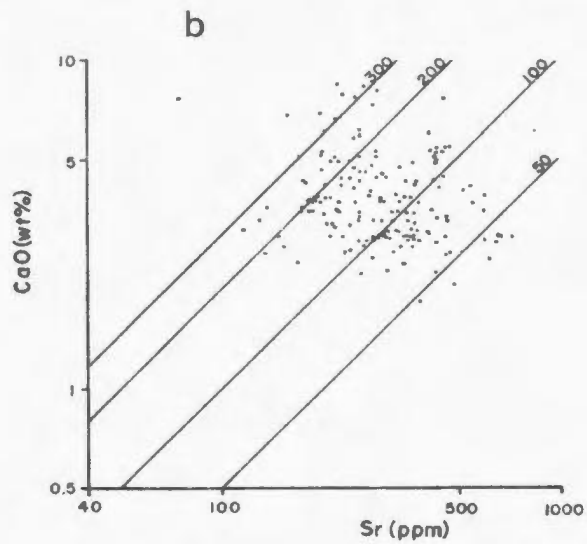
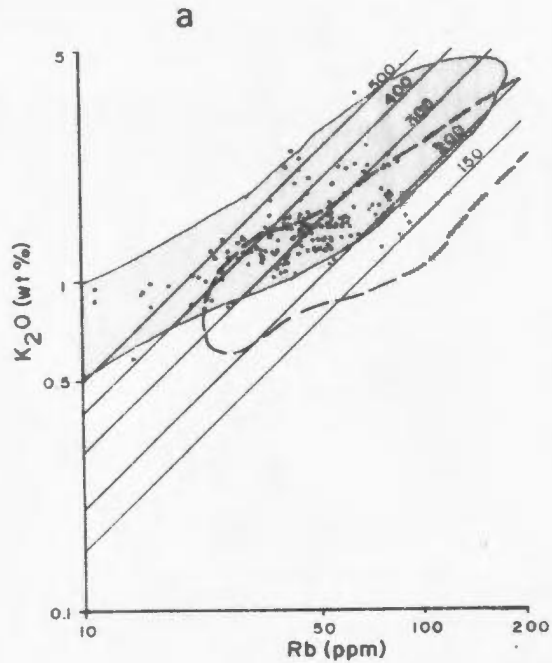


Figure 5.8: Element ratio diagrams.

- a) K_2O vs Rb - The shaded region is the field for the Nuk Gneiss, SW Greenland (Compton, 1978b). The data for the Ulvak I gneiss, northern Labrador (Collerson and Bridgwater, 1979) is enclosed by the dashed line.
- b) CaO vs Sr
- c) K_2O vs Ba.



variation from 165 to 984 (Figure 5.8a). Shaw (1968) predicted that normal igneous suites undergoing differentiation would have a near constant K/Rb ratio. The wide range in Maggo gneiss K/Rb ratios suggests that these elements have been mobile during development of the gneiss complex. On a plot of K/Rb vs K_2O (not shown) the Maggo gneiss data exhibit considerable scatter. The lack of a good correlation between K_2O and K/Rb is interpreted to reflect changes in the distribution of these two elements after the gneiss protolith was formed.

The variation in K/Rb ratio of the Maggo gneiss is similar to that reported for the Nuk gneiss of southwest Greenland (shaded field on Figure 5.8a, from Compton, 1978b). Nuk gneiss K/Rb ratios, approach 4000 in samples which have undergone granulite facies metamorphism. This extreme depletion of Rb, and to a lesser degree K, is not recorded in the Maggo gneiss. The K/Rb ratios are higher than those for the Uivak gneiss of northern Labrador, which define a very tight field (Figure 5.8a) about a mean K/Rb value of 230 (Collerson and Bridgwater, 1979).

The CaO/Sr ratio (40 to 400, Figure 5.8b) and K/Ba ratios (16 to 143, Figure 5.8c) likewise exhibit a wide scatter. If the Maggo gneiss protolith chemistry were unaffected by later metamorphic events, i.e. isochemical metamorphism, the CaO/Sr ratios would vary, however they should still define a smooth trend. The wide scatter exhibited for this ratio (Figure 5.8b) is interpreted to

reflect the mobility of these two elements in response to metamorphic events. Similarly, no correlation exists between K and Ba, as evidenced by the variable K/Ba ratios, and Ba and Rb (not shown).

The lack of any inter-element correlations and the variable ratios exhibited by the Maggo gneiss are the opposite of that expected if the element distributions reflect some primary crystallization or melting process which gave rise to the gneiss protolith. The element distributions and ratios recorded for the Maggo gneiss are interpreted then to reflect the mobility of these species during subsequent deformation and metamorphism. The extent to which this mobility results from the Hopedalian and/or Flordian events will be discussed in Section 6.2.

5.2.5 Rare Earth Elements

Rare earth elements (REE) were determined using the thin film X-ray fluorescence method of Eby (1972) as modified by Fryer (pers. comm., 1984). The relative precision and accuracy of this method are discussed in Appendix B.

REE distributions in the Maggo gneiss have been determined in order that the parental composition, the mode of origin for the gneiss precursors and any primary trends preserved in the gneiss may be studied. As well the REE are believed to be relatively immobile during greenschist to amphibolite facies metamorphism. The Hopedale Block, with the transition from the Hopedalian to Flordian domain

provides an opportunity to examine the effects of reworking at amphibolite facies on the REE.

REE abundances and chondrite normalized plots of representative Maggo gneiss samples, from the chemically defined gneiss subgroups, are presented in Tables 5.6 to 5.9 and Figures 5.9 to 5.12, respectively. The Maggo gneiss REE data exhibits a rather restricted range of distributions. Another feature of the REE patterns is the nature of the Eu anomaly. Overall, Maggo gneiss samples exhibit no consistent pattern, i.e. enriched, depleted and normal Eu contents are all recorded. The nature of the Eu anomaly may be used to further subdivide all gneiss subgroups into two classes;

- 1) Class I - display negative Eu anomalies.
- 2) Class II - display positive to normal abundances.

REE data for analyzed samples of the diorite subgroup, (Table 5.6, Figure 5.9) display the least fractionated REE patterns. Typically this subgroup has LREE from 14 to 75X chondrites and HREE contents at 1.3 to 8.7X chondrite. The two classes of REE pattern types are observed for the diorite subgroup. Class I diorite patterns, represented by samples 83-252 and 274, are characterized by a marked negative Eu anomaly (mean $\text{Eu}/\text{Eu}^* = 0.42$) and depleted HREE. The remaining samples, defining the class II diorites, are characterized by near linear (83-203, 299), to convex upward patterns, (83-182).

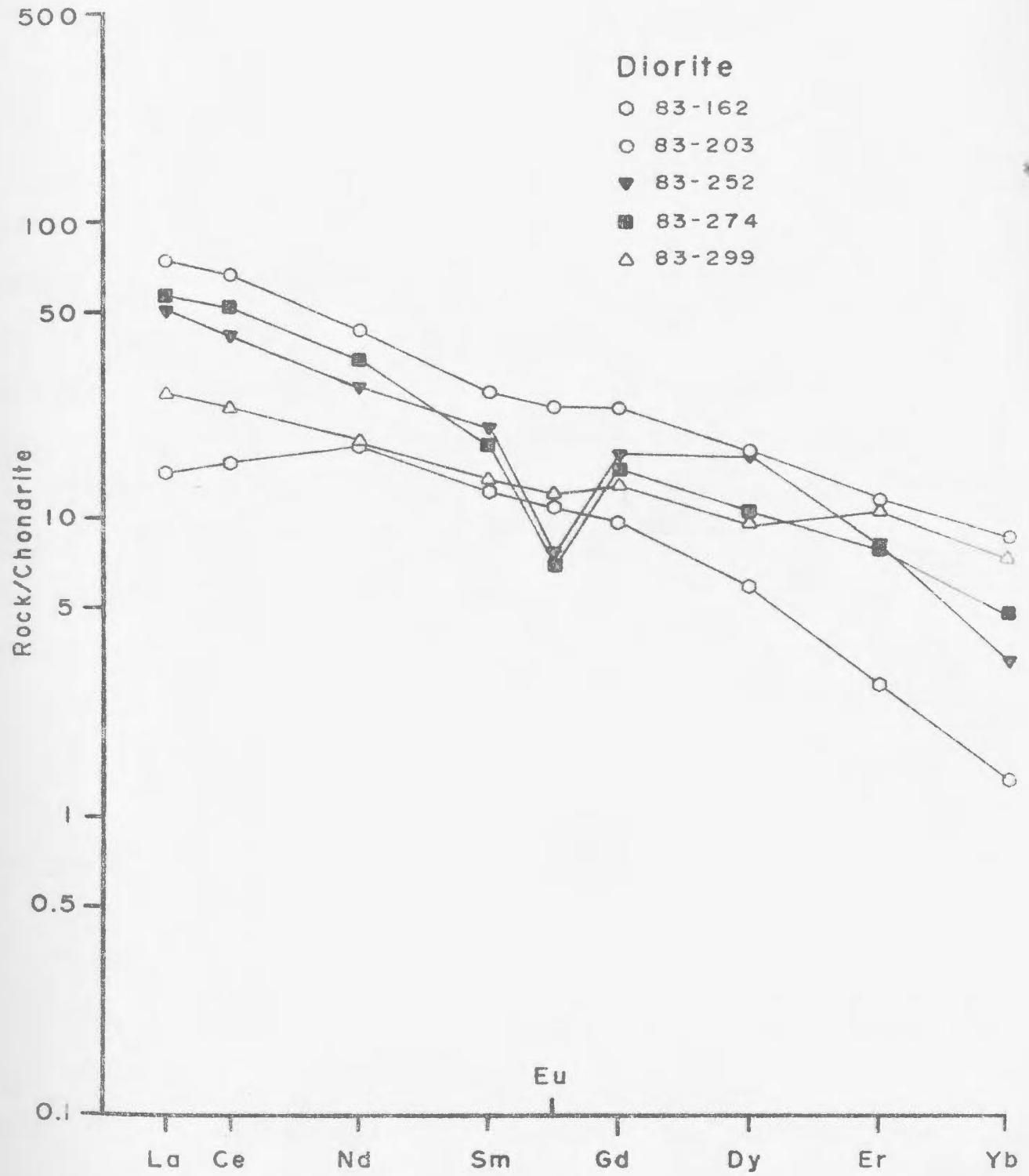
00197

Table 5.6: Rare Earth Element concentrations, in parts per million, for the Diorite Subgroup, Maggo gneiss.

Sample	83-162	83-203	83-252	83-274	83-299
La	4.5	23.4	15.8	17.7	8.3
Ce	12.6	54.0	33.8	42.2	19.0
Pr	2.1	6.5	4.5	5.3	2.4
Nd	10.4	25.7	16.5	20.5	10.7
Sm	2.4	5.2	3.9	3.4	2.6
Eu	0.8	1.7	0.5	0.5	0.9
Gd	2.5	6.0	4.1	3.8	3.3
Dy	1.9	5.4	5.3	3.4	3.0
Er	0.6	2.4	1.7	1.6	2.2
Yb	0.3	1.8	0.7	1.0	1.5
Σ REE	38.1	132.1	86.8	99.4	53.9
(Ce/Er) _N	5.5	5.89	5.21	6.91	2.26
Eu/Eu*	1.0	0.94	0.42	0.42	0.92

28100

Figure 5.9: Chondrite normalized REE distribution patterns for dioritic gneiss subgroup samples (Data in Table 5.4). All REE presented are normalized using the values (given in Appendix B) of Masuda et al. (1973).



A measure of the relative degree of fractionation of the REE can be obtained by examining the normalized ratio of a LREE to a HREE (O'Nions and Pankhurst, 1974a). For example, a sample derived from a chondritic source, i.e. the mantle, displaying a normalized ratio of 1 indicates that the REE have not been subjected to any fractionation affects during formation of the analyzed unit. A ratio of < 1 indicates that the HREE are fractionated into the liquid over the LREE. If the LREE are preferentially incorporated into the liquid and the HREE retained in the solid, then the ratio will be > 1 . In this study the $(Ce/Er)_N$ ratio is used to indicate the degree of REE fractionation recorded for the Maggo gneiss.

The $(Ce/Er)_N$ ratios for the diorite subgroup lie between 5 and 7, indicating the REE have undergone some fractionation during the formation of this subgroup. One sample (83-299) has a weakly fractionated pattern ($(Ce/Er)_N = 2.26$) representing a low degree of REE fractionation for this sample.

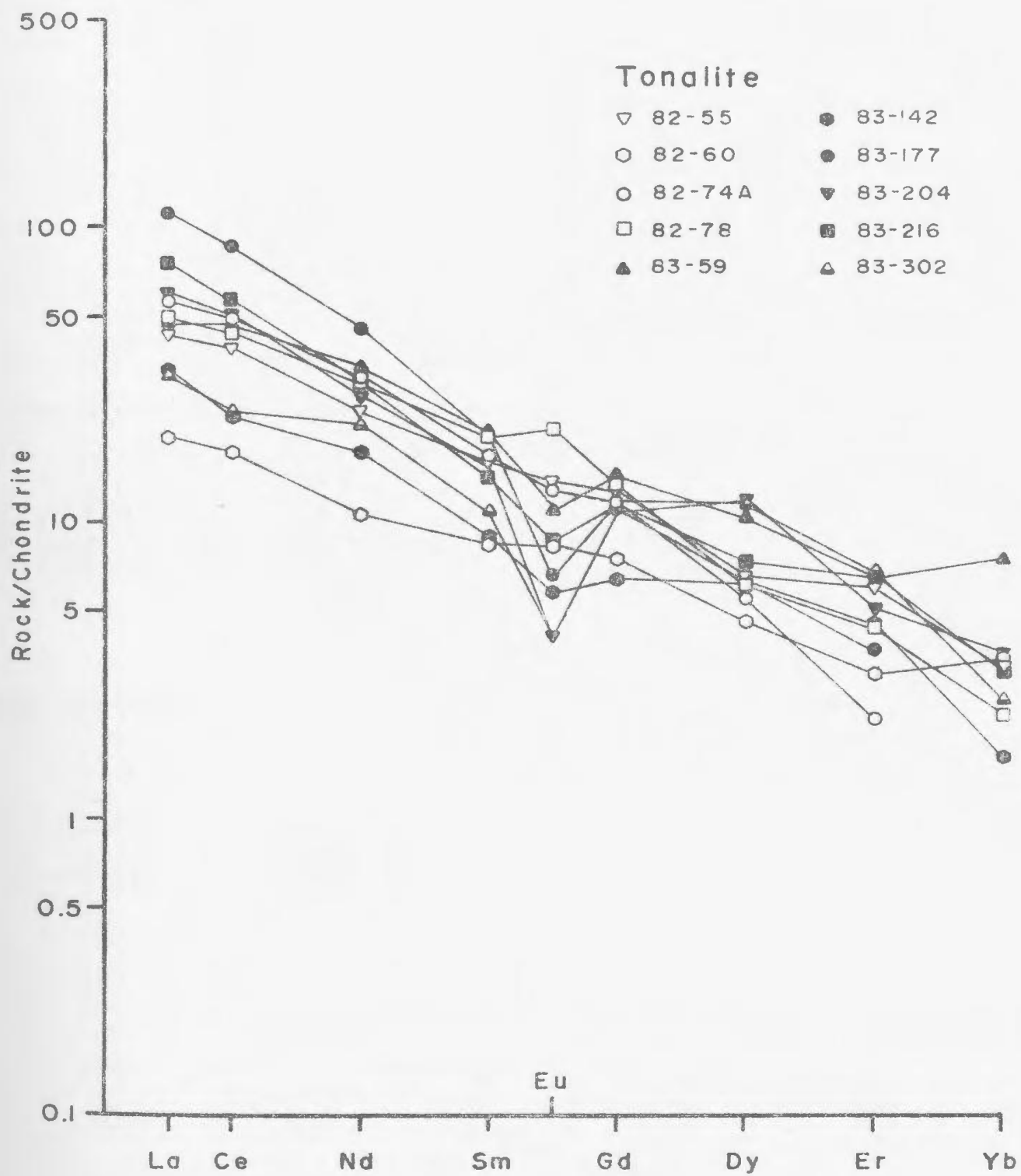
Representative REE concentrations and normalized REE patterns for the tonalitic gneiss subgroup are presented in Table 5.7 and Figure 5.10, respectively. The tonalite subgroup can be subdivided on the basis of the observed Eu anomaly. Class I tonalites, (solid symbols, Figure 5.10) have moderate, negative Eu anomalies, Eu/Eu^* from 0.10 to 0.77, are enriched in LREE (29-115X chondrites) and depleted in HREE (1.6-8.8X chondrites). The $(Ce/Er)_N$

Table 5.7: Representative Rare Earth Element concentrations, in parts per million, Tonalite Subgroup, Maggo gneiss.

Sample	82-55	82-60	82-74A	83-78	83-59
La	13.7	6.1	17.7	15.7	15.2
Ce	31.8	14.1	39.9	25.8	37.8
Pr	3.5	1.7	4.7	4.0	4.5
Nd	14.2	6.3	18.3	17.8	20.0
Sm	3.2	1.7	3.3	3.9	3.9
Eu	1.0	0.61	0.9	1.5	0.8
Gd	3.1	2.0	2.8	3.5	3.7
Dy	2.1	1.5	1.8	2.0	3.3
Er	1.3	0.7	0.5	0.9	1.4
Yb	0.7	0.7	0.2	0.5	1.6
Σ REE	74.6	35.5	90.4	76.2	92.2
(Ce/Er) _N	6.6	5.7	22.2	7.2	7.1
Eu/Eu*	0.97	1.05	0.90	1.28	0.64
Sample	83-142	83-177	83-204	83-216	83-302
La	10.3	35.3	18.9	23.8	7.1
Ce	18.4	70.6	40.8	46.3	11.2
Pr	2.6	7.6	4.8	4.3	2.9
Nd	10.3	27.0	16.4	17.5	10.5
Sm	1.7	3.8	3.0	2.8	2.0
Eu	0.4	0.5	0.3	0.6	0.3
Gd	1.7	3.0	2.8	2.8	3.2
Dy	2.0	2.0	3.8	2.4	2.7
Er	1.0	0.8	1.1	1.4	1.5
Yb	0.3	n.d.	0.7	0.7	0.5
Σ REE	48.7	150.6	92.6	102.6	41.9
(Ce/Er) _N	4.8	23.1	9.7	8.7	2.0
Eu/Eu*	0.75	0.45	0.32	0.68	0.32

n.d. - not detected

Figure 5.10: Chondrite normalized REE distribution patterns for representative tonalitic gneiss samples (Data in Table 5.1). Solid symbols - Class I tonalite, open symbols Class II tonalite (See text for discussion).

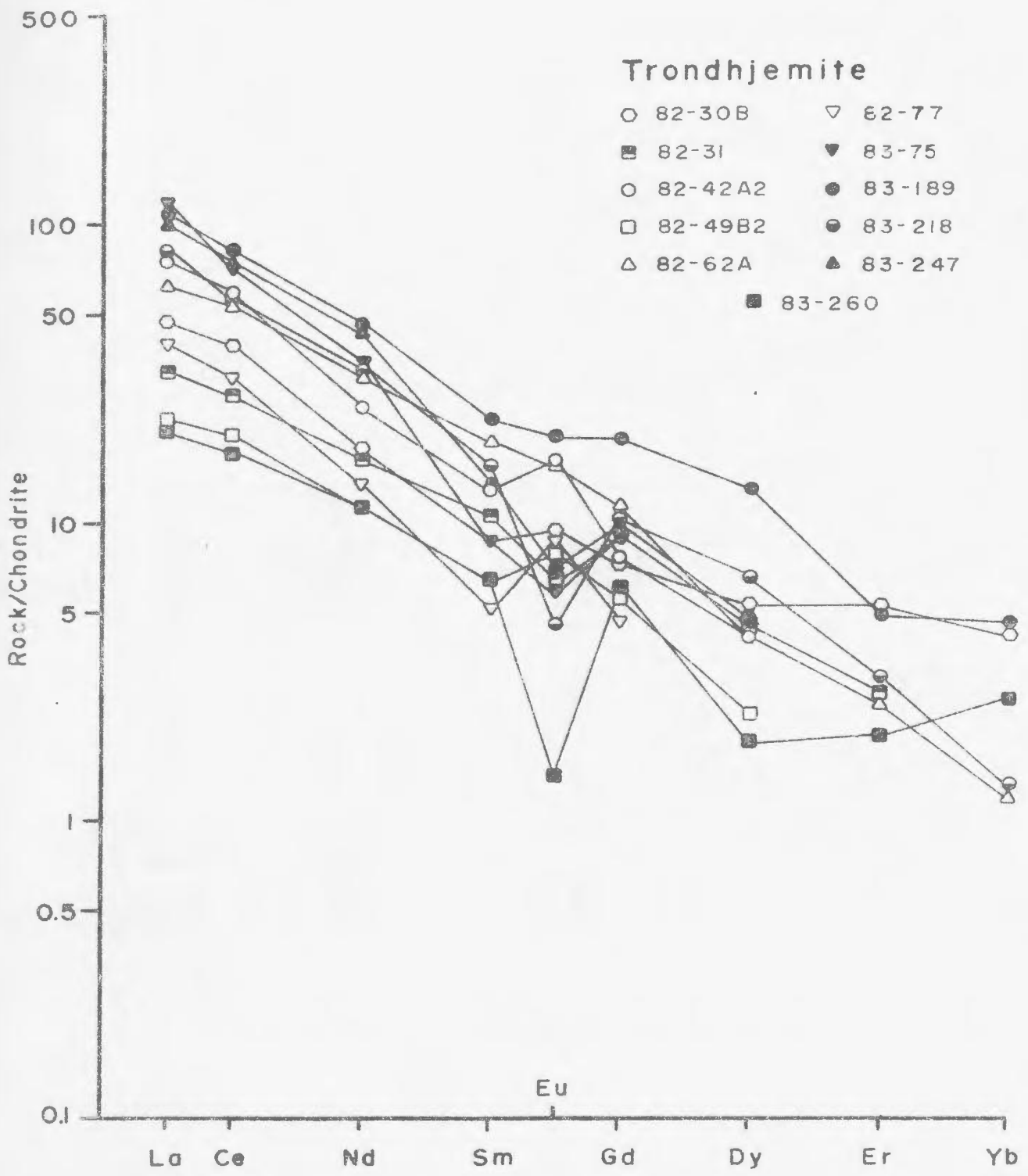


ratios vary from 2 to 23, indicating a range in the relative degree of fractionation for the class I tonalites. This enrichment-depletion gives the tonalites a steeper REE pattern than the dioritic gneiss samples on average. REE patterns for class I tonalites are comparable to amphibolite facies gneiss samples of the Lewisian Complex (Drury, 1978).

Class II tonalite samples (open symbols, Figure 5.10) exhibit positive to absent Eu anomalies, with Eu/Eu^* from 1.0 to 1.38. The degree of LREE enrichment (19.5 to 75X chondrites) and HREE depletion (0.92 to 4.5X chondrites) in this class is comparable to that in class I samples. There is a tendency for lower, average LREE abundances in class II tonalites. However, the range of $(\text{Ce}/\text{Er})_N$ ratios, 5.7 to 7.2, for this class indicate lower degrees of fractionation. The degree of enrichment-depletion observed in the REE patterns for the class II tonalites are similar to the granulite facies gneiss samples of the Lewisian Complex (Drury, 1978), but Hopedale Block samples have a less pronounced, positive Eu anomaly.

The trondhjemitic subgroup of the Maggo gneiss have steeper LREE enriched-HREE depleted patterns than the previous subgroups (Figure 5.11, Table 5.8). As with the tonalites, the trondhjemitic subgroup can be subdivided into two classes, based on the nature of the Eu anomaly. Class I trondhjemitic gneiss samples are characterized by negative Eu anomalies ranging from 0.94 to 0.22 (solid

Figure 5.11: Chondrite normalized REE distribution patterns for representative trondhjemitic gneiss samples (Data in Table 5.2). Solid symbols - Class I trondjemite, open symbols - Class II trondjemite.



00207

Table 5.8: Representative Rare Earth Element concentrations, in parts per million, Trondhjemite Subgroup, Maggo gneiss.

Sample	82-30B	82-31	82-42A2	82-49B2	82-46
La	15.0	10.1	23.5	7.0	19.7
Ce	32.0	22.0	48.4	16.1	44.3
Pr	2.4	2.2	3.8	1.9	5.0
Nd	10.5	9.8	14.9	6.8	18.9
Sm	1.7	2.1	2.6	1.3	3.7
Eu	0.7	0.5	1.2	0.6	1.1
Gd	1.9	2.1	2.6	1.3	3.7
Dy	1.7	1.4	1.3	0.72	1.3
Er	1.1	0.55	0.16	0.19	0.5
Yb	0.9	n.d.	n.d.	n.d.	0.24
Σ REE	68.0	50.75	98.46	35.96	98.44
(Ce/Er) _N	7.5	10.5	71.0	22.3	22.8
Eu/Eu*	1.18	0.70	1.63	1.36	1.04

Sample	82-77	83-75	83-189	83-218	83-247
La	12.7	36.6	33.7	25.5	31.9
Ce	25.3	60.7	66.4	46.4	62.1
Pr	2.3	6.4	6.6	5.2	6.2
Nd	8.0	20.3	27.9	20.2	26.1
Sm	1.0	1.7	4.4	3.0	2.7
Eu	0.6	0.4	1.4	0.3	0.5
Gd	1.2	2.3	5.0	2.6	2.5
Dy	0.2	1.6	4.2	2.1	1.6
Er	n.d.	n.d.	1.0	0.6	n.d.
Yb	n.d.	n.d.	1.0	0.3	n.d.
Σ REE	51.3	130.0	151.6	106.2	133.7
(Ce/Er) _N			17.4	20.3	
Eu/Eu*	1.79	0.57	0.94	1.32	0.63

n.d. - not detected

02208

symbols, Figure 5.11), and the degree of LREE enrichment (20-119X chondrites) is greater than that of class II samples. The HREE abundance distribution for class I trondhjemite (0.5-4.6X chondrites) overlap with those of class II.

Class II trondhjemites (open symbols, Figure 5.11) are characterized by positive Eu anomalies, with a more restricted range of LREE (22-75X chondrites) than class I samples. This trondhjemite class is depleted in HREE to a greater degree than class I samples with HREE abundances from 4 to < 1X chondrites. The $(Ce/Er)_N$ ratios (20 to > 71) for the trondhjemitic subgroup are greater than those of the previous two subgroups. The increased ratio reflects a higher degree of fractionation of the REE during the formation of this chemical subgroup.

The granodioritic gneiss subgroup display the most fractionated REE patterns of all Maggo gneiss samples (Figure 5.12, Table 5.9) with $(Ce/Er)_N$ ratios ranging from 24 to 134. Class I granodiorites (solid symbols, Figure 5.12) have LREE abundances from 125-285X chondrites, HREE abundances from 1-10X chondrites and negative Eu anomalies. These samples exhibit the largest $(Ce/Er)_N$ ratios of all gneiss samples analyzed.

Class II granodiorites show a lower degree of LREE (31-65X chondrites) enrichment and are more strongly depleted in HREE. Er values are less than those for the class I granodiorite samples (Er from 0.55-1.92X

Figure 5.12: Chondrite normalized REE distribution patterns for representative granodioritic gneiss samples (Data in Table 5.3). Solid symbols - Class I granodiorite, open symbols - Class II granodiorite.

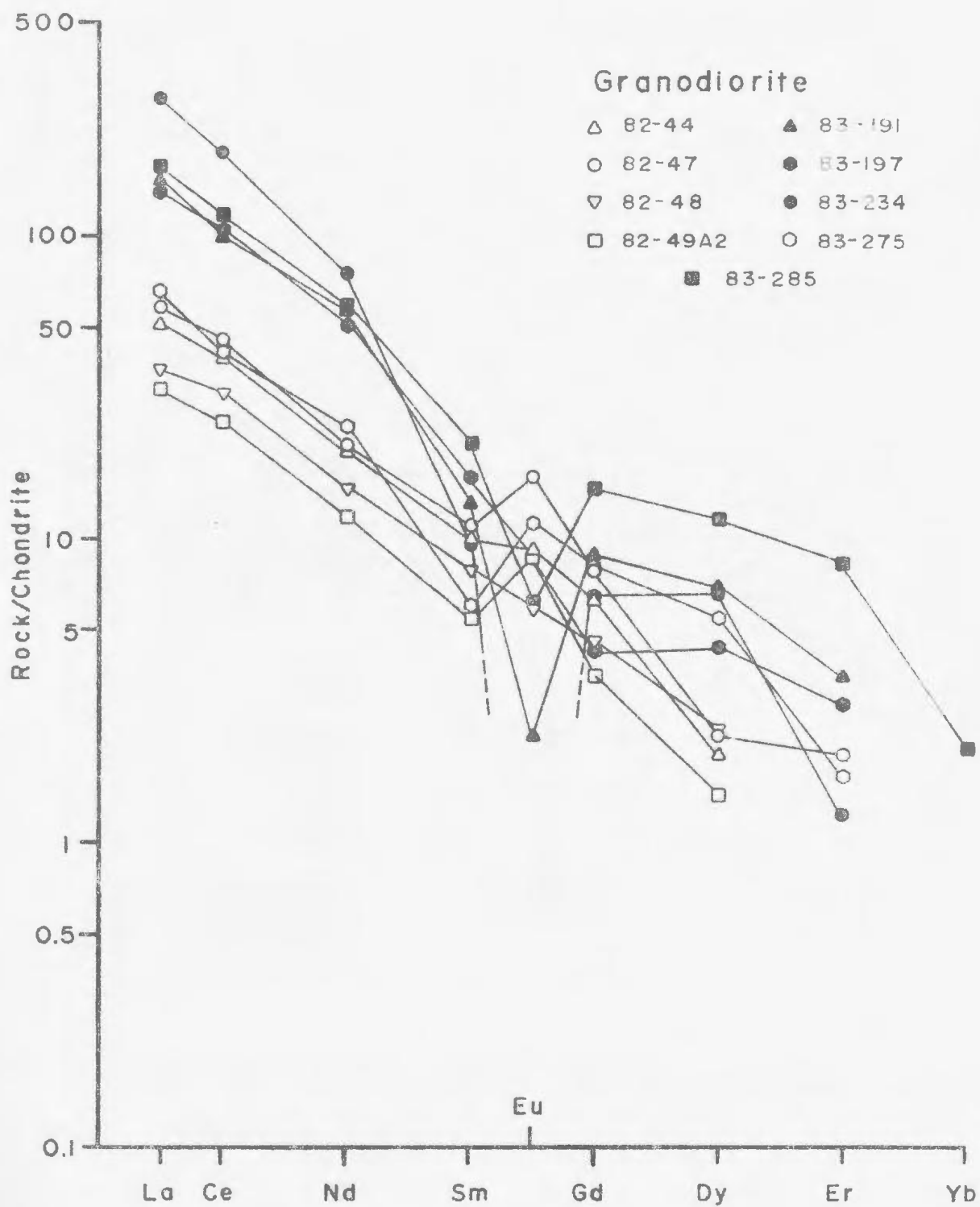


Table 5.9: Rare Earth Element concentrations, in parts per million, for the Granodiorite Subgroup, Maggo gneiss.

Sample	82-44	82-47	82-48	82-49A2	83-191
La	16.2	18.3	11.5	9.9	48.0
Ce	32.2	37.5	24.5	19.8	81.2
Pr	3.3	2.9	2.5	1.6	9.5
Nd	11.7	12.2	8.8	7.1	33.4
Sm	2.0	2.2	1.6	1.05	2.6
Eu	0.7	1.2	0.4	0.6	0.2
Gd	1.8	2.05	1.2	1.2	2.3
Dy	0.6	0.7	0.8	0.5	2.2
Er	0.12	0.4	0.15	n.d.	0.7
Yb	n.d.	n.d.	n.d.	n.d.	n.d.
Σ REE	68.42	77.56	51.45	41.75	180.1
(Ce/Er) _N	70.3	24.0	42.8		30.4
Eu/Eu*	1.17	1.76	0.94	2.05	0.19

Sample	83-197	83-234	83-275	83-285
La	43.2	88.8	20.7	53.2
Ce	84.6	153.2	33.4	95.6
Pr	8.6	14.4	4.4	10.1
Nd	30.1	44.2	14.2	35.2
Sm	3.2	1.9	1.2	4.1
Eu	0.7	n.d.	0.8	0.4
Gd	1.1	1.6	2.1	3.8
Dy	1.4	2.2	1.8	3.7
Er	0.6	0.2	0.3	1.8
Yb	n.d.	n.d.	n.d.	0.4
Σ REE	173.5	306.6	78.9	208.3
(Ce/Er) _N	36.9	133.8	28.2	62.6
Eu/Eu*	1.15		1.7	0.35

n.d. - not detected

chondrites). The Eu anomaly for class II granodiorites is positive with Eu/Eu^* from 1.17 to 2.05.

5.2.5.1 Discussion

The increase in the degree of REE fractionation is reflected in the fields of REE distribution for each gneiss subgroup. The fields shown on Figure 5.13 encompass all REE patterns for all analyzed samples from each subgroup. With an increase in the degree of 'fractionation', i.e. from diorite to granodiorite, the REE fields steepen, becoming more LREE enriched and HREE depleted.

The further subdivision of the gneiss subgroups into two classes based on the nature of the Eu anomaly is possible. Class I samples display negative Eu anomalies and have higher total REE contents, as compared to class II samples which exhibit positive to normal Eu anomalies and lower total REE contents. The recognition of grey gneisses characterized by positive and negative Eu anomalies has been reported for tonalitic gneisses of southern India (Condle et al., 1982) and the Lewisian gneiss of Scotland (Drury, 1978).

The presence of the two classes of REE patterns for Maggo gneiss indicates that either the two classes represent two distinct, different lithologies intimately intermixed on the outcrop scale, or an evolutionary link exists between the two classes. The evolutionary link may reflect either differentiation of the original, primary composition or some means of differentiation under

1230

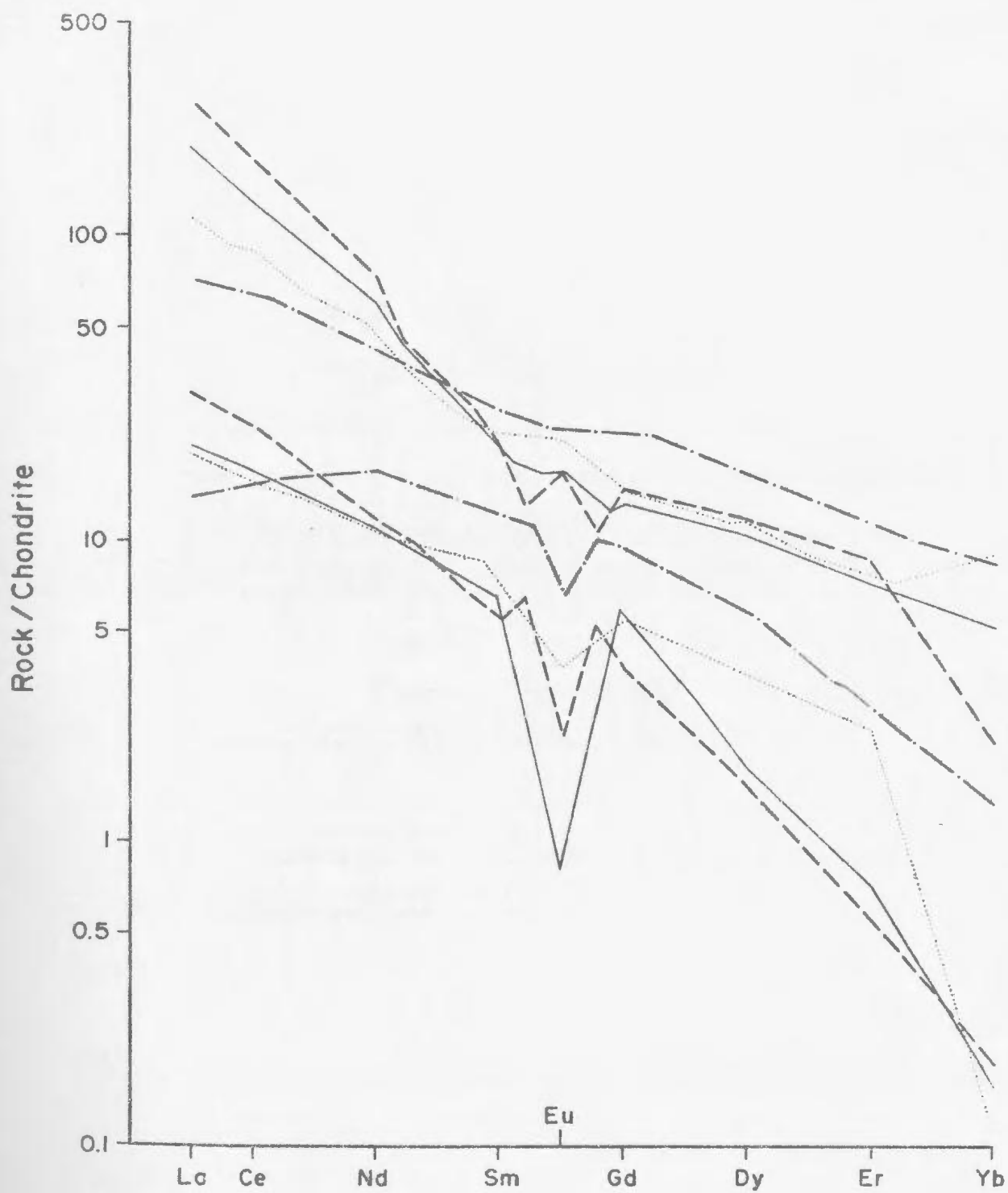
Figure 5.13: Ranges of REE distribution for chemically defined gneiss subgroups of the Maggo gneiss. The individual groups overlap, however, there is a progressive enrichment in LREE (La to Sm) and depletion in HREE (Gd to Yb) with increasing fractionation. Symbols:

dioritic gneiss - - - - -

tonalitic gneiss

trondhjemitic gneiss _____

granodioritic gneiss - - - - -

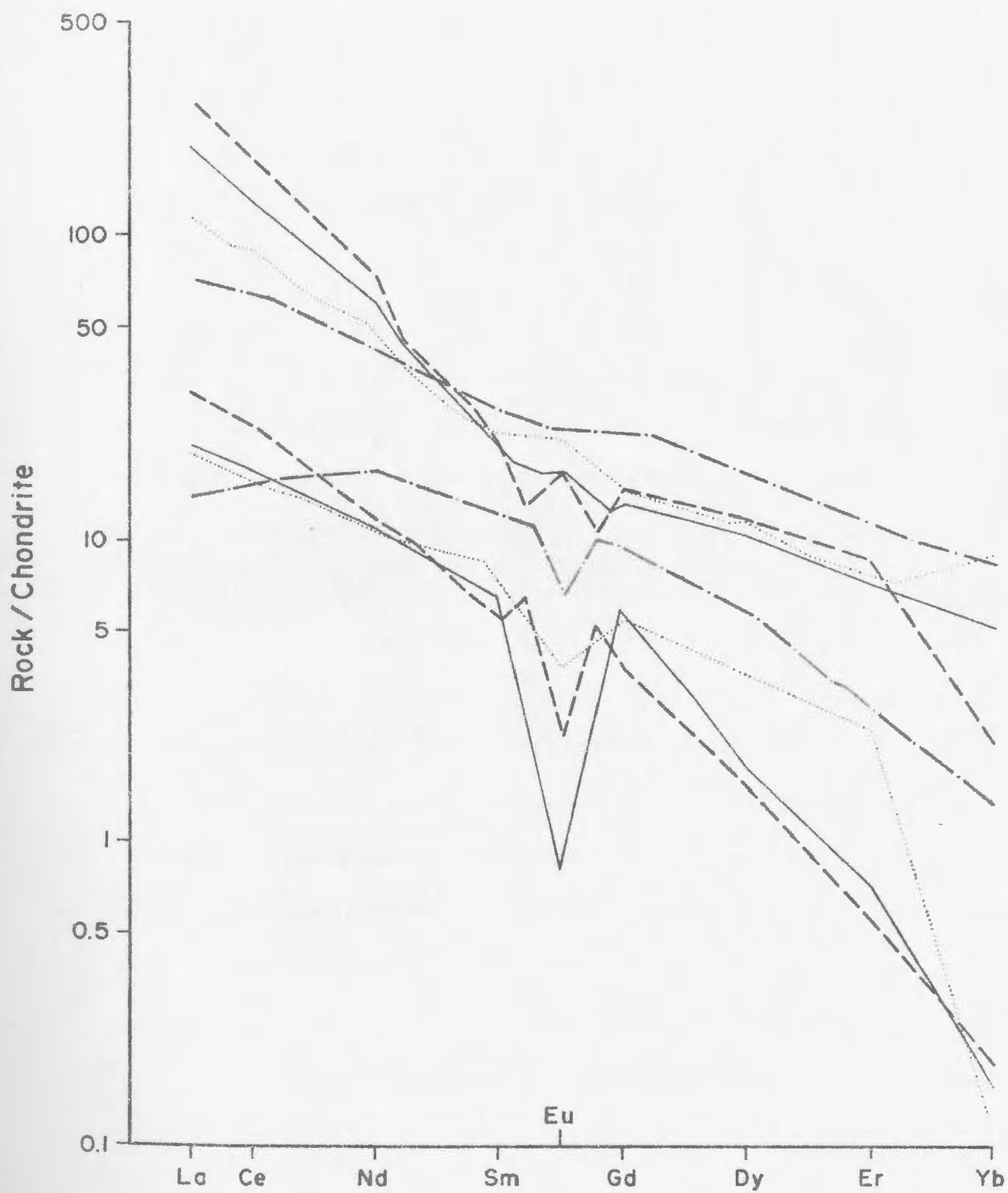


metamorphic conditions. Consideration of the field relationships and geochemical results (major, trace and REE data) for samples from the Black Head Tickle geochronology suite are considered in documenting the link between the two class types.

Black Head Tickle samples 83-264 and 265 consist of hornblende tonalite which occurs as concordant boudins within the dominant biotite tonalite (Samples 83-261 and 263; See Figure A.6 and Plate 5E). All samples fall within the trondhjemite subgroup, with the former displaying negative Eu anomalies and the latter positive (Eu/Eu^*) values (Figure 5.14). On various 2-component variation diagrams (not shown) all samples from Black Head Tickle plot in a single field, with no clear separation of the two classes. The results of the isotopic analysis of these samples, when regressed, yield an errorchron (MSWD = 5.7) which is attributed to resetting after the gneiss complex has stabilized. The Black Head Tickle samples are interpreted to represent a suite of genetically related samples. Using the same criteria similar results can be obtained for class I and II REE analyses for groups of localized samples.

With the establishment that a genetic link may exist between the two classes within each subgroup, what fractionation mechanism or mechanisms would produce the observed REE patterns for the Maggo gneiss samples? The contrast in REE patterns suggests that either 1)

Figure 5.14: REE patterns for the two trondhjemite classes, as represented by samples from Black Head Tickle. The dichotomy in REE patterns for the two classes are interpreted to reflect variations in the source material to the Maggo gneiss and magmatic processes affecting the derived liquid.



metamorphic differentiation during development of the Hopedale Block, or 2) variable source composition and/or magmatic differentiation prior to metamorphism and deformation may be responsible for the different classes.

5.2.5.2 Metamorphic Differentiation

If metamorphic differentiation is responsible for the two REE classes, which event, of those recognized, is responsible for the REE patterns recorded for the Maggo gneiss samples? Within the Hopedalian (D_{n+2}) and Flordian (D_{n+3}) domains there is no evidence for two distinct metamorphic grades (e.g. granulite and amphibolite facies), of similar age, which would result in the separation of the two classes. Further, both classes of REE patterns are recorded for localized samples within a single domain, e.g. Black Head Tickle (Figure 5.14). Discussion of the effects of Flordian reworking on the Hopedalian domain lithologies and the response of the REE are considered in Section 6.2.

Metamorphic differentiation seems an unlikely mechanism to produce the observed dichotomy in Maggo gneiss REE patterns because of the complex metamorphic and tectonic history recorded for the Hopedale Block.

5.2.5.3 Magmatic Differentiation

The contrasting REE patterns for class I and II gneiss samples are characteristic of those expected during removal of plagioclase (class II) by fractional crystallization of a parent magma, leaving a residual melt (class I). The REE patterns reported for the Maggo gneiss are comparable to

those reported for unmetamorphosed Archaean granitic plutons (Condle *et al.*, 1985; 1986).

The separation of the two class types also reflects, to some extent, mineralogical variations in the parent material to the Maggo gneiss. Partial melting of mineralogically different sources can result in comparable REE patterns, displaying Eu enrichment and depletion, controlled by variations in source mineralogy (see Section 6.5.4).

Derivation of the Maggo gneiss from a variety of parent compositions followed by magmatic processes, i.e. fractionation, can explain the two types of REE patterns observed.

Based on the REE patterns (Figure 5.14) the hornblende tonalite (83-265) represents a phase of the gneiss precursor which has 1) accumulated hornblende (reflected in the enriched HREE) and 2) undergone plagioclase fractionation (negative Eu anomaly). The effects of the hornblende retention and plagioclase removal are seen in the pattern for Sample 83-265, i.e. enriched HREE with respect to 83-263 and the negative Eu anomaly, reflecting the residual liquid composition. The REE patterns for these two samples, from the two trondhjemite classes, appear to be complimentary to each other.

5.2.5.4 Comparison With NAC Grey Gneiss Complexes

Maggo gneiss REE abundances exhibit a restricted range of distribution, similar to those reported for grey gneiss

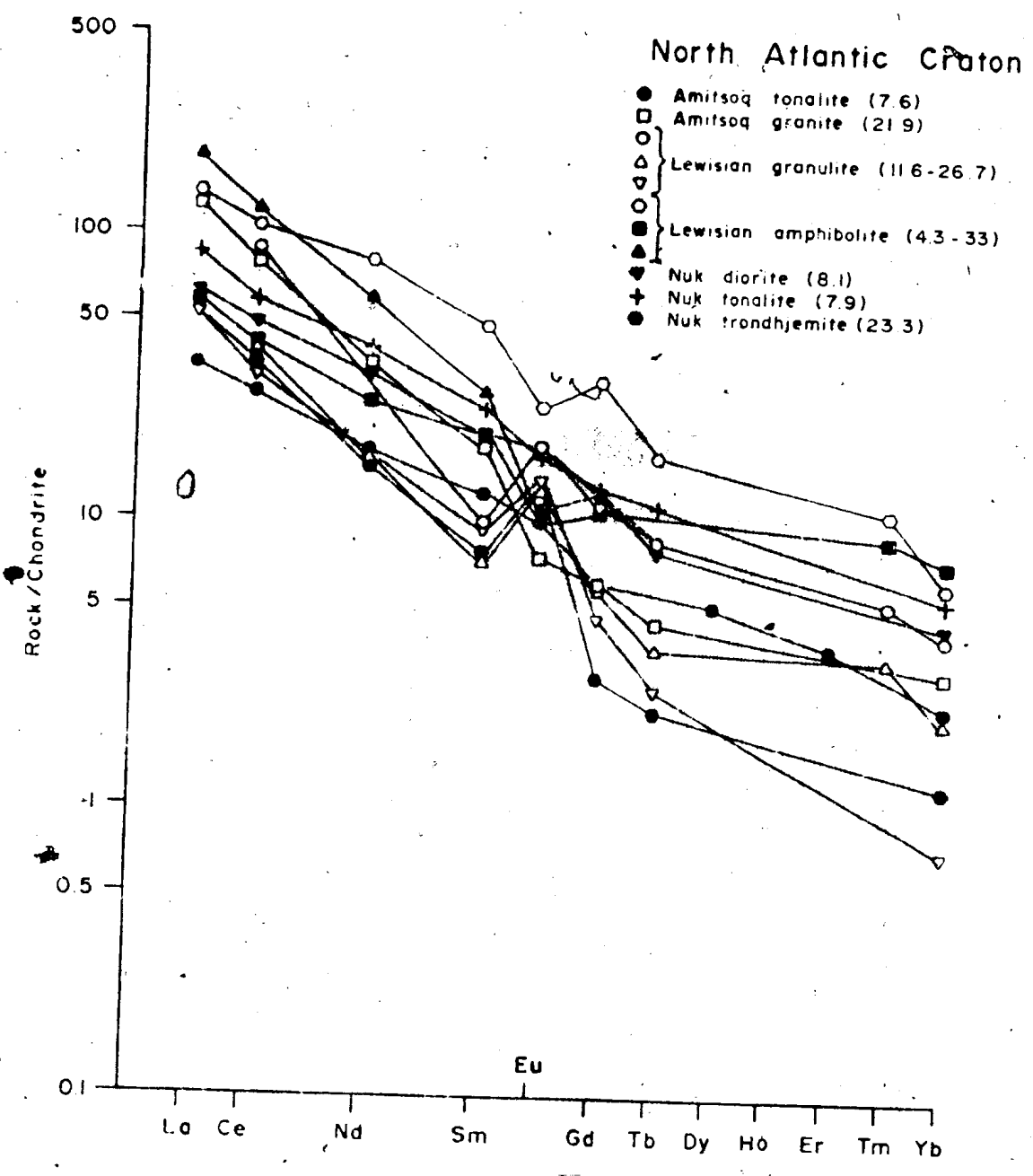
complexes elsewhere in the NAC. All NAC REE patterns exhibit moderate to strong HREE depletion, accompanied by positive, normal and negative Eu anomalies (Figure 5.15). Compared with two representative samples of the tonalite and granite phases of the Amitsoq gneiss of Southwest Greenland, the Maggo gneiss patterns exhibit similar shapes (weak positive and negative Eu anomalies) and $(Ce/Er)_N$ ratios (7.6 - 22). Nutman et al. (1984) interpret these leucocratic sheets as resulting from local heating of the contact rocks during the intrusion of the iron-rich suite of Amitsoq gneiss. Larger scale studies of Amitsoq gneiss show them to result from either fractional crystallization of garnet or, partial melting of a basic source, leaving a garnet-rich residue (O'Nions and Pankhurst, 1974a).

Representative abundances for the early diorite, tonalite and trondhjemite phases of the Nuk gneiss are shown in Figure 5.15. Compton (1978a) interprets the mildly fractionated diorite and tonalite phases to result from partial melting of garnet amphibolite or garnet granulite. The trondhjemites are related to the diorite and tonalite by residual hornblende in the partial melt residue or fractional crystallization of this phase (Compton, 1978a).

The REE patterns for the Maggo gneiss closely resemble those for the Lewisian granulite and amphibolite facies gneiss, reported by Drury (1978), in terms of the dichotomy and magnitude of the Eu anomalies. The granulite facies gneiss are interpreted to represent melts derived directly

Figure 5.15: Comparison of REE data for the Maggo gneiss (shaded field) with published REE data for other NAC grey gneiss complexes I) Amitsoq gneiss (Nutman et al., 1984); II) Lewisian gneiss (Drury, 1978); III) Nuk gneiss (Compton, 1978a). The bracketed values are the $(Ce/Er)_N$ ratios for the pattern shown.

00722



from metabasaltic (eclogite, garnet amphibolite, and garnet granulite) sources (Drury, 1978): The amphibolite facies Lewisian gneiss, were produced by either fractionation of plagioclase, resulting in anorthosites or, the crystallization of a granulite facies mineral assemblage (Drury, 1978). The melts required are the same as those which give rise to the granulite facies gneiss.

From the above comparisons with other grey gneiss complexes it is evident that they are all interpreted to be derived by some degree of partial melting of a 'basaltic' parent. Upon derivation, each may then have been subjected to later fractionation mechanisms which further enriched and/or depleted the REE concentrations in later phases. These interpretations as applied to the Maggo gneiss are discussed in the following chapter (Section 6.5). The final conclusion that all of the above studies have in common is that the REE are interpreted to have remained immobile during subsequent metamorphic events which affected the grey gneiss complex (O'Nions and Pankhurst, 1974a; Compton 1978a; Drury, 1978).

5.3 Hopedale Dykes

5.3.1 Introduction

The Hopedale dykes, ubiquitous throughout the study area, and present within both the Hopedalian and Flordian domains, form an easily recognizable unit in the field. In appearance and local chronologic position the Hopedale dykes resemble the Saglek dykes of northern Labrador

(Bridgwater et al., 1975) and the Ameralik dykes of Southwest Greenland (McGregor, 1973).

This section presents major, trace and REE results for the Hopedale dykes. The geochemical data presented are only considered in examining the effects of Flordian reworking on the Hopedale dykes. No attempt is made here to work out a complete petrogenetic, i.e. the Pre-Hopedalian, history for the origin of the dykes.

Representative analyses of selected Hopedale dykes are given in Table 5.10. The mean composition and standard deviation for each element, given in Table 5.10, is calculated using all dyke analyses (Appendix D). Chemical data for the Hopedale dykes are plotted on Figure 5.16, along with the fields for the Ameralik and Malene dykes of Greenland (from Chadwick, 1981) for comparison. These two dyke swarms, emplaced into the Greenland Archaean craton, are significant chronologic markers used in interpreting the history of this portion of the NAC (McGregor, 1973; Chadwick and Coe, 1976).

5.3.2 Major and Trace Elements

CIPW normative calculations show that the dykes can be separated into two groups. Four samples are quartz normative (0.92 to 10.31 wt %) with K_2O values from 0.92 - 2.8 wt.%, and lie within the quartz tholeiite field. The remaining samples are olivine normative (K_2O values from 0.6 to 1.7 wt %), with 6 of these samples containing normative nepheline (0.7 to 4.29 wt %). Gill and Bridgwater

TABLE 5.10. Representative analyses and mean composition of Hopedale Dykes

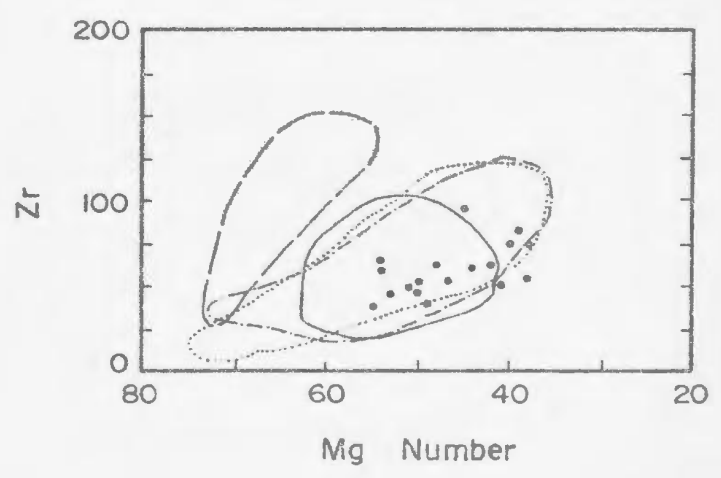
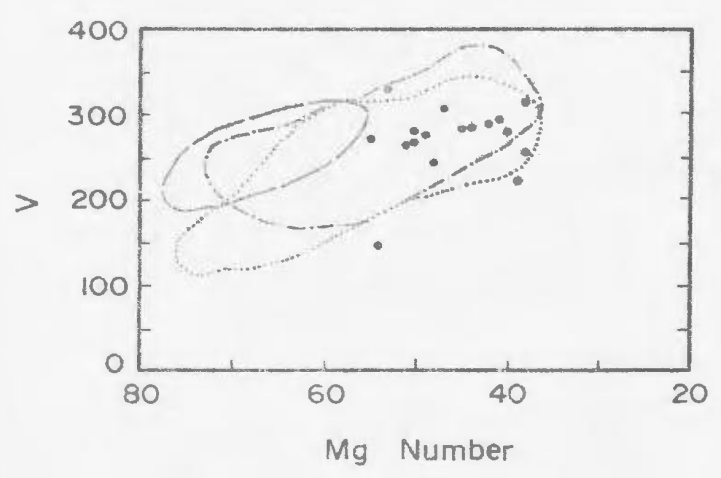
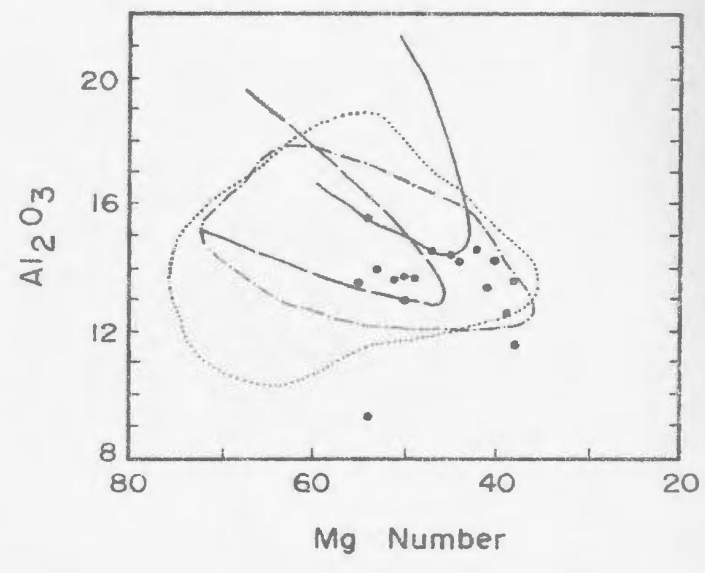
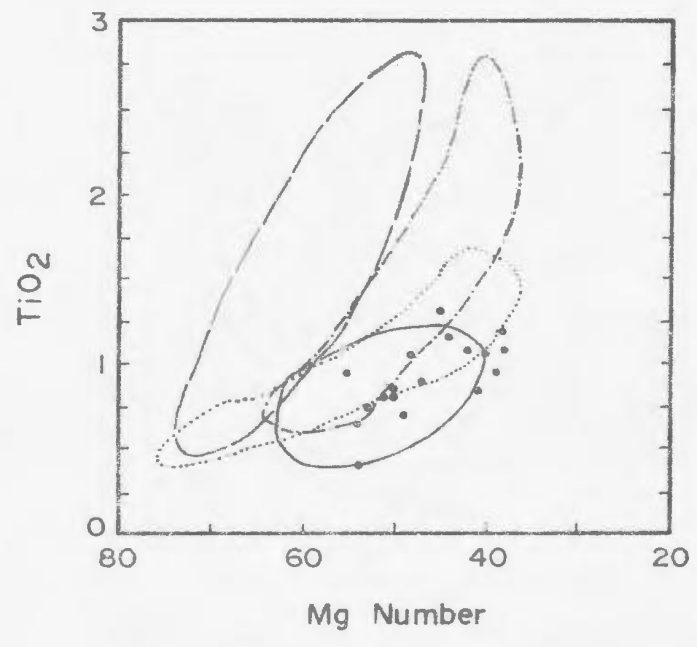
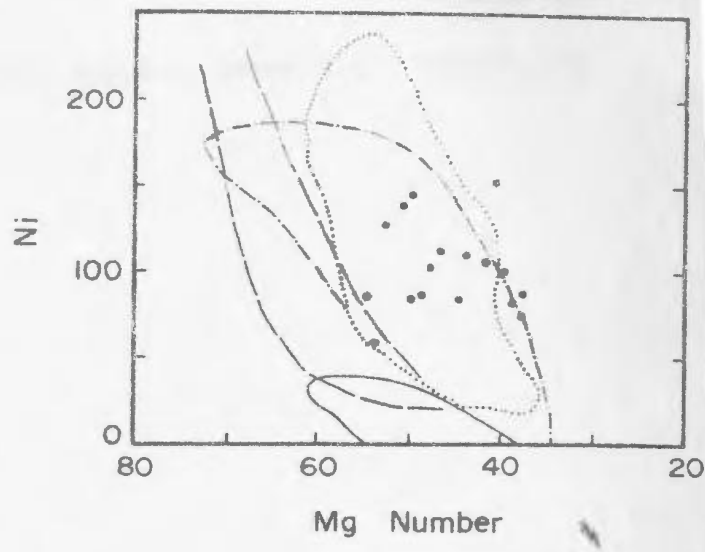
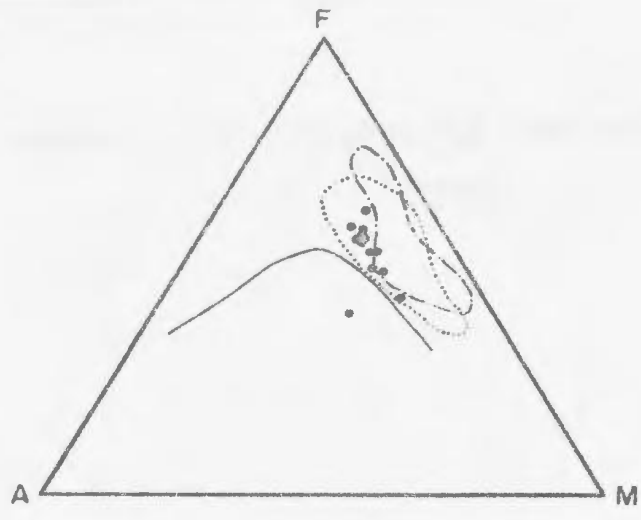
Sample	87-436	82-655	82-695	83-192	83-212	82-228	83-314	$\bar{X}(n=17)$ s.d.
SiO ₂	44.80	51.80	49.10	49.30	49.70	46.90	48.20	47.32 (3.56)
TiO ₂	.95	1.08	.89	1.18	.93	.80	1.06	0.93 (0.22)
Al ₂ O ₃	12.60	11.60	14.20	13.60	13.50	13.00	14.20	13.21 (1.08)
Fe ₂ O ₃	2.70	3.90	4.67	2.96	2.91	4.05	2.20	2.13 (1.07)
FeO	9.04	13.27	8.65	10.29	8.58	8.44	10.68	9.12 (1.49)
MnO	.20	.24	.20	.22	.19	.26	.21	0.21 (0.03)
MgO	5.69	6.87	7.69	6.44	8.00	8.31	7.14	7.60 (0.89)
CaO	7.84	9.36	10.27	9.86	10.68	10.08	9.80	9.76 (0.75)
Na ₂ O	2.35	1.85	2.22	2.52	2.34	2.57	3.11	2.74 (0.43)
K ₂ O	1.01	1.14	1.04	1.38	1.20	.98	.93	1.10 (0.28)
P ₂ O ₅	.13	.08	.03	.11	.05	.08	.04	0.07 (0.03)
LOI	2.09	1.80	1.40	1.59	2.33	1.79	1.68	
TOTAL	99.46	102.59	101.41	99.41	100.41	99.26	99.25	
Pb		13				8	2	6 (3.9)
Th		10		4	7	7		5 (3.1)
U		7				1		
Rb	20	17	8	24	21	23	8	20 (8.2)
Sr	231	195	70	94	134	140	104	134 (51)
Y	27	26	28	34	19	30	28	27 (8.3)
Zr	82	55	50	75	38	46	74	59 (15.5)
Nb	5	5	3	9	7	6	6	6 (3.3)
Zn	126	106	87	103	90	115	108	105 (26)
Cu	117	122	70	63	39	144	54	64 (38)
Ni	82	88	112	74	86	84	101	102 (26)
Ba	215	94	76	41	106	40	25	93 (70)
V	225	255	207	313	271	281	281	271 (41)
Cr	39	98	130	143	221	133	96	158 (72)
Ga	18	8	17	19	14	15	18	17 (4)
La	10.66	13.30	3.12	6.70	5.20	9.20	7.10	
Ce	25.84	30.50	7.90	16.80	12.00	22.60	16.70	
Pr	3.13	3.80	1.41	2.40	1.20	2.90	3.40	
Nd	13.90	18.00	6.54	12.70	8.00	12.80	14.20	
Sm	1.46	4.50	2.44	4.70	2.70	2.70	3.70	
Eu	1.27	1.40	1.00	1.00	.50	.90	1.20	
Gd	2.82	2.60	3.28	6.00	3.40	5.00	6.50	
Dy	3.52	5.50	3.84	7.00	4.00	5.40	7.40	
Er	1.76	3.10	2.00	3.90	2.30	2.90	3.30	
Yb	1.72	1.50	1.67	3.00	1.20	2.10	1.20	
Lu	.25							
ΣREE	70.72	87.70	34.67	84.20	41.20	66.50	64.70	
Mg#	39	38	47	38	35	50	40	

00285

Figure 5.16: Selected variation diagrams for the Hopedale dyke lithology.

a) AFM ternary projection with the tholeiite boundary (solid line) from Irvine and Baragar (1971). The fields for Ameralik (.....) and Malene (-.-.-.-) dykes of SW Greenland are shown for comparison (From Chadwick, 1981).

b) to f) Oxide and trace element variation with Mg number. Mg number = $(\text{MgO}/\text{MgO}+\text{FeO})$. MORB (-----) and IAT (————) fields are taken from Gill (1979). The fields for the Ameralik and Malene dykes are shown for comparison.



(1979). In examining the Ameralik dykes, consider norms to be too sensitive to changes in alkali content to provide a reliable means of indicating the original magma type where metasomatism has occurred. Due to the susceptibility of the Hopedale dykes to post-emplacment alteration, the immobile elements (TiO_2 , V, Ni, Zr and the REE) are considered in determining the range in primary chemical composition of the dykes.

Hopedale dyke data, when plotted on an AFM diagram, lie above the boundary between the tholeiitic and calc-alkaline fields of Irving and Baragar (1971), and within the field of the Ameralik dykes (Figure 5.16a). The Mg number (Mg Number = $100(\text{MgO}/\text{MgO}+\text{FeO})$) for the dykes varies from 38 to 55, spanning a narrow compositional range, suggesting that the dykes form a single trend, with a common origin. In Figure 5.16 b-f, data for TiO_2 , Al_2O_3 , Ni, V and Zr are plotted against Mg number. In all cases the Hopedale dyke data defines a single field which falls within or overlaps with the fields for both the Ameralik and Malene dykes. Chemically the Hopedale dykes are similar to both dyke suites from Southwest Greenland, but appear to be compositionally more similar to the Ameralik dykes.

Also shown in Figure 5.16 b-f are the fields for mid-ocean ridge basalts (MORB) and island arc tholeiites (IAT) from Gill (1979). Hopedale dyke data for TiO_2 vs. Mg number and Zr vs. Mg number fall within or near the IAT field. Al_2O_3 contents fall below while Ni contents lie

above the IAT field, when plotted against Mg number. It should be noted that on all these plots the Hopedale dyke data falls outside the MORB field. The variation of Al_2O_3 and Ni with Mg number may reflect fractionation mechanisms during the formation of the dykes. This possibility has been suggested by Chadwick (1981) for the Ameralik and Malene dykes.

Using a plot of CaO/Al_2O_3 vs K_2O , Gill and Bridgwater (1979) identified distinct types of Ameralik dykes. Dykes with K_2O and CaO/Al_2O_3 values > 0.85 wt % and < 0.72 , respectively, formed a distinct geochemical subgroup. These authors attribute the enriched K_2O values and lower CaO/Al_2O_3 ratios to result from alteration or a distinct magma type. Half of the Hopedale dyke samples lie within this same field (Figure 5.17).

The dyke samples exhibit a narrow range of volatile contents, as seen in the LOI values (1.05 to 2.3 wt%), which are enriched over volatile contents in primary magmas (Sun *et al.*, 1979). The lack of a correlation between CaO/Al_2O_3 and Mg number is interpreted to indicate that the variations in the CaO/Al_2O_3 ratio result from alteration processes. The point here is that the chemical composition of some Hopedale dykes has been influenced by alteration processes.

5.3.3 Rare Earth Elements

Rare earth element distribution patterns for 7 Hopedale dyke samples are plotted on Figure 5.18. For comparison the

Figure 5.17: $\text{CaO}/\text{Al}_2\text{O}_3$ ratio vs K_2O content in the Hopedale dykes. Gill and Bridgwater (1979) suggest that Ameralik dykes with $\text{K}_2\text{O} > 0.85$ and $\text{CaO}/\text{Al}_2\text{O}_3 < 0.72$ have undergone post emplacement alteration.

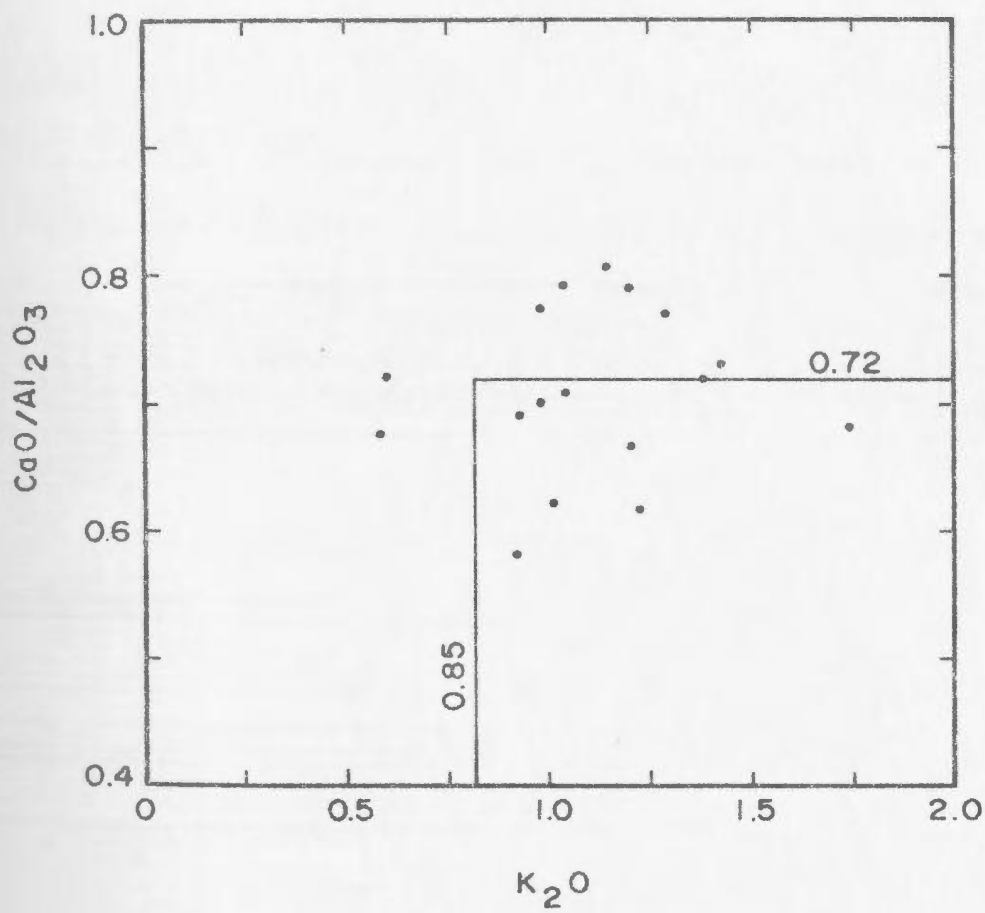
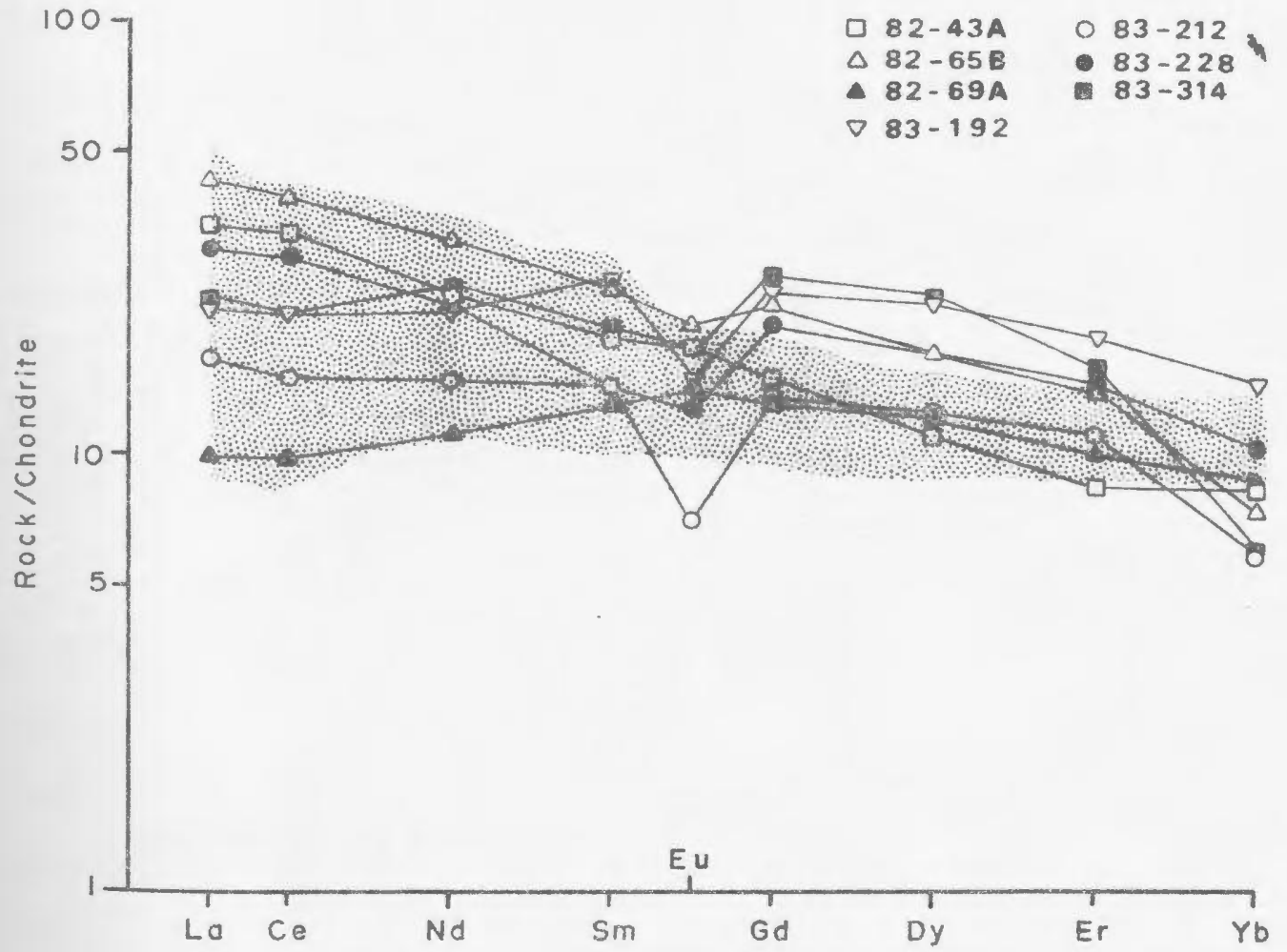


Figure 5.18: Chondrite normalized REE distribution patterns for Hopedale dyke samples in Table 5.10. The shaded region is the field for the type B, C and D Ameralik dykes, defined by Chadwick (1981).



field for groups B, C and D Ameralik dykes as defined by Chadwick (1981) are also shown.

All Hopedale dykes exhibit regular patterns varying from nearly flat (83-212; $(Ce/Er)_N = 1.4$) to LREE enriched (83-65B; $(Ce/Er)_N = 2.6$), with some having slightly convex upward shapes (82-69A; $(Ce/Er)_N = 1.0$). Fourteen of the 17 dyke samples analyzed display a negative Eu anomaly, with (Eu/Eu^*) ranging from 0.5 to 1.0. The remaining three samples (82-43A, 82-58, 82-69A) display weak positive Eu anomalies. The predominance of negative Eu anomalies is seen in the Group A, Variant 1 Ameralik dykes and the Malene dykes, of Southwest Greenland, examined by Gill and Bridgwater (1979) and Chadwick (1981), respectively.

The presence of the negative Eu anomaly for the Hopedale dykes may be accounted for by the formation and fractionation of plagioclase during the crystallization of the parent magma. The fractionation of plagioclase would be sufficient to cause the negative Eu anomaly. Evidence for plagioclase fractionation is reflected in the presence of plagioclase phenocrysts within the Hopedale dykes at various localities within the study area, e.g. Dyke Island, and elsewhere in the Hopedale Block.

Further evidence that the Hopedale dyke source magma underwent some degree of fractionation is the range of Mg numbers recorded for the dykes. To account for observed variation in Mg number requires that a mafic phase (clinopyroxene, olivine, etc.) fractionate from the magma.

5.3.4 Summary

Hopedale dyke geochemical data, i.e. immobile trace and REE, suggests that the range of original magma chemistry for the Hopedale dykes is not as great as suggested by the normative results. Most intra-suite element variation, especially K, probably results from post-magmatic alteration, although the importance of crustal contamination at the time of intrusion may have been significant. The REE appear to have been unaffected by alteration as patterns for samples from the Hopedalian and Flordian domains are similar. Compare sample 83-192, from the Hopedalian domain, with Flordian sample 83-212 (Figure 5.18).

In summary, the Hopedale dykes are interpreted to represent a suite of diabasic dykes, with a tholeiitic composition, emplaced into the crust. The source magma underwent some degree of differentiation resulting in the Eu anomalies and the range in Mg numbers.

The combined affect of variable assimilation and fractional crystallization, although not discussed here, to some extent influences the chemical composition of the Hopedale dykes magma. After emplacement the dykes were subjected to at least two periods of deformation and metamorphism which resulted in further changes in their chemical composition.

Chapter 6

DISCUSSION - ORIGIN AND EVOLUTION OF THE

MAGGO GNEISS

6.1 Introduction

In the previous chapters, the geological setting, metamorphic history, geochronology and geochemistry of the Maggo gneiss were presented independently of each other. In this chapter the data will be integrated to provide a history of the Hopedale Block as reflected in the Maggo gneiss. In particular the following will be considered:

- 1) Examination of the geochemical characteristics of Hopedalian domain Maggo gneiss and the affects of the Flordian reworking on the gneiss. The geochemical characteristics of the reworked Maggo gneiss will be presented.
- 2) Examination of the Flordian overprinting and retrogression as it affects Hopedale dykes.
- 3) Discussion of the Sr evolution of the Maggo gneiss as it has been affected by the Hopedalian and Flordian events.

00836

4) Petrogenetic modelling, using REE, LILE and HFS element data, to determine the composition of the source material to the Maggo gneiss.

6.2 Hopedallian vs Flordian Domain Maggo Gneiss

6.2.1 Introduction

Chapter 5 presented the major, trace and REE geochemical results for all samples of Maggo gneiss, analyzed in this study, irrespective of the structural domain from which the sample was collected. Maggo gneiss samples from both structural domains span the range of chemically defined gneiss subgroups (Section 6.2.1). In this section the geochemistry of the Maggo gneiss from the Hopedallian and Flordian domains is examined. Only whole rock data for samples used in the geochronology study are considered, as the ages of these suites are known. It will be shown that without knowledge of the isotopic age of a suite of samples, assignment to a specific structural domain, purely on the basis of chemical composition, is dubious.

6.2.2 Major and Trace Elements

Geochemical results for the MI, HI and PP geochronology suites are interpreted as representative of Maggo gneiss from the Hopedallian domain. The SEDI suite yields a Hopedallian age yet displays a geochemical signature distinctly different from the other Hopedallian suites. Samples from the MC, DP and BH suites are used to define the geochemical characteristics of the Flordian

domain Maggo gneiss. The HG, HH and DI suites yield Flordian ages. However, they display distinct chemical differences when compared with the other four Flordian suites above.

The mean whole rock major and trace element composition for each geochronology suite is presented in Table 6.1. Major element data show minor variation in mean chemical composition between the Hopedallian and Flordian geochronology suites; compare the HI and HG data in Table 6.1. However, it must be noted that for individual suites of the same geochronological domain, the major elements exhibit a spread of values, e.g. Flordian suites MC and BH. The only major element oxide which can be seen to exhibit a distinct chemical variation between the two geochronologic domains is K_2O . Hopedallian suites are enriched in K_2O with respect to the four Flordian suites. The K_2O enrichment is born out by examination of Table 6.2, where the mean K_2O content of the Hopedallian domain gneiss is 0.5 wt % higher than in samples from the Flordian domain.

Mean trace element data (Table 6.2) for the majority of elements exhibit little variation, with a similar range of values for each domain and/or the elements have a large standard deviation associated with them, e.g. Nb, Cr, V. In Table 6.2, Rb and Ba exhibit the widest variation in content between the two domains. These elements are depleted within the Flordian domain when compared to the Hopedallian average composition. The final point to be made

Table 6.1: Average whole rock chemical composition of each geochronology suite. The standard deviation for each oxide/element is given in brackets. Total Fe is reported as Fe₂O₃.

	Hopedalian Suites			
	MI (8)	PP (5)	HI (8)	SEDI (5)
SiO ₂	68.72(4.2)	69.38(1.7)	70.69(3.7)	63.48(0.63)
TiO ₂	0.39(0.17)	0.33(0.03)	0.27(0.15)	0.54(0.02)
Al ₂ O ₃	15.42(0.84)	15.56(0.86)	14.96(0.68)	16.32(0.23)
Fe ₂ O ₃	3.08(1.84)	2.86(0.59)	2.35(1.63)	5.29(0.19)
MnO	0.05(0.03)	0.04(0.02)	0.04(0.02)	0.08(0.0)
MgO	1.53(0.92)	1.42(0.1)	1.31(0.8)	2.55(0.12)
CaO	4.01(1.23)	3.43(0.69)	3.18(1.17)	5.38(0.09)
Na ₂ O	4.31(0.26)	4.41(0.16)	4.55(0.28)	4.14(0.06)
K ₂ O	1.44(0.14)	1.62(0.18)	1.66(0.27)	1.07(0.14)
P ₂ O ₅	0.09(0.05)	0.07(0.03)	0.08(0.05)	0.15(0.05)
Pb	6.7(4.3)	6.8(2.2)	5.1(2.5)	3.0(2.8)
Rb	48.0(11.1)	65.4(13.7)	54.8(10.5)	24.2(2.8)
Sr	379.7(85.2)	298.6(64.1)	341.5(35.3)	436.2(11.2)
Y	7.4(5.2)	8.6(3.4)	5.9(4.7)	12.6(0.6)
Zr	102.7(35.4)	92.4(11.3)	87.8(11.1)	83.8(7.4)
Nb	4.3(1.0)	4.4(1.1)	4.1(0.5)	3.4(0.6)
Zn	40.3(16.1)	42.8(9.9)	37.1(11.4)	59.4(2.0)
Cu	21.3(7.8)	18.6(7.6)	17.6(8.3)	21.8(3.4)
Ni	13.4(7.7)	15.8(11.3)	17.0(4.8)	17.6(2.6)
Ba	428.7(161.1)	344.4(116.5)	416.9(117.4)	372.8(49.7)
V	49.8(37.1)	35.6(9.9)	33.9(35.0)	92.8(5.6)
Cr	22.8(12.9)	24.0(19.1)	22.0(12.7)	31.4(11.9)
Ga	17.8(3.0)	17.4(1.1)	17.0(2.3)	19.2(0.9)

* - Number of samples

00210

Table 6.1: continued

	Floridan Suite			
	HH (4)	MC (8)	HG (5)	BH (5)
SiO ₂	71.93(1.3)	65.64(4.5)	71.80(6.7)	71.72(1.78)
TiO ₂	0.23(0.01)	0.49(0.18)	0.29(0.38)	0.32(0.17)
Al ₂ O ₃	14.70(0.81)	15.0(0.68)	13.76(1.02)	14.82(0.59)
Fe ₂ O ₃	1.70(0.23)	4.95(2.35)	2.52(3.34)	2.32(1.05)
MnO	0.02(0.01)	0.08(0.03)	0.05(0.06)	0.04(0.02)
MgO	0.63(0.13)	2.28(1.3)	1.12(1.91)	0.69(0.37)
CaO	2.77(0.21)	4.67(1.47)	2.72(1.43)	3.33(0.42)
Na ₂ O	5.09(0.51)	4.28(0.33)	3.73(0.54)	4.78(0.19)
K ₂ O	1.57(0.26)	1.27(0.65)	2.83(2.01)	1.07(0.18)
P ₂ O ₅	0.05(0.03)	0.14(0.09)	0.07(0.06)	0.11(0.04)
Pb	8.8(2.6)	6.3(5.0)	7.5(7.4)	7.4(2.0)
Rb	39.5(10.9)	37.5(15.2)	58.4(41.5)	30.2(15.1)
Sr	537.3(176.1)	269.3(91.5)	314.8(67.9)	360.0(48.8)
Y	2.5(0.6)	16.9(3.3)	8.7(13.3)	8.3(1.3)
Zr	100.8(42.7)	112.1(33.1)	103.8(65.9)	152.6(51.7)
Nb	2.3(0.6)	7.1(2.3)	4.8(4.2)	5.3(1.7)
Zn	32.3(10.6)	49.8(22.7)	28.6(39.1)	39.0(18.3)
Cu	14.5(1.7)	17.2(5.1)	20.8(14.7)	19.4(11.6)
Ni		25.4(20.0)	22.0(26.9)	1.5(0.7)
Ba	384.5(258.0)	190.6(177.3)	773.4(802)	181.2(52.0)
V	21.5(3.7)	79.5(44.8)	45.0(80.3)	20.6(16.9)
Cr	4.0(2.2)	38.8(25.0)	16.0(20.0)	13.0(6.5)
Ga	21.3(2.1)	16.8(2.6)	16.4(3.2)	16.2(1.6)

00241

Table 8.1: continued

	Flordian Sulfes		
	DP (4)	PB (4)	DI (7)
SiO ₂	67.83(3.29)	68.76(1.37)	71.0(0.80)
TiO ₂	0.52(0.07)	0.39(0.17)	0.35(0.11)
Al ₂ O ₃	15.13(0.43)	15.8(0.57)	14.73(0.18)
Fe ₂ O ₃	3.84(1.47)	2.6(1.28)	3.14(0.44)
MnO	0.06(0.03)	0.04(0.02)	0.04(0.01)
MgO	1.82(0.69)	1.07(0.48)	1.00(0.10)
CaO	4.59(0.92)	3.59(0.71)	3.68(0.12)
Na ₂ O	4.18(0.13)	4.77(0.51)	4.15(0.23)
K ₂ O	1.23(0.23)	1.65(0.43)	1.28(0.15)
P ₂ O ₅	0.09(0.02)	0.12(0.02)	
Pb	6.0(1.8)	8.4(3.4)	6.1(3.1)
Rb	37.8(13.2)	45.6(13.9)	65.3(17.0)
Sr	359.8(42.8)	424.2(176.1)	189.4(33.0)
Y	8.3(4.0)	5.8(3.0)	9.0(3.2)
Zr	99.5(27.5)	115.2(31.1)	126.9(22.2)
Nb	2.5(1.3)	3.5(0.6)	5.6(1.0)
Zn	43.5(12.6)	37.4(19.1)	43.4(9.7)
Cu	32.3(8.3)	22.2(6.2)	13.4(4.5)
Ni	19.0(8.3)	13.0(7.8)	3.4(1.4)
Ba	233.0(64.8)	443.0(262.8)	315.1(91.7)
V	71.3(29.2)	40.8(22.1)	32.1(4.1)
Cr	42.5(28.0)	14.6(16.5)	3.2(1.8)
Ga	16.3(2.2)	18.0(2.0)	16.9(1.2)

Table 8.2: Mean compositions for Hopedalian and Flordian domain Maggo gneiss. For the Hopedalian composition, the values used are from the MI, HI and PP suites. The Flordian composition is based on data from the MC, DP and BH suites. Total Fe is reported as Fe₂O₃.

	Hopedalian (n=18)			Flordian (n=18)		
	Mean	S.D.	Range	Mean	S.D.	Range
SiO ₂	69.99	3.08	60.5-73.0	67.96	4.2	57.5-73.8
TiO ₂	0.32	0.10	0.26-0.58	0.43	0.18	0.09-0.62
Al ₂ O ₃	15.06	0.69	14.0-16.8	14.97	0.57	13.9-16.1
Fe ₂ O ₃	2.67	1.44	1.44-7.65	3.85	2.06	0.47-8.74
MnO	0.04	0.02	0.02-0.13	0.05	0.03	0.01-0.13
MgO	1.39	0.72	0.63-4.08	1.67	1.14	0.20-4.44
CaO	3.44	1.10	2.3-7	4.25	1.20	2.6-6.86
Na ₂ O	4.44	0.33	3.41-4.84	4.42	0.36	3.13-4.99
K ₂ O	1.70	0.82	0.87-2.24	1.19	0.44	0.01-2.35
P ₂ O ₅	0.01	0.03	0.01-0.16	0.12	0.07	0.05-0.21
Pb	6.5	2.8	3-14	6.36	3.0	2-13
Rb	55.3	15.6	10-77	33.2	14.5	5-51
Sr	333	81.8	202-541	320.3	81.1	161-490
Y	7.6	4.7	5-22	13.1	6.0	5-25
Zr	96.1	28.3	65-170	119.2	41.5	40-204
Nb	4.5	0.9	3-6	4.9	2.9	1-11
Zn	40.1	10.7	28-68	43.3	17.5	8-64
Cu	17.4	5.1	12-35	21.2	10.9	6-44
Ni	17.2	14.6	5-66	17.3	16.2	1-53
Ba	358.4	111.7	122-571	194.3	122.2	68-614
V	39.4	34.5	15-169	58.9	41.7	5-164
Cr	24.9	27.9	1-126	34.2	24.4	1-74
Ga	16.6	1.9	14-21	16.7	2.4	13-21

with reference to Table 5.2 is the similar mean Sr contents for the two domains, although this element exhibits a large standard deviation and a wide range of values.

6.2.2.1 Large Ion Lithophile Elements (LILE)

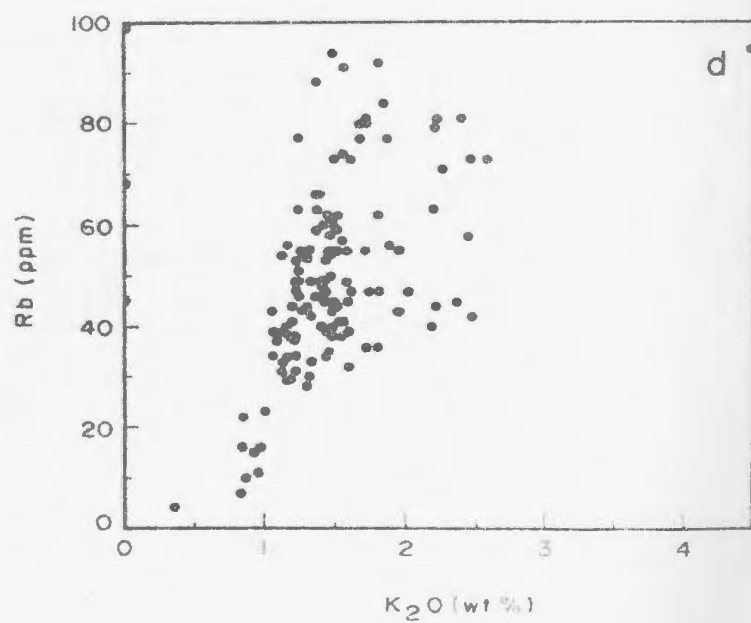
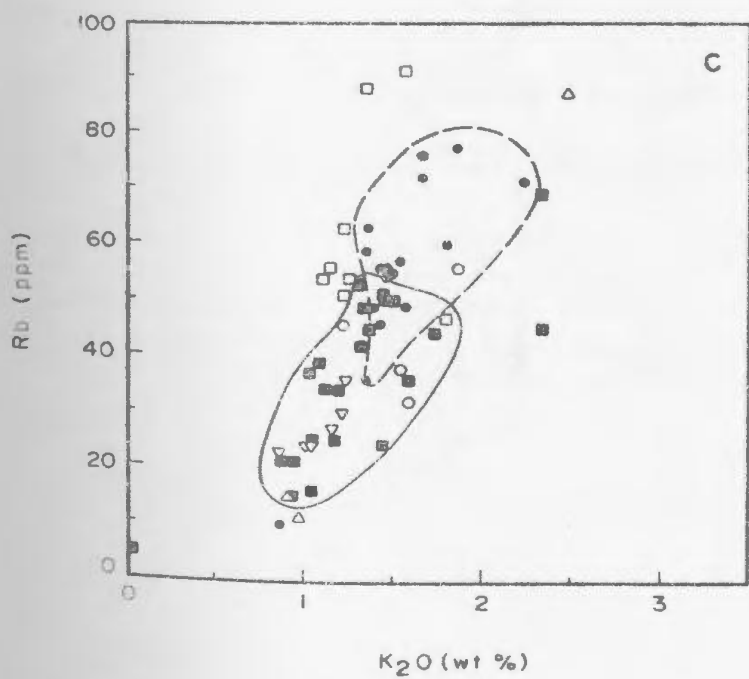
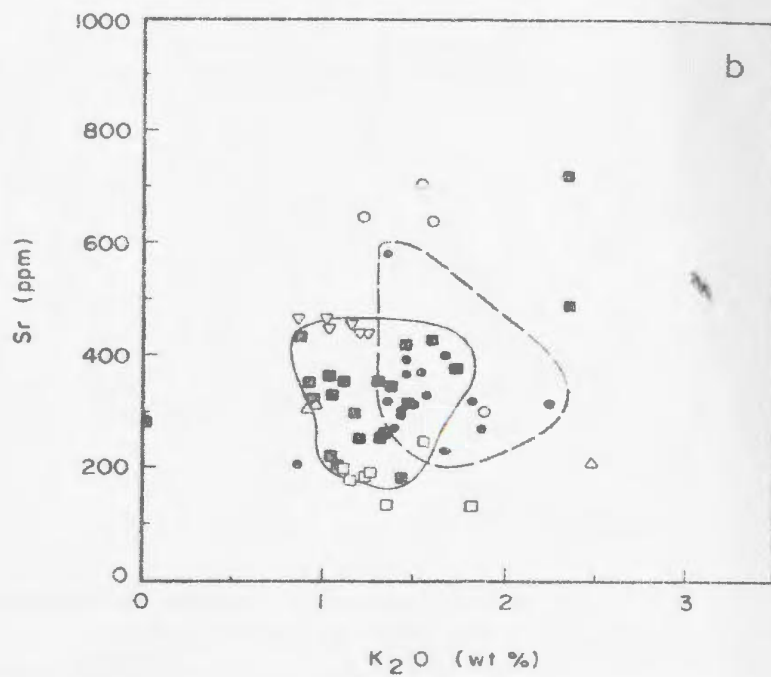
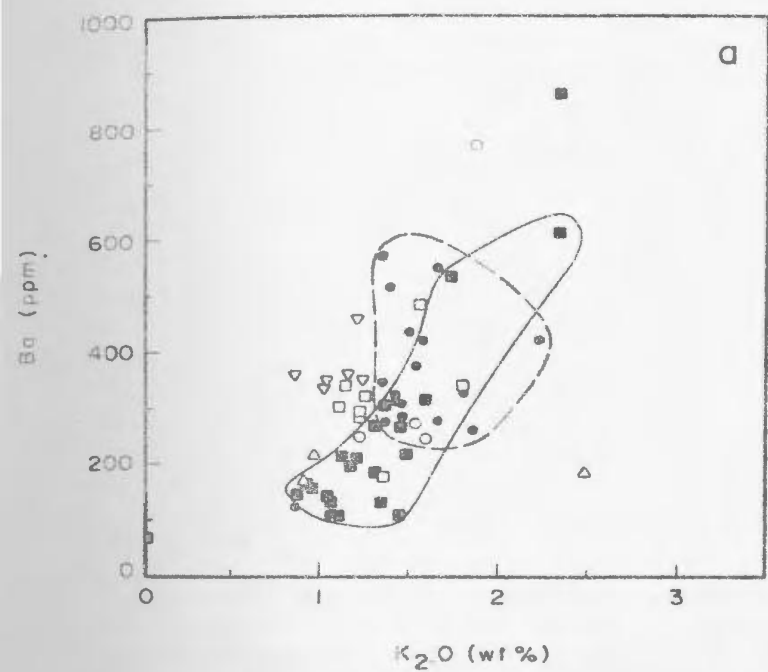
The mean data for the LILE (K_2O , Rb, Ba, and Sr) can be used as a starting point to identify the geochemical characteristics of the two, geochronologically distinct domains. The LILE data, taken with the $^{87}Rb/^{86}Sr$ ratio and the initial Sr_0 ratio (Table 4.1) for the Hopedalian and Flordian suites exhibit the most variability.

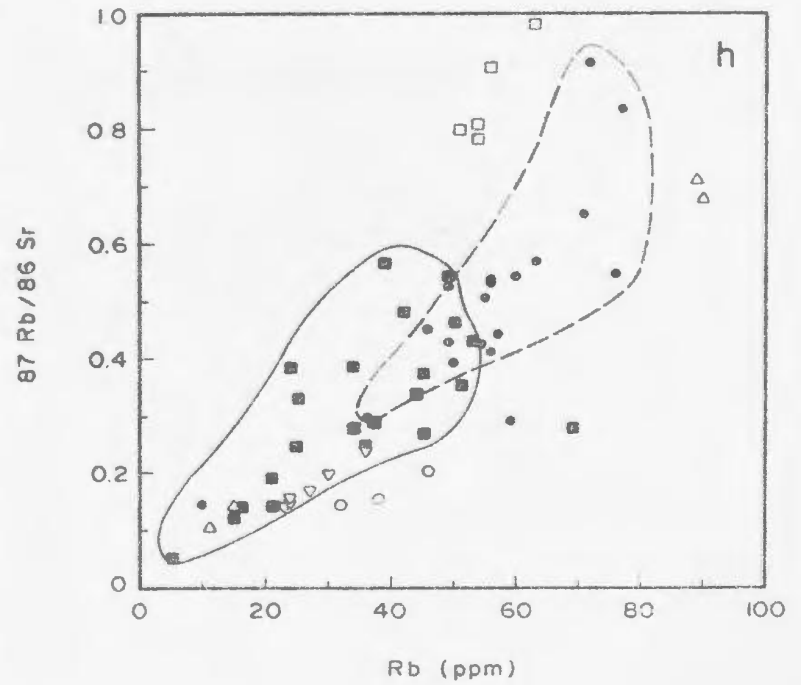
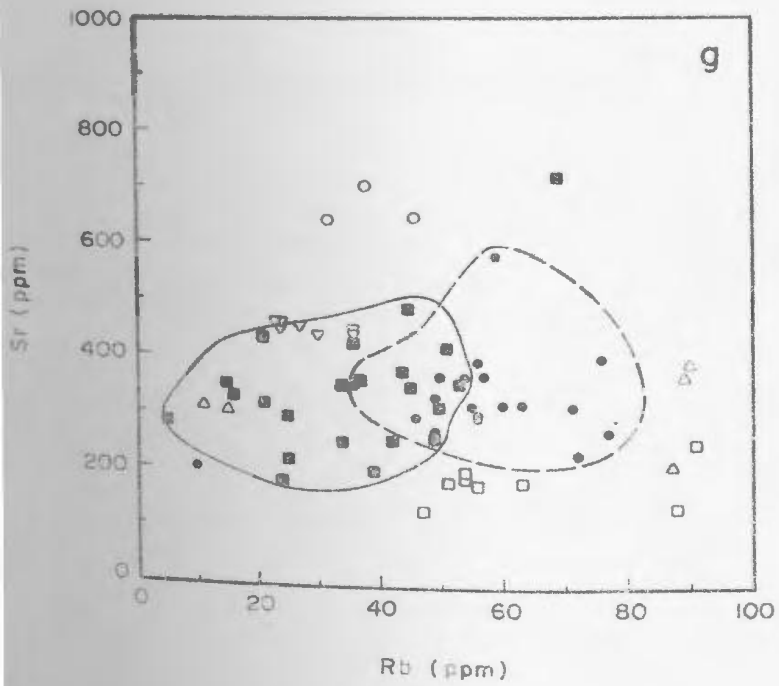
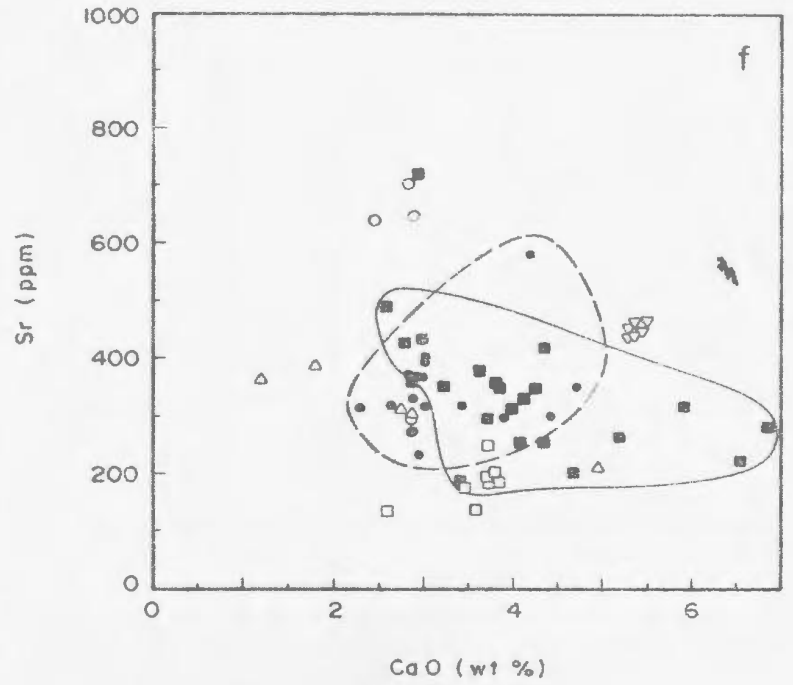
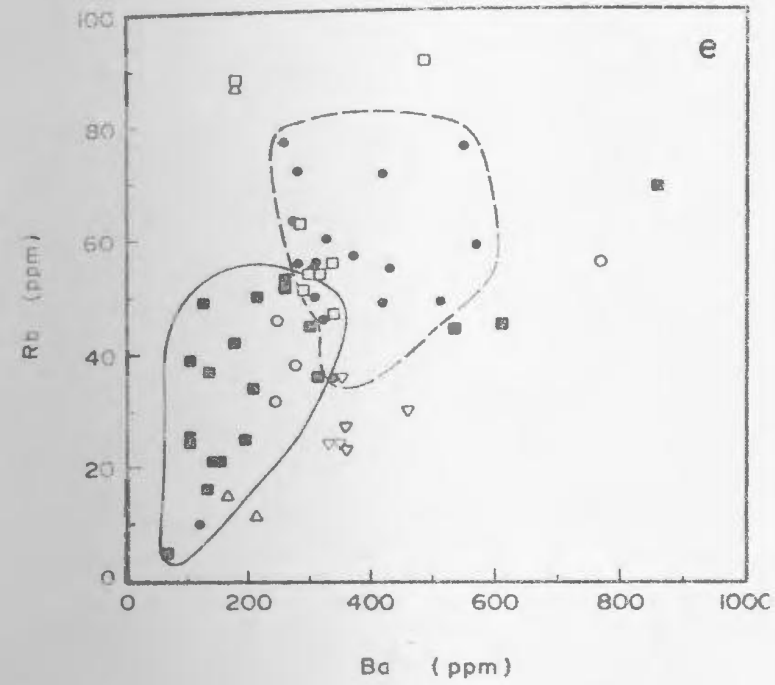
Variation diagrams for the LILE data from Hopedalian and Flordian domain suites are presented in Figure 6.1. Figure 6.1a, b and c plot Ba, Sr and Rb contents, respectively, against K_2O for the geochronology suite samples. Figure 6.1d shows the distribution of Rb with K_2O for all Maggo gneiss samples analyzed in this study. Figure 6.1e, f, g and h plot the distribution of Rb vs. Ba, Sr vs. CaO, Sr vs. Rb and $^{87}Rb/^{86}Sr$ vs. Rb, respectively. The fields defining the two domains are shown on all plots.

The Hopedalian domain samples (solid circles) exhibit a tight distribution distinctly different from the Flordian samples (solid squares) on most of the plots (Figure 6.1). The SEDI samples (inverted triangles) are not considered in defining the Hopedalian geochemical signature as these analyses consistently plot as a distinct group, away from the Hopedalian samples. The SEDI samples display higher Sr

Figure 8.1: Variation diagrams for selected LILE from the geochronology suites used to characterize the chemical composition of the Hopedallian and Flordian domain Maggo gneiss. The Hopedallian field (-----) is based on 18 samples from the MI, HI and PP suites. 18 Samples from the MC, BH, and DP suites define the Flordian chemical composition (-----) a) Ba vs. K_2O ; b) Sr vs. K_2O ; c) Rb vs. K_2O ; d) Rb vs. K_2O for all Maggo gneiss samples analyzed; e) Rb vs. Ba; f) Sr vs. CaO; g) Sr vs. Rb; h) $^{87}Rb/^{86}Sr$ vs. Rb.

Symbols - solid circles - Hopedallian domain samples; solid squares - Flordian domain samples; open triangles - HG suite; inverted triangles - SEDI suite; open circles - HH suite; open squares - DI suite.





contents, with correspondingly lower K_2O and Rb values (Figure 6.1b, g) and higher CaO contents (Figure 6.1f) compared with Hopedalian samples. This suite exhibits lower $^{87}Rb/^{86}Sr$ ratios compared to the Hopedalian suites. The depletion in Rb and K_2O , the lower $^{87}Rb/^{86}Sr$ ratios combined with the increased Sr and CaO contents for this suite result from either 1) mobility of these elements in response to the Hopedalian event, as this suite retains a Hopedalian age, or, 2) this suite represents a different primary composition, with a distinct chemical signature, compared with other Maggo gneiss suites.

The LILE data for Flordian domain samples is consistently displaced away from the Hopedalian domain field. The displacement is interpreted to result from LILE mobility in response to Flordian metamorphism, at lower to middle amphibolite facies conditions (see Section 3.3). LILE changes during metamorphism of the Maggo gneiss is in agreement with the element mobility studies of Tarney (1976), Tarney and Windley (1977), and Compton (1978a and b). These LILE mobility studies, however, deal with the transition from amphibolite to granulite facies (see Section 5.2.3), with the LILE depleted samples characterized by granulite facies mineralogy. This is not the case for the Maggo gneiss, which was retrogressed during the Flordian event.

The LILE depletion observed in the Maggo gneiss is interpreted to result from a combination of the development

of a non K-bearing mineral assemblage in response to the Flordian metamorphism combined with a fugitive metasomatic fluid which was capable of removing these elements. The LILE depletion recorded for the gneiss suggests that Flordian metamorphism took place in an open system environment.

The HG, HH and DI suites, which yield Flordian ages (Section 4.14) can be utilized to document the various aspects of the Flordian event as seen by their chemical composition. The HG suite samples (open triangles, Figure 6.1) plot as two distinct groups distinguished by;

- 1) depletion of Rb, Ba and K_2O , to a degree similar to that observed for the other Flordian samples.

- 2) enrichment of these elements, compared with other Flordian samples, to abundances greater than those recorded for the Hopewellian domain gneiss, i.e. Ba up to 1700 ppm, Rb up to 90 ppm and K_2O up to 5.33 wt. %.

The depleted samples are interpreted to represent the parent material which yielded the enriched samples in response to the Flordian event. The enriched samples consist entirely of, or contain abundant, discrete layers of migmatitic material (Plate 10B).

On the scale of sampling for the HG suite, over a 2 m width perpendicular to strike, the LILE are interpreted to have moved between individual samples in response to the presence of a fluid phase accompanying the Flordian event.

Examination of Figures 6.1c, g and h show that the DI data, which plots away from that for other Flordian suites, exhibits Rb and Ba enrichment, Sr depletion and increased $^{87}\text{Rb}/^{86}\text{Sr}$ ratios for similar K_2O values, compared with other Flordian suites. On the remaining plots the separation of the DI data from the Flordian suites is not as pronounced.

The Rb and Ba enrichment and Sr depletion for the DI suite, compared with the Rb depletion and constant Sr for the other Flordian suites can be used to examine the large scale transport of LILE during the Flordian event. The DI locality is interpreted to represent an area of LILE enrichment in response to the Flordian event. The source for the Rb is envisaged to be areas, such as those represented by the remaining Flordian suites, which have been depleted in Rb and Ba during the Flordian event. The Rb and Ba removed from these localities is transported via a fluid phase, present during the Flordian metamorphism, to the DI locality, where these elements are no longer soluble in the fluid and are removed. The DI samples have biotite as the dominant mafic phase, which preferentially incorporates Rb and Ba. In contrast, the other Flordian suites are characterized by having hornblende as the dominant mafic phase. The actual mechanism responsible for the formation of biotite and deposition of the LILE at localities such as DI remains unknown.

The $^{87}\text{Rb}/^{86}\text{Sr}$ ratios for the geochronology suites exhibit a variation between Hopedallian and Flordian domains (Figure 6.1h), with Flordian suites exhibiting lower overall $^{87}\text{Rb}/^{86}\text{Sr}$ ratios with respect to Hopedallian suites. Examination of the mean $^{87}\text{Rb}/^{86}\text{Sr}$ ratios (Table 4.5) for the Hopedallian suites MI, HI and PP, show these ratios vary from 0.633 to 0.349. Flordian suites (MC, BH, and DP) have consistently lower values, from 0.380 to 0.213. The lower overall $^{87}\text{Rb}/^{86}\text{Sr}$ ratios for the Flordian suites result from the Rb depletion associated with the reworking event, whereas the Sr contents remain nearly constant for the two domains.

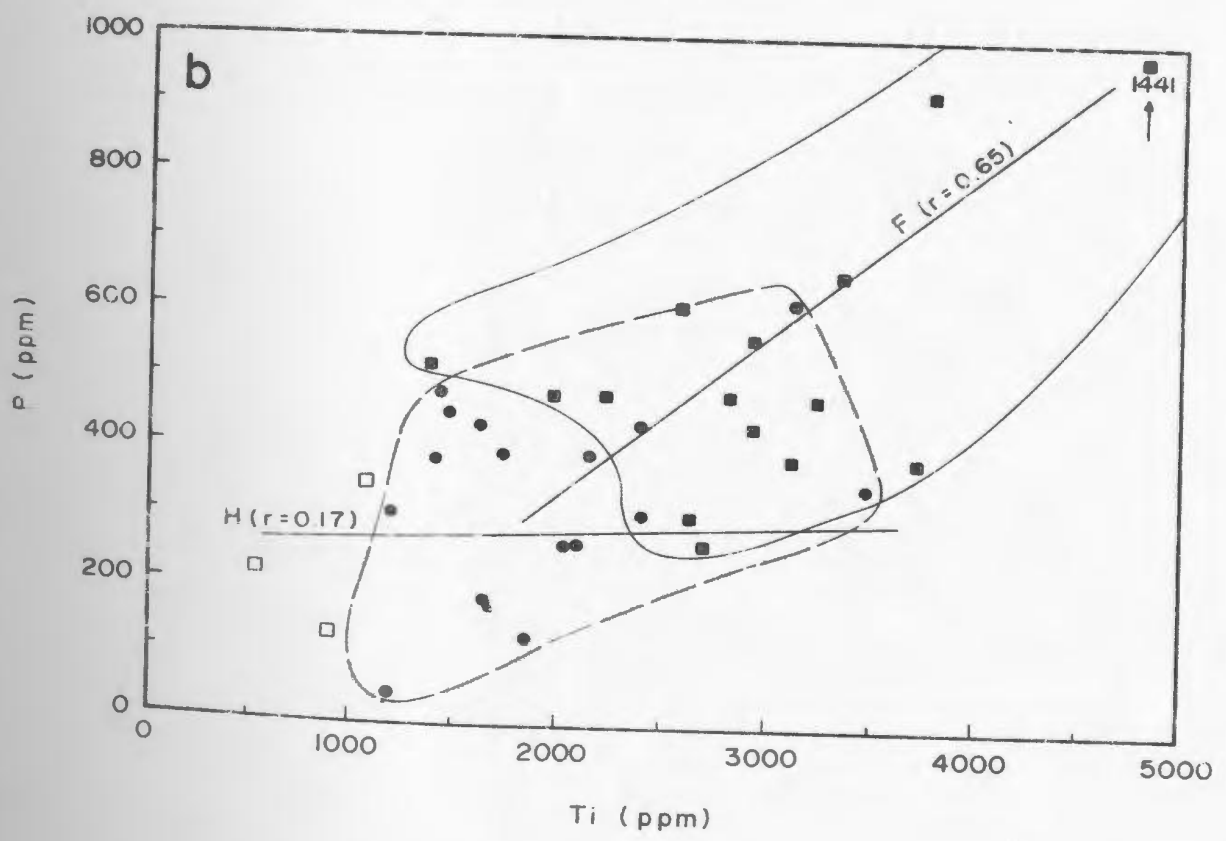
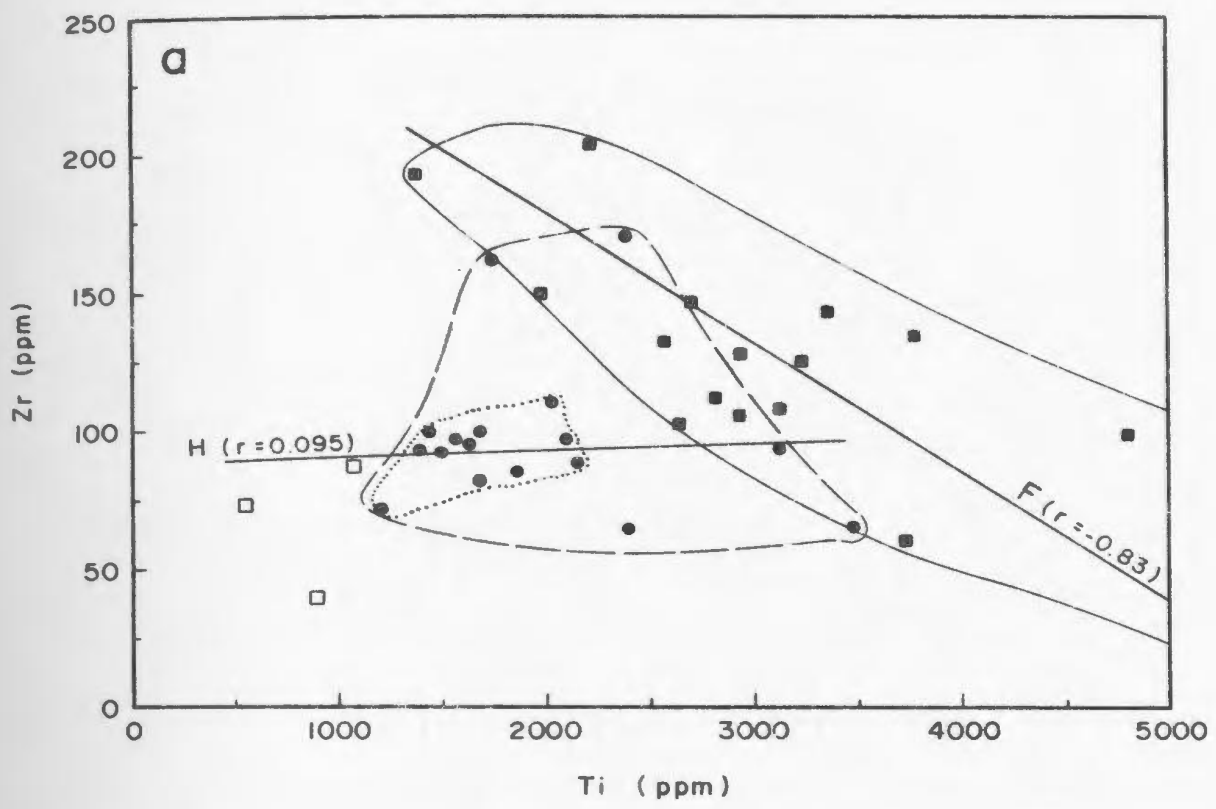
The Sr_0 values for the geochronology suites (Table 4.1) indicate that the Hopedallian suites have ratios < 0.7020. Flordian suites exhibit initial Sr_0 ratios in the range 0.7021 to 0.7035. The Sr evolution of the Maggogneiss is discussed in Section 3.3.

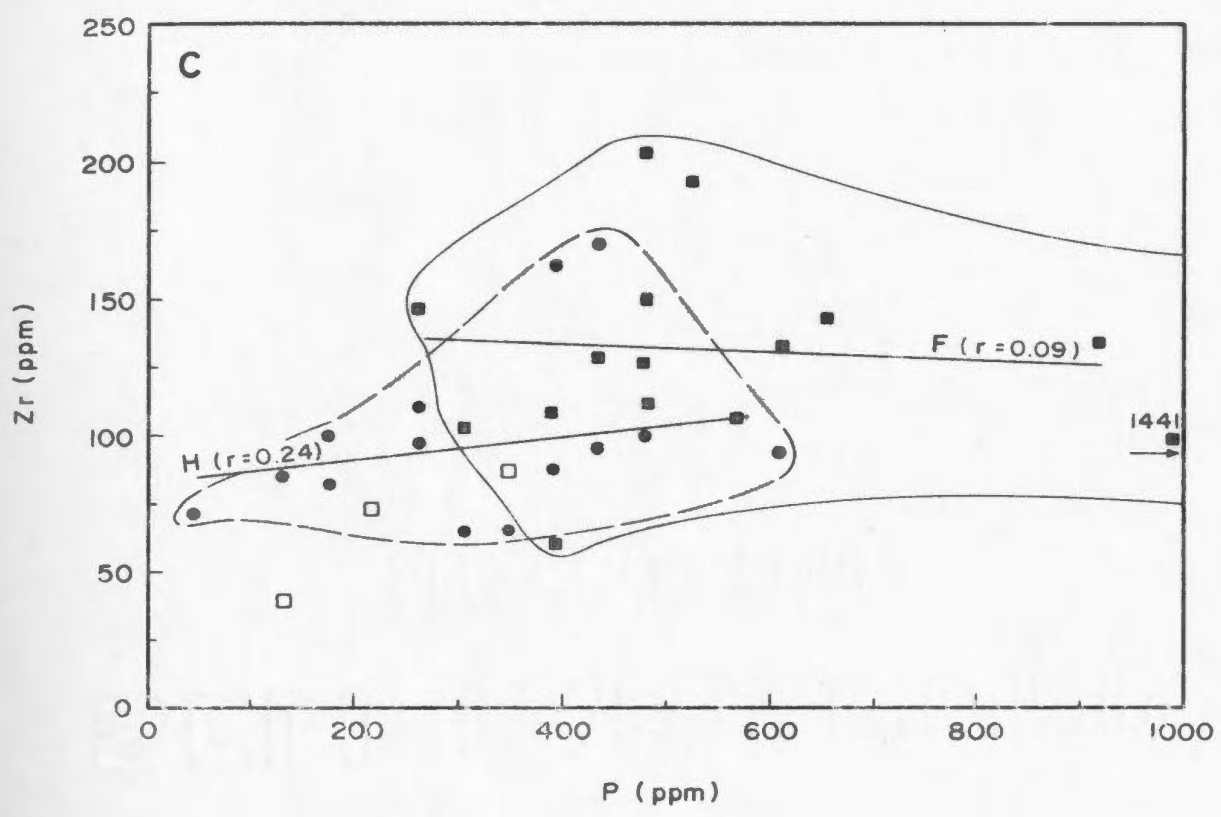
6.2.2.2 High Field Strength (HFS) Elements

Examination of the results for other analyzed trace elements, e.g. high field strength (HFS) elements (Ti, Zr, P, Y, and Nb) can be used to further examine element mobility in response to Flordian reworking. Plots of Zr vs. Ti, P vs. Ti and Zr vs. P are shown in Figure 6.2.

On Figure 6.2a (Zr vs. Ti) all Hopedallian samples can be seen to exhibit a weak positive correlation of increasing Zr with increasing Ti. The majority of Hopedallian samples, enclosed by the dotted line on Figure

Figure 6.2: Variation diagrams for selected HFS elements from the geochronology suites used to characterize the Hopedallian (solid circles; enclosed by the dashed line) and Flordian (solid squares; enclosed by the continuous line) domain Maggo gneiss. a) Zr vs. Th; The dotted line encloses the majority of the Hopedallian domain samples, see text for discussion; b) P vs. Th; and c), Zr vs. P. The regression lines were calculated using the Cricket graph program package run on a Macintosh SE computer. The correlation coefficient (r) is an estimate of the fit of the data points to a straight line distribution: H- Hopedallian; F- Flordian. The open squares represent strongly migmatized gneiss or leucosomes separated from Flordian domain gneiss. The value of $r=0.095$ results from the consideration of all Hopedallian samples. The restricted Hopedallian field, enclosed by the dotted line, yields an r value of 0.54.





6.2a, define a restricted field and exhibit a moderate to strong positive correlation ($r=0.54$). This restricted field may result from either mobility of these elements in response to the Hopedalian event, or reflect an original igneous trend. Without knowledge of the composition of the Hopedalian domain gneiss parental material it is not possible to discern which of these origins might dominate.

Flordian samples are enriched in both Ti and Zr with respect to Hopedalian samples and exhibit a strong negative correlation of decreasing Zr with increasing Ti. The Flordian samples exhibit a wider spread of values with respect to the Hopedalian samples.

Three Flordian domain gneiss samples (open squares on Figure 6.2), consisting of strongly migmatized gneiss or leucosomes separated from the gneiss, exhibit depleted Zr and Ti values with respect to Hopedalian and Flordian samples. Due to the strongly migmatized nature of these samples they are not considered in defining the Flordian field.

Hopedalian samples exhibit a weak positive correlation of P with Ti (Figure 6.2b), while Flordian samples exhibit higher P contents for equivalent Ti compared with the Hopedalian samples. The Flordian samples display a moderate to strong positive correlation for these elements. The fields for both domains overlap to some extent. The migmatitic Flordian samples are depleted in P with respect to other Flordian samples. Similarly the Hopedalian and

Flordian fields overlap on a plot of Zr vs. P (Figure 6.2c). Samples from the Hopedalian domain exhibit a weak positive correlation of increasing Zr with increasing P, while Flordian samples exhibit a poor negative correlation.

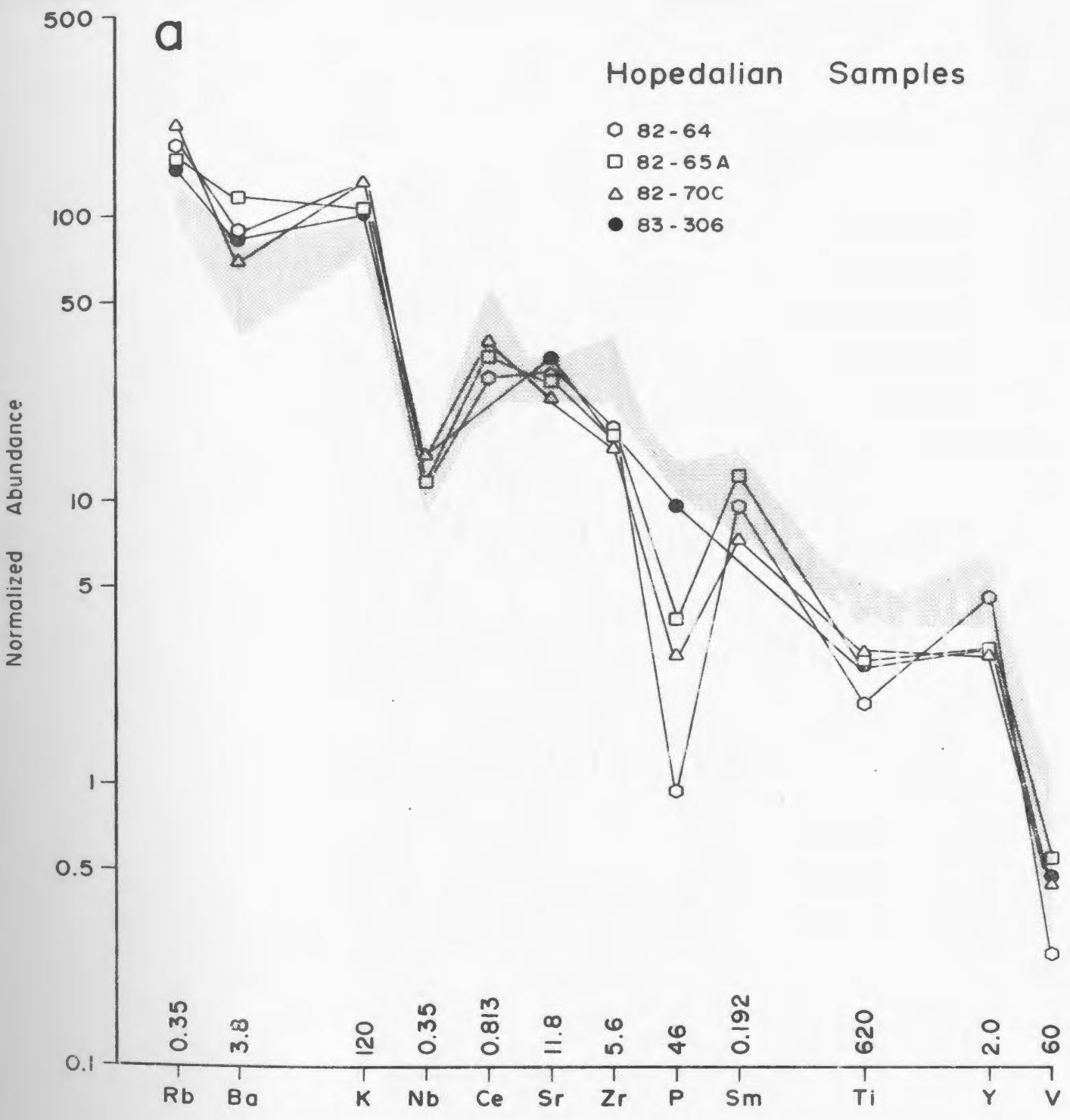
A means of qualitatively representing the degree of relative enrichment and depletion of the LILE and HFS elements between the Hopedalian and Flordian domains can be obtained using normalized values for these elements plotted against their increasing degree of incompatibility (Figure 6.3). With respect to the Hopedalian samples, Flordian domain gneiss samples are depleted in Rb, Ba and K, enriched in Ti, Zr, P, Y and V and exhibit no change in Nb, Ce, Sr and Sm contents.

6.2.2.3 Rare Earth Elements

From Figure 6.3, the Ce and Sr contents of the Maggo gneiss appear to be unaffected by Flordian reworking of the Hopedalian domain gneiss. Complete REE distribution patterns for representative Hopedalian and Flordian domain samples are presented in Figures 6.4 and 6.5, respectively. Examination of these figures reveals that both domains exhibit moderate LREE enrichment (19 to 200 X chondrites), weak to moderate HREE depletion (1.9 to 11 X chondrites and $(Ce/Er)_N$ ratios which vary from 2.3 (Sample 83-299) to 49.1 (Sample 83-276). Enriched, depleted and normal Eu contents are present in samples from both domains. Overall the REE patterns for the two geochronology domains are indistinguishable from each other, suggesting that the REE

4000

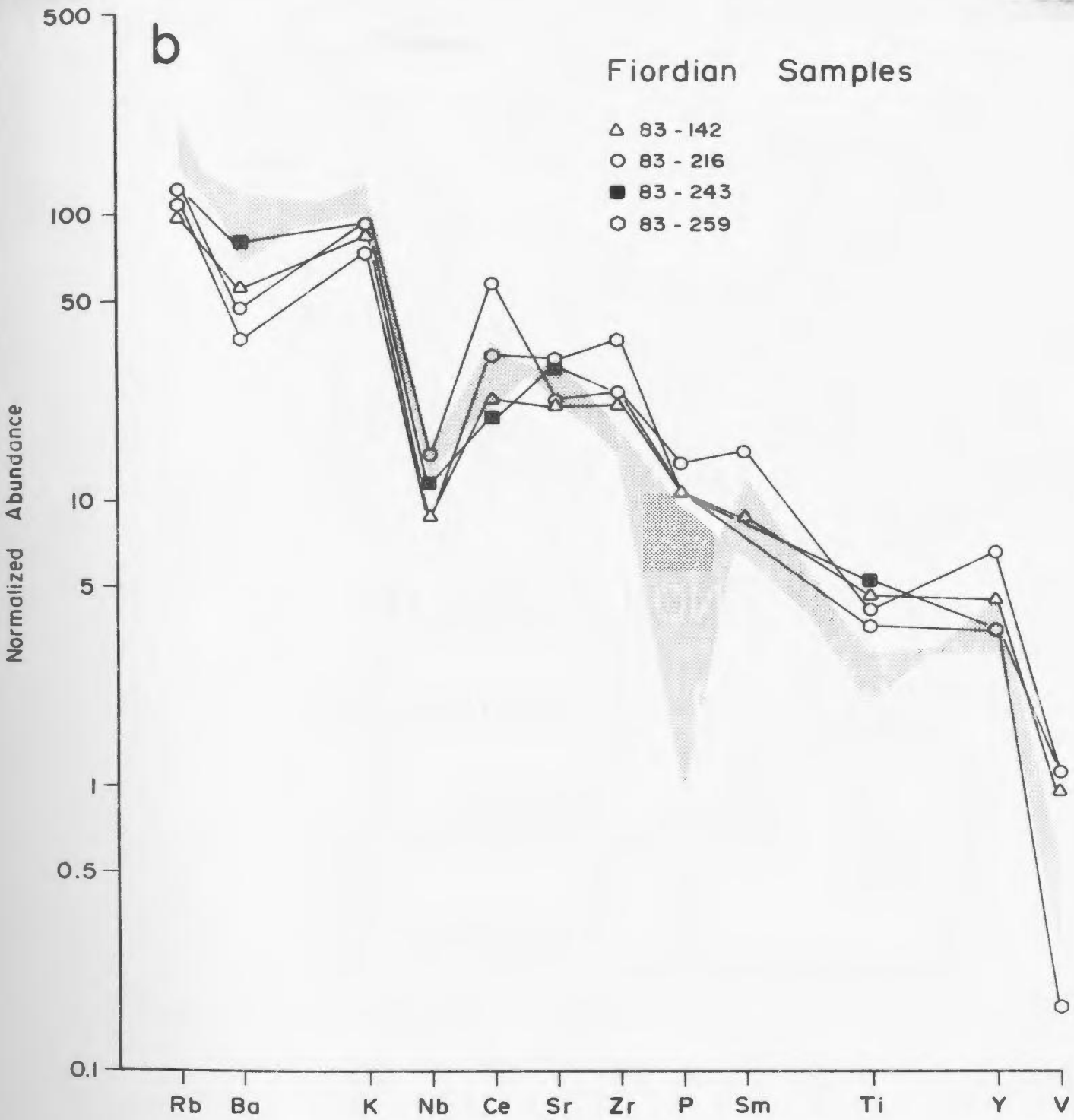
Figure 8.3: Normalized values of LILE and HFS elements for representative a) Hopedalian and b) Flordian domain Maggo gneiss samples. The shaded portion of each diagram represents the field defined for the other domain. I.e. Flordian field on Hopedalian data. The normalizing factors are from Sun (1980).



b

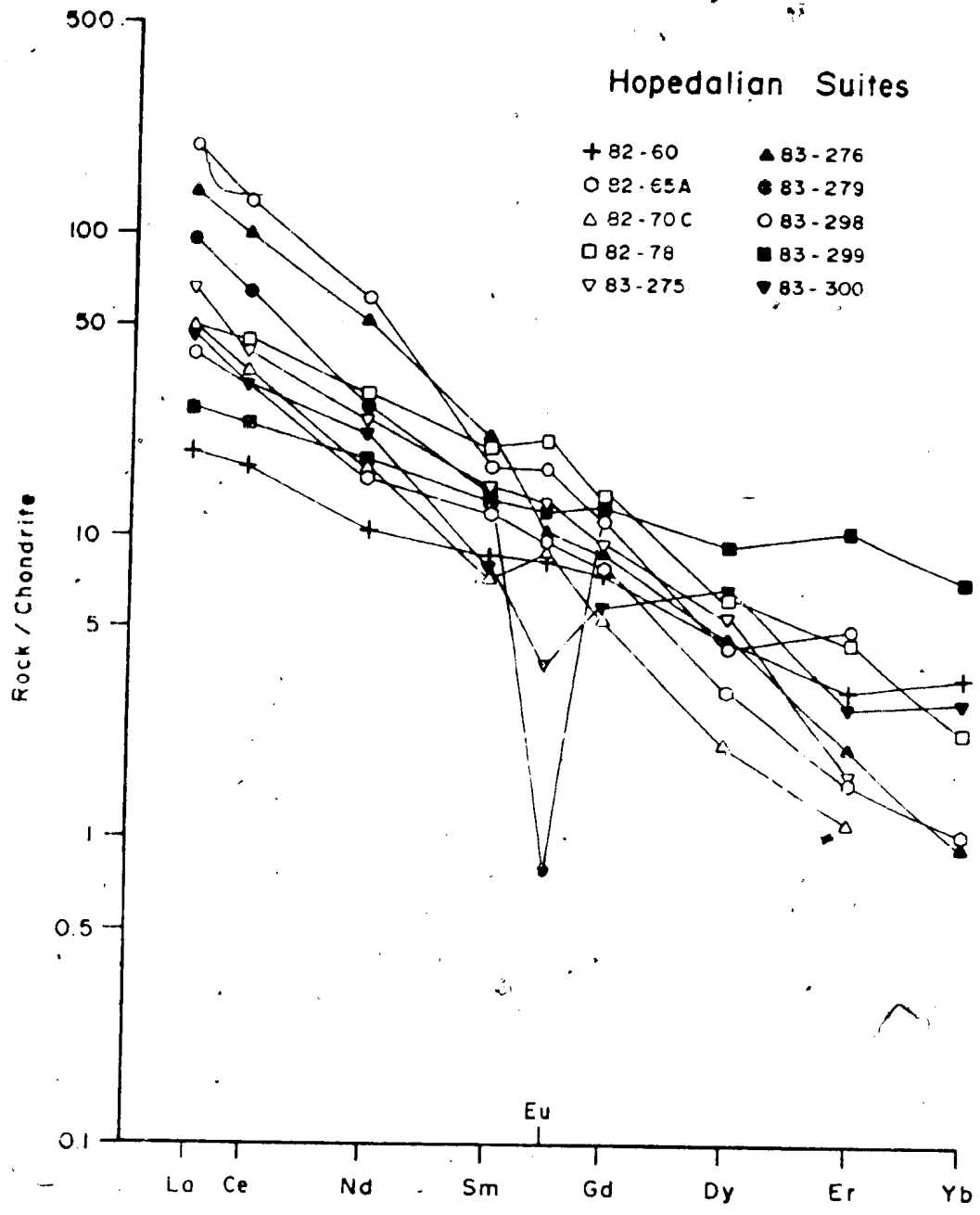
Fiordian Samples

- △ 83 - 142
- 83 - 216
- 83 - 243
- 83 - 259



00300

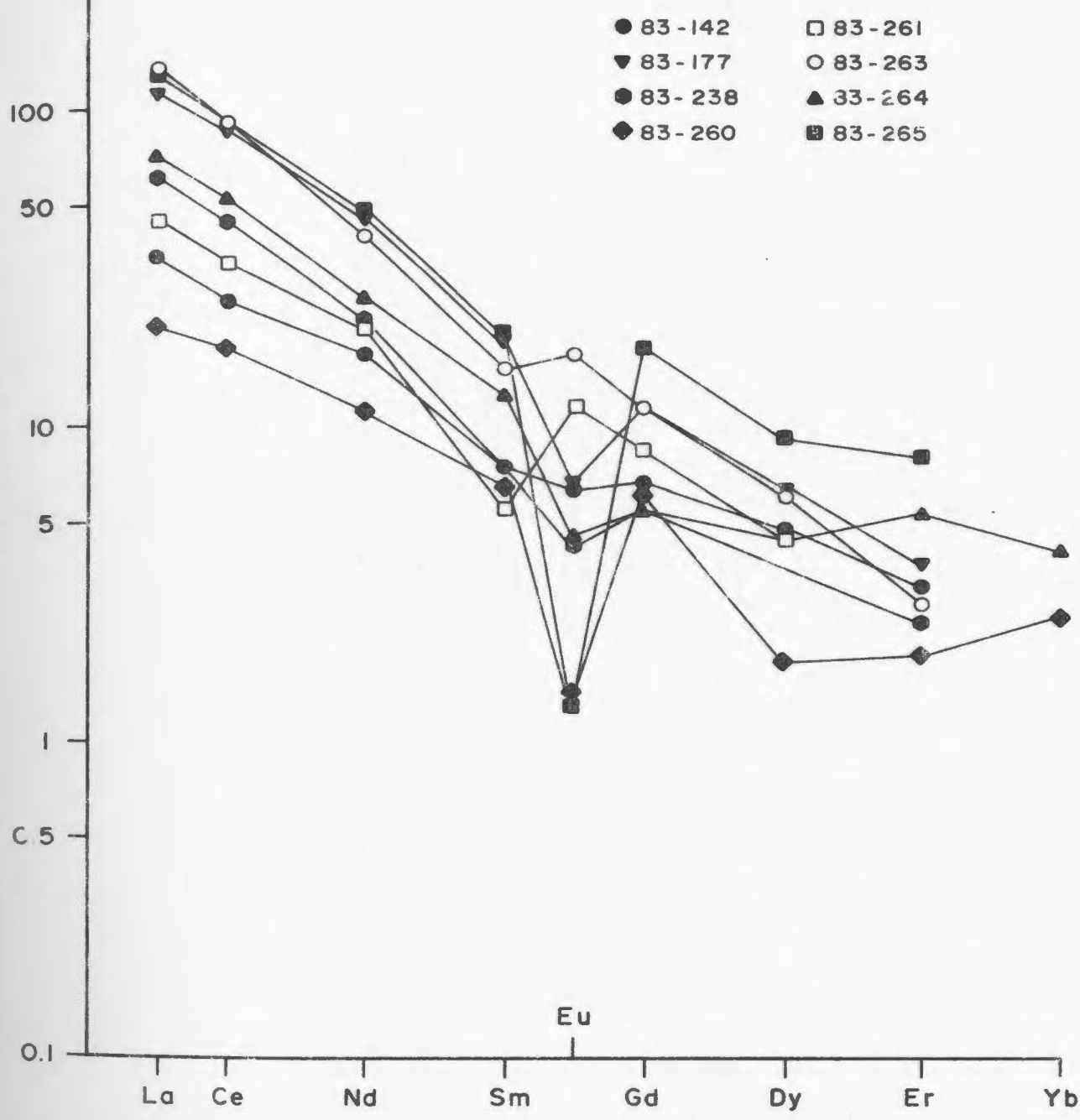
Figure 6.4: Representative REE distribution patterns for Hopedalian domain Maggo gneiss samples. Compare with Figures 6.5.



10200

Figure 6.5: Representative REE distribution patterns for Flordian domain Maggo gneiss samples. Compare with Figure 6.4.

Fiordian Suites



have remained immobile during the Flordian event, despite distinct differences in P and Ti contents.

6.2.3 Quantitative Aspects of Flordian Reworking

Flordian reworking has been shown to result in the relative depletion in LILE, enrichment in HFS elements and no change in REE contents of the Maggo gneiss. Gresens (1967) proposed a quantitative means of determining chemical changes, based on composition-volume relationships, which accompany the transformation of a given parent to its complement daughter. Visual inspection and comparison of results for a given parent-daughter pair yield numerous and often conflicting results. By incorporating whole rock analyses with specific gravity data and volume changes accompanying the parent to daughter transition a unique solution estimating the quantitative changes in bulk chemical compositions is possible. Gresens (1967) mass balance equation may be written in the form:

$$X_n = 100(f_v[g(D)/g(P)] \cdot x_n^D - x_n^P) \quad (6.1)$$

where:

X_n = chemical change in component 'n'

f_v = volume factor

$g(D)$, $g(P)$ = specific gravity of daughter and parent suites, respectively

x_n^D = weight fraction of component 'n' in the daughter suite

x_n^P = weight fraction of component 'n' in the parent suite

Equation 6.1 has been applied to assess the chemical changes, in response to Flordian reworking of Maggo gneiss and Hopedale dykes.

6.2.3.1 Maggo Gneiss

Major and trace element data for individual samples and mean compositions for Manuel Island and Black Head Tickle suites, representing Hopedalian and Flordian domains, respectively, have been used in the mass balance calculations. These two suites were selected for comparison due to their geographic proximity and similar field relationships. Three sets of analyses were compiled, two use individual analyses of samples with similar major element compositions, from both suites (Table 6.3). The third data set employs the mean compositions of the two suites, calculated using all analyses from each suite (Table 6.1).

Following the method of Gresens (1967) composition-volume diagrams were used to determine the volume factor (f_v) for each set of analyses. The f_v values, based on major element data, were determined where composition-volume curves for several components simultaneously cross the zero gain-loss line. These same f_v values were applied to the trace element results.

Using data for Samples 82-76 and 83-259, representing Hopedalian and Flordian domains, respectively, and applying Equation 6.1 with an $f_v = 1.03$, i.e. a slight volume increase, results in the relative gains and losses

Table 6.3- Analyses used for mass balance calculations to estimate changes in composition for the Hopedalian (H) to Floridian (F) transition. The values shown were calculated using Equation 6.1 (from Greens, 1967).

	H -----> F			H -----> F		
	82-76	83-259	x_N	83-304	83-263	x_N
SiO ₂	72.8	73.1	1.06	71.6	71.8	.79
TiO ₂	0.29	0.37	0.08	0.24	0.23	-0.01
Al ₂ O ₃	14.5	14.2	-0.15	14.8	14.6	-0.10
Fe ₂ O ₃	2.74	2.59	-0.12	1.97	2.62	0.67
MnO	0.04	0.04	0	0.04	0.04	0
MgO	0.63	0.52	0.10	10.7	0.61	-0.46
CaO	2.87	2.89	0.05	2.98	3.23	0.27
Na ₂ O	4.22	4.98	0.51	4.58	4.98	0.43
K ₂ O	1.44	1.05	-0.38	1.47	0.93	-0.53
P ₂ O ₅	0.09	0.11	0.02	0.11	0.12	0.01
Pb	5	8	3	9	5	-4
Rb	45	37	-8	54	53	1
Sr	256	364	112	352	356	6
Y	11	7	-4	7	8	1
Zr	162	204	44	100	142	44
Nb	5	3	2	5	7	2
Ba	513	139	-373	307	265	-33
V	19	10	-9	28	38	10
Ni				13	2	-11
Cr	1	21	20	21	5	-16
S.G.	2.62	2.57		2.51	2.58	

* - x_N calculated using $f_V = 1.03$.

! - x_N calculated using $f_V = 0.95$.

presented in Figure 6.6a. For this calculation Na_2O , SiO_2 , P_2O_5 , TiO_2 , CaO , Cr , Sr , Zr and Nb have positive values indicating addition to the system in response to Flordian retrogression. Elements which exhibit depletion for this calculation are MgO , Al_2O_3 , K_2O , Total Fe as Fe_2O_3 , V, Rb, Y, and Ba.

Results of applying Equation 6.1 to analyses for Samples 83-304 and 83-263, with $f_V = 0.95$, are shown in Figure 6.6b. This transition is characterized by depletion in MgO , Al_2O_3 , K_2O , Ba, Cr and Ni, with no change in TiO_2 , Rb and Y. The remaining oxides and elements are enriched for this transition.

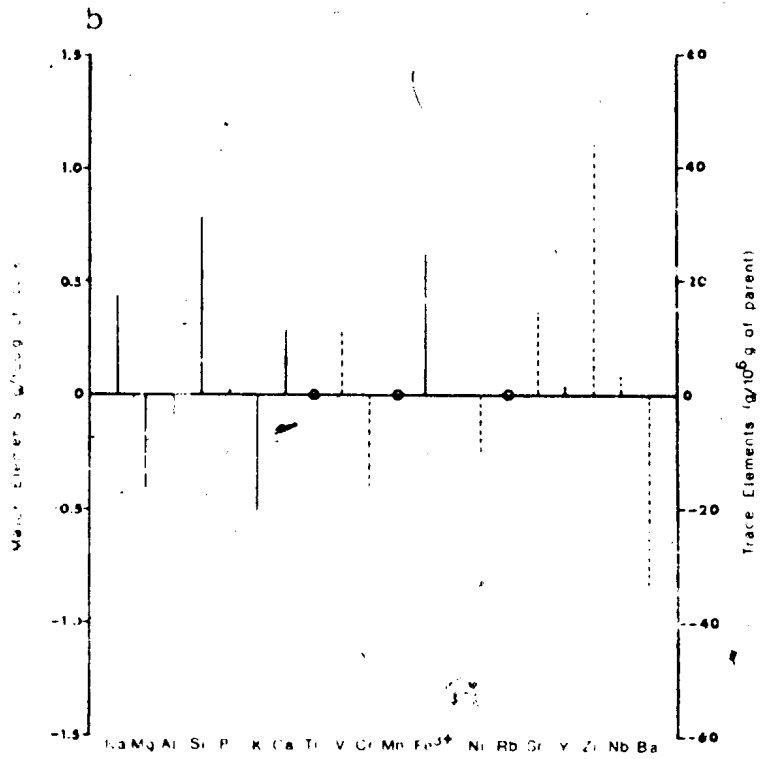
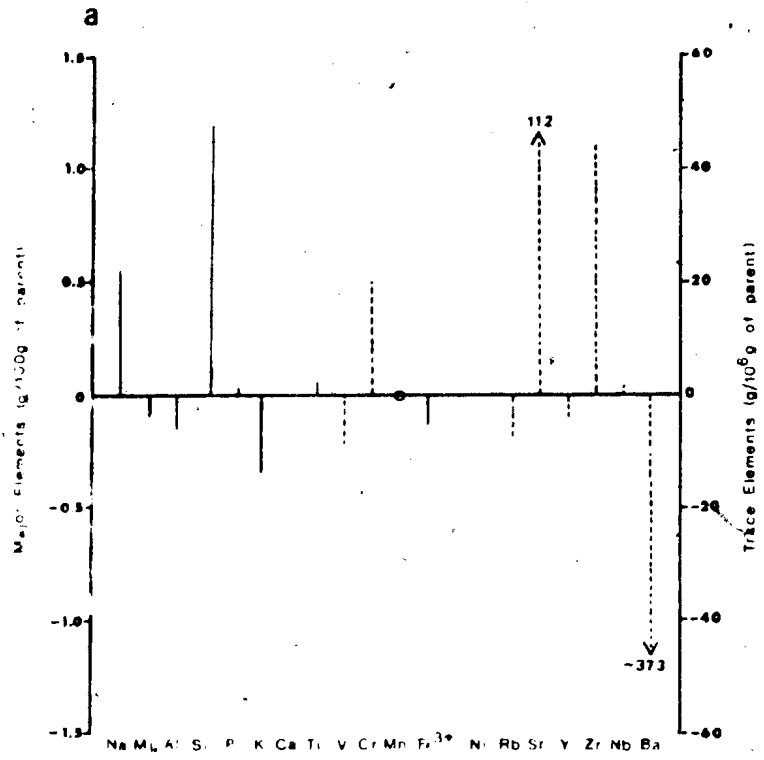
The gains and losses depicted for the two transitions assume the parent and daughter samples were originally identical in composition. Both transitions use samples from the chemically defined trondhjemitic gneiss subgroup. The parent samples, which fall in the middle of the SiO_2 range for this subgroup were chosen with the view that any SiO_2 mobility, during the transition, would result in a daughter within the same subgroup. The possibility still exists that the parent-daughter samples used do not have a direct genetic relationship.

To overcome the lack of a possible direct genetic relationship between the parent-daughter pairs, the mean composition of the Manuel Island and Black Head Tickle suites (Table 6.1) were used in similar mass balance calculations. The mean compositions for each suite

73208

Figure 6.6: Composition-volume relationships showing relative gains and/or losses, calculated after Gresens (1967), of major (solid lines) and trace elements (dashed lines) in response to Flordian reworking of Hopedalian domain Maggo Gneiss. The values plotted are taken from Table 6.3. a) parent-daughter pair 82-76 and 83-259. b) parent-daughter pair 83-304 and 83-263.

00268



represent the range of bulk compositions of Maggo gneiss at each locality, displaying similar field relationships. The specific gravities used, calculated as the mean for the suite, were 2.65 ± 0.10 and 2.63 ± 0.12 for Manuel Island and Black Head Tickle suites, respectively.

A volume increase is assumed for this change ($f_v = 1.03$). The transition from Hopedalian to Flordian domains has been shown to be retrogressive in nature, requiring the addition of water (see Section 3.3). The hydration of Hopedalian assemblages results in a volume increase for this transition. The magnitude of the volume increase is difficult to determine from composition-volume diagrams as the major elements exhibit a range of f_v values from 0.90 for Na_2O to 1.3 for Total Fe, with no clear grouping of the data. The volume factor used corresponds to Al_2O_3 immobility for this transition.

The results of the composition-volume relationships for the Hopedalian to Flordian transition are shown in Figure 6.7a. Flordian retrogression involves enrichment in Na_2O , SiO_2 , P_2O_5 , Y, Zr, and Nb, depletion in MgO, K_2O , CaO, TiO_2 , V, Cr, Total Fe, Ni, Rb and Ba, with no change in Sr contents.

In Section 6.2.2 it was suggested that Flordian reworking of Maggo gneiss involves depletion in Rb, Ba and K_2O with no significant change in Sr. This result was based on a visual examination of the data for Hopedalian and Flordian samples. Composition-volume results, which

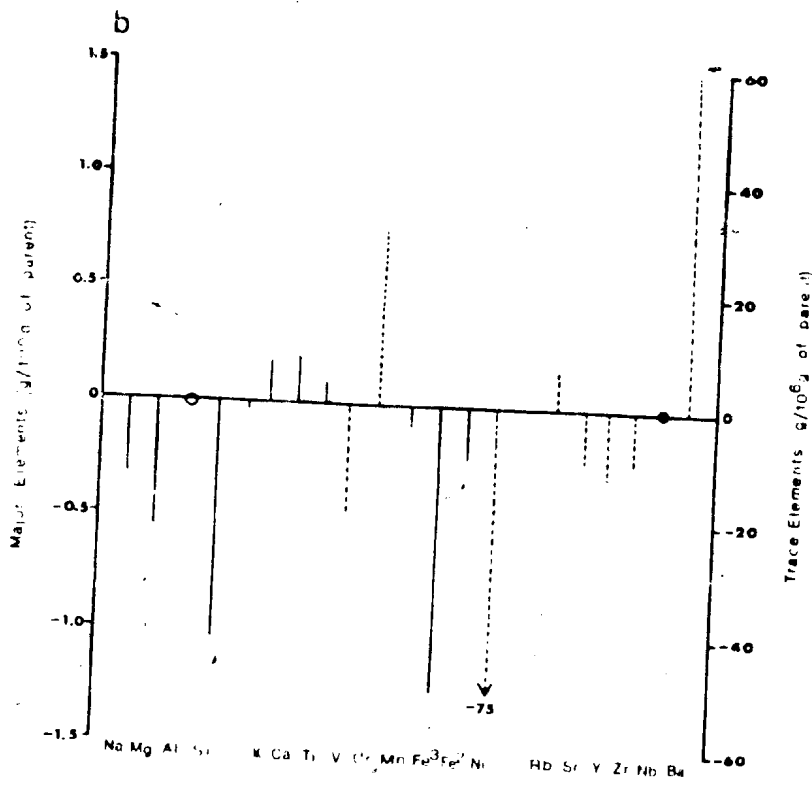
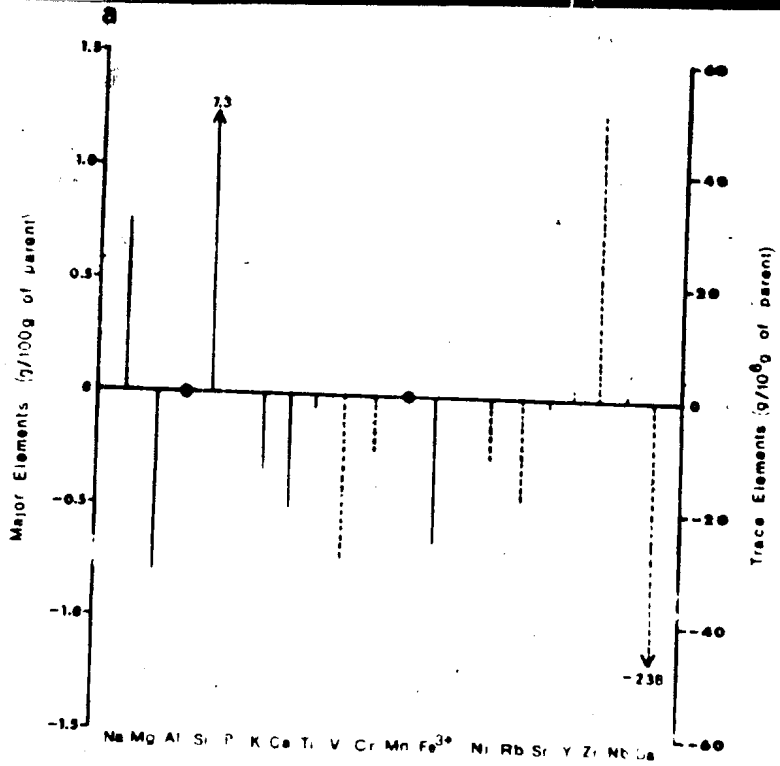
Figure 6.7: Composition-volume relationships showing relative gains and/or losses, calculated after Gresens (1967), of major (solid lines) and trace elements (dashed lines).

a) Relations for chemical changes observed for the Flordian reworking of Maggo gneiss, using mean compositions of Manuel Island and Black Head Tickle suites.

b) Relations for chemical changes in Hopedale dykes in response to Flordian reworking.



00271



put values on the relative gains and/or losses for all elements during the Flordian reworking, substantiate this earlier conclusion.

6.2.3.2 Hopedale Dykes

Hopedale dykes have been subjected to Flordian retrogression, which involves the development of an epidote-actinolite-plagioclase (An 20) assemblage from the Hopedalian, hornblende-plagioclase (An 27) assemblage (See Plates 8B and 8E). Mass balance calculations have been used to examine chemical changes in bulk composition in response to the retrogression. The dyke samples used are from areas of Maggo gneiss where geochronology suites record Hopedalian and Flordian ages. The Hopedalian domain dyke sample (83-228; S.G. = 3.06 g/cc) is from Manuel Island, where Maggo gneiss yields an age of 3,125 Ma. A Hopedale dyke sample (83-212; S.G. = 2.79 g/cc) from Marsha's Cove, is hosted by gneiss dated at 2,894 Ma, and records evidence of Flordian retrogression.

Composition-volume relations for the dykes suggest that a volume increase ($f_v = 1.06$) is indicated for this transition. The relative gains and losses, calculated using Equation 6.1 and employing chemical compositions listed in Table 5.10, are presented graphically in Figure 6.7b. Flordian retrogression of the Hopedale dykes results in enrichment of K_2O , CaO , Cr , TiO_2 , Rb and Ba , no change in Al_2O_3 and V and depletion in all other analyzed elements.

The indicated enrichment in Cr, based on mass balance, accompanying the retrogression of the dykes is interpreted to be an anomalous feature. The Cr content of the analyzed dyke samples exhibit a range from 39 to 311 ppm, and are interpreted to reflect variations in the original chemistry of the dyke magma resulting from primary fractionation processes.

The elements which exhibit enrichment patterns for the Hopedale dykes are also those elements which are depleted in the Maggo gneiss during the Flordian retrogression. The elements which are enriched within the dykes are interpreted to be derived from the host gneisses in response to the retrogression. This exchange between the dykes and gneisses is here interpreted to reflect an attempt to maintain chemical equilibrium between the two lithologies during the retrogression.

The enrichment of LILE, for basic dykes swarms, accompanying prograde metamorphism to amphibolite and granulite facies have been reported for the Saglek dykes, northern Labrador (Collerson et al., 1984), the Ameralik dykes, Southwest Greenland (Gill and Bridgwater, 1979) and the Scourie dykes, northwest Scotland (Weaver and Tarney, 1981a & b).

6.3 Sr₀ Evolution of the Hopedale Block

6.3.1 Maggo Gneiss

Evidence for a genetic link between Hopedalian and Flordian domain Maggo gneiss can be assessed with reference

to a Sr evolution diagram relating age, Sr_0 and mean $^{87}Rb/^{86}Sr$ ratios (Figure 6.8). All Hopedale Block suites display a normal, inverse correlation between age and Sr_0 . As a reference, the mantle evolution curve corresponding to a Rb/Sr ratio of 0.025 (Peterman, 1979) is shown.

The geochronology results (Table 4.1) for the suites analyzed in this study, with corresponding 1 sigma errors are plotted in Figure 6.8a. The errors for each suite overlap to such an extent that a clear separation of the Hopedalian and Flordian suites is not possible. The older suites, i.e. the Hopedalian, have lower Sr_0 ratios than the younger Flordian suites. Application of a Student t-test to the age and Sr_0 values, for the Hopedalian and Flordian suites, indicates that at the 99% confidence limit the age and Sr_0 are significantly different.

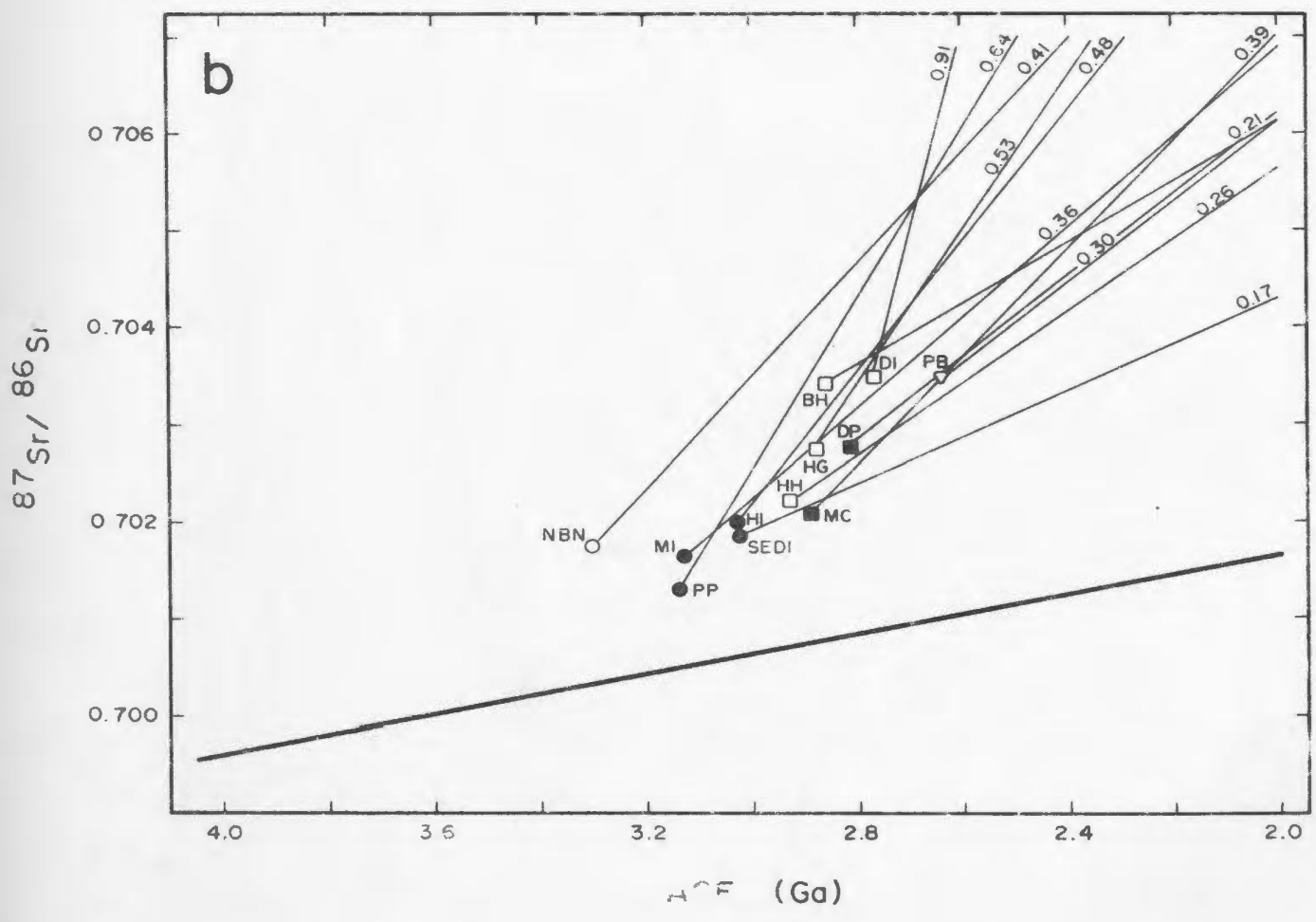
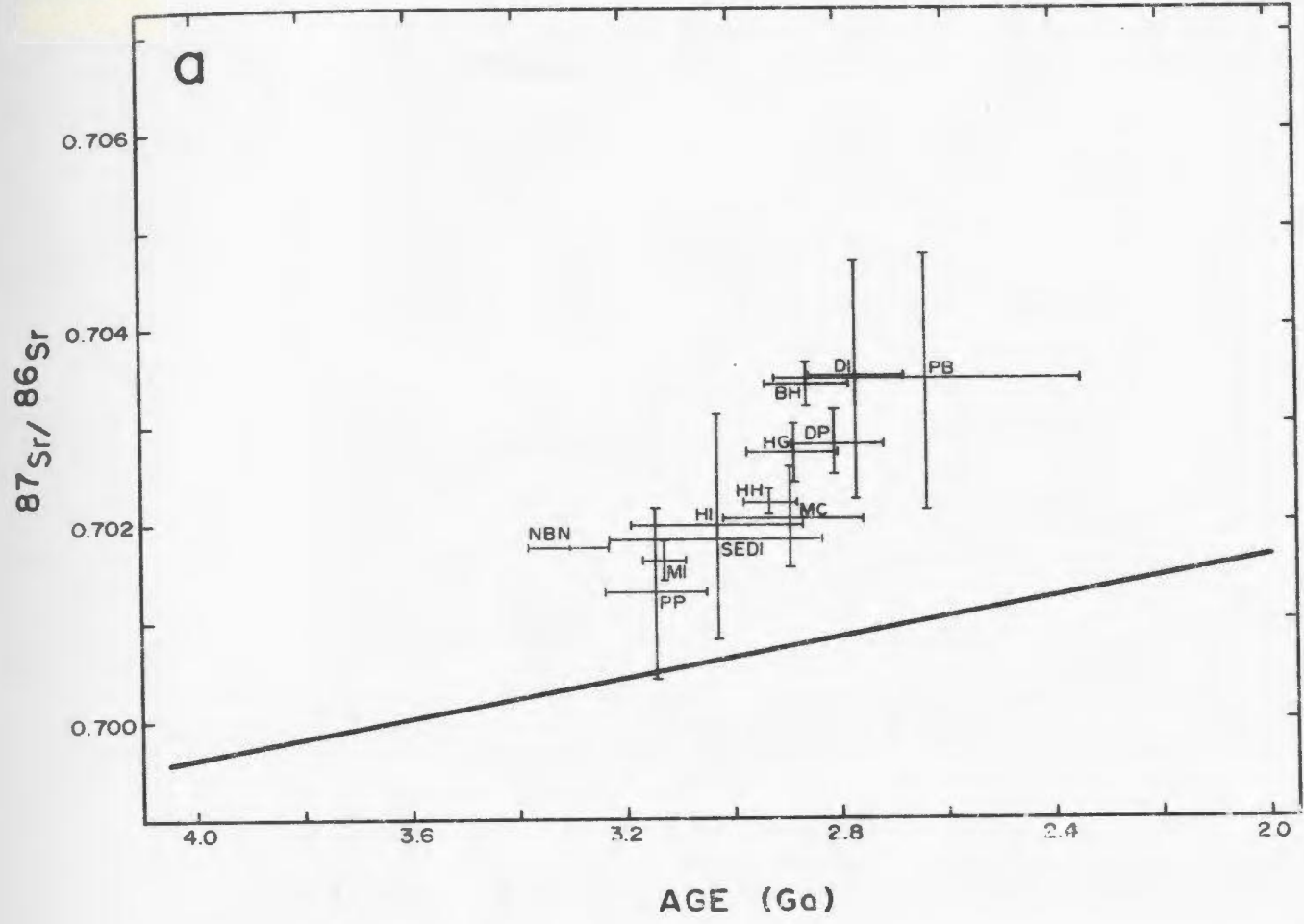
On Figure 6.8b individual suites are grouped according to age and structural fabric (see Section 4.14) preserved at each field locality, i.e. suites with Hopedalian ages are shown with open and closed circles representing localities with Hopedalian and Flordian fabrics, respectively. Sr isotope evolution lines for mean $^{87}Rb/^{86}Sr$ ratios, on Figure 6.8b, represent the increase in $^{87}Sr/^{86}Sr$ with time as ^{87}Rb decays for each suite. The Hopedalian suites have higher mean $^{87}Rb/^{86}Sr$ ratios than the younger Flordian suites. The lower mean $^{87}Rb/^{86}Sr$ ratios for the Flordian suites

Figure 6.8: Sr Evolution diagram, plotting Sr_0 versus age, for Maggo Gneiss suites analyzed in this study. a) Individual suites, showing errors (1 sigma) for determinations. b) Individual suites showing the mean $^{87}Rb/^{86}Sr$ ratio for each suite and their isotopic evolution with time. The suites are grouped according to recorded age and preserved tectonic fabric (see Section 4.14). Abbreviations for suites are given in Chapter 4.

Symbols: solid circle - Hopedallian age and Hopedallian fabric; open circle - Hopedallian age and Flordian fabric; solid square - Flordian age and Flordian fabric; open square - Flordian age and Hopedallian fabric.

The PB suite (inverted triangle) is interpreted to represent Maggo gneiss which has been effected by Proterozoic metamorphism.

The solid heavy line represents the mantle evolution line of Peterman (1979), corresponding to a Rb/Sr ratio of 0.025.



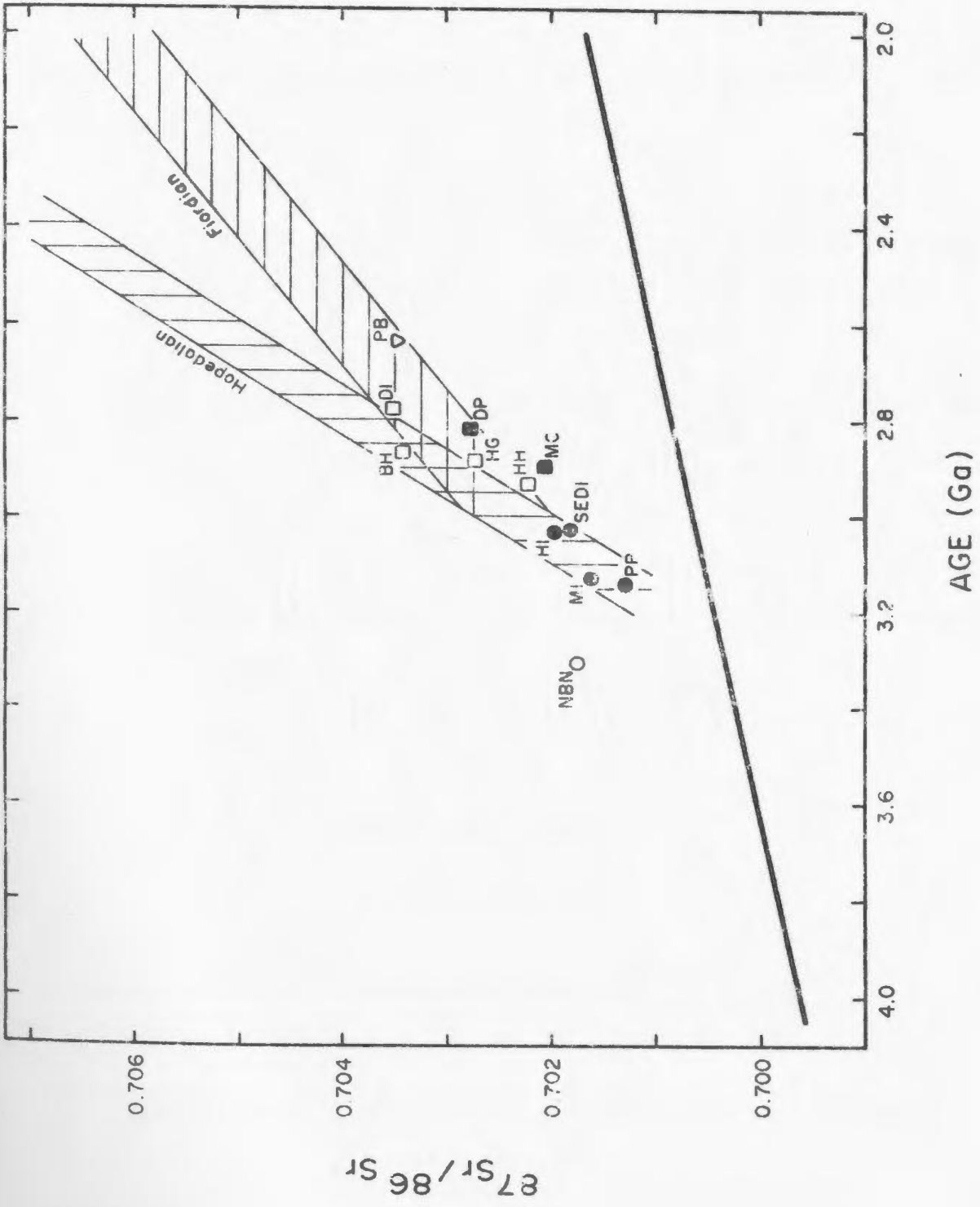
reflect the depletion of Rb, with constant Sr contents (see Figure 6.1h), in the Maggo gneiss in response to the Flordian reworking.

Two suites, SEDI and DI, stand out as being exceptions to the above statement. The SEDI suite, yielding a Hopedalian age, exhibits the lowest mean $^{87}\text{Rb}/^{86}\text{Sr}$ ratio of all suites analyzed. Compared with the remaining Hopedalian suites, SEDI exhibits Rb depletion and Sr enrichment (See Figure 6.1f) in response to the Hopedalian event. In contrast, the Flordian DI suite records the highest mean $^{87}\text{Rb}/^{86}\text{Sr}$ ratio (0.91). Examination of Figure 6.1f and h shows the DI suite to be enriched in Rb and depleted in Sr with respect to other Flordian and the Hopedalian suites. The Rb behaviour (enrichment) recorded for this suite is opposite to that observed for the Flordian event as a whole (see Section 6.2.2).

6.3.1.1 Hopedalian Domain Suites

Hopedalian suites (solid circles on Figure 6.8b) lie above the mantle growth curve (from Peterman, 1979), have Sr_0 values ranging from 0.7013 to 0.7020 and define the Sr evolution path for the Hopedalian domain (vertical ruling Figure 6.9). The slope of this evolution path, determined by least squares fit, corresponds to a mean $^{87}\text{Rb}/^{86}\text{Sr}$ ratio of 0.52. Each of the Hopedalian domain suites closed at different times, as seen by the different ages, however the Hopedalian "evolution" path on Figure 6.9 represents the mean change in the $^{87}\text{Sr}/^{86}\text{Sr}$ ratio with time for these suites.

Figure 6.9: Sr evolution diagram for the Maggo Gneiss suites analyzed in this study. The vertical ruling defines the evolution of Sr for the Hopedalian domain suites, corresponding to a mean $^{87}\text{Rb}/^{86}\text{Sr}$ value of 0.52. Horizontal ruling defines the evolution of Sr for the Flordian suites, corresponding to a mean $^{87}\text{Rb}/^{86}\text{Sr}$ ratio of 0.30. The Flordian suites result from reworking of the older Hopedalian suites between 2,900 and 2,804 Ma. Symbols for individual suites given in Figure 6.8.



The age for the NBN suite (3,305 Ma), compared to other Hopedalian domain suites, is the oldest age reported for the Hopedale Block. Schløtte et al. (in prep.) report an ion-probe age of 3,258 +/- 25 Ma (2 σ) for zircon separated from the pelitic subunit of the Weekes association. This sample was collected at the same locality as the NBN suite samples analyzed here. The old age of Schløtte et al. (in prep.) further demonstrates the presence of Early to Early-Middle Archaean crust in the Hopedale Block.

The zircon age is interpreted by Schløtte et al. (in prep.) to represent a minimum age either of the sediment source or the recrystallization of the sediment under granulite facies conditions. A comparable period of high grade metamorphism has not been recognized in the NAC.

Field relationships within the study area, e.g. Pre-Hopedalian and older fabrics within the gneiss and supracrustals, displaying discordant structural and metamorphic relationships to the gneiss, are interpreted to support the possibility that segments of the Hopedale Block crust are older than Hopedalian.

Model age calculations for Hopedalian domain suites (MI, HI and PP) range from 3,350 to 2,204 Ma (Table 6.4). These ages indicate crustal residence times of at least 200 Ma for these suites, if derived from a mantle-like, i.e. low Rb/Sr, source.

00281

Table 6.4 Model ages, quoted in Ma, for Hopedale Block, Maggo gneiss suites. The ages, calculated using the equations of McCulloch and Wasserburg (1978), assume an initial $^{87}\text{Sr}/^{86}\text{Sr}$ ratio of 0.7039* and a $^{87}\text{Rb}/^{86}\text{Sr}$ ratio of 0.0729. The ages are calculated using $\lambda^{87}\text{Rb} = 1.42 \times 10^{-11}$.

Suite	Mean Rb/Sr	Sr ratio	ϵ_{Sr}^1	$f_{\text{Rb/Sr}}^2$	Model Age ³	Isochron Age
MI	0.349	0.71693	185.2	3.82	3242	3125
PP	0.623	0.73056	378.8	7.60	3330	3140
HI	0.48	0.72287	269.5	5.63	3204	3025
SEDI	0.174	0.70956	80.5	1.40	3820	3024
NBN	0.393	0.72126	248.7	4.43	3714	3305
MC	0.38	0.71874	210.8	4.23	3318	2899
DP	0.297	0.71496	157.1	3.10	3385	2804
PB	0.292	0.71510	159.1	3.10	3502	2632
HH	0.252	0.71574	163.2	2.48	4497	2927
BH	0.213	0.71251	122.3	1.94	4185	2874
HG	0.531	0.72640	319.6	6.33	3373	2884
DI	0.98	0.74445	576.1	12.54	3078	2764

The following equations, from McCulloch and Wasserburg (1978), are used in calculating the model ages:

1) $\epsilon_{\text{Sr}} = [((\text{Sr Ratio})/0.7039) - 1] \times 10^4$

2) $f_{\text{Rb/Sr}} = ((\text{Mean Rb/Sr ratio}) - 0.0729) - 1$

3) Model Age = $1/\lambda \ln[1 + (\epsilon_{\text{Sr}} \times 0.7039 \times 10^{-4}) / f_{\text{Rb/Sr}} \times 0.0729]$

* - These values correspond to a Rb/Sr ratio of 0.025, producing a initial Sr_0 value of 0.7039 for the present day mantle (Peterman, 1979), assuming that the mantle represents an unfractionated source.

Model age calculations for the SEDI and NBN suites are 3,820 and 3,714 Ma (Table 6.4), respectively, suggesting the presence of excess ^{87}Sr in these suites derived from an evolved reservoir. This evolved reservoir is interpreted to represent a preexisting crustal component, which at present is not recognized and/or exposed within the Hopedale Block. Such an evolved reservoir is interpreted to be comparable to Amitsoq gneiss of southern West Greenland, which has undergone a period of Early Archaean granulite facies metamorphism.

An alternative interpretation for the SEDI model age is that it results from a decrease in the mean Rb/Sr ratio of this suite due to metamorphism. This would result in the back extrapolation necessary for the model age to correspond with an erroneous age for the correct crustal age. At present it is not possible to clearly state which of these two possibilities is correct for the SEDI model age.

The results of the Hopedalian area isochron yields an age of 3,366 Ma (Section 4.15.2), indicating a petrogenetic event which is older than the last Sr homogenization event recorded for the whole rocks, i.e. older than the Hopedalian event. Koehler and Mueller-Sohnius (1980) interpret such a period of homogenization to represent either the age of formation or the age of metamorphism of the samples examined. For the Hopedale Block this period of Sr homogenization is interpreted to correspond to the Pre-Hopedalian event.

Collerson et al. (1981; 1982) have identified a suite of Middle Archaean age, quartzo-feldspathic gneisses, the Kiyuktok gneiss, in the Saglek area which consist of 'new' and 'relict' components: Field relationships for the Kiyuktok gneiss, e.g. fragmented and partially resorbed Saglek dykes, indicate an origin of these gneisses by processes involving remobilization of the older Uivak gneiss (Collerson et al., 1981). Isotopic results show that the Kiyuktok gneiss results from mixing of aqueous fluids, enriched in ^{87}Sr and Pb, with the in situ granitic mobilizates of the Uivak gneiss (Collerson et al., 1982).

The Hopedalian domain Maggo gneiss is here interpreted to be derived from preexisting silicic crustal material in a manner similar to that proposed for the Kiyuktok gneiss. Examination of possible precursors to the Hopedalian domain Maggo gneiss is presented in Section 5.5.

6.3.1.2 Flordian Domain Suites

With the closing of the isotopic systematics at the end of the Hopedalian event, the Rb-Sr clock for the Maggo gneiss continued its evolution, resulting in the increase in $^{87}\text{Sr}/^{86}\text{Sr}$ with time. The Flordian event, which spans the time range from 2,880 to 2,804 Ma, began with disturbance of the isotopic systematics in the Maggo gneiss. The time period spanned by the Flordian event or events is comparable to that reported here for the Hopedalian event and that recorded for Archaean orogenic periods in South Africa (Harris et al., 1987). The Sr₀

284

ratios for the Flordian suites ($Sr_0 = 0.7021$ to 0.7035) result from evolution of the Maggo gneiss from 3,091 to 2,900 Ma. Accompanying the resetting was LILE depletion of the gneiss, resulting in the lower mean $^{87}Rb/^{86}Sr$ ratios for the Flordian suites. The Sr evolution path for the Flordian suites (horizontal ruling, Figure 6.9) corresponds to a mean $^{87}Rb/^{86}Sr$ ratio of 0.30.

6.3.2 Published Results for Maggo Gneiss and Kanairiktok Intrusions

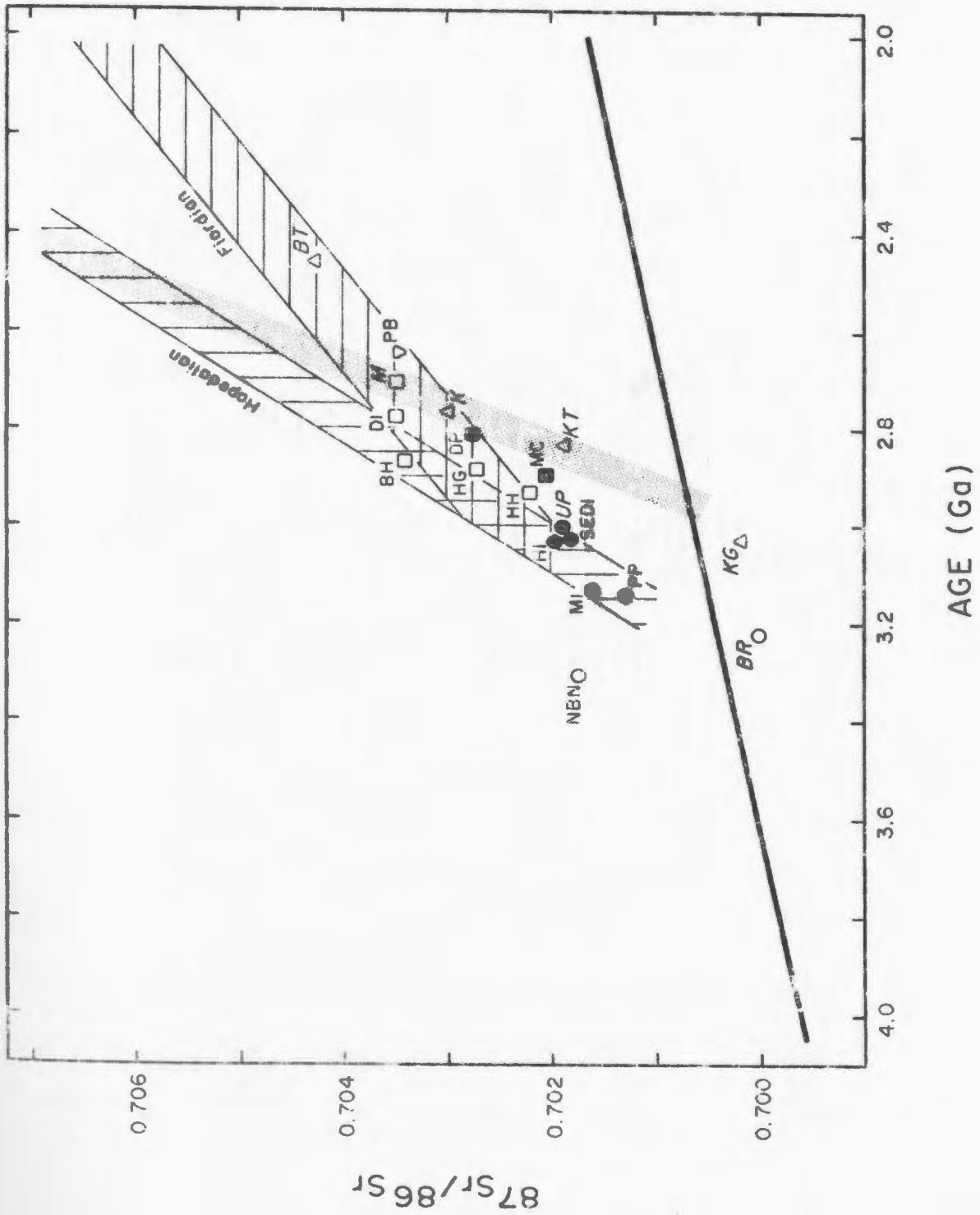
On Figure 6.10 results of isotopic analyses of Maggo gneiss and Kanairiktok intrusive suites examined by Grant et al. (1983) are plotted with the isotopic results from this study. Grant et al. (1983) suggested that the Archaean rocks of the Hopedale Block separated from the mantle 2,900 to 3,100 Ma ago; forming two distinct crustal segments. The older segment, defined by their Hunt River Belt (BR) and Uivak Point (UP) suites, is comparable to the Hopedalian evolution path defined in this study. The younger crustal segment is defined by Maggo gneiss (KG, M) and Kanairiktok intrusive suites (KT, K, BT). The latter represent pre- to syn- Flordian tonalitic to granodioritic intrusions, which yield a U-Pb discordia age of 2,830 Ma (Ermanovics et al., 1982). The Kanairiktok intrusive suites are interpreted here to represent the younger segment.

Of the Maggo gneiss suites analyzed by Grant et al. (1983) to define the younger crustal segment, the Maggo Island (M) suite is here interpreted to represent Flordian

Figure 6.10: Sr evolution diagram incorporating data from this study with the results of Grant et al. (1983) for Maggo gneiss and Kanairiktok Intrusions from the Hopedale Block. The Flordian event is characterized by 1) reworking of Hopedalian domain gneiss and 2) emplacement of new material, the Kanairiktok Intrusions, into the Hopedale Block. The crustal segment represented by the Kanairiktok Intrusions is shown by the light stipple. See text for discussion.

Data points from Grant et al. (1983) shown in Italics: BR - Hunt River Belt; UP - Uivak Point; M - Maggo Island; KT, K and BT - Kanairiktok Intrusions. The KG suite is here interpreted to represent a deformed, early phase of the Kanairiktok Intrusions.

Symbols as in Figure 6.8, plus open triangle - Kanairiktok Intrusions.



reworked Maggo gneiss similar to the BH and DI suites of this study. Without knowledge of the field relationships of the Kanairiktok Bay (KG) suite of Grant et al. (1983) its significance to the evolution of the Hopedale Block is far from certain. Based on the little information available, this suite may represent an early phase of the Kanairiktok Intrusions, and not Maggo gneiss, emplaced prior to the Flordian event. The KT and K suites are interpreted to be cogenetic and represent the crustal segment corresponding to the addition of new material to the Hopedale Block (shaded pattern, Figure 6.10). The lower end of the Kanairiktok Intrusive evolutionary path intersects the KG data point and as such this suite is interpreted to be cogenetic, in terms of Rb-Sr isotopic systematics, with the other Kanairiktok suites.

The emplacement of new material and the reworking of preexisting crust during the Flordian was preceded by the deposition of the Florence Lake supracrustals. This period of volcanism and sedimentation represents a time of relatively little tectonic activity between the Hopedalian and Flordian events resulting in the growth of ^{87}Sr within the Maggo gneiss.

6.4 Characteristics of the Flordian Event

6.4.1 Introduction

Based on the isotopic results from this study it is apparent that the Flordian event comprises the reworking of preexisting material in response to dynamothermal processes

occurring between 2,880 and 2,804 Ma. Accompanying the Flordian reworking is emplacement of the Kanairiktok intrusions into the Hopedale Block. In this section the nature of the Flordian event is considered with emphasis on:

- 1) the role played by the Kanairiktok intrusions;
- 2) the chemical and physical changes accompanying Flordian reworking, with emphasis on metamorphism and its relationship to the contemporaneous high grade metamorphism observed elsewhere in the NAC;
- 3) the nature of the fluid phase accompanying the Flordian reworking, and;
- 4) how these features relate to the depletion and enrichment patterns observed in the Maggo gneiss.

6.4.2 Role of the Kanairiktok Intrusions

Within the study area no outcrops of the Kanairiktok intrusions were observed, however to the south and west, within the Hopedale Block, this lithology accounts for at least 35 % of all exposed rock types (see Figure 2.2). The Kanairiktok intrusions, based on geochronology results (Grant et al., 1983; Loveridge et al., 1987) and field relationships (Ermanovics et al., 1982), were emplaced into the Hopedale Block crust during the Flordian event.

The initiation of Flordian reworking of the Maggo gneiss is interpreted here to have been the inaugural mechanism for the derivation and emplacement of the Kanairiktok intrusions. Following emplacement the

[REDACTED]

Intrusions were subsequently deformed and metamorphosed in response to the latter phases of the Flordian event. It is not possible to state whether the Kanariktok intrusions represent either new, juvenile material or reworked preexisting material added to the Hopedale Block crust in response to the Flordian event. Based on Rb-Sr isotopic results Grant et al. (1983) favour the former hypothesis for the origin of the intrusions. This aspect of Hopedale Block geology requires further study.

Structural, metamorphic and isotopic evidence from South Africa suggests that Archaean orogenic periods begin with the formation and introduction of a new crustal component and end with the reworking of preexisting continental crustal material (Harris et al., 1987). The Flordian event differs from the South African case in that reworking accounts for a more pronounced effect on the crustal component at Hopedale.

6.4.3 Chemical and Physical Changes Accompanying the Flordian Reworking

The Maggo gneiss underwent LILE depletion in response to the Flordian reworking, resulting in lower Rb/Sr and higher K/Rb ratios, compared with the Hopedalian domain gneiss. Low Rb/Sr and high K/Rb ratios are considered to 'fingerprint' evidence of granulite facies metamorphism (Heler, 1973; Griffin et al., 1980; Sheraton and Black, 1983). Granulite facies mineral assemblages and relict textures have not been recognized in the exposed Flordian or the Hopedalian domains of the Hopedale Block.

For Rb depletion observed in the Flordian domain gneiss to result from a pre-Hopedalian (i.e. > 3,091 Ma) granulite facies metamorphism, comparable to the 3,600 Ma event recognized in the Amitsoq gneiss of Greenland (Griffin et al., 1980), requires;

- 1) preservation of the depleted character of the gneiss throughout the Hopedalian event,
- 2) closing of the Rb-Sr isotopic systematics only as a result of the Flordian event, and
- 3) a strong sampling bias towards these preserved samples.

All of these criteria must be met in order for the depleted gneiss to result from an old, i.e. 3,600 Ma, granulite facies event.

6.4.4 Flordian Metamorphism and the Contemporaneous NAC High Grade Event

In West Greenland and northern Labrador evidence for a major period of granulite facies metamorphism at 2,800 Ma has been reported by Wells (1976; 1979) and Collerson et al. (1981). The LILE depletion and HFS element enrichment observed for the Flordian domain Maggo gneiss is interpreted to result from this widespread period of deformation and metamorphism.

Metamorphic conditions, i.e. P and T estimates, during the Flordian reworking have yet to be examined in detail and are beyond the scope of the present study. Preliminary data for the Hopedale dykes (Section 3.3.3) indicate

retrogression of the Hopedalian domain assemblages under low to middle amphibolite facies conditions in response to the Flordian event. T, P and fluid composition data for the synchronous granulite to amphibolite facies metamorphism recorded in West Greenland, is examined to identify the nature of the fluid phase that may have accompanied the Flordian reworking.

Wells (1976; 1979) has examined the chemical and thermal evolution of the Greenland Archaean in response to the 2,800 Ma metamorphism. Wells (1976) has shown that P_{H_2O} accompanying the metamorphism is equivalent to $0.5P_{Solid}$ and $<0.3P_{Solid}$ for the amphibolite ($P_{Solid} = 7.0$ kb; $T = 630^{\circ}C$) and granulite ($P_{Solid} = 10.5$ kb; $T = 810^{\circ}C$) facies, respectively. The major and trace element redistribution patterns associated with the granulite facies metamorphism in the Buksefjorden region results from the action of a vapour phase rather than the removal of an anatectic melt (Wells, 1979).

6.4.5 Nature and Role of the Flordian Fluid Phase

The vapour phase accompanying Flordian metamorphism must have been a mixture of several species, mainly H_2O and CO_2 , to account for $P_{H_2O} < P_{Total}$. If the vapour phase is a mixture of H_2O and CO_2 and provided P_{Vapour} equals P_{Solid} , which is not unreasonable considering the high metamorphic P and T (Wells, 1979), then the low P_{H_2O} accompanying metamorphism implies a low $H_2O:CO_2$ ratio. The low $H_2O:CO_2$ ratio has been

██████████

Interpreted to result from a CO₂-rich vapour phase being pumped into the lower crust, from deeper sources during granulite facies metamorphism, effectively diluting the H₂O fluid phase (Wells, 1979). The relationship between granulite facies metamorphism and a CO₂-rich fluid phase has further been examined by Newton et al. (1980).

For the contemporaneous amphibolite facies metamorphism, in West Greenland, the higher P_{H₂O} and H₂O:CO₂ ratio results from the lack of deeper level CO₂ diluting the vapour phase. Wells (1979) has shown that at pressures of 5 - 10 kb the CO₂:H₂O ratio reaches a maximum and at P < 5 kb the vapour phase CO₂:H₂O ratio is markedly decreased.

The documented trace element enrichment and depletion patterns for the Flordian domain Maggo gneiss can be explained using the fluid composition of Wells (1979) and the observed mineralogical changes in the Maggo gneiss.

The Hopedalian to Flordian transition observed for the Maggo gneiss points to minor amounts of migmatite within the Flordian domain (see Plate 6D, 10B). This feature is in part due to the conditions of Flordian metamorphism (low to middle amphibolite facies) which occurred at P and T conditions below the water saturated granite solidus. The migmatites developed during the Flordian event are interpreted to have been derived at depth, i.e. above the granite solidus, and subsequently emplaced into the Maggo gneiss. The minor amounts of migmatite development recorded

In the study area for the Flordian domain, and the contemporaneous high grade metamorphism (Wells, 1979) may reflect the low activity of water at depth, resulting from CO₂ dilution. The lack of partial melting accompanying high grade metamorphism is indicative of low activity of water (Wells, 1979; Stahle et al., 1987). The observed element enrichment and depletion patterns for the Flordian reworking suggests that solid-solid reactions occurring in equilibrium with a transient fluid phase are mainly responsible for the new mineral assemblages.

Wells (1979) data for the 2,800 Ma amphibolite facies metamorphism (P = 7 kb; T = 630°C) places an upper limit on conditions for the Flordian metamorphism. This falls into the P range (4 to 7 kb) proposed by Wells (1979) which corresponds with the decrease in the CO₂:H₂O ratio in the fluid phase (Kadik and Eggler, 1975). The implications of this are that the Flordian fluid system was characterized as a dry (H₂O-poor) system, which was diluted to some extent with CO₂. The depth at which the Flordian event occurred represents the deeper portion of this transition zone, corresponding to the change from high to low CO₂:H₂O ratios. The loss of CO₂ from the fluid phase affects the ability of the fluid to transport element species, e.g. the LILE, HFS and REE.

Various workers (Collerson and Fryer, 1976; Wells, 1979; Murphy and Hynes, 1986; Stahle et al., 1987) have suggested that given high CO₂:H₂O ratios a fluid phase

would have the ability to cause the LILE, HFS and REE to become mobile. Flordian domain Maggo gneiss exhibits LILE depletion, HFS enrichment and no change in REE contents (Section 8.2) when compared with the Hopedalian domain gneiss. The results of the element mobility/immobility study suggest that the fluid phase present during the Flordian event was a mixture of CO₂ and H₂O and had an intermediate to low CO₂:H₂O ratio (i.e. CO₂:H₂O < 0.5). The CO₂:H₂O ratio within the fluid phase was low enough not to cause significant mobility of the REE, but was sufficiently high to cause some mobility of the HFS elements, e.g. Ti, Y, P and Zr (see Murphy and Hynes, 1986).

The fluid phase present during the Flordian reworking is inferred to have been derived during high grade metamorphism at depth and with movement upward through the crust, the CO₂ content had decreased. The decrease in CO₂ content could have been due to a decrease in CO₂ solubility with a decrease in pressure (Kadik and Eggler, 1975). A migrating fluid, displaying increasing CO₂ with depth, would carry the HFS elements necessary to cause their observed enrichment. HFS elements would be released in response to dehydration reactions, involving hornblende, accompanying high grade metamorphism. The same fluid phase would be capable of removing the LILE, resulting in the depleted nature of these elements in the Flordian domain gneiss. The actual mechanism for the HFS elements coming

out of solution at the level corresponding to the Flordian is inferred to be a function of the decreasing $\text{CO}_2:\text{H}_2\text{O}$ ratio.

The lack of any significant difference in REE distribution patterns between the Hopedalian and Flordian domain gneiss is taken to indicate that the CO_2 content of the fluid phase was not sufficient to produce a $\text{CO}_2:\text{H}_2\text{O}$ ratio which would cause the mobility of the REE. This conclusion fits with Wells (1979) data which shows decreasing $\text{CO}_2:\text{H}_2\text{O}$ ratios with decreasing pressure equivalent to those inferred for the Flordian reworking.

6.4.6 Observed Mineralogical Changes

The recorded behaviour of the HFS and LILE is reflected to some extent in the change in mineralogy of the Maggo gneiss during the Flordian reworking. The lack of K-feldspar, in Maggo gneiss from both domains, suggests that other minerals, i.e. the mafic minerals, are responsible for controlling the LILE distribution. The dominant mafic mineral in the Hopedalian domain gneiss is biotite with minor hornblende and garnet. Flordian domain gneiss is characterized by the growth of hornblende (Ermanovics et al., 1982) which is dominant over minor biotite and epidote. The replacement of a biotite dominant assemblage by a hornblende dominant assemblage can be used to explain the element enrichment and depletion patterns.

Hornblende growth during the Flordian preferentially incorporated K over Rb, both of which were liberated by breakdown of biotite. Hornblende is capable of taking up some of the K, with the remainder being lost from the system, as seen in the lower K_2O contents for the Flordian domain gneiss. The larger Rb ion does not fit the hornblende structure, resulting in the marked decrease in Rb from the Hopedalian to Flordian domains. The end result is that the Flordian domain gneiss is depleted in K and Rb, released by biotite breakdown, but not incorporated into growing hornblende. These elements are removed from the system by transport within the Flordian fluid phase.

The biotite to hornblende transition takes place at a static position, with the elements exchanged between the solids and the fluid phase. The elements, with low partition coefficients for hornblende are removed by the fluid, those elements with high partition coefficients, are selectively removed from the fluid. Partition coefficient data for silicate-fluid systems are not available at present mainly due to the number of variables required to attain equilibrium. The main variables to be considered are the fluid composition, especially the affect of minor constituents, e.g. H_2S , F^- , Cl^- , CO , H_2 , O_2 , the different mineral structures for the phases involved and the solubility relations of the silicates.

The growth of hornblende in response to Flordian reworking can explain the enrichment in Y recorded for the

Flordian domain gneiss. This element is preferentially incorporated into hornblende over biotite, with the Y required coming from the fluid phase. The enrichment in P is reflected in the increase in the observed apatite content of the Flordian domain gneiss.

6.4.7 Summary

The Flordian orogenic period spans the time range from 2,900 to 2,804 Ma with early and late phases characterized by reworking of preexisting crust, separated by a period dominated by the derivation and emplacement of the Kanairiktok intrusions. The time between the Hopedalian and Flordian events, within the Hopedale Block, is characterized by the extrusion and deposition of the Florence Lake supracrustals (Ermanovics *et al.*, 1982). It is during this tectonically quiet period that the Rb-Sr isotopic systematics of the Maggo gneiss, established during the Hopedalian event, evolved with time, such that during the Flordian reworking the isotopic systematics were reset.

In response to reworking, Flordian domain gneiss exhibits LILE depletion, HFS element enrichment and no change in REE content, compared with the Hopedalian domain gneiss. The enrichment-depletion patterns for the Maggo gneiss are 1) reflected in the change in mineralogy as a result of the retrogression associated with the reworking, and 2) a reflection of the fluid phase composition accompanying the reworking. The Flordian fluid phase

composition is characterized by $P_{fluid} < P_{total}$ and the $CO_2:H_2O$ ratio having an intermediate to low value, ($0 < CO_2:H_2O < 0.5$), by analogy with Well's (1979) study. The last point to be made concerning the Flordian event is that the geochemical reworking (enrichment-depletion and isotopic systematics) occurred later than and, in the case of some analyzed localities, independently of structural reworking.

6.5 Origin of the Maggo Gneiss Precursor

6.5.1 Introduction

In the previous sections the evolution of the Maggo gneiss and the evolution of the Hopedale Block for the post-Hopedalian period were examined. Looking in the other direction, at the pre-Hopedalian history of the gneiss, i.e. its origin and evolution, provides a more complete history of the gneiss, information on its relationship to similar grey gneisses of the NAC and the nature of the processes leading to the growth and stabilization of the Hopedale Block.

Workers are divided into two schools of thought to explain the origin of grey gneiss lithologies (Amitsoq, Nuk, Ulvak and Hebron gneisses) within the NAC. The major differences between the two schools relates to the composition of, and the source region for, the parental material to the dominant grey gneisses in these terrains. The most contentious point of debate is whether the old gneisses display evidence of a crustal prehistory prior to

metamorphism, which closed the gneiss to further changes in Rb-Sr isotope systematics.

Moorbath (1975, 1977, 1978), among others, believes the grey gneisses are igneous in origin, derived directly from a mantle source. The evidence cited in support of this hypothesis is that the gneisses record evidence of relatively short (<150 Ma) crustal residence periods prior to their emplacement.

Bridgwater and Collerson (1976, 1977) invoke inter-related mechanisms to interpret the origin of grey gneiss complexes. These mechanisms involve long crustal residence periods prior to derivation of the gneiss and/or remobilization of older crust, accompanied by Rb metasomatism during emplacement. Rb metasomatism masks preexisting isotopic inhomogeneities in the gneiss and render crustal residence time calculations, based on Rb contents, invalid as the Rb content does not represent the true concentration in the original parent.

The conclusions of Bridgwater and Collerson (1976, 1977) suggest that the model age calculations, presented in Table 6.4, for the suites of this study be treated with some scepticism. McCulloch and Wasserburg's (1978) calculations date the time of addition of new material to the crust. This is not the case for the Flordian suites.

Geochemical and isotopic results (Sections 6.2 to 6.4) show that Flordian domain Maggo gneiss has been derived from older, Hopedalian domain, gneiss by reworking. The

older gneiss component represents preexisting crustal material. Grant et al. (1983), based on Rb-Sr isotopic studies, suggest that the Kanairiktok Intrusive magma represents new material derived from a mantle source and added to the crust at this time, however no geochemical modelling of this relationship has been carried out.

The origin and evolution of grey gneiss complexes, not just restricted to the NAC but in other Precambrian terrains, is directly related to the origin of granite magmas. Of the processes of granite formation outlined in Chapter 1, fractional crystallization and partial melting occurring independently or in unison are most often cited to explain granitic (s.l.) lithologies in Precambrian terrains. Fractional crystallization of basaltic magmas has been suggested by Arth et al. (1978) and Smith et al. (1983) to explain the observed basalt (gabbro) - granite (tonalite, trondhjemite, quartz monzonite) association in Proterozoic and Archaean terrains. The major problem with this mechanism is the small volume of granitic magma produced (Grout, 1926). To account for the observed volume of Precambrian granitic (s.l.) material requires the presence of at least 10 times as much basaltic (s.l.) material to have been produced and disposed of over the course of earth history.

A more likely mechanism, which explains the observed quantities of granitic (s.l.) lithologies in exposed high grade terrains is for partial melting, of a variety of

~~SECRET~~

lithologic sources, in the generation of grey gneiss complexes. The following lithologies, which undergo varying degrees of partial melting, have been suggested as possible parents to Archaean grey gneiss complexes:

1) Mantle Sources (Moorbath, 1975; Peterman and Barker, 1976).

2) Crustal Sources

a) Immature greywackes (Arth and Hanson, 1975).

b) metabasaltic lithologies

i) eclogite (Arth and Hanson, 1975)

ii) mafic granulite (Compton, 1978a; Drury, 1978)

iii) garnet-rich and garnet-absent amphibolite (Martin, 1987).

c) Intermediate lithologies (This Study)

i) Intermediate granulite facies gneiss

ii) Intermediate amphibolite facies gneiss.

Petrogenetic modelling of REE compositions, from Hopedallan domain Maggo gneiss, has been undertaken to assess the relevance of the above sources as parental material to the gneiss.

6.5.2 Petrogenetic Models - Introduction

REE petrogenetic modelling provides a means of estimating parent-daughter compositions developed in response to evolutionary processes (Haskin, 1984). Petrogenetic modelling involves the consideration of two concepts in the derivation of suitable parent-daughter

██████████

compositions as a result of complex geological processes. First, that the theoretical behaviour of trace elements during melting and crystallization be known. Shaw (1970) proposed equations which consider the distribution of individual elements, between solid and liquid, in response to anatexis.

The second concept involves the availability of suitable measurements of partition coefficients for elements between phenocrysts and matrices for lithologies of comparable composition to the parent being considered (Arth, 1976). The resulting models are limited as they attempt to duplicate complicated, often poorly understood processes occurring in nature. Drury (1978, p. 247) points out the fallibility of attempting to model natural processes and trying to come up with a reasonable geological solution.

Parent - daughter REE compositions have been modelled using an unpublished BASIC program, employing the equations of Shaw (1970), written by D. Furey (MUN). Partition coefficient values for the source materials considered are listed in Appendix E. Parent mineralogical compositions of the various source materials considered to give rise to the Hopedalian domain Maggo gneiss are listed in Tables 6.5 and 6.6.

6.5.3 Mantle Source

The mantle source used as a parent to the Maggo gneiss is inferred to have a flat chondrite normalized REE

Table 6.5: Metabasaltic modal mineralogies, approximating early Archaean quartz tholeiite, used as source materials in melting models. Mineral proportions in volume percent. Mineral abbreviations are: opx - orthopyroxene; cpx - clinopyroxene; hbl - hornblende; plag - plagioclase; garn - garnet; qtz - quartz; mag - magnetite; ilm - ilmenite.

	opx	cpx	hbl	plag	garn	qtz	mag	ilm
Eclogite		56.5			41			2.5
Garnet Granulite I		45		25	30			
II	20	25		35	20			
Garnet Amphibolite I		10	40	40	10			
II			30	30	30	8	2	
Amphibolite			50	50				

Table 8.6: Intermediate composition, modal mineralogies, approximating early Archaean granulite (Part A) and amphibolite (Part B) facies gneiss, used as source material in melting models. Mineral proportions in volume percent. Mineral abbreviations as in Table 6.5 plus blo - biotite; kspar - K feldspar; ap - apatite. Representative bulk chemical compositions for these source materials are given in Table 6.7.

Part A - Granulite Facies Gneiss

	opx	cpx	hbl	plag	garn	blo	kspar	qtz	mag
I	5	15	10	60	10				
II	5	15	10	55	10		5		
III	15	4	5	60	10		5		1
IV	15	5	5	50	15	2	5	2	1
V	10	20	5	55	5		5		
VI	15	20	2	55	3		5		
VII	15	20		55	2		8		

Part B - Amphibolite Facies Gneiss

	hbl	plag	garn	blo	kspar	qtz	ap	mag
I	20	55		10	3.5	10	0.5	1
II	10	55	10	10	3.5	10	0.5	1
III	10	50	10	10	8.5	10	0.5	1
IV	15	55	5	10	3.5	10	0.5	1
V	15	50	10	10	8.5	10	0.5	1
VI	10	55		20	3.5	10	0.5	1
VII	10	55	5	15	3.5	10	0.5	1
VIII	8	55	5	8	8	14.5	0.5	1

4422

distribution, with abundances at 2X chondrites, similar to that used by Martin (1987). A variety of possible parental mineralogies were tested with all compositions yielding similar results. The results obtained for a garnet hornblende parent (56% olivine, 30% orthopyroxene, 8% clinopyroxene and 6% garnet) are presented as representative for a mantle source (Figure 6.11a).

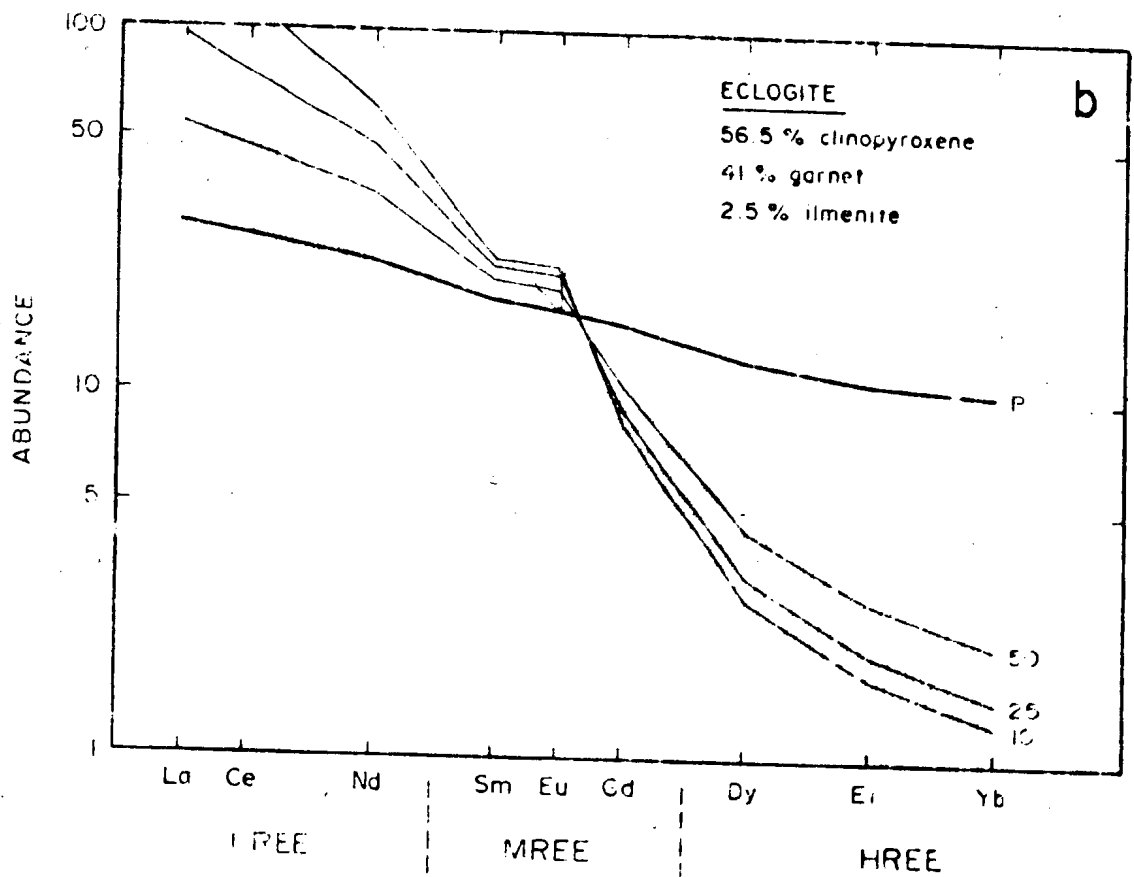
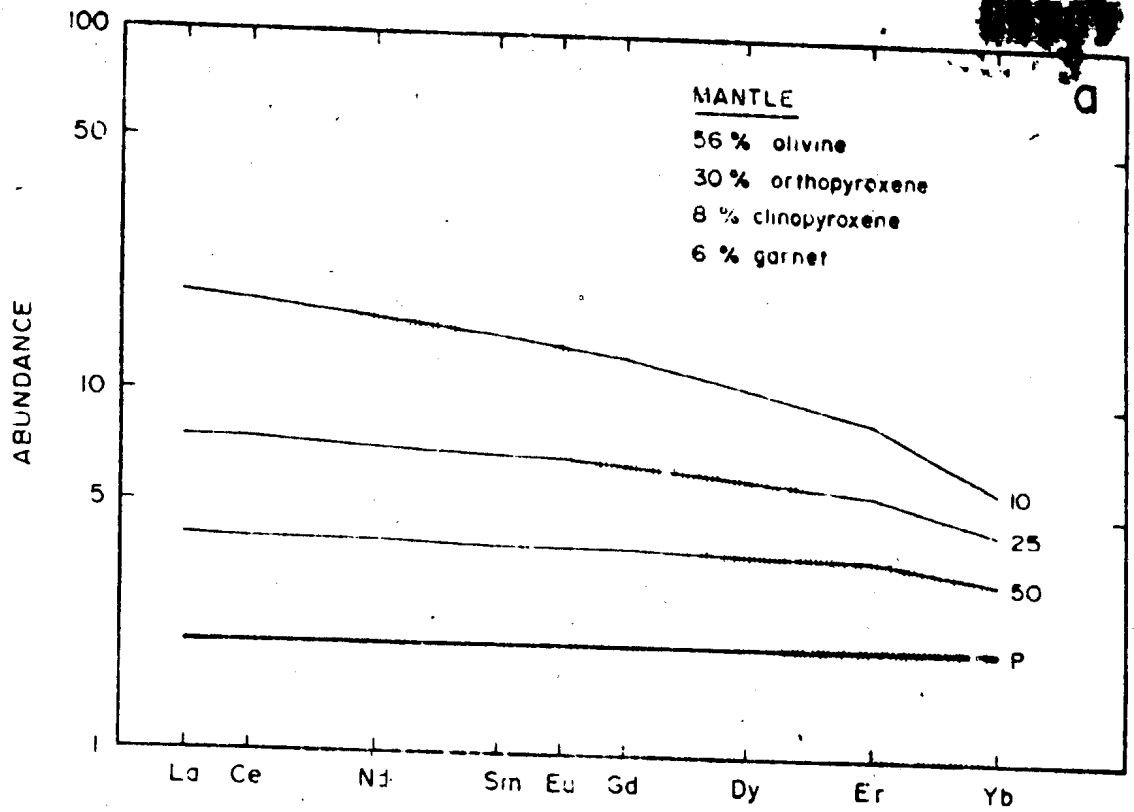
Equilibrium modal melting of the above mineralogy (Figure 6.11a) does not yield REE distribution patterns comparable to those observed for Hopedalian domain Magog gneiss (shaded field on Figure 6.11). The resulting REE patterns for this model are weakly fractionated, lack LREE enrichment, HREE depletion and any evidence of Eu anomalies. The effects of changing the modal mineralogy of the parent and/or the chondritic abundance of the source affects the REE abundance in the melt produced and not the general overall shape of the resulting patterns. For the Hopedalian domain gneiss the mantle is an improbable source.

6.5.4 Crustal Sources

As outlined above three possible crustal protolith lithologies have been suggested as sources for granitic (s.l.) magmas by partial melting. Arth and Hanson (1975) suggested that immature greywackes will, on 25-50% melting, yield a quartz monzonite composition. However, this composition has not been recognized in the Hopedale Block, or in lithologies of comparable age within the N/C, hence

Figure 6.11: Results of equilibrium modal melting of compositions shown for a) mantle peridotite and b) eclogite sources.

P - Parent composition. Numbers correspond to the degree of melting which the parent undergoes to yield the observed pattern. The shaded region is the field defined by 9 Hopedalian domain Maggo Gneiss samples.



~~SECRET~~

this is an improbable parent for the Maggo gneiss. This leaves two possibilities for the Hopedalian domain Maggo gneiss parent.

6.5.4.1 Metabasaltic Sources

Partial melting of metabasaltic sources is the most often cited means of deriving Archaean grey gneiss, comprised of tonalite, trondhjemite and granodiorite (Arth and Hanson, 1975; Compton, 1978a; Drury, 1978; Martin, 1987). Parent mineralogies, representing a range of metamorphic grades, used in modelling a metabasaltic source to the Maggo gneiss are presented in Table 6.5. The variation in mineralogical content, reflecting a range of metamorphic grades, represents hypothetical minerals and their proportions developed in a quartz tholeiite subjected to amphibolite to eclogite facies metamorphism. The quartz tholeiite parent (P on Figure 6.11b) exhibits a mildly LREE enriched pattern $(La/Yb)_N = 2.8$, comparable to Early Precambrian tholeiites from northeastern Minnesota (Arth and Hanson, 1975). The REE source composition and partition coefficient data used are listed in Appendix E.

Parental material with REE abundances comparable to present day MORB (Sun et al., 1979) were modelled. A MORB parent to the Maggo gneiss was rejected because of the low degrees of melting (< 2%) required to yield LREE enrichment patterns comparable to those observed for the gneiss.

Results of equilibrium modal melting of an eclogite parent (Table 6.5), with a source composition P (Figure

8.11b) for 10, 25 and 50% melting yield REE patterns which exhibit strong LREE enrichment (175X chondrites), positive Eu anomalies ($\text{Eu}/\text{Eu}^* = 1.5$) and HREE depletion (1.3X chondrites). All values quoted are for 10% melting. The overall slope of the model results are steeper than the observed slopes for REE patterns from Hopedalian domain Maggo gneiss.

For low degrees of melting the model LREE and MREE (middle REE) enrichment is greater than that observed for Hopedalian domain gneiss. With an increase in the degree of melting, the MREE abundances are too great compared to Maggo gneiss. The HREE depletion recorded for all degrees of melting are comparable to observed HREE depletion. The distinctly different model REE patterns compared with the Maggo gneiss suggests that an eclogite is an improbable source for the gneiss.

The garnet granulite and garnet amphibolite source mineralogies (Table 6.5) yield similar results when modelled (Figure 6.12). The model results are characterized by enriched LREE and MREE and steeper overall patterns when compared with Hopedalian domain gneiss. The HREE results are again comparable to observed patterns for Maggo gneiss.

The amphibolite source (Table 6.5) yields a mildly fractionated pattern with a strong negative Eu anomaly ($\text{Eu}/\text{Eu}^* = 0.6$) for a 10% melt (Figure 6.13), with the magnitude of the Eu anomaly decreasing with an increasing degree of melting. The amphibolite source does not produce

Figure 8.12: Results of equilibrium modal melting of (a) garnet granulite I and (b) garnet amphibolite II sources (Table 6.5). The dashed line corresponds to the melt produced after 25% melting of the given parent, with 1% apatite in the residue. The dot-dashed line corresponds to the melt produced after 25% melting of the given parent, with 1% titanite in the residue. See text for discussion. P - Parent composition. Numbers correspond to the degree of melting. Shaded region is the field defined by 9 Hopedalian domain Maggo Gneiss samples.

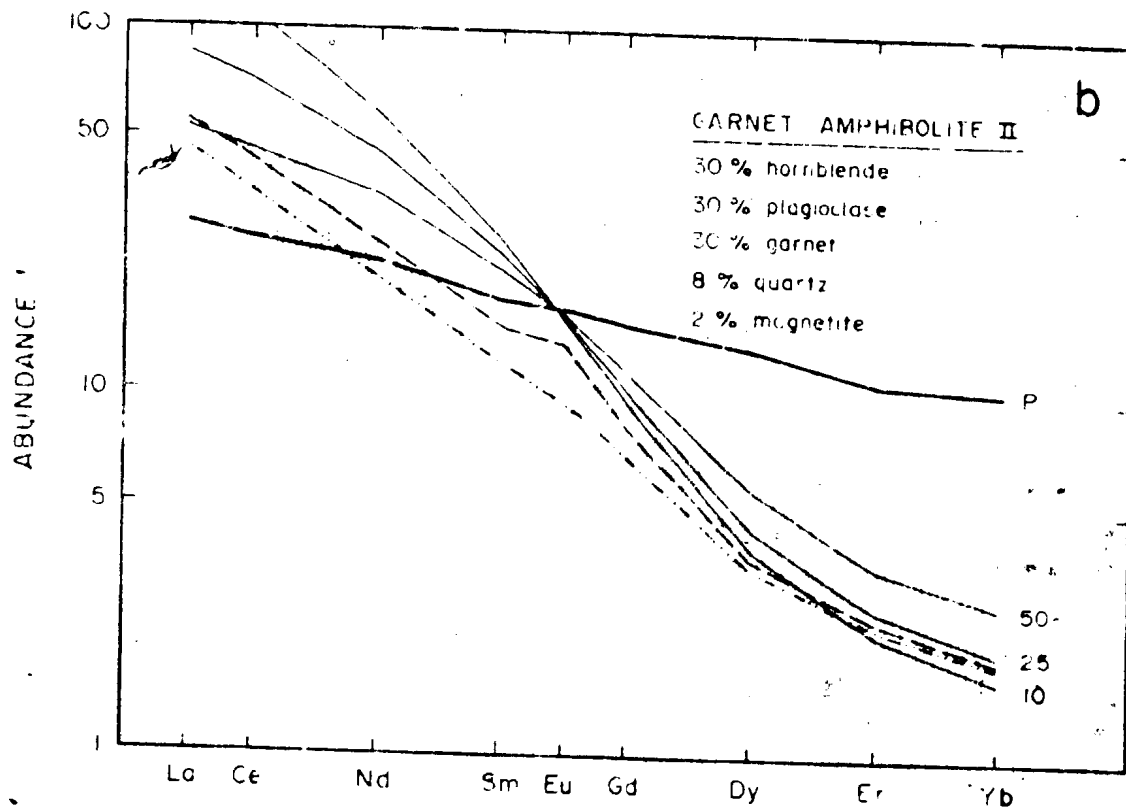
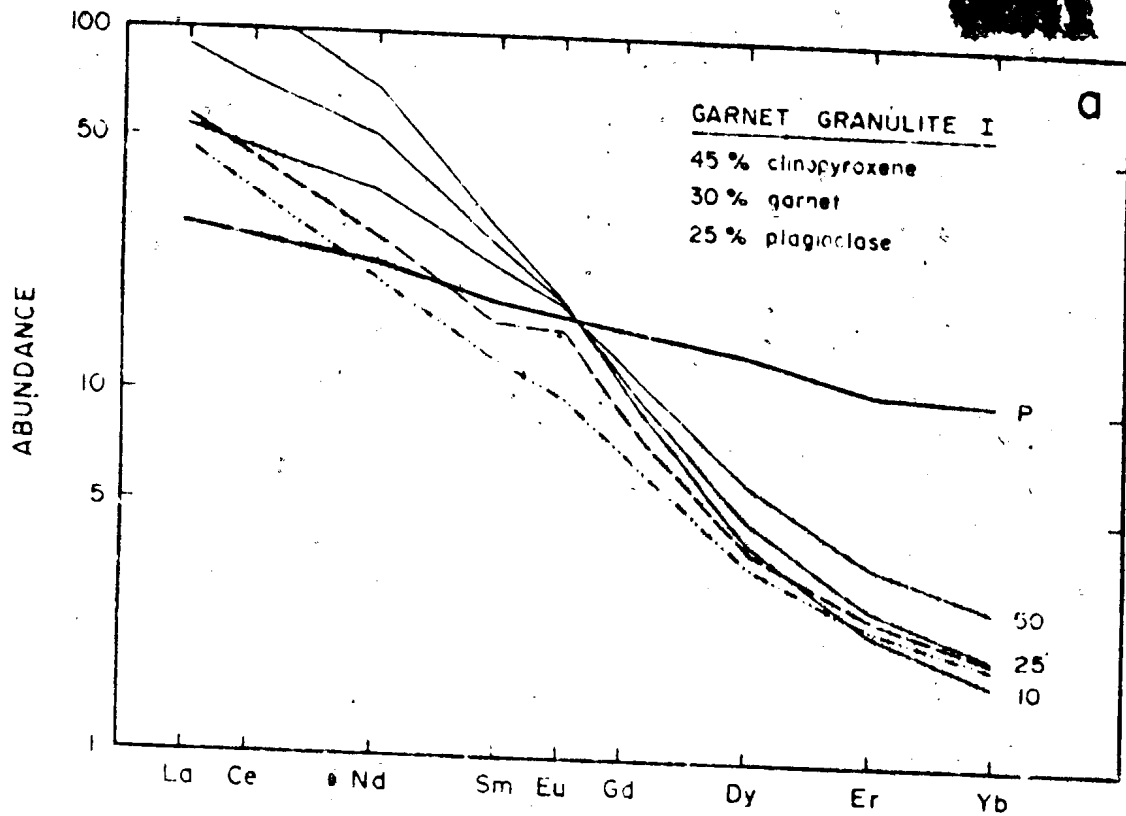
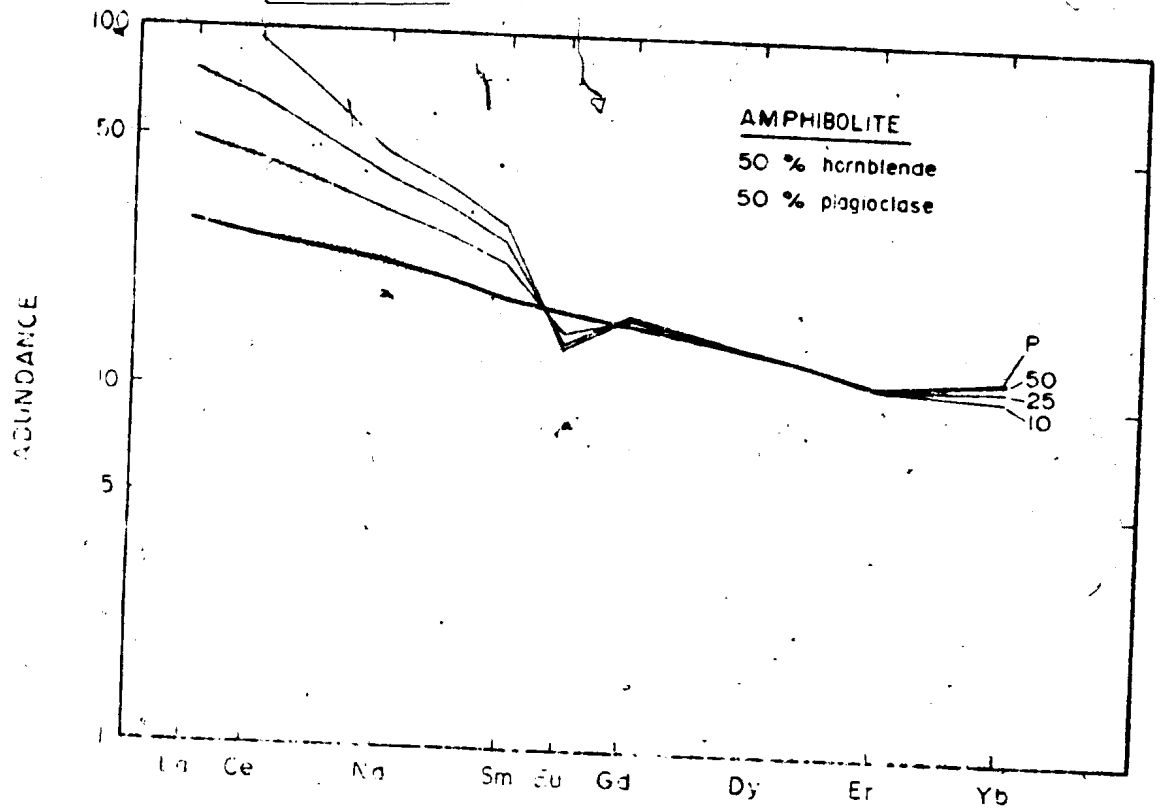


Figure 6.13: Results of equilibrium modal melting of amphibolite (Table 6.5).

P = Parent composition. Numbers correspond to the degree of melting. Shaded region is the field defined by 9 Hopedalian domain Maggo Gneiss samples.



0000

the degree of HREE depletion observed for Maggo gneiss. These results point to the presence of a residual phase, e.g. garnet, in the source which selectively retains the HREE during melting.

6.5.4.1.1 Trace Mineral Control on REE Contents

The influence of trace mineral phases (apatite and titanite) on the REE contents of coexisting melts derived by partial melting and fractional crystallization have been pointed out by Simmons and Hedge (1978), Heliman and Green (1979) and Gromet and Silver (1983). These authors all stress the control of trace minerals on the REE patterns of derived melts, reflecting their large partition coefficients for REE.

The results for 25% melting of garnet granulite (Table 6.5) with 1% apatite in the residue is represented by the dashed line on Figure 6.12a. For this model the REE have lower abundances and the pattern has a shallower slope [$(\text{Ce/Er})_N = 17$] compared with the model lacking apatite. The control of apatite on the LREE is reflected by a 39% decrease in absolute La abundances for the apatite-bearing residue, resulting in the LREE falling within the Maggo gneiss field. The MREE are also depleted, compared with the apatite-absent residue, however they are enriched over the Maggo gneiss field. The HREE results are not significantly affected by the presence of apatite, their abundance being controlled by other phases, e.g. garnet.

~~CONFIDENTIAL~~

The results for 25 % melting of garnet amphibolite 11 (Table 6.5) with 1% apatite in the residue is represented by the dashed line on Figure 6.12b. The results are comparable to those outlined above.

The presence of 1% apatite in the residue of the garnet granulite and garnet amphibolite sources requires a P_2O_5 content of 0.78 weight percent in the source. This amount of P_2O_5 is unreasonably high for this parent composition and suggests that other phases may play a role in controlling the REE content.

Titanite is well known as a potential host for REE (Hellman and Green, 1979). Gromet and Silver (1983) suggest that 80% to 95% of each REE resides in titanite and allanite, which control the MREE to HREE and LREE respectively.

Titanite partition coefficient data, for dacitic to rhyolitic compositions (Simmons and Hedge, 1978) is used here, due to the lack of appropriate partition coefficient data for mafic parents, to examine the control of this phase on the REE content of derived melts. This seems justifiable, as pointed out above, as titanite has the ability to incorporate large quantities of REE and effectively control their distribution during melting. The actual titanite partition coefficient data for a metabasaltic source will be different from that used here, but the influence of this phase in controlling the REE abundances will remain relatively the same.

~~00013~~

The results for 25% melting of garnet granulite I and garnet amphibolite II with 1% titanite (no apatite) in the residue are shown in Figure 6.12 a and b, respectively. The model REE patterns are identical for both sources $[(Ce/Er)_n = 14]$ with the LREE, MREE and HREE abundances falling within the field for the Maggo gneiss. The strong potential controlling influence of titanite is clearly evident from the modelling results and suggest that with this phase present, these metabasaltic sources could give rise to the observed REE patterns in the Maggo gneiss.

6.5.4.2 Intermediate Sources

Intermediate composition (diorite, tonalite) crustal sources, metamorphosed to granulite and amphibolite facies, are considered here as possible parental material to the Maggo gneiss. If intermediate compositions comprise the Maggo gneiss parent then this material was in existence prior to the Hopedallian event, i.e. older than 3,091 Ma. In the NAC the Amitsoq and Ulvak gneisses, at granulite and amphibolite facies, formed stable crust at this time, and provide a possible parent material from which the Maggo gneiss could be derived.

6.5.4.2.1 Parent REE Composition

Normalized REE abundances for Amitsoq banded gneiss display generally flat to slightly LREE enriched and HREE depleted $[(Ce/Yb)_N = 2.1 - 18.9]$ patterns with positive and negative Eu anomalies (O'Nions and Pankhurst, 1974). The material considered here to be parental to the

Pre-Hopedalian Maggo gneiss exhibits the following REE characteristics:

I) a LREE enriched and HREE depleted pattern with

$$(Ce/Yb)_N = 4$$

II) a positive Eu anomaly ($Eu/Eu^* = 1.3$).

This parent material is considered to be analogous to some Amitsoq gneisses and as such is representative of intermediate composition crustal material in existence when the Maggo gneiss precursor was derived. O'Nions and Pankhurst (1974) present patterns for Amitsoq gneiss from Qllangarsuit and Praestefjord, southern West Greenland, which are comparable to the parent REE distribution used here. The hypothetical parent is also comparable to unpublished data for granulite facies Amitsoq gneiss from the Kangimut saingmissoq area, Ameralik fjord, southern West Greenland (Nutman, pers. comm., 1985).

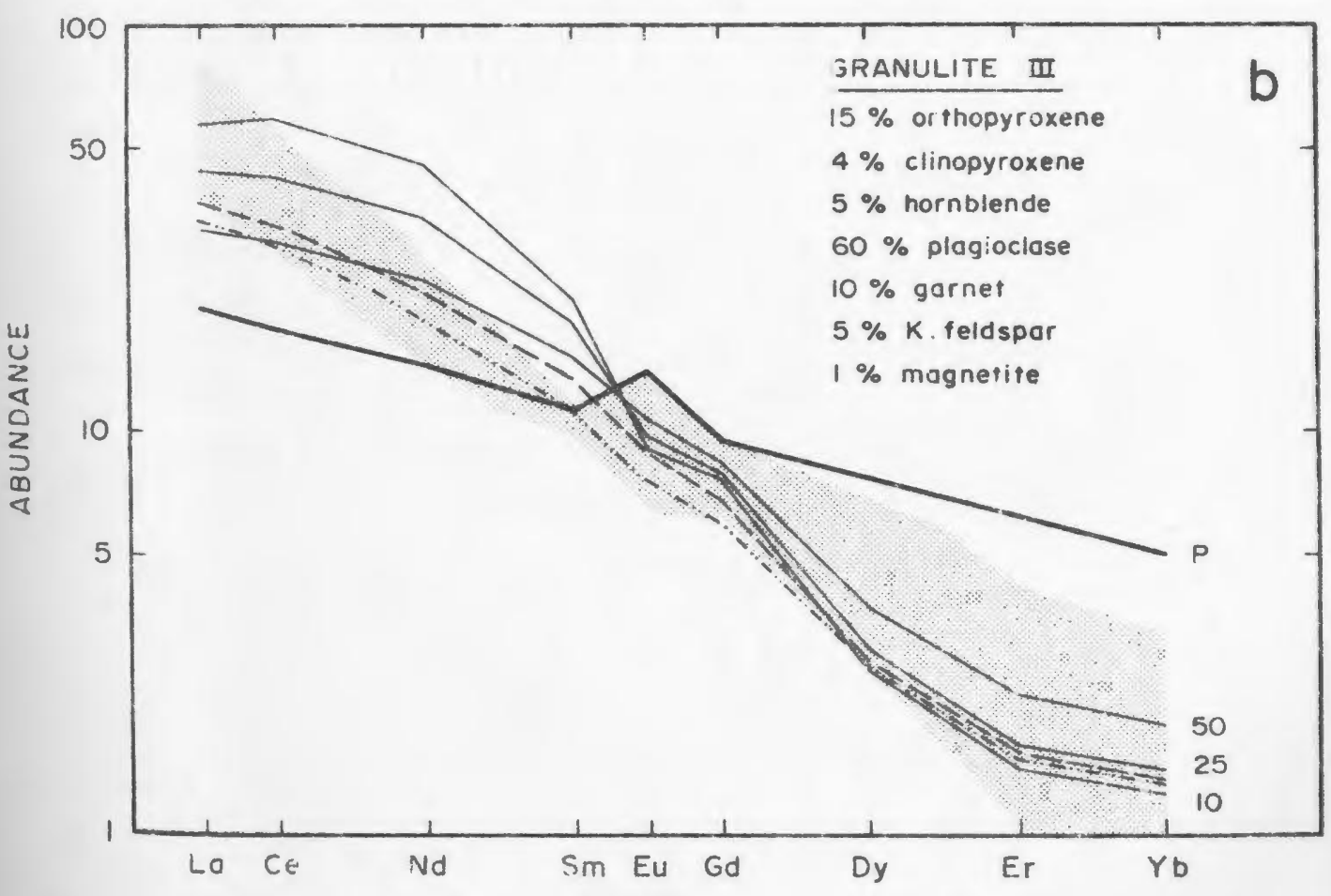
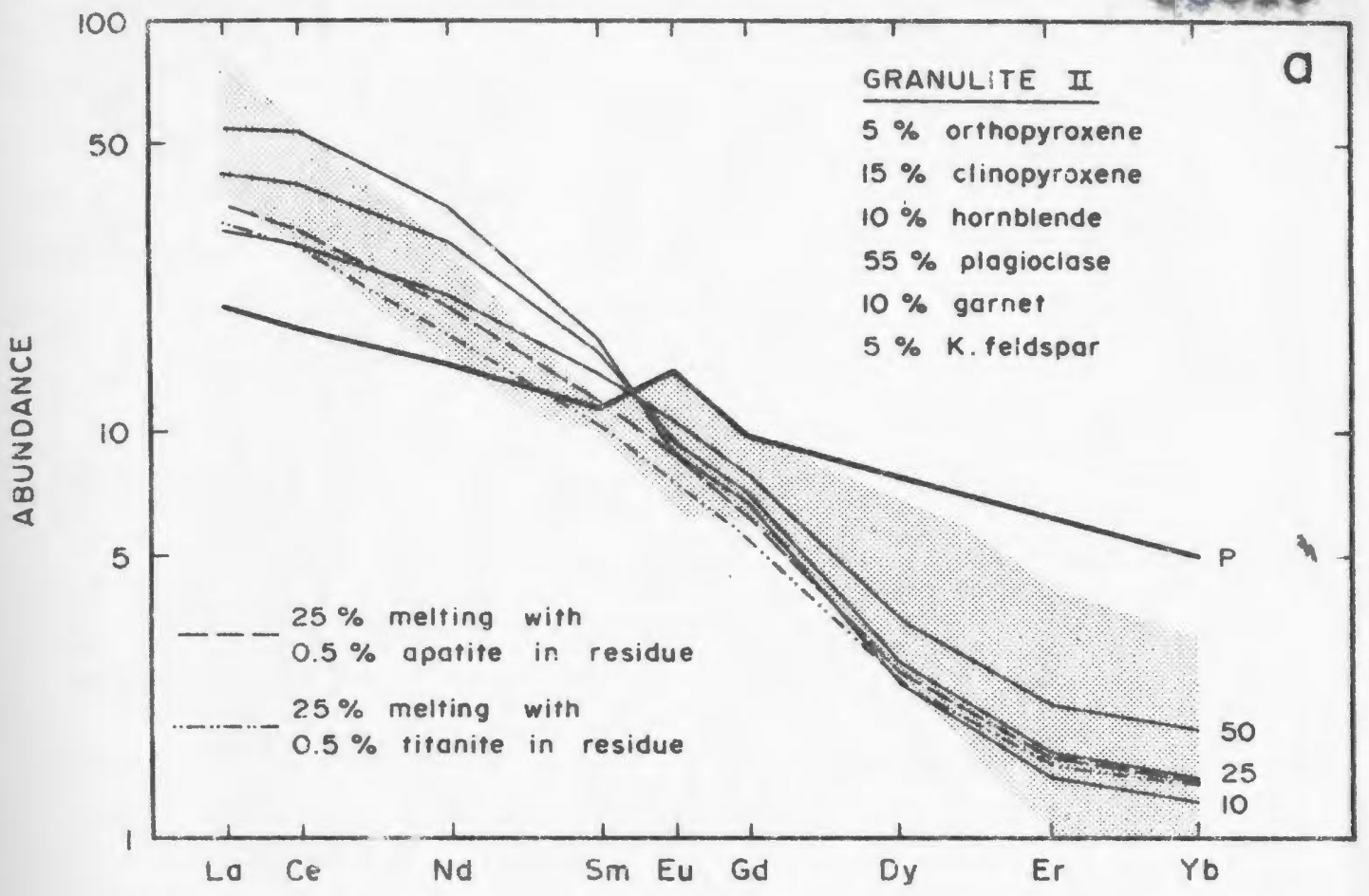
The Amitsoq gneiss has also been affected by a period of high grade metamorphism, resulting in granulite and amphibolite facies mineral assemblages, prior to intrusion of the Ameralik Dykes at approximately 3,200 Ma (Nutman et al., 1984). The mineral assemblages produced within the gneiss in response to this metamorphism are used as starting mineralogies for possible Maggo gneiss parents (Table 6.6).

6.5.4.2.2 Granulite Facies Parent

Intermediate composition modal mineralogies,
approximating hypothetical granulite facies mineral

Figure 6.14: Results of equilibrium modal melting of intermediate composition granulite facies gneiss (Table 6.6, Part A); a) granulite II and b) granulite III. The results for 25% melting of granulite II and III with 0.5% apatite and 0.5% titanite are represented as the dashed and double dot-dashed lines, respectively.

P - Parent composition. Numbers correspond to the degree of melting. Shaded region is the field defined by 9 Hopedalian domain Maggo Gneiss samples.



assemblages, used as sources for modelling Maggo gneiss REE distributions are given in Table 6.6. Equilibrium modal melting results for granulite facies gneisses II and III are shown in Figure 6.14 a and b, respectively.

For all mineralogies examined there is good agreement between the calculated abundances and overall slopes for the REE from Gd to Yb. To account for the concave upward shape of the HREE segment of the curves and the depletion of the HREE from Gd to Yb requires the presence of 5 to 10% garnet, and an equal amount of hornblende, in the residue for varying degrees of melting. The slope of the LREE segment of the curve, up to and including Sm, is gentler ($(La/Sm)_N = 1.7$ for 25% melting versus 5.0 for the Maggo gneiss) with the LREE segment displaying a convex upward shape.

The effects of including minor amounts (0.5%) of trace minerals, e.g. apatite and titanite, in the source mineralogy, on the model results are shown on Figure 6.14a and b. The convex upward shape for the LREE segment of the model results is eliminated with the incorporation of the trace minerals. The model $(La/Sm)_N$ ratios for apatite- and titanite-bearing parents range from 2.3 to 3.6 and 3.3 to 3.8, respectively, and are in close agreement with the observed Maggo gneiss patterns. The trace minerals also cause the MREE and HREE segments of the model results to shift to lower abundances, compared with parent compositions lacking these phases for equivalent degrees of melting (Figure 6.14).

The presence of up to 0.5% apatite in the residue requires that at least 0.4 wt % P_2O_5 be present in the source. Lower proportions of apatite in the residue require lower amounts of P_2O_5 , which is in agreement with the range of recorded P contents (0.05 to 0.43 wt % P_2O_5 ; Collerson and Bridgwater, 1979) in grey gneisses. The inclusion of titanite in the residue does not result in the parent requiring an anomalous chemical composition.

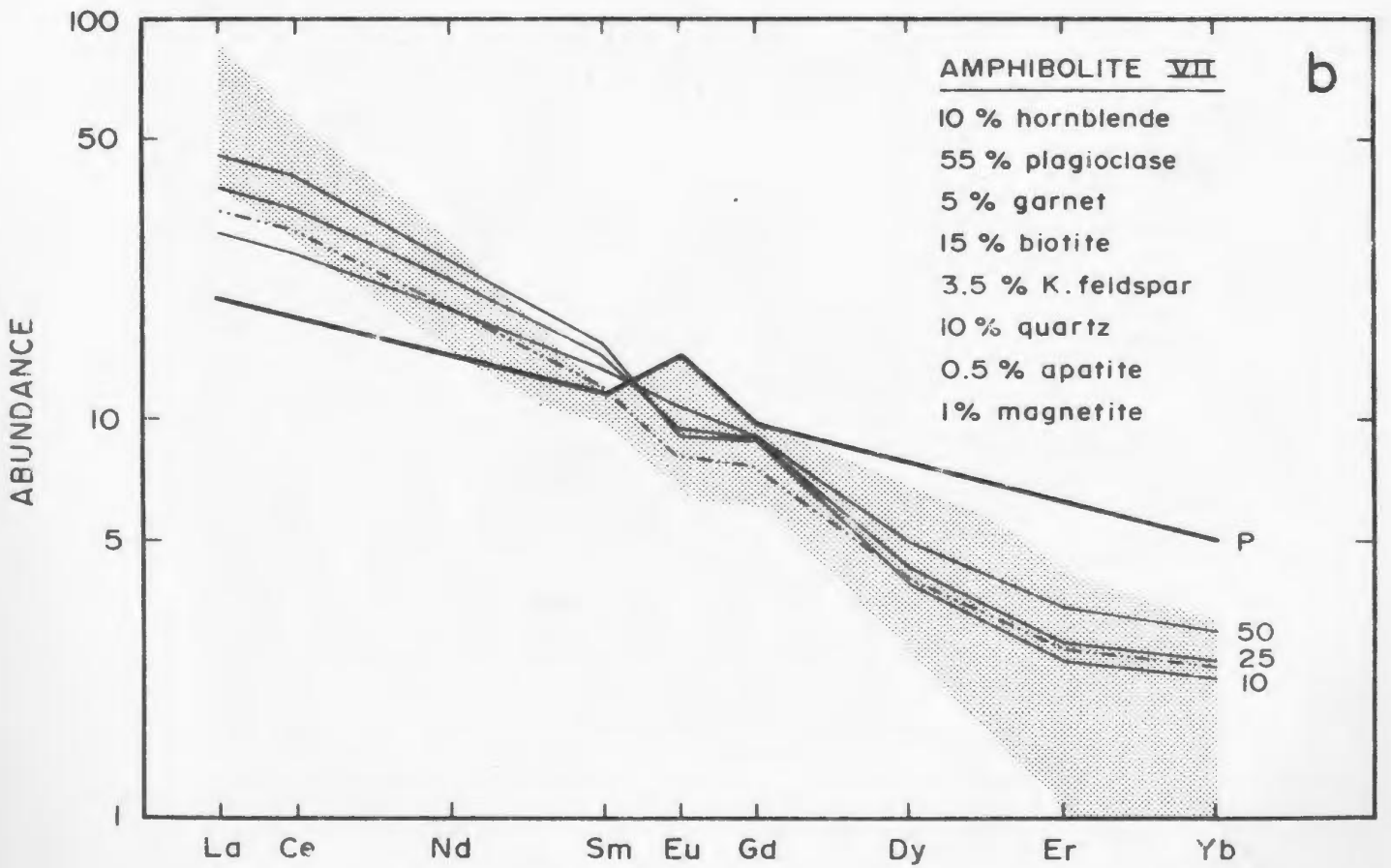
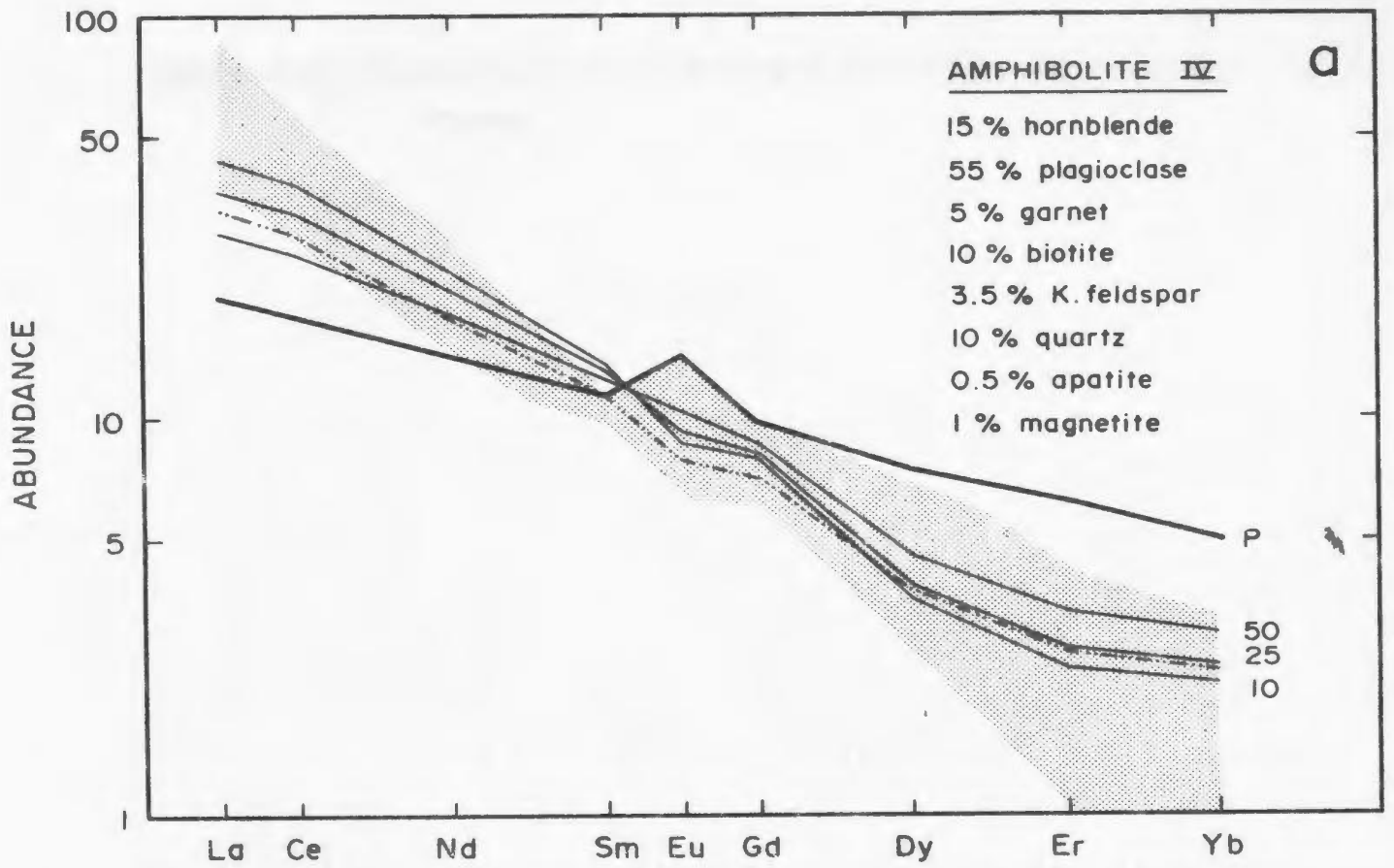
6.5.4.2.3 Amphibolite Facies Parent

Equilibrium modal melting results of intermediate composition, amphibolite facies gneiss (Table 6.6) are shown in Figure 6.15. The mineralogy of the source is based on data presented by Moorbath et al. (1972) for Amitsoq basic dioritic gneiss. The variation in mineral proportions results from varying proportions of mafic minerals, e.g. hornblende- and biotite-rich phases of the gneiss. Estimates of the bulk composition for the amphibolite facies gneiss parent (Table 6.7) show these samples to be comparable, in part, to the Amitsoq Fe-rich diorite of Nutman et al. (1984).

The modelling results for the amphibolite facies parent which yield REE abundances comparable to those recorded for the Maggo gneiss are shown in Figure 6.15. These model results require minor garnet (5%) along with moderate hornblende (8 to 15%) to account for the observed HREE depletion (Figure 6.15). At low degrees of melting (10 - 25%), for the compositions shown, agreement between the

Figure 6.15: Results of equilibrium modal melting of intermediate composition amphibolite facies gneiss (Table 6.6, Part B); a) amphibolite IV, b) amphibolite VII, and c) amphibolite VIII. The double dot-dashed line corresponds to the results for 25% melting of the given parent with 0.5% titanite in the residue.

P - Parent composition. Numbers correspond to the degree of melting. Shaded region is the field defined by 9 Hopedalian domain Maggo Gneiss samples.



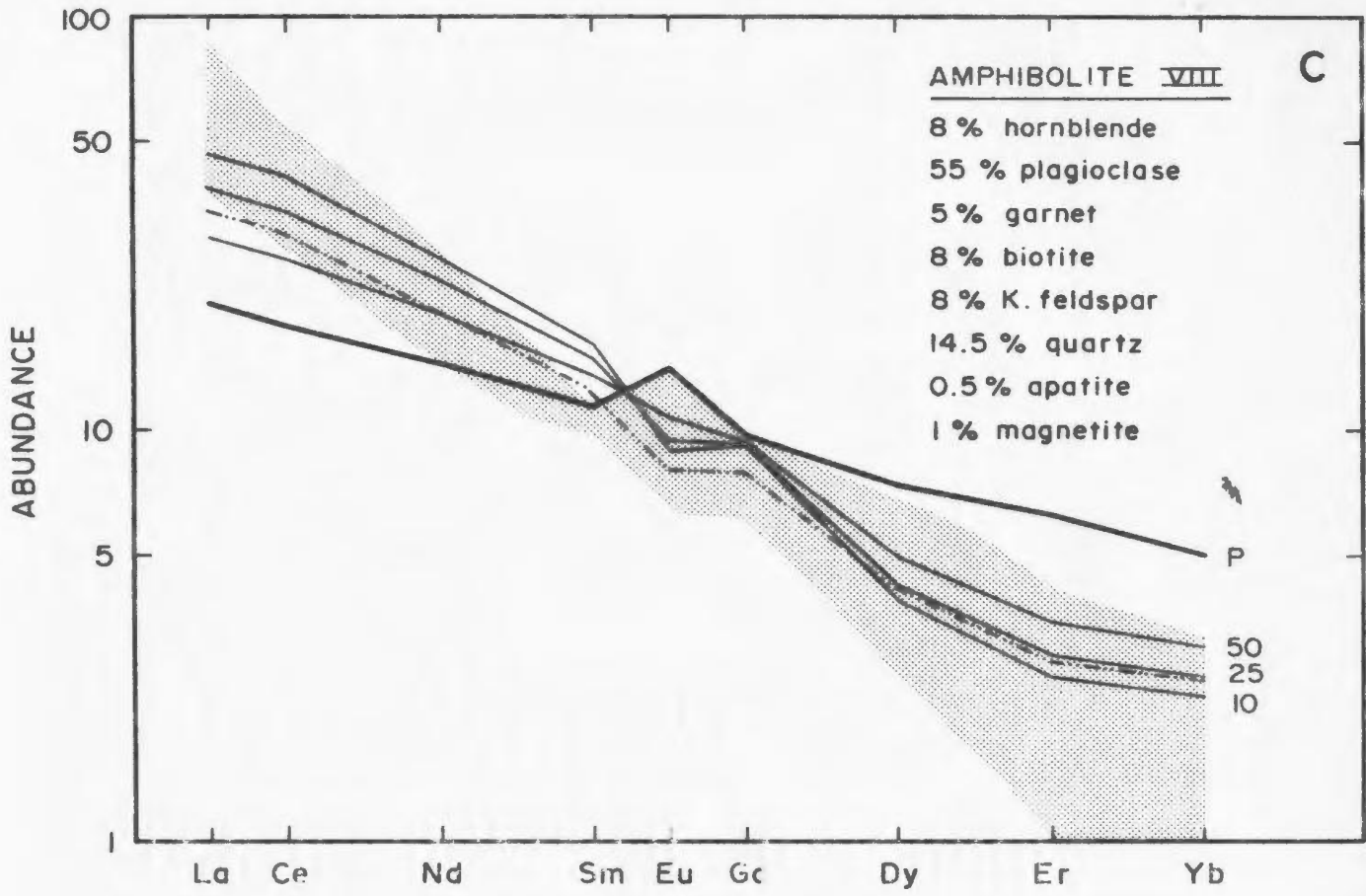


Table 6.7. Estimate of the bulk chemical composition of intermediate composition granulite and amphibolite facies gneiss used as parent material to the Hopedalian domain Maggo gneiss. The parent material corresponds to modal proportions given in Table 6.6.

Bulk compositions were calculated using a BASIC language computer program - GRCHEM written by Urdansky (1985).

	<u>Granulite Facies</u>		<u>Amphibolite Facies</u>		
	II	III	IV	VII	VIII
SiO ₂	52.39	52.74	55.93	55.40	59.37
Al ₂ O ₃	17.55	18.1	18.84	18.80	18.43
FeO	13.86	15.50	10.25	10.78	7.79
MgO	2.59	2.90	1.92	2.02	1.46
CaO	9.39	6.36	6.67	5.97	5.81
Na ₂ O	3.31	3.61	3.56	3.56	3.64
K ₂ O	0.69	0.69	1.61	2.15	2.10
P ₂ O ₅			0.46	0.46	0.47
H ₂ O	0.21	0.21	0.76	0.86	0.53

NOTE: The effects of including 0.5 % titanite in the parent modal mineralogy results in the addition of 0.25 wt % TiO₂ along with an increase in CaO, a decrease in SiO₂ and minor decreases in all other oxides.

0000

LREE, Eu and Gd is good. However, Sm abundances are consistently high for the model compared to the Maggo gneiss.

The inclusion of 0.5% titanite in the parent material results in a lowering of the LREE and MREE abundances, for 25% melting, with the resulting model composition being in close agreement with the observed Maggo gneiss REE distributions (Figure 6.15).

From Figure 6.15 it is clear that a variety of parent material metamorphosed to amphibolite facies, containing varying proportions of hornblende and biotite with minor garnet and trace titanite, will on 25% melting give rise to REE distributions comparable to those observed for Hopedalian domain Maggo gneiss.

6.5.5 Discussion

Based on REE modelling the observed Maggo gneiss REE patterns can be generated by 25% melting of a variety of crustal source materials. Likely sources are:

- 1) basaltic compositions, metamorphosed at medium to high grade resulting in garnet granulite and garnet amphibolite lithologies, and
- 2) Intermediate compositions metamorphosed to granulite and amphibolite facies.

Using the LILE and HFS element contents of the various sources and modelling their abundances in the resulting melt would narrow the list of possible parental compositions suggested above.

The Maggo gneiss parent has been subjected to a period of high grade metamorphism at c. 3,600 Ma (Griffin et al., 1980). Schlotte et al. (in prep.), based on zircon U-Pb systematics, have hypothesized a period of granulite facies metamorphism affecting the Hopedale Block at c. 3,300 Ma. These two periods of high grade metamorphism, prior to the Hopedalian event, would be sufficient to mask the 'original' LILE content of the Maggo gneiss parent.

LILE modelling results must be treated with caution, due to the complex history of the parent and precursor lithologies. The LILE are not useful in determining which parent source is dominant in the generation of the Maggo gneiss precursor.

The HFS elements (Nb, Ti, Zr, and P) may be immobile or mobile during metamorphism, depending on the composition of the accompanying fluid phase (Section 5.2.3, 6.2. and 6.4). As well each HFS element may behave independently of the others, with the behaviour of individual elements reflecting the fluid phase composition (Murphy and Hynes, 1986; Section 6.4). The behaviour of the HFS elements during partial melting is controlled more by minor phases than by major phases in the parent, e.g. Zr in zircon, Ti in titanite, P in apatite. If these elements are considered to be immobile during high grade metamorphism then their distribution in the Hopedalian domain gneiss may be useful in identifying the Maggo gneiss precursor.

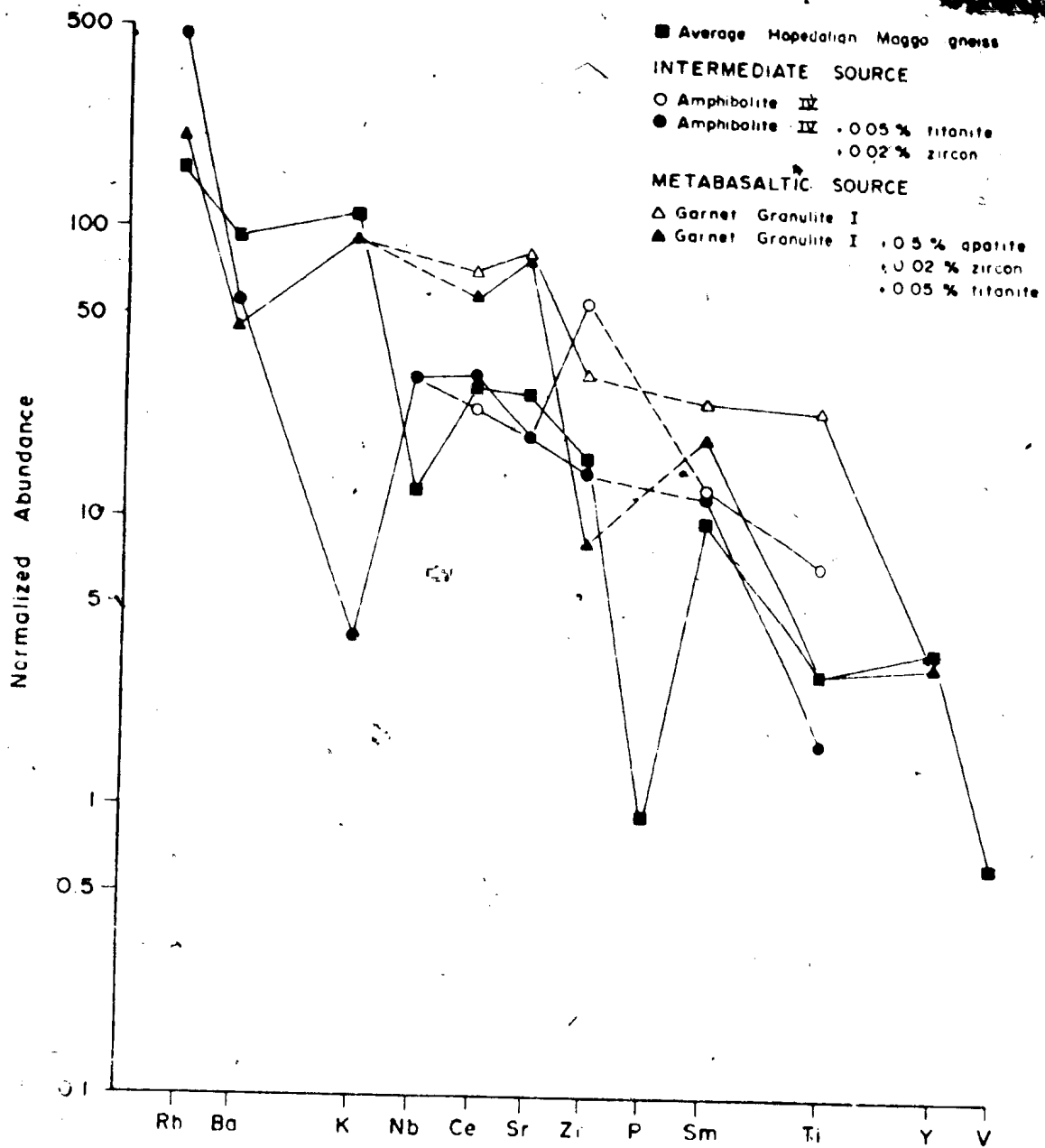
00000

The importance of trace (< 0.5 %) quantities of titanite and apatite in controlling the REE content of the melt was considered in Section 6.5.4.1.1. These trace phases in effect control the distribution of a single HFS element during partial melting, e.g. Ti in titanite, Zr in zircon. LILE and HFS element modelling results for amphibolite IV parent (Table 6.6) and the same parent with the addition of 0.05% titanite and 0.02% zircon are presented in Figure 6.16. The average Hopedalian domain Maggo gneiss composition (Table 6.6) is also shown.

The addition of titanite and zircon to the source does not affect the abundances of Rb, Ba, K, Nb and Sr in the resulting melts, compared to the source lacking these phases (Figure 6.16). Only the Sr contents are in agreement with the mean Hopedalian domain gneiss composition. The lack of agreement for Rb, Ba, K and Nb is interpreted to reflect the mobility of these elements during early Archaean high grade metamorphism. The Ce and Sm abundances are increased and decreased, respectively, in the resulting melt, bringing them into closer agreement with the average Hopedalian domain gneiss. This is in agreement with the REE modelling results (Section 6.5.4).

With the addition of trace titanite and zircon to the amphibolite IV source the resulting Ti and Zr contents for the melt are lowered to within the range for the average gneiss composition. Modelling results using Amphibolite VII and VIII sources (Table 6.6) including trace amounts of

Figure 6.16: Comparison of LILE and HFS elements for average Hopedalian Domain Maggo gneiss with the model results for intermediate and metabasaltic source compositions shown. The effect of including minor amounts of trace phases, in the source, on element distributions is readily visible, e.g. Zr abundances in Amphibolite IV with 0.05% titanite and 0.02% zircon. Similar results were obtained for other source lithologies from Tables 6.5 and 6.6. Parent chemical compositions used in the model for intermediate and metabasaltic sources are from Nutman (unpublished data) and Martin (1987), respectively. Normalizing factors used are from Sun (1980).



~~SECRET~~

titanite and zircon yield results similar to those for Amphibolite IV.

The HFS elements and REE patterns obtained for modelling Granulite II and III sources (Table 6.6) are also comparable to the Amphibolite IV results. Modelling of the LILE contents for the granulite sources result in lower Rb (50X) and K (1.2 X), and higher Ba abundances (115X), compared with the amphibolite source. This difference in LILE contents is interpreted to reflect the differing chemical compositions of the two sources.

The LILE and HFS element modelling results for a metabasaltic source, as represented by garnet granulite I (Table 6.5), are shown on Figure 6.16. Results for other metabasaltic source mineralogies (Table 6.5) are comparable to those obtained for the source shown.

Rb and K results are in close agreement with the average Hopedallan domain gneiss, while Ba is depleted over that expected for the possible daughter product. The close agreement for Rb and K suggests minor post emplacement mobility of these elements, which is unlikely considering the protracted history of the Maggo gneiss.

The modelling results for the remaining elements show them to be enriched over the expected results for the Hopedallan domain gneiss (Figure 6.16). The inclusion of minor amounts of trace phases only affects those HFS elements with large partition coefficients for the minerals involved. Even though REE modelling indicates the

possibility that a metabasaltic source may be parental to the Maggo gneiss precursor, the LILE and HFS element modelling does not agree with this conclusion.

6.5.6 Summary

A range of possible crustal sources representing a variety of bulk chemical compositions were examined as possible parental material to the Hopedalian domain Maggo gneiss.

Based on the modelling results for the REE, LILE and HFS elements the Maggo gneiss source must contain:

- 1) essential phases in the residue with large partition coefficients for the HREE, e.g. garnet and hornblende, to account for the observed degree of HREE depletion, and
- 2) trace phases with a) high partition coefficients for the LREE, which exercise a strong control on the LREE and Sm abundances, and b) high partition coefficients for specific HFS elements.

Intermediate composition sources metamorphosed to granulite facies, with trace amounts of apatite, titanite and zircon in the residue, will on 25% or less melting yield REE abundances comparable to Hopedalian domain Maggo gneiss abundances. Amphibolite facies, intermediate composition sources, with minor titanite and zircon, result in REE abundances comparable to Hopedalian domain Maggo gneiss when subjected to approximately 25% melting.

1222

The results for model REE abundances for the crustal sources display enriched, depleted and normal Eu abundances. These features, observed for the chemically defined gneiss subgroups, were used to distinguish Class I and Class II REE patterns (Section 5.2.5). The presence of the various Eu anomalies in the model melts may further be enhanced by subsequent plagioclase fractionation and/or hornblende crystallization.

6.6 Conclusions

Based on the results presented in this chapter the following conclusions dealing with the origin and evolution of the Maggo gneiss are presented.

- 1) The Flordian event, spanning < 130 Ma, is characterized by early and late periods during which reworking of preexisting crust is dominant and an intervening period during which the Kanairiktok intrusions were derived and emplaced. The Flordian domain Maggo gneiss is derived by reworking of the Hopedalian domain gneiss.
- 2) Changes associated with the chemical reworking of the Hopedalian domain gneiss to produce the Flordian domain gneiss are: a) LILE (K, Rb and Ba) depletion and relatively constant Sr contents resulting in lower Rb/Sr and higher K/Rb ratios for Flordian domain gneiss, b) HFS element (Ti, Zr, P, Y and V) enrichment, and c) no change in REE contents. Geochemical reworking associated with the Flordian occurs later than and independently of structural reworking.

~~SECRET~~

3) Based on 1) the age obtained for the NBN suite, 2) model age calculations for Maggo gneiss suites, and 3) the Hopedalian areal isochron a crustal history for the Maggo gneiss older than the Hopedalian is indicated. This suggests that the Hopedale Block has a more complex history than first indicated. This history is interpreted to be comparable to that recorded for other areas of the NAC. Further detailed isotopic studies involving the Nd-Sm and Pb-Pb systematics of the Maggo gneiss are required to substantiate or disprove this point.

4) The Maggo gneiss precursor was derived predominantly by 25% melting of an intermediate composition, granulite to amphibolite facies parent prior to the Pre-Hopedalian event. The hypothesized parent to the gneiss precursor is considered to be preexisting Early Archaean crust, equivalent to depleted granulite and amphibolite facies Amitsoq gneiss.

Chapter 7

SIGNIFICANCE OF THE MAGGO GNEISS IN THE DEVELOPMENT OF THE NORTH ATLANTIC CRATON

The Hopedale Block forms the southwest corner of the North Atlantic Craton (NAC), as such its growth and development should be comparable to other areas of the NAC. Field relationships and geochronologic results yield conflicting conclusions as to the origin of the Hopedale Block.

7.1 Field Relationships

Field relationships exhibited by the Maggo gneiss are comparable to those observed in southern West Greenland and northern Labrador (Figure 7.1) for Amitsoq and Ulvak I and II gneisses, respectively (Collerson *et al.*, 1981). The Maggo gneiss contains minor amounts of supracrustal material (Hunt River Belt, Weekes association). In terms of supracrustal rocks a major difference between the Hopedale Block and other areas of the NAC is the lack of recognition of two distinct supracrustal sequences, which in part may reflect a lack of sufficient information for the supracrustal component at Hopedale.

8104

Figure 7.1: Reconstruction of a portion of the North Atlantic Craton, showing the location of geographic features mentioned in the text. The dashed line encloses the NAC.

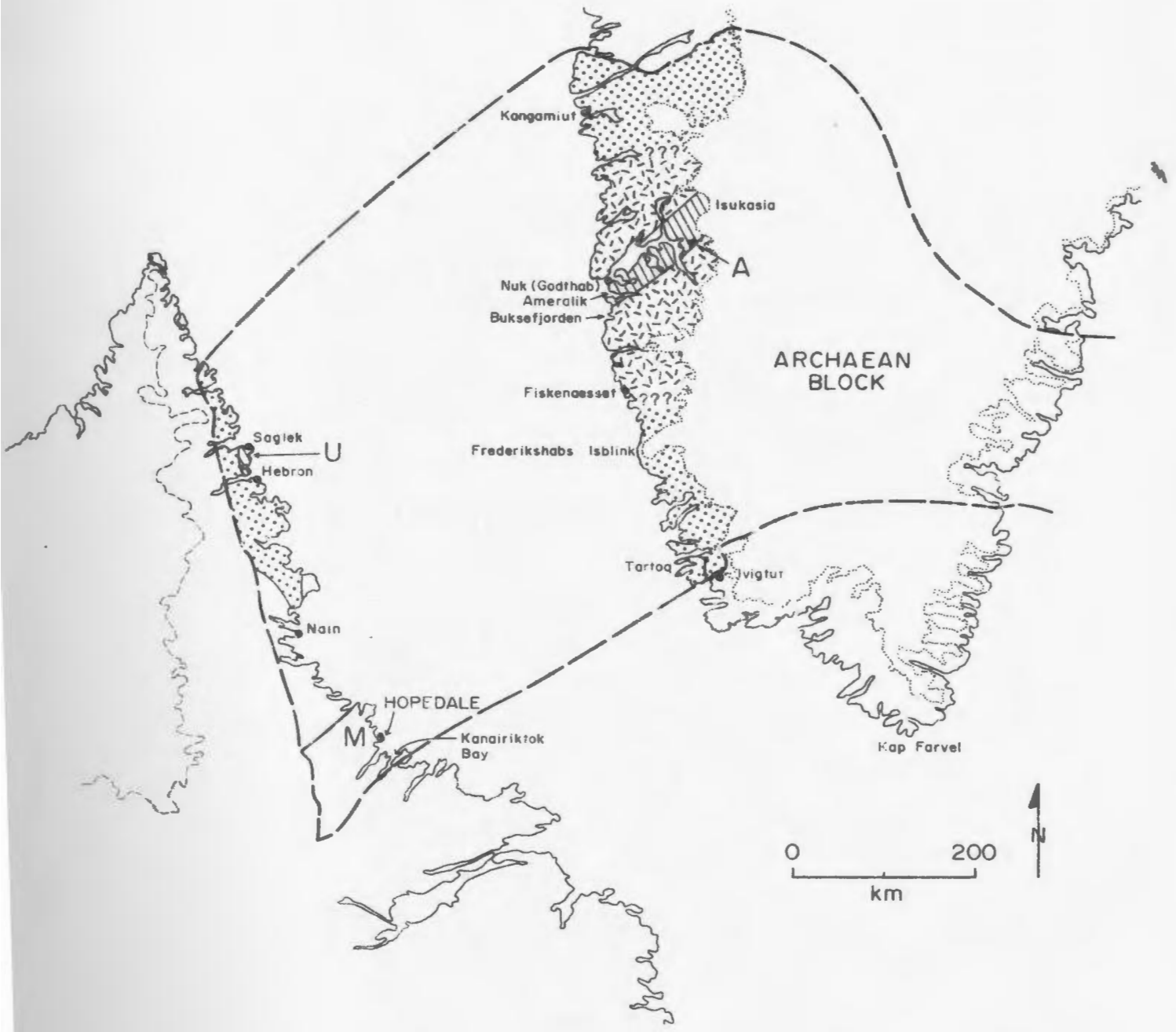
. LEGEND

|||| Tracts containing Early Archaean Amitsoq (A) and Uivak (U) gneiss.

Late Middle Archaean Maggo gneiss (M) outcrops at Hopedale.

⊛ Extent of Late Archaean Nuk gneiss.

⊞ Area underlain by Late Middle to Late Archaean grey gneiss - Ivigtut gneiss (I).



~~SECRET~~

Elsewhere in the NAC supracrustal sequences of Early and Early Middle Archaean ages have been recognized. The West Greenland sequences (the Akilia association and the Malene supracrustals) have been the subject of more detailed work (Beech and Chadwick, 1980; Chadwick, 1981; Friend et al., 1981; Gill et al., 1981; Nutman, 1986) compared with the sequences of northern Labrador (Nuiliak association and Upernavik supracrustals; Bridgwater et al., 1975; Ryan et al., 1983; 1984). The older Akilia and Nuiliak associations retain evidence of a more protracted metamorphic and structural history compared with the younger Malene and Upernavik supracrustals. The recognition of the two supracrustal sequences in northern Labrador was not readily apparent during the early stages of the work in this area (Bridgwater, pers. comm., 1984). Schiøtte et al. (1988), based on ion probe U-Pb zircon analyses, have shown that the Malene supracrustals, as previously defined, consist of two distinct sequences, which were laid down before and after emplacement of the Nuk gneiss.

In the Hopedale Block some Weepes association inclusions retain evidence of two periods of deformation prior to their inclusion within the Maggo gneiss. The more intensely deformed inclusions also retain evidence of relict, higher grade mineral assemblages. Other Weepes association inclusions exhibit a weak penetrative fabric, accompanied by low to middle amphibolite facies metamorphism. Schiøtte et al. (in prep.) have carried out

00000

an ion probe U-Pb study of detrital zircon grains, separated from Weekes association pelites, collected along the north shore of Kangiluasukoluk Tagani (in the vicinity of the NBN suite). Ages for these grains range from 3,260 to 3,280 Ma, placing an upper limit on the time of derivation of this pelitic subunit of the Weekes association.

The data presented here for the Weekes association are not conclusive, but may suggest the presence of two supra-crustal sequences at Hopedale. Detailed metamorphic, structural, geochemical and geochronological studies of the Weekes association are required before this problem can be resolved.

The most obvious, common feature between the Hopedale Block and other localities in the NAC is the presence of a suite of early diabase dykes. Ermanovics et al. (1982), based on field relationships, speculated that the Hopedale dykes were analogous to the Saglek and Ameralik dykes of northern Labrador and southern West Greenland, respectively. Grant et al. (1983), based on Rb-Sr geochronology, concluded that the Hopedale dykes were not correlative with the other early dyke swarms in the NAC.

The Hopedale dykes must be older than 3,091 Ma (the pooled Hopedalian age; see Section 4.14.1) as they are folded, rotated, boudinaged and metamorphosed during the Hopedalian event. The time of emplacement of the dykes is unknown, however they do cut a Pre-Hopedalian fabric in the Maggo gneiss.

The Saglek dykes, based on field relationships and geochronology studies of their hosts, are interpreted to have been emplaced between 3,400 Ma and 3,200 Ma (Collerson et al., 1981).

Diabase dykes, of mid-Archaean ages, are prevalent throughout much of the West Greenland portion of the NAC. These dykes are referred to as the Ameralik (McGregor, 1973), Isua (Gill and Bridgwater, 1979) and/or Tarssartoq (Nutman, 1986) dykes. The Tarssartoq dykes, preserved in the Isukasia area (Figure 7.1), are between 3,400 Ma and 2,550 Ma old as they cut 3,400 Ma old pegmatites and are cut by 2,550 Ma old pegmatites. Pb-Pb and Rb-Sr isotopic studies (Wagner, 1982) of the Tarssartoq dykes suggest that they are older than 3,100 Ma and correlate with the > 3,000 Ma Ameralik dykes present in ~~coastal~~ exposures (Nutman, 1986).

Based on the results of this study and comparing the field and geochronologic position of correlative dykes (Saglek, Ameralik, Isua and Tarssartoq) in the NAC, the similarity of the Hopedale dykes to the above as proposed by Ermanovics et al. (1982) appears to hold up.

The only other major gneiss unit in the NAC is the Nuk gneiss, identified in the vicinity of Nuk (Godthab), Greenland (Figure 7.1). Correlation of the Maggo gneiss, on the basis of field relationships, with Nuk lithologies seems unlikely. The Nuk gneiss, as defined by McGregor (1973), does not contain remnants of Ameralik dykes, yet Maggo

gneiss contains Hopedale dykes. The Maggo gneiss, on the basis of field relationships, more closely resembles the relationships observed for the older grey gneiss component (Amitsoq and Uivak gneisses) with associated, early to middle Archaean dyke swarms (Ameralik and Saglek dykes, respectively).

7.2 Geochronological Results

The Rb-Sr isotopic results from this study, along with the results of Grant et al. (1983), do not confirm the observed similarity of field relationships for the Hopedale Block and other NAC localities outlined above.

The Hopedalian event, as recorded in the Maggo gneiss, has been dated at 3,140 Ma to 3,025 Ma, more than 500 Ma younger than ages obtained for Amitsoq and Uivak gneisses (Figure 7.2). Maggo gneiss Hopedalian ages are closer to the oldest recorded age for Nuk gneiss (3,076 Ma; Baadsgaard and McGregor, 1981). This Rb-Sr age for the Nuk gneiss overlaps the upper limit of a bracket of U-Pb zircon ages (2,800-3,070 Ma) reported by Baadsgaard and McGregor (1981). An age of 2,900 Ma ($Sr_0 = 0.7014$) for Nuk-type gneisses, incorporating samples which record evidence of Pb and Nd contamination, has been obtained by Taylor et al. (1984). Also shown on Figure 7.2 are Rb-Sr results for eight suites of Nuk gneiss reported by Taylor et al. (1980), recalculated from data of Moorbath and Pankhurst (1976). Rb-Sr results for Nuk gneisses invariably lie to the right of the Hopedalian evolutionary path and are hence

01800

Figure 7.2: Compilation of Rb-Sr isotopic results for the North Atlantic Craton plotted on a Sr evolution diagram. Hopedalian (vertical ruling), Flordian (horizontal ruling) and Kanairiktok Intrusion Sr evolution paths are taken from Figure 6.9.

Symbols and data sources are:

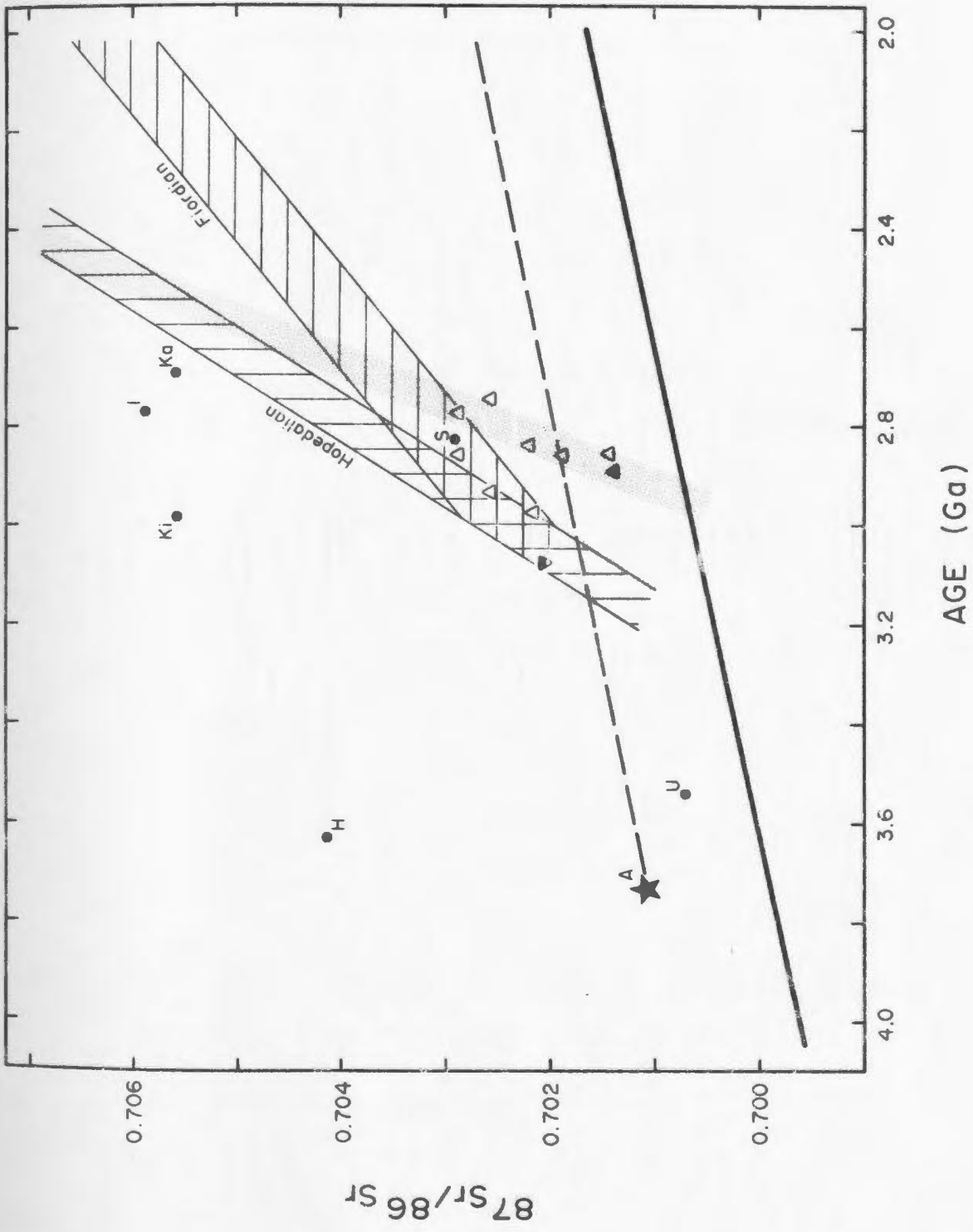
West Greenland

- A . Amitsoq gneiss - Hurst (1978)
- ▼ Nuk gneiss, townsite - Baadsgaard and McGregor (1981)
- ▲ Nuk gneiss - Taylor et al. (1984)
- △ Nuk gneiss - Taylor et al. (1980)

Labrador (data from Collerson et al., 1982, unless otherwise stated)

- U Ulvak gneiss
- H Hebron gneiss - Barton (1976)
- KI Kiyuktok gneiss
- I Ikurat gneiss
- Ka Kammarsuit gneiss
- S Saglek tonalite-granodiorite sheets

See text for details.



younger than the Hopedalian domain Maggo gneiss suites (Figure 7.2). The Nuk gneisses generally lie along the evolutionary path for the Kanariktok intrusions (light stipple, Figure 7.2) and are here interpreted to be chronologically equivalent lithologies.

Clearly, field relationships and geochronological results for Maggo gneiss do not correlate with recorded relationships observed in comparable regions of the NAC. This lack of correlation must result from the Hopedale Block either having formed elsewhere in the Archaean and then becoming attached to the NAC, or, more likely, being derived by reworking of preexisting NAC lithologies. This latter possibility is discussed in Section 7.3.

The geochronological results obtained in this study for the NBN suite, the model age calculations and the Hopedalian areal isochron indicate an event at c. 3,300 Ma which reset the Rb-Sr isotopic systematics of the Maggo gneiss precursor. This age and the event it records is interpreted to be the Pre-Hopedalian event. An event of similar age has not been recognized elsewhere in the NAC. Schlötte et al. (in prep.), using ion probe zircon results for Hopedale Block lithologies, support the uniqueness of this event. These authors interpret their results as indicating that the zircons grew in response to high grade metamorphism.

Isotopic, geochemical and field evidence, supports derivation of Flordian domain Maggo gneiss from Hopedalian domain Maggo gneiss, by reworking between 2,927 Ma and

0000

2,804 Ma. The initial Sr_0 ratios for the Flordian domain suites are higher than Nuk gneiss initial ratios. The development of Flordian characteristics (LILE depletion, HFS element enrichment and REE immobility) in the Maggo gneiss occurred during the time span when the Kanairiktok intrusions and Nuk gneisses were being emplaced into the Hopedale Block and southern West Greenland, respectively.

7.3 Proposed Developmental History of the Maggo Gneiss

In this section the proposed developmental history of the Hopedale Block, as recorded by field relationships and geochronological results for the Maggo gneiss, is presented. Figure 7.3 compares the growth and development of the Hopedale Block with the documented evolution of the West Greenland Archaean. Figure 7.4 provides a diagrammatic summary of the stages of development of the Hopedale Block, based on the results of this study.

Hopedalian domain Maggo gneiss was derived from preexisting crustal material between 3,140 Ma and 3,025 Ma ago. Petrogenetic modelling (Section 6.5) indicates that crustal sources, metamorphosed to amphibolite or granulite facies, will, on 25% partial melting, yield REE and HFS element compositions comparable to Hopedalian domain Maggo gneiss.

7.3.1 Early to Early Middle Archaean (> 2,900 Ma)

The exposed Early Archaean segments of the NAC are a heterogeneous mixture consisting predominantly of grey gneisses with minor quantities of other lithologies (meta

01-010

Figure 7.3: Summary of the Archaean events in the development of the Hopedale Block, based on work carried out in this study and the work of Ermanovics et al. (1982) compared with crustal development in the West Greenland Archaean (McGregor, 1973; Berthelsen and Henriksen, 1975; Bridgwater et al., 1976; Nutman et al., 1984; Nutman, 1986).

Solid brackets - span the time range defined (*) or inferred (?) for each event.

No direct evidence exists, in the Hopedale Block, for events which lie below the dashed line.

6007

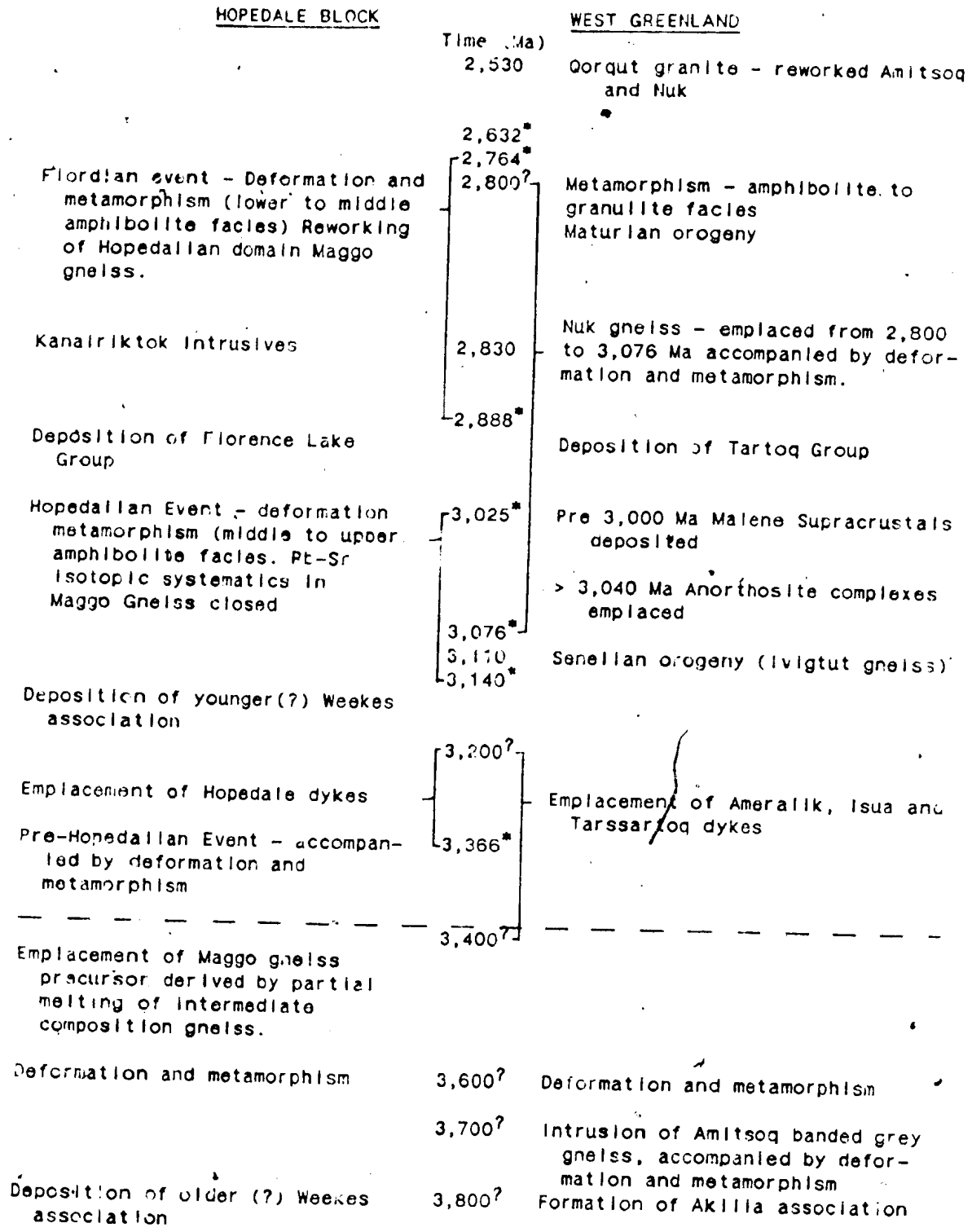


Figure 7.4: Diagrammatic representation of the stages of development of the Hopedale Block from Early Archaean (> c. 3,300 Ma) through Flordian (c. 2,853 Ma) time. The horizontal axis is not to scale. See text for discussion.

LEGEND

Stage I: > c. 3,300 Ma

- v - supracrustals (Hunt River, Weekes)
 - A - anorthosite
 - +++ - granitic intrusions
 - - mantle
 - /// - deep level metabasaltic composition
- The unshaded portion consists of intermediate composition, LILE depleted granulite to amphibolite facies crust. The dashed line represents the amphibolite to granulite facies transition.

Stage II: Pre-Hopedalian (c. 3,300 Ma)

- ⋈ - Maggo gneiss precursor, with Pre-Hopedalian fabric

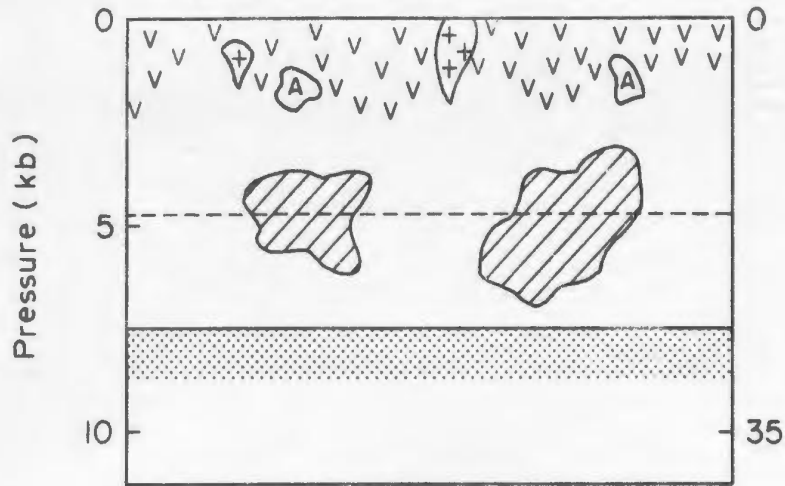
Stage III: Hopedalian (c. 3,090 Ma)

- ⋈ - Hopedalian domain Maggo gneiss

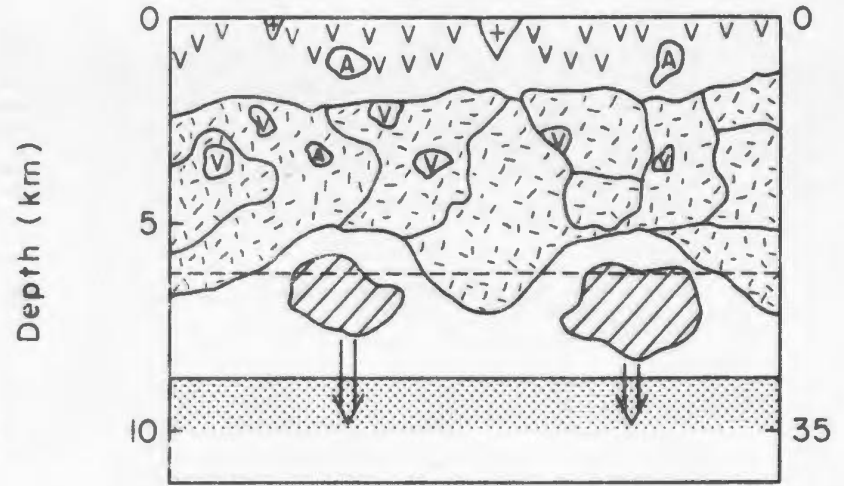
Stage IV: Flordian (c. 2,853 Ma)

- ≈ - Florence Lake supracrustals
- ⋈ - Flordian domain Maggo gneiss
- xxx - Kanairiktok intrusions

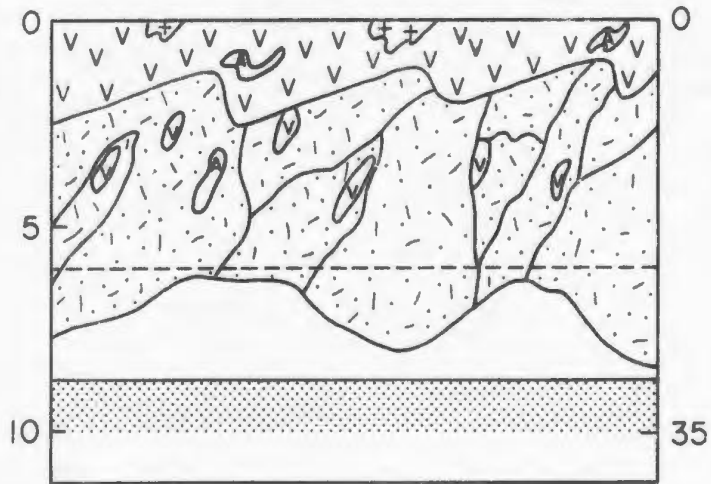
Stage I (> c.3,300 Ma)



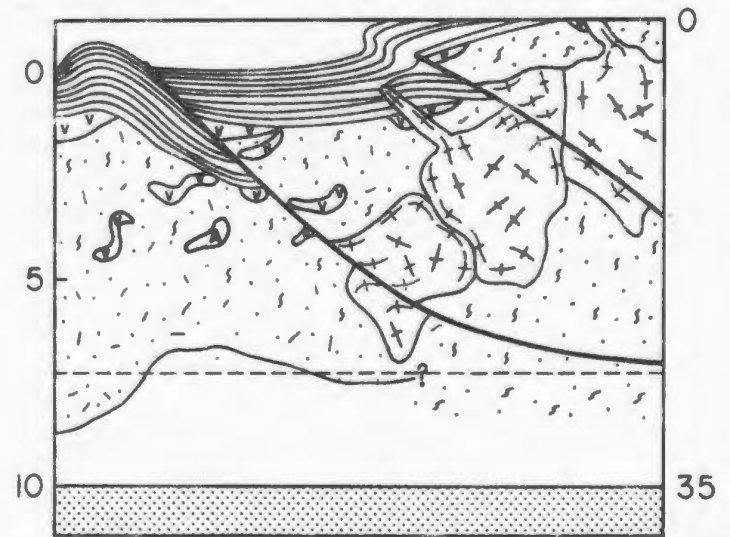
Stage II Pre-Hopedalian (c.3,300 Ma)



Stage III Hopedalian (c.3,091 Ma)



Stage IV Fiordian (< c.2,853 Ma)



~~0130~~

basaltic and metasedimentary supracrustal rocks and anorthosite; Figure 7.4, Stage 1). Partial melting of granulite and/or amphibolite facies, intermediate composition parent produced a melt with REE and HFS element distribution comparable to that observed for the Maggo Gneiss (Section 6.5).

In West Greenland and northern Labrador a pre-3,600 Ma high grade metamorphic event, documented by McGregor (1973) and Griffin et al. (1980) could have produced the required Maggo gneiss parent. During this high grade event the Amitsoq gneiss, present at this time, underwent LILE depletion. Parental material to the Maggo gneiss precursor can be represented by a depleted, granulite facies Amitsoq gneiss. The Kangimut sangmissoq gneiss, a phase of Amitsoq gneiss has been interpreted to represent a relict granulite facies Amitsoq gneiss (Nutman, pers. comm., 1985). The REE pattern for the Kangimut sangmissoq gneiss is similar to that used as a parent composition in Section 6.5.

Within the NAC, Early Archaean gneisses have only been recognized in the Godthab and Saglek regions. Elsewhere, i.e. the Hopedale Block and southern portions of the, Greenland Archaean, no direct evidence exists for the presence of these ancient rocks at surface. In the southern portion of the the Greenland Archaean Taylor and Kalsbeek (1986) have carried out an extensive program of Pb isotope geochemistry on the grey gneisses. The Ivigtut gneisses, which on a pre-drift reconstruction of the NAC (Figure 7.1), are

contiguous with the Maggo gneiss, yield a Pb-Pb date of 3,110 +/- 65 Ma and have a low model μ_1 value (7.19; Taylor and Kalsbeek, 1986). The low model μ_1 value implies that this area has been the site of several episodes of reworking of older U-depleted continental crust. These authors estimate a minimum age of 3,330 Ma for the source of the crustal Pb component in the Ivigtut gneisses. This age is in agreement with the results for the NBN suite and Hopedalian area of this study and the results of Schiøtte et al. (In prep.). The Pb isotopic data are interpreted as strong indirect evidence of the occurrence of early Archaean, U-depleted, crust, approximating granulite facies Amitsoq gneiss, at depth in southern West and South Greenland.

After derivation, during the pre-3,600 Ma metamorphism, the high grade, intermediate composition parent remained at a deep crustal level, at a high temperature and pressure (Figure 7.4, Stage II). Under these conditions the parent behaved as an open system resulting in further mobility of the LILE, especially Rb. This two stage depletion produces a parent with a low Rb/Sr ratio, equal to, or lower than, the assumed mantle ratio (0.025, Peterman, 1979).

The Maggo gneiss parent remained at depth and open to LILE mobility until 3,366 Ma. This age, corresponding to the Hopedalian area, is interpreted to date the Pre-Hopedalian deformation. This event resulted in a thickening of the crust (due to horizontal (?) movements) and

Increasing P_{load} and temperature on the parent material as it was displaced to deeper crustal levels. This increase in pressure and temperature induced partial melting, approximately 25% of a granulite and/or amphibolite facies parent (Section 6.5). This partial melting episode is interpreted to be responsible for generating the majority of the Maggo gneiss precursor (Figure 7.4, Stage II).

Greater or lesser degrees of melting would produce a Maggo gneiss precursor with flatter to steeper REE abundances, respectively. The variable degree of melting combined with the variable parental compositions combine to account for the range of REE distribution patterns observed for Hopedalian domain Maggo gneiss (See Figure 6.4).

The Maggo gneiss precursor was emplaced at a higher level in the crust under the influence of a directed stress, producing the Pre-Hopedalian fabric in the gneiss. This material incorporates inclusions of previously deformed, older supracrustal material which retains evidence of a high grade metamorphism.

Having derived the Maggo gneiss precursor and with its subsequent emplacement, the Rb-Sr systematics in the precursor began to stabilize, i.e. closed to further LILE mobility. After the Pre-Hopedalian fabric developed, Hopedale dykes were emplaced into the crust, between 3,366 and 3,091 Ma, the ages for precursor derivation and the Hopedalian event, respectively. This time span corresponds to that inferred for the emplacement of the Saglek.

00000

Ameralik and Tarssartog dykes (Collerson et al., 1981; Nutman, 1986).

After emplacement of the Hopedale dykes, the entire sequence underwent middle to upper amphibolite facies metamorphism, the Hopedalian event (Figure 7.4, Stage III). Up to this point the Rb-Sr systematics of the Maggo gneiss precursor were in a state of flux. Based on modelling results, Rb contents of 17 ppm, in the precursor, result from 25% melting of the granulite facies parent which originally contained 5 ppm Rb. For the amphibolite facies parent, comparable Rb contents can be attained at lower degrees of melting. This Rb level in the gneiss precursor is maintained, i.e. depletion no longer affects the LILE content of the gneiss, resulting in the Hopedalian domain Maggo gneiss being enriched in Rb with respect to its parent. Further enrichment in the gneiss results from the continued depletion of Rb from the granulite parent and the migration of the Rb up through the crust into the Maggo gneiss during the Hopedalian event. The degree of LILE enrichment at this time was sufficient to increase the Rb, Ba and K₂O content of the Maggo gneiss to values comparable to those observed in other grey gneiss terrains, e.g. Northern Light Gneiss, NW Ontario (Arth and Hanson, 1976).

The NBN suite is interpreted to represent Maggo gneiss in which the Rb-Sr systematics closed at 3,305 Ma, in response to the Pre-Hopedalian event. Evidence for the

unstable nature of the Rb-Sr systematics in the gneiss after derivation of the precursors can be seen in the SR suite of Grant et al. (1983). This suite yields an age of 3,226 Ma and has a low Sr_0 value, which overlaps the mantle evolution line. The age is interpreted to represent the first effects of the Hopedalian event and closure of this suite with respect to Rb addition, characteristic of other Hopedalian suites.

7.3.2 Late Middle to Late Archaean (< 2,900 Ma)

After these events the Hopedalian domain Maggo gneiss was stabilized in the crust and deposition of the Florence Lake supracrustal lithologies occurred. At c. 2,853 Ma the Flordian tectonothermal event began to affect the gneiss (Figure 7.4, Stage IV). The Flordian reworking occurred at a time when the NAC was subjected to another complex period in its development. Accompanying the Flordian event, elsewhere in the NAC, was the derivation and emplacement of the Nuk gneiss. In southern West Greenland (Taylor et al., 1980, 1984), the Kanairiktok intrusives south and west of Hopedale (Grant et al., 1983) and ending with emplacement of the Qorqut granite at 2,520 Ma (Moorbath et al., 1981). Between 2,900 and 2,700 Ma the NAC underwent granulite (Greenland and northern Labrador; Collerson et al., 1981) and lower amphibolite facies (Hopedale Block; Korstgard and Ermanovics, 1984; 1985; This Study) metamorphism.

In response to Flordian reworking the Hopedalian Maggo gneiss fabric was reoriented into a NE-SW orientation. Accompanying this physical change in the gneiss was a chemical change (LILE depletion and HFS element enrichment; Section 6.2) as a result of reworking of the Hopedalian domain gneiss. The depletion in Rb along with Sr immobility (Section 6.2.2.1) in turn caused the isotopic systematics of the gneiss to reset such that $^{87}\text{Rb}/^{86}\text{Sr}$ ratios for the Flordian gneiss were lowered.

Metamorphism, at lower to middle amphibolite facies, associated with the Flordian event, caused retrogression in the gneiss and other lithologies, e.g. Hopedale dykes. In the Godthab region of West Greenland high grade metamorphism at this time resulted in granulite facies assemblages in Nuk gneiss (Wells, 1979). Further south, in the Ivigtut region, Berthelsen and Henriksen (1975) recognized a primary middle to upper amphibolite facies metamorphism and a secondary retrogression to greenschist and lower amphibolite facies. Korstgard and Ermanovics (1985) correlated these metamorphic events, the Senillian and Maturian orogenies, with the Hopedalian and Flordian events of the Hopedale Block. The range in metamorphic conditions at this time indicate that the southern portion of the NAC was at a higher crustal level than areas further north.

Reworking of the Maggo gneiss during the Flordian event does not require the addition of large volumes of new material to form the Flordian domain gneiss. However, in the

Hopedale Block the Kanairiktok Intrusions were emplaced during the Flordian event (Figure 7.4, Stage IV). The Kanairiktok Intrusions were derived from either a mantle source or preexisting crustal material (Figure 7.2). If the first hypothesis is correct, the Kanairiktok Intrusions represent new material added to the crust after derivation from the mantle (Grant et al., 1983). Alternatively the Intrusions could have been derived from an older, depleted granulite facies crust, in a manner similar to that proposed for the Maggo gneiss precursor (Section 6.5). In this instance the parent could again be Amitsog gneiss, having a Rb/Sr ratio (0.025) comparable to the mantle value. Further isotopic and geochemical work on the Kanairiktok Intrusions is necessary before this aspect of Hopedale Block geology can be settled.

The Kanairiktok Intrusions may be chronologically equivalent to the Nuk gneiss, but the former have not been subjected to the post-emplacment deformation and metamorphism which has affected the latter suite.

Reworking of the Maggo Gneiss during the Flordian event is accompanied by synchronous tectonic, metamorphic and chemical changes elsewhere in the NAC. Crustal thickening, by thrusting and folding, has recently been identified as a major feature in the late Archaean (Brown et al., 1986) responsible for the complex and contrasting relationships observed for this time period.

7.4 Summary

The Maggo gneiss of the Hopedale Block retains evidence of a protracted developmental history extending from c. 3,300 to c. 2,600 Ma. The gneiss precursor, interpreted to be derived from an Amitsoq-like parent, was subjected to three tectonothermal periods during this time span. The oldest, the Pre-Hopedalian, event has not been recognized in other, more studied, areas of the NAC.

The field relationships for the Hopedalian domain Maggo gneiss are comparable to those observed in other NAC lithologies (Amitsoq and Uivak gneisses) representing a similar time frame. The youngest Archaean tectonothermal event to affect the Maggo gneiss is the Flordian event or series of events. The Flordian is responsible for the reworking of the Hopedalian domain gneiss and is correlative with the Late-Middle Archaean, high grade metamorphism recognized in other areas of the NAC. The syn-Flordian Kanariktok intrusions are tentatively correlated with the Nuk gneiss of southern West Greenland.

PHOTOGRAPHIC PLATES

00800

Plate 1

- A Gently plunging antiformal structure preserved within amphibolite subunits 1 to 3 of the Weekes association (WA), in Maggo gneiss (MG). The layering reflects varying proportions of plagioclase and garnet. Contacts with the enclosing gneiss are marked by foliated pegmatites. Person for scale, on left limb of fold. Station 83-224 - Manuel Island.
- B Cigar shaped inclusion of Weekes association (WA) within foliated to banded tonalitic Maggo gneiss (MG). Inclusions of Weekes association vary in size between that depicted here and in Plate 1A. Station 83-129 - east shore of Pilliarusik Bay.
- C Inclusion of layered metavolcaniclastic unit (V) and various amphibolite (A) subunits of the Weekes association. The contact between the Weekes and the Maggo gneiss is marked by a wide pegmatite zone (Peg) with inclusions of supracrustals. Plate 4B is a close up of the volcanoclastic unit taken to the right of centre. Hammer on antiformal closure (centre) is 35 cm long. Station 82-50 - Zacharius Island.
- D Granoblastic equigranular texture in clinopyroxene (cpx) bearing amphibolite (Subunit 2). Clinopyroxene is in equilibrium with plagioclase (pl) and hornblende (hbl). Sample 83-311 - Manuel Island. Scale bar is 0.25 mm.
- E Lepidoblastic texture in amphibolite subunit 1, defined by the alignment of hornblende (hbl) with interstitial plagioclase (pl). Sample BF-82-1B - Maggo Island. Scale bar is 0.5 cm.
- F Garnet (gt) poikiloblast with inclusion of plagioclase (pl), opaques (op) and hornblende (hbl). Clinopyroxene, in this sample, and garnet were not observed in contact with each other suggesting inequilibrium between these phases. The garnet is rimmed by successive zones of sericitized plagioclase (pl) and hornblende (hbl) inferred to have been produced by the instability of the garnet and clinopyroxene. Sample 83-193 - Garnet Island. Scale bar is 0.5 cm.

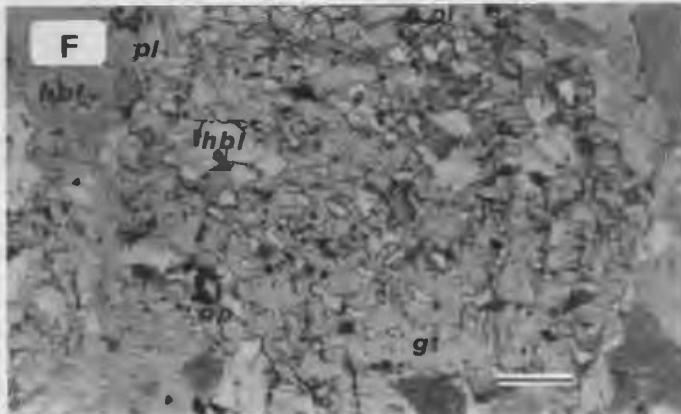
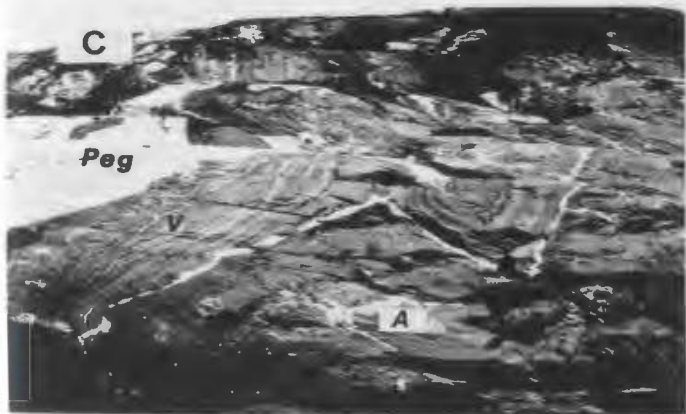
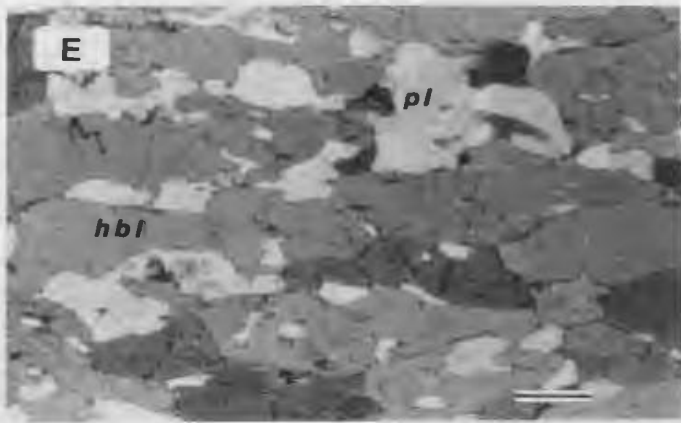
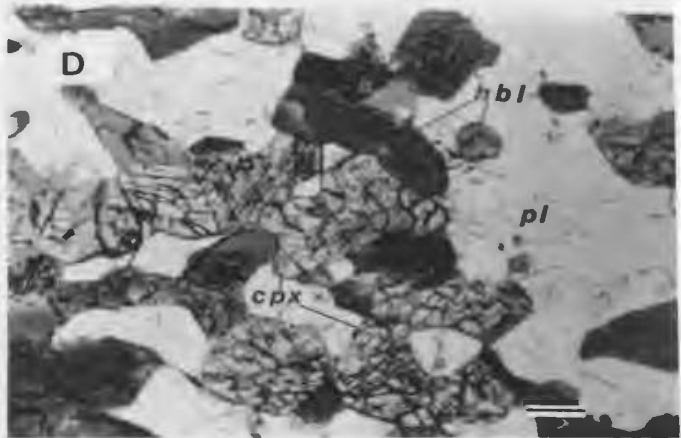


Plate 2

- A Equilibrium texture between clinopyroxene (cpx), plagioclase (pl) and hornblende (hbl) in Weekes association subunit 4. Garnet and clinopyroxene were observed in contact in this sample, however these two species are not stable and react to form plagioclase and hornblende coronas on the garnet (lower left corner). Sample 83-84 - northwest of Camp Island. Scale bar is 0.25mm.
- B Coronas of plagioclase (pl) and hornblende (hbl) surrounding garnet (gt). The coronas effectively isolate the garnet and prevent further reaction with clinopyroxene (cpx). Sample 83-84 - northwest of Camp Island. Scale bar is 0.5 cm.
- C Ultramafic unit of Weekes association. The ultramafic occurs as boudins within a larger enclave of Weekes subunits 1 to 3. The ultramafic displays relict harriitic textures similar to those described by Collerson *et al.* (1976). Station 83-131 - east shore Piliiarusik Bay.
- D Composite inclusion of Weekes association in Maggo gneiss. The long axis of the inclusion parallels the Hopedalian fabric (S_{n+2}). The inclusion consists of calcite (cc) + pyrite (py) separated from talc (tc) + tremolite (tr) by a narrow transition zone (dashed line). The inclusion has a mono-mineralic rim of radiating actinolite (ac) needles. Station 83-84 - south of Camp Island. Scale bar is 8 cm.
- E Alteration of olivine porphyroblast in ultramafic unit of Weekes association. The olivine (ol - high relief) is being replaced by serpentine (serp) + magnetite (mag). Tremolite (tr) forms the matrix supporting the olivine. Sample 83-51 - north shore of Kangliuasualuk Tapani. Scale bar is 0.1 mm.

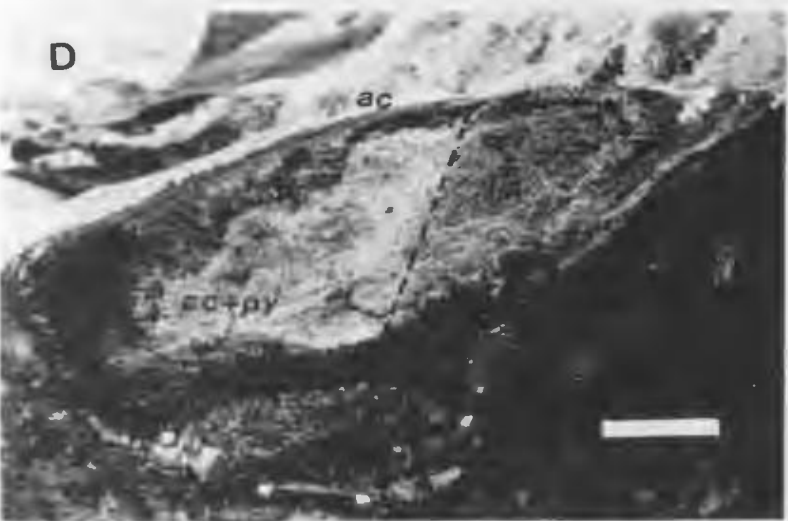
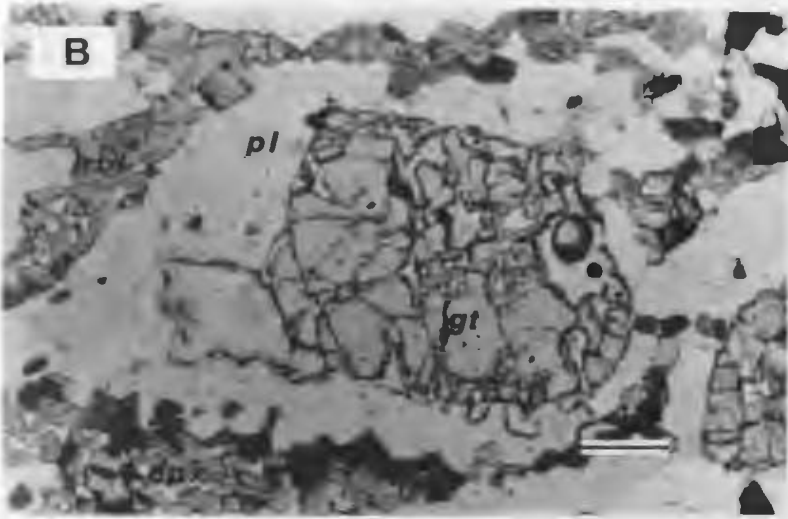


Plate 3

- A Inclusion of marble, Weekes association unit 8, within Maggo gneiss (MG) from Manuel Island. The long axis of the inclusion parallels the Hopedalian fabric (S_{n+2}). The inclusion is enveloped by a mono-mineralic rim of foliated phlogopite (phlog). The core of the inclusion is layered with varying proportions of dolomite, olivine, phlogopite and magnetite. Plate 3B is a close up view taken at the hammer. This is the largest inclusion of marble material found in the study area. Station 83-308 - Manuel Island.
- B Close up of layering in marble inclusion. The foliated phlogopite rim (phlog) is visible at the top of the photo. The inclusion proper consists of dolomite rich (cc), (cc + mag + ol +/- phlog) and phlogopite-rich (ph), (phlog + cc + mag +/- ol) layers. Station 83-308 - Manuel Island.
- C Olivine (ol) porphyroblast, altering to serpentine along fractures, in a dolomite-rich layer from the marble inclusion (plate 3A and B). Dolomite (cc) exhibits a well developed cleavage, while phlogopite (phlog) is foliated parallel with the long axis of the inclusion. Sample 83-308C - Manuel Island. Scale Bar is 0.5 cm.
- D Inclusion of staurolite (st) in garnet (gt) from a pelitic horizon of the metasedimentary unit of the Weekes association. Where observed staurolite always occurred as an inclusion in garnet. Biotite (bio) occurs as inclusions within the garnet and with chlorite (chl) in the matrix surrounding garnet. Sample BF-82-4E - Woody Island. Scale bar is 0.25 mm.
- E Some pelitic horizons of the Weekes association are characterized by the presence of corundum (co) indicating an SiO_2 -poor bulk composition. The garnet in the lower left corner contains staurolite (Plate 3D). The corundum is separated from the garnet (gt) by biotite (bio) and chlorite (chl). The latter appears to be the result of retrogression of garnet and biotite. Sample BF-82-4E Woody Island. Scale bar is 0.5 cm.

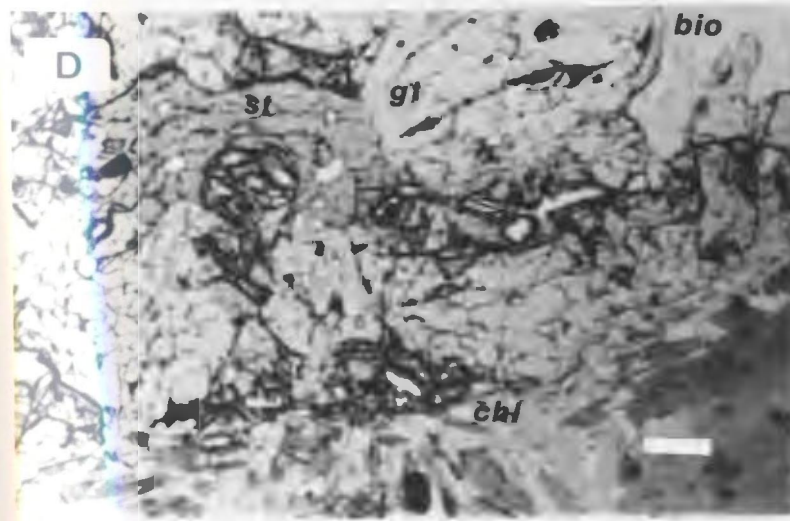
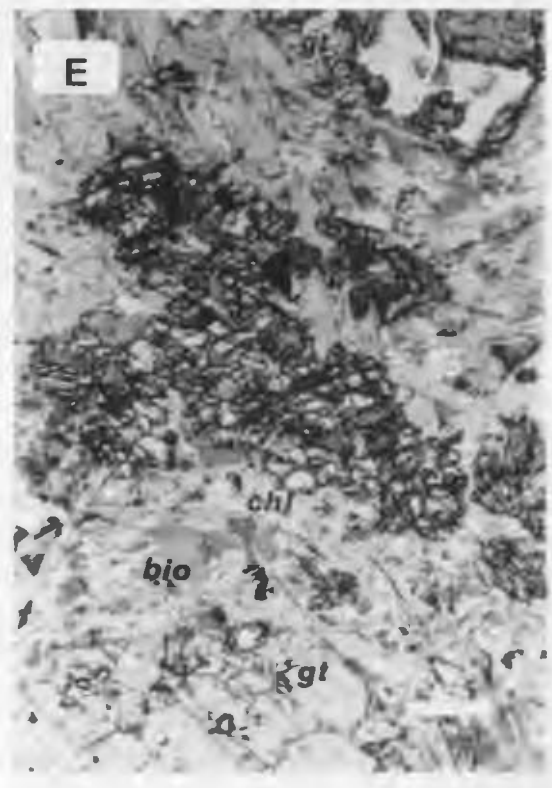
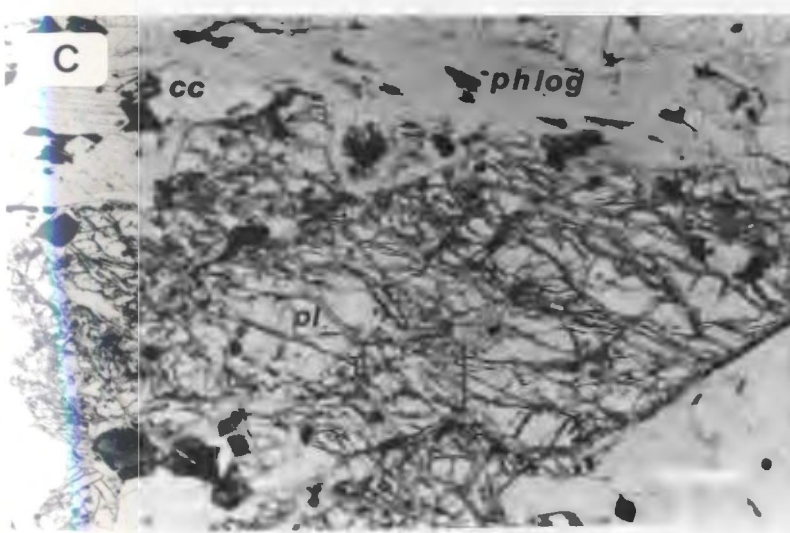
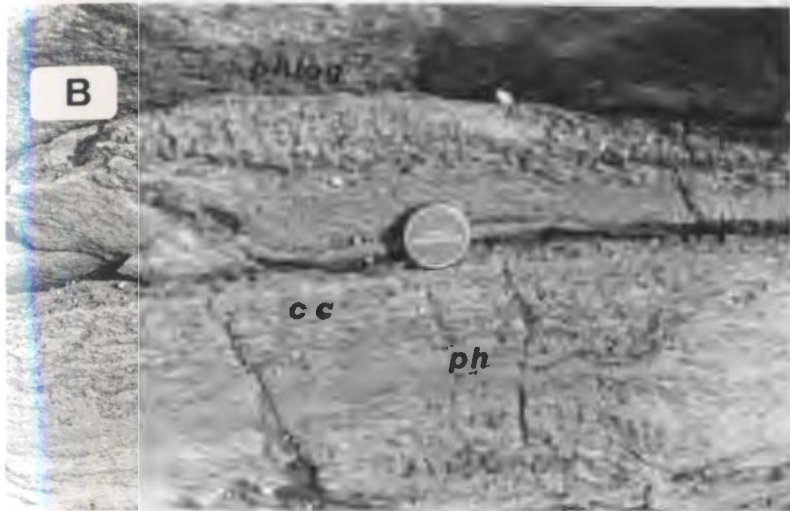


Plate 4

- A Cumingtonite (cum) - garnet (gt) - biotite (bio) assemblage within pelite. Chlorite (chl) occurs along fractures cutting through the garnet and as a retrogression product of biotite. Sample BF-82-4F - Woody Island. Scale bar is 0.5 cm.
- B Metamorphically enhanced, primary (?) layering in metavolcaniclastic unit of the Weekes association. The more competent amphibole-rich layers are thinned and boudinaged by post-peak metamorphic, tectonic events. Station 82-50 - Zacharius Island.
- C Leucocratic layers within the metavolcaniclastic unit (Plate 4B) are characterized by the assemblage anthophyllite (anth) - garnet (gt) - plagioclase (pl) - biotite (bio) - quartz (qtz). The anthophyllite is sub-poikiloblastic and cuts the foliation defined by biotite. Sample 82-50B-1 - Zacharius Island. Scale bar is 0.5 cm.
- D Rounded to angular inclusions of megacrystic and foliated anorthosite within Maggo gneiss. The foliation in the anorthosite (S_2) is discordant to the Hopedalian fabric (S_{n+2}) in the gneiss. Anorthositic lithologies form a minor but important component of the Hopedale Block. Sample BF-81-56.
- E Anorthosite, anorthositic gabbro and hornblendite inclusions within variably migmatized Maggo gneiss. Large, recrystallized plagioclase accumulations (1) are common in the mafic-rich lithologies. With increasing deformation the plagioclase crystals become flattened (2). Station 83-30 - north shore of Kangluasuakoluk Tagani.

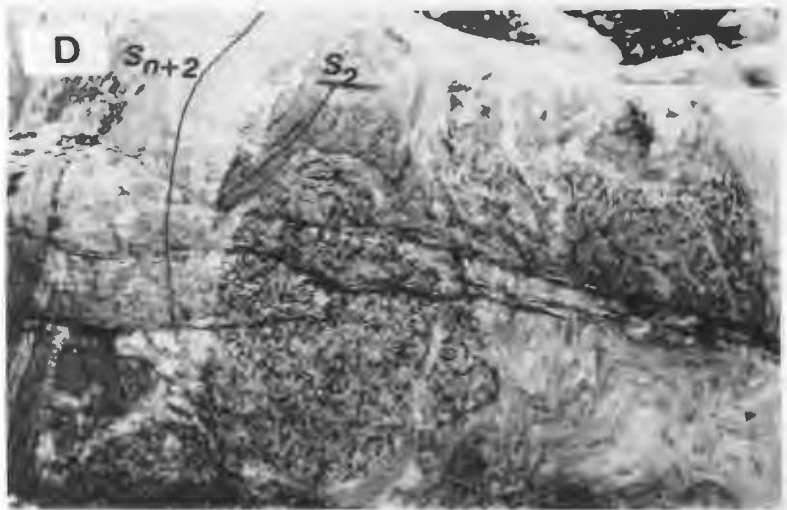
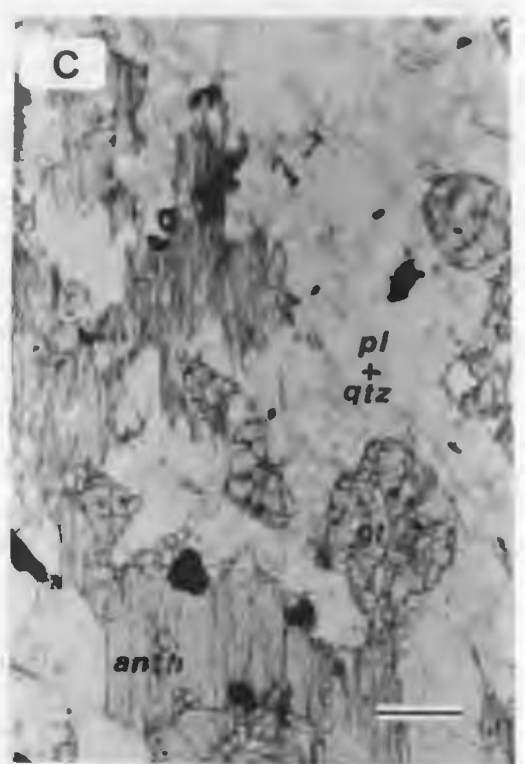
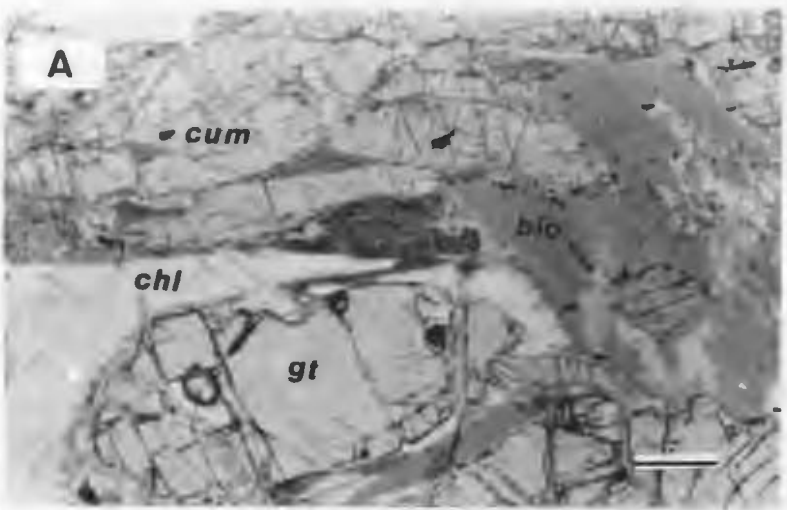


Plate 5

- A Rootless intrafolial fold (arrow) within Maggo gneiss. These structures are inferred to have developed prior to Hopedalian deformation (D_{n+2}). Station 83-303 - Manuel Island.
- B Discordant contact between foliated biotite tonalite phase of the Maggo gneiss (MG) and Hopedale dyke (HD). The Pre-Hopedalian fabric (S_{n+1}) in the gneiss developed prior to emplacement of the dyke. The gneiss-dyke contact lies between the two arrows. Station 83-315 - Hopedale Harbour.
- C Maggo gneiss displaying a well developed Hopedalian fabric (banding). This exposure is typical of the weakly migmatized Maggo gneiss (Compare with Plate 6A). Station 83-172 - south of Camp Island.
- D Fine grained inclusion of foliated tonalite in Maggo gneiss. The inclusion, one of several at this locality, is enclosed in a coarser grained tonalitic phase of the gneiss displaying a well developed Hopedalian fabric. The inclusion has undergone some post-Hopedalian deformation resulting in the displacement and rotation of the right end of the block (arrow). Station 82-39 - Kernertalik Island.
- E Fine grained layer of foliated tonalite within medium grained tonalite to trondhjemite phase of the Maggo gneiss. The layer is displaced by a sinistral shear (arrow) attributed to the Flordian event. Station 83-265 - Black Head Tickle.

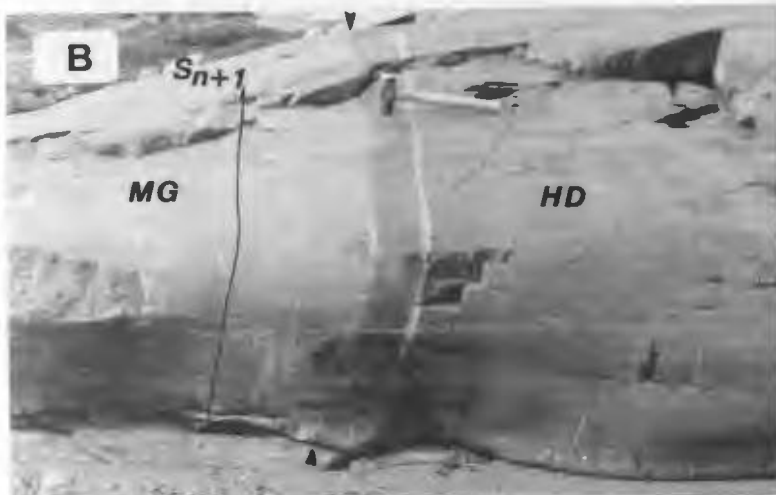


Plate 6

- A Stromatic, phlebitic and pygmatic migmatites developed during the Hopedalian event. Individual migmatites display concordant and discordant relationships with the Hopedalian fabric. Station 83-130 - Pilliarusik Bay.
- B Hopedalian lit-par-lit migmatites producing a banded Maggo gneiss which subsequently becomes folded during later stages of the Hopedalian deformational event. The migmatites develop tight chevron folds in the hinge zones and become stretched along the fold limbs. Station 83-55A - north of Camp Island.
- C Diktyonitic migmatite developed along a shear cutting foliated biotite tonalite. The terminations of the shear parallel the foliation in the tonalite and are characterized by the development of nebulitic migmatites. Station 83-261 - Black Head Tickle.
- D Coarse grained diktyonitic migmatite (1) developed in banded tonalitic to granodioritic gneiss. The nature of the non-migmatized gneiss at this locality is shown in Plate 10A. Samples 83-214 and 215 are used in the geochronological determinations (SW end, Marsha's Cove; see Sections 4.6 and A.2.5). These samples date the early effects of Flordian overprinting on the gneiss. The terminations of the shear are marked by nebulitic migmatites. Patchy nebulitic migmatites are present as well (2). Station 83-214, 215 - Marsha's Cove.
- E Hornblende-rich trondhjemite phase of the Maggo gneiss from the Hopedalian domain. The gneiss consists of hornblende (hbl) -plagioclase (pl) -biotite (bio) - quartz (qtz) displaying a granoblastic texture. Hornblende is optically aligned defining the foliation, with minor amounts of biotite exhibiting the same orientation. Sample 83-299-1 - Manuel Island. Scale bar is 0.5 cm.

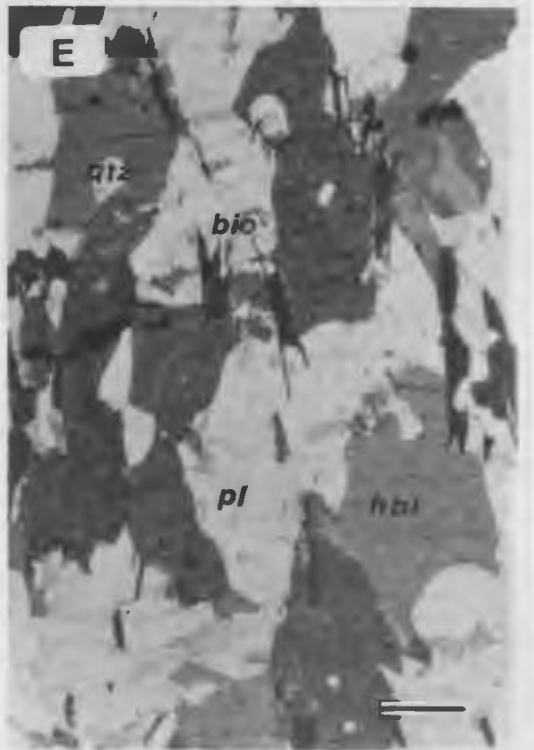
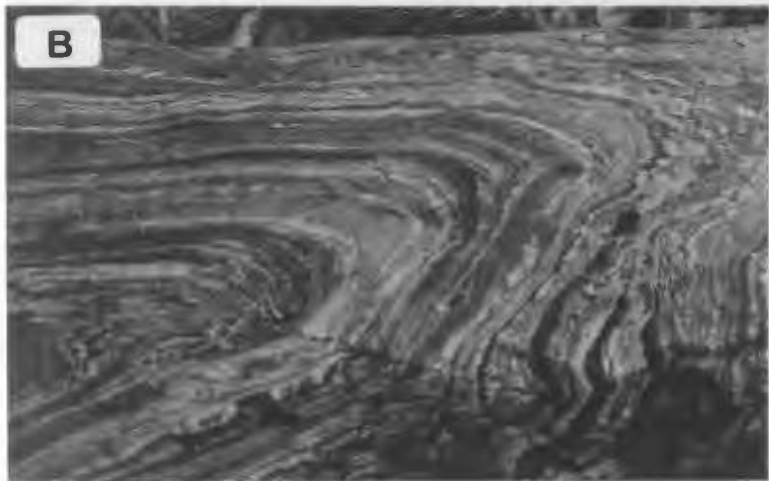
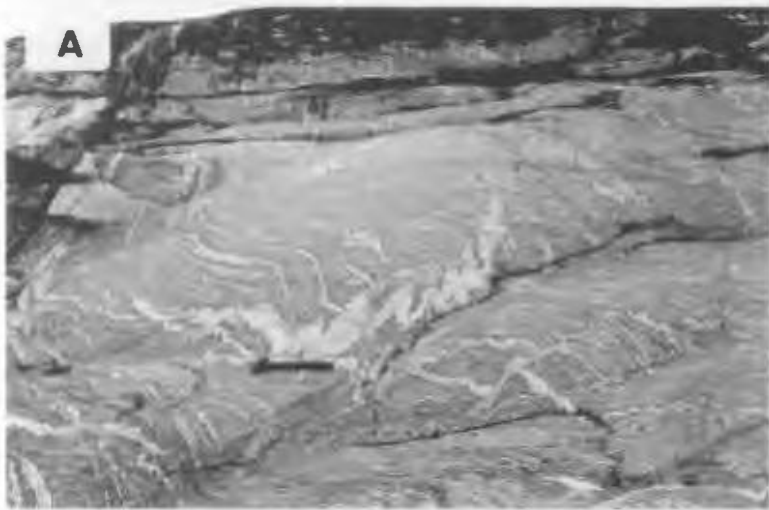


Plate 7

- A Biotite (bio)-rich, foliated trondhjemitic Maggo gneiss displaying two generations of biotite. Primary (1^o) biotite which defines the foliation, with hornblende (not shown), is cut by secondary (2^o) biotite. Plagioclase (pl) is twinned, with alteration to sericite along twin planes visible. Quartz and untwinned plagioclase make up the remainder of the field of view. Titanite (sph) is a common accessory mineral in all phases of the Maggo gneiss. Sample 83-38 - north shore of Kangliuasukoluk Tagani. Scale bar is 0.25 mm.
- B Interstitial K-feldspar (Kspar), displaying tartan twinning, within the foliated biotite tonalite phase of the Maggo gneiss. In this sample the K-feldspar forms a continuous interstitial mosaic to the larger plagioclase (pl) and quartz (qtz) grains. Sample 83-99 - south shore of Iganiakuk Bay. Scale bar is 0.25 mm.
- C Garnet-bearing, banded to foliated trondhjemitic Maggo gneiss. Garnet (gt) in all gneiss samples is irregular in shape and forms pseudo-poikiloblastic grains which show evidence of retrogression to chlorite and biotite. Plagioclase (pl), hornblende (hbl) and quartz (qtz) are abundant phases in this lithology. Sample 83-78A - southwest of Camp Island. Scale bar is 0.5 cm.
- D Hopedale dyke folded during the Hopedalian deformation with foliated biotite tonalite (MG). The Hopedalian fabric (S_{n+2}), parallel to the hammer handle, is coplanar with the axial plane of the folded dyke. The dyke contains relict plagioclase accumulations (arrow) which are atypical of this lithology within the study area. To the left and right of the antiform-synform pair the dyke becomes boudinaged, with the boudins parallel to the Hopedalian fabric. Station 83-192 - Garnet Island.
- E Boudinaged Hopedale dyke with the boudins aligned parallel to the Hopedalian fabric (S_{n+2}) within the Maggo gneiss (MG). The interboudin regions (arrow) have been filled by the flowage of gneiss material into the void created by the stretching of the dyke (Compare with Plate 8A). The amphibolite boudins, above and below the hammer, are inferred to represent adjacent limbs of a folded dyke. Station 82-65A - Hypothesis Island.
- F Parallel limbs of a folded Hopedale dyke displaying two responses to the Hopedalian deformation. At the top (1) the dyke responds by stretching with recrystallization, while the lower dyke (2) is boudinaged with the development of migmatitic material around the boudins. Station 82-70 - Double Island.

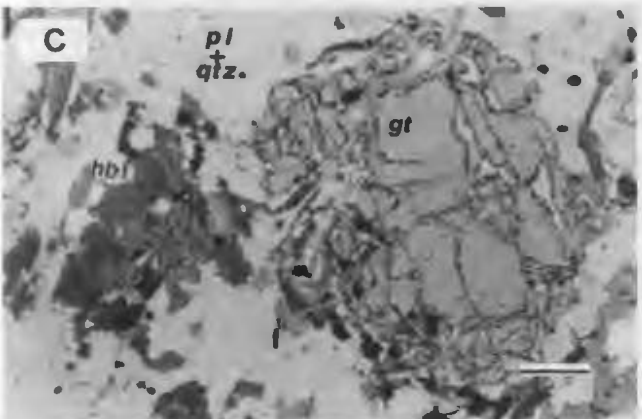
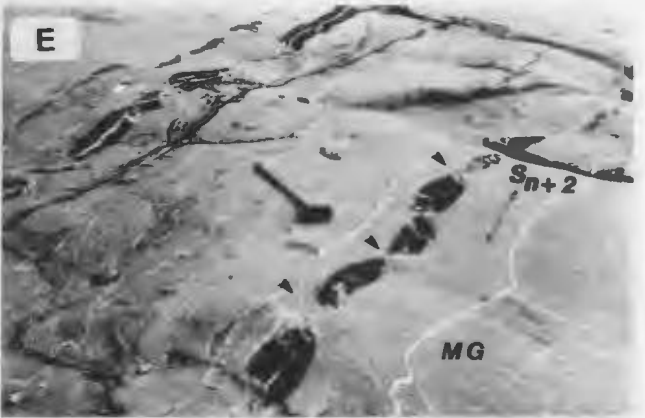
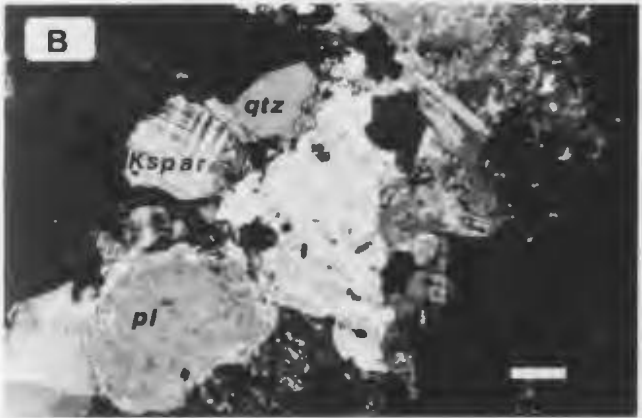
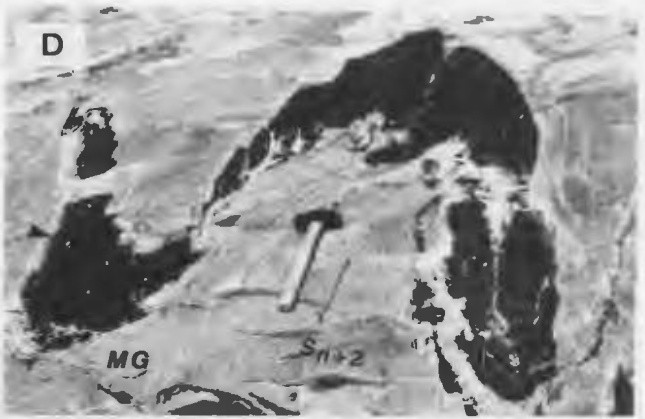


Plate 8

- A Rectangular boudins of Hopedale dyke with interboudin zones filled by minimum melt material, of unknown origin, within foliated Maggo gneiss (MG). The rectangular boudins are one response of the dykes to the Hopedalian deformation. Station 83-225 - Manuel Island.
- B Granoblastic equigranular texture in clinopyroxene (cpx) bearing Hopedale dyke. Clinopyroxene occurs as discrete grains within a mosaic of hornblende (hbl) and plagioclase (pl) and accounts for < 5 volume % of the dyke mineralogy. Sample 83-314 - Hopedale Harbour. Scale bar is 0.5 cm.
- C Plagioclase (pl) accumulations within Hopedale dyke. The arrows point to an accumulation which has a core of garnet surrounded by plagioclase. The latter mineral effectively armours the garnet from further reaction with clinopyroxene in the dyke. The assemblage garnet-clinopyroxene represents the highest grade assemblage preserved in the Hopedale dykes (see Section 3.3.3). Station 83-192 - Garnet Island.
- D Clinopyroxene (cpx) bearing amphibolite from Weekes association subunit 2, for comparison with the clinopyroxene-bearing Hopedale dyke lithology. Station 83-311 - Manuel Island. Scale bar is 0.25 mm.
- E Retrogressed Hopedalian mineral assemblage within the Hopedale dyke lithology. The retrogression, attributed to the Flordian event produces symplectic epidote (ep) with quartz inclusions at the expense of plagioclase (pl). The An content of the plagioclase decreases from 27 to 20 with the retrogression. Hornblende (hbl) reacts to form actinolite (act) in response to the Flordian event. (see Section 3.3.3). Sample 83-212 - Marsha's Cove. Scale bar is 0.25 mm.

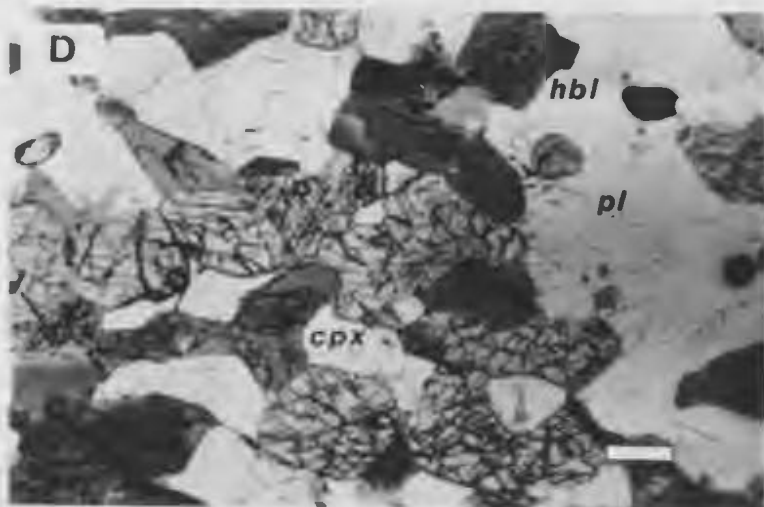
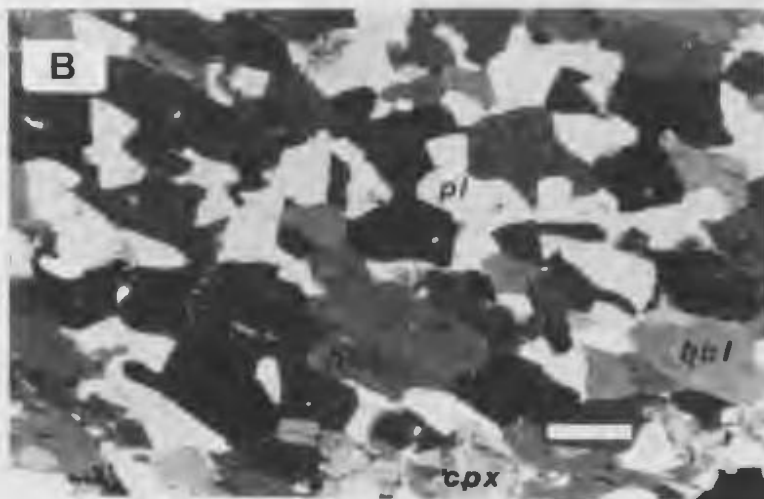
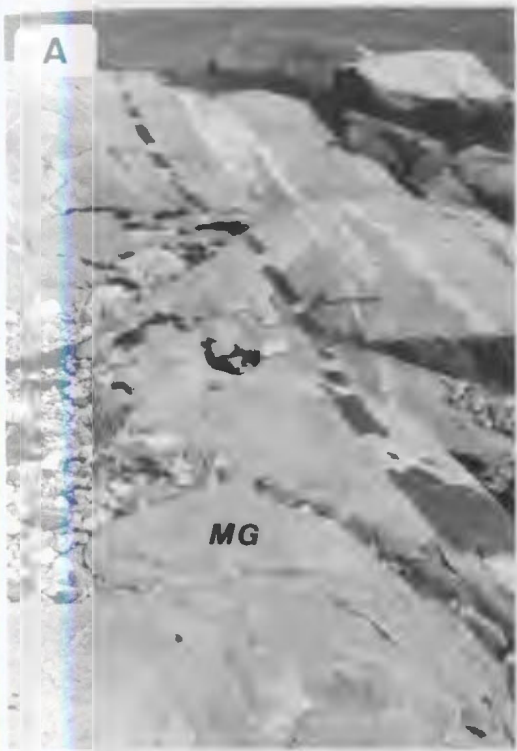


Plate 9

- A Hopedale dykes (arrow) become thinned and intensely folded during Hopedalian deformation. The dyke shown here is 200 m, along strike, from the dyke shown in Plate 8A. Station 83-223 - Manuel Island.
- B Gently folded foliated hornblende tonalite phase of the Maggo gneiss (MG). Lit-par-lit pegmatites, displaying evidence of pinch and swell structures, parallel the foliation. The foliation and pegmatites are displaced by dextral shears which produce the folding. Station 82-64 - Hypothesis Island.
- C Homogeneous foliated tonalite with lit-par-lit pegmatite swaths (below ledge) producing a banded tonalite. The "banded" gneiss is displaced by dextral shears, arrows show the sense of shear. Numbers refer to samples used in the geochronology portion of the study. Station 83-312, 316 - Hopedale Harbour.
- D to F - Field relationships and localities for samples from Marsha's Cove geochronology suite. Station 83-146.
- D Locations of two samples (83-202, 203) of Maggo gneiss which preserve Hopedalian mineralogy and textures. The varying shades of grey on the outcrop surface are interpreted to represent primary features of the gneiss protolith.
- E The clipboard (middle-top) is at the same position as the pack in Plate 9D. Samples 83-204 and 205 represent Maggo gneiss lithology which is progressively reoriented into a NE-SW orientation during the Flordian event. Plate 9F is from the area marked by the arrows.
- F Samples 83-208 and 209 represent Maggo gneiss which has been completely reoriented and retrogressed during the Flordian event. The collection of all geochemistry samples used in this study was facilitated by the use of a gas powered diamond drill shown here.

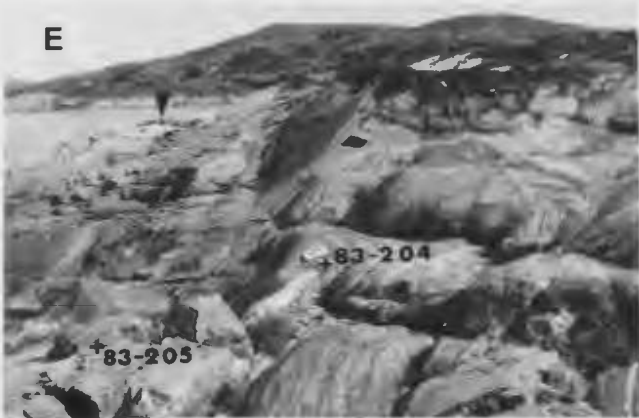
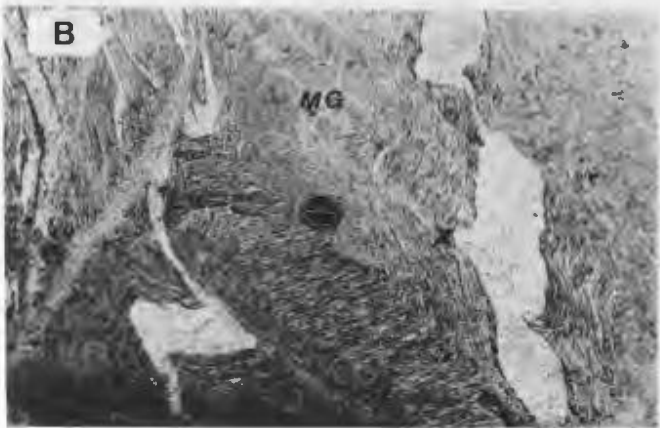
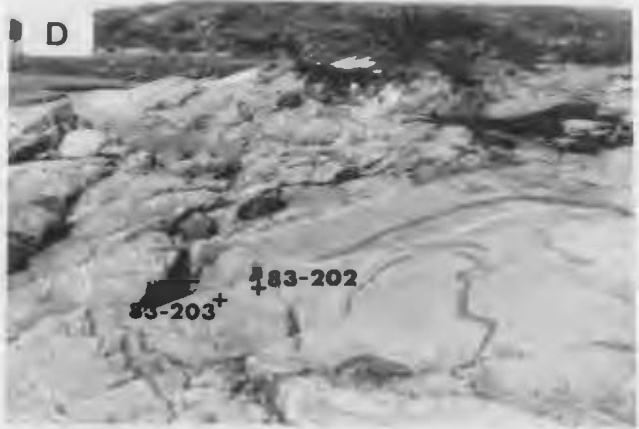


Plate 10

- A Banded tonalite phase of the Maggo gneiss from the SW end of Marsha's Cove. The banded tonalite is cut by diktyonitic migmatites (see Plate 6D) developed during the Flordian event. The location of samples 83-216 and 217, with respect to other samples in this suite, is shown in Figure A.5.
- B Field locations and relationships between samples from the Hopedale Gneiss geochronology suite. Sample 83-232 contains thin biotite foliae separated from Sample 83-233, a mafic-rich layer, by a zone of medium to coarse grained, biotite-poor migmatite (83-237). Sample 83-234 is a homogeneous biotite tonalite, with the biotite displaying a random orientation, cut by granitic (s.s.) pegmatite, 83-235. Station 83-1 - mainland shore due south of Manuel Island.
- C Field location for three samples of the Dead Dog Point geochronology suite. Sample 83-242, collected directly under the notebook, is banded gneiss. Samples 83-243 and 244 are individual bands within the gneiss. 83-243 is a fg to mg, foliated, hornblende-poor, band situated between mg to cg, massive, hornblende-rich bands (83-244). In the latter case the hornblende forms porphyroblasts up to 0.5 cm long. Station 83-4 - Dead Dog Point, due south of Manuel Island.
- D Refolded isoclinal fold within layered Weekes association amphibolite. The layering, folded about F_1 , is interpreted to be relict primary layering enhanced by metamorphic recrystallization. The F_1 structure subsequently becomes refolded (F_2). Note the parallelism of the F_1 and F_2 fold limbs away from the F_1 hinge zone. In other outcrops of the Weekes association recognition of the early folding is difficult because of the lack of F_1 hinge zones. Station BF-82-3 - Manuel Island.
- E Hopedale dyke displaying evidence of coplanar folding resulting from Hopedalian deformation. The refolding of the Hopedale dykes may be explained by a continuum of deformation where isoclinal folds are produced early in the deformation and subsequently become refolded at a later stage of the same event. The fabric within the host Maggo gneiss parallels the dyke-gneiss contact. Hinge zones of folded Hopedale dykes are only rarely preserved and exposed, so what is normally observed are the limbs of the folds as parallel dykes (see Plate 7E). Station 82-37 - Kernertalik Island.

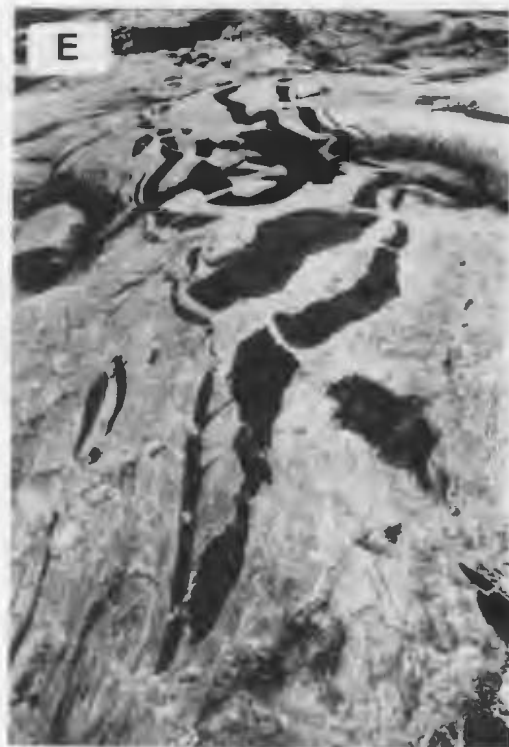
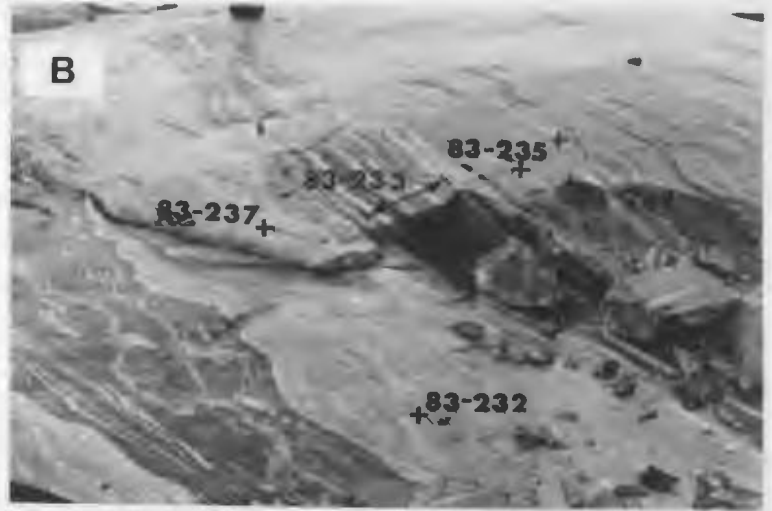
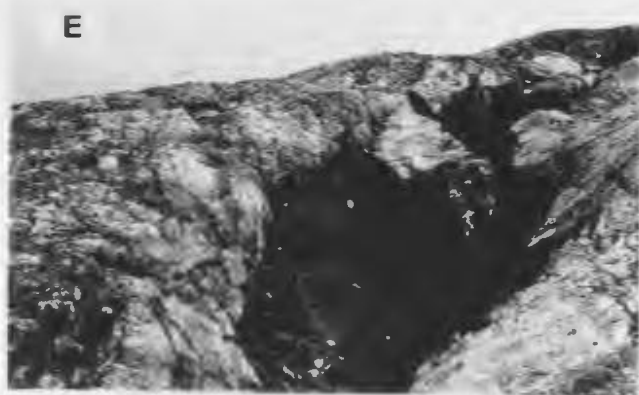
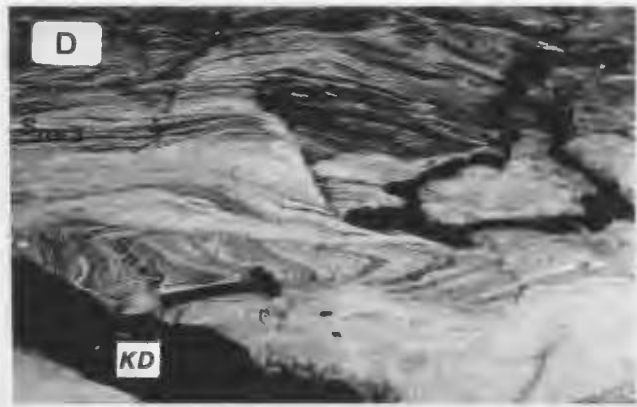
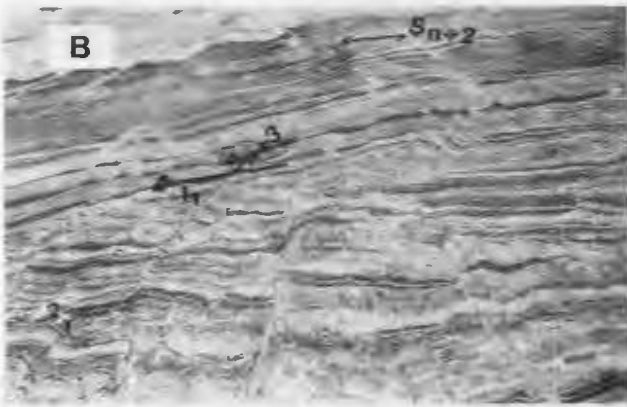


Plate 11

- A to D - Progressive affects of Flordian reorientation of the Hopedallian fabric within the Maggo gneiss.
- A Maggo gneiss from the Hopedallian domain cut by minor discordant (1) and concordant (2) migmatitic swaths. Station 83-99 - south shore, Inganialuk Bay.
- B The first manifestation of Flordian overprinting is the development of localized sinistral shears (S_{n+3}) which disrupt the Hopedallian fabric (S_{n+2}) within the Maggo gneiss. The shears, < 1 m long, display evidence of brittle (1) and ductile (2) deformation along their length. Station 82-51 - Zacharius Island. Hammer is 0.9 m long.
- C With increasing intensity of Flordian overprinting the Hopedallian fabric (S_{n+2}), defined by the banding in the Maggo gneiss, begins to reorient parallel to the shearing direction (S_{n+3}). Station 83-138 - east shore, Piliiarusik Bay.
- D Completely reoriented Maggo gneiss within the Flordian Domain. The predominant fabric (S_{n+3}) is oriented in a NE-SW direction. An enclave of Maggo gneiss with preserved Hopedallian fabric (S_{n+2}) which has not been rotated with the Flordian deformation is shown. A Kikkertavak dyke (KD), of Proterozoic age, cuts all previous fabrics in the gneiss. Station 83-6 - east shore, Piliiarusik Bay.
- E A faulted Kikkertavak dyke, cutting Flordian domain Maggo gneiss, records evidence of the last structural event to affect the Hopedale Block. The faulting is associated with Proterozoic deformation. Station 83-5 - east shore, Piliiarusik Bay.



REFERENCES

- Abbey, S., 1983. Studies in "Standard Samples" of silicate rocks and minerals 1969-1982. Geological Survey of Canada, Paper 83-15; 114 pp.
- Alderton, D.H.M., Pearce, J.A. and Potts, P.J., 1980. Rare earth element mobility during granite alteration: evidence from southwest England. *Earth and Planetary Science Letters* 49; 149-165.
- Anhaeusser, C.R., Mason, R., Viijoen, M.J., Viijoen, R.P., 1969. A reappraisal of some aspects of Precambrian shield geology. Geological Society of America, *Bulletin* 80; 2175-2200.
- Arth, J.G., 1976. Behaviour of trace elements during magmatic processes - A summary of theoretical models and their application. *Journal of Research, United States Geological Survey* 4; 41-47.
- Arth, J.G. and Hanson, G.N., 1972. Quartz diorites derived by partial melting of eclogite or amphibolite at mantle depths. *Contributions to Mineralogy and Petrology* 37; 161-174.
- Arth, J.G. and Hanson, G.N., 1975. Geochemistry and origin of the early Precambrian crust of Northeastern Minnesota. *Geochimica et Cosmochimica Acta* 39; 325-362.
- Arth, J.G., Barker, F., Peterman, Z.E. and Friedman, I., 1978. Geochemistry of the gabbro-diorite-tonalite-trondhjemite suite of southwest Finland and its implications for the origin of tonalitic and trondhjemitic magmas. *Journal of Petrology* 19; 289-316.
- Baadsgaard, H. and McGregor, V.R., 1981. The U-Th-Pb systematics of zircons from the type Nuk gneisses, Godthabsfjord, West Greenland. *Geochimica et Cosmochimica Acta* 45; 1099-1109.
- Barker, F. and Arth, J.G., 1976. Generation of trondhjemitic-tonalitic liquids and Archaean bimodal trondhjemitic-basalt series. *Geology* 4; 596-600.
- Barth, T.F.W., 1959. Principles of classification and norm calculations of metamorphic rocks. *Journal of Geology* 67; 135-152.
- Barth, T.F.W., 1962. A final proposal for calculating the mesonorm of metamorphic rocks. *Journal of Geology* 71; 497-498.

00000

- Barton, J.M., 1975. Rb-Sr characteristics and chemistry of the 3.6 by Hebron gneiss, Labrador. *Earth and Planetary Science Letters*, 27; 427-435.
- Bates, R.L. and Johnson, J.A., 1980. Glossary of Geology. American Geological Institute, Falls Church, Virginia, 751 pages.
- Beach, A., 1973. The mineralogy of high temperature shear zones at Scourie, NW Scotland. *Journal of Petrology*, 14; 231-248.
- Beach, A., 1974. Amphibolitization of Scourie granulites, Scotland. *Journal of Geology*, 10; 35-43.
- Beach, A., 1976. The inter relations of fluid transport, deformation, geochemistry and heat flow in early Proterozoic shear zones in the Lewisian complex. *Philosophical Transactions of the Royal Society*, London, A280; 569-604.
- Beach, A., 1980. Retrogressive metamorphic processes in shear zones with special reference to the Lewisian complex. *Journal of Structural Geology*, 2; 257-263.
- Beach, A. and Fyfe, W.S., 1972. Fluid transport and shear zones at Scourie, Sutherland: Evidence of overthrusting? *Contributions to Mineralogy and Petrology*, 36; 175-180.
- Beach, A. and Tarney, J., 1978. Major and trace element patterns during retrogressive metamorphism of granulite facies gneisses, NW Scotland. *Precambrian Research*, 7; 325-348.
- Reech, E.M. and Chadwick, B., 1980. The Malene supracrustal gneisses of northwest Buksefjorden: their origin and significance in the Archaean crustal evolution of southern West Greenland. *Precambrian Research* 11; 329-355.
- Berthelsen, A. and Henriksen, N., 1975. Descriptive text and geological map of Greenland, 1:100,000, Ivigtut 61V.1 Syd. Grønlands geologiske Undersøgelse 169 pages.
- Black, L.P., Moorbath, S., Pankhurst, R.J. and Windley, B.F., 1973. $^{207}\text{Pb}/^{208}\text{Pb}$ whole rock age of the Archaean granulite facies metamorphic event in West Greenland. *Nature, Physical Sciences* 244; 50-53.

00383

- Bridgwater, D. and Collerson, K.D., 1976. The major petrological and geochemical characters of the 3600 m.y. Ulvak Gneisses from Labrador. Contributions to Mineralogy and Petrology 54; 43-59.
- Bridgwater, D. and Collerson, K.D., 1977. On the origin of early Archaean Gneisses: a reply. Contributions to Mineralogy and Petrology 62; 179-191.
- Bridgwater, D., Collerson, K.D., Hurst, R.W. and Jesseau, C.W., 1975. Field characteristics of early Precambrian rocks from Saglek, coast of Labrador. Geological Survey of Canada, Paper 75-1A; 287-296.
- Bridgwater, D., Fryer, B.J. and Gorman, B.E., 1985. Proterozoic basic dykes in southern Greenland and the coast of Labrador; Tectonic setting, intrusion forms and chemistry. Abstract, International Conference - Mafic Dyke Swarms, University of Toronto, Erindale Campus; 15-21.
- Bridgwater, D., Keto, L., McGregor, V.R. and Myers, J.S., 1976. Archaean gneiss complex of Greenland. In Escher, A and Watts, W.S. (editors) Geology of Greenland. Geological Survey of Greenland, Copenhagen; 18-75.
- Bridgwater, D., Watson, J. and Windley, B.F., 1973. The Archaean of the North Atlantic region. Philosophical Transactions of the Royal Society, London, A-273; 493-512.
- Brinex, 1964. Shapiro/Ugjuktok concession, Labrador geology; Map G6401c; scale approx. 1 inch = 3,333 feet.
- Brinex, 1970. Geological survey Ugjuktok Bay 6-03/1970; Map G71006; scale 1 inch = 2,000 feet.
- Brooks, C., Wendt, I. and Harre, W., 1968. A two-error regression treatment and its application to Rb-Sr and initial $^{87}\text{Sr}/^{86}\text{Sr}$ ratios of younger Variscan Granitic rocks from the Schwarzwald Massif, southwest Germany. Journal of Geophysical Research 73; 6071-6084.
- Brooks, C., Hart, S.R. and Wendt, I., 1972. Realistic use of two error regression treatments as applied to Rb-Sr data. Journal of Geophysics and Space Sciences 10; 551-577.

- ~~SECRET~~
- Brown, M., Davies, A., Friend, C.R.L. and Perkins, W.T., 1986. A model for the Qorqut granite complex, southern West Greenland. Geological Association of Canada, Programs with Abstracts 11; 49.
- Cann, J.R., 1970. Rb, Sr, Y, Zr and Nb in some ocean floor basaltic rocks. Earth and Planetary Science Letters 10; 7-11.
- Chadwick, B. 1981. Field relations, petrography and geochemistry of Archaean amphibolite dykes and Malene supracrustal amphibolites, northwest Buksefjorden, southern west Greenland. Precambrian Research 14; 221-259.
- Chadwick, B. and Coe, K., 1976. New evidence related to Archaean events, in southern west Greenland in Windley, B.F. (editor) The Early History of the Earth. John Wiley and Son, London; 203-212.
- Christie, A.M., Roscoe, S.M. and Fahrig, W.F., 1953. Preliminary map central Labrador coast, Newfoundland (Descriptive notes) Geological Survey of Canada, Paper 53-14.
- Coleman, A.P., 1921. North eastern part of Labrador and New Quebec. Geological Survey of Canada, Memoir 124.
- Collerson, K.D. and Bridgwater, D., 1979. Metamorphic development of early Archaean tonalitic and trondhjemitic gneisses: Saglek area, Labrador. In Barker, F. (editor) Trondhjemites, Dacites and Related Rocks. Elsevier, Amsterdam; 182-204.
- Collerson, K.D. and Fryer, B.J., 1978. The role of fluids in the formation and subsequent development of early continental crust. Contributions to Mineralogy and Petrology 67; 151-167.
- Collerson, K.D., Jesseau, C.W. and Bridgwater, D., 1976a. Crustal development of the Archaean gneiss complex: eastern Labrador, In Windley, B.F. (ed) The Early History of the Earth. John Wiley and Sons, London; 237-253.
- Collerson, K.D., Jesseau, C.W. and Bridgwater, D., 1976b. Contrasting types of bladed olivine in ultramafic rocks from the Archaean of Labrador. Canadian Journal of Earth Sciences, 13; 442-450.
- Collerson, K.D., Jesseau, C.W., Ryan, A.B. and Hawkins, D.W., 1974. Mineral potential evaluation in the Makkovik and Hopedale areas, Labrador; In Smyth, W.R. (ed) Report of Activities for 1973.

09485

Newfoundland Department of Mines and Energy,
Mineral Development Division, 24-31.

- Collerson, K.D., Kerr, A. and Compston, W., 1981. Geochronology and evolution of Late Archaean gneisses in northern Labrador: An example of reworked stialic crust. *Special Publications, Geological Society of Australia* 7; 205-224.
- Collerson, K.D., Kerr, A., Vocke, R.D. and Hanson, G.N., 1982. Reworking of stialic crust as represented in Late Archaean age gneiss, northern Labrador. *Geology* 10; 202-208.
- Collerson, K.D., McCulloch, M.T. and Bridgwater, D., 1984. Nd and Sr isotopic crustal contamination patterns in an Archaean metadiabase dyke from northern Labrador. *Geochimica et Cosmochimica Acta* 48; 71-83.
- Compton, P., 1978a. Rare earth evidence for the origin of the Nuk gneisses, Buksefjorden Region, southwest Greenland. *Contributions to Mineralogy and Petrology* 66; 283-293.
- Compton, P., 1978b. A Study of the Nuk Gneisses and Qorqut Granite in the Buksefjorden Region, southwest Greenland. Unpublished PhD thesis. University of Exeter.
- Condle, K.C., 1978. Trace element geochemistry of Archaean greenstone belts. *Earth Science Reviews*, 12; 393-417.
- Condle, K.C., Allen, P. and Narayana, B.L., 1982. Geochemistry of the Archaean low- to high- grade transition zone in Southern India. *Contributions to Mineralogy and Petrology* 81; 157-167.
- Condle, K.C., Bowling, C.P. and Allen, P., 1985. Missing Eu anomaly and Archaean high grade granites. *Geology* 13; 633-636.
- Condle, K.C., Bowling, G.P. and Allen, P., 1986. Origin of granites in an Archaean high-grade terrain; Southern India. *Contributions to Mineralogy and Petrology* 92; 93-103.
- Condle, K.C. and Hunter, D.R., 1976. Trace element geochemistry of Archaean granitic rocks from the Barberton region, South Africa. *Earth and Planetary Science Letters* 9; 389-400.

- 00388
- Cullers, R.L., Yeh, L-T., Chaudhuri, S. and Guidotti, C.V., 1976. Rare earth elements in Silurian pelitic schists, NW Maine. *Geochimica et Cosmochimica Acta* 38; 389-400.
- Davies, R.D. and Allsopp, H.L., 1976. Strontium isotopic evidence relating to the evolution of the lower Precambrian granitic crust in Swaziland. *Geology* 4; 553-556.
- Deer, W.A., Howie, R.A. and Zussman, J., 1982. Rock Forming Minerals - Orthosilicates; Volume 1A. Longmans, London. 919 pages.
- Douglas, G.V., 1953. Notes on localities visited on the Labrador coast in 1946 and 1947. Geological Survey of Canada, Paper 53-1.
- Drury, S.A., 1973. The geochemistry of Precambrian granulite facies rocks from the Lewisian complex of Tiree, Inner Hebrides, Scotland. *Chemical Geology* 11; 167-188.
- Drury, S.A., 1978. REE distributions in a high-grade Archaean complex in Scotland: Implications for the genesis of ancient sialic crust. *Precambrian Research* 7; 237-257.
- Easton, R.M., 1982. Tectonic significance of the Akaitcho Group Wopmay Orogen, Northwest Territories, Canada. unpublished PhD thesis, Memorial University of Newfoundland, St. John's.
- Eby, G.N., 1972. Determination of rare earth, yttrium and scandium abundances in rocks and minerals by an ion-exchange procedure. *Analytical Chemistry* 44; 2137-2143.
- Emslie, R.F., 1980. Geology and petrology of the Harp Lake Complex, central Labrador: An example of Eisonian magmatism. Geological Survey of Canada, Bulletin 293; 136 pages.
- Ermanovics, I.F., 1980. Geology of the Hopedale Block of the Nain Province, Labrador: Report 2, Nain-Makkovik boundary zone. Geological Survey of Canada, Paper 80-1B; 11-15.
- Ermanovics, I.F. and Korstgard, J.A., 1981. Geology of the Hopedale Block and adjacent areas, Labrador: Report 3. Geological Survey of Canada, Paper 81-1A; 69-76.

- 0037
- Ermanovics, I.F., Korstgard, J.A. and Bridgwater, D., 1982. Structural and lithological chronology of the Archaean Hopedale Block and adjacent Proterozoic Makkovik Subprovince, Labrador; Report 4. Geological Survey of Canada, Paper 82-1B; 153-165.
- Ermanovics, I.F. and Raudsepp, M., 1979. Geology of the Hopedale Block of eastern Nain Province, Labrador; Report 1. Geological Survey of Canada, Paper 79-1B; 341-348.
- ▲Etheridge, M.A. and Cooper, J.A., 1981. Rb/Sr isotopic and geochemical evolution of a recrystallized shear zone (mylonite) at Broken Hill. Contributions to Mineralogy and Petrology, 78; 74-84.
- Field, D. and Clough, P.W.L., 1976. K/Rb ratios and metasomatism in metabasites from a Precambrian amphibolite-granulite transition zone. Journal of the Geological Society, London 132; 277-288.
- Frey, F.A., Green, D.H. and Roy, S.D., 1978. Integrated models of basalt petrogenesis: a study of quartz tholeiites to olivine melilitites from south eastern Australia utilizing geochemical and experimental petrological data. Journal of Petrology 19; 463-513.
- Frey, F.A., Haskin, M.A., Poetz, J.A. and Haskin, L.A., 1968. Rare earth abundances in some basic rocks. Journal of Geophysical Research 73; 6085-6098.
- Frey, F.A., Bryan, W.B. and Thompson, G., 1974. Atlantic Ocean Floor: Geochemistry and petrology of basalts from legs 2 and 3 of the Deep-Sea Drilling Project. Journal of Geophysical Research 79; 5507-5529.
- Friend, C.R.L., Hall, R.P. and Hughes, D.J., 1981. The geochemistry of the Malene (mid-Archaean) ultramafic-mafic amphibolite suite, southern West Greenland. Special Publication, Geological Society of Australia 7; 301-312.
- Fryer, B.J., 1977. Rare earth evidence in iron-formations for changing Precambrian oxidation states. Geochimica et Cosmochimica Acta 41; 361-367.
- Fryer, B.J. and Taylor, R.P., 1985. Comment and Reply on "Sm-Nd direct dating of the Collins Bay hydrothermal uranium deposit, Saskatchewan". Geology 13; 749.

- 04383**
- Gellinas, L., Brooks, C. and Trzcinski, W.E., 1976. Archaean variolites - quenched immiscible liquids. *Canadian Journal of Earth Sciences* 13; 210-230.
- Gill, R.C.O., 1979. Comparative petrogenesis of Archaean and modern low-K tholeiites: a critical review of some geochemical aspects. In Ahrens, L.H. (editor) Origin and Distribution of the Elements. Pergamon Press, Amsterdam; 431-488.
- Gill, R.C.O. and Bridgwater, D., 1979. Early Archaean basic magmatism in West Greenland: The geochemistry of the Ameralik Dykes. *Journal of Petrology* 20; 635-726.
- Gill, R.C.O., Bridgwater, D. and Allart, J.H., 1981. The geochemistry of the earliest known basic metavolcanic rocks, at Isua, West Greenland: A preliminary investigation. *Special Publication, Geological Society of Australia* 7; 313-325.
- Glickson, A.Y., 1972. Early Precambrian evidence of a primitive ocean crust and island nuclei of sodic granite. *Geological Society of America, Bulletin* 83; 3323-3344.
- Glickson, A.Y., 1979. Early Precambrian tonalite - trondhjemite sialic nuclei. *Earth Science Reviews* 15; 1-73.
- Gower, C.F., 1981. The geological and geochemical characteristics of the Benedict Mountains Intrusive Suite, Labrador. *Geological Association of Canada, Program with Abstracts*, 8; A-22.
- Gower, C.F., Ryan, A.B., Bailey, D.G. and Thomas, A., 1980. The position of the Grenville Front in Labrador. *Canadian Journal of Earth Sciences* 17; 784-788.
- Graham, C.M., 1976. Petrochemistry and tectonic significance of Dalradian metabasaltic rocks of the SW Scottish Highlands. *Journal of the Geological Society, London*. 132; 61-84.
- Grant, N.K., Voner, F.R., Marzano, M.S., Hickman, M.H. and Ermanovics, I.F., 1983. A summary of the Rb-Sr isotope studies in the Archaean Hopedale Block and adjacent Proterozoic Makkovik Subprovince, Labrador: Report 5. *Geological Survey of Canada, Paper* 83-1B; 127-134.
- Gray, C.M., 1977. The geochemistry of central Australian granulites in relation to the chemical and isotopic effects of granulite facies metamorphism. *Contributions to Mineralogy and Petrology* 65; 79-89.

- Green, T.H., Brunfelt, A.O. and Heler, K.S., 1969. Rare earth element distribution in anorthosites and associated high grade metamorphic rocks, Lofoten-Vesteraalen, Norway. *Earth and Planetary Science Letters* 7; 93-98.
- Green, T.H., Brunfelt, A.O. and Heler, K.S., 1972. Rare earth element distribution in granulites, mangerites and anorthosites, Lofoten-Vesteraalen, Norway. *Geochimica et Cosmochimica Acta* 36; 241-257.
- Greene, B.A., 1974. An outline of the geology of Labrador. Department of Mines and Energy, Mineral Development Division. Information Circular 15. 66 pages.
- Gresens, R.L., 1967. Composition - volume relationships of metasomatism. *Chemical Geology*, 2; 47-65.
- Griffin, W.L., McGregor, V.R., Nutman, A.P., Taylor, P.N. and Bridgwater, D., 1980. Early Precambrian granulite facies metamorphism south of Ameralik, West Greenland. *Earth and Planetary Science Letters* 50; 59-74.
- Gromet, L.P. and Silver, L.T., 1983. Rare earth element distributions among minerals in a granodiorite and their petrogenetic implications. *Geochimica et Cosmochimica Acta* 47; 925-939.
- Haack, U., Hoefs, J. and Gohn, E., 1982. Constraints on the origin of Damaran granites by Rb/Sr and ^{18}O data. *Contributions to Mineralogy and Petrology* 79; 279-289.
- Hart, S.R. and Allegre, C.J., 1980. Trace element constraints on magma genesis. In R. Hargraves (editor) Physics of Magmatic Processes. Princeton University Press, Princeton, 121-160.
- Haskin, L.A., 1984. Petrogenetic modelling - use of rare earth elements in Henderson, P. (editor) Rare Earth Element Geochemistry. Elsevier, Amsterdam; 115-152.
- Hatch, F.H., Wells, A.K. and Wells, M.K., 1972. Petrology of igneous Rocks. George Allen and Unwin, London; 551 pages.
- Heler, K.S., 1973. Geochemistry of granulite facies rocks and problems of their origin. *Philosophical Transactions, Royal Society of London*, A273; 429-442.

0030

- Heler, K.S. and Thoresen, K., 1971. Geochemistry of high grade metamorphic rocks, Lofoten-Vesterdaalen, North Norway. *Geochimica et Cosmochimica Acta* 35; 89-99.
- Hellman, P.L. and Green, T.H., 1979. The role of sphene as an accessory phase in the high-pressure partial melting of hydrous mafic compositions. *Earth and Planetary Science Letters* 42; 191-201.
- Hellman, P.L., Smith, R.E. and Henderson, P., 1979. Rare earth element investigation of the Cliefden Outcrop, N.S.W. Australia. *Contributions to Mineralogy and Petrology* 65; 155-164.
- Hildreth, W., 1981. Gradients in silicic magma chambers: Implications for lithospheric magmatism. *Journal of Geophysical Research* 86; 10153-10192.
- Hill, J.D., 1981. Geology of the Flowers River area, Labrador. Mineral Development Division, Department of Mines and Energy, Government of Newfoundland and Labrador, Report 81-6.
- Hobbs, B.E., Means, W.D. and Williams, P.F., 1976. An Outline of Structural Geology. John Wiley and Son, Toronto. 521 Pages.
- Huang, W.L. and Wyllie, P.J., 1981. Phase relationships of S-type granite with H₂O to 35 kbar: Muscovite granite from Harnery Peak, South Dakota. *Journal of Geophysical Research* 86; 10515-10529.
- Hunter, D.R., Barker, F. and Millard, H.T., 1978. The geochemical nature of the Archaean Ancient Gneiss Complex and granodiorite suite, Swaziland: a preliminary study. *Precambrian Research* 7; 105-127.
- Hurst, R.W., 1973. The early Archaean of coastal Labrador, in Morse, S.A. (editor) *The Main Anorthosite Project, Labrador: Field Report 1973*. Geology Department, University of Massachusetts, Amherst, Massachusetts, Contribution No. 13, 29-32.
- Hurst, R.W., 1978. Sr evolution of the West Greenland - Labrador craton; a model for early Rb depletion in the Mantle. *Geochimica et Cosmochimica Acta* 42; 39-44.
- Hurst, R.W., Bridgwater, D., Collerson, K.D., and Wetherill, G.W., 1975. 3,600 m.y. Rb-Sr ages from very early Archaean gneisses from Saglek Bay.

- Labrador. *Earth and Planetary Science Letters* 27; 393-403.
- Hynes, A.J., 1980. Carbonatization and mobility of Ti, Y, and Zr in Ascot Formation metabasalts, SE Quebec. *Contributions to Mineralogy and Petrology* 75; 79-87.
- Irvine, T.N. and Baragar, W.R.A., 1971. Guide to the chemical classification of the common volcanic rocks. *Canadian Journal of Earth Sciences* 8; 523-548.
- Jesseau, C.W., 1976. A structural, metamorphic and geochemical study of the Hunt River supracrustal belt, Nain Province, Labrador; unpublished MSc thesis, Memorial University of Newfoundland, St. John's.
- Kadik, A.A. and Egger, D.H., 1975. Melt-vapour relations on the join $\text{NaAlSi}_3\text{O}_8\text{-H}_2\text{O-CO}_2$. *Yearbook, Carnegie Institute, Washington* 74; 479-484.
- Kalsbeek, F., 1976. Metamorphism of Archaean rocks of west Greenland. In Windley, B.F. (editor) The Early History of the Earth. Wiley and Son, London; 225-236.
- Kalsbeek, F. and Leake, B.E., 1970. The chemistry and origin of some basement amphibolites between Ivigtut and Frederickshab, southwest Greenland. *Meddelelser om Gronland Bd. 190, Nr. 4*, 1-47.
- Kerr, A., 1980. Late Archaean Igneous, metamorphic and structural evolution of the Nain Province at Saglek, Labrador; unpublished MSc thesis, Memorial University of Newfoundland, St. John's.
- Koehler, H. and Mueller-Sohnius, D., 1980. Rb/Sr systematics on paragneiss series from the Bavarian Moldanubicum, Germany. *Contributions to Mineralogy and Petrology* 71; 387-392.
- Korstgard, J.A. and Ermanovics, I., 1984. Archaean and early Proterozoic tectonics of the Hopedale Block, Labrador, Canada. In Kroner, A. and Greiling, R. (editors) Precambrian Tectonics Illustrated. E. Schweizerbartische Verlagbuchhandlung, Stuttgart. 295-318.
- Korstgard, J.A. and Ermanovics, I., 1985. Tectonic evolution of the Archaean and early Proterozoic of the Hopedale Block, Labrador, Newfoundland. In L.D. Ayres, P.C. Thurston, K.D. Card and W. Weber (editors) Evolution of Archaean Supracrustal

00002

Sequences. Geological Association of Canada, Special Paper 28; 223-238.

- Kranck, E.H., 1953. Bedrock geology of the seaboard of Labrador between Domino Run and Hopedale, Newfoundland. Geological Survey of Canada, Bulletin 26; 41p.
- Lambert, I.B. and Heler, K.S., 1988. Geochemical investigations of deep-seated rocks in the Australian shield. Lithos 1; 30-53.
- Leeman, W.P. and Dasch, E.J., 1978. Strontium, lead and oxygen isotopic investigation of the Skaergard intrusion, East Greenland. Earth and Planetary Science Letters 41; 47-59.
- Lieber, O.M., 1860. Notes on the geology of the coast of Labrador. Report of the United States Coast Survey for 1860; 402-408.
- Loveridge, W.D., Ermanovics, I.E. and Sullivan, R.W., 1987. U-Pb ages on zircon from the Maggo Gneiss, the Kanariktok Plutonic Suite and the Island Harbour Plutonic Suite, coast of Labrador, Newfoundland. Geological Survey of Canada, Paper 87-2; 59-66.
- Marzano, M.S., 1981. Rb/Sr whole rock geochronology of six rock suites from the Hopedale Block, Main Province, Labrador, Canada. unpublished MSc thesis, Miami University, Oxford, Ohio; 103 pages.
- Masuda, A., Nakamura, N. and Tanaka, T., 1971. Rare earth elements in metagabbros from the Mid-Atlantic Ridge and their possible implications for the genesis of alkali olivine basalt as well as the Lizard peridotite. Contributions to Mineralogy and Petrology 32; 295-306.
- Masuda, A., Nakamura, N. and Tanaka, T., 1973. Fine structures of mutually normalized rare-earth patterns of chondrites. Geochimica et Cosmochimica Acta 37; 239-248.
- Mathews, D.W., 1967. Zoned ultrabasic bodies in the Lewisian of the Moine Nappe in Skye. Scottish Journal of Geology 3; 17-33.
- Maxwell, J.A., 1968. Rock and Mineral Analysis. Wiley-Interscience, New York. 584 pp.

- 0000
- McGregor, V.R., 1973. The early Precambrian gneisses of the Godthab District, west Greenland. Philosophical Transactions, of the Royal Society, London A-273; 343-358.
- McGregor, V.R., 1979. Archaean gray gneisses and the origin of the continental crust: Evidence from the Godthab Region, west Greenland. In Barker, F. (editor) Trondhjemites, Dacites and Related Rocks. Elsevier, Amsterdam; 169-204.
- Mehnert, K.R., 1968. Migmatites and the Origin of Granitic rocks. Elsevier, Amsterdam, 405 p.
- Miyashiro, A., 1973. Metamorphism and Metamorphic Belts. George Allen & Unwin, London, 429 p.
- Moorbath, S., 1975. Evolution of Precambrian crust from strontium isotopic evidence. Nature 254; 395-398.
- Moorbath, S., 1975a. Geological interpretation of whole-rock isochron dates from high grade gneiss terrains. Nature 255; 391.
- Moorbath, S., 1977. Ages, isotopes and evolution of Precambrian continental crust. Chemical Geology 20; 151-187.
- Moorbath, S., 1978. Age and isotope evidence for the evolution of continental crust. Philosophical Transactions of the Royal Society, London A288; 401-413.
- Moorbath, S.A., O'Nions, R.K., Pankhurst, R.J. and Gale, N.H., 1972. Further Rb-Sr age determinations on the very early Precambrian rocks of the Godthab District, West Greenland. Nature 240; 78-82.
- Moorbath, S., O'Nions, R.K. and Pankhurst, R.J., 1975. The evolution of early Precambrian crustal rocks at Isua, West Greenland - Geochemical and isotopic evidence. Earth and Planetary Science Letters 27; 229-239.
- Moorbath, S. and Pankhurst, R.J., 1976. Further rubidium - strontium age and isotope evidence for the nature of the Late Archaean plutonic event in West Greenland. Nature 262; 124-126.
- Moorbath, S. and Taylor, P.N., 1981. Isotopic evidence for continental growth in the Precambrian. In Kroner, A. (editor) Precambrian Tectonics. Elsevier, Amsterdam; 491-525.

- ~~SECRET~~
- Moorbath, S., Taylor, P.N. and Goodwin, R., 1981. Origin of granitic magma by crustal remobilization: Rb/Sr and Pb/Pb geochronology and isotope geochemistry of the late Archaean Qorqut Granite Complex of southern West Greenland. *Geochimica et Cosmochimica Acta* 45; 1051-1060.
- Mose, D.G., 1982. 1,300-million year old rocks in the Appalachians. *Geological Society of America, Bulletin* 93; 391-399.
- Muecke, G.K., Pride, C. and Sarkar, P., 1979. Rare earth element geochemistry of regional metamorphic rocks. In Ahrens, L.H., (editor) Origin and Distribution of the Elements. Pergamon Press; 449-464.
- Murphy, J.B. and Hynes, A.J., 1986. Contrasting secondary mobility of Ti, P, Zr, Nb and Y in two metabasalt suites in the Appalachians. *Canadian Journal of Earth Sciences* 23; 1138-1144.
- Nesbitt, H.W., 1979. Mobility and fractionation of rare earth elements during weathering of a granodiorite. *Nature* 279; 206-210.
- Nesbitt, R.W., 1971. Skeletal crystal forms in the ultramafic rocks of the Yilgarn Block, Western Australia: Evidence for an Archean ultramafic liquid. *Special Publication, Geological Society of Australia* 3; 331-347.
- Newton, R.C., Smith, J.W. and Windley, B.F., 1980. Carbonic metamorphism, granulites and crustal growth. *Nature* 288; 45-5.
- Nicholls, J.A. and Harris, K.L., 1980. Experimental rare earth element partition coefficients for garnet, clinopyroxene and amphibole coexisting with andesitic and basaltic liquids. *Geochimica et Cosmochimica Acta* 44; 287-308.
- Nutman, A.P., 1984. Early Archaean crustal evolution of the Isukasia area, southern West Greenland. In Kroner, A. and Greiling, R. (editors) Precambrian Tectonics Illustrated. E. Schweizerbortische Verlagbuchhandlung, Stuttgart; 79-83.
- Nutman, A.P., 1986. The early Archaean to Proterozoic history of the Isukasia area, southern West Greenland. *Grønlands geologiske Undersøgelser Bulletin* 154; 80 pages.

- 9375
- Nutman, A.P., Bridgwater, D. and Fryer, B.J., 1984. The iron-rich suite from the Amitsoq gneiss of southern West Greenland: Early Archaean plutonic rocks of mixed crustal and mantle origin. *Contributions to Mineralogy and Petrology* 87; 24-34.
- Nystrom, J.O., 1984. Rare earth element mobility in vesicular lava during low-grade metamorphism. *Contributions to Mineralogy and Petrology* 88; 328-331.
- O'Connor, J.T., 1965. A classification for quartz-rich igneous rocks based on feldspar ratios. *United States Geological Survey, Professional Paper* 525-B; B79-B84.
- O'Nions, R.K. and Pankhurst, R.J., 1974a. Rare-earth element distribution in Archaean gneisses and anorthosites, Godthab area, West Greenland. *Earth and Planetary Science Letters* 22; 328-338.
- O'Nions, R.K. and Pankhurst, R.J., 1974b. Petrogenetic significance of isotope and trace element variations in volcanic rocks from the Mid-Atlantic. *Journal of Petrology* 15; 603-634.
- Packard, A.S., 1891. The Labrador Coast. Hodges, N.D.C., New York, 513p.
- Pearce, J.A. and Cann, J.R., 1971. Ophiolite origin investigated by discriminant analysis using Ti, Zr and Y. *Earth and Planetary Science Letters* 12; 339-349.
- Pearce, J.A. and Cann, J.R., 1973. Tectonic setting of basic volcanic rocks determined using trace element analysis. *Earth and Planetary Science Letters* 19; 290-300.
- Pearce, J.A., Harris, N.B.W. and Tindle, A.G., 1984. Trace element discrimination diagrams for the tectonic interpretation of granitic rocks. *Journal of Petrology* 25; 956-983.
- Pearce, J.A. and Norry, M.J., 1979. Petrogenetic implications of Ti, Zr, Y and Nb variations in volcanic rocks. *Contributions to Mineralogy and Petrology* 69; 33-47.
- Peterman, Z.E., 1979. Strontium isotope geochemistry of late Archaean to late Cretaceous tonalites and trondhjemites. In Barker, F. (ed) Trondhjemites, Dacites and Related Rocks, Elsevier, Amsterdam; 133-147.

04908

- Peterman, Z.E., and Barker, F., 1976. Rb-Sr whole-rock age of trondhjemites and related rocks of the southwestern Trondheim region, Norway. U.S. Geological Survey open File Report 76-670; 1-17.
- Philpotts, J.A., Schnetzler, C.C. and Hart, S.R., 1969. Submarine basalts: some K, Rb, Sr, Ba, REE, H₂O and CO₂ data bearing on their alteration modification by plagioclase and possible source materials. Earth and Planetary Science Letters 7; 293-299.
- Potts, P.J., Thorpe, O.W. and Watson, J.S., 1981. Determination of the rare earth element abundances in 29 international rock standards by instrumental neutron activation analysis: a critical appraisal of calibration errors. Chemical Geology 34; 331-352.
- Pyke, D.R., Naldrett, A.J. and Eckstrand, O.R., 1973. Archean ultramafic flows in Munro Township, Ontario. Geological Society of America, Bulletin 84; 955-78.
- Ramsay, J.G., 1967. Folding and Fracturing of Rocks. McGraw-Hill, New York. 568 pages.
- Roedder, E., 1978. Silicate liquid immiscibility in magmas and the system K₂O-FeO-Al₂O₃-SiO₂, an example of serendipity. Geochimica et Cosmochimica Acta 42; 1597-1617.
- Rutland, R.W.R., 1981. Structural framework of the Australian Precambrian. In Hunter, D.R. (editor) Precambrian of the Southern Hemisphere. Elsevier, Amsterdam; 1-32.
- Ryan, A.B., 1974. Metamorphic and structural investigation of the Hopedale Gneiss, Flowers Bay, Labrador; unpublished BSc thesis, Memorial University of Newfoundland, St. John's.
- Ryan, A.B., 1977. Progressive structural reworking of the Uivak gneisses, Jerusalem Harbour, northern Labrador; unpublished MSc thesis, Memorial University of Newfoundland, St. John's.
- Ryan, A.B. and Kay, A., 1982. Basement-cover relationships and plutonic rocks in the Makkovik Subprovince, north of Postville, coastal Labrador (13 J/13, 13 O/4), Mineral Development Division, Department of Mines and Energy, Government of Newfoundland and Labrador, Report 82-1; 109-121.

00807

- Ryan, A.B., Martineau, Y., Bridgwater, D., Schiøtte, L. and Lewry, J., 1983. The Archaean-Proterozoic boundary in the Saglek Flord area, Labrador, Report 1; In Current Research, Part A, Geological Survey of Canada, Paper 83-1A; 297-304.
- Ryan, A.B., Martineau, Y., Korstgard, L. and Lee, D., 1984. The Archaean-Proterozoic boundary in northern Labrador, Report 2; In Current Research, Part A Geological Survey of Canada, Paper 84-1A; 545-551.
- Schiøtte, L., Compston, W. and Bridgwater, D., 1988. Late Archaean ages for the deposition of the clastic sediments belonging to the Malene supracrustals, southern West Greenland; evidence from an ion probe U-Pb zircon study. *Earth and Planetary Science Letters* 87; 45-58.
- Schiøtte, L., Compston, W., Williams, I.S. and Bridgwater, D., (In prep.). Ion probe U-Th-Pb zircon dating of Archaean supracrustals from Labrador, Canada.
- Shaw, D.M., 1968. A review of K/Rb fractionation by covariance analysis. *Geochimica et Cosmochimica Acta* 32; 573-601.
- Shaw, D.M., 1970. Trace element fractionation during anatexis. *Geochimica et Cosmochimica Acta* 34; 237-243.
- Sheraton, J.W. and Black, L.P., 1983. Geochemistry of Precambrian gneisses: relevance for the evolution of the East Antarctic Shield. *Lithos* 16; 273-296.
- Sheraton, J.W., Skinner, A.C. and Tarney, J., 1973. The geochemistry of the Scourian gneisses of the Assynt district. In Park, G. and Tarney, J. (editors) *The Early Precambrian of Scotland and Related Rocks of Greenland*. University of Keele; 13-30.
- Shimizu, H., 1980. Experimental study on rare earth element partitioning in minerals formed at 20 and 30 kb for basaltic systems. *Geochemistry Journal* 14; 185-202.
- Simmons, E.C. and Hedge, C.E., 1978. Minor-element and Sr-isotope geochemistry of Tertiary stocks, Colorado mineral belt. *Contributions to Mineralogy and Petrology* 67; 379-396.

Smith, T.E., Choudhry, A.G. and Huang, C.H., 1983. The geochemistry and petrogenesis of the Archaean Gamitagama lake igneous complex, Southern Superior Province. *Precambrian Research* 22; 219-244.

Stahle, H.J., Ralsh, R., Hoernes, S. and Delfs, A., 1987. Element mobility during incipient granulite formation at Kabbaldurga, Southern India. *Journal of Petrology* 28; 803-834.

Steiger, R.H. and Jaeger, E., 1977. Subcommission on geochronology convention on the use of decay constants in geo- and cosmochronology. *Earth and Planetary Science Letters* 38; 359-362.

Stockwell, C.H., 1982. Proposals for time classification of Precambrian rocks and events in Canada and adjacent areas of the Canadian Shield; Part I: A time classification of Precambrian rocks and events. Geological Survey of Canada, Paper 80-19.

Sun, S.-S., 1980. Lead isotope study of young volcanic rocks from mid-ocean ridges, ocean islands and island arcs. *Philosophical Transactions, Royal Society of London* A297; 409-445.

Tarney, J., 1976. Geochemistry of Archaean high-grade gneisses, with implications as to the origin and evolution of the Precambrian crust. In Windley, B.F. (editor) The Early History of the Earth. Wiley and Son, London; 405-418.

Tarney, J., Weaver, B. and Drury, S.A., 1979. Geochemistry of Archaean trondhjemitic and tonalitic gneisses from Scotland and east Greenland. In Barker, F. (editor) Trondhjemites, Dacites and Related Rocks. Elsevier, Amsterdam; 275-299.

Tarney, J. and Windley, B.F., 1977. Chemistry, thermal gradients and evolution of the lower continental crust. *Journal of the Geological Society, London* 134; 153-172.

Taylor, F.C., 1969. Reconnaissance geology of a part of the Precambrian Shield, northeastern Quebec and northern Labrador. Geological Survey of Canada, Paper 68-43.

Taylor, F.C., 1970. Reconnaissance geology of a part of the Precambrian Shield: northeastern Quebec and Labrador Part II. Geological Survey of Canada, Paper 70-24.

00100

- Taylor, F.C., 1971. A revision of Precambrian structural provinces in northeastern Quebec and northern Labrador. *Canadian Journal of Earth Sciences* 9: 930-932.
- Taylor, F.C., 1972. Reconnaissance geology of part of the Precambrian Shield, northeastern Quebec and northern Labrador, Part II. Geological Survey of Canada, Paper 70-24.
- Taylor, F.C., 1979. Reconnaissance geology of part of the Precambrian Shield, northeastern Quebec, northern Labrador and Northwest Territories. Geological Survey of Canada, Memoir 393.
- Taylor, P.N. and Kalsbeek, F., 1986. Pb isotopic evidence for Early Archaean crust in South Greenland. In Ashwal, L.D. (editor) Workshop on Early Crustal Genesis: The World's Oldest Rocks. LPI Technical Report 86-04. Lunar and Planetary Institute, Houston; 103-106.
- Taylor, P.N., Moorbath, S., Goodwin, R. and Petrykowski, A.C., 1980. Crustal contamination as an indicator of the extent of early Archaean continental crust: Pb isotopic evidence from the late Archaean gneisses of West Greenland. *Geochimica et Cosmochimica Acta* 44; 1437-1453.
- Taylor, P.N., Jones, N.W. and Moorbath, S., 1984. Isotopic assessment of relative contributions from crust and mantle sources to the magma genesis of Precambrian granitoid rocks. *Philosophical Transactions of the Royal Society, London* A310; 605-625.
- Taylor, R.P. and Fryer, B.J., 1980. Multiple-stage hydrothermal alteration in porphyry copper systems in northern Turkey: the temporal interplay of potassic, propylitic and phyllic fluids. *Canadian Journal of Earth Sciences* 17; 901-926.
- Taylor, R.P. and Fryer, B.J., 1983. Rare earth element litho geochemistry of granitoid mineral deposits. *Canadian Institute of Mining and Metallurgy, Bulletin* 76; 1-11.
- Trommsdorff, V. and Evans, B.W., 1972. Progressive metamorphism of antigorite schist in the Bergell tonalite aureole (Italy). *American Journal of Science* 272; 423-437.

00400

- Turner, F.J., 1968. Metamorphic Petrology: Mineralogical and Field Aspects. McGraw-Hill, New York. 403 pages.
- Usdansky, S.I., 1985. GRCHEM: A BASIC program to calculate granite mineralogy from modal mineralogy. Computers and Geosciences 11; 229-233.
- Vernon, R.H. and Ransom, D.M., 1971. Retrograde schists of the amphibolite facies at Broken Hill, New South Wales. Journal of the Geological Society of Australia, 18; 267-277.
- Wagner, P.A., 1982. Geochronology of the Ameralik dykes at Isua, West Greenland; unpublished MSc thesis, University of Alberta, Edmonton.
- Walsh, J.N., Buckley, F. and Barker, J., 1981. The simultaneous determination of the rare-earth elements in rocks using inductively coupled plasma source spectrometry. Chemical Geology 33; 141-153.
- Weaver, B.L. and Tarney, J., 1981a. Chemical changes during dyke metamorphism in high grade basement terrains. Nature 289; 47-49.
- Weaver, B.L. and Tarney, J., 1981b. The Scourie dyke suite: Petrogenesis and geochemical nature of the Proterozoic sub-continental mantle. Contributions to Mineralogy and Petrology 78; 175-188.
- Wells, P.R.A., 1976. Late Archaean metamorphism in the Buksefjord region, West Greenland. Contributions to Mineralogy and Petrology 56; 229-242.
- Wells, P.R.A., 1979. Chemical and thermal evolution of Archaean sialic crust, southern West Greenland. Journal of Petrology 20; 187-226.
- Wilson, A.F., 1968. Granulite terrains and their tectonic setting and relationship to associated metamorphic rocks in Australia. Special Publications of the Geological Society of Australia 2; 243-258.
- Wilton, D.H.C., 1984. Metallogenic, tectonic and geochemical evolution of the Cape Ray Fault Zone with emphasis on electrum mineralization; unpublished Ph.D. thesis, Memorial University of Newfoundland, St. John's.
- Windley, B.F., 1972. Regional geology of the early Precambrian high-grade metamorphic rocks in west Greenland. Part 1: Kangnaitsoq to Ameralik. Geological Survey of Greenland, Report 46, 46p.

00401

- Windley, B.F., 1973. Crustal development in the Precambrian. Philosophical Transactions of the Royal Society, London A273; 321-341.
- Wyllie, P.J., 1977. Crustal anatexis: An experimental review. Tectonophysics 43; 41-71.
- Zindler, A., Staudigel, H. and Batiza, R., 1984. Isotope and trace element geochemistry of young Pacific seamounts: Implications for the scale of upper mantle heterogeneity. Earth and Planetary Science Letters 70; 175-195.

Appendix A
FIELD LOCATION AND DESCRIPTIONS OF
GEOCHRONOLOGY SUITES

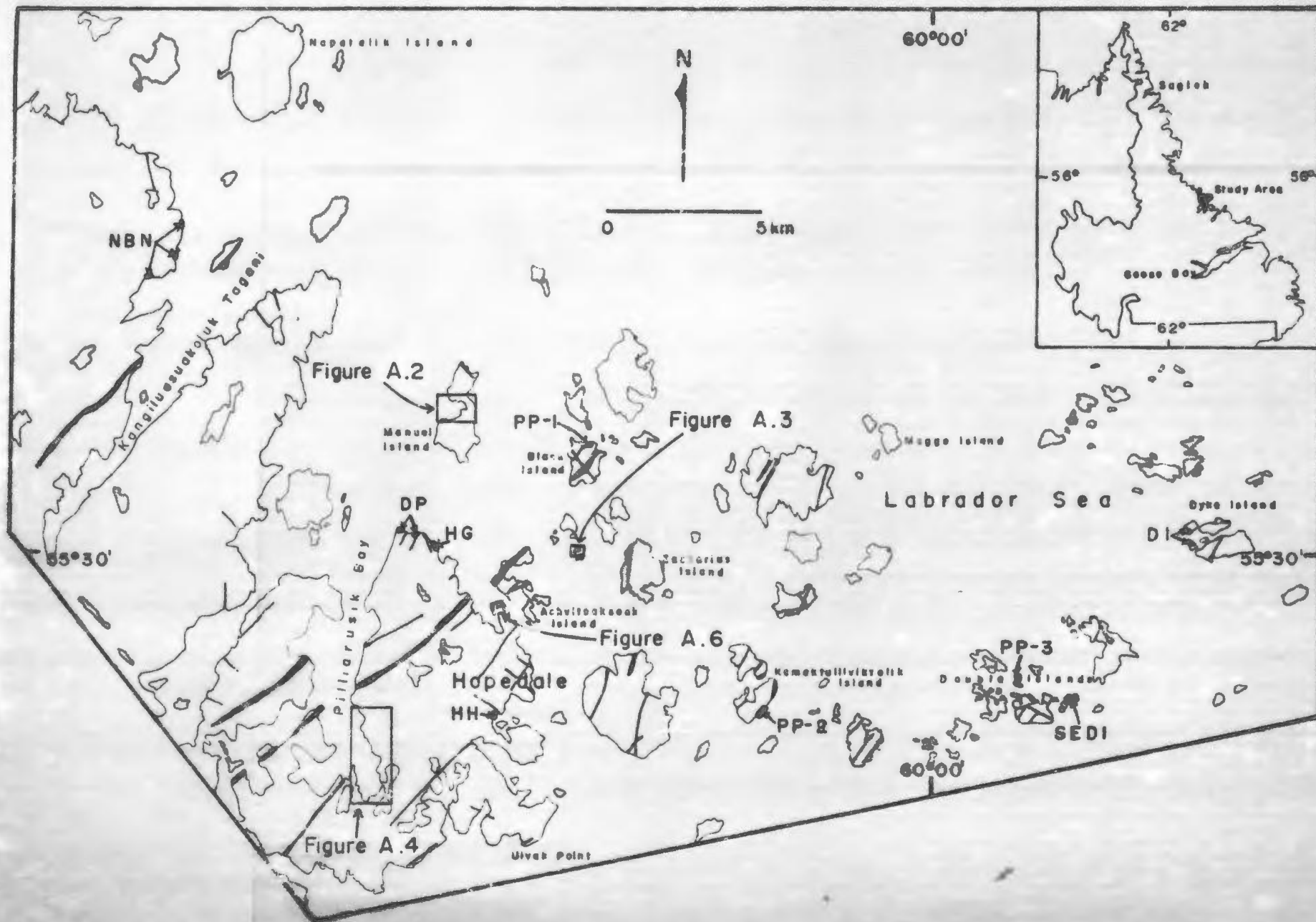
A.1 Introduction

Twelve suites of samples of Maggo gneiss were collected for Rb-Sr geochronology. The geological setting and salient features of each suite are described in this Appendix. The field locations of all suites are given in Figure A.1. Abbreviations are used throughout this work to refer to the individual geochronology suites. The suites were taken at localities that had been previously mapped and are representative of the lithologies at each locality. Sampling was carried out on a variety of scales, from detailed sampling over 5 - 10 m, to samples taken over several kilometres. This variable scale of sampling was undertaken to provide evidence on the extent to which the isotopic systematics were affected by metamorphism and deformation associated with the Flordian, and to a lesser extent the Hopedaian, events. The sample localities were

09402

2010

Figure A.1: Field locations of the twelve suites of Maggo
gneiss used in the Rb-Sr geochronology study.



selected to document Hopedalian isotopic characteristics of the gneiss and the progressive effects of Flordian overprinting.

A.2.1 Manuel Island

Manuel Island (MI), located north of Hopedale village (Figure A.1), samples were collected from the large bay on the west side of the island, informally named West Bay.

The geology of West Bay and sample locations are presented in Figure A.2. Three MI samples, collected from the south tip of the island, are not shown on Figure A.2. Biotite and hornblende tonalite, the dominant lithology of the island, has a well developed Hopedalian fabric (S_{n+2}). Evidence of Pre-Hopedalian fabric (S_{n+1}) is preserved as intra- and inter-folial folds (Plate 5A). The Maggo gneiss trondhjemitic phase is banded. The banding results from metamorphic differentiation during the Hopedalian event. Geochronology samples are from the tonalite and trondhjemite phases of the Maggo gneiss.

Along the north shore of West Bay all lithologies have been migmatized. The degree of migmatization varies from small diktyonitic migmatites associated with shear zones which cut the Hopedalian fabric to agmatitic zones with rare nebulitic zones. Some migmatites were emplaced lit-par-lit into the gneiss giving the latter a banded appearance. Larger pegmatite segregations in the gneiss are foliated, with evidence of two foliations. The early fabric (S_{n+1}) is reoriented by the predominate Hopedalian (S_{n+2}) foliation.

Figure A.2: Sample locality and local geology, West Bay
Manuel Island.

LEGEND

Weekes association

- 1 Normal Amphibolite
 - W W Layered to banded
 - 00 Weekes association pods in gneiss
 - / Carbonate-ultramafic enclave

Maggo gneiss

- 3a Biotite Tonalite
- 3c Hornblende Tonalite
- 4a Biotite Trondhjemite
- 4c Hornblende Trondhjemite

/ Hopedale dyke

⊗ Migmatites developed in Maggo gneiss

/ Kikkertavak dyke

x Sample Location

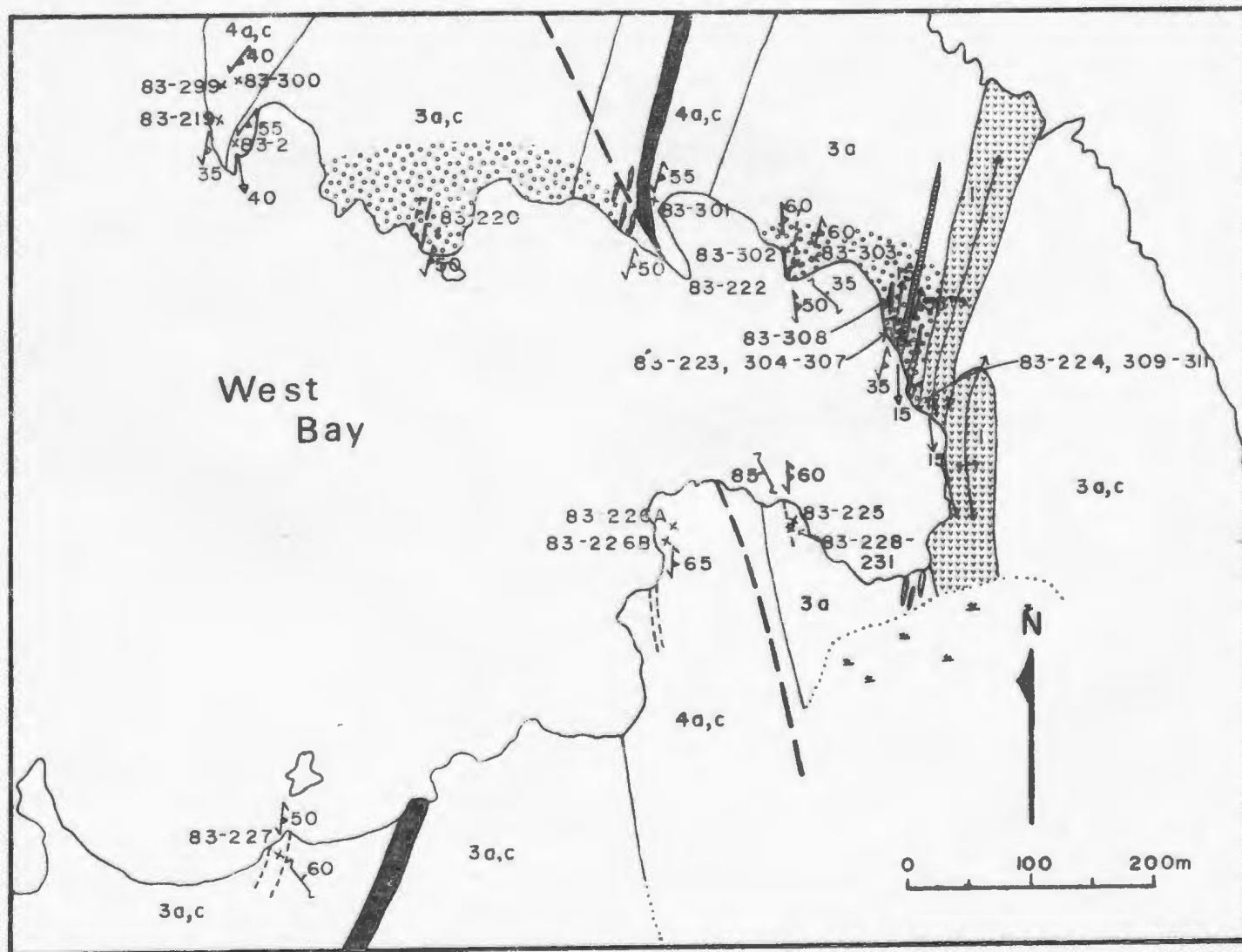
^
45 Shear Plane and Dip

10 Mineral Lineation

←
45 Folliation and Dip

/ Fault

10 ← Fold Axis



00407

00488

Around West Bay, numerous, variably sized enclaves of Weekes association are present within the gneiss. Clinopyroxene-bearing Hopedale dykes are numerous throughout the area shown in Figure A.2. During the Hopedalian (D_{n+2}) event the dykes were boudinaged, giving rise to rectangular, blocky shapes (Plate 8A). Not all dykes are boudinaged in response to Hopedalian deformation, some are (Plate 9A) thinned and folded about Hopedalian fold axes (F_{n+2}). The foliation within the gneiss is parallel to the fold structure defined by the dykes.

A.2.2 Porphyroblastic Phase

Samples of the Porphyroblastic Phase (PP) of the Maggo gneiss were collected from three widely separated localities, Kernertaluk (Black) Island, Kemaktulliviktalik Island and central Double Island (Figure A.1). The samples all display a Hopedalian (S_{n+2}) fabric defined by biotite. Samples in this suite consist of biotite tonalite and hornblende trondhjemite. Plagioclase is coarse grained and typically porphyroblastic in contrast with the remaining minerals. These samples were selected for geochronological study because they are similar in all respects to each other, they cover a wide area, exhibit a well developed Hopedalian fabric and display no visible evidence of Flordian shearing and migmatization.

A.2.3 Hypothesis Island

Hypothesis Island (HI; an informal name) is located midway between the NE tip of Achvitoaksoak Island and

Zacharius Island, NNE of Hopedale village (Figure A.1). Biotite tonalite, (Figure A.3) is massive to weakly foliated, with K-feldspar interstitial to the predominant assemblage (plagioclase - quartz - biotite - hornblende). The gneiss is homogeneous, with the proportion of mafic minerals, biotite and hornblende, exhibiting the greatest variation. The gneiss foliation (S_{n+2}) is oriented NW-SE and is cut by E-W shears that fold the foliation (Plate 9B). Boudinaged Hopedale dykes are concordant to the Hopedalian fabric.

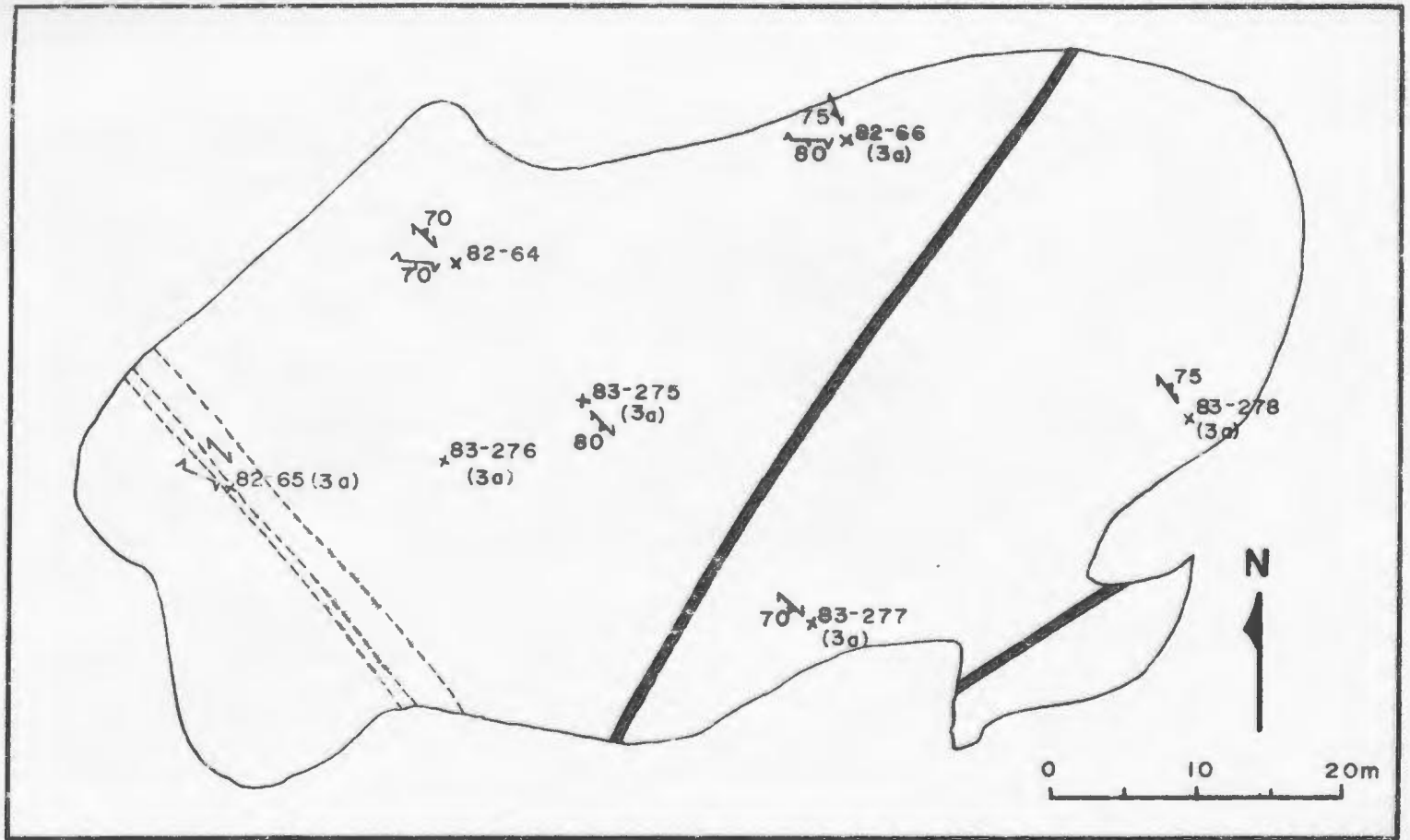
Migmatites, forming a minor component of the gneiss, are found in a variety of environments. Small, recrystallized migmatitic swaths, parallel the foliation and are deformed with the gneiss by E-W shears (Plate 9B). Nebulitic migmatites, in conjunction with dictyonitic migmatites, disrupt the foliation within the gneiss. The former are found along the edges and the terminations of shear zones associated with dictyonitic migmatite.

A.2.4 Hopedale Harbour

Four samples were collected on the west side of Hopedale Harbour (HH) (Figure A.1) from an area exhibiting only minor effects of migmatization. At this locality a Hopedale dyke is in discordant contact with the preserved pre-Hopedalian fabric (S_{n+1}) indicating a Hopedalian low strain zone. The dyke, 1.5 m thick, can be traced over a length of 5 m before disappearing under cover. Where the dyke becomes covered its thickness has decreased to < 0.4 m

01-00

Figure A.3: Geology of Hypothesis Island showing the location of geochronology samples.



LEGEND

3a Biotite Tonalite
 - - - Hopedale Dyke
 — Kikkertavak Dyke

x Sample Location
 ↘₇₀ Foliation and Dip
 ↘₇₀ Shear Plane and Dip

and becomes concordant to the gneissic foliation. The gneiss-dyke contact is sharp, marked by the growth of minor biotite parallel to the contact.

The Hopedale dyke host is a foliated biotite tonalite, with minor lit-par-lit pegmatites parallel to the gneissic foliation. The swaths effectively change the nature of the gneiss from a homogeneous foliated tonalite to a more banded variety (Plate 9C). The samples of gneiss exhibit a range of grain sizes from fine to medium grained tonalite to a coarser, porphyroblastic texture.

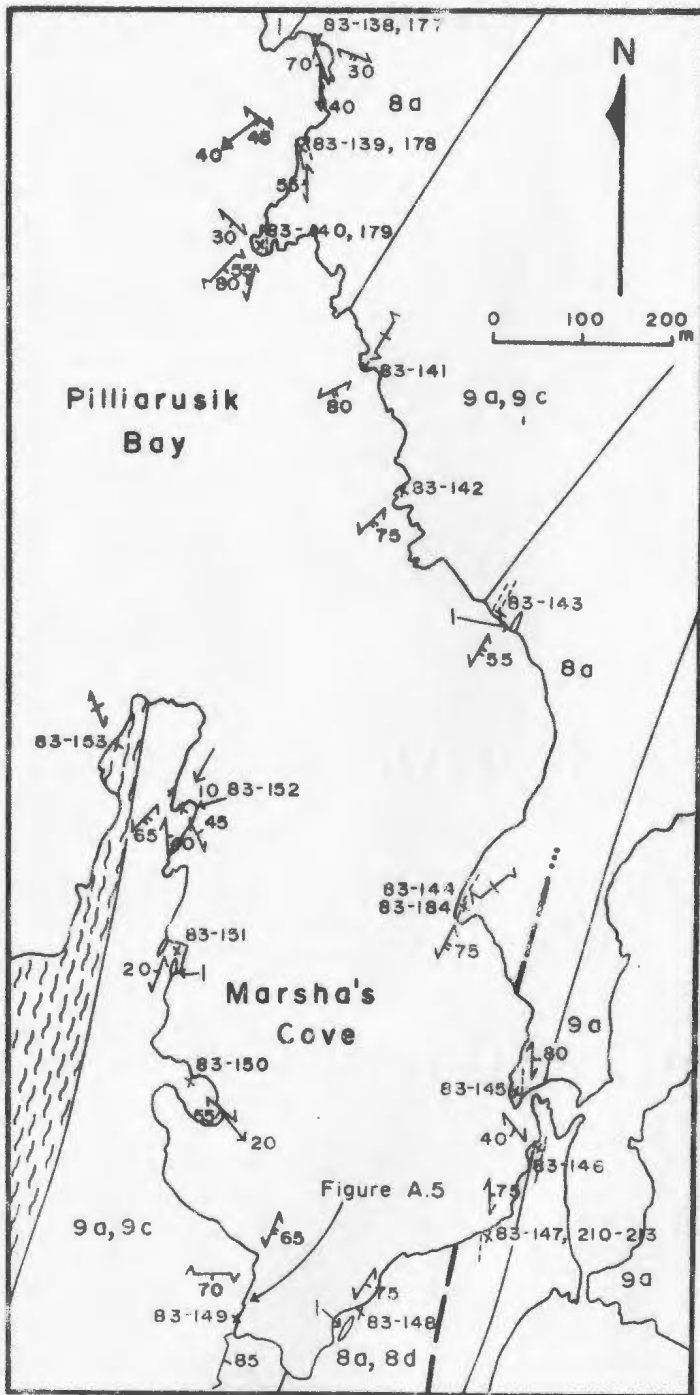
A.2.5 Marsha's Cove

Marsha's Cove (MC; an informal name) is located at the extreme southeastern end of Pilliarusik Bay, west of Hopedale village (Figure A.1). Along the east side of Pilliarusik Bay (Figure A.4) the progressive effects of Flordian reworking of the Hopedalian gneiss and fabric can be examined. In Marsha's Cove a large augen of Maggo gneiss, preserving Hopedalian mineralogy and fabric, has been rotated into a NE-SW orientation, during Flordian deformation. The boundaries of the augen are marked by a change in the character of the gneiss, reflected in the mineralogy. Biotite alters to chlorite, plagioclase to epidote and sericité and the proportion of K-feldspar increases.

Figure A.4 presents the geology of Marsha's Cove, as well as the location of Maggo gneiss samples used for geochronological determinations. Three separate areas were

61700

Figure A.4: Geology of Piliilarusik Bay. Sample localities for Piliilarusik Bay and Marsha's Cove geochronology suites are shown.



LEGEND

- | Weekes association
- Maggo Gneiss
- 8a Biotite Tonalite
- 8d Hornblende Tonalite, garnetiferous
- 9a Biotite Trondhjemite.
- 9c Hornblende Trond.
- Hopedale Dykes
- x Sample Location
- x/45 Hopedalian fabric & dip
- V/45 Fiordian fabric & dip
- V/45 Shear plane & dip
- x/45 Mineral lineation
- x/45 Minor fold axis
- Fault
- /// Mylonite zone

sampled for geochronology. (Plate 6D, 9D, 9E, 9F and 10A, Figure A.5)

Locality 1, (Plate 9D, 9E and 9F) consists of Maggo gneiss preserving Hopedalian mineralogy, but the Hopedalian (S_{n+2}) fabric has been rotated into a NE-SW orientation during the Flordian deformational event (D_{n+3}). The relict Hopedalian gneiss is composed of tonalite with variable proportions of biotite and hornblende. Mineralogically the gneiss changes from a slightly recrystallized, foliated hornblende tonalite (right side, Plate 9D), to a completely recrystallized epidote-chlorite-sericite-K-feldspar rich gneiss (left side, Plate 9D). Epidote is present in two forms 1) as a symplectic intergrowth with quartz, and, 2) as thin veins (<2 mm) which crosscut the foliation. Pegmatites become reoriented and recrystallized (plagioclase-quartz-K-feldspar-epidote-sericite) away from the augen core (Plate 9F).

Hopedale dykes in this vicinity exhibit evidence of retrogression from hornblende-plagioclase to epidote-actinolite-plagioclase. Retrogression and reorientation of the gneiss, pegmatites and dykes are attributed to Flordian deformation.

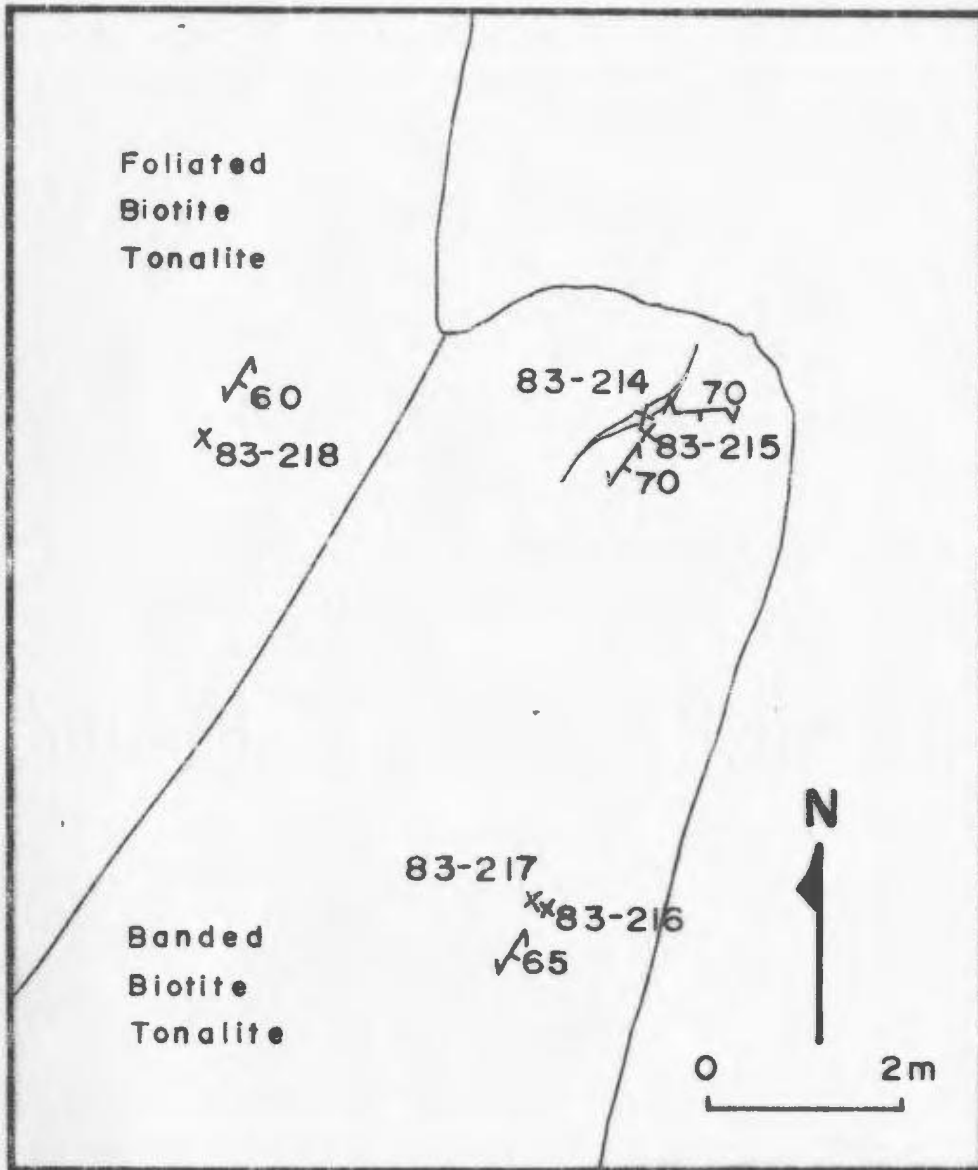
Two samples, collected at station 83-147 (Figure A.4), come from the extension of the augen preserved at the previous station. The samples are hornblende tonalite, one containing, the other lacking, garnet (83-210 and 83-211). The samples show no evidence of recrystallization

associated with the Flordian event, with K-feldspar occurring interstitially to plagioclase-quartz-hornblende and/or garnet.

At locality 3 (Figure A.5) banded and foliated biotite tonalite predominates, with banded tonalite most abundant. The banding (2 to 10 cm thick) is defined by alternating leucocratic (83-217) and melanocratic (83-218) layers (Plate 10A). The leucocratic bands contain relatively more K-feldspar, resulting from metamorphic differentiation which produced the banded gneiss. The plagioclase in the leucocratic bands is twinned, the twins being curved, and only mildly altered to epidote and sericite.

In the mafic-rich layers, K-feldspar forms interstitially to the plagioclase-quartz mosaic as a minor constituent. The biotite in the mafic bands is optically aligned, defining the foliation within the band. Epidote forms euhedral to subhedral grains, that exhibit a symplectic intergrowth with quartz. The gneiss at this locality is folded about NE plunging fold axes. Numerous small scale faults, having a sinistral sense of displacement are parallel to the fold axes. The banding in the gneiss is cut by sinistral (E-W), sigmoidal shears with associated diktyonitic migmatites (Plate 6D). The migmatite-gneiss contacts are sharp, with the diktyonitic migmatites reaching widths of up to 15 cm. Nebulitic migmatites within the banded gneiss, are inferred to represent the terminations or boundaries of diktyonitic

Figure A.5: Geology and sample location, SW Marsha's Cove
geochronology suite.



migmatites. The foliated tonalite (83-218) is less abundant than the banded tonalite having a total thickness of 3 m.

A.2.6 Hopedale Gneiss

The Hopedale Gneiss suite (HG) comes from the mainland shore, due south of Manuel Island (Figure A.1). Five samples were collected over a 1.5 m section of banded, migmatized gneiss, with band parallel pinch and swell pegmatites (Plate 10B).

The five samples at this locality represent a wide variation in bulk composition and mineralogy. Sample 83-232 is characterized by 1) biotite and other mafic minerals concentrated in wispy lenses and 2) the presence of thin, intensely folded migmatitic material, disrupted by dextral shears (Plate 10B). One of the larger migmatite layers (83-237) occurs along the contact between the migmatized unit of grey gneiss and a mafic-rich, migmatite poor unit (83-233). Sample 83-233 consists of plagioclase-biotite-hornblende-epidote-quartz, interpreted to be a relatively mafic-rich horizon developed in the protolith of the grey gneiss. The migmatites within this sample parallel the contact with the gneiss, are recrystallized and exhibit a foliation. In Plate 10B the dark band at the lower left portion of the photo appears identical to sample 83-233 except the latter contains several calc-silicate pods, concordant to the foliation within the layer.

In contrast sample 83-234 is a biotite tonalite lacking extensive migmatites, with biotite displaying a random

orientation. Granophyric and myrmekitic intergrowths of felsic minerals are common. K-feldspar in this sample occurs interstitially to plagioclase and quartz, and as larger grains (up to 0.75 mm). This sample is cut by non-recrystallized phlebotic to stromatic migmatitic material (sample 83-235).

Korstgard and Ermanovics (1984) interpret these lithologic associations, i.e. migmatized Maggo gneiss with amphibolite inclusions cut by Hopedale dykes, as constituting the elements, which during Hopedalian (D_{n+2}) deformation formed the Hopedale Gneiss.

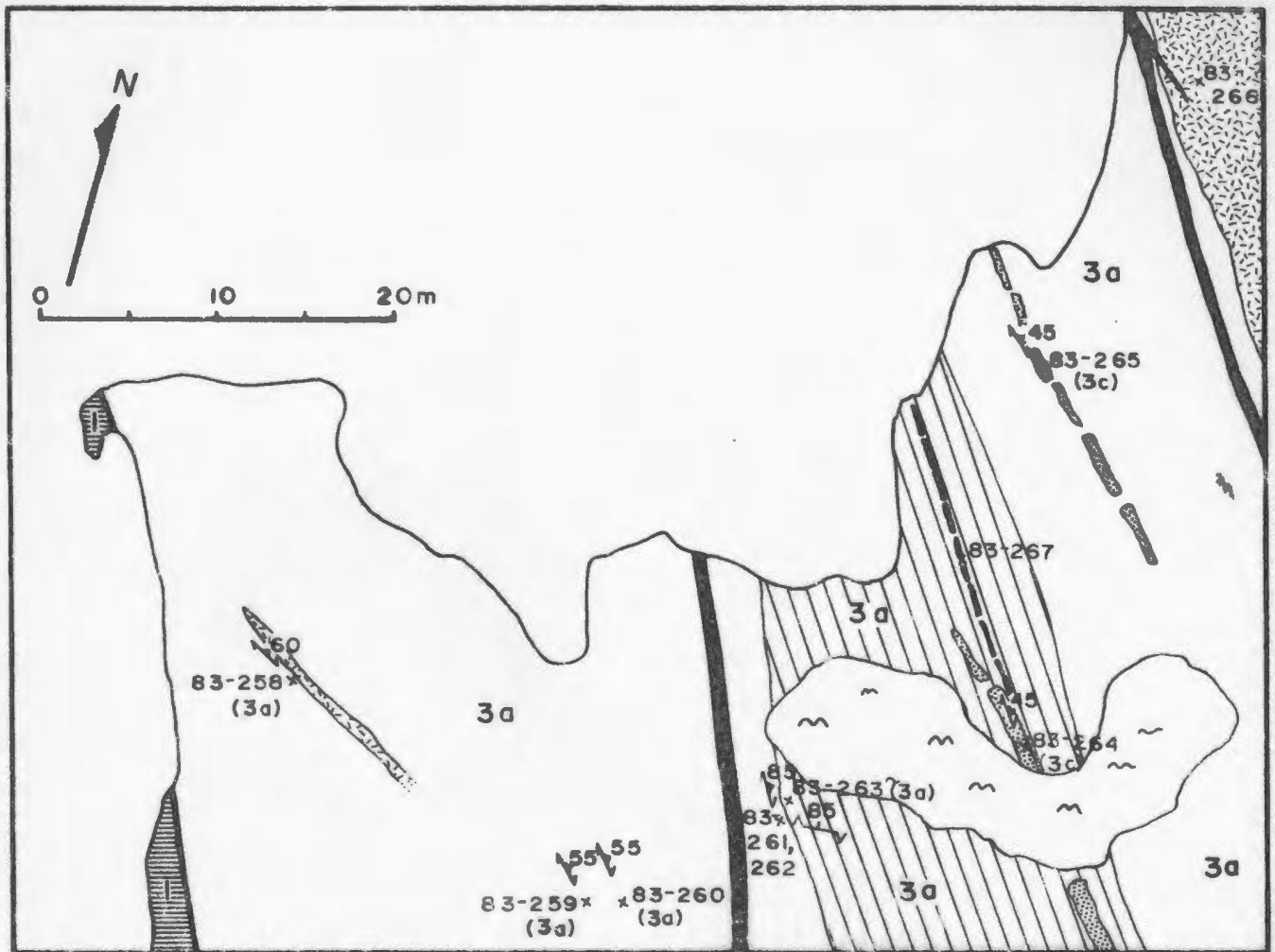
A.2.7 Black Head Tickle

The Black Head Tickle suite (BH) comprises 8 samples of foliated to banded biotite and hornblende tonalite. Biotite tonalite, identical to that exposed on Hypothesis Island, is the predominant lithology (Figure A.6) with the foliated variety being the most common. Hornblende tonalite occurs as boudins within the biotite tonalite (Plate 5D). The boudins vary in size, (0.5 m wide X 1.2-1.5 m long), are traceable along strike and are concordant to the foliation in the biotite-rich tonalite. The biotite-rich lithologies from Black Head contain sagentic biotite, (see Section 3.2.3.2). Hopedale dykes at this locality are clinopyroxene-bearing and concordant to the foliation within the gneiss.




The degree of shearing at this locality is minor, only one shear, with associated dicytonitic migmatite was

1100

Figure A.6: Geology and sample location for the Black Head geochronology suite.


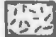




LEGEND

-  Weekes association
Normal Amphibolite
Garnet Amphibolite
-  3a Foliated Biotite Tonalite
-  3a Banded Biotite Tonalite

x Sample Location

 Foliation and Dip
85

-  Foliated Hornblende Tonalite
-  Recrystallized Pegmatite
-  Hopedale Dyke
-  Kikkertavak Dyke

 Fault

 Shear Plane and Dip
85

00423

observed (Plate 6C). The shear, 1.5 m long, exhibits a sigmoidal shape with a sinistral shear sense. The terminations of the shear, marked by nebulitic migmatites, are concordant to the foliation in the gneiss. In all respects, this locality resembles the MI, HI and PP sample sites. The presence of this shear is the only visible evidence of Flordian overprinting. Several foliated, recrystallized pegmatites parallel the foliation in the tonalite at this locality.

A.2.8 Dead Dog Point

Dead Dog Point (DP; an informal name; Figure A.1) represents an area of extreme Flordian overprinting of the Hopedalian Maggo gneiss. The gneiss at this locality is well banded, migmatized, hornblende tonalite. The samples for this suite come from two localities near Dead Dog Point, separated by 350 m. Two samples, 83-238 and 83-239, consisting of foliated to banded hornblende (up to 1 cm) tonalite are inferred to result from Flordian metamorphism. At this locality there are massive coarse grained amphibolite pods (Weekes association?) and softball sized anorthosite inclusions.

The remaining samples represent three distinct lithologies, separated from a single large block, collected from the extreme tip of Dead Dog Point (Plate 10C). Sample 83-242, a wispy foliated to banded hornblende tonalite, exhibits two generations of hornblende growth. The first occurs in the thin wispy layers, has a grain size of 0.2 mm

and is commonly associated with biotite. The second generation hornblende, is coarser grained (up to 2.5 mm) and occurs in distinct layers within the gneiss. This later hornblende is attributed to result from Flordian metamorphism.

The remaining samples result from separation of the above distinct lithologies from each other. Sample 83-243 consists of the finer grained hornblende gneiss and 83-244, contains the coarser grained hornblende.

A.2.9 Pilliarusik Bay

This suite (5 samples) was collected, along a 2.5 km stretch on the east side of Pilliarusik Bay (PB) (Figure 2.7), to document the progressive effects of Flordian overprinting. Samples in this suite are foliated biotite tonalite, with two samples having up to 10 % (visual estimate) K-feldspar, which reaches 3 mm in size. Samples in this suite exhibit varying degrees of alteration in the form of epidote and sericite after plagioclase, and chlorite after biotite.

Sample 83-142 is a banded gneiss, with stromatic and phlebitic migmatites characterized by the presence of hornblende, produced during the Flordian metamorphism. At this locality the gneiss has a granular weathering texture whereas the remainder of the localities are more resistant to weathering. At other localities, migmatitic material emplaced into the gneiss during the Hopedalian and earlier events becomes extensively recrystallized and foliated during the Flordian event.

A.2.10 Dyke Island Suite

The Dyke Island suite was collected by D. Bridgwater, during the 1981 field season, from the extreme eastern edge of the map area (Figure A.1). The sample site was visited by the author during the 1982 season. The samples from Dyke Island (DI) represent a homogeneous suite of weakly foliated biotite trondhjemite to biotite tonalite. The percentage of K-feldspar in the Dyke Island samples is low. The K-feldspar occurs as small, < 0.1 mm, grains interstitial to the more abundant plagioclase and quartz. Hopedale dykes at this locality are boudinaged, folded and contain accumulations of plagioclase crystals. The deformation observed to affect the dykes has been attributed to the Hopedalian event (D_{n+2}), with no visible effects of Flordian deformation (Ermanovics, pers. comm., 1983).

A.2.11 South East Double Island

This suite of 5 samples comes from a small island at the southeastern end of the Double Islands (SEDI) chain (Figure A.1).

The samples are dominantly hornblende trondhjemite with minor amounts of biotite trondhjemite. This lithology has been interpreted by Ermanovics *et al.* (1982) to intrude the Dyke Island lithology. The grain size of the gneiss at this locality is coarser (0.5 to 3 mm) than at other localities throughout the study area. Hornblende has a random orientation and displays irrational grain boundaries with

other mineral species. Biotite exhibits rare sagenitic textures and defines a weak foliation within the gneiss. The trondhjemite is cut by minor amounts of migmatitic leucosomes that vary from 0.5 m to 2.0 m in length and 5.0 to 10.0 cm in width. The leucosomes are wispy in places, form weak nebular patches with margins characterized by new hornblende growth, up to 1.0 cm in size. The gneiss is also cut by very fine to fine grained, weakly recrystallized aplitic dykes parallel to the foliation.

A.2.12 Next Bay North

The Next Bay North (NBN) geochronology suite was collected at three localities, over 2 km, along the mainland coast southwest of Napataik Island along the north shore of Kangluaksuakoluk Tagani (Figure A.1). The 6 samples were collected from within an area of preserved Hopedalian domain (D_{n+2}) bordered by zones of Flordian reworking (D_{n+3}). Sample 83-269, from the Hopedalian side of one region of Flordian overprinting, is a garnet-bearing biotite trondhjemite, which hosts abundant enclaves of anorthosite and related lithologies.

Three samples (83-272 - 274) come from an area displaying well developed Hopedalian migmatites. These samples are banded to foliated hornblende trondhjemite, with hornblende, up to 0.75 mm long, hosting rounded anorthosite xenoliths. The final sample locality (83-293, 294) is 800 m to the north of the previous location. The gneiss consists of banded biotite trondhjemite (83-293)

00437

with concordant, clinopyroxene-bearing Hopedale dykes (83-292). Minor amounts of foliated biotite tonalite (83-294) form concordant sheets within the banded trondhjemite. This lithology retains evidence of an internal fabric (Pre-Hopedalian D_{n+1}) that is not seen to affect the banded gneiss hosting it.

Appendix B

SAMPLING AND ANALYTICAL TECHNIQUES

B.1 Sampling

Samples were collected for all lithologies present in the study area. The majority of samples were collected by the author, these samples have no initials as a prefix. Samples collected by B.J. Fryer and D. Bridgwater are prefixed by BF and DB respectively.

All samples, whether to be used for major, trace, REE or Rb/Sr isotopic studies were collected with the aid of an Atlas Copco "Cobra Super" gas powered drill employing the plug and feather method. The drill facilitated the collection of otherwise inaccessible samples, i.e. from relatively smooth surfaces, which were generally the least visibly effected by late fracturing, alteration and epidote veining. These first stage samples, weighing up to 75 kg, were reduced to < 4 cm size chips on the outcrop to ensure an adequate supply of fresh material was available and to reduce one possible source of laboratory contamination. At

00428

00429

the same time a hand sample, for sectioning and staining was collected. Upon returning from the field, samples were passed through a Braun Chipmunk Jaw Crusher to reduce the chips to < 1 cm size. Each sample was then passed through a riffle splitter to reduce the sample volume to <150 ml; prior to pulverizing in a Siebtechnik "Tema" swing mill using a tungsten carbide bowl. Samples were run in the pulverizer for 60 seconds or less to produce a homogeneous powder of < 200 mesh.

Between each sample the jaw crusher, after stripping down, and the riffle splitter were vacuumed, washed down with methanol and blown dry with compressed air. The shatterbox was vacuumed out, washed down with water, blown dry, rinsed with methanol and blown dry between each sample. During all stages in the crushing procedure a high level of cleanliness was maintained to reduce possible sources of inter-sample contamination.

B.2 Major Element Analysis

Major elements were determined by atomic absorption (AA) spectrometry using a Perkin Elmer digitized spectrometer. on 0.1 g aliquots of rock powder that had been subjected to a hot hydrofluoric acid digestion followed by dilution in a saturated boric acid - distilled water solution (1:3 vol.:vol.). Determination of Si, Ti, Al, Total Fe as Fe³⁺, Mn, Na and K were carried out on this solution, while Ca and Mg were determined on a 5 ml aliquot of the boric acid solution plus 10 ml La₂O₃ diluted to

00430

50 ml. Ferrous Iron was determined by titration with standard potassium dichromate solution (Maxwell, 1968). P_2O_5 was determined by colorimetry (Maxwell, 1968). "Loss on Ignition", (LOI) values were determined on all samples after heating in porcelain crucibles at 1000 °C for 2 hours in a muffle furnace. G. Andrews, Department of Earth Sciences, Memorial University performed the AA analyses.

Accuracy of the AA analysis is determined through repeated analysis of international standards. The results of repeated analysis of USGS standard rock powder GSP-1 are given in Table B.1.

B.3 Trace Element Analyses

Trace elements were determined with a Philips 1450 X-ray fluorescence spectrometer, with on line data reduction, calibrated against international rock standards. Samples were run as 40 mm diameter, pressed pellets prepared from a homogeneous mixture of 10 g of rock powder and 1.3-1.4 g of phenol formaldehyde subjected to 50 MPa pressure for 10 seconds. The resulting pellets were heated in a muffle furnace for 20 minutes at 200 °C.

USGS standard powder pellets were run as unknowns interspersed with samples from this study. Average results of 14 replicate determinations on GSP-1, with one standard deviation and the accepted values (Abbey, 1982) in brackets are: Pb 54.1 (4.0; 54); Th 107.2 (4.4; 105); U 4.3 (2.4; 2.1); Rb 251.8 (4.2; 250); Sr 226.2 (2.2; 240); Y 29.2

00431

Table B.1. Accuracy and precision results calculated from replicate analysis of USGS standard GSP-1 as determined by AAS.

	Published Value*	No. of Analyses	Mean (wt %)	Standard Deviation
SiO ₂	67.32	7	68.65	0.80
TiO ₂	0.66	7	0.6	0.03
Al ₂ O ₃	15.28	7	14.77	0.22
Fe ₂ O ₃	4.28	8	4.22	0.07
MnO	0.04	8	0.04	0.01
MgO	0.97	7	0.96	0.03
CaO	2.03	8	1.94	0.07
Na ₂ O	2.81	8	2.74	0.08
K ₂ O	5.51	8	5.44	0.12

* From Abbey (1983)

00492

(5.2; 29); Zr 495.2 (8.20; 500); Nb 28.71 (0.9; 23); Zn 99.7 (2.4; 105); Cu 44.1 (5.7; 33); Ni 10.2 (2.6; 9); Ba 1329.1 (75.4; 1300); V 53.5 (7.3; 54); Cr 7.8 (5.2; 12); Ga 20.4 (2.0; 23).

Easton (1982) has demonstrated that the effects of deliberate cross contamination of samples and both field and laboratory duplicates are within the limits of analytical uncertainty.

B.4 Rare Earth Elements Analysis

Rare earth elements were analyzed by the thin film X-ray fluorescence method of Eby (1972) as modified by Fryer (1977; 1984 pers. comm.). The method employed in this study is outlined in Table B.2.

Samples were calibrated against international rock standards. Results for USGS standard G-2, a granite, are presented in Figure B.1. The MUN determinations are within 30% of the published values except for Sm and Gd. The higher error on these elements is the result of fractionation of these elements within the columns and/or low sample yields. The estimated precision of the XRF REE method is $\pm 10\%$ (Fryer, 1977). A measure of the precision of this method is given in Figure B.2, where 10 determinations on a Brazilian basalt, supplied by B.J. Fryer, are presented. The samples with lower yields (<50%) fall outside the limits of precision for this method due to fractionation of the REE in the columns. All samples are within analytical uncertainty of one another, excepting Dy

Table B.2: Procedure for Rare Earth Earth Separation

Sample Dissolution

- 1) Weigh 0.5 to 2.0 g into a 100 ml Teflon beaker
- 2) Add 15 ml HF + 2 ml HClO₄, evaporate to dryness
- 3) Add 15 ml HF, evaporate to dryness
- 4) Add 15 ml 2N HCl + 2 ml HClO₄, evaporate to dryness
- 5) Add 15 ml 2N HCl, evaporate to dryness
- 6) Add 5 ml 2N HCl, warm beaker until sample is in solution
- 7) Dilute solution to 1N HCl with distilled water

Ion Exchange separation of the REE

Ion exchange separation is carried out in glass columns - 18 X 1 cm filled to a height of 15 cm with a strong cation exchange resin (Amberlite CG 120, Na form, 100-200 mesh). Prior to placing the sample onto the column, the resin has been cleaned with 6N HCl, repacked with distilled water and re-equilibrated with 2N HCl.

- 8) Sample solution is filtered onto the column. After addition the filter paper is rinsed with 2N HCl, elution proceeds as follows.
- 9) Remove funnel and wash sides of the columns with 5 ml 2N HCl to remove droplets and ensure sample is absorbed onto resin bed. Repeat
- 10) To remove all cations up to and including Sr add 105 ml 2N HCl. Discard eluted solution.
- 11) Clean stopcock and column tip with distilled water. Place clean teflon beaker under column.
- 12) Add 5 ml 6N HCl to equilibrate resin with 6N HCl.
- 13) Add 115 ml 6N HCl to complete elution of REE group into beaker.
- 14) Add 1 drop HClO₄ to each beaker and evaporate solution to dryness.

Sample Clean Up

To ensure a clean sample a second pass through a small glass column, 10 X 0.75 cm, filled to a height of 8 cm with Amberlite resin is performed. In the sample clean up procedure HNO₃ is employed as the elutant. The resin is cleaned with 8N HNO₃, repacked and equilibrated with 2N HNO₃.

- 15) Preparing samples for the columns. Add 20 ml 8N HNO₃ to the samples and evaporate to dryness. Add 1-2 ml 2N HNO₃ to each sample to put them into solution. The samples are ready to be loaded onto the columns.
- 16) Pour solution directly onto the columns, rinsing in with 2N HNO₃, approximately 5 ml.
- 17) Separation of the REE. Wash down the sides of the columns with 1-2 ml 2N HNO₃. Repeat.

Table B.2: continued

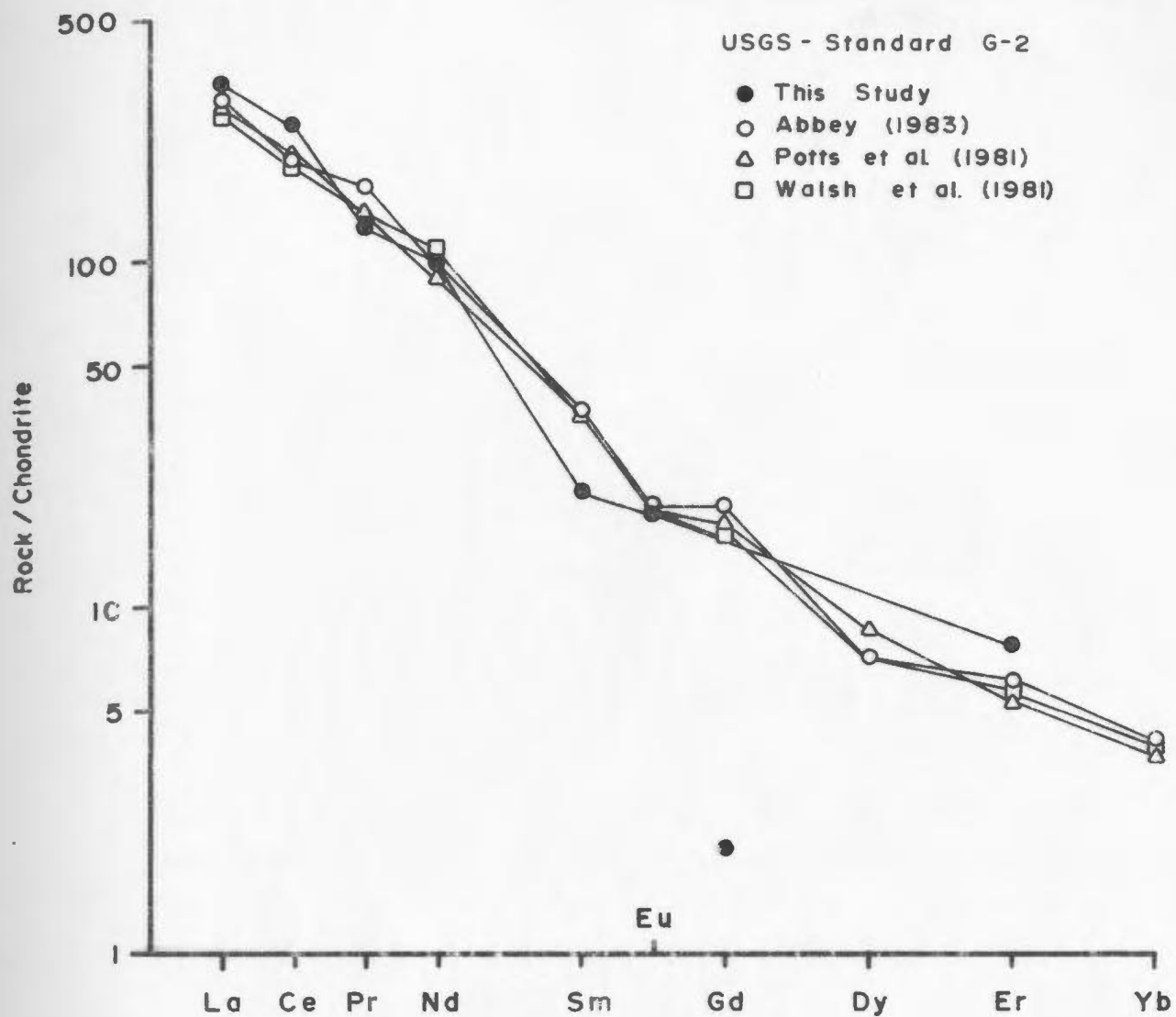
- 18) Add 21 ml 2N HNO_3 to each column and let drain. Discard.
- 19) Place a clean labelled 30 ml Teflon beaker under the columns. Add 14 ml 8N HNO_3 and let drain.
- 20) Place beakers on a hotplate and evaporate to dryness. Dilute the solution to 1N HCl with distilled water

Loading samples onto Ion Exchange Papers.

Samples are picked up in $\approx 0.25\text{N}$ HCl, using a 50 μl Eppendorf automatic pipette, and placed in the centre of an ion exchange paper (Reeve Angel SA-2) that has been cut and fitted onto a cardboard backing ring. When the paper has dried it is stored in a labelled coin envelope prior to analysis on the XRF.

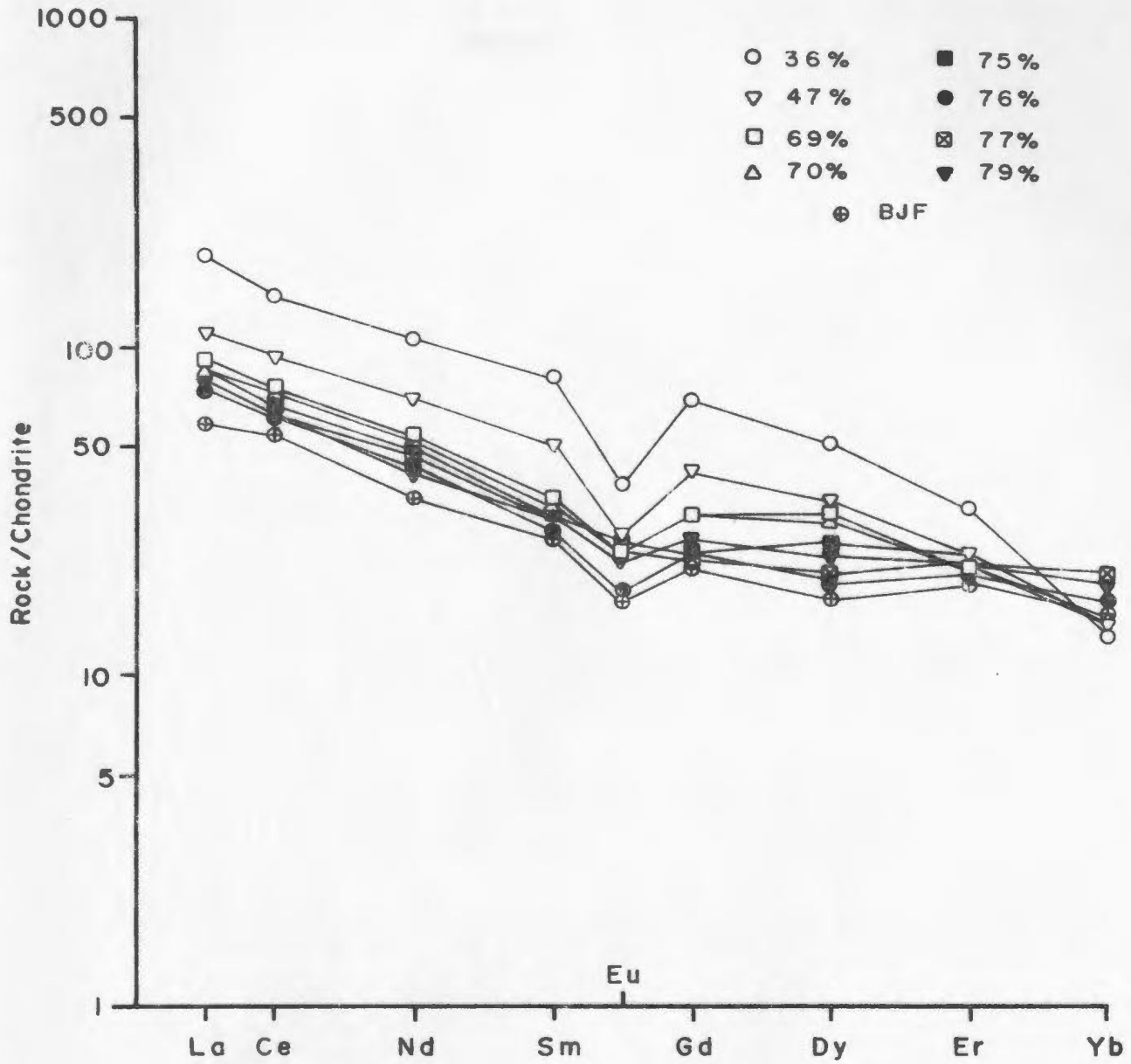
3100

Figure B.1: REE results for USGS standard sample G-2 as determined in this study by the thin film XRF method. Results are compared to published values.



73100

Figure B.2: Precision of the thin film XRF method of determining REE distributions. The sample run is a Brazilian basalt supplied by B.J. Fryer. The values accompanying the symbols refer to the percent of sample yield, as determined using a Tm spike. The samples with lower Tm yields result in higher abundances for the same sample.



00489

values which are within 30% of each other. REE plots are normalized to the chondritic values reported by Masuda et al. (1973) divided by 1.2. Chondrite normalizing factors (in ppm) are La 0.315; Ce 0.813; Nd 0.597; Sm 0.192; Eu 0.0722; Gd 0.259; Dy 0.325; Er 0.213; Yb 0.208.

In all petrogenetic discussions only samples with chemical yields >60% are considered. The low yields, in 20% of all samples analyzed, are the result of either loss of sample solution during processing or fractionation of the REE on the columns, i.e. over elution and loss of Tm and HREE.

Appendix C

RUBIDIUM - STRONTIUM ISOTOPIC DATING METHODS

C.1 Rubidium-Strontium Analysis

Rubidium - strontium ratios were determined by X-ray fluorescence on the same pressed powder pellets used for trace element determinations. Rubidium and strontium values and the $^{87}\text{Rb}/^{86}\text{Sr}$ ratios are based on a minimum of ten replicate analyses and calibrated against International rock standards. USGS standard sample W-1 was run with each set of Maggo Gneiss samples. A total of 120 determinations on W-1 (Table C.1) yield mean values for Rb and Sr of 22.1 +/- 0.5 and 188.5 +/- 0.8 ppm, respectively. Estimated precision of the rubidium and strontium contents is 1% (1 sigma) or 0.5 ppm, whichever is lower. The precision of the rubidium - strontium ratios is 1.5% (1 sigma) or better. Table C.2 presents results of duplicate determinations of Rb and Sr and the corresponding $^{87}\text{Rb}/^{86}\text{Sr}$ ratios for samples from this study used to define the precision of the determinations.

00440

00441

Table C.1. Results of replicate analyses on USGS standard sample W-1 for Rb and Sr, in ppm, with the corresponding $^{87}\text{Rb}/^{86}\text{Sr}$ ratio. The errors quoted are for 1 standard deviation about the mean.

Run	Cycles	Rb	Sr	$^{87}\text{Rb}/^{86}\text{Sr}$
1	15	22.3	188.5	0.343
2	10	22.1	187.5	0.341
3	10	21.2	188.9	0.325
4	10	22.2	188.3	0.341
5	10	21.5	190.3	0.328
6	15	21.7	187.7	0.324
7	15	22.7	188.8	0.347
8	15	22.6	189.0	0.347
9	10	22.1	188.3	0.340
10	10	22.6	187.3	0.349
Mean		22.1 +/- 0.5	188.5 +/- 0.8	0.339
Accepted Values*		21	190	0.320

* - From Abbey (1982)

05442

Table C.2. Results of duplicate analyses of Rb and Sr, in ppm, and the corresponding $^{87}\text{Rb}/^{86}\text{Sr}$ ratio for geochronology samples from this study. Contents are based on a minimum of 10 replicate determinations by XRF analysis. Errors (s) quoted are for 1 standard deviation about the mean.

Sample	Rb	s	Sr	s	$^{87}\text{Rb}/^{86}\text{Sr}$	s
82-76						
(15)	48.5	0.3	270.0	0.8	0.520	0.003
(10)	48.4	0.3	270.1	0.7	0.519	0.004
82-78						
(15)	42.8	0.2	421.9	1.1	0.294	0.002
(10)	41.7	0.3	418.7	1.2	0.288	0.002
83-184						
(10)	68.6	0.4	752.6	2.4	0.264	0.001
(10)	68.4	0.4	752.0	2.8	0.263	0.001
83-216						
(15)	42.2	0.2	253.3	0.5	0.483	0.002
(10)	41.7	0.3	250.6	1.0	0.481	0.002
83-238						
(15)	49.7	0.4	431.8	1.2	0.333	0.002
(10)	49.6	0.2	428.6	1.8	0.335	0.002
83-258						
(10)	40.5	0.4	643.0	2.5	0.183	0.001
(10)	39.8	0.4	641.7	2.4	0.180	0.002
83-294						
(10)	35.7	0.4	349.0	1.0	0.296	0.003
(10)	35.8	0.4	347.8	1.7	0.298	0.003
83-315						
(10)	45.8	0.3	649.9	1.3	0.204	0.001
(10)	45.9	0.4	643.6	1.7	0.206	0.002

C.2 Strontium Analysis

Throughout the strontium separation the concentration of HCl used was 2N, (S.G. = 1.035 +/- 0.001) made from quartz distilled 6N HCl. Strontium separation was carried out on 0.2 to 0.4 g aliquots of rock powder. Table C.3 is a summary of the sample dissolution and ion exchange procedure employed for strontium separation.

Strontium from the final solution was loaded as the phosphate onto a degassed, single tantalum filament using H_3PO_4 . Six samples were loaded on each turret and analyzed on a Vacuum Generators Micromass 30 mass spectrometer. Samples were run at filament currents from 2.0 to 2.8 amperes, in blocks of 10 cycles, with 4 to 20 blocks counted for each sample. Each cycle involved counting backgrounds 8X, and the following Sr peaks: 86; 11X, 87; 8X, 88; 4X. At the end of each cycle the following ratios are calculated: 1) $^{86}Sr/^{88}Sr$, 2) the raw $^{87}Sr/^{86}Sr$ and 3) the $^{87}Sr/^{88}Sr$ normalized to $^{86}Sr/^{88}Sr$ ratio of 0.1194.

At the completion of 10 cycles of data collection, the mean $^{87}Sr/^{86}Sr$ ratio for that block was calculated. The $^{87}Sr/^{86}Sr$ ratio for a sample is taken as the mean of the mean values for each block. Errors quoted for each isotopic determination are at the 1 sigma level. Analyses of the NBS 987 strontium carbonate at MUN yielded a mean value of 0.71030 +/- 0.00001 (1 sigma) for 28 determinations between October 8, 1984 and April 16, 1985 by 3 analysts.

00444

Table C.3: Procedure for Sr Separation.

Sample Dissolution

- 1) Weigh 0.2 to 0.4 g into a 100 ml Teflon beaker
- 2) Add 15 ml HF + 2 ml HClO₄, evaporate to dryness
- 3) Add 15 ml HF, evaporate to dryness
- 4) Add 15 ml 2N HCl + 2 ml HClO₄, evaporate to dryness
- 5) Add 15 ml 2N HCl, evaporate to dryness
- 6) Add 5 ml 2N HCl, warm beaker until sample is in solution
- 7) Dilute solution to 1N HCl with distilled water

Ion Exchange Separation

Ion exchange separation is carried out in glass columns - 18 X 1 cm filled to a height of 15 cm with a strong cation exchange resin (Amberlite CG 120, Na form, 100-200 mesh). Prior to placing the sample onto the column the resin has been cleaned with 6N HCl, repacked with distilled water and reequilibrated with 30 ml 2N HCl.

- 8) Sample solution is filtered onto the column, the funnels being removed after the sample has drained completely onto the resin.
- 9) Elution with 2; 3; 5; 10; 10; 5 ml of 2N HCl. Each individual aliquot has drained completely prior to the addition next aliquot. Solution is discarded
- 10) Add 30 ml 2N HCl, collect and evaporate to dryness.

Sample Clean Up

To ensure a clean sample a second pass through a small glass column, 10 X 0.75 cm, filled to a height of 8 cm with Amberlite resin is performed. The small columns are cleaned, repacked and re-equilibrated in the same manner as the large columns, however reduced acid volumes are required.

- 11) Add 5 ml 5N HCl to sample to bring it into solution
- 12) Dilute the solution to 1N HCl with distilled water
- 13) Pour the sample directly onto the resin
- 14) Elute with 1; 1; 5; 5; 5 ml 2N HCl, allowing each aliquot to drain completely. Solution is discarded.
- 15) Add 5 + 5 ml 2N HCl, collect and evaporate to dryness
- 16) Upon completion of the evaporation the sample is picked using a 50 μ l Eppendorf pipette and a dilute H₃PO₄ acid solution and stored in a labelled, tightly capped vial for analysis on the mass spectrometer.

The author performed the Sr separations on all 1982 samples. T. Finn, Department of Earth sciences, Memorial University, performed the Sr separations on all 1983 samples.

C.3 Regression Analysis

All samples analyzed for $^{87}\text{Sr}/^{86}\text{Sr}$ are normalized to a $^{87}\text{Sr}/^{38}\text{Sr}$ value of 0.1194. Isochrons were regressed using a least squares fit similar to Brooks et al. (1968). The regressions were carried out on a Hewlett Packard system 9845A desktop computer and plotted on a Hewlett Packard 7470A plotter using programs written by D. Press and H. Longerich, Department of Earth Sciences, Memorial University.

A measure of the geological error associated with an individual regression is given by the MSWD (Mean Square of the Weighted Deviates). The MSWD is a statistical function which evaluates the contribution of analytical error (machine, analyst) vs. the geological error to age determination. The higher the MSWD the greater is the geological error. Brooks et al. (1972) suggest that for an $\text{MSWD} > 2.5$ the samples used in the regression define an errorchron rather than a true isochron.

Appendix D

MAJOR, TRACE AND RARE EARTH ELEMENT RESULTS
FOR MAGGO GNEISS AND HOPEDALE DYKES

00446

4400

	Diorite Gneiss Phase of the Maggo Gneiss									Tonalite Gneiss 83-184
	83-78a	83-1e2	83-203	83-233	83-252	83-274	83-297	83-299	83-310	
SiO2	58.70	57.20	59.19	60.30	59.30	60.20	58.70	60.50	57.50	67.00
TiO2	.73	.54	.70	.94	.58	.70	.69	.58	.80	.52
Al2O3	15.8	18.76	15.26	15.10	15.60	15.50	15.10	13.00	15.10	15.70
Fe2O3	8.51	5.01	9.21	6.38	7.17	6.83	7.97	7.65	9.74	2.58
MnO	.10	.04	.12	.15	.15	.12	.14	.13	.13	.07
MgO	3.71	3.97	3.95	4.52	3.85	3.73	7.52	4.08	4.40	1.08
CaO	3.72	7.4	6.94	1.75	7.36	5.88	7.80	7.00	6.86	2.95
Na2O	4.69	5.12	4.91	3.12	4.08	4.23	3.10	3.41	4.42	4.58
K2O	.36	.83	.97	2.48	.96	1.49	1.72	.87	.91	2.34
P2O5	.23	.18	.21	.14	.09	.12	.11	.08	.33	.14
LOI	.44	.71	.52	.87	.38	.41	.75	.54	.35	.68
TOTAL	99.19	99.67	99.93	101.55	99.52	99.21	98.60	98.84	99.64	98.62

Trace Elements (ppm)										
Pb	3	2	7	4	9	2	7	4		
Th		3		6	3		4	1		11
U					1			2		11
Rb	4	7	16	90	11	38	55	10		
Sr	258	446	160	217	269	255	74	202	5	59
Y	27	7	21	24	19	14	25	22	282	718
Zr	125	43	144	110	58	77	78	77	17	5
Nb	6	1	8	11	6	6	7	6	99	159
Zn	52	66	83	94	78	69	78	6	11	
Cu	38	31	14	10	44	78	68	68		58
Ni	41	43	62	41	90	13	51	22		27
Ba	91	73	68	181	88	42	76	66		
V	132	110	133	188	179	132	166	122	68	860
Cr	42	17	95	39	175	117	257	169	164	45
Ga	19	22	14	21	17	21	116	126	16	3

Rare Earth Elements (ppm)										
La	4.50	23.40			15.80	17.70		8.30		
Ce	12.60	54.00			33.80	42.20		19.00		
Pr	2.10	6.50			4.50	5.30		2.40		
Nd	10.40	25.70			16.50	20.50		10.70		
Sm	2.40	5.20			3.90	3.40		2.60		
Eu	.80	1.70			.50	.50		.90		
Gd	2.50	6.00			4.10	3.80		3.30		
Dy	1.90	5.40			5.70	3.40		3.00		
Er	.60	2.40			1.70	1.60		2.20		
Yb	.30	1.80			.70	1.00		1.50		
Lu										

SumREE	-1.00	38.10	132.10	-1.00	86.80	99.40	-1.00	53.90		
Na/K	13.03	6.17	4.13	1.38	4.25	2.84	1.80	3.92	442	1.96
Y/Rb	747.09	984.02	447.22	236.57	724.28	334.20	259.53	656.38	15.32	303.79
K/Ba	58.60	94.36	118.38	113.71	90.53	93.68	85.99	59.18	1.13	20.94

80448

	Tonalite phase of the Maggo Gneiss											
	82-55	82-60	82-74A	82-74B	82-74C	82-74D	82-74E	82-74F	82-78	83-15	83-59	83-62
SiO ₂	47.77	47.77	60.00	62.70	64.00	62.90	63.80	61.60	61.80	64.40	62.80	65.60
TiO ₂	1.40	1.34	1.33	1.56	.51	.55	.53	.55	.63	.53	.88	.60
Al ₂ O ₃	15.20	16.30	16.10	16.10	16.60	16.50	16.50	16.20	16.60	15.30	16.10	15.40
Fe ₂ O ₃	5.97	7.54	5.31	5.15	4.98	5.43	5.47	5.34	6.32	5.02	6.18	5.23
MnO	1.0	1.05	1.09	1.08	1.08	1.08	1.08	1.09	1.10	1.08	1.09	1.06
MgO	2.29	2.46	2.52	2.52	2.39	2.72	2.59	2.66	3.20	3.05	2.42	2.16
CaO	2.95	4.31	5.30	5.30	5.37	5.51	5.44	5.38	6.01	5.58	6.16	5.17
Na ₂ O	3.69	4.46	4.13	4.13	4.24	4.10	4.15	3.99	3.98	3.08	3.85	3.72
K ₂ O	1.18	1.44	1.17	1.22	1.03	1.87	1.04	1.25	1.37	1.38	1.01	1.14
P ₂ O ₅	1.13	1.11	1.10	1.10	.17	.21	.16	.16	.13	.13	.17	.12
LOI	1.22	1.41	1.79	1.66	.78	.65	.80	.72	.62	1.53	.25	.46
TOTAL	98.59	100.63	100.04	98.59	100.15	99.32	100.56	98.17	100.76	99.95	99.91	99.66

Trace Elements (ppm)												
Pb		9	7	1	1		3	8	2	10	6	9
Th												5
U			4			2		1		6		1
Rb	34	54	27	30	24	23	24	36	43	36	26	41
Sr	147	312	456	440	467	467	448	441	422	384	200	282
Y	17	10	12	13	13	12	13	16	16	8	24	13
Zr	118	110	86	86	93	73	81	91	68	64	120	131
Nb	5	6	3	4	3	3	4	3	5	5	7	4
Zn	62	53	57	58	60	62	60	61	64	59	59	60
Cu	36	11	20	25	25	22	17	26	37	41	27	28
Ni	28	11	20	14	18	20	16	21	26	33	27	21
Ba	724	311	360	460	336	359	347	333	397	262	131	204
V	95	42	97	97	88	100	92	92	119	98	102	78
Cr	46	22	39	44	22	32	15	25	44	70	37	47
Ga	18	16	18	19	20	20	19	21	21	24	18	17

Rare Earth Elements (ppm)												
La	13.70	6.12	17.67	17.48	23.95	18.38	14.65	18.75	15.74	9.20	15.20	27.70
Ce	31.78	14.12	39.89	40.56	50.71	42.13	35.67	42.87	25.77	19.70	37.80	53.90
Pr	2.53	1.84	4.71	4.78	5.33	4.48	4.19	4.78	3.97	2.50	4.50	5.10
Nd	14.24	6.38	18.34	18.97	21.93	19.63	17.54	20.02	17.83	14.10	20.00	22.50
Sm	3.15	1.67	3.33	3.19	4.28	3.81	3.09	3.74	3.86	2.50	3.90	3.10
Eu	.99	.61	.93		1.53	1.52	1.30	1.27	1.51	.60	.80	.20
Gd	3.10	1.97	2.79	2.88	3.62	3.37	2.82	3.11	3.45	2.70	3.70	3.10
Dy	2.14	1.49	1.78	1.76	1.91	2.15	1.78	2.02	1.96	2.30	3.30	2.60
Er	1.27	.65	.47	.72	1.15	.96	.81	.52	.94	.80	1.40	.80
Tb	.68	.72	.19	.32	.86	.85	.28	.27	.47	.50	1.60	.70

SumREE	74.38	35.52	91.36	91.29	116.44	98.43	83.14	97.97	76.19	56.00	92.20	119.70
Nb/Rb	3.17	3.10	3.57	3.36	4.12	4.71	3.99	3.19	2.91	2.23	3.81	3.26
K/Rb	287.07	213.40	359.62	374.99	388.54	300.84	411.00	314.36	258.40	318.13	322.38	230.75
K/Ba	43.73	30.44	26.95	22.01	25.44	20.11	24.73	29.11	28.64	43.71	63.98	46.58

00448

Tonalite Phase of the Maggo Gneiss

	83-116	83-120	83-142	83-169	83-174	83-177	83-187	83-202	83-204	83-205	83-207	83-211
TiO2	65.7	65.96	67.2	65.70	67.70	66.00	65.10	66.40	65.90	64.20	62.60	66.90
Al2O3	17.30	15.50	14.0	15.00	14.90	15.20	15.10	14.80	14.20	15.40	15.10	13.90
Fe2O3	5.26	4.47	4.28	4.49	3.92	3.45	4.61	4.96	4.94	5.65	5.80	4.90
MnO	.09	.07	.06	.06	.06	.05	.07	.08	.08	.07	.11	.06
MgO	2.34	1.91	1.47	2.68	2.13	1.47	1.75	2.07	2.27	2.41	3.43	2.72
CaO	5.29	4.27	4.34	4.92	4.44	4.06	4.58	4.99	4.68	5.19	6.55	3.44
Na2O	4.13	4.11	4.09	3.87	4.12	4.15	4.09	4.17	3.92	4.11	4.14	3.91
K2O	1.26	1.67	1.21	1.33	1.42	.59	.84	.86	1.10	1.35	1.05	1.45
P2O5	.12	.12	.11	.13	.14	.12	.14	.14	.10	.13	.11	.11
LOI	.26	.47	.54	.92	.71	1.16	1.51	.76	.85	.82	.77	.75
TOTAL	100.12	99.27	99.49	99.32	99.78	96.55	99.12	99.69	98.53	99.84	101.45	98.61

Trace Elements (ppm)

Pb	4	10	7	11	5	9	9	3	3	7		
Th		9	4	7		9	11	3	2			
U		6							1		3	10
Rb	24	64	36	32	42	15	27	27	39	49	25	24
Sr	281	368	262	331	426	543	292	230	199	260	220	181
Y	16	16	9	7	8	8	12	17	17	20	22	13
Zr	73	144	120	119	62	163	118	126	128	106	134	112
Nb	3	9	3	6	5	6	7	6	6	6	5	9
Ta	63	46	32	34	40	63	64	47	53	64	63	
Cu	19	12	28	45	33	22	11	46	25	16	12	
Ni	32	14	18	25	20	7	15	23	33	29	53	
Ba	319	367	211	307	365	365	187	126	108	128	106	107
V	85	52	57	61	68	65	70	77	84	93	105	70
Cr	58	24	36	71	44	16	12	23	43	33	74	
Ga	18	17	17	21	16	10	11	16	19	14	13	18

Rare Earth Elements (ppm)

La		10.30	9.80	35.80	35.30		18.00	18.90				
Ce		18.40	17.20	66.90	70.60		39.50	40.80				
Pr		2.60	2.20	6.10	7.60		4.40	4.80				
Nd		10.30	11.60	29.20	27.00		17.40	16.40				
Sm		1.70	1.90	2.90	3.80		3.30	3.00				
Eu		.40	.60	.30	.50		.30	.30				
Gd		1.70	2.10	3.10	3.00		2.90	2.80				
Dy		2.00	2.60	2.40	2.00		2.00	3.80				
Er		1.00	1.60	1.00	.80		1.40	1.10				
Yb		.30	.70	.40			1.80	.70				
Lu												

SumREE	-1.00	-1.00	48.70	50.30	148.10	150.60	-1.00	91.00	92.60	-1.00	-1.00	-1.00
Na/K	3.28	2.46	3.55	3.15	2.90	7.03	4.87	4.85	3.56	3.04	3.94	2.70
K/Rb	435.70	216.55	329.35	318.99	280.59	349.74	258.19	254.90	240.23	224.07	335.15	501.52
K/Ba	32.78	37.76	42.47	33.25	32.29	13.41	37.28	56.64	84.53	87.53	82.21	112.49

00450

Tonalite Phase of the Maggo Gneiss

	83-215	83-216	83-238	83-272	83-255	83-272	83-273	83-295	83-296	83-300	83-301	83-302
SiO2	67.80	67.20	66.60	66.50	65.60	66.00	66.90	65.80	64.90	65.90	63.80	65.20
TiO2	.45	.43	.52	.43	.62	.43	.44	.16	.40	.52	.77	.61
Al2O3	15.10	15.00	15.20	14.70	16.10	14.30	14.50	16.00	11.60	16.10	15.90	16.50
Fe2O3	3.77	4.02	3.69	4.70	4.34	5.49	4.69	2.14	5.30	4.25	5.18	4.16
MnO	.06	.07	.05	.07	.06	.11	.10	.05	.11	.05	.08	.06
MgO	1.49	1.23	1.04	3.66	1.64	2.60	2.52	2.63	3.71	1.87	2.52	2.18
CaO	3.98	4.08	4.72	4.90	5.88	5.14	4.68	4.92	5.25	4.71	5.27	4.67
Na2O	4.53	4.18	4.15	3.73	4.39	3.89	4.10	4.40	3.61	4.48	4.12	4.71
K2O	1.49	1.73	1.46	1.58	.46	1.36	1.33	1.21	1.35	1.36	1.44	1.49
P2O5	.06	.14	.09	.13	.19	.10	.08	.02	.06	.14	.13	.16
LOI	.57	.68	.53	.70	.16	.55	.42	.55	.67	.40	.75	.35
TOTAL	99.30	98.36	98.59	98.15	99.44	99.97	99.76	98.63	99.56	99.78	99.96	100.09

Trace Elements (ppm)

Pb		13	8	8	6	7		7	4	5	3	7
Th	14	5		3	7	4						
U	7			2	2				1	6		4
Rb	50	42	50	58	9	33	40	33	33	32	44	54
Sr	313	253	472	435	274	239	251	469	199	353	407	465
Y	16	13		6	9	19	18	6	16	7	12	14
Zr	146	132	108	127	261	97	92	89	89	94	111	92
Nb	8	5	1	3	6	5	9	4	7	3	2	4
Zn		59	40	50	43	64	61	35	49	57	40	47
Cu		19	44	37	15	22	18	19	35	18	36	14
Ni		9	21	60	2	35	34	96	56	12	23	16
Ba	215	179	264	295	4	111	146	216	207	343	398	328
V	52	57	61	88	56	90	98	31	91	62	100	56
Cr	55	27	41	121	50	50	74	58	175	12	43	22
Ga	21	15	19	15	18	20	22	17	17	15	17	19

Rare Earth Elements (ppm)

La	23.80	18.90			25.70	22.40		4.10	7.60	14.10		7.10
Ce	46.30	35.50			49.60	46.00		4.90	15.70	26.00		11.20
Pr	4.30	3.60			4.60	7.30		1.10	2.20	3.60		2.90
Nd	17.50	12.50			19.90	27.90		4.40	9.70	12.90		10.50
Sm	2.80	1.40			3.10	7.60			2.20	1.60		2.00
Eu	.60	.20			.60				.70	.30		.30
Gd	2.80	1.40			3.90	8.90		1.20	2.40	1.50		3.20
Dy	2.40	.10			3.50	9.30		1.30	3.40	2.20		2.70
Er	1.40	.50			1.20	2.30		.80	1.60	.60		1.50
Yb	.70								.90	.60		.50

SumREE	1.00	102.60	74.20	-1.00	111.50	131.70	-1.00	17.80	46.40	63.40	-1.00	41.90
Na/K	3.04	3.14	2.84	2.36	9.54	2.88	3.08	3.64	2.67	3.29	2.86	3.16
K/Rb	247.37	262.80	277.58	218.54	424.27	376.22	290.47	304.20	339.51	313.52	271.60	228.99
K/Ba	57.53	61.66	65.90	44.45	954.62	101.68	75.60	46.49	54.11	32.91	30.03	37.70

15451

Trochylite Phase of the Magg Gneiss

	82-36A	82-36B	82-37	82-38	82-42A	82-42B	82-41B	82-45A	82-46A	82-49B	82-51B	82-62A
SiO ₂	49.4	49.66	47.75	47.20	71.10	70.60	69.40	69.40	68.20	71.50	70.10	68.90
TiO ₂	1.4	1.17	1.47	1.47	1.40	1.40	1.23	1.35	1.35	1.18	1.40	1.38
Al ₂ O ₃	15.9	14.11	15.10	14.60	15.70	15.50	15.60	15.20	15.60	15.40	15.10	15.90
Fe ₂ O ₃ T	1.66	1.57	1.67	1.61	2.83	2.49	2.37	2.75	3.34	1.49	2.77	3.33
MnO	1.00	1.06	1.04	1.01	1.04	1.04	1.03	1.05	1.06	1.05	1.04	1.05
MgO	1.38	1.80	1.54	1.55	1.43	1.21	1.44	1.00	1.31	1.58	1.53	1.58
CaO	3.20	3.13	3.37	3.47	3.30	3.42	3.55	2.95	3.91	2.91	2.95	2.84
Na ₂ O	4.22	4.12	4.26	4.04	4.35	4.27	4.35	4.55	4.26	4.86	4.30	4.76
K ₂ O	1.56	1.24	1.61	1.47	1.50	1.49	1.42	1.72	1.44	1.94	1.72	1.81
P ₂ O ₅	.10	.14	.10	.09	.13	.08	.07	.06	.06	.08	.08	.08
LOI	.49	.34	.59	.47	.57	.49	.77	.79	.37	.79	.39	.58
TOTAL	98.65	100.47	99.77	98.97	101.15	99.99	99.23	98.80	99.10	99.56	99.38	100.23

Trace Elements (ppm)

	5	6	1	5	4	1	7	2	10	9
Pb	3	4	1	5	4	1	7	2	10	9
Th	3	4	1	5	4	1	7	2	10	9
U	3	4	1	5	4	1	7	2	10	9
Rb	74	49	73	56	73	61	49	81	47	43
Sr	238	230	235	264	259	351	434	291	307	456
Y	8	9	9	17	6	5	9	9	9	4
Zr	106	170	103	116	112	115	123	145	97	77
Nb	7	4	5	6	4	5	2	4	3	3
Zn	48	37	46	43	42	34	41	42	46	33
Cu	14	11	24	11	13	12	18	14	17	21
Ni	15	5	16	10	25	10	25	2	6	6
Ba	360	341	340	451	366	397	415	237	323	399
V	29	18	36	35	41	34	35	26	41	21
Cr	16	13	10	9	16	7	14	25	7	7
Ga	17	14	15	17	17	17	16	16	17	20

Rare Earth Elements (ppm)

La	19.90	15.03	10.19	15.90	25.27	23.46	9.27	31.17	9.88	7.01	19.73
Ce	41.54	31.99	21.98	35.73	50.63	48.38	82.60	62.90	21.07	16.14	44.33
Pr	3.87	2.43	2.16	3.99	3.73	3.82	1.71	5.10	1.24	1.92	4.98
Nd	14.77	10.55	9.80	14.06	15.45	14.91	7.64	19.88	8.97	6.82	18.92
Sm	2.46	1.72	2.07	2.60	2.08	2.59	1.97	3.18	1.97	1.26	3.73
Eu	.77	.67	.47	.76	.64	1.18	1.63	.86	.51	.57	1.10
Gd	2.31	1.89	2.08	2.55	1.95	1.99	2.46	2.68	1.76	1.43	2.95
Dy	1.17	1.68	1.39	1.50	.98	1.32	.70	1.07	1.00	.72	1.32
Er	.25	1.12	.55	.75	.23	.16	.15	.26	.29	.19	.51
Yb	.27	.89	.05	.32	.03	.03	.44	.27	.05	.05	.24
Lu											

SumREE	87.59	67.97	51.44	78.59	101.58	98.19	107.66	128.14	47.16	36.11	-1.00	97.81
Na/K	2.71	3.32	2.65	2.75	2.90	2.87	3.06	2.65	2.96	2.51	2.50	2.63
K/Rb	174.95	210.02	188.19	206.77	165.98	202.71	250.74	176.23	259.80	374.42	178.43	163.27
K/Ba	24.07	30.19	39.30	28.31	34.01	31.15	28.40	60.23	37.00	40.36	57.34	45.39

00432

Trondhjemite Phase of the Maggo Gneiss

	82-57A	82-64	82-10A	82-66	72-70A	82-70C	82-76	82-77	83-26	83-75	83-96A	83-121
SiO2	69.20	72.70	71.30	70.50	70.00	71.90	72.80	73.00	70.40	69.20	70.20	71.00
TiO2	.75	.20	.28	.23	.28	.31	.29	.16	.30	.25	.38	.34
Al2O3	15.70	15.00	14.80	15.20	14.90	14.50	14.50	14.60	14.90	14.80	15.40	14.20
Fe2O3	2.87	1.57	2.05	1.84	2.34	2.21	2.74	1.50	2.58	2.89	2.27	2.96
MnO	.05	.04	.04	.04	.03	.02	.04	.03	.03	.03	.02	.04
MgO	1.31	.99	1.21	1.12	1.46	1.54	.63	.55	.91	1.72	.93	.96
CaO	3.00	2.65	3.02	2.98	2.95	2.86	2.87	2.72	3.24	3.30	3.23	3.47
Na2O	4.67	4.65	4.49	4.79	4.35	4.31	4.22	4.31	4.55	4.29	4.53	4.06
K2O	1.67	1.61	1.51	1.59	1.67	1.87	1.40	1.72	1.49	1.62	1.95	1.19
F2O5	.09	.01	.04	.08	.04	.03	.09	.01				
LOI	.51	.44	.55	.46	.76	.60	.36	.52	.54	.70	.10	.06
TOTAL	99.45	100.06	99.29	98.87	98.78	100.25	99.94	99.18	98.95	98.80	99.71	98.65

Trace Elements (ppm)

Pb	6	5	4	4	4	8	5	4	10	13	11	10
Th												
U			4	4	1				6	12	8	8
Rb	80	62	55	55	77	77	1	2			2	1
Sr	413	340	333	363	243	285	49	36	45	47	55	41
Y	13	9	6	7	7	4	41	352	297	282	355	183
Zr	88	71	120	59	82	85	162	99	2	1	1	14
Nb	4	4	4	7	4	5	5	109	109	79	140	111
Zn	49	35	34	34	38	28	45	5	5	6	37	5
Cu	28	14	17	7	11	24	35	20	23	23	66	34
Ni	7	13	17	10	23	32			12	32	11	18
Ba	548	329	432	379	279	361	513	679	294	437	698	259
V	45	15	33	21	23	27	19	16	41	54	29	33
Cr	1	5	31	1	45	42	1		43	85	9	9
Ga	19	17	17	17	17	16	14	19	20	14	15	17

Rare Earth Elements (ppm)

La	11.83	11.04	12.58	17.15	15.61	16.07	12.67	18.60	36.60	51.20	33.80
Ce	34.53	21.76	25.98	33.65	28.85	32.08	25.29	35.70	60.70	81.80	66.10
Pr	3.95	2.13	2.87	2.70	1.96	2.94	2.27	4.40	6.40	8.00	6.60
Nd	14.46	8.39	9.61	11.54	9.78	11.89	8.01	14.00	20.30	28.30	25.70
Sm	2.86	1.70	2.32	1.93	1.42	2.24	1.01	1.40	1.70	2.00	3.90
Eu	.92	.46	.71	.60	.65	1.03	.62	.40	.40	.40	.70
Gd	2.42	1.53	2.01	1.58	1.39	2.06	1.19	1.50	2.30	2.30	3.40
Dy	1.74	.86	1.00	.55	.67	1.58	.22	1.60	1.60	1.00	3.30
Er	.53	.20	.35	.04	.24	.64	.01	.30		.80	1.50
Yb	.53									.10	1.00
Lu	.24		.08		.03	.65					

SumREE	79.67	48.39	57.79	71.00	70.11	60.67	71.76	51.29	76.30	130.00	175.50	146.00
Na/K	2.80	2.57	2.97	3.01	2.60	2.30	3.01	2.51	3.06	2.65	2.32	3.41
K/Rb	182.7	250.35	227.85	237.92	192.49	201.55	258.19	396.51	274.79	286.05	294.24	240.87
K/Ba	21.29	45.68	29.01	34.82	49.68	59.46	22.65	21.03	42.06	30.77	23.18	38.13

80453

	Tephroite Phase of the Magg Sphess											
	83-128	83-172	83-173	83-179	83-179	83-180	83-182	83-186	83-188	83-189	83-209	83-217
SiO ₂	72.1	68.80	68.10	69.80	70.50	71.40	70.10	69.60	70.20	70.50	68.50	73.50
TiO ₂	1.15	1.47	1.10	1.20	1.20	1.28	1.28	1.38	1.20	1.26	1.38	1.22
Al ₂ O ₃	15.00	14.10	14.10	14.80	15.50	15.70	15.50	14.50	15.80	14.20	15.00	14.00
Fe ₂ O ₃	1.11	1.61	1.31	1.34	1.39	1.79	2.19	3.13	1.76	3.46	3.60	1.89
MnO	1.01	1.05	1.10	1.02	1.02	1.03	1.02	1.04	1.03	1.05	1.05	1.02
MgO	1.40	1.43	1.77	1.59	1.59	1.68	1.67	1.15	1.65	1.39	1.42	1.27
CaO	2.10	4.34	4.16	3.82	2.90	3.94	3.49	3.74	3.66	3.85	3.00	2.92
Na ₂ O	5.57	7.96	4.23	5.23	5.39	4.89	4.94	4.28	4.57	3.73	4.53	4.53
K ₂ O	1.33	1.22	1.44	1.74	1.60	1.95	1.06	1.17	1.46	1.00	1.84	1.30
P ₂ O ₅	1.01	1.01	1.01	1.01	1.01	1.01	1.01	1.01	1.01	1.01	1.01	1.01
LOI	1.79	1.89	1.84	1.04	1.02	1.52	1.44	1.19	1.06	1.33	1.62	1.84
TOTAL	98.47	99.47	99.85	100.38	99.01	99.98	98.76	99.18	99.17	99.99	99.04	98.51
Trace Elements (ppm)												
Pb	3	5	5	13	6	13	8	6	8	8	8	7
Th	3	4	4	7	3	3	6	3	2	5	4	2
U												
Rb	33	31	39	47	39	22	37	29	35	23	84	28
Sr	491	175	375	397	450	595	610	293	339	270	405	315
Y		9	10	2	1	1	3	6	1	9	8	8
Zr	69	129	98	73	79	87	84	113	79	133	105	65
Nb		4	5	3	4	3	1	5	5	7	3	3
Zn	4	46	58	18	17	24	29	46	24	41	67	15
Cu	17	19	23	15	16	21	26	13	13	55	13	17
Ni		10	19	4	4	6	6	1	6	6	10	10
Ba	281	278	439	535	314	187	244	276	293	206	292	259
V	9	53	64	19	17	24	21	50	25	60	54	13
Cr		19	32	2	3	5	18	2	11	6	18	13
Ga	18	20	21	19	21	22	15	12	19	19	16	15
Rare Earth Elements (ppm)												
La		21.20	19.60				33.40			33.70		2.30
Ce		38.10	34.00				66.90			66.40		1.60
Pr		4.50	4.70				6.80			6.60		1.60
Nd		14.70	18.00				27.10			27.90		1.40
Sm		2.00	2.30				3.10			4.40		1.40
Eu		1.70	1.70				1.40			1.40		1.40
Gd		2.00	3.10				1.80			5.00		1.70
Dy		2.70	3.40				1.40			4.20		1.30
Er		1.80	1.70				1.60			1.00		1.60
Yb			1.70				1.10			1.00		1.00
Lu							1.10			1.00		1.00
SumREE	1.00	95.70	87.20	-1.00	-1.00	-1.00	141.60	-1.00	-1.00	151.60	-1.00	6.90
Na/K	4.19	3.25	2.94	3.01	3.37	5.75	4.57	3.66	3.13	3.73	2.46	3.48
K/Rb	334.48	326.61	306.43	328.19	368.84	320.64	224.07	334.82	346.19	360.83	191.79	372.02
K/Ba	19.28	16.42	27.22	26.99	42.29	37.72	36.73	35.18	41.35	40.29	52.30	41.66

00434

	Trondhjemite Phase of the Maggo Gneiss											
	83-218	83-219	83-242	83-243	83-247	83-249	83-250	83-253	83-258	83-259	83-260	83-261
SiO ₂	70.40	70.10	72.00	70.50	71.60	70.50	70.10	70.10	71.60	73.10	72.00	71.80
TiO ₂	.29	.28	.44	.54	.34	.20	.31	.34	.23	.37	.25	.23
Al ₂ O ₃	15.60	14.40	14.50	15.50	15.70	15.6	15.40	15.70	15.60	14.20	16.00	15.70
Fe ₂ O ₃	1.89	1.66	2.57	3.41	1.88	1.91	2.20	3.30	1.46	2.59	1.55	1.42
MnO	.03	.02	.04	.05	.03	.02	.03	.06	.03	.04	.05	.02
MgO	.79	.32	1.10	1.61	.73	.77	1.04	1.32	.48	.52	.67	.55
CaO	2.97	2.99	3.82	4.25	3.31	3.21	3.31	3.92	2.50	2.89	2.78	2.70
Na ₂ O	5.21	4.48	4.18	4.34	4.79	5.23	4.80	4.35	5.47	4.68	5.40	5.45
K ₂ O	1.29	1.41	1.15	1.38	1.36	1.59	1.48	1.40	1.54	1.05	1.43	1.41
P ₂ O ₅	.18	.04	.07	.11	.08	.15	.10	.09	.06	.11	.07	.07
LOI	.50	.78	.60	.60	.12	.24	.31	.41	.26	.28	.44	.28
TOTAL	99.25	99.30	100.25	100.29	99.94	99.37	99.08	100.49	99.23	99.83	100.52	99.63

Trace Elements (ppm)												
Pb	9		4	5	8	3	13	5	5	8	6	3
Th		15	7	3	6	6	3	2	5	1	1	
U		3					2	1	9	1	2	
Rb	43	50	33	46	46	45	55	48	41	34	34	40
Sr	372	345	361	367	437	464	467	332	643	374	636	400
Y	1	1	7	7	2		3	5	2	7	7	2
Zr	89	70	103	126	80	79	120	93	74	204	54	61
Nb	2	5	2	4	1	1	2	2	3	3	2	
Zn	33		31	42	36	33	41	47	26	42	28	31
Cu	19		22	25	17	15	17	20	14	16	12	14
Ni	4		9	17	5	2	9	10	10	16	12	14
Ba	171	244	211	303	236	327	246	219	287	139	190	272
V	27	21	45	66	23	22	28	57	14	10	15	21
Cr	11	55	18	29	15	5	35	47	14	21	4	15
Ga	18	17	14	17	21	10	16	19	15	15	20	16

Rare Earth Elements (ppm)												
La	25.50				31.90						6.50	14.00
Ce	46.40				62.10						14.20	26.50
Pr	5.20				6.20						1.90	3.40
Nd	20.20				26.10						6.70	12.50
Sm	3.00				2.70						1.30	1.10
Eu	3.30				.50						.10	.80
Gd	2.60				2.50						1.50	2.20
Dy	2.10				1.60						.60	1.40
Er	.60										.40	
Yb	.50										.50	
Lu					.10							

SumREE	106.20	-1.00	-1.00	-1.00	133.70	-1.00	-1.00	-1.00	-1.00	-1.90	33.70	61.90
Na/K	4.12	3.18	3.70	3.14	3.52	3.29	3.24	3.11	3.55	4.46	3.78	3.87
K/Rb	237.91	195.07	275.87	254.50	245.36	293.23	223.32	242.05	327.70	235.51	329.66	285.41
K/Ba	62.61	47.97	44.41	37.80	47.82	90.35	49.93	53.05	44.53	62.69	62.46	43.02

00455

Thondhjeite Phase of the Magg Greiss

	83-267	83-264	83-265	83-269	83-275	83-277	83-278	83-279	83-281	83-282	83-293	83-294
SiO ₂	71.80	69.70	70.20	72.50	70.50	72.10	71.10	70.40	72.10	72.10	70.90	71.60
TiO ₂	.13	.56	.33	.33	.26	.22	.23	.34	.19	.25	.38	.16
Al ₂ O ₃	14.80	15.80	14.70	14.20	14.50	14.90	14.70	15.00	14.80	14.60	15.00	15.90
Fe ₂ O ₃	2.81	2.90	3.08	1.75	2.22	1.76	1.66	2.38	2.13	2.57	3.17	1.05
Mn	.04	.05	.05	.04	.05	.03	.03	.05	.02	.04	.05	.01
MgO	1.41	1.04	1.09	1.04	1.37	1.12	1.14	1.52	1.29	.82	1.19	.41
CaO	3.27	3.81	3.71	3.43	2.89	3.02	2.83	3.05	3.02	2.87	3.50	3.17
Na ₂ O	4.98	4.68	4.58	4.03	4.64	4.84	4.72	4.73	4.87	4.30	4.44	4.93
K ₂ O	.93	1.32	1.13	1.20	1.58	1.47	1.55	1.49	1.45	1.56	1.30	1.80
P ₂ O ₅	.12	.15	.11	.10	.09	.16	.10	.12	.09	1.10	.08	.04
LOI	.43	.27	.30	.58	.72	.37	.26	.45	.21	.72	.29	.29
TOTAL	99.57	100.28	99.24	99.18	98.94	99.89	98.52	99.53	100.27	99.93	100.30	99.36

Trace Elements (ppm)

Pb	6	5	10	6	10	3	7	8	6	6	10	7
Th	6	3	3	4	9	2			2	7		
U	4				6	1		1			5	
Rb	15	54	29	38	49	55	57	60	55	41	44	36
Sr	367	373	314	387	330	393	372	335	319	281	220	349
Y	13	8	8	2	4	2	3	4	2	10	12	1
Zr	193	143	150	157	96	90	85	112	85	145	70	56
Nb	6	7	5	3	4	5	4	2	4	8	6	2
Zn	43	57	45	22	37	34	35	44	40	36	42	13
Cu	40	13	14	25	12	12	15	16	12	16	15	16
Ni		2	1		20	14	12	20	16	7	17	1
Ba	163	265	196	415	419	284	374	361	268	608	180	477
V	10	38	40	23	24	21	23	31	29	39	52	16
Cr		5	13	11	17	13	21	40	21	27	59	8
Ga	15	16	19	18	18	15	1	18	19	17	19	18

Rare Earth Elements (ppm)

La	42.40	22.50	41.20		43.90	14.70	15.10	29.50	25.90			
Ce	73.20	42.80	73.40		80.10	24.40	20.90	50.70	43.60			
Pr	5.40	3.80	6.80		8.60	2.70	3.20	6.60	5.90			
Nd	23.50	15.00	27.90		31.30	9.20	10.80	21.90	16.10			
Sm	3.00	2.50	4.00		4.10	1.30	1.10	2.80	2.00			
Eu	1.20	.30	.20		.70	.40	.70	.10	.10			
Gd	3.00	1.30	4.60		2.30	.90	1.60	2.90	1.70			
Dy	2.00	1.40	3.00		1.50	.40	1.20	1.40	1.30			
Er	.60	1.10	1.70		.40	.20		.60	.40			
Yb	.10	.80			.20							
Lu					.20		.10					

SumPEF	154.40	91.50	162.80	-1.00	173.10	54.20	54.70	116.50	97.00	-1.00	-1.00	-1.00
Na/K	5.35	3.55	3.88	3.36	2.95	3.29	3.05	3.17	3.36	2.76	3.42	2.74
K/Rb	514.54	206.69	391.71	269.16	242.82	206.77	214.39	216.94	218.79	315.77	245.20	481.89
K/Ba	47.35	41.34	49.96	24.00	31.29	42.96	34.39	34.25	44.90	21.36	59.94	34.18

88456

Trochjemitic Phase of the Maggo Gneiss

	83-298	83-303	83-304	83-306	83-312	83-313	83-315	83-316
SiO2	68.90	71.20	71.50	71.40	70.50	73.00	71.10	73.10
TiO2	.40	.40	.24	.27	.24	.23	.24	.22
Al2O3	15.70	14.70	14.80	15.00	15.80	14.00	14.80	14.20
Fe2O3	2.16	2.21	1.97	1.96	1.72	1.98	1.67	1.41
MnO	.02	.04	.04	.03	.02	.04	.02	.01
MgO	1.14	1.35	1.07	1.04	.86	.77	.42	.45
CaO	4.20	3.42	2.98	2.93	2.84	2.86	2.92	2.66
Na2O	4.00	4.49	4.58	4.56	5.65	4.41	5.20	4.00
K2O	1.36	1.37	1.47	1.46	1.55	1.86	1.24	1.60
P2O5	.10	.07	.11	.10	.02	.07	.06	.06
LOI	.37	.48	.49	.18	.26	.18	.37	.30
TOTAL	98.35	99.73	99.25	98.93	99.26	99.42	98.24	98.83

Trace Elements (ppm)

Pb	6	14	9	6	5	10	11	9
Th	4	11	5	6	2	15	3	1
U		2						
Rb	59	63	54	50	38	56	46	32
Sr	581	319	368	366	703	301	650	642
Y		5	7	6	2	3	3	2
Zr	170	65	100	95	80	162	92	63
Nb		4	5	5	2	2	2	2
Zn	31	31	34	33	31	47	29	22
Cu	17	17	19	15	13	16	16	13
Ni	5	11	13	14				
Ba	571	275	307	309	275	771	248	244
V	33	36	28	28	25	20	24	17
Cr	15	24	21	22	15	4	6	1
Ga	21	14	17	18	23	20	23	19

Rare Earth Elements (ppm)

La	61.20	21.10	25.70					
Ce	104.10	35.60	41.70					3.20
Pr	12.90	5.10	4.70					2.90
Nd	36.10	15.60	16.50					.08
Sm	3.30	1.20	1.80					2.20
Eu	1.20	.70						.10
Gd	2.90	2.10	2.40					.30
Dy	1.40	1.80	2.20					.80
Er	1.00	.50	.90					
Yb			.30					.40
Lu								

SumREE	224.10	83.70	96.20	-1.00	-1.00	-1.00	-1.00	9.98
Na/K	2.94	3.28	3.12	3.12	3.65	2.35	4.19	3.18
K/Rb	205.21	180.47	225.92	247.28	338.79	279.68	225.77	415.05
K/Ba	19.77	41.34	39.74	39.21	46.79	20.44	41.51	54.43

00487

	Granodiorite Phase of the Maggo Gneiss											
	82-44	82-47	82-48	82-49A	82-51C	82-51D	82-51E	83-176	83-191	83-194	83-195	83-197
SiO ₂	72.70	72.26	72.06	72.30	71.60	70.90	71.10	71.50	69.60	73.30	72.90	70.60
TiO ₂	.27	.27	.21	.15	.20	.31	.17	.17	.32	.18	.20	.45
Al ₂ O ₃	14.70	14.86	15.26	15.60	14.90	15.00	15.30	15.00	15.30	13.60	14.50	15.00
Fe ₂ O ₃	1.54	1.49	1.37	1.57	2.12	2.35	1.96	1.60	1.72	1.76	2.12	2.21
MnO	.07	.02	.02	.03	.03	.03	.04	.03	.07	.04	.05	.03
MgO	.50	.52	.52	.58	1.07	1.26	1.05	.54	.79	.50	.72	1.01
CaO	2.30	2.60	2.66	2.74	2.66	2.69	2.79	2.60	2.98	2.48	2.48	2.88
Na ₂ O	4.46	4.38	4.82	4.05	4.31	4.60	4.49	4.85	4.40	4.37	4.15	4.39
K ₂ O	2.56	2.46	2.17	2.01	2.39	2.19	2.20	2.48	2.42	2.32	3.08	2.18
P ₂ O ₅	.04	.04	.03	.07	.04	.16	.09	.06	.08	.06	.10	.14
LOI	.67	.35	.47	.59	.44	.40	.40	.78	.74	.25	.29	.57
TOTAL	99.93	99.09	99.59	100.29	99.76	99.87	99.59	99.71	98.37	98.86	100.59	99.46

Trace Elements (ppm)

Pb	9	5		3	19	15	14	28	3	12	19	7
Th					5	5	4			10	7	5
U				4				6	1			
Rb	73	42	40	47	81	79	81	45	58	68	99	63
Sr	448	458	512	365	231	236	261	423	667	192	227	652
Y		3	3	5	16	9	12	4	3	11	16	4
Zr	94	114	106	92	82	93	90	95	104	102	104	143
Nb	2				5	6	8	6	4	5	13	5
Zn	35	45	36	39	36	37	32	58	33	31	29	50
Co	16	38	14	16	11	10	8	12	24	14	11	20
Ni				2	10	12	11	1		2	4	3
Ba	608	655	350	355	433	410	484	832	888	494	547	699
V	20	24	18	22	23	28	22	24	37	15	23	43
Cr	1	12		9	8	4		3	8	10	2	9
Ga	18	21	20	18	16	13	16	20	20	15	16	21

Rare Earth Elements (ppm)

La	16.23	18.30	11.47	9.89								
Ce	32.20	37.49	24.48	19.77					48.00			43.20
Pr	3.31	2.92	2.51	1.61					81.20			84.60
Nd	11.65	12.18	8.80	7.07					9.50			8.60
Sm	1.96	2.17	1.56	1.05					33.40			30.10
Eu	.66	1.18	.41	.64					2.60			3.20
Gd	1.62	2.05	1.20	1.17					.20			.70
Dy	.63	.72	.77	.46					2.30			1.10
Er	.12	.41	.15						2.20			1.40
Yb		.11							.70			.60
Lu												

ΣREE	68.60	77.53	51.35	41.66	-1.00	-1.00	-1.00	-1.00	180.10	-1.00	-1.00	173.50
Na/K	1.74	1.78	2.22	2.41	1.80	2.10	2.04	1.96	1.82	1.88	1.35	2.01
K/Rb	303.51	486.08	450.22	354.92	244.87	230.06	225.41	457.48	346.27	283.21	258.25	287.17
K/Ba	34.94	31.18	51.47	47.00	45.82	44.34	37.73	27.74	22.62	39.98	46.74	25.88

01458

Granodiorite Phase of the Maggo Gneiss

	83-208	83-234	83-275	83-285	83-288	83-289
SiO ₂	73.00	71.30	73.00	73.80	68.70	68.10
TiO ₂	.15	.28	.20	.20	.56	.27
Al ₂ O ₃	15.20	14.00	14.60	13.90	13.70	14.50
Fe ₂ O ₃	.73	1.99	1.44	.38	4.76	4.38
MnO	.02	.03	.03	.04	.07	.08
MgO	.25	.53	.92	1.00	2.10	2.35
CaO	2.60	1.81	2.30	2.25	2.43	3.35
Na ₂ O	4.89	3.48	4.73	4.28	3.49	3.72
K ₂ O	2.35	4.46	2.24	2.20	2.54	2.10
P ₂ O ₅	.03	.12	.07	.06	.05	.10
LOI	.66	.29	.55	.96	.40	.83
TOTAL	99.88	98.29	100.08	99.07	98.80	99.78

Trace Elements (ppm)

Pb	2	16	6	8	6	8
Th		17	1	7	1	10
U						
Rb	45	95	71	44	113	104
Sr	490	402	316	258	175	33
Y		1	5	14	2	8
Zr	40	216	73	134	136	97
Nb		3	5	6	9	9
In	10	36	33	28	77	68
Cu	14	14	14	17	16	26
Ni	3		17	7	35	21
Ba	614	1626	421	667	351	141
V	11	21	15	38	84	91
Cr	1		23	43	138	54
Ga	17	16	14	16	20	18

Rare Earth Elements (ppm)

La	.60	88.80	20.70	53.20		
Ce		153.20	33.40	95.60		
Pr	.40	14.40	4.40	10.10		
Nd	1.00	44.20	14.20	35.20		
Sm		1.90	1.20	4.10		
Eu	.30		.80	.40		
Gd	.60	1.60	2.10	3.80		
Tb	.70	2.20	1.80	3.70		
Er	.20	.30	.30	1.80		
Yb				.40		
Lu						

SumREE	3.80	306.60	78.90	208.30	0.00	-1.00
Na/K	2.08	.78	2.11	1.95	1.37	1.77
K/Rb	443.24	411.26	265.57	414.95	189.91	169.20
K/Ba	31.76	22.76	44.16	27.37	60.06	123.60

00480

D. Bridgwater 1981 Samples of Magg Gneiss from Dyle Island

	DB-81-1A	DB-81-1B	DB-81-1C	DB-81-1D	DB-81-1E	DB-81-1F	DB-81-1G	DB-81-1H	DB-81-2A	DB-81-2C	DB-81-4C	DB-81-4D
SiO2	70.18	71.20	70.50	71.70	69.80	71.70	71.00	78.10	70.90	70.20	67.80	63.40
TiO2	.21	.24	.25	.26	.60	.29	.38	.05	.17	.42	.41	.36
Al2O3	14.80	14.70	14.60	14.60	15.10	14.70	14.60	13.00	14.90	14.20	15.00	15.20
Fe2O3	3.71	2.91	2.63	2.91	3.81	3.04	2.98	.73	2.94	3.23	4.24	3.47
MnO	.06	.04	.04	.04	.05	.04	.04	.02	.05	.04	.06	.05
MgO	1.05	.98	.85	.96	1.17	1.03	.99	.25	.90	1.22	1.81	1.46
CaO	3.54	3.68	3.79	3.71	3.71	3.83	3.47	2.59	3.64	3.51	5.07	4.35
Na2O	4.14	4.65	4.07	4.01	4.10	4.01	4.00	3.97	4.18	3.93	4.01	3.77
K2O	1.36	1.27	1.12	1.24	1.57	1.24	1.16	1.81	1.24	1.49	1.33	1.72
Li2O	.10	.08	.06	.09	.15	.06	.08		.08	.09	.11	.08
LOI	.42	.39	.28	.35	.44	.42	1.27	.70	.69	.71	.71	.82
TOTAL	99.67	100.24	98.53	99.87	100.50	100.36	100.70	101.52	99.69	99.04	101.20	99.49

Trace Elements (ppm)

Pb	11	4	9	5	7	2	5	8	15	8	4	7
Th	6	6	8	7	6	5	6	9	10	9	7	9
U												
Rb	88	54	54	51	91	83	56	2	77	3	42	4
Sr	136	194	199	185	248	185	179	47	94	94	237	53
Y	14	8	8	13	4	8	6	134	169	168	237	228
Zr	152	119	103	115	164	116	119	3	7	6	7	5
Nb	7	6	4	6	4	5	5	41	127	138	121	108
Zn	51	42	37	36	67	40	36	4	9	7	5	4
Cu	10	14	12	12	23	10	13	13	49	37	49	36
Ni	4	2	4	5	5	2	2	16	11	48	28	59
Ba	179	321	302	290	437	286	341	339	281	363	334	11
V	35	29	28	30	40	31	32	2	29	31	53	45
Cr	5	5	1	1	3		4		1	1	18	15
Ga	16	16	18	18	19	17	15	14	16	15	21	18

Rare Earth Elements (ppm)

La	8.37	10.56	3.86	7.72	12.39	8.76	9.59	10.11	11.84	6.85	7.75	7.75
Ce	20.29	23.16	10.88		28.30	18.69	23.29	21.17	23.77	16.08	20.70	20.70
Pr	3.19	2.84	1.34	1.28	3.13	2.29	2.74	1.23	2.65	2.50	2.20	2.20
Nd	10.46	11.11	6.36	10.08	13.98	9.22	11.16	7.66	10.50	8.26	12.63	12.63
Eu	2.20	2.45	1.90	3.93	2.14	1.97	2.19	1.38	1.93	1.82	2.22	2.22
Gd	.36	.53	.47	.68	.20	.52	.70	1.38	1.93	1.82	2.22	2.22
Dy	1.74	1.84	1.46	4.07	1.97	1.93	1.88	1.22	1.79	2.16	3.07	3.07
Er	1.97	1.24	1.18	1.16	1.61	1.93	1.68	1.79	1.81	2.36	6.93	6.93
Yb	1.30	.95	.77	6.05	1.10	1.70	1.19	.61	1.48	2.65	4.29	4.29
Lu	1.45	.84	.74	3.07	.84	1.58	1.23	.74	1.38	1.33	2.45	2.45
SumRE	.96	.93	.66	6.58	.54	1.72	.84	.70	1.00	1.49	2.97	2.97

SumRE	54.17	58.05	30.44	50.69	67.01	51.60	57.89	46.66	60.03	48.04	71.75	71.75
Na/K	3.04	3.66	3.63	3.25	2.61	3.23	3.49	2.19	3.37	2.64	3.02	3.25
K/Rb	128.26	195.18	172.13	201.78	143.18	163.35	171.91	319.60	133.65	131.55	262.80	191.03
K/Ba	67.05	32.83	30.78	35.47	26.75	35.98	28.23	44.31	36.62	34.06	33.05	34.32

00460

	D. Bridgwater 1981 Maqgo Gneiss Samples											
	DB81-5A	DB81-5B	B81-21A	B81-21B	DB81-22	B81-23A	B81-23E	DB81-24	DB81-25	DB81-27	DB81-28	DB81-29
SiO2	76.40	71.50	71.40	73.70	72.70	65.90	68.20	68.70	69.60	56.90	55.50	57.80
TiO2	.20	.20	.27	.22	.31	.49	.51	.37	.32	.83	1.03	.70
Al2O3	12.77	15.20	14.60	14.20	14.50	15.50	15.20	15.80	16.20	16.70	16.80	15.60
FeO	.50	.70	.10		3.10	.40	.30	.10	.10	2.20	2.40	2.30
MnO	1.41	1.90	2.60	2.30		4.10	4.40	3.10	3.10	5.50	6.10	5.00
MgO	.05	.05	.05	.05	.03	.08	.09	.05	.04	.13	.13	.13
CaO	.68	.87	.89	.71	.99	1.95	2.06	1.31	1.17	3.96	3.37	4.47
Na2O	3.10	3.72	3.75	3.44	4.24	5.25	5.37	4.81	4.65	7.73	8.12	7.86
K2O	2.90	3.30	3.50	3.60	3.20	3.10	2.90	3.20	4.20	3.40	3.10	2.90
P2O5	1.05	1.39	1.36	1.37	1.05	1.31	1.30	1.12	1.12	1.48	1.48	1.16
LOI	.11	.10	.10	.09	.11	.14	.16	.14	.16	.23	.31	.16
	.40	.50	.10	.10	.10	.20	.20	.20	.20	.70	.70	.90
TOTAL	99.07	99.55	98.72	99.78	100.34	98.42	98.69	98.90	100.56	99.76	99.04	98.98

	Trace Elements (ppm)											
Pb	7	9	8	5	3	3	4	4	9	2	3	8
Th	5	5	7	3	5	3	4	1	2	2	5	4
U												
Rb	43	66	66	59	39	55	53	39	31	43	40	34
Sr	210	219	184	199	200	148	109	285	252	246	288	225
Y	6	5	10	8	10	10	15	6	7	23	28	18
Zr	79	110	104	111	140	122	132	127	149	132	217	103
Nb	3	5	6	5	4	6	6	4	4	8	9	6
Cu	35	43	40	34	33	64	67	50	43	95	102	84
Ni	22	2	36	30	120	61	50	118	75	47	41	39
Li	5	7	8	7	/	29	31	13	11	59	27	81
Ba	11	12	21	26	21	20	31	13	17	15	19	14
V	297	210	309	426	258	306	287	261	262	269	353	149
Co	20	29	29	19	23	58	61	35	35	126	18	136
Cr	16	17	36	75	28	24	19	12	23	18	19	38
Ca	15	17	23	24	18	52	54	26	34	87		141
Ga	12	16	17	17	15	16	20	18	17	15		18

	Element Ratios											
Na/K	3.76	2.37	2.57	2.63	3.05	2.37	2.23	2.86	3.75	2.30	2.09	2.50
K/Rb	202.70	174.82	171.05	192.75	223.47	197.72	203.61	238.39	299.91	285.71	307.14	283.21
K/Ba	29.35	54.94	36.54	26.70	33.78	35.54	37.60	35.62	35.49	45.67	34.80	64.63

00482

D. Bridgwater 1981 Maggo Swiss Samples

	DB91-30	DB91-31	DB91-32	DB91-9A	DB91-9B	DB91-9C	DB91-9D	DB91-9E	DB91-9F	DB91-9G	DB91-10A	DB91-10B
SrO2	55.30	56.60	69.40	62.70	61.80	69.50	67.90	72.60	67.90	72.70	72.30	69.60
TiO2	.90	.69	.32	.45	.49	.35	.41	.17	.29	.07	.26	.32
Al2O3	18.42	14.60	15.00	17.00	16.80	15.00	15.60	15.80	15.70	16.50	15.40	15.20
Fe2O3	2.73	2.50	.73	.70	.80	.20	.20	.30	.60	.20	.20	.20
FeO	6.09	5.50	2.00	4.30	4.40	2.80	3.70	1.00	2.30	.70	2.30	3.00
MnO	.14	.14	.04	.09	.10	.05	.07	.02	.06	.01	.04	.04
MgO	4.36	5.57	.99	2.47	2.40	1.07	1.71	.42	1.48	.23	.71	.93
CaO	3.41	3.54	4.58	5.96	6.11	4.18	4.44	3.51	4.13	3.65	3.63	4.26
Na2O	2.99	2.60	3.40	4.10	4.00	4.00	3.90	4.30	4.10	5.20	4.40	3.90
K2O	1.32	.97	1.15	1.23	1.21	1.25	1.32	1.42	1.20	.84	1.27	1.22
F2O5	.23	.12	.12	.11	.12	.10	.12	.06	.06	.02	.09	.11
LOI	.80	.77	.50	.20	.20	.20	.40	.40	.70	.30	.10	.20
TOTAL	79.26	98.71	99.00	99.32	98.43	99.20	99.77	99.40	98.52	100.22	100.70	98.78

Trace Elements (ppm)

	3	6	4	8	5	5	7	8	8	10	4	6
Pb	3	6	4	8	5	5	7	8	8	10	4	6
Th	3	1	2	2	5	5	4	5	6	3	6	5
U												
Rb	30	16	40	38	37	55	49	45	44	16	43	49
Sr	260	213	268	253	255	276	283	328	437	355	186	222
Y	23	17	6	13	14	7	16	2	6		4	8
Zr	108	84	140	84	108	135	126	90	82	59	113	116
Nb	8	6	4	5	4	31	4	2	2		4	3
Zn	96	95	42	72	74	49	64	29	50	12	51	52
Cu	47	43	2	14	2	6	3	10	2	2	2	6
Ni	50	126	7	22	22	9	18	2	17	2	2	7
La	15	14	13	7	13	24	25	4	8	1	14	15
Ba	319	147	285	265	315	389	303	263	285	159	288	236
V	166	137	23	61	88	35	59	14	50	4	22	35
Ce	37	33	8	19	25	32	39	9	16	2	20	15
Cr	100	212	10	51	35	20	42	10	34	8	10	17
Ga	19	17	13	20	19	16	18	15	17	13	15	17

Element Ratios

Na/K	2.20	2.68	2.96	3.33	3.31	3.20	2.95	3.03	3.42	6.19	3.46	3.20
K/Rb	365.24	503.25	238.65	268.69	271.47	188.66	223.62	261.94	226.39	435.80	245.17	206.68
K/Ba	34.35	54.78	33.50	38.53	31.89	35.90	36.16	44.82	34.95	43.85	36.61	42.91

88788

D. Bridgwater 1981 Magg's Gneiss Samples

	BB1-10C	BB1-10D	BB1-10E	BB1-10F	BB1-35A	BB1-35B	BB1-35C	BB1-35D
SiO2	50.10	50.40	51.80	52.20	51.40	51.00	52.40	51.90
TiO2	.25	.33	.26	.27	.25	.24	.21	.24
Al2O3	21.80	15.30	15.30	14.50	14.90	15.00	13.10	15.10
Fe2O3	3.00				.40			
FeO	3.00	2.90	2.70	2.40	1.40	1.80	1.40	1.90
MnO	.07	.04	.03	.03	.04	.04	.04	.03
MgO	.11	.87	.70	.57	1.10	1.09	1.02	1.16
CaO	17.80	3.79	3.82	3.27	3.10	3.12	2.83	2.98
Na2O		3.90	3.80	3.90	3.70	4.00	4.40	4.20
K2O	2.44	1.43	1.22	1.52	1.50	1.52	1.45	1.52
F2O5	.10	.10	.10	.09	.09	.09	.09	.12
LOI	.70	.20	.10	.10	.40	.40	.50	.50
TOTAL	99.15	99.26	99.83	98.85	98.38	98.30	99.84	99.65

Trace Elements (ppm)

Pb	23	5	5	6	11	12	11	12
Th	9	4	7	4	5	9	5	2
U								
Rb	73	53	47	44	55	59	62	62
Sr	302	204	186	203	369	360	273	297
Y	5	6	4	5	7	7	7	4
Zr	84	131	102	114	95	98	101	110
Nb	4	4	4	3	4	3	7	4
Zn	108	55	50	40	34	44	49	47
Cu	9							
Ni		3	4	6	18	22	19	2
La	17	15	24	17	21	17	13	18
Ba	225	318	281	400	324	277	161	10
V	71	30	26	19	21	17	17	169
Ce	29	14	37	11	21	13	13	20
Cr	15	13	13	12	23	27	23	12
Ga	31	16	17	11	13	13	15	36

Element Ratios

Na/K		2.73	3.11	2.57	2.47	2.63	3.03	2.76
K/Rb	277.46	223.97	215.47	286.76	226.70	213.86	194.14	203.51
K/Ba	90.07	37.33	36.04	31.54	38.43	43.96	74.76	74.66

82-683

	Hopedale Dyles											
	82-43A	82-58	82-59	82-69A	82-70B	82-65B	83-137	83-170	83-192	83-199	83-206	83-212
SiO ₂	54.66	50.00	56.10	49.10	52.90	51.80	51.00	45.60	49.30	49.00	49.50	49.70
TiO ₂	.95	.67	.40	.99	.84	1.06	1.05	1.31	1.18	.80	.84	.95
Al ₂ O ₃	15.66	13.70	15.60	14.50	9.30	11.82	14.50	14.40	13.60	13.60	13.70	13.50
Fe ₂ O ₃	2.75	5.50	1.05	4.87	11.82	3.50	2.50	4.00	2.98	2.33	2.90	2.91
FeO	7.84	8.89	5.74	8.63		11.27	8.20	10.14	10.29	8.46	8.57	8.58
MnO	.20	.26	.14	.70	.27	.24	.17	.27	.22	.19	.19	.19
MgO	5.69	8.52	6.26	7.69	11.08	6.87	7.52	8.31	6.44	8.74	8.53	8.00
CaO	7.84	7.14	7.08	10.27	5.70	9.30	8.96	9.84	9.80	9.54	10.02	10.68
Na ₂ O	2.55	2.55	3.65	2.99	1.05	1.85	3.13	2.28	2.52	2.57	2.74	2.34
K ₂ O	1.01	1.20	.92	1.04	2.80	1.14	1.22	1.74	1.38	.98	1.42	1.20
P ₂ O ₅	.13	.03	.04	.03	.09	.08	.07	1.74	1.38	.98	1.42	1.20
LOI	2.09	1.47	1.12	1.40	1.05	1.80	1.69	2.86	1.59	2.25	2.21	2.33
TOTAL	99.40	99.95	99.70	101.41	99.61	100.59	100.01	100.97	99.41	98.51	100.71	100.41

Trace Elements (ppm)												
Pb			6			13	4	8	9	5	3	7
Th						10	1	9	4	2		
U						7						
Rb	20	22	8	8	115	17	17	34	24	27	33	31
Sr	221	149	154	70	64	108	253	182	94	123	142	142
Y	22	25	18	28	26	26	27	55	34	19	23	19
Zr	82	40	64	53	60	55	62	96	75	50	52	38
Nb	5	7	3	7	11	5	4	16	9	5	12	7
In	126	143	64	97	107	106	94	176	103	85	99	90
Cu	113	13	15	70	186	122	64	34	63	69	36	39
Ni	82	87	59	112	309	86	103	85	74	139	145	86
Ba	215	128	156	76	340	94	204	205	41	73	64	106
V	223	275	144	307	145	255	245	285	313	265	269	271
Cr	39	221	155	130	812	98	216	429	143	311	234	221
Ga	18	17	17	17	15	8	17	31	19	16	14	14

Rare Earth Elements (ppm)												
La	10.66	3.20	6.84	3.12	4.64	13.30	4.20	38.00	6.70	4.00	11.00	5.20
Ce	25.84	7.82	14.61	7.90	12.66	30.50	5.20	81.60	16.80	9.10	27.60	12.00
Pr	3.13	1.14	1.69	1.41	1.67	3.80	1.70	11.00	2.40	1.70	2.60	1.20
Nd	13.90	5.31	7.05	6.54	7.72	18.00	3.10	47.20	12.70	7.70	16.10	8.70
Sm	3.46	1.79	1.77	2.44	2.90	4.50	2.40	10.80	4.70	2.00	3.60	2.70
Eu	1.27	.70	.58	1.00	.74	1.40	1.10	2.00	1.00	.60	1.20	.50
Gd	3.82	2.31	2.11	3.28	3.40	5.60	5.00	10.70	6.00	3.40	4.80	3.40
Dy	3.52	2.39	1.77	3.84	3.26	5.50	5.20	10.50	7.00	4.10	5.60	4.00
Er	1.76	1.39	1.19	2.10	1.93	3.10	2.70	5.70	3.90	1.60	2.50	2.30
Yb	1.70	.97	.91	1.67	1.56	1.50	1.50	3.60	3.00	1.20	1.50	1.20
Lu	.25		.02									
SumRE	70.72	28.24	39.14	34.67	41.46	87.20	37.10	221.10	64.20	35.40	76.50	41.20
Hg#	33.16	41.44	49.90	37.47	51.02	32.27	41.85	37.35	33.18	45.29	43.28	41.67

00484

	Honedale Dykes					
	83-228	83-245	83-246	83-267	83-292	83-311
SiO ₂	48.90	48.70	47.80	47.60	47.40	48.20
TiO ₂	.80	1.08	1.16	.73	.83	1.06
Al ₂ O ₃	13.00	14.60	14.20	13.90	13.40	14.20
Fe ₂ O ₃	4.05	3.70	4.01	3.57	.66	2.20
FeO	8.44	9.82	9.08	7.58	11.56	10.68
MnO	.26	.21	.21	.19	.20	.21
MgO	8.31	7.23	7.46	8.39	8.08	7.14
CaO	10.08	9.88	10.27	11.04	10.32	9.80
Na ₂ O	2.57	3.01	3.12	3.06	2.69	3.11
K ₂ O	.98	.58	.60	1.04	1.27	.93
P ₂ O ₅	.08	.11	.11	.05	.04	.04
LOI	1.79	1.73	1.43	1.34	1.60	1.63
TOTAL	99.26	100.65	99.95	98.51	98.27	99.25

Trace Elements (ppm)						
Pb	8	1	12	1	5	2
Th	7	2	5	5		
U	1		1	1		
Rb	23	22	16	19	14	8
Sr	140	100	90	94	108	104
Y	30	25	27	27	22	28
Zr	46	62	61	46	50	74
Nb	6	4	3		5	6
Zn	115	101	97	87	107	108
Cu	144	96	82	36	36	54
Ni	84	107	110	128	152	101
Ba	40	11		51	4	25
V	281	288	285	330	294	251
Cr	183	76	92	250	212	56
Ga	15	19	17	15	17	18

Rare Earth Elements (ppm)						
La	9.20	4.90		3.10	4.00	7.10
Ce	22.60	10.40		6.40	9.50	16.70
Pr	2.90	1.20		1.60	1.30	3.40
Nd	12.80	8.30		5.50	7.40	14.20
Sm	2.70	2.60		2.10	2.20	3.70
Eu	.90	.70		.60	.80	1.20
Gd	5.00	4.60		3.10	3.10	6.50
Dy	5.40	5.20		4.90	5.10	7.40
Er	2.90	2.60		2.80	2.40	3.30
Yb	2.10	1.80		1.90	1.60	1.20
Tu						

SumRE	66.50	42.30	-1.00	32.00	37.90	64.70
Mg#	40.75	35.48	36.13	43.70	39.93	36.06

00485

	Anorthosite Enclaves						
	83-50	83-101	83-241	83-254	83-268	83-270	83-271
SiO ₂	58.70	73.70	47.10	74.70	49.90	44.30	50.10
TiO ₂	.23	.16	.29	.02	.25	.16	.44
Al ₂ O ₃	17.00	17.50	13.10	13.90	24.30	19.00	16.70
Fe ₂ O ₃	3.58	1.54	7.07	.75	3.86	8.40	4.77
FeO							
MnO	.04	.03	.13	.07	.07	.14	.07
MgO	2.96	.90	8.41	.05	2.91	8.08	3.79
CaO	7.57	4.02	11.37	1.60	13.05	11.23	7.02
Na ₂ O	3.63	4.08	2.66	3.93	2.75	1.63	4.14
K ₂ O	1.53	.58	1.48	4.78	.87	2.32	.95
P ₂ O ₅	.04		.01	.01	.02	.06	.10
LOI	1.70	.47	1.98	.33	1.25	2.89	.44
TOTAL	99.20	98.98	98.70	99.74	99.23	98.23	98.72
							0.00

Trace Elements (ppm)							
Pb	11	11	3	15	12	13	
Th	6	4	8	14	3	1	
U			2				
Rb	53	6	47	84	20	101	11
Sr	255	365	240	171	176	174	369
Y	6	3	11	11	6	7	8
Zr	42	12	2	52	13	15	90
Nb	3	2	1		4	2	3
Zn	38	17	68	3	31	68	41
Cu	11	25	6	20	11	4	34
Ni	60	2	170		34	177	57
La	3	4			6		9
Ba	253	124	84	503	55	148	131
V	37	22	73		98	87	113
Ce	16	29			32	5	70
Cr	74	4	256	7	125	73	147
Ga	17	14	15	14	19	13	18

Element Ratios							
Na/K	2.37	7.03	1.80		3.15	.70	4.36
K/Rb	239.63	802.43	251.39		361.09	190.68	716.91
K/Ba	50.20	38.83	146.26		131.31	130.12	60.20

00486

Pegmatites from the Maggo Gneiss

	82-428	82-49A	82-49C	82-61	82-62C	82-69C	83-96B	83-183	83-235	83-237	83-251	83-198
SiO2	74.30	72.90	78.60	73.80	72.90	72.30	70.50	74.30	76.00	75.90	73.60	73.00
TiO2	.09	.05		.09	.06	.20	.20	.12	.03	.06	.06	.01
Al2O3	14.30	14.70	12.00	14.60	14.20	15.20	15.00	14.20	12.80	13.50	13.10	13.80
Fe2O3	.31	.40	.73	.66	.48	1.91	1.09	.50	.34	1.03	.48	.51
MnO	.01	.01	.01	.01	.01	.04	.01	.01	.01	.02	.00	.00
HgO	.12	.13	.09	.10	.10	.61	.44	.11	.09	.20	.18	.11
CaO	1.99	2.16	2.04	1.18	1.18	2.56	2.45	3.09	1.20	2.76	2.77	.80
Na2O	3.99	4.35	3.53	3.85	3.36	4.27	3.97	4.77	3.16	4.44	4.38	3.39
K2O	4.16	3.58	2.51	5.62	5.99	2.70	3.48	.66	5.33	.98	.69	6.96
P2O5	.02	.02		.02	.05	.03	.09	.03	.04	.01	.02	.02
LOI	.70	.62	.36	.43	.73	.55	1.16	.32	.42	.44	.24	.22
TOTAL	99.97	98.92	99.48	100.35	99.06	100.37	98.39	98.11	99.42	99.36	95.52	98.80

Trace Elements (ppm)

Pb	9	9	7	12	6		8	12	24	14	9	16
Th				1	4		5	7	13	9		2
U				1	5		1		1			
Rb	86	54	39	115	71	68	59	11	84	11	10	144
Sr	283	344	256	236	396	296	351	481	362	312	316	269
Y	1		2	3	2	14	3		1			
Zr	12	38	20	24	68	66	81	166	63	70	15	70
Nb	1		2	1	8	4				2		1
Zn	3	11	5	11	22	24	20	4	6	4	5	1
Cu	16	40	67	12	17	33	15	13	13	46	24	12
Ni						4						
Ba	1083	648	725	864	824	607	1549	125	1677	216	119	2145
V	5	4	3	2	15	19	15	4		10	4	6
Cr				4	9	3	3	11		3	4	
Ga	12	20	16	21	22	17	13	13	13	14	13	14

Rare Earth Elements (ppm)

La	2.65	2.56	1.52	13.71	14.88	9.27						
Ce	4.03	4.65	2.56	27.64	31.26	18.15						
Pr												
Nd	1.08	2.01	.92	10.56	13.42	6.56						
Sm	.27	.74	.23	1.84	2.55	1.35						
Eu	.19	.70	.42	.36	.74	.51						
Gd	.24	.61	.55	1.33	2.36	1.29						
Tb	.08	.50	.07	.44	1.01	1.27						
Er		.21			.12	.78						
Yb	.11	.02			.13	1.05						
Lu												

SUMRE

Na/K	0.65	12.02	6.27	55.88	66.50	40.23	-1.00	-1.00	-1.00	-1.00	-1.00	-1.00
K/Rb	403.47	550.33	534.24	405.67	700.32	325.60	1.14	7.23	.59	4.53	6.35	.49
K/Ba	32.04	45.86	28.74	53.99	60.34	36.92	18.65	43.83	26.38	37.66	48.13	26.93

08487

Metagaites from the Maggo Gneiss

	83-266	83-268	83-283	83-287	83-307
SiO2	73.80	75.30	73.50	73.50	74.30
TiO2	.01	.06	.11	.08	.13
Al2O3	14.80	14.30	13.80	15.10	13.77
Fe2O3	.47	.23	.88	.44	.40
MnO	.01	.00	.02	.08	.01
MgO	.20	.09	.24	.07	.20
CaO	2.99	1.79	1.36	1.59	1.60
Na2O	4.99	4.21	3.49	4.23	3.32
K2O	.88	3.82	5.52	4.64	5.18
P2O5	.05	.00	.03		.07
LOI	.68	.27	.32	.33	.29
TOTAL	98.96	99.81	99.26	100.06	99.20

Trace Elements (ppm)

	8	14	15	20	16
Pb					
Th			7	2	3
U					
Rb	21	67	107	94	82
Sr	433	250	274	245	333
Zr	73	32	6	34	2
Nb		1	4	2	3
Zn	8	1	12	7	5
Cu	14	17	18	19	17
Ni					
Ba	143	1239	1833	543	2104
V	5	4	11	5	4
Cr	13	1	9	11	
Ga	16	17	18	18	17

Rare Earth Elements (ppm)

La					
Ce					
Pr					
Nd					
Sm					
Eu					
Gd					
Dy					
Er					
Yb					
Lu					

SumRE	-1.00	-1.00	-1.00	-1.00	-1.00
Na/K	5.67	1.10	.63	.91	.64
K/Rb	347.85	473.28	478.24	409.75	524.38
K/Ba	51.08	25.59	25.00	70.93	20.42

Metagaited Gneiss

	82-498	82-514	82-590	83-118	83-171	83-185
SiO2	72.90	73.30	71.30	70.20	64.90	72.50
TiO2	.15	.03	.28	.30	.36	.19
Al2O3	14.80	13.60	14.80	15.30	15.50	14.90
Fe2O3	1.01	.91	2.70	2.45	4.22	1.12
MnO	.02	.03	.07	.03	.07	.02
MgO	.35	.30	.83	1.30	2.25	.75
CaO	2.00	.43	2.89	3.35	5.46	3.12
Na2O	3.95	3.27	4.41	4.25	4.24	5.01
K2O	4.17	5.15	1.73	2.01	.87	1.27
P2O5	.06	.02	.05	.07		
LOI	.43	.52	.42	.48	.29	.28
TOTAL	99.86	98.66	99.48	99.74	98.86	99.36

Trace Elements (ppm)

	8	16	5	9	12	11
Pb						
Th	4	3	2	6	7	
U	5		5			2
Rh	71	112	67	57	14	30
Sr	396	242	278	378	349	348
Y	2	6	19	4	14	
Zr	68	135	117	82	120	67
Nb	8		9	2	5	2
Zn	22	10	34	38	40	12
Cu	17	24	23	14	45	20
Ni		1	6	20	25	
Ba	824	1149	315	707	211	260
V	15	14	30	39	76	15
Cr	9		1	35	48	5
Ga	22	14	15	19	13	18

Rare Earth Elements (ppm)

La	9.82	24.68	23.03			
Ce	20.68	47.48	48.19			
Pr						
Nd	8.32	16.79	16.17			
Sm	1.71	3.01	2.59			
Eu	.64	1.10	.57			
Gd	1.49	2.52	2.59			
Dy	.68	1.25	1.67			
Er		.53	1.08			
Yb		.19	.99			
Lu						

SumRE	43.34	97.75	96.88	-1.00	-1.00	-1.00
Na/K	.95	.63	2.55	2.11	4.87	3.94
K/Rb	487.54	381.70	214.34	292.72	515.85	351.41
K/Ba	42.01	37.21	45.59	23.60	34.23	40.55

80468

Recrystallized Pegmatites within the Maggo Gneiss

	B3-175	B3-231	B3-248	B3-700	B3-232	B3-213
SiO2	72.10	72.70	74.20	88.80	71.56	77.10
TiO2	.13	.13	.09	.12	.10	.04
Al2O3	15.40	14.30	13.10	3.43	13.10	13.00
Fe2O3	.34	.29	1.07	2.15	.81	.38
MnO	.01	.01	.07	.04	.02	.00
MgO	.08	.12	.30	1.82	.28	.13
CaO	1.12	1.19	1.31	2.10	2.86	2.36
Na2O	3.33	3.59	3.18	.72	4.17	5.12
K2O	7.13	5.76	4.83	.30	.92	.59
P2O5	.01	.01	.10	.02	.04	.04
LOI	.35	.34	.43	.04	.74	.48
TOTAL	100.00	98.44	98.68	99.55	98.14	99.23

Trace Elements (ppm)

	B3-175	B3-231	B3-248	B3-700	B3-232	B3-213
Pb	11	21	19	9	9	1
Th	3	2	10	8	6	3
U			5	2		5
Rb	144	120	109	8	15	5
Sr	315	300	368	33	305	167
Y		3	4	4		2
Zr	6	9	40	13	60	17
Nb			2	3	?	3
Zn	2	6	13	10	3	
Cu	15	75	32	15	21	5
Ni		4		23	3	
Ba	2914	1066	1380		167	38
V	4	1	8	48	5	6
Cr	4		11	60	6	14
Ga	9	4	14	6	15	16

Rare Earth Elements (ppm)

La
Ce
Pr
Nd
Sm
Eu
Gd
Dy
Er
Yb
Lu

	1.00	-1.00	-1.00	-1.00	-1.00
SumRE					
Na/K	.47	.62	.66	2.40	4.53
K/Rb	411.02	398.45	367.83	511.29	469.79
K/Ba	20.31	44.85	29.05		42.20
					128.88

Discordant Leucosomes

	B3-244	B3-214	B3-267	B3-309
SiO2	64.20	68.20	72.90	73.20
TiO2	.62	.18	.18	.05
Al2O3	15.90	14.80	14.50	13.70
Fe2O3	5.87	2.80	1.40	2.05
MnO	.10	.01	.02	.04
MgO	2.74	1.06	.41	1.54
CaO	5.92	4.12	2.50	4.46
Na2O	4.03	4.76	5.40	3.80
K2O	.96	1.06	1.36	.62
P2O5	.09	.08	.05	.00
LOI	.56	.73	1.20	.47
TOTAL	100.29	97.80	99.98	97.90

Trace Elements (ppm)

	B3-244	B3-214	B3-267	B3-309
Pb	7		7	6
Th		21	2	
U		2		
Rb	1			
Sr	21	16	35	10
Y	319	328	571	220
Zr	14	25		15
Nb	61	87	72	32
Zn	3	3		4
Cu	61	32	27	17
Ni	28	6	19	25
Ba	29			17
V	154	135	196	90
Cr	113	37	11	57
Ga	82	58	10	73
	15	21	17	16

Rare Earth Elements (ppm)

La
Ce
Pr
Nd
Sm
Eu
Gd
Dy
Er
Yb
Lu

	-1.00	-1.00	-1.00	0.00
SumRE				
Na/K	4.20	4.49	4.01	6.13
K/Rb	379.47	549.74	322.55	514.66
K/Ba	51.75	65.18	57.60	57.15

8-1-77

Appendix E

PARTITION COEFFICIENT DATA

Table E.1: Partition coefficients for REE in hypothetical mantle source minerals used in partial melting calculations. The chemical composition of the source is also given in ppm. Data from Martin (1987).

	ol	opx	cpx	garr.	source
La	0.0004	0.002	0.070	0.015	0.63
Ce	0.0005	0.003	0.098	0.021	1.62
Nd	0.0010	0.0068	0.21	0.087	1.19
Sm	0.0013	0.010	0.26	0.217	0.38
Eu	0.0016	0.013	0.31	0.320	0.144
Gd	0.0015	0.016	0.30	0.498	0.52
Dy	0.0017	0.022	0.53	1.06	0.65
Er	0.0015	0.030	0.30	2.00	0.44
Yb	0.0015	0.049	0.28	4.03	0.42
Lu	0.0015	0.058	0.27	5.05	0.065

Table E.2: Partition coefficients for REE in hypothetical Archaean tholeiite source minerals used in partial melting calculations. The chemical composition of the source is given in ppm. Data is compiled from the following sources: Arth and Hanson (1975); Frey et al. (1978); Pearce and Norry (1979); Nicholls and Harris (1980); Shimizu (1980); Martin (1987).

	opx	cpx	hbl	plag	garn	mag	zirc	apat	ilm	tit	source
La	0.0005	0.1	0.2	0.13	0.04	0.22	2.45	13.5	0.005	0	9.14
Ce	0.0009	0.2	0.3	0.11	0.08	0.28	2.29	18.0	0.006	55.3	21.5
Nd	0.0019	0.4	0.8	0.07	0.2	0.30	1.97	27.4	0.008	88.3	13.73
Sm	0.0028	0.6	1.1	0.05	1.0	0.35	3.14	62	0.01	102	3.46
Eu	0.0036	0.6	1.3	1.3	0.98	0.26	3.14	30.4	0.007	101	1.23
Gd	0.0045	0.7	1.8	0.04	3.8	0.32	12	56.3	0.017	102	4.01
Dy	0.0074	0.7	2.0	0.031	11	0.28	45.7	50.7	0.028	80.6	4.4
Er	0.0130	0.6	1.9	0.026	16	0.22	135	37.2	0.046	58.7	2.30
Yb	0.0286	0.8	1.7	0.024	21	0.18	270	23.9	0.077	37.4	2.14
Lu	0.038	0.6	1.5	0.023	21	0.18	323	20.2	0.10	26.9	0.31
K	0.01	0.02	0.33	0.11	0.02	0	0	0	0	0	3070
Rb	0.02	0.03	0.22	0.06	0.034	0	0	0	0	0	20
Sr	0.02	0.2	0.36	2.0	0.013	0	0	1	0	0	666
Ba	0.02	0.02	0.09	0.16	0.02	0	0	0	0	0	50
Y		0.03	1.9	0.6	16	0	0	0	0	0	25
Tl	0.25	0.4	3	0.05	0.5	34	0	0	0	10000	7807
Zr	0.08	0.25	1.4	0.03	0.5	0	10000	0	0	0	95

Table E.2: Partition coefficients for REE in a hypothetical intermediate composition source lithology used in partial melting calculations. The chemical composition of the source is also given in ppm. Data is compiled from the following sources: Arth and Hanson (1975); Frey et al. (1978); Simmons and Hedge (1978); Pearce and Norry (1979); Nicholls and Harris (1980).

	opx	cpx	hbl	plag	garn	bio	Kspar	apat	zirc	mag	tit	source
La	0.028	0.25	0.4	0.35	0.28	0.034	0.054	23.7	2.8	0.098	40.0	6.3
Ce	0.038	0.3	0.51	0.24	0.35	0.037	0.044	34.7	2.64	0.11	53.3	14.8
Nd	0.058	0.49	1.2	0.17	0.53	0.044	1.025	57.7	2.2	0.13	88.3	8.7
Sm	0.1	0.7	2.0	0.13	2.66	0.058	0.01	62	3.14	0.15	102	2.2
Eu	0.01	0.79	0.87	2.11	1.5	0.145	1.13	30.4	3.04	2.1	101	1.01
Gd	0.171	0.96	2.5	0.09	10.5	0.082	0.011	56.3	3.12	0.12	102	2.5
Dy	0.293	1.2	3.5	0.086	28.6	0.097	0.006	50.7	45.7	0.14	80.6	2.47
Er	0.46	1.2	2.75	0.084	42.8	0.162	0.006	37.2	135	0.155	58.7	1.32
Yb	0.67	0.9	2.0	0.077	39.9	0.179	0.012	23.9	270	0.17	37.4	1.04
Lu	0.84	0.8	1.7	0.062	29.6	0.185	0.006	20.2	323	0.19	26.9	0.09
K	0.01	0.02	0.33	0.11	0.02	2.6	1000	0	0	0	0	11505
Rb	0.02	0.02	0.05	0.07	0.01	3.3	0.034	0	0	0	0	87
Sr	0.02	0.08	0.23	1.8	0.02	0.12	3.87	1	0	0	0	263
Ba	0.02	0.02	0.09	0.16	0.02	6.4	6.12	0	0	0	0	199
Nb	0.35	0.3	1.3	0.025	0.17	1.8	0.006			50.7	45.7	8
Tl	0.25	0.4	3	0.05	0.5	1.5	0.04	0	0	34	10000	4969
Zr	0.08	0.25	1.4	0.03	0.5	1.2	0.1	0	10000	0	0	169

